TEMPO AND MODE: USING GENOMIC, ANATOMICAL, AND LIFE-HISTORY DATA TO INTEGRATE THE MICRO- AND MACROEVOLUTION OF BIRDS

A Dissertation

Presented to the Faculty of the Graduate School

of Cornell University

In Partial Fulfillment of the Requirements for the Degree of

Doctor of Philosophy

by

Jacob Samuel Berv

August 2019

© 2019 Jacob Samuel Berv

TEMPO AND MODE: USING GENOMIC, ANATOMICAL, AND LIFE-HISTORY DATA TO INTEGRATE THE MICRO- AND MACROEVOLUTION OF BIRDS

Jacob Samuel Berv Ph. D.

Cornell University 2019

My research agenda as a Ph.D. Candidate has been primarily driven by a fascination with the boundary between micro- and macroevolution. While these intellectual domains are most commonly studied separately from of one another, I do not regard them as products of distinct phenomena; to me, they are different manifestations of the same underlying evolutionary processes. As such, I am motivated to understand the mechanisms linking microevolutionary processes to macroevolutionary patterns. Some of the questions that guide my research program include: What are the roles of evolutionary contingency and convergence in generating patterns of biodiversity? Why might certain modes of evolution predominate over others? What are the drivers and constraints on evolutionary change? Are there evolutionary 'laws'?

My first two dissertation chapters focus on evolutionary questions at relatively recent timescales. The most significant of these interests focuses on the biogeography and evolution of neotropical suboscine passerines, a speciose group of modern birds representing ~10% of living bird diversity. In particular, I focus on two South American avian clades, Cotingidae (Berv and Prum 2014), and Pipridae (forthcoming work, Berv *et al* 20xx), which are characterized by a fascinating diversity of plumages, vocalizations, and display behaviors. These works evaluate several hypotheses about the origins of diversity in the Amazonian and Andean regions of Latin America.

While the first half of my dissertation reports on avian microevolution, I am also deeply fascinated by macroevolutionary patterns. Birds are one of the most broadly appreciated groups of living organisms, but the origins of modern birds are shrouded in mystery. After the Chicxulub asteroid struck the Yucután peninsula 66 million years ago (the K-Pg event), up to

75% of life on Earth was lost. It took millions of years for ecosystems to recover from this geologically instantaneous contingency. We know that at least a few early lineages of modern birds survived and rapidly diversified in the wake of this event—but *how*? My dissertation research in this area leverages advances in DNA sequencing to investigate the impact of the mass extinction on bird evolution. In one chapter, I worked with a team of researchers to construct a new phylogenetic framework for understanding bird diversification (Prum, Berv *et al* 2015). In my final chapter (Berv and Field 2018), I propose and evaluate a new hypothesis—that the K-Pg event drove a macroevolutionary shift in the rate of avian genome evolution.

BIOGRAPHICAL SKETCH

Jacob Samuel Berv was born in Stamford, Connecticut to Kenneth and Spring Berv. Jacob's father fostered an initial appreciation for science, and both of his parents provided countless opportunities for him to learn and explore. Early trips to the Stamford Nature Center, as well as the American Museum of Natural History in New York, cemented what would become a life-long pursuit of science. After completing his early education in Stamford at Westover Magnet Elementary School, Cloonan Middle School, and then Westhill High School in 2006, Jacob entered Yale College, in New Haven Connecticut. While at Yale, Jacob discovered Evolutionary Biology as an intense interest, and sought out opportunities to do field work in Latin America and Africa. He received a Bachelor of Science in Biology, with a focus in Ecology and Evolution, in 2010. During the following three years, he was employed as a research technician in Richard Prum's lab, which had been his home for his undergraduate research. In August 2013, Jacob entered the Ecology and Evolutionary Biology Ph. D. program at Cornell University in Ithaca, New York, under the guidance of Dr. Irby Lovette, Dr. Amy McCune and Dr. Anurag Agrawal. Jacob successfully defended his dissertation on May 20, 2019, and accepted a post-doctoral position as a Life Sciences Fellow at the University of Michigan.

Dedicated to my undergraduate scientific mentors, Richard Owen Prum and Kristof Zyskowski, for their boundless enthusiasm, support, and encouragement. Thank you for opening my eyes to the immensity and splendor of life.

ACKNOWLEDGMENTS

Scientific work is never done in isolation. There are so many people who have supported me over the years that it will strain my memory to provide a compressive accounting. First, I must thank my parents, Spring and Kenneth Berv, for understanding that medical school was not right for me, and for supporting me in finding my own path. Thank you for all of the pets, books, freedom, field trips, and science camps. To the rest of my immediate family – I thank my brother Mahlon for listening to my stories from graduate school, my uncles Irving and Sam for trains, legos, and RC cars, and my grandparents for their encouragement in my early years.

My first research experiences in a laboratory were in molecular neuroscience, in the lab of Dr. Arie Kaffman, at the Yale School of Medicine. I spent much time with Arie in high school, and for some time in college before getting pulled toward other pursuits. I attribute my first lab bench skills, as well as my first real appreciation for the scientific method to him, and for that I am extremely grateful.

Later, after I rediscovered an interest in the natural history sciences at Yale, I met Dr. Richard Prum, Dr. Kristof Zyskowski, Dr. Edgar Benavides, Dr. Jon Beadell, as well as future Drs. Jacob Musser, Teresa Feo, Daniel Field, and others through coursework and later research opportunities. I cannot overstate the impact these individuals had and continue to have on my personal development as a scientist, so I will simply say that I would not be here without them.

I also would not be here without the support of my Ph.D. committee, and in particular my Ph.D. committee chair Dr. Irby Lovette. Dr. Lovette recruited me to join the Cornell Laboratory of Ornithology community, and during my time at Cornell he has been a thoughtful mentor, encouraging me to develop my communication skills and pushing me when I needed to be. Dr. Lovette offered a unique perspective that has added tremendously to my graduate education, particularly with respect to understanding university administration and running a large lab: I hope to fully appreciate it one day. Throughout my Ph.D., Dr. Lovette supported a nurturing environment for me to grow as a scientist, and I attribute many ideas to conversations with

associated graduate students and postdocs. I am very grateful for all of his support, both direct and indirect. Dr. Amy McCune and Dr. Anurag Agrawal have also been sources of inspiration throughout my Ph. D., and I thank them for their time in reading paper drafts, their willingness to help me develop my dissertation ideas, and for the many occasions in which they lent me their ears when an outside perspective was needed.

While at Cornell, I have had the privilege of getting to know and work with Dr. Leonardo Campagna, who arrived at Cornell around the same time that I did. Leo and I bonded over a shared passion for Latin American birds, and we have been working together for a large portion of my Ph.D. on one of my dissertation chapters (enclosed). It has been great fun to learn from and travel with Leo.

Another individual I need to highlight is Dr. Daniel Field, now Lecturer at Cambridge in the United Kingdom. Though I met Daniel when I had just finished my undergraduate education at Yale and he was starting as a Ph.D. student there, I only got to know him later, when working on my third and fourth dissertation chapters (enclosed). In working on those projects (and others), Daniel has become one of my greatest friends and mentors and continues to be a truly invaluable sounding board for all aspects of my academic life. I look forward to many years of future collaboration and friendship.

I must thank the universally agreed upon unsung hero of Cornell EEB's program, Dr. Monica Geber. There are few people who have done as much good for graduate students in our community as Monica. Dr. Geber, as well as Dr. Kelly Zamudio are also owed an enormous debt for leading a specialized course on grant writing, to which I fully attribute my success at obtaining my first NSF grant. To other EEB staff, I would like to thank Carol Damm, Patty Jordan, John Howell, and Brian Mlodzinski for administrative and technical support.

I have also had the great pleasure of getting to know some extraordinarily friends while I have been a graduate student at Cornell. In no particular order: Erin Larson, Emily Funk, Lina Arcila-Hernandez, Sue Pierre, Aubrie James, James Lewis, Karin van der Burg, Jenny Uheling, Timmothy Salazar, Collin Edwards, Holly Lutz, J. Ryan Shipley, and Lily Twinning, have all

made this an unforgettable experience. I cherish our friendships and memories. I also thank close friends from earlier periods of my life, including Akshay Mehra, Cole Sickler, Daniel King, Michele Trickey, Roger Kim, Derek Zhao, and Blair Benham-Pyle, for being unconditional and always able to make me smile. You made the slough of grad school endurable.

The present work was funded by a variety of sources which are acknowledged in the acknowledgement sections for separate chapters. However, my primary sources of funding in graduate school have come from the Cornell Laboratory of Ornithology (graduate student Athena research grants), as well as a Graduate Research Fellowship from the National Science Foundation and a Doctoral Dissertation Improvement Grant, also from the National Science Foundation. Additional funding came from the Society for the Study of Evolution, The Society for Molecular Biology and Evolution, The Society of Systematic Biologists, Sigma Xi, Cornell University (Mellon Grant, Feeny Fund, Orenstein Fund), and elsewhere.

Lastly, in the word of Carl Sagan, “In the vastness of space and the immensity of time, it is my joy to share a planet and an epoch...” with Amelia.

TABLE OF CONTENTS

LIST OF FIGURES

LIST OF TABLES

PREFACE

> *"The affinities of all the beings of the same class have sometimes been represented by a great tree. I believe this simile largely speaks the truth. The green and budding twigs may represent existing species; and those produced during each former year may represent the long succession of extinct species…At each period of growth all the growing twigs have tried to branch out on all sides, and to overtop and kill the surrounding twigs and branches, in the same manner as species and groups of species have tried to overmaster other species in the great battle for life…Of the many twigs which flourished when the tree was a mere bush, only two or three, now grown into great branches, yet survive and bear all the other branches; so with the species which lived during long-past geological periods, very few now have living and modified descendants…As buds give rise by growth to fresh buds, and these, if vigorous, branch out and overtop on all sides many a feebler branch, so by generation I believe it has been with the great Tree of Life, which fills with its dead and broken branches the crust of the earth, and covers the surface with its ever branching and beautiful ramifications."*
>
> — Charles Darwin, 1859

As the origins of Earth's biodiversity come into clearer focus, the 21st century is becoming an increasingly exciting time to be studying evolution. One of the reasons for this sustained enthusiasm is the closure of the genomic data-gap—the sequencing revolution that has enabled us to peer into the blueprint of life with resolution perhaps unimaginable to researchers of earlier eras. Evolutionary biologists are now often faced with the challenge of processing and understanding an inundation of data, creating new imperatives for the training of researchers in the life sciences: in addition to studying classical genetics, we must now train in computing to analyze the datasets we generate.

I have been extremely fortunate to have entered into my doctoral studies at a point in time in which the development of sequencing technologies has enabled evolutionary biologists to generate such datasets germane to evaluating fascinating questions that we could not previously

address. For example, in 2019, it has become almost routine to query the entire genome and its derivatives, to search for genotype-phenotype associations in non-model organisms. The study of speciation itself has also grown tremendously, and the paradigm of species as products of gradually accumulating genic variation shaped mostly abiotic forces has begun to give way to the perspective that novel combinations of ancestral variation can also punctuate gradients of diversity with new forms.

In my subfield of phylogenetic systematics, a parallel revolution has occurred in the development of statistical methods which help us evaluate hypotheses about the timing and correlates of evolutionary patterns. These developments can be traced to the first rigorous attempts to use computers to infer the relationships among organisms in the 80s by Joe Felsenstein, David Hillis and their contemporaries. But today, 20 years into the new century, the unification of sophisticated computer science and natural history science has led to a truly remarkable ability to query the history of life. While we may never know the 'truth' about some things, the mathematical language which enables us to use the available evidence to test interesting hypotheses is maturing and becoming more accessible.

It has indeed been awe-inspiring to observe the pace at which my field has developed since I entered graduate school in 2013, and since I began seriously thinking about evolution a decade ago. One important lesson I have learned over the course of my Ph.D.is that even the most impressive genomic datasets sometimes do not provide clear answers. While we can now address some long-standing questions with more data, more data may not help if you are asking the wrong question—indeed it can be positively misleading. This is strongly exemplified by recent efforts to elucidate the higher-level relationships among bird families, which is the focus of one dissertation chapter (below). The complexity of genome-scale data has highlighted to me

the fundamental inadequacy of many commonly used models, and that the assumptions underlying such models are sometimes better described as exceptions.

My own growing awareness of this issue has led me to think about the way we acquire knowledge in my discipline less in terms of the discovery of absolute truths, but in terms of evaluating competing models, each with different assumptions which may or may not be met, and each with parameters which may or may not be sufficient. In this era of big data science it is worth emphasizing that a good model with limited data may produce a better inference than a poor model with unlimited data, and that good models for limited data may not be the same models as those that would be best for unlimited data. Future breakthroughs will come from identifying the aspects of our models which fail to explain the pronounced heterogeneity of process and pattern required by the unlimited genomic data we now collect. Moreover, if Stephen Jay Gould's perspective that nature is "so hierarchically ordered in a causal sense…that distinct processes emerge at a series of ascending breakpoints in time and magnitude" (Gould 1994) is true, then we might expect to require fundamentally different models to describe observations made at different scales, even if the phenomena which ultimately generated those scales are fundamentally the same (below).

Given these challenges, it amazes me that we do as well as we do at modeling complex evolutionary phenomena, considering that often we cannot easily derive experimental evidence to validate our models and their implications. Neontologists who study evolutionary systematics are much like cosmologists in that we often have no direct evidence of the inherently historical phenomena we are studying—only their contemporary products, most often in the form of DNA sequences or anatomical and other traits. We may also only have a single slice of time on which to apply our models to divine the process which generated our contemporary observations [of

course, this is a somewhat weak analogy because cosmologists have the added benefit of actually being able to see directly and literally into the past].

The only direct evidence of evolution on geologic timescales, indeed the evolutionary process at all, is the fossil record. While the fossil record is of course invaluable, our ability to answer specific evolutionary questions is first conditioned on the combination of luck and skill required to find and correctly identify fossils germane to those questions, and/or in identifying natural experiments with independent historical replication. In this respect, paleontologists are perhaps more like archaeologists: there often are no longer contemporary examples of their research foci, so inferences must be drawn from a patchy historical record.

Therefore, if we are to understand the evolutionary process, we must recognize that we are constrained by the adequacy of the models we use, which aim to interpolate and integrate a patchy record of different data types through time and space, even when we are lucky enough to have multiple timepoints represented.

My own perspective on the history of life is certainly biased, as it comes primarily from neontological studies of avian phylogeny. I am not overly familiar with the invertebrate, vertebrate, and non-animal fossil records, though my understanding of the avian fossil record is steadily improving. I still have much to learn from these areas, and as I transition to the next phase of my career at the University of Michigan Museum of Vertebrate Paleontology, I am very grateful that I can continue to be a student of paleontological and neontological tools with which I hope to help bridge the intellectual and parametric gaps that characterize our present state of knowledge.

Introduction

My research agenda as a Ph.D. Candidate has been mostly driven by a fascination with the boundary between micro- and macroevolution. Microevolutionary processes are those which are commonly identified as those occurring within species, perhaps even within a single population—mutation, drift, selection, and migration, each mediated by the life histories and unique physiologies of organisms. By contrast, macroevolutionary patterns can only be observed through a wider lens—these are patterns evident across multiple species or taxa, often through deep evolutionary time: speciation, extinction and patterns thereof. While these intellectual domains are commonly studied in isolation of one another, they are not products of distinct phenomena; they are different manifestations of the same underlying evolutionary processes. As argued by Stephen Jay Gould and George Gaylord Simpson in various works, micro- and macro-evolution should not be viewed as opposed, but as truly complimentary (Gould 1994). While the purpose of this introduction is not to summarize the immense body of theory that exists on that topic, it is fair to say I have grown particularly motivated in my Ph.D. to contribute to our developing understanding of the links between microevolutionary processes and macroevolutionary patterns.

I can trace my initial interest in these topics to work I did as an undergraduate and post-graduate at Yale University ~2008-2013. I started my university education on a pre-medical track, having volunteered in a molecular neuroscience lab when I was in high school (also at Yale, having been a local student). Most of my friends in biology were also pre-med, though I lived with a few who would go on to become engineers, financiers, and entrepreneurs.

My first real exposure to evolutionary biology happened in 2008. I record this brief story only to highlight how my entire career trajectory may have hinged on a single serendipitous

decision made a long time ago. When I was a sophomore in college, I had an open slot in my course schedule because I had placed out of an otherwise required pre-med course. I still recall leafing through 'the blue book' (which has by now migrated online), and finding a course called "Ornithology," taught by a professor named Richard Prum, whom I had never previously heard of. I remember reading something about the dinosaur ancestry of birds in the course description and feeling like a bomb had been dropped in my world.

That was 11 years ago this year. I ended up taking the course (an upper level elective, without having taken the pre-requisites) mostly because it sounded fun, and for the first time in my academic life I was exposed to material that was fascinating on its own, not because it felt like a means to some other career-related end. I loved this experience and subject matter, and I didn't have to work to enjoy it. Though it might be cliché, people talk about 'finding their calling,' and this was it for me, though it took another year or so for me to formally transition to declaring myself an Ecology and Evolution major, and for me to work up the nerve to ask Rick if he would take me on as an undergraduate researcher.

I worked a number of bird evolution projects with Rick as an undergraduate, and for a few years after as a technician. Working with Rick, as well as Kristof Zyskowsi (a collections manager at the Yale Peabody Museum) I was eventually invited to participate in several field collecting trips that each left me awe-struck, and I continued to seek out field opportunities, mostly for the adventure; between 2007 and 2013, I helped with field research in Ecuador, South Africa, Suriname, Papua New Guinea, Guatemala, and Honduras. I became interested in Neotropical grassland birds, some of which have intriguing patterns of disjunct distributions across the Amazon Basin, and we came up with an idea to study the comparative biogeography of these birds. I was able to pursue that to an extent while working on other projects in Rick's

lab, but ultimately several of these early projects remain unfinished.

I applied to graduate school in 2012, and after accepting a position in Irby Lovette's lab at Cornell University and the Cornell Laboratory of Ornithology, I deferred a year to start in the Fall of 2013. After a tough first semester teaching a writing intensive seminar, and a phenomenal trip as a TA to Kenya, Irby graciously allowed and encouraged me to continue pursuing ideas that had germinated earlier—including the ideas I had been developing on Neotropical birds.

These early projects on grassland birds, among other things, led me to think about why co-distributed species may or may not share aspects of their evolutionary histories. With Irby's input, I wrote an NSF Graduate Research Fellowship proposal focused on these ideas, and proposed a mechanism linking individual dispersal ability to macroevolutionary patterns. While I didn't realize it at the time, these concepts directly connected a microevolutionary phenomenon (the actions or behaviors of individuals) to the evolutionary fate of the lineages of which they are members in a way that may have mechanistically explained some broad scale (macroevolutionary) observations. I recall conversations with Amy McCune and Anurag Agrawal, two obliging and invaluable members of my Ph.D. committee, in which we discussed the idea that differences in an organisms' intrinsic life-history characters, such as generation length, may also contribute to macroevolutionary patterns. Soon after, I read George Gaylord Simpson's 'Tempo and Mode in Evolution' on Amy's recommendation, and it completely changed the way I think about evolutionary biology. In general, I was excited by the idea of being able to connect observations made at different temporal and spatial scales, and the idea that simple rules could generate complex emergent patterns.

My GRFP proposal was funded, guaranteeing three years of uninterrupted research support. In the following year however, an enormous dataset I had worked to generate earlier fell

into my lap, and Irby encouraged me to pursue that project in the short term (summarized below). Ultimately, while my ideas about neotropical grassland taxa have not directly turned into dissertation chapters, I can now clearly see the links between those early conceptual ideas and the projects I ended up actually doing.

Dissertation themes

Though I have focused much of my research on birds, I now identify first as an evolutionary biologist. The lens through which I view biodiversity and the study thereof is the lens of Darwin's conception of the "Tree of Life." Though I do find birds immensely fun and fascinating and useful as a system to investigate various hypotheses, I aspire to be more question-based than I am taxon-focused. Some of the broader thematic questions that have inspired my Ph.D. research have included: What are the roles of evolutionary contingency and convergence in generating patterns of biodiversity? Why might certain modes of evolution predominate over others? What are the drivers and constraints on evolutionary change? Are there evolutionary 'laws', and how can we discover them? These topics have required an appeal to both micro- scale and macro-scale observations, and my dissertation chapters have thus required that I consider information from natural history, systematics, genomics, and paleontology, sometimes simultaneously, and often through the language of Bayesian statistics.

Dissertation summary

Part I: Two of my dissertation chapters focus on evolutionary questions at relatively recent timescales. The most significant of these interests focuses on the biogeography and evolution of neotropical suboscine passerines, a speciose group of modern birds that comprises ~10% of

living bird diversity. In particular, I have focused on two South American avian clades, Cotingidae and Pipridae, which are both characterized by a captivating diversity of plumages, vocalizations, display behaviors, and mating systems. In one chapter, I investigate how breeding system may affect the evolution of plumage coloration, in order to test Darwin's hypothesis that polygyny drives the evolution of avian color dichromatism (Berv and Prum 2014). This project required that I generate the first comprehensive time calibrated phylogenetic tree for the Cotingidae (~70 species) based on DNA sequences, and then apply comparative methods to address a macroevolutionary hypothesis. One of the major challenges of this work was generating compatible DNA sequence data from old museum skins, and I spent several years focused on generating this dataset using sanger sequencing technology (next-generation methods have made this incomparably easier in the years since). While we did not find statistical support for Darwin's original hypothesis, subsequent unpublished analyses I have performed have questioned this result and await either another student or more time for me to follow up.

In another chapter that has been my prime focus at various points since 2011 (and most of the last two years in collaboration with Leo Campagna, Teresa Feo, Camila Ribas, Ivandy-Castro Astor, Richard Prum, and Irby Lovette), I investigate the historical biogeography and evolution of the cryptic neotropical species complex, *Pseudopipra*. While the intellectual seeds of this work were planted in some ways before I formally started graduate school, most of its development has been a consequence of a close collaboration with Leonardo Campagna, who helped tirelessly with all aspects of it, and without whom it would not have become nearly as interesting.

Although many Neotropical birds have complicated distribution patterns, this taxon is particularly appropriate for assessing patterns of phylogenomic differentiation across a nested set

of spatial scales, as it is found on both sides of a variety of known dispersal barriers, including elevational gradients of the Andes, major Amazonian rivers, dry open habitats, tepuis, and the Isthmus of Panama. In this study, I apply a genomic technique to sample thousands of markers across a continental-scale sample of hundreds of individuals. My primary goal was to evaluate several hypotheses about the provenance of diversity in the Amazonian and Andean regions of Latin America, and to elucidate the history of a continental scale radiation, from the scale of individuals to multiple differentiated species. In particular, I address the hypothesis that lowland Amazonian rainforest diversity within this complex may have originated from montane Andean lineages. My investigations of *Pseudopipra* have also provided me two opportunities to study this species in the field, initially in Suriname (before I started graduate school in 2009—specimen collecting), and then later in collaboration with Latin American scientists at the Instituto Nacional de Pesquisas da Amazônia (INPA) in Manaus, Brazil in 2015. In Brazil, I collected data on vocalizations and courtship behavior, which has helped provide phenotypic context to my studies of genomic variation.

Part II: I have also used my Ph.D. as an opportunity to study broader scale patterns of avian phylogeny. As the only extant group of theropod dinosaurs, birds are one of the most broadly appreciated groups of living organisms, but despite the disproportionate scientific effort in elucidating bird biology, the origins of modern birds are still somewhat shrouded in mystery.

In 2012, while working as a technician for Richard Prum, I began contributing to a team-effort to generate a new phylogenetic hypothesis at the family level for all birds. The history and context of this project is somewhat complicated, so I have provided a brief summary here. First, we wanted to leverage advances in DNA sequencing technology previously developed by Alan

and Emily Lemmon, that had made it suddenly much easier to collect a genome-wide sample of long, high quality stretches of DNA. Next, we were propelled forward by knowledge of two independent groups of scientists working to publish on a similar topic. Our main goal was to try to generate a new genomic dataset quickly, to serve partly as an infrastructure project, and also to generate a new backbone for comparative analyses. We knew that one of the groups working in parallel was focused on generating whole-genome data for about 50 taxa, so our strategy was to complement their ongoing work with a larger taxon sample, but with lower data coverage. We eventually settled on a sample of 198 species of living birds, representing all major avian lineages, as well as two crocodilian outgroups. Then, in collaboration Alan and Emily, as well as Alex Dornberg, Daniel Field, and Jeffrey Townsend, it became my job to generate a phylogenetic hypothesis, as well as to estimate a new timescale of avian evolution. Fast forward three years, and in late 2015 in my third year of graduate school, I published this work as a co-lead author in *Nature* (Prum et al. 2015). While I was not the sole lead author of this work (and it certainly could not have been finished without major contributions from all collaborators), my Ph.D. committee kindly offered to allow me to include this work as an additional chapter of my dissertation. In the few years since we published, a number of important works have questioned some of our results – so I emphasize that at this time (May 2019) there are still many unanswered (maybe even unanswerable) questions about the early evolution of birds.

One of the conclusions of our 2015 study was that the age of modern birds may have been about ~72 Ma, considerably younger than some previous estimates, which ranged up to ~160 Ma. However, issues of logical circularity became apparent soon after we published: sensitivity analyses of molecular data which did not include prior information on the age of the entire clade generated substantially older (~100 Ma) estimates which were incongruous with

what the fossil record would have us believe (closer to the K-Pg boundary ~66 Ma). This discrepancy between the signal from the fossil record and the signal from molecular data makes it difficult to reliably assess the impact of the K-Pg event on bird evolution. This incongruence, as well as patterns I noted when I had initially performed the divergence time analysis for Prum et al. (2015), led me to consult again with Daniel Field (then Ph.D. Candidate in Jacques Gauthier's lab, now Lecturer at the University of Cambridge, UK). Daniel describes himself as a paleo-ornithologist and having come from a more traditional background of paleontology, we began discussing the context in which early birds must have evolved.

A key observation was that our previous divergence time analysis indicated pronounced heterogeneity (~20x) in the rate of molecular evolution (that is, the underlying rate of sequence evolution on a per-lineage basis) across the avian tree of life in our new dataset. At the time, I didn't appreciate how much research had been done on understanding heterogeneity in rates of molecular evolution across the Tree of Life, and I began reading intensively on the topic. Several names popped out as contemporary leaders in this sub-field of molecular systematics: Lindell Bromham, Simon Ho, Robert Lanfear, and many others. It quickly became apparent that one of the prime correlates of rate variation was generation length, often proxied via adult body size (observational data on generation length are hard to come by, even in birds). After a quick preliminary analysis, it became clear that adult body mass was highly predictive of the rate of molecular evolution across our dataset.

Of course, in hindsight this makes sense – for instance, we intuitively accept that organisms like bacteria evolve quickly because of their dramatically shorter generation lengths. However, I had never before considered the idea that such differences in individual life histories of macro-organisms could leave clear fingerprints on model-based inferences of phylogenetic

history. This personal epiphany changed the way I look at phylogenies—I remember thinking to myself that while phylogenies are in many ways a gross abstraction of an incredibly complex process, their nested hierarchy of *branch lengths* contains much more information than just a set of topological *branching order*. In essence, model-based phylogenies derived from genomic sequence data are summary reconstructions of the entire population genetic history of clades.

I sometimes like to use the analogy of pulling on a thread. In science, we sometimes identify threads of inquiry that are interesting for a particular reason, or perhaps have some intrinsic interest. But when you pull on that thread, it is sometimes hard to predict where you will end up. In this case, the thread was an observation of heterogeneity of pattern within a large dataset. I ended up with a new mindset with which to assess a perplexing conundrum surrounding the early history of bird evolution.

When the Chicxulub impactor struck the Yucután peninsula 66 million years ago (the K-Pg event), some estimates suggest that up to 75% of life on Earth was lost. Millions of years passed before ecosystems fully recovered from this geologically instantaneous environmental contingency. As we continue to learn from deposits all over the world (and increasingly from China), an incredibly diverse community of ancestral early birds went extinct at the K-Pg boundary. And while there must have been an element of chance in which lineages survived, we are learning that deterministic ecological factors also likely played a role. In other work from my Ph.D., I argued that ancestral ecological habit (terrestrially or arboreality) may have played an important role in avian survivorship (Field et al. 2018). But the question of the timing of bird evolution, one of the primary results from the 2015 study, required further treatment.

My discussions with Daniel progressed, and we eventually arrived at a previously proposed idea, that the K-Pg event itself may have driven a macroevolutionary shift in the rate of

avian genome evolution in survivors of the K-Pg event. We know that at least a few early lineages of modern birds survived and rapidly diversified in the wake of this event—but *what actually happened to those lineages which survived?* I don't remember if it was me or Daniel, but at some point during our discussions, one of us remarked that the observations I had made about rates of molecular evolution could be a convenient way to explain the divergence time issue, *if birds got smaller at the K-Pg boundary*. I recall Daniel excitedly mentioning that that mass extinctions had been previously proposed to filter out large bodied organisms through a poorly understood process paleontologists call the "Lilliput Effect." Smaller bodied birds tend to have faster evolving genomes, and if only small birds survived, such a "Lilliput Effect" may explain part of the divergence time discrepancy. At this time, Daniel had become an authority on estimating the body mass of extinct birds, by comparing anatomical measures of living birds to different kinds of preserved skeletal elements in the fossil record. We realized that by joining forces, we could test the hypothesis of an 'avian Lilliput Effect' at the K-Pg boundary, directly integrating paleontological evidence with molecular data from living birds.

From that point, we proceeded with an intensive investigation of these ideas that ultimately turned into one of my dissertation chapters (Berv and Field 2018). In brief, we found that an avian Lilliput Effect was a plausible explanation, at least in part, for over-estimations of divergence times in prior studies of avian phylogeny.

Concluding thoughts

I hope that this introduction has provided some useful context for anyone reading in the future – it has been a fun exercise for me to reflect on the personal intellectual journey that has led me to the synthesis of ideas, disciplines and tools discussed above. In this final section, I

would like to make some predictions about where I think my field may go over the next decades.

First, my studies of neotropical diversification have re-emphasized to me something which we already accept—that patterns of diversity in the tropics are likely dramatically underestimated. My focal studies of tropical diversity in several avian clades have concentrated on the New World tropics, which may have some peculiarities, but I think some reasonable generalizations can be made. Though I have not studied conservation biology from a theoretical perspective (and am not well informed on the latest trends within that field), the conservation of tropical biodiversity will be extremely difficult without better documentation of the patterns of diversity which exist to be conserved. For example, if we aim to protect evolutionarily distinct forms of whatever degree we eventually decide is most important, knowledge of historical and contemporary genetic diversity, as well as contemporary and historical relationships, is essential. Acquiring this knowledge demands rejuvenated and sustained effort in specimen collection and curation, as well as standardized analyses of patterns of genetic diversity.

It might seem like taxonomic breadth may be more important than detailed investigations of single taxa at this point. However, if a majority of tropical taxa contain unrecognized and deeply divergent cryptic species (which is certainly true of many tropical birds, and probably true of all other major organismal groups), we will need to cover both taxonomic breadth across recognized species, as well as depth within recognized species, to fully characterize patterns of extant diversity. Given that most theoretical and empirical work attempting to understand the drivers of neotropical diversification are conditioned on taxonomy-based hypotheses, it is difficult to gauge where these investigations may be falling short. I fear that current trends and nationalist politics may preempt the acquisition of this knowledge before we can learn enough to make informed conservation decisions and protect our global heritage.

Second, and on a generally more positive note, I think that the ongoing synthesis of neontology and paleontology is going to lead to a new renaissance in comparative biology. At present, I think it is fair to say that a majority of neontological comparative biologists working with DNA sequence data have only considered using fossils in terms of parameterizing models of divergence time analyses. But I think that perhaps in some ways we have missed the forest for the trees. Clearly fossils provide invaluable information about the timing of events, but fossils also inherently possess an astonishing amount of information beyond their geologic context which pertains directly to analyses of molecular sequence data. For instance, fossils can tell us many things which are directly correlated to population genetic or demographic parameters; genome size, body size, population size, generation length, metabolic parameters, ecological habit, and much more, all leave tell-tale fingerprints (though some no doubt clearer than others). I anticipate that ongoing advances in statistical approaches will increasingly enable neontological and paleontological datasets to talk to each other, thereby allowing us to address fascinating questions such as:

1) What does the relationship between the rate of molecular evolution and life history traits look like, across the genome?
    a. Are there particular types of loci which are more correlated to life history traits than others? Why or why not?
    b. Can we detect candidate loci for complex phenotypes by looking for shifts in the rate of molecular evolution across the genome?
2) Can we use models of DNA sequence evolution to study the history of life history diversity?

a. Does mass extinction leave a deterministic imprint on the genomes of surviving lineages?
b. Can we use models of sequence evolution to ground truth estimates of ancestral state reconstructions?
c. Can we use models of sequence evolution to inform predictions of phenotypes or life history characters for recently extinct or living taxa that cannot easily be measured?

3) What must we believe about molecular evolution in order to believe or disbelieve the fossil record? What must we believe about the fossil record in order to believe or disbelieve patterns of molecular evolution?

Each of these related questions and sub questions encompass broad domain of intellectual inquiry and will keep me and many other scientists busy for many years.

PREFACE REFERENCES

Berv JS, Field DJ. 2018. Genomic Signature of an Avian Lilliput Effect across the K-Pg Extinction. Systematic Biology, 67:1-13.

Berv JS, Prum RO. 2014. A comprehensive multilocus phylogeny of the Neotropical cotingas (Cotingidae, Aves) with a comparative evolutionary analysis of breeding system and plumage dimorphism and a revised phylogenetic classification. Molecular Phylogenetics and Evolution, 81:120-136.

Field DJ, Bercovici A, Berv JS, Dunn R, Fastovsky DE, Lyson TR, Vajda V, Gauthier JA. 2018. Early Evolution of Modern Birds Structured by Global Forest Collapse at the End-Cretaceous Mass Extinction. Current Biology, 28:1825-1831.e1822.

Gould SJ. 1994. Tempo and mode in the macroevolutionary reconstruction of Darwinism. Proceedings of the National Academy of Sciences, 91:6764-6771.

Prum RO, Berv JS, Dornburg A, Field DJ, Townsend JP, Lemmon EM, Lemmon AR. 2015. A comprehensive phylogeny of birds (Aves) using targeted next-generation DNA sequencing. Nature, 526:569-573.

CHAPTER 1

A comprehensive multilocus phylogeny of the Neotropical cotingas (Cotingidae, Aves) with a comparative evolutionary analysis of breeding system and plumage dimorphism and a revised phylogenetic classification[I]

Jacob S. Berv[1], Richard O. Prum[2]

1. Department of Ecology and Evolutionary Biology, Fuller Evolutionary Biology Program, Cornell University, and Cornell Laboratory of Ornithology, Ithaca, New York 14853, USA
2. Department of Ecology and Evolutionary Biology and Peabody Museum of Natural History, Yale University, P.O. Box 208105, New Haven, CT 06520, USA

Keywords: Phylogenetics, Bayesian inference, Species-tree, Sexual selection, Polygyny, Monogamy

[I] Reviewed, formatted, and accepted for publication as Berv, J.S, Prum R.O. A comprehensive multilocus phylogeny of the Neotropical cotingas (Cotingidae, Aves) with a comparative evolutionary analysis of breeding system and plumage dimorphism and a revised phylogenetic classification. Molecular Phylogenetics and Evolution. 1055-7903, (2014). Reprinted here with permission.

ABSTRACT: The Neotropical cotingas (Cotingidae: Aves) are a group of passerine birds that are characterized by extreme diversity in morphology, ecology, breeding system, and behavior. Here, we present a comprehensive phylogeny of the Neotropical cotingas based on six nuclear and mitochondrial loci (~7500 bp) for a sample of 61 cotinga species in all 25 genera, and 22 species of suboscine outgroups. Our taxon sample more than doubles the number of cotinga species studied in previous analyses, and allows us to test the monophyly of the cotingas as well as their intrageneric relationships with high resolution. We analyze our genetic data using a Bayesian species tree method, and concatenated Bayesian and maximum likelihood methods, and present a highly supported phylogenetic hypothesis. We confirm the monophyly of the cotingas, and present the first phylogenetic evidence for the relationships of *Phibalura flavirostris* as the sister group to *Ampelion* and *Doliornis*, and the paraphyly of *Lipaugus* with respect to *Tijuca*. In addition, we resolve the diverse radiations within the *Cotinga*, *Lipaugus*, *Pipreola*, and *Procnias* genera. We find no support for Darwin's (1871) hypothesis that the increase in sexual selection associated with polygynous breeding systems drives the evolution of color dimorphism in the cotingas, at least when analyzed at a broad categorical scale. Finally, we present a new comprehensive phylogenetic classification of all cotinga species.

1. Introduction

The cotingas (Cotingidae) are a diverse radiation of Neotropical, suboscine frugivores and omnivores that includes 66 species in 25 genera (Snow, 1982, 2004; Kirwan and Green, 2012). Cotingas are well known for their diversity in sexual dimorphism, plumage coloration and ornamentations, vocalizations, display behaviors, and breeding systems. The family includes species with concentrated leks (e.g. Guianan Cock-of-the-Rock, *Rupicola rupicola*), dispersed leks (e.g. *Phoenicircus* red cotingas), solitary leks (e.g. *Procnias* bellbirds), socially monogamous species (e.g. *Ampelion* cotingas, *Phytotoma* plantcutters, and *Pipreola* fruiteaters, etc.), and even group living territorial species with helpers at the nest (Purple throated Fruitcrow, *Querula purpurata*).

Cotingas also encompass a great diversity of avian plumage coloration mechanisms. Various cotingas produce plumage colors with (1) eumelanin and phaeomelanin pigments, (2) a tremendous diversity of dietary and physiologically modified carotenoid pigments, (3) spongy, medullary structural coloration in barb rami, (4) iridescent barbule structural coloration (in *Cephalopterus* umbrellabirds), and (5) combinations of barb structural coloration and carotenoid pigments (e.g. green plumages in *Pipreola* and female *Procnias*) (Prum et al., 1998, 1999; Prum et al., 2012; Saranathan et al., 2012).

Variation in cotinga plumage is not restricted to the coloration alone. Many male cotingas have unusual plumage ornaments like the vertical crests of Cocks-of-the-Rock, or the forward-bending crown feathers that give the *Cephalopterus* umbrellabirds their common name. Cotingas also exhibit a wide diversity of fleshy skin ornaments which includes the structurally colored bare blue crowns of *Perisocephalus* tricolor, the blue face and neck skin of *Gymnoderus foetidus*, the bare green throat skin of *Procnias nudicollis* (Prum and Torres, 2003), the bare black throat patch with dozens of thin, wormy wattles of *Procnias averano*, the single, feathered nasal wattle of *Procnias alba* (Burton, 1976), the three, bare black nasal and rictal wattles of *Procnias tricarunculata*, and the elongate bare or feathered breast wattle of the umbrellabirds.

Cotingas also vary strikingly in their vocal behavior and acoustic signaling. A few species vocalize very infrequently (*Carpodectes nitidus*, *C. antoniae*, and *Xipholena* sp.) (Kirwan and Green, 2012). However, the *Procnias* bellbirds and *Lipaugus* pihas produce some of the loudest bird vocalizations in the world (Nemeth, 2004). *Procnias* bellbirds are also the only members of the suboscine clade demonstrated to exhibit vocal learning (Saranathan et al., 2007; Kroodsma et al., 2013). In order to produce these diverse and variable vocal signals, the cotingas are tremendously diverse in syringeal morphology, and many genera are identifiable by unique syringeal morphology (Prum, 1990, Prum, unpubl. data). Several cotinga species also produce conspicuous mechanical wing-sounds as part of their courtship displays (e.g. *Rupicola*, *Phoenicircus*, and *Cotinga*) (Snow, 2004).

Further, cotingas vary in the relation between breeding system and sexual plumage dimorphism. Cotingas include polygynous, sexually monomorphic species that advertise with largely acoustic signals (eg. *Lipaugus*), monogamous, monomorphic species (eg. *Ampelion*, *Zaratornis*), monogamous, dimorphic species (eg. *Pipreola*, *Phytotoma*), and polygynous, dimorphic species (e.g. *Procnias*, *Cotinga*). Ohlson et al. (2007) first tested the hypothesis that the sexually dimorphic, polgynous state in the cotingas was derived from a sexually monomorphic, monogamous root state (Snow, 1973) but limited taxon sampling and poor resolution at the base of their tree resulted in equivocal reconstructions.

Comparative analysis of the evolution of the morphological, behavioral, and ecological diversity of cotingas requires a comprehensive species-level phylogeny of the family. Anatomical and molecular phylogenetic studies have largely resolved the previously confusing limits of the cotinga clade (Prum, 1990; Prum et al., 2000; Johansson et al., 2002; Ohlson et al., 2007, 2013; Tello et al., 2009), but previous phylogenetic analyses have not attempted to reconstruct the relationships among a comprehensive sample of cotinga species. Previous studies have also focused on analyzing single locus or concatenated data sets that assume gene-tree concordance.

Here, we present a comprehensive phylogeny of the cotingas based on molecular data for up to ~7500 base pairs of nuclear introns (MYO, G3PDH), exons (RAG-1, RAG-2), and mitochondrial genes (CYT-B, ND2) for a sample of 61 species in all 25 cotinga genera, and 22 species of suboscine outgroups. Our cotinga sample includes all but four currently recognized species in the family: Handsome Fruiteater *Pipreola formosa* and Golden-breasted fruiteater *Pipreola aureopectus*, Chestnut-capped Piha *Lipaugus weberi*, and Grey-winged Cotinga *Tijuca condita* (all are narrow endemics with few specimens available). We analyze these phylogenetic data using a Bayesian species tree method, and concatenated Bayesian and maximum likelihood methods. We then present a comparative phylogenetic analysis of the evolution of cotinga breeding systems and sexual plumage dimorphism. Specifically, we test the hypothesis that

increased levels of sexual selection associated with polygyny have fostered the evolution of sexual dimorphism in plumage coloration.

1.1. Taxonomic history of cotingas

Traditionally, the cotinga family has included an even wider diversity of species than are currently placed in Cotingidae (Ridgway, 1907; Hellmayr, 1929; Snow, 1973, 1979). The historically broader limits to the family included becards (*Pachyrampus*), tityras (*Tityra*), purpletufts (*Iodopleura*), various genera of mourners (*Laniisoma*, *Laniocera*, *Rhytipterna*, and *Casiornis*), and often the Sharpbill (*Oxyruncus cristatus*). The traditional cotingas excluded the plantcutters (*Phytotoma*), which were often placed in the Phytotomidae (Snow, 1973, 1982; Lanyon and Lanyon, 1988), and *Rupicola* which was placed in Rupicolidae (Hellmayr, 1929).

On the basis of syringeal anatomy, Ames (1971) removed *Pachyrampus*, *Tityra*, *Rhytipterna*, and *Casiornis* from the cotingas, and transferred them to the tyrant flycatchers (Tyrannidae). Using cladistic analysis of syringeal characters and protein electrophoresis, Lanyon and Lanyon (1988) moved *Phytotoma* into the Cotingidae near the Andean *Ampelion* species, as first suggested by Küchler (1936). In the first phylogenetic test of the monophyly of cotingas, Prum (1990) identified a clade of cotingas based on a derived insertion of an extrinsic syringeal muscle – *M. tracheolateralis* – on the lateral syringeal membrane between the A1 and B1 supporting elements. However, unrecognized evolutionary derivation (*Lipaugus*) and loss (*Tityra*) of complex intrinsic syringeal muscles contributed ambiguity to diagnosis of cotinga monophyly. Prum et al. (2000) largely confirmed the monophyly of the cotinga clade with an analysis of sequences of the mitochondrial gene cytochrome-B (CYT-B). However, they erroneously placed *Oxyruncus* within the cotinga clade based on an untranscribed nuclear copy of CYT-B (Johansson et al., 2002). Prum et al. (2000) confirmed Ames' hypothesis that *Tityra* is closely related to *Pachyramphus* within the *Schiffornis* group– a novel clade made of former members of the cotinga, manakin, and flycatcher families (Prum and Lanyon, 1989).

Ohlson et al. (2007) provided a well-resolved phylogeny of 26 cotinga species in 22 genera based on ~2100 base pairs of nuclear and mitochondrial DNA (Fig. 1). They identified four main clades: (1) a montane fruiteater clade including *Pipreola* and *Ampelioides* as the sister group to the rest of the family, (2) the *Ampelion* clade including *Ampelion*, *Doliornis*, *Zaratornis*, and the *Phytotoma* plantcutters as the next sister group to the remainder of the family, (3) the *Rupicola–Phoenicircus* clade, and (4) a diverse clade of the 'core' cotingas including the fruitcrows, two clades of pihas, and a clade of 'canopy' cotingas. Tello et al. (2009) analyzed ~4000 bases of the nuclear RAG-1 and RAG-2 genes for a slightly different sample of 25 cotinga species in 23 cotinga genera. The Tello et al. (2009) phylogeny identified many of the same broad clades as Ohlson et al. (2007) but with a few slight differences: *Snowornis* was placed as the sister group to the *Rupicola–Phoenicircus* clade; this clade was sister group to the *Ampelion* clade; and the genus *Carpornis* was placed as the sister group to this larger clade. Within the fruiteaters, the *Ampelion* clade, and the fruitcrows, the phylogenetic relationships of Tello et al. (2009) and Ohlson et al. (2007) are highly congruent, but relationships between *Lipaugus*, *Cotinga*, and *Procnias* were inconsistent between the two studies (Fig. 1).

Most recently, Ohlson et al. (2013) analyzed three introns and two exons (~6300 bp) across 14 cotinga species (14 genera), and supported different phylogenetic relationships from both Tello et al. (2009) and Ohlson et al. (2007); the *Ampelioides–Pipreola* fruiteater clade was reconstructed as sister to all other cotingas in all three, but they inferred different relationships among the *Snowornis–Rupicola* clade, the 'core' cotinga clade, and the *Ampelion* clade. Further, Ohlson et al. (2013) placed *Lipaugus* within the 'core' cotingas, while Tello et al. (2009) placed it as the sister group to the rest of the clade. Regardless, inadequate taxon sampling in all prior analyses has limited overall resolution (Fig. 1).

A few recent taxonomic changes have been recommended. Based on substantial genetic differentiation (Prum et al., 2000) and differences in syringeal morphology, Prum (2001) proposed the genus *Snowornis* for two Andean piha species-*cryptolophus* and *subalaris* – that were formerly in the genus *Lipaugus*. Ohlson et al. (2007) confirmed that *Snowornis* is

monophyletic, and not closely related to *Lipaugus*. In sum, previous phylogenetic studies of cotingas have not included enough taxa to test the monophyly of cotinga genera. This is partly because cotinga genera are so highly split – an average of only 2.6 species per genus – as a consequence of taxonomic splits that reflect extreme diversity in secondary sexual traits.

2. Materials and Methods

2.1 *Taxon and character sampling*

We sampled frozen or preserved tissue samples of 63 specimens of 49 different cotinga species (Table 1). Although we had no tissue for the species, sequences for two nuclear and one mitochondrial genes from this species were available for *Tijuca atra* through GenBank (Ohlson et al., 2007). An additional 12 species were represented by 21 toepad samples from museum study skins (collected 1926–1970). In order to assess geographic variation within some cotinga species, multiple populations were sampled and analyzed for 11 different species (Table 1).

Outgroups include multiple representatives from all major clades of the superfamily Tyranni, three members of the tracheophone Furnarii, and three Old World suboscines. We included four species each of manakins (Pipridae), tyrant flycatchers (Tyrannidae), tityrids (Tityridae), other Tyranni with unresolved relationships to tyrannids (*Oxyruncus cristatus*, *Piprites chloris*, *P. pileatu*s, and *Calyptura cristata*), an antbird (Formicariidae), an ovenbird and a woodcreeper (Furnariidae) (Table 1).

We collected new DNA sequence data for four loci—two mitochondrial genes and two nuclear introns. The nuclear introns included myoglobin intron-2 (MYO) and glyceraldehyde-3-phosphate dehydrogenase intron-11 (G3PDH). The mitochondrial loci included cytochrome B (CYTB) and NADH dehydrogenase subunit 2 (ND2). Sequences of target loci that were already available from prior studies were downloaded from GenBank, as well as sequences of two protein coding nuclear loci, (the recombination activating genes (RAG) 1 and 2), for 25 ingroup species and 16 outgroup species which were produced by Tello et al. (2009). In most cases, these

supplemental data were from the same individuals as in our study, or were from other individuals in the same population. See the Supplemental Appendix for details regarding PCR, DNA extraction and sequencing methods.

2.2. *Tree inference strategies and genetic distance metrics*

We explored our dataset with a three-pronged approach. For Bayesian species tree inference, we used the *BEAST multispecies coalescent method implemented in BEAST 1.7.5 (Heled and Drummond, 2010; Drummond et al., 2012). For phylogenetic analysis of the concatenated super-matrix, we used MrBayes 3.2.1 (Ronquist et al., 2012) and RAxML 7.4.4 (Stamatakis, 2006b; Stamatakis et al., 2008) to perform Bayesian and Maximum Likelihood tree inference. We also used MrBayes to infer gene trees for individual loci. For each analysis, we compared and ranked three partitioning schemes. For all phylogenetic reconstructions, we constrained the monophyly of New World suboscines and rooted trees with the Old World suboscines. With the exception of RAxML maximum likelihood analyses, all computations were carried out on the Omega Linux cluster at Yale West Campus.

To explore empirical variation between and among species and genera, we computed uncorrected p-distance matrices for each locus in MEGA 5.1 (Kumar et al., 2008). We also calculated net distances between genera using the formula $dA = dXY - ((dX + dY)/2)$, where, dXY is the average distance between groups X and Y, and dX and dY are the mean within-group distances (Kumar et al., 2008). These data are discussed in the Supplementary Appendix.

2.3. *Partitioning scheme and evolutionary model selection*

Recent empirical and theoretical studies have demonstrated that the choice of molecular data partitions can have a pronounced effect on the inference of topology and relative divergence times (McGuire et al., 2007; Li et al., 2008; Poux et al., 2008; Papadopoulou et al., 2009; Ward et al., 2010; Leavitt et al., 2013; Powell et al., 2013; Wu et al., 2013). An inappropriate partitioning strategy can also lead to misleading support estimates (Brown and Lemmon, 2007).

To try to control for these issues, we used PartitionFinder v1.01 (Lanfear et al., 2012), which uses several statistical criteria to evaluate and rank alternative partitioning strategies while simultaneously performing nucleotide substitution model selection for each partition. Thus, subsequent usage of the phrase, ‘‘partitioning scheme’’ will refer to both the particular groupings of data partitions for a given dataset, and the best-fit nucleotide substitution models applied to those groupings.

Our general approach was to use PartitionFinder to choose an ‘‘optimal’’ partitioning scheme from a set of a priori schemes according to the Bayesian information criterion, or BIC (Schwarz, 1978). The BIC is defined as $-2l + K \log n$, where l is the maximized log likelihood of the model, K is the number of estimable parameters, and n is the number of sites in the alignment. The BIC penalizes model complexity for increasing the number of parameters and the sample size. In contrast, the popular Akaike information criterion, or AIC ($-2l + 2K$) (Akaike, 1974), accounts only for the number of model parameters, and tends to favor models that are more complex than those selected by the BIC (Posada and Buckley, 2004). Simulation studies also support the use of the BIC over the AIC for substitution model selection (Luo et al., 2010).

2.4. *Species tree and gene tree inference*

For species tree inference, we first used PartitionFinder to evaluate partitioning schemes for each locus separately. For protein coding loci, we compared three commonly tested schemes: (S1) codon positions 1, 2, and 3 together; (S2) positions 1 and 2 together and position 3 separately; (S3) all codon positions separate. We then estimated a species tree with *BEAST, using the partitioning scheme with the lowest BIC score (best model) for each locus. In order to test the sensitivity of the inferred topology, we also estimated a species tree with alternative schemes.

To allow each locus to evolve along independent topologies, the trees for nuclear loci were unlinked. We applied a lognormal relaxed clock to each locus, and selected the default Yule Process (pure birth) as the species tree prior to minimize the dimensionality of the analysis.

Because no reliable biogeographic or fossil ingroup calibrations are available for all subocine passerines, we calibrated the evolutionary rates of five of the six loci with previously published rates from other studies of passerine birds (Supplementary Table 6). We assumed a normal prior distribution for each rate calibration, and applied the conditional reference prior to the remaining un-calibrated locus (RAG-2) for which no explicit priors were available (Ferreira and Suchard, 2008). We ran six independent analyses for $6.5 * 10^8$ generations, sampling every $1.0 * 10^5$ generations, which gave us $6.5 * 10^3$ trees per simulation (run). After discarding the first $1.5 * 10^3$ trees per run (~23%), we combined the output files for each set of six analyses and summarized the maximum clade credibility (MCC) tree with median node heights across the final posterior distribution of $3.0 * 10^4$ trees.

We inferred individual gene trees in MrBayes using the partitioning schemes with the best BIC score as selected by PartitionFinder (Supplementary Table 5). We allowed each partition to evolve under its own model of evolution in MrBayes by unlinking all parameters across data partitions (using the commands: unlink shape = (all), pinvar = (all), statefreq = (all), revmat = (all)). We also allowed all partitions to evolve under different evolutionary rates by setting ratepr = variable. For each gene tree, we summarized four Metropolis-coupled Markov chain Monte Carlo analyses (MCMCMC), each with four incrementally heated chains. Instead of specifying an upper limit to the chain length, we used the automatic stopping criterion built into MrBayes (stopval = 0.01), and summarized 50% majority rule consensus trees after discarding the first 25% of the sampled trees as burn in. Individual gene trees as estimated by MrBayes are reported as Supplemental Figs. 3–8.

2.5. *Analyses of concatenated loci*

For analyses under the assumption of among gene-tree concordance, we considered two a priori partitioning schemes (C1, C2), and one scheme (C3), which was heuristically chosen by PartitionFinder's ''greedy'' algorithm to optimize the groupings of the 12 codon and 2 intron

partitions. Scheme C1 analyzed each of the six loci under their own models (partitions by locus). In contrast, scheme C2 represented the ‘‘maximally’’ partitioned dataset, with 14 partitions.

For analysis of the concatenated dataset in MrBayes, we applied the settings described in the previous section for individual loci to allow partitions to evolve under their own models and rates. After testing with default mixing settings, we decreased the temp parameter from 0.1 to 0.025 to increase the acceptance rates for swaps between different chains of the analysis. All other parameters and priors were left at their default settings. For each partitioning scheme, we ran two independent analyses of $1.0 * 10^8$ generations with four incrementally heated chains, sampled every $1.0 * 10^4$ generations. This gave us a final distribution of $1.0 * 10^4$ trees for each analysis, from which we generated a 50% majority rule consensus tree after discarding the first 25% of the sampled trees as burn in.

For maximum likelihood analysis of the concatenated dataset, we used the RAxML-HPC2 on XSEDE (Stamatakis, 2006b; Stamatakis et al., 2008) application through the CIPRES Science Gateway (Miller et al., 2010) to compute 1000 rapid bootstrap replicates using partitioning schemes C1–C3. We selected the default option to use the GTRCAT model for the bootstrapping phase and the GTRGAMMA model for the final tree inference (Stamatakis, 2006a). Finally, we summarized bootstrap support values on the best scoring ML tree.

2.6. *Assessing convergence of Bayesian analyses*

For Bayesian inference, including concatenated, individual locus, and species tree approaches, we examined the output log files by plotting log-likelihood values against the number of generations in the MCMC Trace Analysis Tool v1.5, ‘‘Tracer,’’ to assess whether or not the MCMC analysis had run long enough (Rambaut and Drummond, 2009). We also used the online tool AWTY (‘‘Are We There Yet?’’),’’ to graphically assess clade stability (Nylander et al., 2008). Using Tracer, we also ensured that the trace statistics of replicate analyses had converged on the same posterior distributions and that the effective sample sizes for all statistics were greater than 200 (most were greater than 1000). Where appropriate, we used the ‘sump’

command in MrBayes to check that the potential scale reduction factors (Gelman and Rubin, 1992) were close to one, and that the average standard deviation of split frequencies (Ronquist et al., 2012) was close to zero.

2.7. *Evolution of breeding system and sexual dimorphism in color*

Breeding systems and plumage color dimorphism were coded as binary traits (Monogamous = 0, Polygynous = 1; Monomorphic = 0, Dimorphic = 1). We obtained data on cotinga breeding behavior and sexual dimorphism from a recent comprehensive literature review (Kirwan and Green, 2012) and other recent publications (del Hoyo et al., 2004; Avalos, 2011; Belmonte-Lopes et al., 2011). There are scientific studies of breeding biology for some cotinga species; for many species however, there are only scattered observations or no information at all. For poorly known species, observations of female only nest attendance (e.g. *Snowornis cryptolophus*), or male lek display behavior were treated as evidence of polygyny. For some species, breeding systems were inferred from closely related congeners: e.g. all *Carpodectes* were presumed to be polygynous based on their male display behavior and observation of female-only nest attendance in *C. nitidus*. Six of ten species of *Pipreola* have undescribed nests or breeding systems, but all four known species with data have monogamous, biparental care (Kirwan and Green, 2012).

The sister group to the cotingas is a very diverse clade of mostly monogamous tyrannids and tityrids (Ohlson et al., 2013), so by outgroup comparison monogamy was assumed to be primitive to the cotinga clade. Because polgynous species were overrepresented in our original outgroup sample, we pruned all outgroups for ancestral state reconstructions. Additionally, we pruned biogeographic replicates when appropriate.

Sexual dimorphism was coded from visual inspection of study skins from the collections of the Yale Peabody Museum of Natural History and the American Museum of Natural History, which includes all the cotinga species of analyzed. Species were coded as sexually dimorphic if any plumage patches were diagnosably distinct in color or brightness between the sexes. Because

cotingas have four color-cones, including a violet cone with broad sensitivity into the near ultraviolet, they perceive an additional ultraviolet dimension to color diversity (Ödeen and Håstad, 2003; Stoddard and Prum, 2008). Therefore, our analysis based on human visual sensitivity is conservative with respect to possible sexual dimorphism in cotinga coloration.

To reconstruct the evolution of cotinga breeding biology across the MCC species tree, we followed Wiens et al. (2011) and used a maximum likelihood strategy in Mesquite 2.75 (Maddison and Maddison, 2011). For both characters, we compared the fit of a one-parameter (equal transition rates) Markov k-state model (Lewis, 2001), and a two-parameter (unequal transition rates) asymmetrical Markov k-state model (Pagel, 1997; Mooers and Schluter, 1999), and assumed equilibrium root state frequencies. For stand-alone reconstructions, we used likelihood ratio tests and information criteria to discriminate between these two models. In order to account for phylogenetic uncertainty in branch lengths and tree topology, we examined models of trait evolution across the distribution of $3.0 * 10^4$ post-burn-in trees from our Bayesian species tree analyses, and report the mean and 95% confidence intervals of likelihood scores and p-values. Finally, we report preferred reconstructions of trait evolution mapped onto the species tree topology.

To examine the potential co-evolutionary relationship between breeding system and sexual dimorphism, we used Pagel's (1994) correlation test implemented in Mesquite 2.75 (Maddison and Maddison, 2011). This method tests the independent evolution of two binary characters by fitting two models of evolution to the data and the phylogeny with maximum likelihood; one in which transition rates in one character evolve independently of the state of the other (H_o – 4 parameter), and a second in which the transition rates of each character are allowed to depend on the state of the other (H_1 – 8 parameter). To calculate statistical significance, we compared the log-likelihoods derived from 1000 Monte Carlo simulations (with 100 likelihood search iterations each) of the independent and dependent models. As described above, we also examined how topological variation across the posterior distribution of trees affected this test's statistical significance by comparing the log-likelihoods derived from 100 Monte Carlo

simulations (with 10 likelihood search iterations each) of the independent and dependent models, calculated across a random sample of 10,000 post-burn-in trees.

3. Results

3.1. *Data partitioning*

For our species tree analysis, partitioning schemes were evaluated for each locus separately; PartitionFinder indicated that the maximally partitioned scheme S3 (with each codon position on different partitions) was significantly preferred for all protein-coding loci with the exception of RAG2 (ND2, $\Delta BIC_{S2–S3} = 133$; CYTB, $\Delta BIC_{S2–S3} = 94$; RAG1, $\Delta BIC_{S2–S3} = 22$). For RAG2, the intermediately partitioned scheme S2 (with the first two codon positions grouped together and the third separately) was preferred (RAG2, $\Delta BIC_{S1–S2} = 157$). A ΔBIC of 10 units or more is considered to represent a large improvement in model fit (Robert Lanfear, personal communication). Here, ΔBIC refers to the difference in model fit between the preferred scheme and the next best scheme.

In comparing partition schemes for the concatenated analysis, scheme C1 (minimally partitioned) and C2 (maximally partitioned), PartitionFinder indicated scheme C2 was significantly preferred ($\Delta BIC_{C1–C2} = 3370$). Using PartitionFinder's ''greedy'' search algorithm, we identified a novel partitioning scheme (C3; $\Delta BIC_{C2–C3} = 179$) that was further preferred overall, and was composed of seven data partitions: (Partitions 1–3) The first, second, and third codon positions of ND2 and CYTB were each grouped together to form three data partitions, (Partition 4) the first codon positions of RAG-1 and RAG-2, (Partition 5) the second codon positions of RAG-1 and RAG-2, (Partition 6) the third codon positions of RAG-1 and RAG-2 and the MYO intron, (Partition 7) the G3PDH intron. Detailed results from our tests of alternative partitioning schemes are summarized in Supplemental Tables 3–5.

3.2. *Sequence characteristics and distance matrices*

Newly generated sequence data are deposited in GenBank (Accession Nos. KJ810194–KJ810513). Final alignment sizes were: MYO, 790 bp; G3PDH, 440 bp; CYTB, 1143 bp; ND2, 1041 bp; RAG-1, 2871 bp; and RAG-2, 1152 bp. The final concatenated alignment length was 7437 bp. Post-burn-in data characteristics and estimated substitution model parameters are listed in Supplemental Table 2. The ranges of pairwise uncorrected sequence divergences for all loci and ingroup (cotingas) taxa are: ND2 (0.1– 27%), CYTB (0.3–21.1%), G3PDH (0.0–11.1%), MYO (0.1–6.4%), RAG1 (0.2–3%), RAG2 (0.5–4%). Average p-distances for all pairwise comparisons of cotingas are reported in Supplementary Table 9.

3.3. *Species tree topology*

The monophyly of the cotinga clade was supported with a posterior probability of one. As in some previous studies, the cotingas were found to be composed of five monophyletic clades that are the successive sister-groups to the rest of the family (Figs. 2 and 3).

Our analysis reconstructs the fruiteaters as the sister group to all other cotingas. Within the fruiteaters, the monotypic *Ampelioides* is resolved as the sister group to the diverse genus *Pipreola*. Although not currently recognized as separate subspecies, the two east Andean populations of *Ampelioides tschudii* sampled from Ecuador and Peru exhibited an average genetic distance of 1.2%, indicating underestimated diversity within this quite ancient lineage. Within *Pipreola*, a clade including the two smallest-bodied species—*P. chlorolepidota* and *P. frontalis*—is the sister group to all other *Pipreola*. Then, *P. whitelyi*, from the isolated tepuis of southern Venezuela and Guyana, is the sister group to a lineage consisting of two wellresolved Andean clades. The first of these clades contains three mid-sized species, with *lubomiirskii* as the sister group to the welldifferentiated *jacunda*, and *pulchra*. The last clade in *Pipreola* consists of the three large species, with *arcuata* as the sister-group to *intermedia* and *riefferii*. All clades

within *Pipreola* were very highly supported, except for the monophyly of the sister group to *P. whitelyi*, (posterior probability, or PP, = 0.58). *P. formosa* and *P. aureopectus* were not available for this study; however, *formosa* is likely to be a member of the *chlorolepidota-frontalis* clade, and *aureopectus* is likely to be closely related to *lubomirskii*, *jacunda*, and *pulchra* (Snow, 1982).

The next cotinga clade consists of a novel group of four genera— *Rupicola*, *Phoenicircus*, *Snowornis*, and *Carpornis* (PP = 0.78). As in previous studies, *Rupicola* and *Phoenicircus* are sister groups, and we confirm the monophyly of each genus. Their sister group is a new clade consisting of the two Andean *Snowornis* species and the two southeast Brazilian *Carpornis* species (PP = 0.79). Our tree also confirms that *Snowornis* and *Carpornis* are each monophyletic.

The third cotinga clade is the *Ampelion* group, which consists of its now traditional members – *Zaratornis*, *Phytotoma*, *Doliornis*, and *Ampelion* – but with a new addition – the Swallow-tailed Cotinga, *Phibalura flavirostris*. *Zaratornis stresemanni* is the sister group to the other four genera. The three species of *Phytotoma* form the next lineage in the clade, with *rara* as the sister group to *rutila* and *raimondii*. Then, *Phibalura flavirostris* is placed as the sister group to the *Doliornis–Ampelion* clade, and each of these genera is monophyletic. All clades in this assemblage received maximal support, except for the monophyly of the *Phibalura–Doliornis–Ampelion* clade (PP = 0.56).

The fourth cotinga clade consists of the five genera of fruitcrows. The resolution of this clade matches previous studies (Ohlson et al., 2007; Tello et al., 2009), with *Haematoderus militaris*, *Querula purpurata*, and *Pyroderus scutatus* as the successive sister groups to a clade including *Cephalopterus* and *Perissocephalus*. Intriguingly, in this first test of the monophyly of the three species of *Cephalopterus* umbrellabirds, the Capuchinbird *Perissocephalus* tricolor was placed as the sister to the Amazonian Umbrellabird *C. ornatus* (PP = 0.84). This resolution seems to be driven by the increased weighting of mitochondrial genes CYT-B and ND2 in the species tree analysis; *P. tricolor* was grouped with *C. penduliger* in the MYO gene tree, and its

relationships were unresolved in GP3DH. Tello et al. (2009) placed *Perissocephalus* as the sister group to a *Cephalopterus–Pyroderus* clade on the basis of RAG-1 and RAG-2.

The final major clade includes a diverse radiation traditionally recognized as the 'core' cotingas (Prum et al., 2000). We resolve the *Lipaugus* pihas, with *Tijuca atra* embedded within, as the sister group to the other core cotingas. Within *Lipaugus*, *Lipaugus unirufus*, from Central America and the Chocó, is placed as the sister group to all others. The next branching lineage consists of a south-east Brazillian clade containing *L. lanioides* and *T. atra*. Known from only a single specimen, *Tijuca condita* was not available for this study, but based on plumage and behavior, it is likely to be the sister species to *atra*. The rest of *Lipaugus* consists of two clades. One of these clades contains the broadly distributed, lowland *L. vociferans* and the Rose-collared Piha *L. streptophorus* of the tepuis of eastern Venezuela and Guyuna. Their sister group is an Andean clade including *L. fuscocinereus* and *L. uropygialis*. The recently described Chesnut-capped *Piha L. weberi*, from the north Colombian Andes, was unavailable for this analysis, but morphologically and acoustically it appears to be a member of the *fuscocinereus-uropygialis* clade (Cuervo et al., 2001, R. O. Prum, pers. obs.).

The monophyly of the sister group of the *Lipaugus–Tijuca* clade is supported with a posterior probability of 0.94. The first branch within this clade consists of the four species of the genus *Procnias*. Within *Procnias*, there are two well-supported clades, an *averano– nudicolllis* clade, and an *albus–tricarunculata* clade (All PP = 1.0).

The next successive clade consists of the monophyletic genus Cotinga, in which *maynana* and *cayana* are successive sister groups to the rest of the genus. Then, *amabilis* is placed as the sister group to two clades consisting of *nattererii* and *ridgwayi*, and *maculata* and cotinga. These relationships were all well supported (PP $\geqq$ 0.95) except for the placement of *amabilis* (PP = 0.67). This proposed relationship may be affected by the paucity of data for some these taxa (we were only able to sequence ND2 from toe pads of *amabilis*, *nattererii*, and *maculata*).

Throughout our analyses, the most problematic (''rogue'') taxon to place phylogenetically was the Plum-throated Cotinga *Porphyrolaema porphyrolaema* (see Section 3.4

below). In the species tree, *Porphyrolaema* was placed as sister group to a clade of four genera with powder down – a special type of powder producing feathers – that has been identified in previous studies (Prum et al., 2000; Ohlson et al., 2007; Tello et al., 2009). This relationship for *Porphyrolaema* was supported with a posterior probability of 0.59. Within the powder down clade, as in previous studies (all PP = 1.0), *Conioptilon mcilhennyi* and *Gymnoderus foetidus* form a clade that is sister group to a clade including the monophyletic *Xipholena* and *Carpodectes*. Within *Xipholena*, *X. punicea* is the sister group to *lamellipennis* and *atropurpurea*. Within *Carpodectes*, *hopkei* is the sister group to the barely differentiated *nitidus* and *antoniae*.

3.4. *Congruence with concatenated analyses*

The result of the concatenated Bayesian analysis was highly congruent with the species tree analysis (91.5% topological similarity, see Supplemental Appendix), and differed only in regard to the resolution of four clades (Supplementary Fig. 2). The concatenated Bayesian analysis did not recognize the *Rupicola–Phoenicircus* clade and the *Snowornis–Carpornis* clade as sister groups. Rather, these clades were placed as separate, successive sister groups to the large core cotinga clade. Unlike the species tree, the concatenated Bayesian tree placed the *Ampelion* clade as more closely related to the core *cotingas* than the *Rupicola–Phoenicircus* and *Snowornis–Carpornis* clades. Within the core cotingas, the concatenated Bayesian tree placed the genus *Cotinga* outside the *Lipaugus–Tijuca* clade, which was then the sister group to *Procnias*, *Porphyrolaema*, and the power down clade. Lastly, within the genus *Pipreola*, the concatenated Bayesian trees placed *P. jucunda* as sister to *P. lubomirskii* instead of *P. pulchra*.

The results of the concatenated maximum likelihood analysis identified the same trees as the concatenated Bayesian analyses with a single difference. In the maximum likelihood tree, *Tijuca atra* was placed as the sister group to *Lipaugus* excluding *L. unirufus*, while *L. lanioides* was placed as the sister group to the Andean *fuscocinereus–uropygialis* clade.

3.5. *Outgroup relationships*

Our extensive sample of outgroup taxa provided substantial resolution to the phylogenetic relationships among the suboscines, which were identical among all analyses (Supplemental Figs. 1 and 2). Within the New World subsocines, the tracheophone Furnarii were recognized as monophyletic with a Thamnophilus antbird as the sister to two ovenbirds– *Lochmias* and *Lepidocolaptes*. The monophyly of the Tyranni was recognized, with manakins as the sister group to the rest of the Tyranni. The sister group to the cotingas is a diverse clade consisting of the tityrids (Tityridae), *Oxyruncus*, *Piprites*, *Calyptura*, and the tyrant flycatchers (Tyrannidae). The proposed relationships were mostly congruent with the recent broad and better sampled studies of Tello et al. (2009) and Ohlson et al. (2013).

3.6. *Divergence time estimations and evolutionary rates*

Applying calibrations from previous literature, our species tree analysis estimated the age of the split between New World and Old World suboscines at 62.7 MY (95% highest posterior density (HPD): 54.4–71.6 MY), and the age of Cotingidae at 31.2 MY (95% HPD: 26.6–34.3 MY). The updated estimates of substitution rates for the lognormal relaxed clocks per locus are listed in Supplementary Table 7. When viewed in the Tracer software, the ucld.stdev frequency histograms for ND2, RAG1, and RAG2 were abutting against zero, which indicates that we cannot reject the hypothesis of a strict clock for these loci (Drummond et al., 2007). MYO, G3PDH, and CYTB, however, do exhibit a small amount of significant branch rate heterogeneity. ND2 exhibited the least ($\sigma = 0.11$), while G3PDH exhibited the most ($\sigma = 0.54$). As expected, the average estimated mtDNA substitution rate (2.283%/MY) was significantly higher (~16x) than the average estimated nuclear rate (0.15%/MY).

3.7. *Evolution of cotinga breeding system and plumage dimorphism*

All analyses supported a symmetrical rate of breeding system and sexual plumage dimorphism evolution (i.e., equal rates of evolutionary gains or losses). For reconstructions of breeding system evolution, a likelihood ratio test and AIC selection criterion failed to discriminate between symmetrical one-rate (-log l = 17.1; AIC = 36.23) and asymmetrical two-rate (-log l = 16.6; AIC = 37.17) models of character evolution (χ^2_1 = 1.064; p = 0.23; ΔAIC = 0.94). Likewise, reconstructions of sexual dimorphism evolution recovered similar results for symmetrical one-rate (-log l = 26.94; AIC = 55.88) and asymmetrical two-rate (-log l = 25.17; AIC = 54.33) evolutionary models (χ^2_1 = 3.55; p = 0.06; ΔAIC = -1.55), all at a critical value of α = 0.05. When examined across the posterior distribution of 3.0 * 10^4 trees, the model comparisons from the MCC topology were robust to phylogenetic uncertainty (indicative of a high level of consistency across the posterior distribution of trees). Because two-rate models were never statistically preferred, we used the simpler single rate models for ancestral state reconstructions of sexual dimorphism and breeding system.

When averaged across the posterior distribution of trees, the symmetrical rate model inferred at least two origins of polygyny, and three re-gains of monogamy within the cotingas (5 steps) (Fig. 4, left). 71% of the trees in the analyzed posterior distribution predicted monogamy to be the most likely state at the root of the cotinga clade. The ancestor of the fruitcrows, pihas, and core cotinga genera was reconstructed as polygynous in 98% of trees. Within this major cotinga clade, subsequent reversals to monogamy were reconstructed in the lineages leading to *Querula purpurata* (100%) and the *Conioptilon–Gymnoderus* clade (80%). In contrast, the history of breeding system evolution in the *Rupicola–Snowornis* clade was more equivocal. There was an equivalent likelihood of a single common origin of polygyny in the most recent common ancestor of *Rupicola* and *Snowornis* with a subsequent reversal to monogamy in *Carpornis*, or two independent origins of polygyny in the *Rupicola–Phoenicircus* clade and the genus *Snowornis*.

The pattern of sexual plumage dimorphism evolution is more dynamic but less ambiguous than the pattern of breeding system evolution. The preferred hypothesis of

dimorphism evolution supports a sexually dimorphic cotinga ancestor (100%), six independent derivations of sexual monomorphism, and two secondary transitions to sexual dimorphism (8 steps) (Fig 4, right). Gains of monomorphism are predicted along lineages leading to *Zaratornis* (100%), *Ampelion* (95%), *Pyroderus* (100%), *Perissocephalus*, *Lipaugus* (85%), and *Conioptilon* (100%). Within *Lipaugus*, two reversals of sexual dimorphism are predicted in *Tijuca atra* and in *L. streptophorus*.

Pagel's 1994 test of correlated character evolution between breeding system and sexual dimorphism indicated that the transition-dependent eight-parameter model was not a significantly better fit to the data than the transition-independent four-parameter model on the MCC tree $\chi^2_4 = 1.65$; p = 0.30; $\Delta l = 0.83$; ΔAIC = 6.36), or when averaged across 10,000 post-burn in trees—average p = 0.35 [0.1-0.6]. Thus, breeding system and overall plumage dimorphism do not appear to be co-evolving in the cotingas, and this result appears robust to phylogenetic uncertainty.

4. Discussion

This comprehensive study of the relationships among the Neotropical cotingas establishes a strongly supported phylogenetic hypothesis for this highly diverse radiation. Our findings establish the first phylogenetic hypotheses for intrageneric relationships within the *Cotinga*, *Lipaugus*, *Pipreola*, and *Procnias* clades, and the first phylogenetic placement of the highly distinctive Swallow-tailed Cotinga *Phibalura flavirostris*.

4.1. *Phylogenetic approach*

This is the first estimate of the phylogeny of the cotingas or their tyrannoid outgroups using species tree approaches, which have the potential to account for the effects of both mutational and coalescent processes which affect DNA evolution (Barker et al., 2013). Because variance in coalescent processes can give rise to discordance among gene trees, analyzing

discordant loci together may produce misleading phylogenetic results (Edwards et al., 2007; Kubatko and Degnan, 2007; Degnan and Rosenberg, 2009; Song et al., 2012). By estimating a species tree from a collection of gene trees that are allowed to have different topologies, species tree inference can potentially overcome some of the problems of concatenation, and may support emergent relationships that do not appear in any individually estimated gene tree (Barker et al., 2013). A recent simulation study also suggested that the *BEAST species tree algorithm is strikingly robust to missing data and terminals which only represent a single individual (Hovmöller et al., 2013).

Because (1) a fair number of our samples are derived from museum specimens and contribute limited data, (2) most taxa in our study are represented by single individuals, and (3) of apparent gene-tree discordance (see Supplemental Appendix), we believe our species tree analysis (Figs. 2 and 3) should be preferred over our concatenated analyses (Supplemental Fig. 2). Thus, the application of species tree methods to the phylogeny of cotingas and their tyrannoid outgroups provides robust new support for their historical interrelationships. Our species tree was very similar to that derived from mtDNA alone (Supplemental Table 8; 97.8% similarity), which is consistent with the increased weighting given to haploid DNA in a *BEAST analysis (a smaller effective population size means mtDNA is more likely to track speciation, assuming no hybridization or interspecific gene flow).

Tree topologies varied remarkably little across tested partition schemes (not shown), but computation time varied widely. For instance, during our concatenated analyses, we noted that in comparison to typically applied schemes (C1, C2), we achieved a dramatic reduction (~10x) in the number of generations required to reach convergence on the same topology by utilizing the heuristically chosen scheme C3.

On the other hand, computation time was substantially increased in the species tree analyses after selecting the maximally partitioned scheme for most loci (as optimized by PartitionFinder). While topologies in our case were generally robust to the applied scheme, there is no way to evaluate whether or not the signal underlying a given phylogeny is robust to such

methodological assumptions without testing them. Because easily implemented approaches to evaluate alternative partitioning strategies are now available (Li et al., 2008; Lanfear et al., 2012; Wu et al., 2013), they should be included in phylogenetic pipelines, if only to offer an additional level of support for a given result.

4.2. *Congruence with morphology*

The monophyly of the cotinga clade can be diagnosed anatomically by the insertion of the extrinsic syringeal muscle M. tracheolateralis on the lateral A1/B1 syringeal membrane (Prum, 1990). Within the cotinga clade, there are two instances of the evolution of intrinsic syringeal musculature – in Lipaugus and in Procnias; these derived intrinsic muscles retain the plesiomorphic insertion of the M. tracheolateralis on the lateral membranes. Syringeal morphology confirms the proposed phylogenetic placement of *Phibalura*. Lanyon and Lanyon (1988) identified the derived lateral expansion of the syrinx at the membranous insertion of the M. tracheolateralis as a synapomorphy of an *Ampelion*, *Doliornis Phytotoma*, and *Zaratornis* clade. This same derived morphological character is present in the syringes of three *Phibalura flavirostris* specimens (R. O. Prum, unpubl. observ.). In contrast, no syringeal specimens are yet available to assess whether either species of *Tijuca* share the syringeal synapomorphies of the genus *Lipaugus*.

In most birds, including the tyrannids and tracheophone suboscines, the arterial supply to the hindlimb is provided by the ischiadic artery; however, in the manakins, tityrids, and most cotingas, the primary arterial supply to the hind limb is provided by the femoral artery (Garrod, 1876; Midtgård, 1982; Prum, 1990). Prum (1990) found that an eclectic group of cotinga genera – *Ampelioides*, *Pipreola*, *Rupicola*, *Phoenicircus*, *Carpornis*, and *Snowornis* – lack the derived femoral artery state found in other cotingas, and share the primitive ischiadic hindlimb arterial character state. Indeed, this unusual anatomical condition provided the first evidence that the two *Snowornis* species were unrelated to the *Lipaugus* pihas (Prum, 2001). In the context of this

newly resolved molecular phylogeny, it is clear that the six cotinga genera with the primitive ischiadic artery character state consist of the members of the two basal clades of the family, indicating that there was likely a unique derivation of the derived hindlimb femoral artery condition in the most recent common ancestor of *Ampelion* and *Cotinga*. This morphological synapomorphy provides further support for this major cotinga clade, which only received moderate support in the species tree (PP = 0.73).

The morphological diversity of the cotingas provides a great opportunity for future comparative studies of anatomical evolution. Even within the dominant diet of frugivory, cotingas exhibit extensive diversity in bill size and shape, gape width, and body size. For example, a phylogeny of the four species of *Procnias* provides an opportunity to reconstruct the evolution of their *particularly* diverse facial skin ornaments. A sparsely feathered, ‘‘bare’’ throat patch first evolved in the ancestor of the *averano–nudicollis* clade. This novelty subsequently gave rise to the evolution of a green structurally colored throat in *nudicollis* (Prum and Torres, 2003), and to the proliferation of numerous, fleshy, wiggling black throat wattles in *averano*. Given the critical function of dermal melanization in the production of collagen fiber structural color in avian skin (Prum and Torres, 2003), the evolution of dermal melanization likely evolved in the ancestor of *averano* and *nudicollis* before their subsequent differentiation into their unique species morphologies. In contrast, long, muscular facial wattles characterize males of the *albus–tricarunculata* clade. The central nasal wattle located at the base of the clumen at the nasofrontal junction is found in both species. In addition, *P. tricarunculata* sports two additional rictal wattles located at the junctions of the upper and lower mandibles. The nasal wattle apparently evolved first in the common ancestor of *albus* and *tricarunculata*. Then, the novel nasal wattle was duplicated into the rictal wattles of *tricarunculata* in an unusual form of ectopic anatomical expression, or homeotic evolution.

4.3. *Evolution of cotinga breeding biology*

This resolved phylogeny allows us to reconstruct the evolution of sexual dimorphism and breeding system in the cotingas for the first time. The evolutionary history of breeding system diversity in cotingas is highly concordant with their phylogeny. Only five evolutionary transitions between monogamy and polygyny are required to explain the distribution of breeding systems within the 65 species in the family – either two origins of polygyny with three reversals, or three origins of polygyny with two reversals (Fig. 4, left).

The evolutionary loss of extreme display polygyny, or lekking, is rather rare in birds (Prum, 1994). Examples include the Helmeted Manakin *Antilophia galeata* (Pipridae) (Prum, 1994) and the ptarmigans (*Lagopus*, *Tetraoninae*) (Drovetski, 2002). The complete evolutionary loss of paternal care behavior and the associated evolutionary investment in elaborate forms of secondary sexual display may create substantial barriers to the reevolution of monogamy and biparental care (Prum, 1994). Thus, the newly documented reversals from display polygyny to monogamy in the Purple-throated Fruitcrow *Querula purpurata*, and in the last common ancestor of the Bare-necked Fruitcrow *Gymnoderus foetidus* and the Black-faced Cotinga *Conioptilon mcilhennyi* provide two examples of this rare and interesting class of evolutionary reversals. The Purple-throated Fruitcrow is notable for the further evolution of a cooperative breeding system that appears to be unique among all suboscines (Snow, 1971). In contrast, the evolution of sexual dimorphism in plumage coloration in the cotingas has been much more dynamic, but still reveals strong phylogenetic signal. Color dimorphism appears to be primitive to the clade, and has been lost five times and re-evolved twice, both instances within the lekking *Lipaugus* piha clade.

Since Darwin (1871), the increase in sexual selection through mate choice associated with polygynous breeding systems has been hypothesized to foster the evolution of sexual dimorphism in plumage coloration. However, our analysis of the coevolution of breeding system and sexual plumage dimorphism indicates that these traits are evolutionarily uncorrelated in cotingas, at least at a broad categorical scale. Further, transitions between color dimorphism and monomorphism have occurred at approximately twice (Mk1 estimated rates: 0.016/0.009) the

rate at which transitions between monogamy and polygyny have occurred, which further suggests these characteristics may be evolutionarily decoupled.

The two most diverse, monogamous lineages – the fruiteaters and the *Ampelion*–*Zaratornis* clade–consist exclusively or predominantly of sexually dimorphic species. Furthermore, several polygynous lineages have evolutionarily lost sexual plumage dimorphism – i.e. *Pyroderus*, *Perissocephalus*, and *Lipaugus*. Interestingly, as pointed out for other lineages of birds (Irwin, 1994) the loss or acquisition of sexual dimorphism can be achieved by different kinds of evolutionary change. For example, the loss of sexual dimorphism in *Lipaugus* and *Perissocephalus* appear to be a consequence of the loss of male plumage brightness, whereas the loss of sexual dimorphism in *Pyroderus* is a consequence of the derived evolution of female plumage brightness. The few evolutionary transitions that conform to the sexual selection prediction – the gains of sexual plumage dimorphism in polygynous *Tijuca* and *Lipaugus streptophorus*, and the losses of sexual dimorphism in the monogamous *Zaratornis*, *Ampelion*, and *Conioptilon* – are not enough to establish a significant evolutionary correlation across the entire family.

Although the cotingas include some of the most extravagant examples of sexual plumage dimorphism in birds – e.g. Cotinga and *Rupicola* species (Fig. 5) – polygyny itself does not explain our inferred evolutionary origins of plumage dimorphism. Furthermore, the breadth of ornamental advertisements available to birds– including elaborate vocal signals – means that sexual selection may switch to elaborating different classes of ornaments within different lineages. These types of evolutionary transitions among ornament classes are expected to be more frequent if mate choice evolution proceeds by a Fisherian, Lande–Kirkpatrick mechanism rather than by an honest advertisement mechanism (Prum, 1997, 2010).

The comparative analysis of breeding biology presented here is rather conservative because it relies on human vision, and because it does not take into account the heterogeneous evolutionary changes that can produce sexual dimorphism. Future analyses should employ more discriminating measures of sexual dimorphism in plumage coloration – including

spectrophotometric measures of cotinga plumage reflectance and color space modeling of avian color vision (Stoddard and Prum, 2008; Prum et al., 2012) – to explore the effects of sexual selection on cotinga coloration evolution at a finer scale.

4.4. *Historical biogeography*

Although a full biogeographic analysis is outside the scope of this paper, this resolved species phylogeny for cotingas provides a new opportunity for observations about biogeographic history of various cotinga lineages.

Most cotinga clades show a strong pattern of lowland or montane distribution. Thus, the *Ampelioides–Pipreola*, *Snowornis–Carpornis*, and *Ampelion–Zaratornis* clades are all strongly montane or lower montane in distribution. The placement of the montane genus *Phibalura* within a largely montane clade further confirms the historical nature of this eco-biogeographic distribution. Most other cotinga clades are strongly tropical in distribution with a few notably lower montane lineages evolving from within them: i.e. *Pyroderus*, *Perissocephalus*, *Procnias*, and various *Lipaugus* and *Tijuca* species. Interestingly, the sister group to the southeast Brazilian genus *Tijuca* appears to be another southeast Brazilian endemic *Lipaugus lanioides*, indicating the existence of a radiation of pihas in the Serra do Mar area of endemism.

The evolutionary origin of the avifauna of the tepuis of southern Venezuela and the Guianas has been of particular interest in Neotropical ornithogeography (Mayr and Phelps, 1967). There are two cotinga species endemic to the tepuis. The Red-banded Fruiteater *Pipreola whitelyi* is phylogenetically embedded within a radiation of montane, Andean fruiteaters. Thus, *P. whitelyi* was likely derived from a lineage that dispersed from the Andes to the tepuis in the midst of an active evolutionary radiation within the Andes themselves. In contrast, the Rose-collared Piha, *Lipaugus streptophorus*, is the sister group to a broadly distributed Amazonian species, the Screaming Piha *L. vociferans*. It appears to be altitudinally derived from adjacent lowland populations. Thus, the phylogenetic relationships of tepui-endemic cotingas indicate that

this isolated montane avifauna had complex evolutionary origins, and cannot be explained by a single generalized biogeographic mechanism.

4.5. *Divergence times and diversification*

Our inferred divergence estimates (Figs. 3 and 4, Supplemental Fig. 1) are generally consistent with previous studies of passerine diversification that are based on molecular rate or biogeographic calibrations (e.g. Barker et al., 2004; Ohlson et al., 2013). Nonetheless, because there are no suboscine fossils of any kind, and very few significant fossils of any endemic radiation of Neotropical birds, the estimation of divergence times of suboscine passerines and many other Neotropical clades remains challenging and highly problematic. In the absence of any ingroup fossil calibrations, we have followed the molecular rate calibrations used in previous works of passerine molecular systematics, but recalibrations of passerine diversification dates that are consistent with fossil data are clearly needed.

Recent analyses of the temporal distribution of avian crown clade fossils place the divergence dates of the major basal lineages of Neognathous birds at immediately before the Cretaceous-Tertiary boundary (Longrich et al., 2011). Further, the well documented avifauanas of Green River Formation, Wyoming (□50 mya) and the Eocene Messel Formation, Germany (□47 mya) are diverse avifaunas dominated by basal neognathes, and basal lineages of other extant orders (Clarke et al., 2005; Longrich et al., 2011; Mayr, 2013). Thus, it seems improbable our inferred age of the diversification of the basal sub-oscine passerines at ~50MY is correct when there are few if any fossils of this age that can be confidently placed within any extant bird family of anywhere in the world. Likewise, our estimates of 25–30MY (Figs. 3 and 4, Supplemental Fig. 1) for the ages of the earliest cotinga clades seem equally improbable to us.

However, estimates of relative divergence dates can be useful in analyzing patterns of net diversification across time. In our case, the lineage accumulation curve (not shown) is mostly linear over time, with a slightly more rapid rate of lineage accumulation for the first two-thirds of

the radiation. The trajectory shows neither rapid bursts of diversification or a leveling off of diversity, and is close to the prediction of a consistent species 'birth–death' process with some limited historical noise.

4.6. *Species limits*

Sequence data from multiple individuals of eleven species of cotingas allows us to conduct a preliminary review of their monophyly and species limits. All multiply sampled species were monophyletic with respect to the other taxa analyzed. Comparisons of toe pad data from multiple populations of three species detected no DNA sequence differences: *Lipaugus uropygialis* from Peru and Bolivia, *Phibalura flavirostris flavirostris* from Brazil and *P. f. boliviana* from Bolivia and *Procnias albus* from Venezuela, Guyana, and Brazil. Three other pairs of intraspecific comparisons showed differentiation of less than 0.50%, including *Porphyrolaema porphyrolaema* from eastern Ecuador and Peru, *Cotinga cayana* from Rondonia, Brazil and Loreto, Peru, *Cotinga maynana* from Morona-Santiago, Ecuador and Loreto, Peru, and *Lipaugus vociferans* from Venezuela and Bolivia. These low levels of differentiation indicate that these populations are unlikely to be distinct evolutionary lineages that should be recognized as species. Notably, our preliminary data do not provide molecular support for the previously recommended split of the Brazilian and Bolivian subspecies of *Phibalura* into two species (Hennessey, 2011).

However, *Procnias averano averano* from Brazil differed in 0.53% of 932 bp of ND2 from *Procnias averano carnobarba* from Trinidad. These two subspecies are very different in body size, and these initial sequence data indicate that they may be more highly differentiated than currently recognized. Furthermore, the highly polytypic Red-ruffed Fruitcrow, *Pyroderus scutatus*, is broadly distributed in South America, and consists of 5 allopatrically distributed subspecies (Snow, 1979). We measured 0.9% average sequence differentiation between *Pyroderus scutatus scutatus* from Paraguay and *Pyroderus scutatus masoni* from Peru, including

both significant mitochondrial and nuclear variation (ND2-1.5%, MYO-0.0%, G3PDH-0.9%). This level of differentiation indicates that some of the currently recognized forms *Pyroderus* scutatus may be distinct species, and that further research on the polytypic clade is highly recommended.

Although the Scaled Fruiteater, *Ampelioides tschudii* is currently monotypic, individuals of *tschudii* from San Martin, Peru and from Azuay, Ecuador exhibited 1.2% differentiation in mtDNA (CYTB1.5%, ND2-1.1%). These two populations span a relatively short geographic distance within the total distribution of *Ampelioides* in the Andes from Venezuela to Bolivia. This variation may be expected given that *Ampelioides tschudii* is the basal lineage of the basal most clade within the cotingas, and potentially the most ancient species-lineage in the family (Supplementary Fig. 1).

Lastly, we found substantial, previously unappreciated genetic differentiation between two populations of the Green-and-Black Fruiteater *Pipreola riefferii*. Individuals of *Pipreola riefferii confusa* from Cajamarca, Peru and *Pipreola riefferii melanolaema* from Venezuela revealed 4.6% average sequence divergence, including substantial genetic differentiation in one nuclear intron (ND2-6.0%, CYTB-7.0%, G3PDH-5.6%, MYO-0.0%). This level of genetic differentiation strongly indicates the existence of distinct evolutionary lineages indicative of separate species. *Pipreola riefferii melanolaema* is a morphologically distinctive form endemic to the coastal range of Venezuela. *Pipreola riefferii confusa* is one of five subspecies that are distributed in the Andes of western Venezuela and northern Colombia to central Peru, including the type population of *riefferii* (Snow, 1979; Kirwan and Green, 2012). Consequently, we recognize the well marked, allopatric, and genetic differentiated taxon *Pipreola melanolaema* as a distinct, monotypic species, to be called (the) Venezuelan Fruiteater. We recommend that all other recognized subspecies should currently remain in *Pipreola riefferii*, but the taxonomic status of these populations should be further investigated. The distinctive, smaller, red eyed, and allopatric *Pipreola riefferii tallmanorum* found in Dpto. Huánuco, Peru also seems very likely to be a distinct species.

Our results confirm that *Doliornis remseni* (Robbins et al., 1994) is strongly differentiated from *Doliornis sclateri* (4.5% average genetic distance). The allopatrically distributed and morphologically diagnosable Central American species of *Carpodectes nitidus* and *C. antoniae* are only slightly differentiated genetically (0.15%). However, their allopatric distribution, and well marked morphological and habitat differences support their continued recognition as distinct species.

4.7. *Proposed phylogenetic taxonomy*

We propose a hierarchical Linnaean classification of the cotingas based on our Bayesian species tree results. The four unanalyzed species– *Pipreola formosa*, *P. aureopectus*, *Lipaugus weberi*, and *Tijuca condita*– are placed in this classification based on their morphological similarities to other analyzed taxa. These portions of the classification are phylogenetic predictions to be tested by future analyses.

We recognize the same monophyletic subfamiles as Tello et al. (2009), but with one additional subfamily and some different limits. We recognize the new subfamily Cephalopterinae including the members of the fruitcrow clade. We place *Carpornis* in the Rupicolinae, and *Phibalura* in the Phytotominae. Further, given the strong evidence that *Lipaugus* is paraphyletic with respect to the genus *Tijuca*, we place *Tijuca atra* and *T. condita* within the genus *Lipaugus*. The only phylogenetically acceptable alternative would be to split *Lipaugus* into at least three genera for: (1) *unirufus* alone, (2) *lanioides* alone, and (3) all other *Lipaugus* species. This would create unnecessary taxonomic clutter. Indeed, placing *atra* and *condita* within *Lipaugus* communicates effectively that these highly distinctive species have actually evolved from sexually monomorphic piha ancestors.

Our species tree placed *Perissocephalus tricolor* within the genus *Cephalopterus* as the sister group to the Amazonian species *C. ornatus*. The five species of *Cephalopterus*, *Perrisocephalus*, and *Pyroderus* are all extremely closely related; they differ genetically by only

3%-6% (Supplementary Table 9). These three genera could very justifiably be placed within a single genus; Cephalopterus has priority. However, we prefer to wait for confirmation from additional data before placing tricolor in Cephalopterus.

Wherever possible, we follow a phylogenetic sequencing convention in which the first taxon (i.e. subfamily, genus, or species) in a list of taxa is the sister group to the remaining taxa in that list. Thus, the sequence of the five cotinga subfamilies recapitulates the phylogenetic relationships of these clades in the phylogeny. However, we refrain from creating new taxa within subfamilies or genera to precisely recognize each clade within the taxonomy. Authors who wish to refer to these clades can do so by coining names for these clades within specific works: e.g. the *Ampelion* group for members of *Phibalura*, *Doliornis*, and *Ampelion*.

Family Cotingidae Bonaparte, 1849

Subfamily **Pipreolinae** Tello, Moyle, Marchese & Cracraft, 2009

Ampelioides Verreaux 1867

Ampelioides tschudii

Pipreola Swainson 1838

Pipreola chlorolepidota

Pipreola frontalis

Pipreola formosa

Pipreola whitelyi

Pipreola lubomirskii

Pipreola jucunda

Pipreola pulchra

Pipreola aureopectus

Pipreola arcuata

Pipreola intermedia

Pipreola riefferii

Pipreola melanolaema

Subfamily **Rupicolinae** Bonaparte, 1853

Snowornis Prum 2001

Snowornis subalaris

Snowornis cryptolophus

Carpornis G. R. Gray 1846

Carpornis cucullatus

Carpornis melanocephalus

Rupicola Brisson 1760

Rupicola peruviana

Rupicola rupicola

Phoenicircus Swainson 1832

Phoenicircus carnifex

Phoenicircus nigricollis

Subfamily **Phytotominae** Swainson, 1837

Zaratornis Koepcke 1954

Zaratornis stresemanni

Phytotoma Molina 1782

Phytotoma rara

Phytotoma raimondii

Phytotoma rutila

Phibalura Vieillot 1816

Phibalura flavirostris

Doliornis Taczanowski 1874

Doliornis sclateri

Doliornis remseni

Ampelion Tschudi 1845

Ampelion rubrocristatus

Ampelion rufaxilla

Subfamily **Cephalopterinae** Reichenow, 1914

Haematoderus Bonaparte 1854

Haematoderus militaris

Querula Vieillot 1816

Querula purpurata

Pyroderus G. R. Gray 1840

Pyroderus scutatus

Cephalopterus E. Geoffroy Saint-Hilaire 1809

Cephalopterus glabricollis

Cephalopterus penduliger

Cephalopterus ornatus

Perissocephalus Oberholser 1899

Perissocephalus tricolor

Subfamily **Cotinginae** Bonaparte, 1849

Lipaugus Boie 1828

Lipaugus unirufus

Lipaugus ater

Lipaugus conditus

Lipaugus lanioides

Lipaugus streptophorus

Lipaugus vociferans

Lipaugus fuscocinereus

Lipaugus uropygialis

Lipaugus weberi

Procnias Illiger 1811

Procnias albus

Procnias tricarunculata

Procnias nudicollis

Procnias averano

Cotinga Brisson 1760

Cotinga maynana

Cotinga cayana

Cotinga amabilis

Cotinga nattererii

Cotinga ridgwayi

Cotinga maculata

Cotinga cotinga

Porphyrolaema Bonaparte 1854

Porphyrolaema porphyrolaema

Conioptilon Lowery & O'Neill 1966

Conioptilon mcilhennyi

Gymnoderus Geoffroy Saint-Hillaire 1809

Gymnoderus foetidus

Xipholena Gloger 1841

Xipholena punicea

Xipholena lamellipennis

Xipholena atropurpurea

Carpodectes Salvin 1865

Carpodectes hopkei

Carpodectes antoniae

Carpodectes nitidus

5. Acknowledgments

We thank the numerous researchers whose field collection efforts made this research possible including: George F. Barrowclough, Steve Cardiff, Terry Chesser, Mario Cohn-Haft, Tristan Davis, Andrew Kratter, Patricia Escalante Pliego, Cecilia Fox, John O'Neill, Ted Parker, Richard Prum, Nate Rice, Mark Robbins, Gary Rosenberg, Peter E. Scott, Doug Stotz, Tom Schulenberg, David Willard, and others.

Tissue loans were kindly received from the American Museum of Natural History, New York (AMNH), the Academy of Natural Sciences of Philadelphia (ANSP), Colección Boliviana de Fauna, La Paz (CBF), Colección Ornitologica Phelps, Caracas (COP), the Field Museum of Natural History, Chicago (FMNH), the University of Kansas Natural History Museum, Lawrence (KU), the Los Angeles County Museum (LACM), the Louisiana State University Museum of Natural Science (LSU), the Museo Paraense Emílio Goeldi, Belem (MPEG), the United States National Museum of Natural History, Washington, DC (USNM), and the Yale Peabody Museum of Natural History (YPM). We thank the curators and collections managers of these institutions for facilitating these loans: J. Cracraft, G. Barrowclough, P. Sweet, Nate Rice, Álvaro Garitano-Zavala, Miguel Lentino, David Willard, Town Peterson, Mark Robbins, Ken Campbell, Kimball Garrett, Van Remsen, Steve Cardiff, Donna Dittman, Alexandre Aleixo, Gary Graves, and Kristof Zyskowski. Jonas Lai initiated the DNA sequencing effort for the project. The research was paid for by W. R. Coe Funds from Yale University. This work was supported in part by the facilities and staff of the Yale University Faculty of Arts and Sciences High Performance Computing Center. We thank members of the Prum and Lovette labs, as well as two anonymous reviewers, for comments on the research and the manuscript. Illustrations depicted in Fig. 5 are reproduced with permission from Lynx Editions, Barcelona.

Appendix A. Supplementary material

Supplementary data associated with this article can be found, in the online version, at http://dx.doi.org/10.1016/j.ympev.2014. 09.001.

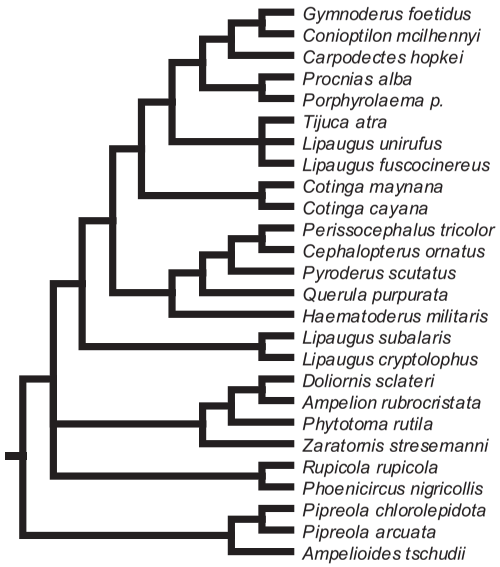

Ohlson 2007

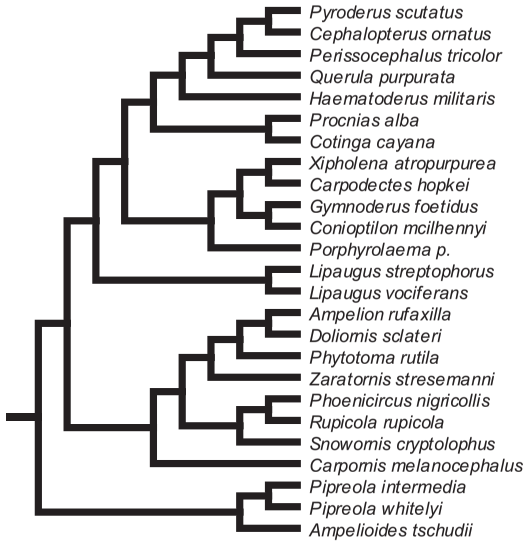

Tello 2009

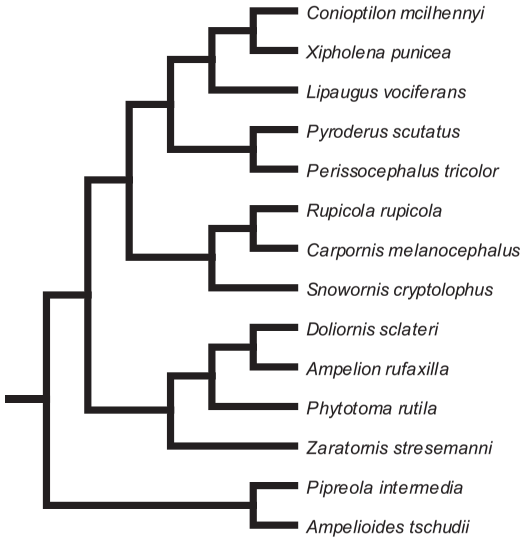

Ohlson 2013

Figure 1.1. Recent phylogenetic hypotheses of the cotingas. Ohlson et al. (2007) provided a well-resolved phylogeny of 26 cotinga species in 22 genera based on ~2100 base pairs of nuclear and mitochondrial DNA. Tello et al. (2009) analyzed ~4000 bases of the nuclear RAG-1 and RAG-2 genes for a slightly different sample of 25 cotinga species in 23 cotinga genera. Later, Ohlson et al. (2013) analyzed three introns and two exons (~6300 bp) across 14 cotinga species (14 genera). **Please refer to the published version of this article for higher quality vector art.**

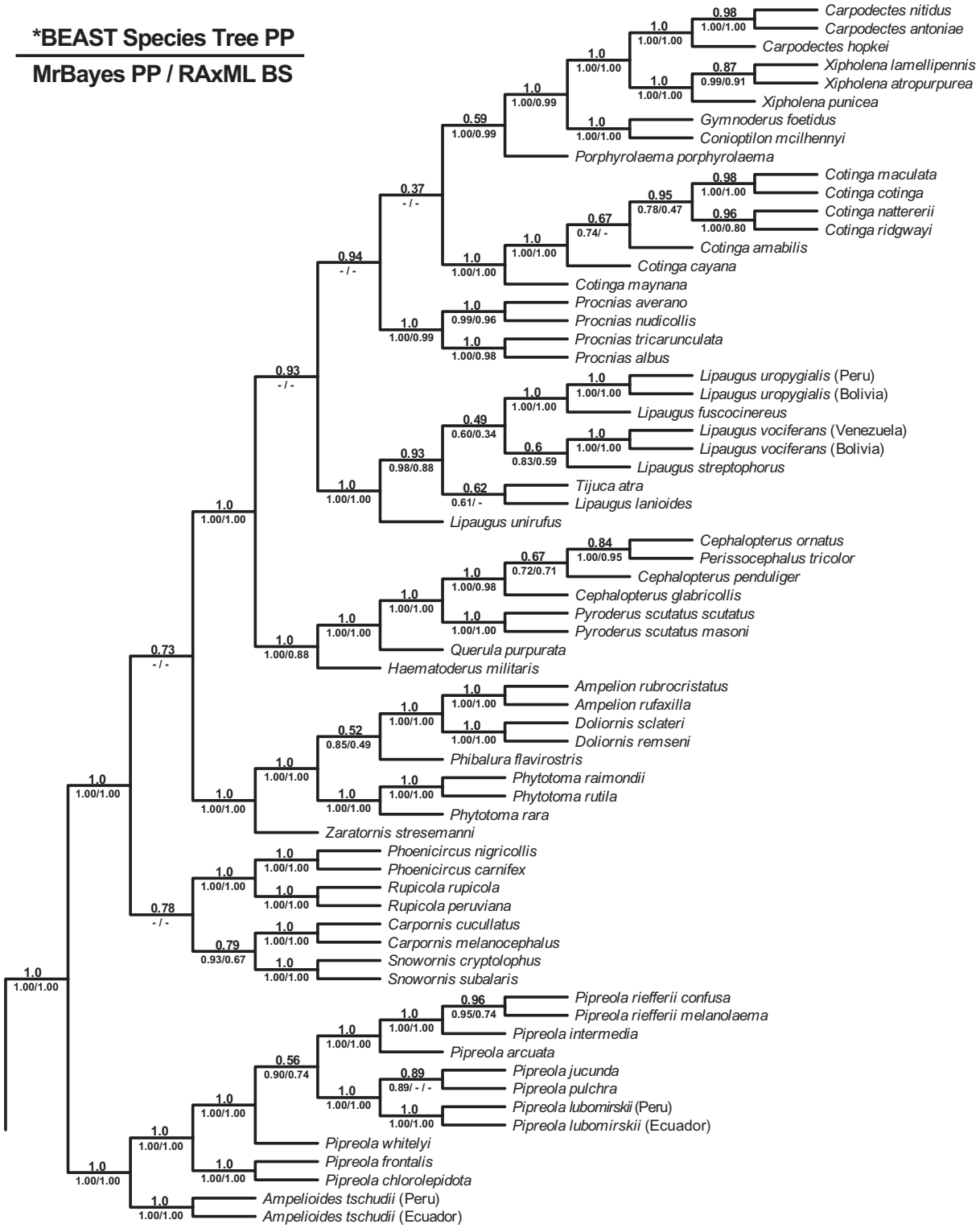
*BEAST Species Tree PP
MrBayes PP / RAxML BS
Carpodectes nitidus
Carpodectes antoniae
Carpodectes hopkei
Xipholena lamellipennis
Xipholena atropurpurea
Xipholena punicea
Gymnoderus foetidus
Conioptilon mcilhennyi
Porphyrolaema porphyrolaema
Cotinga maculata
Cotinga cotinga
Cotinga nattererii
Cotinga ridgwayi
Cotinga amabilis
Cotinga cayana
Cotinga maynana
Procnias averano
Procnias nudicollis
Procnias tricarunculata
Procnias albus
Lipaugus uropygialis (Peru)
Lipaugus uropygialis (Bolivia)
Lipaugus fuscocinereus
Lipaugus vociferans (Venezuela)
Lipaugus vociferans (Bolivia)
Lipaugus streptophorus
Tijuca atra
Lipaugus lanioides
Lipaugus unirufus
Cephalopterus ornatus
Perissocephalus tricolor
Cephalopterus penduliger
Cephalopterus glabricollis
Pyroderus scutatus scutatus
Pyroderus scutatus masoni
Querula purpurata
Haematoderus militaris
Ampelion rubrocristatus
Ampelion rufaxilla
Doliornis sclateri
Doliornis remseni
Phibalura flavirostris
Phytotoma raimondii
Phytotoma rutila
Phytotoma rara
Zaratornis stresemanni
Phoenicircus nigricollis
Phoenicircus carnifex
Rupicola rupicola
Rupicola peruviana
Carpornis cucullatus
Carpornis melanocephalus
Snowornis cryptolophus
Snowornis subalaris
Pipreola riefferii confusa
Pipreola riefferii melanolaema
Pipreola intermedia
Pipreola arcuata
Pipreola jucunda
Pipreola pulchra
Pipreola lubomirskii (Peru)
Pipreola lubomirskii (Ecuador)
Pipreola whitelyi
Pipreola frontalis
Pipreola chlorolepidota
Ampelioides tschudii (Peru)
Ampelioides tschudii (Ecuador)

Figure 1.2 *BEAST species tree topology. Numbers above branches are Bayesian posterior probabilities derived from the species tree analysis. Numbers below branches are (right) posterior probabilities derived from MrBayes, and (left) RaxML bootstrap support values. A hyphen at a particular position indicates a given node was not recovered by that method. **Please refer to the published version of this article for higher quality vector art.**

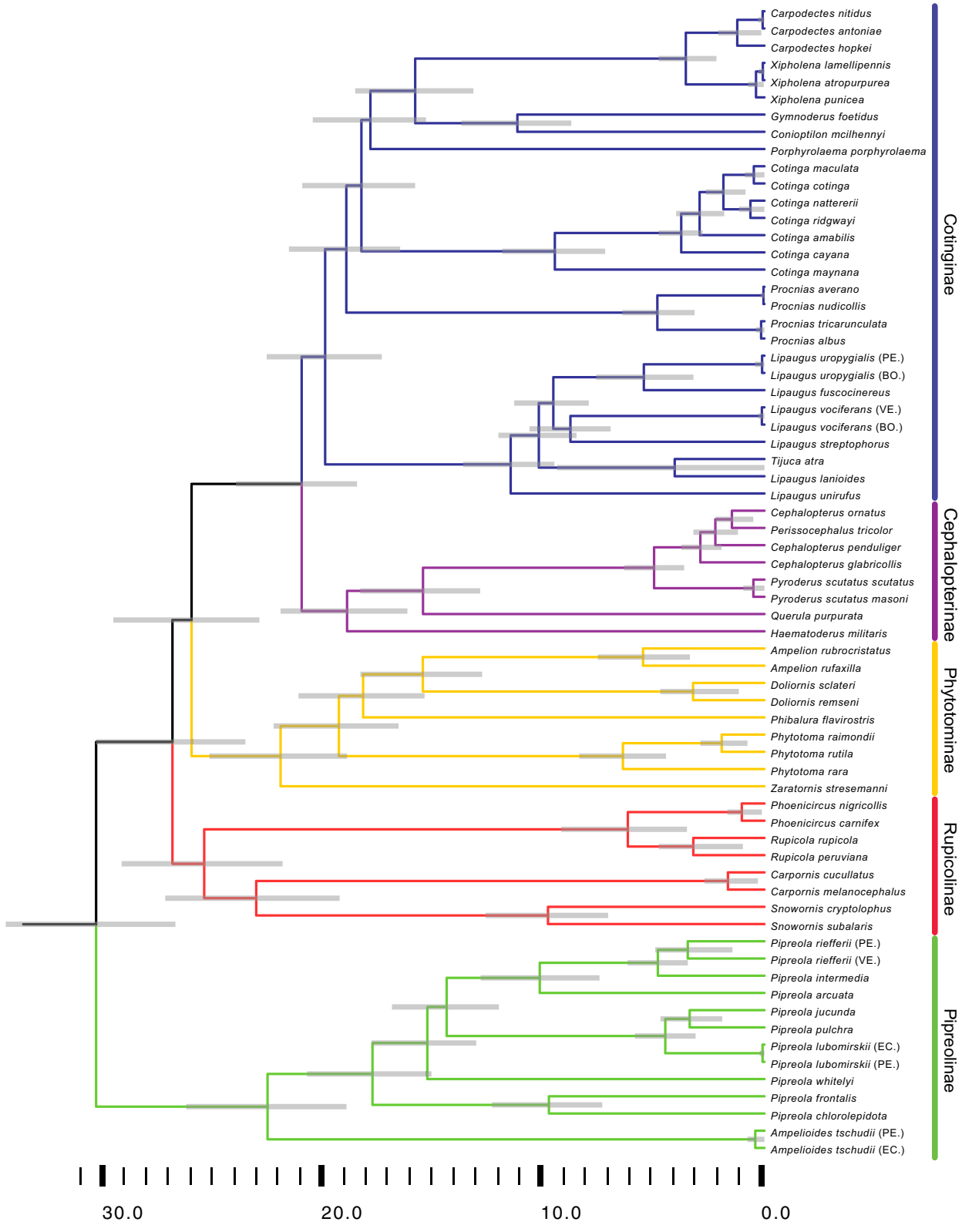
Carpodectes nitidus
Carpodectes antoniae
Carpodectes hopkei
Xipholena lamellipennis
Xipholena atropurpurea
Xipholena punicea
Gymnoderus foetidus
Conioptilon mcilhennyi
Porphyrolaema porphyrolaema
Cotinga maculata
Cotinga cotinga
Cotinga nattererii
Cotinga ridgwayi
Cotinga amabilis
Cotinga cayana
Cotinga maynana
Procnias averano
Procnias nudicollis
Procnias tricarunculata
Procnias albus
Lipaugus uropygialis (PE.)
Lipaugus uropygialis (BO.)
Lipaugus fuscocinereus
Lipaugus vociferans (VE.)
Lipaugus vociferans (BO.)
Lipaugus streptophorus
Tijuca atra
Lipaugus lanioides
Lipaugus unirufus
Cephalopterus ornatus
Perissocephalus tricolor
Cephalopterus penduliger
Cephalopterus glabricollis
Pyroderus scutatus scutatus
Pyroderus scutatus masoni
Querula purpurata
Haematoderus militaris
Ampelion rubrocristatus
Ampelion rufaxilla
Doliornis sclateri
Doliornis remseni
Phibalura flavirostris
Phytotoma raimondii
Phytotoma rutila
Phytotoma rara
Zaratornis stresemanni
Phoenicircus nigricollis
Phoenicircus carnifex
Rupicola rupicola
Rupicola peruviana
Carpornis cucullatus
Carpornis melanocephalus
Snowornis cryptolophus
Snowornis subalaris
Pipreola riefferii (PE.)
Pipreola riefferii (VE.)
Pipreola intermedia
Pipreola arcuata
Pipreola jucunda
Pipreola pulchra
Pipreola lubomirskii (EC.)
Pipreola lubomirskii (PE.)
Pipreola whitelyi
Pipreola frontalis
Pipreola chlorolepidota
Ampelioides tschudii (PE.)
Ampelioides tschudii (EC.)
Cotinginae
Cephalopterinae
Phytotominae
Rupicolinae
Pipreolinae
30.0
20.0
10.0
0.0

Figure 1.3. Ultrametric species tree chronogram. The time scale (below) is in millions of years, and was estimated from five molecular rate calibrations from previous studies of passerine birds using lognormal relaxed clocks. Colors and vertical bars indicate our proposed subfamily classification. Horizontal node bars represent the 95% HPD (highest posterior density) estimate of node height. **Please refer to the published version of this article for higher quality vector art.**

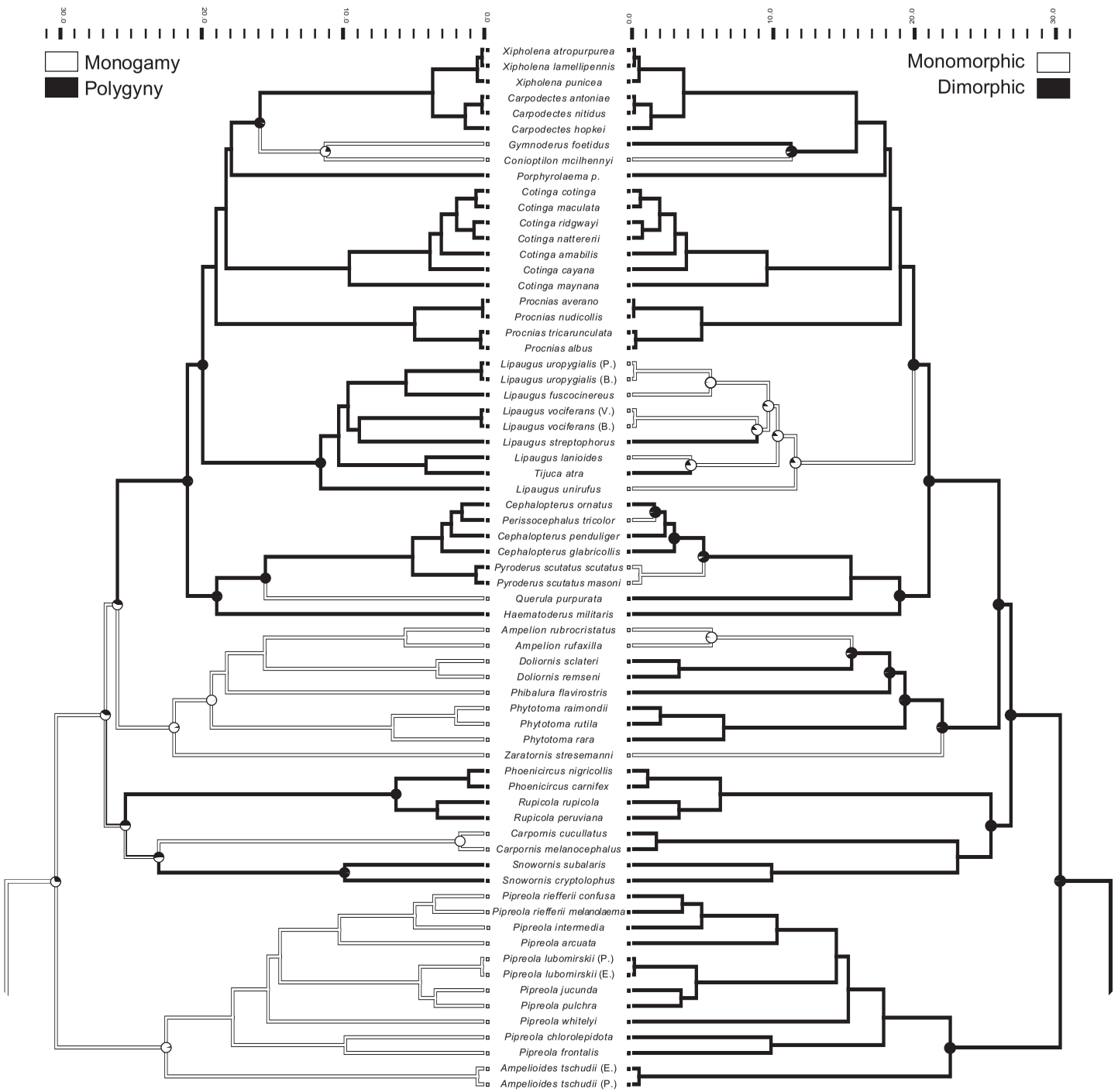
30.0
20.0
10.0
0.0
Monogamy
Polygyny
Xipholena atropurpurea
Xipholena lamellipennis
Xipholena punicea
Carpodectes antoniae
Carpodectes nitidus
Carpodectes hopkei
Gymnoderus foetidus
Conioptilon mcilhennyi
Porphyrolaema p.
Cotinga cotinga
Cotinga maculata
Cotinga ridgwayi
Cotinga nattererii
Cotinga amabilis
Cotinga cayana
Cotinga maynana
Procnias averano
Procnias nudicollis
Procnias tricarunculata
Procnias albus
Lipaugus uropygialis (P.)
Lipaugus uropygialis (B.)
Lipaugus fuscocinereus
Lipaugus vociferans (V.)
Lipaugus vociferans (B.)
Lipaugus streptophorus
Lipaugus lanioides
Tijuca atra
Lipaugus unirufus
Cephalopterus ornatus
Perissocephalus tricolor
Cephalopterus penduliger
Cephalopterus glabricollis
Pyroderus scutatus scutatus
Pyroderus scutatus masoni
Querula purpurata
Haematoderus militaris
Ampelion rubrocristatus
Ampelion rufaxilla
Doliornis sclateri
Doliornis remseni
Phibalura flavirostris
Phytotoma raimondii
Phytotoma rutila
Phytotoma rara
Zaratornis stresemanni
Phoenicircus nigricollis
Phoenicircus carnifex
Rupicola rupicola
Rupicola peruviana
Carpornis cucullatus
Carpornis melanocephalus
Snowornis subalaris
Snowornis cryptolophus
Pipreola riefferii confusa
Pipreola riefferii melanolaema
Pipreola intermedia
Pipreola arcuata
Pipreola lubomirskii (P.)
Pipreola lubomirskii (E.)
Pipreola jucunda
Pipreola pulchra
Pipreola whitelyi
Pipreola chlorolepidota
Pipreola frontalis
Ampelioides tschudii (E.)
Ampelioides tschudii (P.)
0.0
10.0
20.0
30.0
Monomorphic
Dimorphic

Figure 1.4. Ancestral state reconstructions of cotinga breeding biology using the species tree. Left, the evolutionary history of cotinga breeding systems; right, the evolutionary history of sexual plumage dimorphism. Branch lengths are proportional to absolute time, indicated by the scale in millions of years. Branch mappings are derived from reconstructing character evolution on the single MCC topology, using symmetrical transition rate models. Pie charts indicate the character likelihood of a state for a given node, averaged across 10,000 randomly sampled post-burn in trees from the posterior distribution of the species tree analysis. **Please refer to the published version of this article for higher quality vector art.**

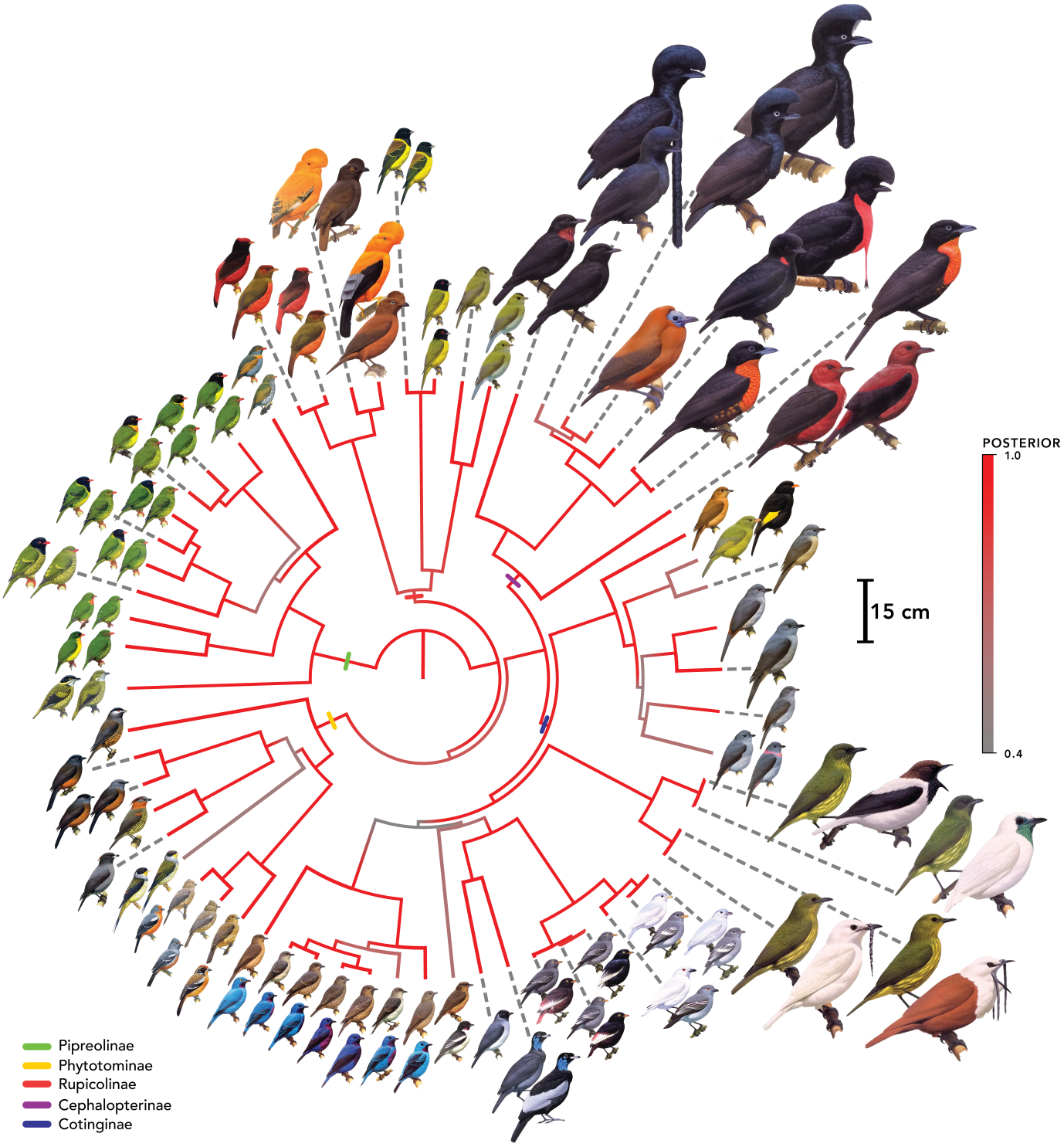
POSTERIOR
1.0
0.4
15 cm
Pipreolinae
Phytotominae
Rupicolinae
Cephalopterinae
Cotinginae

Figure 1.5. Distribution of phenotypes, plumages, and size variation across the Cotingas. Illustrations are reproduced with permission from the Handbook of the Birds of the World. Vol. 9. Cotingas to Pipits and Wagtails, Lynx Editions 2004. Males are depicted towards the outer perimeter, while females are placed more interior. Color monomorphism is indicated by the presence of only a single illustration at a given terminal. Branches are colored according to their posterior probability, and the centimeter scale indicates relative sizes. **Please refer to the published version of this article for higher quality vector art.**

*BEAST species definition	Type	Institution	Institution #; Tissue #	Country	State
Ampelioides tschudii-Peru	T	LSUMZ	–; 5457	Peru	San Martin
Ampelioides tschudii-Ecuador	T	ANSP	–; 18542	Ecuador	Azuay
Ampelioides tschudii-Ecuador	T	ANSP	184088; 18564	Ecuador	Azuay
Pipreola chlorolepidota	T	LSUMZ	–; 5435	Peru	San Martin
Pipreola frontalis	T	LSUMZ	–; 5559	Peru	San Martin
Pipreola whitelyi	T	AMNH	12041; –	Venezuela	Bolivar
Pipreola lubomirskii-Peru	T	LSUMZ	170033; 32720	Peru	Cajamarca
Pipreola lubomirskii-Ecuador	T	ANSP	186238; 19778	Ecuador	Zamora Chinchipe
Pipreola jucunda	T	ANSP	–; 15820	Ecuador	Carchi
Pipreola pulchra	T	LSUMZ	–; 1625	Peru	Pasco
Pipreola arcuata	T	LSUMZ	–; 7654	Peru	Huanuco
Pipreola intermedia	T	LSUMZ	–; 574	Peru	Puno
Pipreola riefferii-Peru	T	LSUMZ	–; 297	Peru	Cajamarca
Pipreola riefferii-Venezuela	T	COP	77717; –	Venezuela	Aragua
Snowornis subalaris	T	ANSP	185671; 19464	Ecuador	Napo
Snowornis cryptolophus	T	ANSP	–; 19141	Ecuador	Zamora-Chinchipe
Carpornis cucullatus	S	LACM	28580, 27611, 28581; –	Brazil	Sao Paulo
Carpornis melanocephalus	T	LSUMZ	–; 35583	Brazil	Bahia
Rupicola peruviana	T	LSUMZ	–; 19004	Houston Zoo	–
Rupicola rupicola	T	AMNH	8790; –	Venezuela	Amazonas
Phoenicircus carnifex	T	LSUMZ	–; 20173	Brazil	Amazonas
Phoenicircus nigricollis	T	LSUMZ	–; 2898	Peru	Loreto
Zaratornis stresemanni	T	LSUMZ	–; 2074	Peru	Lima
Phytotoma rara	T	KUNHM	–; 11748	Argentina	Rio Negro
Phytotoma raimondii	T	LSUMZ	–; 451	Peru	Lambayeque
Phytotoma rutila	T	LSUMZ	–; 1211	Bolivia	La Paz
Phibalura flavirostris	T	CBF	–; 4246-7	Bolivia	Apolo
Phibalura flavirostris	S	LACM	45462; –	Brazil	Goias
Phibalura flavirostris	S	LACM	45432; –	Brazil	Goias
Doliornis sclateri	T	LSUMZ	–; 3562	Peru	Huanuco
Doliornis remseni	T	ANSP	185684; 19525	Ecuador	Zamora Chinchipe
Ampelion rubrocristatus	T	LSUMZ	–; 7664	Peru	Huanuco Department
Ampelion rufaxilla	T	LSUMZ	–; 1673	Peru	Pasco Department
Haematoderus militaris	T	KUNHM	–; 1348	Guyana	Kurupukari
Querula purpurata	T	LSUMZ	–; 2785	Peru	Loreto
Pyroderus scutatus-Paraguay	T	KU	88386; 77	Paraguay	Concepcion
Pyroderus scutatus-Peru	T	LSUMZ	–; 8137	Peru	Pasco
Cephalopterus glabricollis	T	USNM	–; B01560	Panama	Chiriqui
Cephalopterus penduliger	T	LSUMZ	–; 11737	Ecuador	Esmeraldas
Cephalopterus ornatus	T	LSUMZ	–; 12300	Bolivia	Santa Cruz Department
Perissocephalus tricolor	T	AMNH	11946; –	Venezuela	Bolivar
Lipaugus unirufus	T	ANSP	–; 17370	Ecuador	Esmeraldas
Lipaugus lanioides	S	YPM	80714; –	Brazil	Sao Paulo
Lipaugus vociferans-Bolivia	T	LSUMZ	–; 12598	Bolivia	Santa Cruz
Lipaugus vociferans-Venezuela	T	AMNH	11892; –	Venezuela	Bolivar
Lipaugus streptophorus	T	AMNH	11995; –	Venezuela	Bolivar
Lipaugus fuscocinereus	T	ANSP	185672; 19589	Ecuador	Zamora-Chinchipe
Lipaugus uropygialis-Peru	S	LSUMZ	98424; 25308	Peru	Puno
Lipaugus uropygialis-Peru	S	LSUMZ	98425; 25309	Peru	Puno
Lipaugus uropygialis-Bolivia	S	ANSP	–; 120115	Bolivia	La Paz
Tijuca atra	G	ZMUC	128821; –	Brazil	–
Procnias albus	T	KUNHM	–; 1244	Guyana	Kurupukari
Procnias albus	T	AMNH	–; 12002	Venezuela	Bolivar
Procnias albus	S	MPEG	–; 37214	Brazil	Para
Procnias tricarunculata	T	UWBM	–; 56120	Nicaragua	Matagalpa
Procnias tricarunculata	T	ANSP	187540, 187541; 20416, 20431	Panama	Veraguas
Procnias nudicollis	T	KUNHM	–; 1224	Paraguay	Concepcion
Procnias averano	S	ANSP	105021; –	Trinidad	–
Procnias averano	S	MPEG	–; 40911	Brazil	Maranhão
Procnias averano	S	MPEG	–; 40912	Brazil	Maranhão
Procnias averano	S	MPEG	–; 40913	Brazil	Maranhão
Procnias averano	S	ANSP	105021; –	Trinidad	Caura
Procnias averano	S	AMNH	–; 468475	Trinidad	Malajo forest
Cotinga maynana	T	ANSP	181680; 16580	Ecuador	Morona-Santiago
Cotinga maynana	T	LSUMZ	–; 4762	Peru	Loreto
Cotinga maynana	T	LSUMZ	–; 42921	Peru	Loreto
Cotinga cayana	T	FMNH	–; 390011	Brazil	Rondonia
Cotinga cayana	T	LSUMZ	–; 4977	Peru	Loreto
Cotinga amabilis	S	KUNHM	104761; –	Mexico	Veracruz
Cotinga amabilis	S	KUNHM	104762; –	Mexico	Veracruz
Cotinga nattererii	T	LSUMZ	–; 28771	Panama	Colon
Cotinga ridgwayi	S	AMNH	706142; –	Costa Rica	–
Cotinga maculata	S	LACM	66184; –	Brazil	–

(*continued on next page*)

Table 1 (*continued*)

*BEAST species definition	Type	Institution	Institution #; Tissue #	Country	State
Cotinga cotinga	T	ANSP	187801; 21444	Guyana	Upper Takutu-Upper Essequibo
Cotinga cotinga	T	ANSP	187799; 21918	Guyana	Potaro-Siparuni
Porphyrolaema porphyrolaema	T	LSUMZ	–; 6989	Peru	Loreto
Porphyrolaema porphyrolaema	T	ANSP	183371; 18193	Ecuador	Sucumbios
Conioptilon mcilhennyi	T	KU	–; 1416	Peru	Madre de Dios
Gymnoderus foetidus	T	LSUMZ	–; 9586	Bolivia	Pando
Xipholena punicea	T	LSUMZ	–; 20833	Houston Zoo	-
Xipholena lamellipennis	S	KUNHM	52657; –	Brazil	Maranhão
Xipholena atropurpurea	T	FMNH	–; 427187	Brazil	Alagoas
Carpodectes hopkei	T	ANSP	–; 17352	Ecuador	Esmeraldas
Carpodectes antoniae	S	YPM	56777; –	Costa Rica	Puntarenas
Carpodectes nitidus	S	LSUMZ	75501; 25310	Panama	Bocas del Toro
Outgroups	Type	Institution	Institution#; Tissue #	Country	State
Chloropipo unicolor	T	AMNH	11988; –	Venezuela	Bolivar
Manacus manacus	T	LSUMZ	–; 8913	Bolivia	Pando
Lepidothrix suavissima	T	AMNH	12036; –	Venezuela	Bolivar
Pipra cornuta	T	AMNH	–; 11877	Venezuela	Bolivar
Schiffornis virescens	G	NRM	937315; –	Paraguay	–
Laniisoma elegans	T	ANSP	181681; 16543	Ecuador	Morona-Santiago
Iodopleura fusca	T	ANSP	187808; 21600	Guyana	Potaro-Siparuni
Pachyramphus polychopterus	T	YPM	–; 1015	Uruguay	Artigas
Tityra inquisitor	T	LSUMZ	–; 18568	Bolivia	Santa Cruz Department
Hirundinea ferruginea	T	YPM	–; 1183	Uruguay	Cerro Largo
Euscarthmus meloryphus	T	YPM	–; 1044	Uruguay	Artigas
Elaenia parvirostris	T	YPM	–; 978	Uruguay	Artigas
Tyrannus forficatus	T	KU	–; 87603	USA	Kansas
Oxyruncus cristatus	T	KUNHM	–; 220	Paraguay	Caazapa
Piprites chloris	T	KUNHM	–; 329	Paraguay	–
Piprites pileata	G	ZMUC	128817; –	Brazil	–
Calyptura cristata	G	ZMUC	379; –	Brazil	Rio de Janerio
Thamnophilus caerulescens	T	YPM	–; 1016	Uruguay	Artigas
Lochmias nematura	T	YPM	–; 1141	Uruguay	Cerro Largo
Lepidocolaptes angustirostris	T	YPM	–; 1011	Uruguay	Artigas
Pitta baudi	T	ANSP	–; 16224	East Malaysia	Sabah
Smithornis rufolateralis	T	YPM	–; 451	Equatorial Guinea	–
Philepitta castanea	G	ZMUC	S458; –	Madagascar	–

Table 1.1 Taxon sample list. Table of all individuals included in this study. Specimen types: T, tissue; S, skin; G, GenBank. GenBank accession numbers are reported in the Supplemental Appendix. **Please refer to the published version of this article for PDF.**

REFERENCES

Akaike, H., 1974. A new look at the statistical model identification. Autom. Contr., IEEE Transact. 19, 716–723.

Ames, P.L., 1971. The Morphology of the Syrinx in Passerine Birds.

Avalos, V.D.R., 2011. Biparental care and nestling success of the Swallow-tailed Cotinga in northwestern Bolivia. Wilson J. Ornithol. 123, 251–258.

Barker, F.K., Cibois, A., Schikler, P., Feinstein, J., Cracraft, J., 2004. Phylogeny and diversification of the largest avian radiation. Proc. Natl. Acad. Sci. USA 101, 11040–11045.

Barker, F.K., Burns, K.J., Klicka, J., Lanyon, S.M., Lovette, I.J., 2013. Going to extremes: contrasting rates of diversification in a recent radiation of new world passerine birds. Syst. Biol. 62, 298–320.

Belmonte-Lopes, R., Maurício, G.N., Bornschein, M.R., 2011. Description of the nest and egg of an Atlantic forest endemic, the Black-headed Berryeater, Carpornis melanocephala (Cotingidae). Wilson J. Ornithol. 123, 819–822.

Brown, J.M., Lemmon, A.R., 2007. The importance of data partitioning and the utility of bayes factors in bayesian phylogenetics. Syst. Biol. 56, 643–655.

Burton, P.J.K., 1976. Structure and histology of the wattle in the White bellbird (Procnias alba). J. Zool. 178, 285–293.

Clarke, J.A., Tambussi, C.P., Noriega, J.I., Erickson, G.M., Ketcham, R.A., 2005. Definitive fossil evidence for the extant avian radiation in the Cretaceous. Nature 433, 305–308.

Cuervo, A.M., Salaman, P.G.W., Donegan, T.M., Ochoa, J.M., 2001. A new species of piha (Cotingidae: Lipaugus) from the Cordillera Central of Colombia. Ibis 143, 353–368.

Darwin, C., 1871. The Descent of Man, and Selection in Relation to Sex. John Murray, London.

Degnan, J.H., Rosenberg, N.A., 2009. Gene tree discordance, phylogenetic inference and the multispecies coalescent. Trends Ecol. Evol. 24, 332–340.

del Hoyo, J., Elliot, A., Christie, D.A., 2004. Handbook of the Birds of the World. Cotingas to Pipits and Wagtail. Handbook of the Birds of the World, vol. 9. Lynx Editions, Barcelona.

Drovetski, S.V., 2002. Molecular phylogeny of grouse: individual and combined performance of W-linked, autosomal, and mitochondrial loci. Syst. Biol. 51, 930–945.

Drummond, A.J., Ho, S.Y., Rawlence, N., Rambaut, A., 2007. A Rough Guide to BEAST 1.4. Edinburgh: University of Edinburgh.

Drummond, A.J., Suchard, M.A., Xie, D., Rambaut, A., 2012. Bayesian phylogenetics with BEAUti and the BEAST 1.7. Mol. Biol. Evol. 29, 1969–1973.

Edwards, S.V., Liu, L., Pearl, D.K., 2007. High-resolution species trees without concatenation. Proc. Natl. Acad. Sci. 104, 5936–5941.

Ferreira, M.A., Suchard, M.A., 2008. Bayesian analysis of elapsed times in continuous-time Markov chains. Can. J. Stat. 36, 355–368.

Garrod, A.H., 1876. On some anatomical characters which bear upon the major divisions of the passerine birds. Proc. Zool. Soc. Lond. 1876, 506–519.

Gelman, A., Rubin, D.B., 1992. Inference from iterative simulation using multiple sequences. Stat. Sci., 457–472.

Heled, J., Drummond, A.J., 2010. Bayesian inference of species trees from multilocus data. Mol. Biol. Evol. 27, 570–580.

Hellmayr, C.E., 1929. Catalogue of birds of the Americas, Part 6. Oxyruncidae- Pipridae-Cotingidae-Rupicolidae-Phytotomidae. Publ. Field Mus. Nat. Hist., pp. 1–258.

Hennessey, A.B., 2011. Species Rank of Phibalura (flavirostris) boliviana Based on Plumage, Soft Part Color, Vocalizations, and Seasonal Movements. Wilson J. Ornithol. 123, 454–458.

Hovmöller, R., Lacey Knowles, L., Kubatko, L.S., 2013. Effects of missing data on species tree estimation under the coalescent. Mol. Phylogenet. Evol. 69, 1057– 1062.

Irwin, R.E., 1994. The evolution of plumage dichromatism in the new world blackbirds: social selection on female brightness. Am. Nat. 144, 890–907.

Johansson, U.S., Irestedt, M., Parsons, T.J., Ericson, P.G.P., 2002. Basal phylogeny of the Tyrannoidea based on comparisons of cytochrome b and exons of nucelar c-myc and RAG-1 genes. Auk 119, 984–995.

Kirwan, G.M., Green, G., 2012. Cotingas and Manakins. Princeton University Press, Princeton, NJ.

Kroodsma, D., Hamilton, D., Sánchez, J.E., Byers, B.E., Fandiño-Mariño, H., Stemple, D.W., Trainer, J.M., Powell, G.V.N., 2013. Behavioral evidence for song learning in the suboscine bellbirds (Procnias spp.; Cotingidae). Wilson J. Ornithol. 125, 1– 14.

Kubatko, L.S., Degnan, J.H., 2007. Inconsistency of phylogenetic estimates from concatenated data under coalescence. Syst. Biol. 56, 17–24.

Küchler, W., 1936. Anatomische untersuchungen an Phytotoma rara Mol. J. für Ornithol. 84, 350–362.

Kumar, S., Nei, M., Dudley, J., Tamura, K., 2008. MEGA: a biologist-centric software for evolutionary analysis of DNA and protein sequences. Brief. Bioinform. 9, 299–306.

Lanfear, R., Calcott, B., Ho, S.Y., Guindon, S., 2012. PartitionFinder: combined selection of partitioning schemes and substitution models for phylogenetic analyses. Mol. Biol. Evol. 29, 1695–1701.

Lanyon, S.M., Lanyon, W.E., 1988. The systematic position of the Plantcutters, Phytotoma. Auk 106, 422–432.

Leavitt, J.R., Hiatt, K.D., Whiting, M.F., Song, H., 2013. Searching for the optimal data partitioning strategy in mitochondrial phylogenomics: a phylogeny of Acridoidea (Insecta: Orthoptera: Caelifera) as a case study. Mol. Phylogenet. Evol. 67, 494–508.

Lewis, P.O., 2001. A likelihood approach to estimating phylogeny from discrete morphological character data. Syst. Biol. 50, 913–925.

Li, C., Lu, G., Orti, G., 2008. Optimal data partitioning and a test case for ray-finned fishes (Actinopterygii) based on ten nuclear loci. Syst. Biol. 57, 519–539.

Longrich, N.R., Tokaryk, T., Field, D.J., 2011. Mass extinction of birds at the Cretaceous–Paleogene (K–Pg) boundary. Proc. Natl. Acad. Sci. 108, 15253– 15257.

Luo, A., Qiao, H., Zhang, Y., Shi, W., Ho, S.Y., Xu, W., Zhang, A., Zhu, C., 2010. Performance of criteria for selecting evolutionary models in phylogenetics: a comprehensive study based on simulated datasets. BMC Evol. Biol. 10, 242.

Maddison, W., Maddison, D., 2011. Mesquite: A Modular System for Evolutionary Analysis. Version 2.75. Mesquite website. <mesquiteproject.org>.

Mayr, G., 2013. The age of the crown group of passerine birds and its evolutionary significance – molecular calibrations versus the fossil record. Syst. Biodivers. 11, 7–13.

Mayr, E., Phelps Jr., W.H., 1967. The origin of the bird fauna of the south Venezuelan highlands. Bull. Am. Museum Natur. History 136, 269–328.

McGuire, J.A., Witt, C.C., Altshuler, D.L., Remsen, J.V., 2007. Phylogenetic systematics and biogeography of hummingbirds: bayesian and maximum likelihood analyses of partitioned data and selection of an appropriate partitioning strategy. Syst. Biol. 56, 837–856.

Midtgård, U., 1982. Patterns of the blood vascular system in the pelvic limb of birds. J. Zool. 196, 545–567.

Miller, M.A., Pfeiffer, W., Schwartz, T., 2010. Creating the CIPRES Science Gateway for inference of large phylogenetic trees. Gateway Computing Environments Workshop (GCE), 2010. IEEE, pp. 1–8.

Mooers, A.O., Schluter, D., 1999. Reconstructing ancestor states with maximum likelihood: support for one-and two-rate models. Syst. Biol. 48, 623–633.

Nemeth, E., 2004. Measuring the sound pressure level of the song of the screaming Piha Lipaugus Vociferans: one of the loudest birds in the world? Bioacoustics 14, 225–228.

Nylander, J.A., Wilgenbusch, J.C., Warren, D.L., Swofford, D.L., 2008. AWTY (are we there yet?): a system for graphical exploration of MCMC convergence in Bayesian phylogenetics. Bioinformatics 24, 581–583.

Ödeen, A., Håstad, O., 2003. Complex distribution of avian color vision systems revealed by sequencing the SWS1 opsin from total DNA. Mol. Biol. Evol. 20, 855–861.

Ohlson, J.I., Prum, R.O., Ericson, P.G.P., 2007. A molecular phylogeny of the cotingas (Aves: Cotingidae). Mol. Phylogenet. Evol. 42, 25–37.

Ohlson, J.I., Irestedt, M., Ericson, P.G.P., Fjeldså, J., 2013. Phylogeny and classification of the New World suboscines (Aves, Passeriformes). Zootaxa 3613, 1–35.

Pagel, M., 1994. Detecting correlated evolution on phylogenies: a general method for the comparative analysis of discrete characters. Proc. Roy. Soc. Lond. Ser. B: Biol. Sci. 255, 37–45.

Pagel, M., 1997. Inferring evolutionary processes from phylogenies. Zoolog. Scr. 26, 331–348.

Papadopoulou, A., Jones, A.G., Hammond, P.M., Vogler, A.P., 2009. DNA taxonomy and phylogeography of beetles of the Falkland Islands (Islas Malvinas). Mol. Phylogenet. Evol. 53, 935–947.

Posada, D., Buckley, T.R., 2004. Model selection and model averaging in phylogenetics: advantages of Akaike information criterion and Bayesian approaches over likelihood ratio tests. Syst. Biol. 53, 793–808.

Poux, C., Madsen, O., Glos, J., de Jong, W., Vences, M., 2008. Molecular phylogeny and divergence times of Malagasy tenrecs: influence of data partitioning and taxon sampling on dating analyses. BMC Evol. Biol. 8, 102.

Powell, A.F.L.A., Barker, F.K., Lanyon, S.M., 2013. Empirical evaluation of partitioning schemes for phylogenetic analyses of mitogenomic data: an avian case study. Mol. Phylogenet. Evol. 66, 69–79.

Prum, R.O., 1990. A test of the monophyly of the manakins (Pipridae) and of the cotingas (Cotingidae) based on morphology. Occasion. Papers Museum Zool. Univ. Michigan 723, 1–44.

Prum, R.O., 1994. Phylogenetic analysis of the evolution of alternative social behavior in the manakins (Aves: Pipridae). Evolution, 1657–1675.

Prum, R.O., 1997. Phylogenetic tests of alternative intersexual selection mechanisms: macroevolution of male traits in a polygynous clade (Aves: Pipridae). Am. Natur. 149, 668–692.

Prum, R.O., 2001. A new genus for the Andean green pihas (Cotingidae). Ibis 143, 307–309.

Prum, R.O., 2010. The Lande–Kirkpatrick mechanism is the null model of evolution by intersexual selection: implications for meaning, honesty, and design in intersexual signals. Evolution 64, 3085–3100.

Prum, R.O., Lanyon, W.E., 1989. Monophyly and phylogeny of the Schiffornis group (Tyrannoidea). Condor 91, 444–461.

Prum, R.O., Torres, R.H., 2003. Structural colouration of avian skin: convergent evolution of coherently scattering dermal collagen arrays. J. Exp. Biol. 206, 2409–2429.

Prum, R.O., Torres, R.H., Williamson, S., Dyck, J., 1998. Coherent light scattering by blue feather barbs. Nature 396, 28–29.

Prum, R.O., Torres, R.H., Williamson, S., Dyck, J., 1999. Two-dimensional Fourier analysis of the spongy medullary keratin of structurally coloured feather barbs. Proc. Roy. Soc. Lond. B 266, 13–22.

Prum, R.O., Rice, N.H., Mobley, J.A., Dimmick, W.W., 2000. A preliminary phylogenetic hypothesis for the cotingas (Cotingidae) based on mitochondrial DNA. Auk 117, 236–241.

Prum, R.O., LaFountain, A.M., Berro, J., Stoddard, M.C., Frank, H.A., 2012. Molecular diversity, metabolic transformation, and evolution of carotenoid feather pigments in cotingas (Aves: Cotingidae). J. Compar. Physiol. B.

Rambaut, A., Drummond, A., 2009. Tracer. MCMC Trace Analysis Tool, Version 1.5. University of Oxford, UK. http://tree.bio.ed.ac.uk/software/tracer/%5D>.

Ridgway, R., 1907. The birds of North and Middle America, part 4. Bull. United States Natl. Museum 50, 1–973.

Robbins, M., Rosenberg, G.H., Sornoza Molina, F., 1994. A new species of cotinga (Cotingidae: Doliornis) from the ecuadorian Andes, with comments on plumage sequences in Doliornis and Ampelion. Auk 111, 1–7.

Ronquist, F., Teslenko, M., van der Mark, P., Ayres, D.L., Darling, A., Höhna, S., Larget, B., Liu, L., Suchard, M.A., Huelsenbeck, J.P., 2012. MrBayes 3.2: efficient Bayesian phylogenetic inference and model choice across a large model space. Syst. Biol. 61, 539–542.

Saranathan, V., Hamilton, D., Powell, G.V.N., Kroodsma, D.E., Prum, R.O., 2007. Genetic evidence support song learning in the three-wattled bellbird Procnias tricarunculata (Cotingidae). Mol. Ecol. 16, 3689–3702.

Saranathan, V., Forster, J.D., Noh, H., Liew, S.F., Mochrie, S.G.J., Cao, H., Dufresne, E.R., Prum, R.O., 2012. Structure and optical function of amorphous photonic nanostructures from

avian feather barbs: a comparative small angle X-ray scattering (SAXS) analysis of 229 bird species. J. R. Soc. Interface 9, 2563–2580.

Schwarz, G., 1978. Estimating the dimension of a model. Annals Stat. 6, 461–464. Snow, D.W., 1971. Observations on the Purple-throated Fruit-crow in Guyuna. Living Bird 10, 5–15.

Snow, D.W., 1973. The Classification of the Cotingidae (Aves). Breviora 409.

Snow, D.W., 1979. Tityrinae, Pipridae, Cotingidae. In: Traylor, M.A., Jr. (Ed.), Checklist of Birds of the World Museum of Comparative Zoology. Harvard Univ, Cambridge, Massachusetts, pp. 229–308.

Snow, D.W., 1982. The Cotingas. Cornell Univ. Press, Ithaca, N.Y.

Snow, D.W. 2004. Family cotingidae (Cotingidae). In: del Hoyo, J., Elliott, A., Christie, D.A. (Eds.). Handbook of the birds of the world. vol. 9. Cotingas to pipits and wagtails Lynx Edicions, Barcelona, Spain, pp. 32–108.

Song, S., Liu, L., Edwards, S.V., Wu, S., 2012. Resolving conflict in eutherian mammal phylogeny using phylogenomics and the multispecies coalescent model. Proc. Natl. Acad. Sci. 109, 14942–14947.

Stamatakis, A., 2006a. Phylogenetic Models of Rate Heterogeneity: A high Performance Computing Perspective. Parallel and Distributed Processing Symposium, 2006. IPDPS 2006. 20th International. IEEE, 8 pp.

Stamatakis, A., 2006b. RAxML-VI-HPC: maximum likelihood-based phylogenetic analyses with thousands of taxa and mixed models. Bioinformatics 22, 2688– 2690.

Stamatakis, A., Hoover, P., Rougemont, J., 2008. A rapid bootstrap algorithm for the RAxML Web servers. Syst. Biol. 57, 758–771.

Stoddard, M.C., Prum, R.O., 2008. Evolution of avian plumage color in a tetrahedral color space: a phylogenetic analysis of new world buntings. Am. Nat. 171, 755– 776.

Tello, J.G., Moyle, R.G., Marchese, D.J., Cracraft, J., 2009. Phylogeny and phylogenetic classification of the tyrant flycatchers, cotingas, manakins, and their allies (Aves: Tyrannides). Cladistics 25, 429–467.

Ward, P.S., Brady, S.G., Fisher, B.L., Schultz, T.R., 2010. Phylogeny and biogeography of dolichoderine ants: effects of data partitioning and relict taxa on historical inference. Syst. Biol. 59, 342–362.

Wiens, J.J., Sparreboom, M., Arntzen, J.W., 2011. Crest evolution in newts: implications for reconstruction methods, sexual selection, phenotypic plasticity and the origin of novelties. J. Evol. Biol. 24, 2073–2086.

Wu, C.-H., Suchard, M.A., Drummond, A.J., 2013. Bayesian selection of nucleotide substitution models and their site assignments. Mol. Biol. Evol. 30, 669–688.

CHAPTER 2

Genomic phylogeography of the White Crowned Manakin *Pseudopipra pipra* (Pipridae) illuminates a continental-scale radiation out of the Andes[II]

Jacob S. Berv[1], Leonardo Campagna[2], Teresa J. Feo[3], Ivandy Castro Astor[4], Camila Ribas[5], Richard O. Prum[6], Irby J. Lovette[7]

1. Fuller Evolutionary Biology Program, Cornell Lab of Ornithology, 159 Sapsucker Woods Road, Ithaca, NY 14850, USA. Department of Ecology and Evolutionary Biology, Cornell University, 215 Tower Road, Ithaca, NY 14853, USA.

2. Fuller Evolutionary Biology Program, Cornell Lab of Ornithology, 159 Sapsucker Woods Road, Ithaca, NY 14850, USA. Department of Ecology and Evolutionary Biology, Cornell University, 215 Tower Road, Ithaca, NY 14853, USA.

3. Department of Vertebrate Zoology, MRC-116, National Museum of Natural History, Smithsonian Institution, Washington, DC 20013, USA.

4. Department of Biology, City College of New York and CUNY Graduate Center, City University of New York, New York, NY 10031, USA

[II]Formatted for submission to Systematic Biology, final submission version from July 19, 2019.

5. Coordenacão de Biodiversidade, Instituto Nacional de Pesquisas da Amazônia, Manaus, AM, Brazil

6. Department of Ecology and Evolutionary Biology, and Peabody Museum of Natural History, Yale University, New Haven, Connecticut, 06520

7. Fuller Evolutionary Biology Program, Cornell Lab of Ornithology, 159 Sapsucker Woods Road, Ithaca, NY 14850, USA. Department of Ecology and Evolutionary Biology, Cornell University, 215 Tower Road, Ithaca, NY 14853, USA.

Abstract.—The complex landscape history of the Neotropics has generated opportunities for population isolation and subsequent diversification that place this region among the most species-rich in the world. Detailed phylogeographic studies are required to uncover the biogeographic histories of Neotropical taxa, to identify evolutionary correlates of diversity, and to reveal patterns of genetic connectivity, disjunction, and potential differentiation among lineages from different areas of endemism. The White-crowned Manakin (*Pseudopipra pipra*) is a small suboscine passerine bird that is broadly distributed through the subtropical rainforests of Central America, the lower montane cloud forests of the Andes from Colombia to central Peru, the lowlands of Amazonia and the Guianas, and the Atlantic forest of southeast Brazil. *Pseudopipra* is currently recognized as a single, polytypic biological species. We studied the effect of the historical and current Neotropical landscape on genetic and phenotypic differentiation within this species using genomic data derived from double digest restriction site associated DNA sequencing (ddRAD), and mitochondrial DNA. Our analyses identify five ancient clades, which encompass seventeen well-differentiated populations. Most of the breakpoints among populations coincide with physical barriers to gene flow previously associated with avian areas of endemism, and generally coincide with subspecies boundaries. The phylogenetic relationships among these populations imply a unique pattern of a montane Andean origin for the genus, with a subsequent expansion and radiation into the Amazonian lowlands. Analyses of genomic admixture demonstrate a complex history of introgression between some western Amazonian populations, which confound standard concatenated and coalescent phylogenetic analyses, and raise the possibility that a lineage in the western Napo area of endemism is of hybrid origin. Lastly, we analyze variation in vocal phenotypes in the context

of our phylogeny and propose that *Pseudopipra* is a species-complex composed of 15-17 distinct species which have arisen in the last ~2.5 Ma.

Key Words: Neotropics, Amazon, Andes, Areas of Endemism, Suboscine, Speciation Genomics, Phylogeography, Lekking, hybrid speciation

Many kinds of geographic and habitat barriers have been proposed to drive population diversification and speciation in the Neotropics (Wallace 1854, Haffer 1969, Cracraft and Prum 1988, Haffer 2008, Smith et al. 2014). Such ecological barriers partition biodiversity into areas of endemism (Cracraft 1985, Cracraft and Prum 1988, Linder 2001, Da Silva et al. 2005, Crother and Murray 2011, Noguera-urbano 2016) by acting as impediments to gene flow for dispersal-limited organisms (Cheviron et al. 2005, Moore et al. 2008, Brumfield 2012, Ribas et al. 2012, Fernandes et al. 2015). Three of the most prominent features implicated in structuring the biodiversity of Neotropical forest birds (Figure 1) include the Andes Mountains and other montane regions (Figure 1, grey relief); the Chaco, Cerrado, and Caatinga biomes, which collectively form a 'dry diagonal' of open habitat separating the Amazon forest from the Atlantic Forest; and the large rivers of the complex Amazonian drainage system (Brumfield 2012, Smith et al. 2014, Harvey and Brumfield 2015, Naka and Brumfield 2018).

Montane Andean regions in the Neotropics are known to be exceptionally biodiverse, and encompass at least 15 areas of endemism with biotas shaped by a combination of vicariance and dispersal events (Hazzi et al. 2018). Elevational gradients in the Andes contribute substantially to Neotropical diversification metrics and raise fundamental questions about the historical relationships between lowland rainforest and montane endemics in the Neotropics (Weir 2006,

Quintero and Jetz 2018, Musher et al. 2019). From a biogeographic perspective, evolution has proceeded both "into and out of the Andes" (Brumfield and Edwards 2007, Nylander et al. 2008). A number of examples illustrate colonization of Andean regions by lowland ancestors (Fjeldså 1992, Bates and Zink 1994, Ribas et al. 2007), whereas fewer examples suggest colonization of lowlands (grasslands) by Andean ancestors (da Silva 1995, Voelker 1999, van Els et al. 2019). For some tanagers (Aves: Thraupidae), the Northern Andes have been a source of lineages that later dispersed into the Central Andes and Amazonian lowlands (Sedano and Burns 2010). Glacial cycles and climatic fluctuations during the Pleistocene have been implicated as an important factor in montane diversification, disproportionally affecting high elevation forest (Hooghiemstra and Van der Hammen 2004, Weir 2006) and transiently connecting highland and lowland habitats (Brumfield and Edwards 2007, Nylander et al. 2008).

By contrast, in the lowland Amazon basin, a number of areas of endemism have been described, delimited primarily by major tributaries of the Amazon River (Haffer 1974, Cracraft 1985, Da Silva et al. 2005, Borges and Da Silva 2012). Wallace (1854) initially suggested that the Amazon basin could be divided into four wide bioregions (which he termed 'Guyana', 'Ecuador', 'Peru', 'Brazil'), based on primate distributions (see also Lynch Alfaro et al. 2015). These areas were subsequently partitioned by later biogeographers into at least eight major areas of endemism for terrestrial vertebrates (Figure 1) (Haffer 1978, Cracraft 1985, Haffer 1985, Cracraft and Prum 1988, Haffer 1992, Da Silva et al. 2002, Da Silva et al. 2005, Naka 2011, Borges and Da Silva 2012). The aggregate of these geographic partitions has been recognized as the "Amazonian areas of endemism" and is the basis for the riverine barrier hypothesis (Figure 1, Antonelli et al. 2018, Silva et al. 2019 Figure 1A).

Few studies have applied modern phylogeographic techniques leveraging next-generation sequencing datasets to reconstruct the phylogenetic and population genetic history of a Neotropical radiation distributed across many major Neotropical forest areas of endemism. To our knowledge, there has only been one other study to apply a genomic sequencing technique to study continental-scale phylogeography of an Amazonian suboscine passerine bird (*Xenops minutus*; Harvey and Brumfield 2015, also see Harvey et al. 2017). Here, we investigate lineage diversification across the Neotropics using the continentally distributed *Pseudopipra* genus. The monotypic genus *Pseudopipra* (family Pipridae) currently includes a single biological species, the White-crowned Manakin (*Pseudopipra pipra = Dixiphia*). *Pseudopipra* is found on both sides of a variety of known dispersal barriers, including elevational gradients of the Andes, major Amazonian rivers, the dry diagonal, tepuis, and the Isthmus of Panama. Thus, this radiation is particularly appropriate for assessing patterns of phylogenomic differentiation across a nested set of spatial scales in Neotropical forests distributed in both highland and lowland areas of endemism.

In order to assess the historical relationships among Andean and lowland Amazonian populations, and the degree to which population structure corresponds to landscape features, our study design uses fine-scale sampling across a majority of *Pseudopipra's* range. We use double digest restriction site associated DNA (RAD) sequencing (Peterson et al. 2012)—a reduced representation genomic sequencing technique— to sample thousands of independent markers across the genomes of hundreds of individuals spanning many well-known Amazonian and Andean areas of endemism, from Costa Rica to the Atlantic Forest of Brazil. We use these data to infer biogeographic history using a variety of methods, including concatenated data and coalescent-based phylogenetic inference.

Our investigation led us to examine the spatial distribution of genetic diversity across the range of *Pseudopipra* and to investigate the roles of many specific barriers to gene flow on population genomic differentiation. We tested for signals of isolation by distance (IBD) within areas delimited by prominent geographic barriers and assessed the degree to which such barriers generate discontinuities from IBD predictions. Our analyses inferred a spatially explicit model that explains a majority of the observed genetic dissimilarity among sampling localities and of the overall genetic variance, implying a strong connection between landscape features and diversification at multiple scales. Lastly, we investigated congruence between geographic variation in vocal variation, plumage phenotype, and phylogeographic structure, to evaluate the biological mechanisms that may be contributing to population differentiation (e.g. Zamudio et al. 2016), and to reevaluate species delimitation. Overall, these investigations highlight the significant impact of the topography and drainage systems of the Neotropics in structuring genetic diversity across *Pseudopipra*, as well as the complex influence of introgression in generating biogeographic patterns (e.g. Burbrink and Gehara 2018).

Study organism and Taxonomic summary

The White-Crowned Manakin, *Pseudopipra pipra* (Pipridae, hereafter *Pseudopipra*), is a small (10-12 gram), non-migratory, suboscine passerine bird that is broadly distributed within Central America, the lower montane cloud forests of the Andes from Colombia to central Peru, the Amazon basin, and the Atlantic Forest (Figure 2) (Kirwan and Green 2012). The male's striking white crown and jet-black body makes them among the most easily identified manakins, though the grey-green females are often confused with other manakin species in the field. *Pseudopipra* are typically found in dense humid forest, exhibit dispersed lek breeding behavior,

and are predominantly frugivorous. Unlike many manakin species that exhibit concentrated or cooperative lek behavior (e.g. Prum 1990a, Prum 1994), *Pseudopipra* males display in dispersed leks of 2-5 males (Snow 1961, Castro-Astor et al. 2007). Castro-Astor et al. (2007) described at least 11 components in the display repertoire of the Atlantic forest *Pseudopipra* population, including rapid turning, jumping, 'to-and-fro' flights, and an about-face.

For most of its history, the species *pipra* was placed in the genus *Pipra* (Snow 1979). Prum (1990b), Prum (1990a), and Prum (1992) recognized that the traditional *Pipra* (*sensu* Snow 1979) was polyphyletic and placed the species *pipra* in *Dixiphia* (Reichenbach 1850) which was recognized as a junior synonym of *Pipra*. Recently, Kirwan et al. (2016) demonstrated that the genus *Dixiphia* was unavailable for *pipra* because it is actually a junior synonym of the tyrannid genus *Arundinicola*. They named the new genus *Pseudopipra* for *pipra*.

A recent phylogenetic hypothesis of manakins based on mitochondrial and nuclear DNA sequences placed *Pseudopipra* as sister group to the five species of *Ceratopipra* (Ohlson et al. 2013). While the higher level phylogeny and taxonomy of manakins has received significant attention (Tello et al. 2009, Ohlson et al. 2013), work exploring intraspecific genetic variation within manakins has been restricted to a relatively few species (e.g. McDonald 2003, Cheviron et al. 2005, Cheviron et al. 2006, Francisco et al. 2007, Brumfield et al. 2008, Capurucho et al. 2013, Gubili et al. 2016, Luna et al. 2017).

Based on geographic variation in plumage and vocalizations, many previous authors have suggested that the biological species *Pseudopipra pipra* likely includes multiple, distinct phylogenetic species (Ridgely and Greenfield 2001, Snow 2004, Ridgely and Tudor 2009, Kirwan and Green 2012, Spencer 2012, Freile 2014). Thirteen subspecies of *Pseudopipra pipra* have been recognized based primarily on subtle variations in plumage coloration, which are

frequently more marked in females than in males (summarized in Dickinson 2003, Snow 2004, Kirwan and Green 2012). Because suboscine passerines generally do not learn their songs (but see Saranathan et al. 2007), the presence of substantial vocal variation across *Pseudopipra* populations further suggests that the genus may contain unrecognized cryptic species (e.g. Campagna et al. 2012). However, all previous authors awaited new information on genetic differentiation within *Pseudopipra* before making taxonomic recommendations.

It also remains unclear how subspecific designations reflect evolutionary history. The genetic variation within *Pseudopipra* has received prior attention by two studies that used mitochondrial DNA to infer population genetic patterns. Milá et al. (2012) reported intraspecific divergences of up to 3.5% (n=19) across three Amazonian populations, and the highest observed nucleotide diversity ($\pi = 0.266$) among 14 widely distributed Amazonian birds species. Castro-Astor (2014) used a larger sample (n=57), and discovered that at least four *Pseudopipra* subspecies correspond to well supported mitochondrial clades which were generally congruent with Amazonian areas of endemism. Castro-Astor (2014) also estimated the age of the *Pseudopipra* complex to coincide with the onset of the Pleistocene ~2.457 Ma (95% HPD 1.45-3.97).

Materials & Methods

Field and tissue sampling

Muscle tissue samples were obtained from available vouchered avian material from US and Brazilian collections and other institutions (see Acknowledgements and Supplemental Table 1). We sampled from ten of thirteen recognized subspecies (Figure 2) of *Pseudopipra* (Kirwan and Green 2012). Unfortunately, we were unable to obtain material of adequate quality for

ddRAD sequencing from the Andes of Ecuador, Colombia, and for lowland Peruvian populations representing the *coracina*, *bolivari*, *minima*, *unica*, and *pygmaea* subspecies. However, we were able to obtain mtDNA data from *coracina* and *pygmaea*, which allowed us to make a preliminary assessment of their phylogenetic affinities (see discussion on mtDNA). In total, after discarding failed samples and samples with high proportions of missing data, we obtained new genetic data from 277 individuals (232 from ddRAD, 168 from mtDNA), representing ~80 localities and 10 subspecies. We also obtained comparable ddRAD data for two specimens of *Ceratopipra rubrocapilla* as outgroups. See Supplementary Table 1 for details.

Laboratory methods

We extracted DNA from avian tissue specimens (Table S1) using the DNeasy Blood & Tissue Kit (QIAGEN, CA) and generated ddRADtags following the protocol of Peterson et al. (2012), with modifications described in Thrasher et al. (2018). Briefly, we digested equal quantities of genomic DNA from each sample in individual reactions with two restriction enzymes, SbfI and MspI (New England Biolabs, MA), and ligated adapters on both ends. The 5' adapters contained one of 20 unique 5-7 bp barcodes, whereas the 3' adapter was common to all samples. We pooled groups of samples with unique 5' barcodes and subsequently size selected DNA fragments that were between 400-700 bp using a Blue Pippin (Sage Science, MA). For each group of size-selected samples, we incorporated unique Illumina TruSeq adapters by performing 11 cycles of PCR. The combination of 5' barcodes and TruSeq adapters was unique to each sample. A total of 13 groups of pooled samples with different Illumina TruSeq adapters were combined in equimolar proportions into two libraries. We sequenced both libraries on four lanes of Illumina HiSeq 2500 at the Cornell University Institute for Biotechnology, obtaining

single-end 151 bp sequences. We obtained a representative sample of mitochondrial ND2 sequences using standard Sanger Sequencing protocols described in Berv and Prum (2014).

Assembly of sequencing reads into RAD loci

We obtained 497 million raw 151 bp reads (~75 Gb) for 241 individuals. We first assessed the overall read quality with FastQC (Andrews 2010) and trimmed lower quality bases at the 3' end with FASTX-Toolkit (Gordon and Hannon 2010). The trimmed sequences were 145 bp in length. Using FASTX-Toolkit we filtered-out lower quality reads if they had a single base below a Phred quality score of 10 and/or more than 5% of bases with quality between Phred 10 and 20.

The quality filtered reads were demultiplexed with the 'process_radtags' program from the STACKS 1.44 bioinformatics pipeline (Catchen et al. 2013). During the demultiplexing step we also discarded reads that had not passed the Illumina filter, had adapter contamination, lacked barcodes used for multiplexing, or did not contain an SbfI cut site. This step removed the inline barcodes and trimmed all reads to an equal length, the length of the reads that contained a 7 bp barcode. After demultiplexing and filtering, we retained an average of 1.1 ± 0.4 million 138 bp sequences per individual.

We downloaded the *Manacus vitellinus* (GCA_001715985.1) reference genome from www.ncbi.nlm.nih.gov, and aligned the reads from each individual using bowtie2 2.3 (Langmead et al. 2009), as recommended by Paris et al. (2017), Shafer et al. (2017). We assembled the mapped reads into RAD loci using the reference-based pipeline in STACKS, executed with the ref_map script which runs the modules "pstacks/cstacks/sstacks". We subsequently ran the error correction module "rxstacks" and a final iteration of "cstacks/sstacks". We set the parameters to

a minimum coverage of 20 (*m*) and up to two differences among aligned loci of different individuals (*n*). The reference-based assembly produced a catalogue with 47,046 RAD loci. Seven samples were discarded due to high proportions of missing data in the final assemblies; our final data set thus comprised 234 individuals.

We used several filters in the "populations" module from STACKS to export different sets of bi-allelic SNPs: a missing data filter, a minimum depth of coverage filter, a filter that exports only one SNP per RAD locus, and a minor allele frequency filter (MAF). By combining these different filters, we produced three versions of the dataset which varied in important parameters that could potentially bias downstream population genetic inference (Linck and Battey 2017, Paris et al. 2017). Dataset 1 (labeled arbitrarily) included 1,960 SNPs that were generated by setting the MAF to >= 5%, requiring minimum coverage of 20x, requiring the presence of a SNP in at least 80% of individuals, and filtering out all but the first SNP in each RAD locus to minimize linkage across the dataset (Paris et al. 2017). To evaluate the sensitivity of our analyses to rare variants (Linck and Battey 2017, Shafer et al. 2017), dataset 2 was exported with identical parameters to dataset 1, but without a MAF; this generated a dataset of 2,581 SNPs. Lastly, for non-model-based cluster analyses which should be insensitive to linkage, a third dataset was exported which included all SNPs from each locus (dataset 3, 5,099 SNPs). We generated several additional datasets for specific analytical cases when required and describe them later as necessary.

Phylogenetic analysis

Because sparse super-matrices may be more prone to systematic error (e.g. Roure et al. 2013), we explored the sensitivity of our phylogenetic inferences to increasing amounts of

missing data using three different datasets with 20%, 50%, and 80% thresholds for missing data at the RAD locus level (i.e., for the 80% threshold, if the RAD locus is present in at least 20% of individuals, then that locus, containing all variable and invariable sites, was exported). This approach generated datasets comprising 2,584, 4,763, and 7,901 RAD loci, respectively. For each dataset, we obtained complete haplotype data for every locus/individual and generated a concatenated supermatrix using Sequence Matrix (Vaidya et al. 2011). These matrices had up to ~40% missing sites across the entire matrix, irrespective of columns or rows (i.e., using the 80% threshold above).

We estimated phylogenies using each dataset with a concatenated maximum likelihood and a coalescent species-tree approach for a total of six phylogenetic analyses. For analysis of concatenated data, we estimated a maximum likelihood phylogenetic hypothesis using RAxML 8.2.9 (Stamatakis 2014). We estimated 500 bootstrap replicates followed by a full ML search for each dataset, using a GTRGAMMAX substitution model. We avoid the need for ascertainment bias correction by using short-read haplotype alignments including invariant sites (Leaché et al. 2015). We also tested for an effect of data partitioning on phylogenetic inference by generating optimized locus partitioning schemes in PartitionFinder 2 (Lanfear et al. 2017), which were then re-analyzed in RAxML. We found that our topological results were insensitive to data partitioning, and as such we do not present these results.

We evaluated coalescent phylogenetic structure using the SVDquartets method implemented in PAUP* 4.0a159 (Swofford 2002, Chifman and Kubatko 2014, Chifman and Kubatko 2015). SVDquartets may be a useful tool for testing hypotheses of species delimitation because it can be used to generate a lineage-tree under the multispecies coalescent without assigning individuals to species *a priori*. In this approach, each individual in a dataset is

considered to be a separate 'species.' If a clade in such a lineage-tree has high bootstrap support, this would mean that the descendant taxa have strong support as a group under the multispecies coalescent, and may coincide with species boundaries (*Personal communication*, Laura Kubatko). Our SVDquartets analysis evaluated all possible quartets with 500 bootstrap replicates (other settings left to defaults). SVDQuartets has the advantage of working directly on sequence data (above) and has been shown to perform well in comparison to other coalescent models which assume fully and correctly resolved gene trees as input (Chou et al. 2015, Schmidt-Lebuhn et al. 2017). SVDquartets has also been shown to produce reliable results under very general conditions, and is theoretically robust to variation in effective population size, molecular clocks, limited gene flow, and incomplete lineage sorting (Long and Kubatko 2017). Finally, SVDquartets is very computationally efficient compared to other multispecies coalescent models.

While a full statistical exploration of our specific usage of SVDquartets is beyond the scope of the present work, we suggest that this approach may be a useful and efficient way to assess support for hypotheses of species delimitation under the multispecies coalescent. We do not take the perspective that all well supported clades from our coalescent analysis necessarily represent biological species – such an interpretation would likely lead to an over-inflation of species estimates (Sukumaran and Knowles 2017, Leaché et al. 2018, Chambers and Hillis 2019). In general however, we prefer such a species agnostic approach to those which require *a priori* delimitation of species boundaries (e.g SNAPP, Bouckaert et al. 2014), as it enables us to discover well supported coalescent structure without an *a priori* hypothesis. Lastly, we generated a mitochondrial DNA ND2 gene tree using IQ-TREE 1.6.10 (Schmidt et al. 2014, Chernomor et al. 2016, Trifinopoulos et al. 2016, Hoang et al. 2017, Kalyaanamoorthy et al. 2017). We

partitioned by codon position and generated a maximum likelihood tree using the MFP+MERGE model search and partitioning option (Supplemental Appendix).

Descriptive statistics

Estimates of regional variation in allelic richness (Goudet 2005), Hardy-Weinberg equilibrium (Paradis 2010), inbreeding (Goudet 2005), linkage disequilibrium (Kamvar et al. 2014), and an analysis of molecular variance across multiple strata (Kamvar et al. 2014), are reported as supplementary material.

Cluster inference and patterns of genomic admixture

We performed exploratory population genetic analyses intended to quantify the number of similar genetic clusters across the range of *Pseudopipra*. First, we evaluated broad-scale variation across our genomic data using phenetic K-means clustering implemented in the find.clusters function in the adegenet R package (Jombart 2008). This function first transforms the data with a PCA, and then identifies clusters with a phenetic K-means algorithm. Using datasets 1-3, we evaluated K1:20 successively by the Bayesian Information Criterion (BIC). K-means clustering is based on minimizing the variance within clusters, and has the potential advantage of making few prior assumptions about the underlying processes which generated the data (MacQueen 1967). For each analysis, we retained all PC axes, set 200 randomly chosen starting centroids, and ran each search for 10^9 iterations.

We also estimated the number of differentiated populations using STRUCTURE 2.3.4 (Pritchard et al. 2000), a widely-used model-based approach which assigns individuals to populations such that Hardy-Weinberg equilibrium is maximized and linkage among loci is

minimized within groups. By comparing the output of STRUCTURE runs fixed to different numbers of populations (K), one can assess the degree of fit of the data to various models of K and assess genomic admixture among individuals. We ran structure using dataset 1, from K1:20 with 10 iterations per K value. We ran the program for 700,000 generations, discarding the first 200,000 as burn-in, implementing the admixture ancestry model with correlated allele frequencies. We evaluated K by examining Pr($X|K$) or $L(K)$ after summarizing our results using Structure Harvester (Earl and vonHoldt 2012) and CLUMPP (Jakobsson and Rosenberg 2007). We also used the Evanno method to estimate the rate of change in the log probability of data between values of K, which has been suggested to be a useful metric to detect the uppermost hierarchical level of structure in the data (Evanno et al. 2005). Lastly, we generated 95% Bayesian Credible Intervals around admixture coefficients (presented as averages across individuals for population assignment).

To investigate finer scale population genetic differentiation and the genomic composition of populations defined at different hierarchical levels, we used the programs fineRADstructure and RADpainter (Malinsky et al. 2018). RADpainter takes advantage of the information contained in haplotype data and considers each individual in a dataset as a 'recipient' whose genomes are reconstructed using chunks of 'donor' DNA from all other available individuals. This approach generates a 'co-ancestry matrix' which combines the information that can be derived from both PCA and model-based clustering approaches and thus can be more sensitive to subtle population structure (Lawson et al. 2012). The fineRADstructure software uses an MCMC approach to explore the space of population assignments based on the co-ancestry matrix, using an algorithm which merges and splits populations, or moves individuals among populations. We ran fineRADstructure with default priors, but increased the burn in to 200000 iterations,

followed by 1000000 iterations, sampling every 1000. We then assessed convergence by 1) considering the assignment of population membership across multiple independent runs, 2) visualizing the MCMC traces of estimated parameters to ensure convergence on the same posterior distributions, and 3) running each chain long enough to achieve effective parameter sample sizes > 100.

Both RADpainter and fineRADstructure are based on the recently developed chromoPainter and finestructure (Lawson et al. 2012), but are optimized to take advantage of the linkage properties of RAD-like datasets. As our data were assembled relative to a *Manacus* reference genome, the order in which loci appear in our data files are related to positions on assembly scaffolds, even though the ddRAD loci in our data are generally unlinked when considered at the population level (see Supplementary Appendix). We compared the inferred population assignments from fineRADstructure and STRUCTURE with K-means clustering (as above) of the co-ancestry matrix. To determine how much of the variation in our dataset was captured by the RADpainter analysis relative to a standard PCoA on SNP data, we used the normalized PCA approach of (Lawson et al. 2012), using the mypca function provided in 'FinestructureLibrary.R' Library in the fineRADstructure package.

Phylogenetic reticulation in the western Napo lineage

Model-based, cluster, and population genetic analyses revealed that a distinct lineage of individuals restricted to the western Amazonian Napo area of endemism has a complex history of introgression between southern and northern Amazonian clades (see Results). To investigate this pattern, we followed the approach of Barrera-Guzmán et al. (2018) to quantify the degree to

which the inferred co-ancestry of this Napo population reflected the genomic composition of each putative progenitor lineage which contributed genotypes to contemporary individuals.

For these analyses, we exported a separate haplotype dataset of 52 individuals which included all potentially introgressed western Napo individuals (n=10) and their most geographically proximate populations. We used a 5% minor allele frequency cutoff, required 20x minimum coverage, and allowed up to 20% missing data per locus (2,370 loci, including 4,979 SNPs). Potential progenitor populations consisted of 1) the most geographically proximate population inferred to have mostly unadmixed ancestry (Southwestern Amazon: Inambari, n=17), and 2) the primary inferred source of introgressed genotypes (as initially implied by STRUCTURE, north-central Amazonian Jaú + eastern Napo, n=25). This dataset was also analyzed separately with RADpainter as described above.

Heavily introgressed or hybrid populations are expected to have higher mean co-ancestry and lower F_{st} with each of their progenitor lineages than their progenitor lineages will have with each other (Barrera-Guzmán et al. 2018). For co-ancestry comparisons, we used a standard ANOVA and the glht function in the multcomp R package (Hothorn et al. 2013) to test these predictions. We estimated population differentiation due to genetic structure (F_{st}) with Weir and Cockerham's (Weir and Cockerham 1984) F_{st}, and tested the above prediction using 1000 bootstrapped datasets to estimate 95% confidence intervals.

To test whether or not the relationships among these three focal populations may be best represented by a phylogenetic reticulation, we estimated a phylogenetic network using PhyloNet 3.6.4 (Wen et al. 2018, Zhu et al. 2018). PhyloNet takes SNP data and uses a reversible-jump MCMC technique to explore the posterior distribution of phylogenetic networks and bi-furcating topologies, while accommodating both reticulation and incomplete lineage sorting. This

approach searches the set of all possible reticulation models without requiring *a priori* model specification. Starting with dataset 1 (1960 unlinked SNPs), we pruned the dataset to the 52 individuals that comprise the three groups of primary interest (above). We then pruned out all sites with missing data, leaving 572 biallelic SNPs (PhyloNet cannot presently consider sites with missing data). For our final runs of the PhyloNet program MCMC_BiMarkers, we randomly subsampled five diploid individuals from each group, as preliminary program runs indicated a computational bottleneck with more than five individuals. We assigned each group of five individuals to represent a 'species,' allowed for a maximum of one reticulation, set the chain length for 100000 iterations with sampling every 100, set a burn in of 20%, and as our interest is primarily concerned with topology, left all priors as default (i.e. assuming population mutation rates are constant).

Using the final network topology estimated from PhyloNet, we estimated demographic parameters using G-PhoCS version 1.3 (Gronau et al. 2011). We exported haplotype data for the focal samples without a minor allele frequency filter, generating an alignment of 2,947 variant and invariant loci. We ran the program for 750,000 iterations with a 10% burn-in, estimating a total of 13 parameters: the effective population sizes of the three focal lineages, two ancestral population sizes, two splitting times, and six directional migration parameters. Parameter MCMC traces were inspected in Tracer 1.7.1 (Rambaut et al. 2018). We converted the median and 95% Bayesian credible intervals from mutation scale to generations and individuals as described in Campagna et al. (2015), assuming an approximate mutation rate of 10^{-9} per base pair per generation (Kumar and Subramanian 2002, Smeds et al. 2016). We calculated the number of migrants per generation as the product of the per generation migration rate multiplied by ¼θ for the receiving population ($m_{a\text{-}b} * (\theta_b/4)$) (Gronau et al. 2011).

Spatial distribution of genetic variation

In practice, dispersal barriers often create sharp genetic discontinuities between adjacent populations that would otherwise be continuous (Petkova et al. 2015). To assess the degree to which spatial variation in genetic diversity within *Pseudopipra* can be attributed to landscape features, we investigated how patterns of isolation-by-distance (IBD) vary across the landscape. First, we used Mantel and partial Mantel tests to investigate IBD effects within sampling regions delimited by prominent physical barriers, and then separately tested the roles of specific dispersal barriers in structuring genetic variation. Mantel tests evaluate the correlation among two or more matrices, in our case representing pairwise genetic and geographic distance. Significance is assessed by permuting the rows and columns of one of these matrices (Mantel 1967). Partial Mantel tests incorporate a third 'barrier' matrix, which contains information about environmental or ecological distance. By evaluating the correlation between genetic and ecological distance while controlling for geographic distance, a partial Mantel test can be used to investigate the effect of a particular geographic barrier on genetic differentiation. We follow the recommendations of Diniz-Filho et al. (2013), and only reject the null hypothesis of no correlation if $p << 0.05$ (we use a very conservative 0.001 cutoff, ~10x more stringent than a standard correction for multiple tests would require)(also see Legendre and Fortin 2010, Guillot and Rousset 2013).

For these tests and others, we generated a pairwise geographic distance matrix by calculating great circle distances using the distm function in the geosphere R package (Hijmans et al. 2015). Individuals sampled at the same GPS coordinates were set to have an arbitrarily small geographic distance of 0.0001 meters. These geographic distances were paired with a

matrix of pairwise genetic distances estimated in RAxML. We use phylogenetic distance among individuals, rather than F_{st}, because our data is highly hierarchically structured (though exploratory analyses based on F_{st} and other related metrics were qualitatively similar). These procedures, including the non-intuitive generation of an appropriate barrier matrix, are developed in a set of R functions we provide as supplementary material which operate on adegenet GENIND objects (see supplementary R code) and internally use the Mantel implementation from the ecodist R package (Goslee and Urban 2007).

We also analyzed patterns of spatial variation in our data with a more sophisticated population genetic model which relates effective migration rates across geographic space to expected genetic dissimilarities among individuals (Petkova et al. 2015). This recently proposed method termed Estimated Effective Migration Surfaces (EEMS) produces a visualization that emphasizes deviations from isolation by distance to discover 'migratory corridors' and 'barriers to gene flow'. We view this method as complimentary to more explicit hypothesis-testing approaches (such as Mantel tests), as it seeks to identify where local IBD predictions implied by the data are strongly violated in geographic space, and thereby can identify strong barriers to gene flow *de novo*. In brief, a region is covered with a dense regular grid connecting subpopulations (demes), among which individuals can migrate with rates varying by location. EEMS uses an MCMC approach to estimate expected genetic dissimilarity between two individuals, integrating over all possible migration histories, and adjusting migration rates among graph edges to match the genetic differences in the data. A migration surface is then interpolated across a region to indicate where genetic similarities decay faster than what a pure isolation by distance model predicts, visually highlighting barriers to gene flow and migration corridors. An effective diversity parameter is also estimated for every deme, reflecting local deviations in

heterozygosity. We ran several analyses using default priors, iteratively increasing the grid density and chain length, with up to 2000 estimated demes. For each test, we ran three chains, and after examining chain convergence, we assessed model fit by comparing the observed and fitted dissimilarity between and within demes.

Vocal variation

We obtained sound recordings of vocalizations of *Pseudopipra* from the Macaulay Library at the Cornell Lab of Ornithology (https://www.macaulaylibrary.org) and the Xeno-canto (www.xeno-canto.org) collections (Supplementary Table 4). Vocalizations were analyzed in Raven Pro 1.4 (Bioacoustics_Research_Program 2011), and converted into spectrograms using a 512-sample Hann window with 50% overlap. Audio recordings ranged from a cut of a single vocalization to longer recordings of a lek with multiple individuals vocalizing. For our initial assessment, we identified distinct vocalization types based on our own survey of the available recordings, without regard to the geographic location of the recordings. Additional analytical details are reported as supplementary material.

Results

Genetic data collection

Our total genomic data set included an average of 1 ± 0.4 million sequences of 138 bp from 232 individuals of *Pseudopipra* and two *Ceratopipra rubrocapilla,* which were used as an outgroup. Our reference-based assembly produced a catalogue with 47,046 RAD loci. Filtered datasets ranged from 1,960 unlinked SNPs (dataset 1, one SNP per locus with 5% MAF and up

to 20% missing data filter), to 5,099 SNPs (dataset 3, all SNPs in all loci with 5% MAF and up to 80% missing data filter). Dataset 2 comprised the 1,960 SNPs from dataset 1, plus 621 rare variants filtered out with a 5% MAF in dataset 1 (2,581 loci), and up to 20% missing data filter, as described in the methods. We also obtained 168 mtDNA ND2 sequences using PCR methods which broadly overlapped with our ddRAD dataset. Our mtDNA dataset included two subspecies, *pygmaea* and *coracina*, from which we were not able to obtain enough high-quality material for ddRAD sequencing.

Phylogenetic analyses

RAxML and SVDquartets analyses generated a well-supported phylogenetic hypothesis (Figure 3). The monophyletic lineages of *Pseudopipra* identified have distributions that are largely congruent with previously recognized avian areas of endemism, and further reveal much finer scale patterns of local biogeographic differentiation in certain areas. Using the two *C. rubrocapilla* individuals to root the phylogeny, we detected support for at least five major clades across all phylogenetic analyses of nuclear genomic data, with consistently high bootstrap support in both concatenated and coalescent analysis (A-E in Figure 3, 5). We first describe the structure of these major clades, followed by descriptions of well supported substructure within each of these regional groupings. We report six bootstrap values for each clade with at least some high support, from each of the three datasets analyzed in RAxML and SVDquartets (see heatmaps, Figure 3). Figure 4 projects an idealized topology into geographic space, to show how inferred population relationships are related to landscape features.

Phylogenetic structure.—The sister group to all the other *Pseudopipra* is a clade including individuals from subtropical Central America and the northern Andes. The northern

Andes are represented here by a single individual from subtropical forests (~1,000 m) of the eastern slopes of the Andes in San Martín, Peru (Clade A in Figure 3). This subtropical San Martín specimen (identified as *P. pipra occulta*) was the only viable sample in our genomic dataset from the entire northern Andes region (A1 in Figure 3). Mitochondrial data from three additional specimens from the Andes of southern Ecuador (subspecies *coracina*) cluster with the San Martín specimen (See Discussion). Thus, this northern Andean sister lineage to the Central American lineage likely includes all montane Andean populations of *Pseudopipra* in Ecuador, Colombia, and Venezuela. A well supported Central American clade (A2 in Figure 3) was identified in all analyses, with Costa Rican (A3 in Figure 3) and Panamanian subclades (A4 in Figure 3) supported in RAxML.

The second successively nested clade in *Pseudopipra* includes individuals from subtropical forests of the Andes of Central Peru, which are sister to all remaining lineages (Clade B in Figure 3). The Central Peru clade is further subdivided into two very well resolved clades: a northern clade (B2 in Figure 3), sampled here from the Cerro Azul in southwestern Loreto, and a southern clade from Pasco, Junín, and Cusco (labeled B1 in Figure 3). The Central Peru clade is the sister group to a monophyletic, lowland clade (F in Figure 3) that is further subdivided into a southern Amazon clade + Atlantic Forest clade (Clade C in Figure 3), and a Northern Amazonian + Guiana Shield clade (Clade D in Figure 3). In contrast, the analysis of mtDNA with better sampling of subspecies *pygmaea*, from the tropical forest of lower Rio Huallaga Valley, Peru, places this population as sister group to the entire lowland radiation (Clade F; Supplemental Appendix).

Within the broad lowland Northern Amazonian + Guiana Shield clade (Clade D), virtually no phylogenetic substructure is associated with strong bootstrap support. The maximum

likelihood tree however does have substantial biogeographic coherence, which we use as additional justification for subdivision for descriptive statistics (Supplemental Appendix) when coincident with geographic features. For example, all but one individual from coastal Suriname and Amapá form a monophyletic assemblage (D1 in Figure 3), east of the Essequibo river. Likewise, all but one individual from the far eastern Napo area of endemism, east of the Rio Putumayo, form a clade (D2 in Figure 3). We treat these geographic groups, as well as two other Guianan regions, as separate populations for descriptive population genetic analyses (Supplementary Appendix).

A widely distributed set of individuals encompassing the western portion of the Napo area of endemism (from the northern bank of the confluence of the Rio Solimões and the Rio Napo north of Iquitos, then west and south) was recovered as the sister group to the Guiana Shield + Northern Amazon clade (Clade E in Figure 3). In contrast, however, population genetic analyses (below) indicated that this population is a distinct lineage of the southern Amazonian clade that has experienced substantial hybrid introgression from a northern Amazonian population (see Population Genetic analyses and Discussion).

Within the large lowland Southern Amazonia clade (Clade C in Figure 3), we recovered eight moderately supported and hierarchically nested clades, which are successive sister groups to each other, and are congruent in distribution with recognized areas of endemism. First is a moderately supported clade (C1 in Figure 3) of individuals from the western Inambari area of endemism, from west of the Rio Ucayali to the Rio Purus. Although the basal lineages within this clade have low bootstrap support, a monophyletic subgroup of three montane (>1000m) individuals from the highlands between the Rio Huallaga and Rio Ucayali cluster with high bootstrap support (C2 in Figure 3).

The next successively nested clade includes individuals from eastern Inambari, between the Rio Purus and the Rio Madeira (C3 in Figure 3). The next successive clade includes two individuals sampled from the Rondônia area of endemism, between the Rios Madeira and Tapajos (C4 in Figure 3). The next successive clade includes a group of individuals from the Tapajós area of endemism between the Rio Tapajos and the Rio Xingu (C5 in Figure 3). Next, a clade comprised of individuals from the northern Xingu area of endemism, east of the Rio Xingu (C6 in Figure 3), is sister to a well-supported Brazilian Atlantic Forest clade (C7 in Figure 3), which is further subdivided into three successive clades (north to south) in Bahia, Espírito Santo, and Rio de Janeiro, respectively (C8, C9, and C10 in Figure 3). In summary, the subdivisions of the Southern Amazonian clade reflect a stepwise west-east progression, with a hierarchically nested structure:

(West Inambari (East Inambari (Rondônia (Tapajós (Xingu (Bahia (Espírito Santo (Rio de Janeiro))))))).

Cluster inference and patterns of genomic admixture

Broad-scale population structure and admixture.—Overall F_{st} was moderate with respect to *Pseudopipra*: 0.196 [95% CI: 0.188-0.204]. Pairwise population estimates of Weir and Cockerham's F_{st} ranged from essentially undifferentiated, to almost entirely distinct. At the extremes: comparing the geographically proximate eastern Napo and Jaú populations (both weakly resolved in phylogenetic analyses, but likely sister) – F_{st}: 0.0045 [95%CI: 0.0024 - 0.0067]. By contrast, comparing the Atlantic Forest Espírito Santo population to Panama indicates an F_{st} of 0.81 [95%CI: 0.79 - 0.83], or almost entirely differentiated. See Supplementary Figure 10 for a full pairwise F_{st} matrix. Hartl and Clark (1997) indicate $F_{st} > 0.25$ may be considered very great genetic differentiation.

K-means clustering of SNP data identified five clusters of genetically similar individuals as having the lowest BIC score, with membership of one sample varying slightly across datasets: Central America (Clade A2), South Andean Peru (Clade B), Atlantic Forest (Clade C7), Southern Amazon including the western Napo population (the rest of Clade C + Clade E), all Guiana Shield + Northern Amazon (Clade D) (Supplementary Figure 2). These clusters are essentially identical to those detected by STRUCTURE at K=5 (Figure 4, 5, below). In the most restricted dataset (#1, 1960 SNPs; 0.05 MAF), the montane sample from San Martín (North Andean Peru, 5444.PE.MAR) clustered with Central American populations (Clade A), as it does in all phylogenetic analyses. Standard PCoA explained 13-17% of the variance in the SNP data on the first two axes (Supplementary Figure 2).

Visual inspection of Pr(*X*|*K*) from summarized STRUCTURE runs indicated that the likelihood of each successive K from 1:20 plateaued at K = 5, with the standard deviation across runs increasing rapidly after this point (Supplementary Figure 3). We describe patterns of inferred admixture as they appear in Figure 5, reading from top to bottom. For K5, individuals from Central America are unambiguously assigned to their own cluster (Clade A1 in Figure 3, 5). The north Andean montane specimen from San Martín, (North Andean Peru, 5444.PE.MAR) is reconstructed as being highly admixed, with a genomic composition including 4 of the 5 inferred clusters. However, this inference is very weak because we have only one individual to represent this likely distinct and highly diverse north Andean lineage (though see RADpainter below, which is consistent with these results). Samples from the southern Amazon and Atlantic Forest (Clade C), have no admixture with northern populations, except for some individuals from the western (Clade C1), and to a more limited degree, the eastern (Clade C3) Inambari

populations, which are inferred to have limited (~<5%) admixture with individuals assigned to the Northern Amazon + Guiana Shield (Clade D, see Figure 5, 6, and discussion below).

Going from West to East across the Southern Amazon, very limited admixture with individuals from the Atlantic Forest (Clade C7) is first inferred in the Tapajos (Clade C5) area of Endemism. This admixture increases in the Xingu area of endemism (Clade C8) and increases further in a geographic and genetic cline to 100% assignment probability to a distinct cluster in the Rio de Janeiro clade (Clade C10). Given the geographic context of this cline in admixture, we suggest this pattern may a product of isolation by distance, hierarchical structure, and geographic barriers (e.g. Bradburd et al. 2017)(See Supplementary Appendix), and not isolated introgression events.

Next, all individuals from the western portion of the Napo area of endemism are inferred to be heavily admixed (Clade E; Figure 5). On average, at K=5, STRUCTURE assigns these individuals (n=10) with 40.2% probability to the Guiana Shield population (SD 4.7%, average Bayesian credible interval (aBCI): [0.33-0.47]), 50.4% to the Southern Amazon population (SD 3.4%, aBCI: [0.43-0.58]), as well as limited 4.15% probability to Central Peru (SD 3.1%, aBCI: [0.01-0.08]), and 5.2% to Central America (SD 4.8%, aBCI: [0.02-0.1]). The three localities included in this clade– (1) north of Iquitos, on the east bank of the confluence of the Rio Solimões and the Rio Napo, (2) southwest of Iquitos in Allpahuayo Mishana Reserve (represented by three mtDNA samples), and (3) near San Jacinto, Ecuador– indicate that this heavily admixed population (corresponding to subspecies *discolor*) may occur across a large area of the western Napo region of endemism, and likely does not represent a narrow hybrid zone (Figures 2-7).

Lastly, at K=5, all members of the Guiana Shield + Northern Amazon clade (Clade D) are inferred to be virtually undifferentiated. Individuals in the far eastern Napo area of endemism on the east bank of the Rio Putumayo (brown dots in Figure 3, 4) cluster with other Guiana Shield groups in phylogenetic analyses but are detected to have limited (~5%) admixture with pure individuals of Southern Amazon provenance. At higher values of K, the broad-scale population assignments inferred at K=5 are mostly unchanged, however additional admixture components are inferred for most groups. The introgressed western Napo clade is eventually placed into its own cluster at K=9-10 (see Supplementary Figure 4, Supplementary Figure 8).

Fine-scale population structure and admixture.—Admixture analysis using the RAD locus optimized chromosome painting approach in RADpainter and then population assignment with fineRADstructure (Lawson et al. 2012, Malinsky et al. 2018), was congruent with other analyses, and also detected finer partitions of population structure. The fineRADstructure program detected 15 groups of individuals which were each supported with a posterior probability of 100% and which also overlapped with sampling regions which we delimited for population genetic analyses based on clear geographic barriers (Black dots in Figure 3, Supplementary Figure 5): These groups include: 1) Central America (Costa Rica + Panama; Clade A2 in Figure 3), 2) North Andean Peru (grouped with Central America; Clade A), 3) South Andean Peru (north clade; Clade B2), 4) South Andean Peru (south clade: Clade B1), 5) Introgressed western Napo lineage (Clade E), 6) eastern Guiana Shield (Suriname + Amapá; Clade D1), 7) eastern Napo, Jaú and western Guiana (Clade D2+ other members of Clade D), 8) Eastern Inambari (Clade C3), 9) Western Inambari (Clade C1), 10) Rondônia (Clade C4), 11) Tapajós (Clade C5), 12) Xingu (Clade C6), 13) Atlantic Forest – Bahia (Clade C8), 14) Atlantic Forest - Espírito Santo (Clade C9), 15) Atlantic Forest – Rio de Janeiro (Clade C10). The only

sampling regions which fineRADstructure failed to strongly partition into separate groups consisted of a group of individuals in the Jaú area of endemism, and a group of individuals in the eastern Napo area of endemism (both of which are weakly resolved in phylogenetic analyses, but unambiguously members of the broader Northern Amazon + Guiana Shield clade D). The eastern Napo individuals are identified as a low support group (*pp* = 0.49), while the Jaú individuals are lumped in with other western Guiana Shield individuals. See Supplementary Figure 5 (fineRADstructure dendrogram), and the full dataset co-ancestry matrix plot Supplementary Figures 6-7.

Patterns of inferred co-ancestry show a complex mosaic of shared ancestry among populations (Supplementary Figures 6-7). In general, however, these patterns are concordant with higher level patterns detected with STRUCTURE. Notably, the high level of admixture initially inferred for our San Martín sample is recapitulated in RADpainter analysis – this sample has relatively high co-ancestry across most populations. Lastly, the Lawson et al. (2012) 'normalized PCA' approach provided with fineRADstructure captured 89% of the variance in the genetic data on the first four component axes (axis 1: 51.4%, axis 2, 24.9%, axis 3: 7.77%, axis 4: 4.94%) indicating that the co-ancestry matrix reflects substantially more information than standard PCoA/PCA of SNP data (above) (Supplementary Figure 8).

Phylogenetic reticulation in the western Napo lineage

Assessing hybrid introgression.—Separate RADpainter and PhyloNet analysis of the populations in the western Napo area of endemism and their putative progenitor lineages supported the hypothesis that this region has a complex history of introgression. One-tailed tests of mean co-ancestry indicated the null hypothesis that the difference in means among groups is

less than or equal to zero can be strongly rejected (ghlt p < 2e-16), and that individuals from the western Napo population have greater median/mean co-ancestry with each progenitor lineage than their progenitor lineages share with each other (PHvGS/progenitors = ~1.078, PHvInambari/progenitors = ~1.16). These analyses establish the asymmetry in introgression patterns detected by STRUCTURE. On average, western Napo individuals share ~ 7.5% greater co-ancestry with Inambari individuals (southern Amazon) than they do with other Northern Amazon individuals (glht p < 2e-16), indicating that these populations are not likely to be composed of F1 hybrids. We also did not observe clinal variation within our samples of this lineage.

fineRADstructure analysis of the co-ancestry matrix, as well as visualization of the co-ancestry matrix, also indicated that the western Napo population is a differentiated form (Figure 6a-d). Principle components analysis (Figure 6d) of the co-ancestry matrix indicate that the western Napo lineage is intermediate on PC1 (compared to progenitor lineages), and differentiated on PC2, as expected if the Napo lineage has had sufficient time in reproductive isolation for sorting of ancestral alleles or for the evolution of new alleles (Barrera-Guzmán et al. 2018).

Bootstrapped estimates of F_{st} indicated the same general patterns: 95%CI; western Napo vs Eastern Napo (Northern progenitor, 0.07 - 0.090), western Napo v Inambari (Southern progenitor, 0.058 - 0.077): Eastern Napo vs Inambari: (between progenitors, 0.122 - 0.144). These patterns of F_{st} estimates were robust to alternative assignments of source linages (for example, including an additional adjacent population for both of the putative progenitor lineages). Thus, the introgressed western Napo lineage is less differentiated from *each* of its

progenitor lineages than its progenitor lineages are to each other (i.e. it is intermediate, see methods), and it is *also* biased in its ancestry toward Inambari populations.

PhyloNet detected that an evolutionary reticulation is the best model to explain the origin of the western Napo population (Figure 6a). Computational limitations restricted us to evaluating a three-taxon case with a maximum of one reticulation. This included each putative progenitor lineage: (1) western Guiana Shield, northern Amazonian clade (clade D2), (2) a sample of northwestern Inambari individuals, part of the southern Amazonian clade (clade C1) —and (3) the introgressed western Napo population (clade E), each defined as 'species.' The RJMCMC search achieved an ESS of ~300 and detected two network topologies representing 98% of the posterior probability. The top ranked network (*pp* = 51%, Figure 6a) implies the MRCA of the northern Amazonian (Eastern Napo + Jaú) and southern (Inambari + Western Napo) lineages diverged first (clade F). This initial split was followed by a split within the latter lineage that led to the Inambari (S1) and progenitor western Napo (S2a) populations (MRCA of S1 and S2a: Figure 6a). Later, genetically distinct genomes from the Northern lineage (clade D/D2) introgressed into S2a (ancestral western Napo) to give rise to the contemporary western Napo population (S2). The next best network (*pp* = 47%, Supplemental Data) implies that northern and southern lineages of Clade F diverged, as in the top ranked network. Later, S1 and the NW Amazonian lineages merged, forming a hybrid lineage. We base our subsequent discussion on the top ranked network, as this hypothesis is consistent with patterns we detect in other analyses, though we acknowledge that support for these two reticulation scenarios is similar.

Taken in the context of our STRUCTURE (Figure 5) and fineRADstructure (Figure 6) results, the introgression indicated in the top ranked network seems to have been asymmetrical, leaving very little evidence of southern admixture among northern lineages (see Figure 5,

'weakly resolved eastern Napo', which are detected to have very limited (< ~5%) southern admixture). Demographic parameters estimated with G-PhoCS are also consistent with this hypothesis: the only substantial (lower 95% CI > 1 migrant per generation) migration rate was inferred to be from the eastern Napo (member of Guiana Shield lineage) lineage into S2/S2a (Figure 6, Supplementary Table 5).

G-PhoCS also allows us to place a preliminary maximum age bound on the timing of introgression into S2a. Assuming one generation per year and a constant mutation rate, our analysis estimates the splitting time between S2a and S1 to be on the order of 500 Ka (Figure 6, Supplementary Table 5). Though we emphasize that this is a rough approximation, this result is consistent with prior divergence time estimates for several groups in the genus based on mtDNA (Castro-Astor 2014); that study estimated ssp *pipra* (Clade D; Northern Amazon + Guiana Shield lineage) to have branched off from its closest relatives ~ 0.6717 [95% HPD: 0.3506-1.1287] Ma. Therefore, introgression into S2a must have occurred more recently.

Lastly, patterns of admixture (Figure 5) also suggest some evidence of limited introgression of Northern Amazon alleles into the southwestern Amazonian Inambari population (Figure 5). This could be a consequence of limited gene flow into the Inambari population *after* the primary introgression event which formed the introgressed western Napo lineage. Ultimately, the product of this process was a differentiated and introgressed lineage within the western part of Napo area of endemism.

Spatial distribution of genetic variation

Under isolation by distance (IBD), the empirical relationship between geographic distance and genetic distance is related to offspring dispersal distance and population size

(Rousset 1997). Isolation by distance effects are thus predicted when individual dispersal distances are smaller than a species' range (Teske et al. 2018). Fifteen out of eighteen considered areas (see Population Genetics, Figure 4, and Supplemental Appendix for a description of how these areas were defined) contained > 2 individuals, and thus could be evaluated for isolation by distance effects. Within areas, only the western Inambari and Atlantic Forest-Rio de Janeiro populations were detected to show significant signals of IBD at the 0.001 alpha level (Supplementary Table 2a). When geographic distance was log transformed, only the Jaú and Inambari areas were indicated to have significant IBD effects (Supplementary Table 2a). Partial Mantel tests of specific barriers to gene flow indicated that most evaluated river and physical barriers likely play significant roles in structuring genetic variation between areas (Supplementary Table 2b). These patterns are expected if individuals are dispersing within sampling regions but are generally unable to cross barriers delimiting these areas; for our dataset, these barriers are predominantly the major tributaries of the Amazon, or montane regions. Notably, the Rio Negro was the only evaluated barrier which is not detected to exhibit a significant effect—in comparing of Jaú and western Guiana Shield samples (Supplementary Table 2b).

Analysis with EEMS complimented and largely corroborated the specific hypotheses implied by Mantel tests. For our analysis of 2000 fitted demes, the model fit between demes was very high ($R^2 = 0.871$), and within demes somewhat less ($R^2 = 0.579$), indicating that the EEMS model does a very good job of describing spatially structured variation in this dataset (Supplementary Figure 11). EEMS also detected many strong signals (posterior probability > 0.9) of barriers to gene flow and migratory corridors (Figure 7). As expected, the Andes and the

Amazon river were unambiguously detected as the most significant barriers to gene flow and are clearly recovered as landscape features.

EEMS also detected signals of deviation from IBD that likely correspond to several Amazonian tributaries in the Amazon basin, delimiting areas of endemism (Figure 7).
An additional strong barrier to gene flow was inferred in the south-central amazon (south-central brown patch in Figure 7), corresponding to the Caatinga - Cerrado – Chaco 'dry-diagonal' biomes. Strong signals of genetic connectivity are inferred in many localities (blue in Figure 7), notably west of the Andes, connecting north Andean and Central American lineages (despite a dearth of sampling in that region). This link likely reflects the common ancestry among montane Andean lineages between Central America and Central Peru as *Pseudopipra* does not presently occur on the western slopes of the Peruvian Andes. The large Guianan + Northern Amazonian region (E. Napo + Jaú + Guiana) is detected to have relatively weak population structure across a variety of barriers (including the Rio Negro). Several areas of endemism are also detected by EEMS in the Atlantic Forest, likely corresponding to the Coastal Bahia and Serra do Mar areas identified by da Silva et al. (2004) (Figure 7). Introgressed hybrids from the western Napo area of endemism are inferred as being genetically isolated from neighboring populations, with strong barriers to gene flow on all sides, perhaps corresponding to the effects of the Rio Marañón in the south and Rio Putumayo/Içа to the north.

EEMS detected two broad clusters of relatively high genetic diversity (relative heterozygosity: Supplementary Figure 12). One is centered along the Amazon river and was relatively uniform within the northern Amazonian basin, reflecting relatively high genetic diversity in Guiana Shield populations. The other relatively high diversity group is the introgressed western Napo population. Areas of relatively low genetic diversity included the

Atlantic Forest, the Peruvian Andes, and Central American lineages. These results are consistent with estimates of regional variation in allelic richness (Supplementary Appendix for details).

Vocal variation

We examined 198 recordings of *Pseudopipra* and identified 15 distinct vocalizations that can be diagnosed by ear or visual inspection of sonograms (labeled numerically (arbitrarily) in Figure 8 and 9). This set of vocalization types includes both advertisement vocalizations from males at leks, and calls by males and females in other contexts. By examining recordist notes, we generated a preliminary hypothesis which distinguishes 13 highly variable and distinct, male lekking vocalizations (Figure 8) from two broad ranging call types (Figure 9). Work by Castro-Astor et al. (2007) provides important insights of the vocal behavior of Atlantic forest populations, but most *Pseudopipra* populations lack similarly detailed studies. Vocalization types within each category of lekking or call vocalizations can be statistically discriminated based on a combination of the frequency, duration, number of notes, and quality of the sound (buzzy vs pure tone). PCA and logistic regression on lekking vocalizations (n=114, Supplementary Table 3), and call vocalizations (n=33) found significant differences among types ($p < 0.001$). The first three axes of a PCA explained ~90% of the variation in lekking vocalization characters, with PC1 (~64%) primarily explaining variation in note number and frequency (Supplementary Figure 15).

Assigning vocal types to well supported genetic groups is challenging in the absence of matching data (i.e., recordings from the same individuals from which we have genetic samples). Nevertheless, we found that most vocal types have distinct non-overlapping geographic ranges (Figure 8, Figure 9), and that the majority correspond to the geographic range of distinct lineages

we identify (Taxonomic Summary, below). The complex phylogenetic history we have documented with genetic data has clearly had a strong impact on the evolution of male vocal advertisements in *Pseudopipra*. Because lek vocalizations are a focus of female choice in manakins and because suboscine passerines have largely innate vocalizations, the extensive vocal differentiation among populations of *Pseudopipra* strongly indicates the existence of many species with *Pseudopipra*.

Discussion:

In comparison to the great diversity of Neotropical organisms available for study, there have been far fewer studies focused on understanding both fine and broad scale diversity patterns within broadly distributed Neotropical taxa, and this has slowed the biogeographic interpretation of the effects that many landscape features have on the evolution of Neotropical organisms (Marks et al. 2002, Nyári 2007, Milá et al. 2012, Fernandes et al. 2013, Harvey and Brumfield 2015, Harvey et al. 2017). We investigated the phylogenetic and population genetic history of a continentally distributed taxon currently recognized as a single biological species– *Pseudopipra pipra*– using a genomic dataset which samples thousands of loci across the genomes of 232 individuals representing eight of thirteen *Pseudopipra* subspecies. Two additional subspecies, *pygmaea* and *coracaina*, were represented by mtDNA. Our sampling encompasses a majority of the broad range of *P. pipra*, spanning Neotropical forests from Central America to the Atlantic Forest of Brazil, including highland and lowland areas of endemism.

The predominant phylogenetic signal we detect in our dataset is of two successively nested montane clades as the sister groups to several major lowland Amazonian clades (see *Historical Biogeography*, below). This pattern implies that lowland populations of *Pseudopipra*

expanded historically 'out of the Andes,' and that lowland clades of *Pseudopipra* are derived from ancient lineages endemic to the Andes (~ 2.5 Ma; Castro-Astor (2014)). The lowland clade within *Pseudopipra* originated (~1.085 [0.57-1.79] Ma) in southwestern Amazonia (Figure 4) and expanded, occupying Amazonia on both margins of the Amazon river, and eventually reached the Atlantic forest (see below). Therefore, to our knowledge, our study provides a unique example of a widespread suboscine passerine which originated in the Andean highlands.

Population genetic variation

We examined our dataset using a variety of population genetic approaches intended to assess the number of natural genetic groupings that may be present in *Pseudopipra*. Phenetic K-means clustering of SNP data and analysis with STRUCTURE estimated a minimum of 5 broad genetic clusters (Figure 5, Supplementary Figure 2, Supplementary Figure 4). K-means clustering of the co-ancestry matrix (which captured substantially more variation than standard PCoA) more finely partitioned the dataset into at least ~8 broad groups (Supplementary Figure 8), which generally recapitulate phenotypically delimited subspecies boundaries (Figure 2). Phylogenetic (RAxML, SVDquartets) and model-based population genetic (fineRADstructure) analyses of nuclear genomic data detected fifteen clusters of individuals which coincided with sampling regions delimited by clear geographic barriers (results, Figure 3, 4, Supplementary Appendix). Two additional subspecies represented by mtDNA (results) bring the total number of distinct genetic populations delimited by geographic barriers to at least seventeen. The close concordance observed between population structure and landscape features implies that the evolutionary history of *Pseudopipra* within the Neotropics is deeply connected to the South American landscape, adding support to a rich body of literature endorsing this hypothesis

(Cracraft and Prum 1988, Brumfield 2012, Silva et al. 2019). Our analyses of isolation by distance compliment and support these general conclusions (below).

Our analyses also lend themselves to some general conclusions about the sensitivity of various methods to detecting population genetic structure. Overall, methods based on clustering of SNP data were the least sensitive (prone to lumping) to population structure, whereas phylogenetic analyses were the most sensitive to population structure (prone to splitting). Thus, different phylogenetic and population genetic cluster analyses detected different levels of hierarchical structure in the data.

Overall, there was broad congruence in group assignments across methods, and no reciprocally incompatible clusters were recovered—with a notable exception: In phenetic K-means clustering of expanded datasets 2, 3 (Supplementary Figure 2), *and* of the normalized co-ancestry matrix (Supplementary Figure 8), the important and unique North Andean montane individual (5444.PE.MAR) clusters with other South Andean (Central Peruvian) lineages, contra phylogenetic analysis. But in all model based phylogenetic analyses (and fineRADstructure population assignment) 5444.PE.MAR clusters with Central American Lineages. Additional field sampling of these North Andean populations is required to further understand why this lineage may share signals of ancestry with both groups.

Our relatively dense sampling reveals a unique 'horseshoe-like' pattern of genetic differentiation across the Amazon basin (Figure 4). We recover no evidence of gene flow across the Amazon river, except in the western headwaters where the Amazon is narrowest and floodplains are dynamic and young (Räsänen et al. 1987, Haffer 1992, Pupim et al. 2019). Given that the genus originated in the west, we hypothesize that these two clades diverged across the Amazon river in this region. For virtually all evaluated cases, we find significant effects of

geographic barriers on subdividing genetic variation within this species complex, including across the Amazon River and most of its larger tributaries, with the notable exception of the Rio Negro (Figure 7 and Supplementary Table 2a, 2b). As expected, the 'dry-diagonal' Caatinga, Cerrado, and Chaco belt is a strong barrier to gene flow, isolating Atlantic Forest lineages from their southeastern Amazonian Xingu relatives—as are the Andes, which exhibit a disproportionate effect on divergence between Peruvian foothills populations and Central American lineages (see Supplementary Appendix for additional discussion).

Multiple analyses indicate that the western Napo population has a complex history of initial and early differentiation from the broader Southern Amazonian clade, followed by subsequent, asymmetric genetic introgression from Jaú and eastern Napo populations of the Guianan Shield + Northern Amazon clade (Clade D; see discussion below). This result is in conflict with other phylogenetic analyses. When the genetic data are analyzed under either concatenated or coalescent phylogenetic frameworks which do not allow for phylogenetic reticulation, the western Napo population is reconstructed as most closely related to Guiana Shield + Northern Amazon populations (Figure 3, Figure 5, Clade D). In contrast, phylogenetic network analysis strongly indicates that this population is more closely related to individuals of Inambari (southern Amazon) provenance (Figure 6, also summarized in Figure 4). This incongruence between methods is likely due to the complexity of the constituent gene trees in this population-level differentiation induced by asymmetric introgression from the Jaú and eastern Napo populations (Thom et al. 2018). We hypothesize that introgression has introduced more recently derived variation from the Guiana Shield + Northern Amazon clade D into an older, differentiated, population of the Southern Amazonian clade, pulling the phylogenetic affinity toward the northern clade.

History of an introgressed hybrid lineage

Analysis of genomic admixture and phylogenetic reticulation revealed a population of differentiated individuals restricted to the western Napo area of endemism which have highly introgressed genomes and a particularly complex evolutionary history (Figure 6). Our investigation revealed this northwestern lowland Amazonian group is most likely derived from a southwestern Amazonian lineage which experienced introgression from a member of the Guiana Shield +Northern Amazon clade D. The substantial level of observed introgression (>40%), as well as a suite of genomic and phenotypic evidence, suggests that this lineage may be best recognized as a hybrid species.

To date, five prior examples of hybrid species formation in birds have been evaluated with genomic data: (1) the golden crowned manakin (Barrera-Guzmán et al. 2018), (2), the Audubon's warbler (Brelsford et al. 2011), (3) the Italian sparrow (Hermansen et al. 2011), (4) the Hawaiian duck (Lavretsky et al. 2015), and (5) a putative species of Darwin's finches (Lamichhaney et al. 2018). These examples of mosaic genome hybrid speciation, in which the fusion of two or more progenitor lineages leads to a reproductively isolated hybrid species (Jiggins et al. 2008, Counterman 2016), highlight the emerging paradigm that modern patterns of avian diversity may have been significantly influenced by historical phylogenetic reticulation (Suh 2016). Our analyses of genomic data across *Pseudopipra* imply that the western Napo lineage is likely a differentiated, allopatric phylogenetic species which has a genome composition derived from heavy historical admixture with a non-sister lineage. This historical scenario is not the same as those examples cited above, and yet it has produced a population genetic signature which is very similar (compare to Barrera-Guzmán et al. 2018).

Some authors have proposed strict population genetic criteria for identifying homoploid hybrid speciation, including demonstrating (1) evidence of reproductive isolation from parental species, (2) evidence of past hybridization, and (3) evidence that intrinsic reproductive isolation was derived from the hybridization event (Schumer et al. 2014, Barrera-Guzmán et al. 2018).

The first two conditions are easily satisfied by the western Napo *Pseudopipra* lineage. Phylogenetic and population genetic analysis indicate reproductive isolation. All phylogenetic analyses, including concatenated and coalescent analyses (Figure 3 4, 6), recover this lineage as a strongly supported reciprocally monophyletic group. PCA-based and model-based population genetic cluster analyses (Figure 6b, 6c, Supplementary Figures 4-9), also support the hypothesis that this lineage is both intermediate and differentiated when compared its closest living relatives. Analysis of IBD also supports the hypothesis that gene flow around the geographic extents of this population is at least restricted and probably not occurring (Figure 7, Supplementary Figure 12). Estimates of inbreeding coefficients also imply that introgression is probably not ongoing into the western Napo lineage (Supplementary Appendix): The similar levels of inbreeding among *Pseudopipra* populations in the western Amazon (F_{IS}, Supplementary Figure 9, and Supplementary Appendix) imply that the western Napo population is not more outbred (i.e. recently introgressed) than other inbred populations. Notably, the consistently positive level of inbreeding (median ~0.16, 95% CI [0.11-0.21]) among most *Pseudopipra* populations is perhaps attributable to a highly polygynous lek mating system (Smith 1979, Waser et al. 1986, Stopher et al. 2012). In sum, these patterns imply contemporary reproductive isolation of the Western Napo populations.

The second criteria, evidence of past hybridization, is directly supported by model-based analysis of genomic admixture and phylogenetic reticulation (Figure 5, 6), and indirectly

supported by model based and phenetic cluster analysis (Supplementary Figures 4-9). We hypothesize that hybridization initially occurred between progenitor lineage S2a and western lineages of the Guiana Shield + Northern Amazon clade (Figure 6a). S2a then became extinct and was replaced by the novel introgressed lineage, which subsequently exchanged genes with neighboring populations. An intrinsic assumption of our analyses is that S1 (western Inambari) is an appropriate substitute for S2a (which we infer to have existed). We use S1 as proxy for S2a in population genetic analyses because it is the closest and only available relative.

The third criterion, evidence that intrinsic reproductive isolation was derived from the hybridization event, is the most difficult to demonstrate, and perhaps also the most tenuous and dependent on one's concept of species. This criterion is useful for framing the strength of evidence for or against the existence of a homoploid hybrid species if one adheres strictly to the biological species concept, as is frequently adopted for birds (Mayr 1942). However, if one adopts a more evolutionary definition of species, like the metapopulation lineage concept, in which the only necessary requirement is demonstration of separately evolving lineages (de Queiroz 2005), the importance of demonstrating intrinsic reproductive isolation to claim species status for a putative hybrid lineage (or any lineage at all) is less clear to us. Requiring hybridization to be the source of intrinsic reproductive isolation also excludes the possibility that extrinsic reproductive isolation may result from intrinsic changes that enable hybrids access to new niches, which may be also be geographically restricted relative to parental forms (Nieto Feliner et al. 2017). In sum, we cannot yet determine if the genetic signatures of reproductive isolation we observe for western Napo *Pseudopipra* are related to hybridization.

Intriguingly, the evolutionary scenario inferred by phylogenetic reticulation analysis for the introgressed western Napo hybrids is consistent with observed patterns of lekking

vocalizations (Figure 8, Supplementary Appendix). The males from the Napo area of endemism share vocalization type 2 with birds in the southeastern Amazon (Figure 8), and with the restricted Huallaga valley *pygmaea* subspecies (the sister group to all lowland Amazonian forms, according to mtDNA). Manakins are suboscine passerines, have innate vocalizations (though see Saranathan et al. 2007). Therefore, the introgressed Napo lineage inherited its vocalizations from the MRCA of groups S1 and S2 (Figure 6a) and retained it through subsequent introgression with northern lineages that have a different vocal type (Type 3 and/or 5). In this scenario, vocal type 7 in the western Inambari may represent more recently derived variation in the southern Amazonian clade (Figure 8). The observation that the introgressed western Napo hybrids share a greater proportion of their genomes with their southern progenitors is consistent with this hypothesis, as is the observation that the introgressed lineage has mtDNA haplotypes from the southern Amazon (Supplementary Figure 16). This mitochondrial pattern implies that the introgressed Napo lineage may be a product of progenitor female S2a and western males of the Guiana Shield + Northern Amazon clade.

Taking all of the available genetic and phenotypic evidence into account, we propose that the Western Napo lineage is an additional example of the formation of a hybrid species in birds, and one that was produced via an underappreciated historical mechanism. The patterns we observe appear to be most similar to 'hybrid trait speciation,' in which a hybrid species is formed after introgression from one species into a genomic background of a close relative (Jiggins et al. 2008, Counterman 2016, Marques et al. 2019). This type of combinatorial hybrid speciation was originally proposed from studies of *Heliconius* butterflies (Jiggins et al. 2008, Salazar et al. 2010), and suggests introgression of a 'magic trait' can instantaneously lead to hybrid speciation without intrinsic barriers to reproduction (Counterman 2016). While we have no evidence of

'magic traits' representative of the Northern Amazon + Guiana Shield clade (D) that have influenced reproductive isolation in the western Napo lineage, our study predicts that such traits may exist in these populations and are worthy of additional study.

Comparative and Historical Biogeography

The spatial pattern of population structure and evolutionary relationships we identify here are broadly congruent with other recent studies of Neotropical biogeography in upland forest birds, contributing another example of the substantial phylogeographic pseudocongruence across taxa at this wide scale (e.g. Cunningham and Collins 1994, Harvey et al. 2017). As expected, the two main barriers identified for *Pseudopipra* in the South American lowlands are the Amazon River and the dry diagonal. Amazonian tributaries seem to delimit recently isolated populations in southern Amazonia, while northern *Pseudopipra* populations show weaker evidence of being isolated by the Negro and Japurá rivers. By contrast, southern populations seem to be strongly isolated by rivers with smaller discharge, such as the Xingu, Tapajós and Purus.

A comparable survey of the suboscine ovenbirds in the *Xenops* complex (Harvey and Brumfield 2015) identified similar patterns of genetic structuring coincident with major Amazonian tributaries, as did Ribas et al. (2012) in the *Psophia* trumpeters, though the inferred relationships among areas of endemism are not the same. A recent comparative analysis shows that large rivers delimit genetic clusters in as many as 23 groups of upland Amazonian forest birds, strongly arguing in favor of these rivers acting as barriers to gene flow (Silva et al. 2019). The somewhat distinct pattern found for *Pseudopipra* may be related to its recent expansion throughout the eastern Andean lowlands and its habitat tolerance.

Within the manakins, a recent molecular phylogeny (Ohlson et al. 2013) placed *Pseudopipra* as sister to the genus *Ceratopipra*, which includes five well-recognized species that are extensively codistribtuted with *Pseudopipra*. The montane origin of *Pseudopipra* is congruent with the observation that *Pseudopipra* is the sister group to *Ceratopipra,* which is also broadly distributed in the Neotropical lowlands from Central America to the Atlantic Forest, with two secondary expansions into the subtropical forests in the tepuis (*C. cornuta*) and the southern Andes (*C. chloromeros*) (Ohlson et al. 2013). The breakpoints among these *Ceratopipra* species are highly concordant with the breakpoints among the genetic clusters within the *Pseudopipra* complex that we have presented here, implying that these closely related taxa have many components of their phylogeographic history in common. See the Supplemental Appendix for additional notes, as well as Castro-Astor (2014).

A key feature of the phylogeny of *Pseudopipra* is that montane Andean lineages are sister groups to both the montane Central American and the lowland Amazonian-southeast Brazilian lineages. Ancestral character reconstruction with Bayesian stochastic mapping therefore unambiguously reconstructs the most recent common ancestor of *Pseudopipra* as montane (Figure 3, Supplemental Appendix). Thus, it appears that the most recent common ancestor of *Pseudopipra* was an Andean lineage restricted to subtropical, lower montane forest. The earliest diversification event in the genus was likely the differentiation of the ancestral Andean populations north and south of the Rio Huallaga, Peru. The northern lineage gave rise to the subtropical montane lineages of the northern Andes and Central America (Clade A). The southern lineage gave rise to a subtropical montane Southern Peruvian lineage (Clade B) and a southwestern lowland Amazonian lineage (*pygmaea*, represented in our dataset by mtDNA). Subsequently, the Amazonian lineage expanded to the eastern lowlands and differentiated into

the northern lowland Amazonian + Guiana Shield (Clade D in Figure 3) and southern lowland Amazonian/Atlantic Forest (Clade C in Figure 3) clades. Within the Southern Amazonian clade, differentiation proceeded from west to east: (Figure 3, 4):

(West Inambari (East Inambari (Rondônia (Tapajós (Xingu (Bahia (Espírito Santo (Rio de Janerio)))))))).

Contrastingly, the northern Amazonian lineage also expanded all the way to the Atlantic Ocean, but without producing strong phylogenetic structure (Figures 3, 4). In the Napo area of endemism, substantial introgression occurred from east Napo and Jaú populations into the western Napo population, with limited backcrossing into Inambari and east Napo populations.

Intriguingly, a well-supported distinct montane (>1000m) (BS100) (Clade C2 in Figure 3) is recovered as nested within the well supported lowland western Inambari subclade (Cerro Azul, Clade C1 in Figure 3). Thus, there may have been at least one secondary invasion of montane Andean habitats from a lowland ancestor. Patterns of admixture support this hypothesis – montane Cerro Azul individuals are detected to have limited genomic background of derived lineages of the Guiana Shield + Northern Amazon clade (yellow in Figure 5), similar to proximate lowland relatives. The presence of genomic admixture from the Guiana Shield + Northern Amazon clade is consistent with a scenario of secondary invasion of the highlands from lowland Inambari lineages which were secondarily weakly introgressed from the western Napo (see below), which itself experienced significant initial introgression from the Northern Amazon + Guiana Shield clade (D).

North Andean diversity

Our final genomic data set does not include any samples from Andean Ecuador or Colombia, a region that includes four previously recognized subspecies and at least four distinct vocalization types. Unfortunately, the three Andean Ecuadorian tissue (representing subspecies

coracina) specimens in our original sample were not of high enough preservation quality to be viable for ddRAD sequencing (Supplementary Table 1). We were able to obtain mtDNA from these samples however, which unambiguously formed a monophyletic cluster with our single San Martín (North Andean Peru) specimen in mtDNA gene tree analyses (Supplemental Appendix, Supplementary Figure 16). A prior study by Castro-Astor (2014) based on mtDNA also included one Andean Ecuadorian sample and one Central American sample, which unambiguously clustered together (*pp*=100). Thus, it is likely that our unsampled Andean lineages of Ecuador and Colombia (including the subspecies *minimus, bolivari, unica,* and *coracina*) are likely members of the northern Andean clade represented in our genomic data set by our single San Martín specimen.

As noted earlier, our San Martín specimen had approximately equal probability of assignment to multiple populations, which could indicate heavy admixture, or that this is a single sample from a highly distinct population which has its own distinct history. These patterns may also be consistent with the hypothesis that the north Andean clade is the source of montane and lowland *Pseudopipra* diversity. In summary, the genus *Pseudopipra* appears to have radiated 'out of the Andes,' expanding into the Central America highlands, and into the eastern lowland Amazonian and Atlantic forests.

Phenotypic Evolution

Thirteen subspecies have been previously described based on variations in plumage color and, to a lesser extent, size (See Taxonomic Summary in Supplementary Appendix). Male plumage coloration varies among the subspecies of *Pseudopipra* in the glossiness of the black body feathers, the length of the white crown feathers, and the color– white, gray, or black– of the

bases of these crown feathers. Female plumage coloration often shows more striking differentiation among subspecies than does male plumage, including variation in the shade of olive green on the body, the shade and extent of gray on the crown and face, and olive, yellow, or gray coloration on the belly.

Although we did not conduct a detailed analysis of plumage variation among populations of *Pseudopipra*, we note that all of the ten subspecies that were included in our genetic samples were identified as distinct, diagnosable, monophyletic groups. In other words, in all cases that we were able to test, traditional taxonomic practices– conducted between 1758 through 1936– successfully identified and named distinct evolutionary lineages within *Pseudopipra*. We did not have genetic samples of the northern Andean taxa *minima, unica,* and *bolivari*, but the entirely white crown feather bases are shared exclusively by *unica* and *minima,* and on the forecrown feathers of *bolivari,* imply that this plumage character state is derived within *Pseudopipra*, and that *minima* and *unica* form a clade, with *bolivari* as their sister group. One lineage containing two subspecies– *separabilis* and *cephaleucos*- has evolved another unique, shared, derived plumage character– a distinctive, second, predefinitive male plumage which has further differentiated between the two subspecies. In *cephaleucos,* predefinitive males have an olive green back, a white crown, and slate gray face and belly. In *separabilis,* predefinitive males are similar with lighter gray belly, and a medium gray, instead of white, crown. In conclusion, plumage coloration appears to provide highly informative evidence of evolutionary lineage status in this genus.

Our analysis of vocal behavior indicates that vocalizations are also highly informative of lineage identity within *Pseudopipra*. We identified fourteen distinct vocalization types (Figure, 8, 9), and all but one was restricted to and diagnostic of a single previously recognized

subspecies or a broader monophyletic group (See Expanded Taxonomic Summary in Supplementary Appendix for details). The only exception was vocalization type 2 (Fig. 8), which was shared plesiomorphically across the Amazon basin between populations of *pygmaea* in the Huallaga Valley, *discolor* in the western Napo region of Ecuador and Peru, and *separabilis* in Para, Brazil, but not in the intervening southwestern Amazonian populations of *microlopha*. Unfortunately, available vocal sampling is very limited in the intervening regions along the south side of the Amazon Basin, which are populated by a nested series of genetically distinct lineages with successively closer relationships to southern Amazonian *separabilis* and *cephaleucos* from the Atlantic forest of Brazil.

Based on genetic variation, we also identified several additional well-supported clades for which we have limited vocal or plumage coloration data. For example, only one vocal record is known for the South Andean clade (Clade B), which is currently recognized as *P. p. comata*. This lineage is also composed of two well differentiated subclades: a northern clade (B1) from Cerro Azul in Loreto, and a southern clade (B2) from southern Huánuco (AMNH 820866, 820952), Pasco, Junín, and Cusco. Since the type of *comata* is within the southern clade, further investigation is necessary to determine whether the Cerro Azul populations should be recognized as a distinct, new taxon. Our phylogenetic analysis also identified a distinct montane clade from the highlands between the Rio Huallaga and Rio Ucayali (Clade C2) which is closely related to populations from lowland forests of eastern Peru south of the Rio Marañón and east to Rio Purus, Brazil, currently recognized as *P. p. microlopha*. Although it is not certain that this montane clade represents a secondary expansion into the Andes, its phylogenetic distinction implies that it may also exhibit distinct plumage or vocal characters.

Taxonomy and Revised Classification

Our analysis identifies a number of genetically well-differentiated and phenotypically diagnosable lineages and provides compelling new evidence for evaluating the species status of *Pseudopipra*. Although there are gaps in our sampling, we find that there are at least eight genetically well-differentiated, and phenotypically diagnosable lineages of *Pseudopipra*. There is more genetic variation than observed vocal variation implies, and more vocal variation beyond our geographic coverage of genetic samples (especially in northern Andes). Thus, our descriptions of cryptic diversity in *Pseudopipra* are almost certainly an underestimate, underscoring the need for continued reassessment of species limits and of diversity patterns in the Neotropics. Our analysis provides the first comprehensive opportunity to reevaluate species limits within *Pseudopipra* based on phylogenetic, population genetic, vocal, and plumage differentiation among populations and named subspecies (See the Expanded Taxonomic Summary in the Supplementary Appendix). Three of these species are polytypic (i.e. contain multiple subspecies). One of the species we recognize– *P. microlopha* – is paraphyletic with respect to another species, *P. cephaleucos,* because we recognize that speciation may not threaten the lineage identity of a paraphyletic group.

This proposed classification is a conservative treatment that recognizes our limited genetic sampling of populations in the northern Andean clade from Ecuador and Colombia and our limited behavioral data. Three of these unsampled northern Andean subspecies– *coracina, minima,* and *occulta*– have unique, and highly differentiated vocalization types, and diagnosable plumage differences. Our phylogenetic results for other lineages in the genus strongly suggest that each of these subspecies is a distinct evolutionary lineage deserving species status. The vocalization types of one other subspecies– *bolivari*– is currently unknown, but it may also be

distinct species. Further research will be required to assess whether the unexpected vocal diversity among populations of *unica* (types 11a and 11b) from the central Andes of Colombia indicates the existence of additional, undescribed taxa. Plumage and vocal data from other newly identified clades may support the recognition of additional species including populations from the highlands between Rio Huallaga and Rio Ucayali (Clade C2; Fig. 3), and the currently unnamed lineages from the southern Amazon Basin (Clades C3, C4, and C5). In conclusion, *Pseudopipra* may include 15-17 distinct species that have rapidly arisen in the last ~2.5 Ma, but further reclassification will require more vocal data and detailed analyses of plumage variation.

Pseudopipra coracina (Sclater 1856) **Andean White-crowned Manakin**

Distribution: Subtropical Andes from Venezuela south to Esmeraldas, Ecuador and San Martín, Peru.

Phylogenetic Position: Clade A1

P. c. coracina (Sclater 1856)

Distribution: Subtropical forests of the eastern slope of the Andes from western Venezuela to Morona-Santiago, Ecuador.

Phylogenetic Position: (mtdna) Member of Clade A1

Lek Vocal Type: 8 (*errrwer*).

Call Vocal Type: unknown

P. c. minima (Chapman 1914)

Distribution: Subtropical forests of western Cauca, Colombia south to Esmeraldas, Ecuador

Phylogenetic Position: (unsampled) Member of Clade A1

Lek Vocal Type: 9 (*reeee*)

Call Vocal Type: unknown

P. c. bolivari (de Schauensee 1950)

Distribution: Subtropical forests of southern Córdoba, Colombia. (Not Sampled)

Phylogenetic Position: (unsampled) Member of Clade A1

Lek Vocal Type: Unknown

Call Vocal Type: unknown

P. c. unica (de Schauensee 1945)

Distribution: Subtropical forests of Magdalena Valley, Antioquia to Huila, Colombia.

Phylogenetic Position: (unsampled) Member of Clade A1

Lek Vocal Type: 11a (weer-dink) and 11b (shureeep)

Call Vocal Type: unknown

P. c. occulta (Zimmer 1936)

Distribution: Eastern slope of the Andes from Zamora-Chinchipe, Ecuador (Freile 2014) south to San Martín, and Huánuco, Peru, west of the Rio Huallaga

Phylogenetic Position: Member of Clade A1 (represented by

Lek Vocal Type: 1 (*trill-dink*) and 10 (*bree*)

Call Vocal Type: unknown

Pseudopipra anthracina (Ridgway 1906) **Western White-crowned Manakin**

Distribution: Subtropical Costa Rica to Western Panama

Phylogenetic Position: Clade A2

Lek Vocal Type: 4 (*jureeee*)

Call Vocal Type: unknown

Pseudopipra comata (Berlepsch and Stolzmann 1894) **Junín White-crowned Manakin**

Distribution: Subtropical Andes of Peru from Cerro Azul, Loreto (east and south of the Rio Huallaga) to southern Huánuco Pasco, Junín, and northern Cusco.

Phylogenetic Position: Clade B

Lek Vocal Type: One record, statistically similar to type 1 (*trill-dink*)

Call Vocal Type: unknown

Pseudopipra pygmaea (Zimmer 1936) **Huallaga White-crowned Manakin**

Distribution: Tropical forest of lower Rio Huallaga Valley, Peru

Phylogeneic Position: (mtDNA) Sister to Clade F

Lek Vocal Type: 2 (*deeeer*)

Call Vocal Type: 13

Pseudopipra discolor (Zimmer 1936) **Napo White-crowned Manakin**

Distribution: Tropical forest in Napo, Ecuador and Loreto, Peru south to the Rio Marañón.

Phylogenetic Position: Clade E

Lek Vocal Type: 2 (*deeeer*)

Call Vocal Type: 13

Pseudopipra pipra (Linneaus 1758) **Northern White-crowned Manakin**

Distribution: Tropical forest of eastern Colombia, southern Venezuela, the Guianas, and Brazil north of the Amazon and west to the right (west) bank of the Rio Putumayo, Colombia.

Phylogenetic Position: Clade D

Lek Vocal Type: 3 (*buzzzz*)

Call Vocal Type: 5 (*zeee*)

Pseudopipra microlopha (Zimmer 1929) **Southern White-crowned Manakin**

Distribution: Tropical forest of eastern Peru south of the Rio Huallaga, Rio Marañón, and the Amazon River east to Pará, Brazil, and subtropical forests between the Rio Huallaga and Rio Ucayali.

Phylogenetic Position: Paraphyletic, including Clade C without Clade C7

P. m. **undescribed subspecies**

Distribution: Subtropical forest from the highlands between Rio Huallaga and Rio Ucayali

Phylogenetic Position: Clade C2

Lek Vocal Type: Unknown

Call Vocal Type: 13

P. m. microlopha (Zimmer 1929)

Distribution: Eastern Peru south of the Rio Marañón and Rio Huallaga, west to Rio Juruá and Rio Purus, Brazil.

Phylogenetic Position: Clade C1 excluding C2

Lek Vocal Type: 7 (*jeer*)

Call Vocal Type: 13

***P. m.* undescribed subspecies**

Distribution: Right (east) bank of the Rio Purus to the left (west) bank Rio Madeira

Phylogenetic Position: Clade C3

Plumage: Not examined

Lek Vocal Type: Unknown

Call Vocal Type: 13

***P. m.* undescribed subspecies**

Distribution: Right (east) bank of the Rio Madeira to the left (west) bank the Rio Tapajos.

Phylogenetic Position: Clade C4

Plumage: Not examined

Lek Vocal Type: Unknown

Call Vocal Type: 13

***P. m.* undescribed subspecies**

Distribution: Right (east) bank of the Rio Tapajos to the left (west) bank of the Rio Xingu

Phylogenetic Position: Clade C5

Plumage: Not examined

Lek Vocal Type: 6b

Call Vocal Type: 13

P. m. separabilis (Zimmer 1936)

Distribution: Tropical forest of Rio Xingu east to central and southern Pará.

Phylogenetic Position: Clade C6

Lek Vocal Type: 2

Call Vocal Type: 13

Pseudopipra cephaleucos (Thunberg 1822) **Atlantic White-crowned Manakin**

Distribution: Tropical forest from Bahia south to northern Rio de Janeiro, Brazil.

Phylogenetic Position: Clade C7

Lek Vocal Type: 6a (*zeeeee-tonk*)

Call Vocal Type: 13

Supplementary Material: Supplementary material, including data files and online-only appendices, can be found in the Dryad Digital Repository: http://dx.doi.org/10.5061/dryad.[NNNN], and GenBank XXX-XXX.

Funding: J. S. B. was supported by a National Science Foundation Graduate Research Fellowship and NSF Doctoral Dissertation Improvement Grant [DGE-1650441, DEB-1700786]. L. C. was supported by NSF grant DEB-1555754 to I.J.L. T. J. F. was supported by an NSF Post-doctoral Fellowship in Biology [DBI-1523857]. C. C. R. was funded by CNPq (308927/2016-8),

FAPEAM, FAPESP/NSF (NSF DEB-1241066, FAPESP, grant #2012/50260-6) and USAID (PEER AID-OAA-A-11-00012, cycle 5). J. S. B. and R. O. P. were funded by the W. R. Coe Fund of Yale University. Data collection was paid for by Athena Funds from the Cornell Laboratory of Ornithology, and W. R. Coe Fund from Yale University. This work was also supported in part by the facilities and staff of the Yale University Faculty of Arts and Sciences High Performance Computing Center, and with the resources of the Cornell University BRC Bioinformatics Facility, which is partially funded by Microsoft Corporation.

Acknowledgements:

We thank the numerous researchers whose field collection efforts made this research possible including: Angelo P. Capparella, Camila Ribas, Ivandy Castro-Astor, Cecilia Fox, David E. Willard, Diego Ocampo, Donna Dittmann, Jacob S. Berv, John P, O'Neill, Karla Conejo, Katya Balta, Kenneth V Rosenberg, Louise M. Augustine, Peter E. Scott, Richard O. Prum, Steven W. Cardiff, Susan Allen-Stotz, Thomas Valqui, Tristan J. Davis, Ivan Prates and others. Tissue loans were kindly received from Divisão de Aves do Museu de Zoologia da Universidade Estadual de Feira de Santana (MZFS), Field Museum of Natural History (FMNH), Instituto Nacional de Pesquisas da Amazônia (INPA), Kansas University Natural History Museum (KUNHM), Louisiana Museum of Natural History (LSUMZ), Museu de Zoologia da Universidade de São Paulo (MZUSP), Museu Paraense Emilio Goeldi (MPEG), The Academy of Natural Sciences of Drexel University (ANSP), Universidade do Estado do Rio de Janeiro (UERJ), University of Alaska Museum (UAM), University of Nevada, Las Vegas (UNLV), the Yale Peabody Museum of Natural History (YPM), and the Cornell Museum of Vertebrates (CUMV). We thank the curators and collections managers of these institutions for facilitating these loans: Camila Ribas,

John Bates, Mark Robbins, Donna Dittman, Alexandre Aleixo, Caio Graco Machado, Joel Cracraft, Luís Fábio Silveira, Kevin Winker, Maria Alice Santos Alves, Kristof Zyskowski, Nate Rice, Charles Dardia, John Klicka, and others. We thank Eliot Miller, Emma Greig, Matthew Medler, Greg Budney, Eduardo Iñigo and Andrew Spencer at the Macaulay Library for assistance with audio recordings. We thank members of the Lovette Lab, as well as **XXXX** anonymous reviewers, for comments on the research and the manuscript. The illustration depicted in Fig. 3 is reproduced with permission from the Handbook of Birds of the World, Lynx Editions, Barcelona. J. S. B. and R. O. P. conceived of the research in 2011. J. S. B. and L. C. performed laboratory and bioinformatic processing, with input and support from I. J. L. We thank Bronwyn Butcher for help with laboratory protocols. J. S. B. and L. C. analyzed the genomic data and interpretation of the results was supported by input from all authors. T. J. F. organized and analyzed lekking vocalization data. C. C. R. and I. C. R. facilitated critical sample acquisitions from Amazonia and the Atlantic Forest. I. J. L. and R. O. P. provided detailed guidance and feedback on the manuscript. R. O. P. proposed a revised taxonomy. The manuscript was written by J.S.B. with input from all authors.

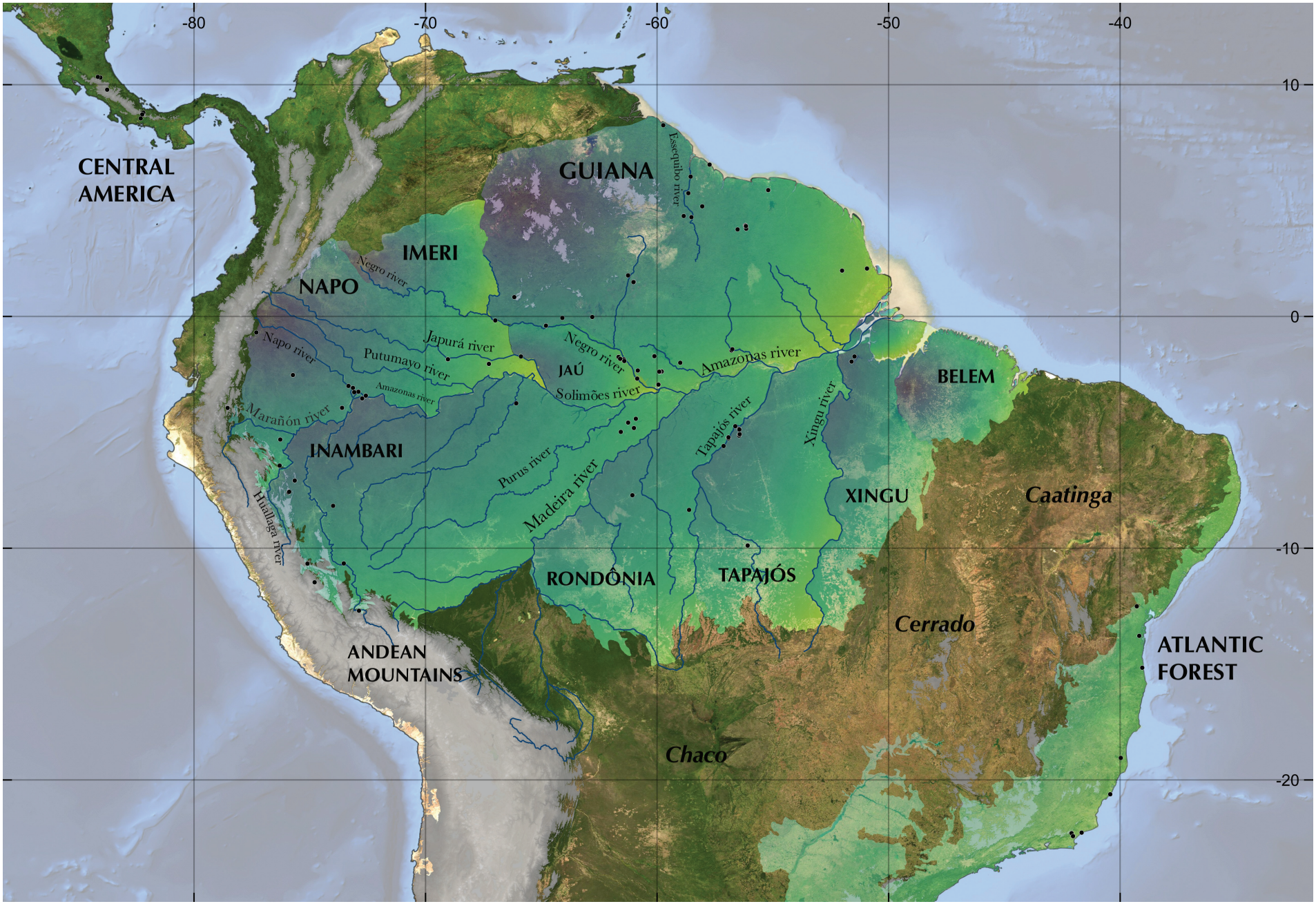
-80
-70
-60
-50
-40
10
0
-10
-20
CENTRAL AMERICA
GUIANA
Essequibo river
IMERI
Negro river
NAPO
Napo river
Japurá river
Putumayo river
Amazonas river
Marañón river
JAÚ
Negro river
Solimões river
Amazonas river
BELEM
Tapajós river
Xingu river
INAMBARI
Purus river
Madeira river
Huallaga river
XINGU
Caatinga
RONDÔNIA
TAPAJÓS
Cerrado
ATLANTIC FOREST
ANDEAN MOUNTAINS
Chaco

Figure 2.1. Neotropical areas of endemism and field sampling. Amazonian lowland areas of endemism as portrayed in Da Silva et al. (2005) are highlighted in shades of green, as well as the Jaú area of endemism (Borges and Da Silva 2012). Montane Andean, Central American, Guianan, and dry diagonal regions (>1000m) are emphasized in grey. As summarized in Da Silva et al. (2005), a sequence of authors identified seven areas of endemism for lowland birds that retained Wallace's 'Guyana' (Wallace 1854), split 'Ecuador' into 'Imeri' and 'Napo,' renamed 'Peru' to 'Inambari', and split 'Brazil' into 'Rondônia', 'Pará', and 'Belém' (Haffer 1978, Cracraft 1985, Haffer 1985, Cracraft and Prum 1988, Haffer 1992). 'Pará' was subsequently further partitioned into two regions, 'Tapajós' and 'Xingu,' (Da Silva et al. 2002). Recently, additional sub-partitions have been proposed for the 'Napo' (Jaú - Borges and Da Silva 2012), and Guianan areas of endemism (Naka 2011). Plotted points indicate field sampling localities for 277 *Pseudopipra* individuals sequenced for genomic analysis in the present study.

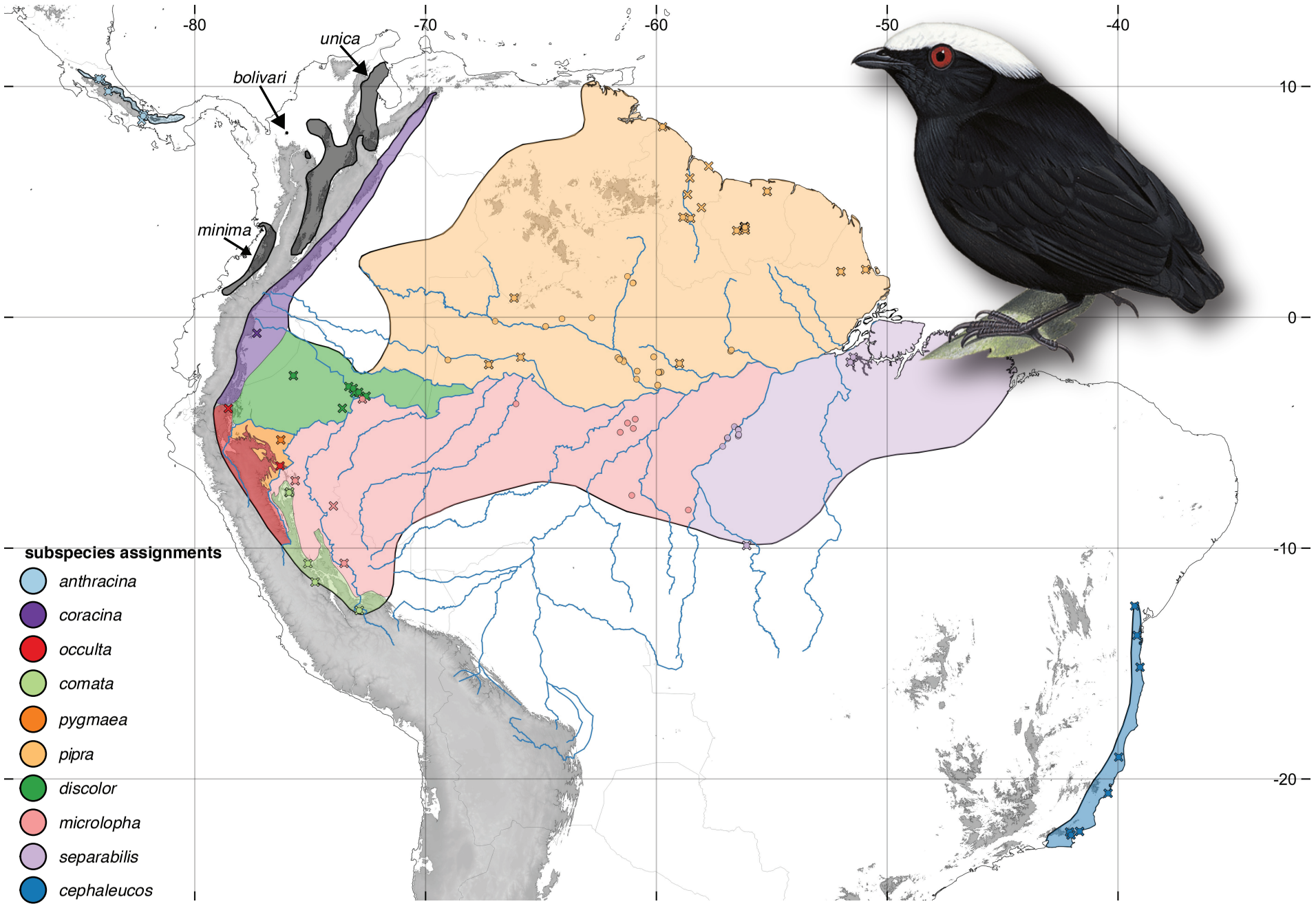
-80
-70
-60
-50
-40
10
0
-10
-20
unica
bolivari
minima
subspecies assignments
anthracina
coracina
occulta
comata
pygmaea
pipra
discolor
microlopha
separabilis
cephaleucos

Figure 2.2. Subspecies sampling. Our sampling of *Pseudopipra pipra* intersects with the ranges of ten named subspecies. In this figure we color code our sampling localities as they overlap with described subspecies ranges. Areas greater than 1000m in elevation are shown in light grey; major Amazonian rivers are indicated in light blue; political boundaries in light grey. Outlined in black: genus range map reflecting the BirdLife International approximation updated to reflect current knowledge (BirdLife International Species factsheet: *Pseudopipra pipra*, 2018, also see Supplemental Figure 1). Hypothetical subspecies ranges are based on descriptions in Kirwan and Green (2012) and indicate maximal potential ranges to highlight proposed barriers delimiting subspecies. Circles indicate sampling for ddRADseq, X's indicate sampling for mtDNA ND2. Our sampling encompasses the majority of the lowland extents of the recognized range of *Pseudopipra*, as well as key montane populations in Peru, Ecuador, and Central America. Ssp *comata*, *anthracina,* and *occulta* are exclusively montane. Inset top right is an illustration of the *pipra* subspecies, reproduced from the Handbook of the Birds of the World, Lynx Edicions.

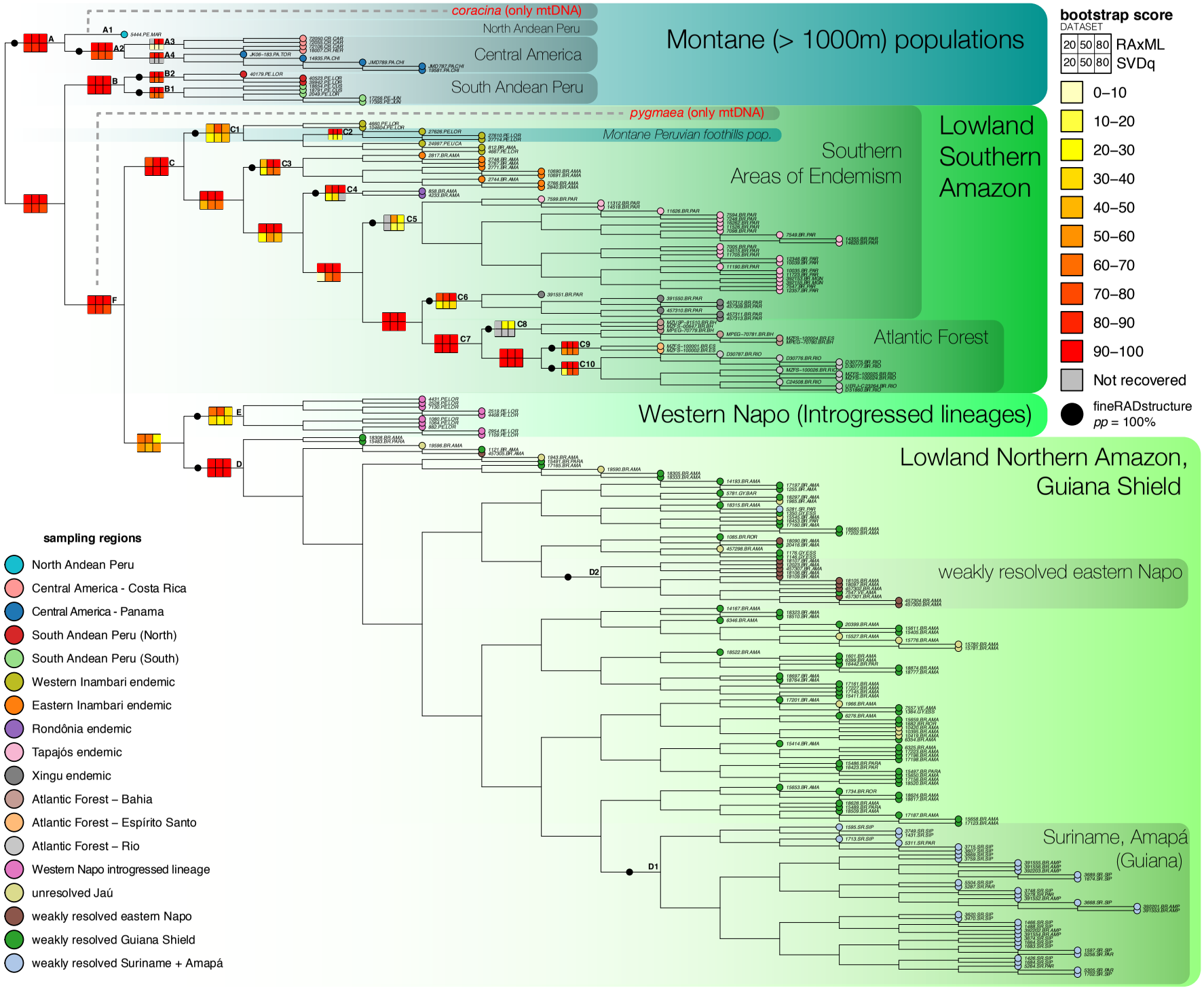
coracina (only mtDNA)
North Andean Peru
Central America
South Andean Peru
Montane (> 1000m) populations
pygmaea (only mtDNA)
Montane Peruvian foothills pop.
Southern Areas of Endemism
Lowland Southern Amazon
Atlantic Forest
Western Napo (Introgressed lineages)
Lowland Northern Amazon, Guiana Shield
weakly resolved eastern Napo
Suriname, Amapá (Guiana)
bootstrap score
DATASET
20 50 80 RAxML
20 50 80 SVDq
0–10
10–20
20–30
30–40
40–50
50–60
60–70
70–80
80–90
90–100
Not recovered
fineRADstructure
pp = 100%
sampling regions
North Andean Peru
Central America - Costa Rica
Central America - Panama
South Andean Peru (North)
South Andean Peru (South)
Western Inambari endemic
Eastern Inambari endemic
Rondônia endemic
Tapajós endemic
Xingu endemic
Atlantic Forest – Bahia
Atlantic Forest – Espírito Santo
Atlantic Forest – Rio
Western Napo introgressed lineage
unresolved Jaú
weakly resolved eastern Napo
weakly resolved Guiana Shield
weakly resolved Suriname + Amapá

Figure 2.3. Phylogenetic hypothesis for *Pseudopipra*. Phylogenetic analysis of short read ddRAD sequence haplotypes generated a well-resolved phylogenetic hypothesis which was largely congruent across datasets and analytical approaches. Montane clades, including a Northern Andean (A1) + Central American (A2) clade (A), and a central Peruvian clade (B), are recovered as nested sister groups to two wide ranging lowland clades (C and D), indicating that the lowland clades are descended from Andean lineages. Shown is the RAxML topology generated using the 50% haplotype dataset. Branch lengths are set to equal for graphical interpretability (see supplementary material for original newick formatted tree files). Colored circles at tips indicate group membership to one of eighteen population-areas (matching Figure 4 and 5). Heatmaps printed at well-supported nodes indicate bootstrap scores from each of six phylogenetic analyses for 20/50/80% datasets, as indicated in the legend. Black dots indicate populations which are identified with 100% posterior probability in fineRADstructure analysis. Most of the major and substructure is recovered by both RAxML and SVDquartets (see text), though RAxML recovers additional low-support substructure in the Northern Amazonian + Guiana Shield clade (D) which is coincident with several geographic features (clades D1 and D2). A clade of introgressed western Napo individuals (E) is recovered by all standard phylogenetic analyses as sister to the northern Amazonian + Guiana shield clade (D). As the history of this clade is characterized by a complex introgression scenario between northern and southern lineages, a purely bifurcating tree model is inadequate to describe its relations with other groups (see text) (Figure 6). Also shown are the well supported phylogenetic positions of two distinct subspecies lineages (*pygmaea* and *coracaina*) from which we were able to obtain mtDNA (Supplemental Appendix).

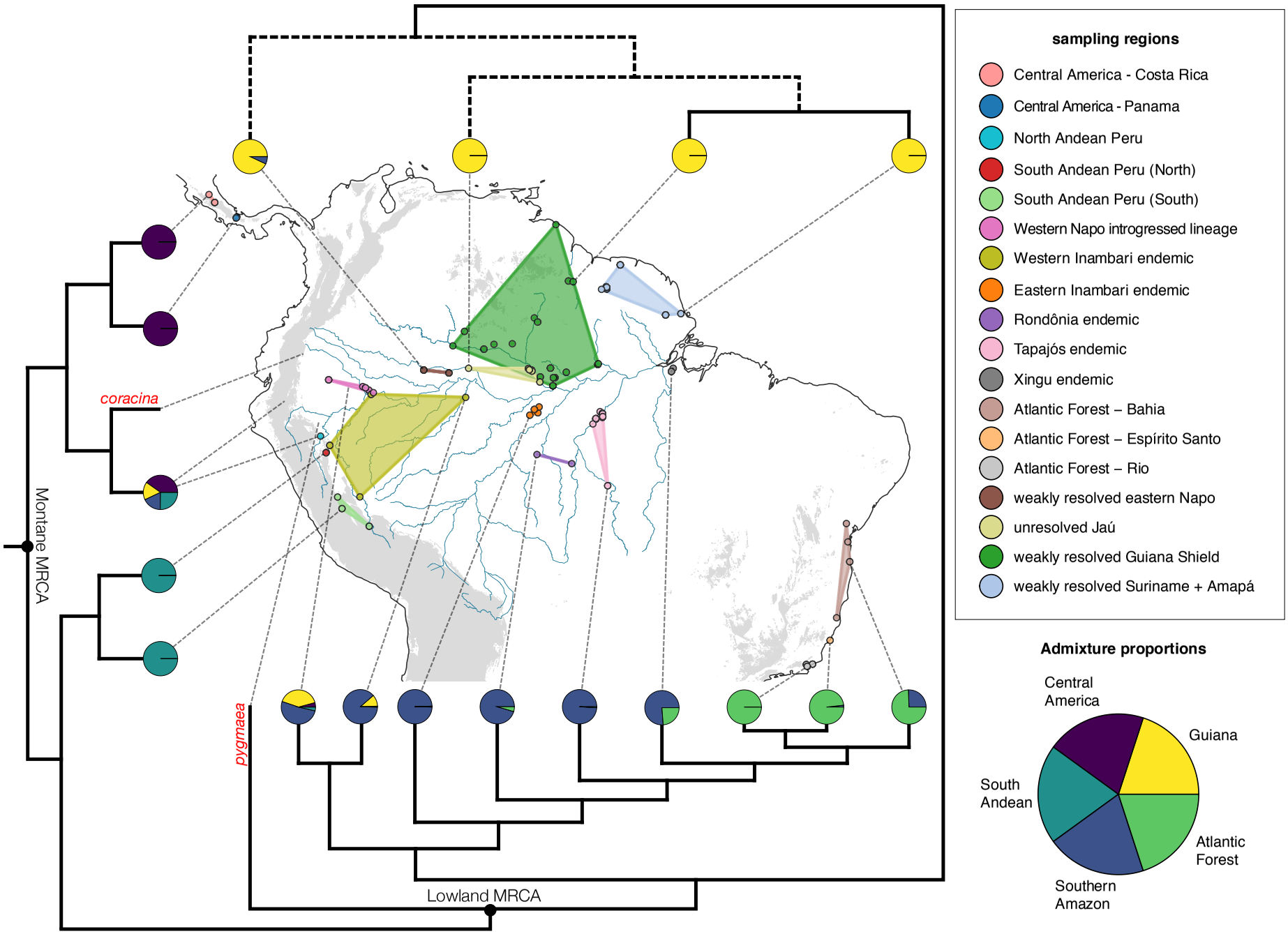
coracina
pygmaea
Montane MRCA
Lowland MRCA
sampling regions
Central America - Costa Rica
Central America - Panama
North Andean Peru
South Andean Peru (North)
South Andean Peru (South)
Western Napo introgressed lineage
Western Inambari endemic
Eastern Inambari endemic
Rondônia endemic
Tapajós endemic
Xingu endemic
Atlantic Forest – Bahia
Atlantic Forest – Espírito Santo
Atlantic Forest – Rio
weakly resolved eastern Napo
unresolved Jaú
weakly resolved Guiana Shield
weakly resolved Suriname + Amapá
Admixture proportions
Central America
Guiana
South Andean
Atlantic Forest
Southern Amazon

Figure 2.4. Phylogeospace mapping of topological relations in geographic space. Here, an idealized topology is plotted with tips attached to sampling coordinates. The colors of circles at sample localities matches those in Figure 3 and 5, and are enclosed by minimum convex hulls (i.e., hypotheses of minimum clade ranges) of the same colors. All of these colored hulls represent distinct non-overlapping geographic areas delimited by physical barriers (though this is somewhat visually confounded in the Northern Amazon + Guiana Shield clade (D), with two weakly resolved lineages (e.g. pale yellow Jaú and green Guiana Shield population groups appear to have some overlap in this figure, but they are delimited by the Rio Negro). Clade D bipartitions are shown with dashed branches (top) to indicate low support for phylogenetic structure (Figure 3, results). The ancestral habit of the genus is inferred to be montane (Supplementary Appendix), with a single origin of lowland lineages (*pp*=100). Also shown at the tips are median admixture proportions across sampling localities as inferred with STRUCTURE (Figure 5 for full detail).

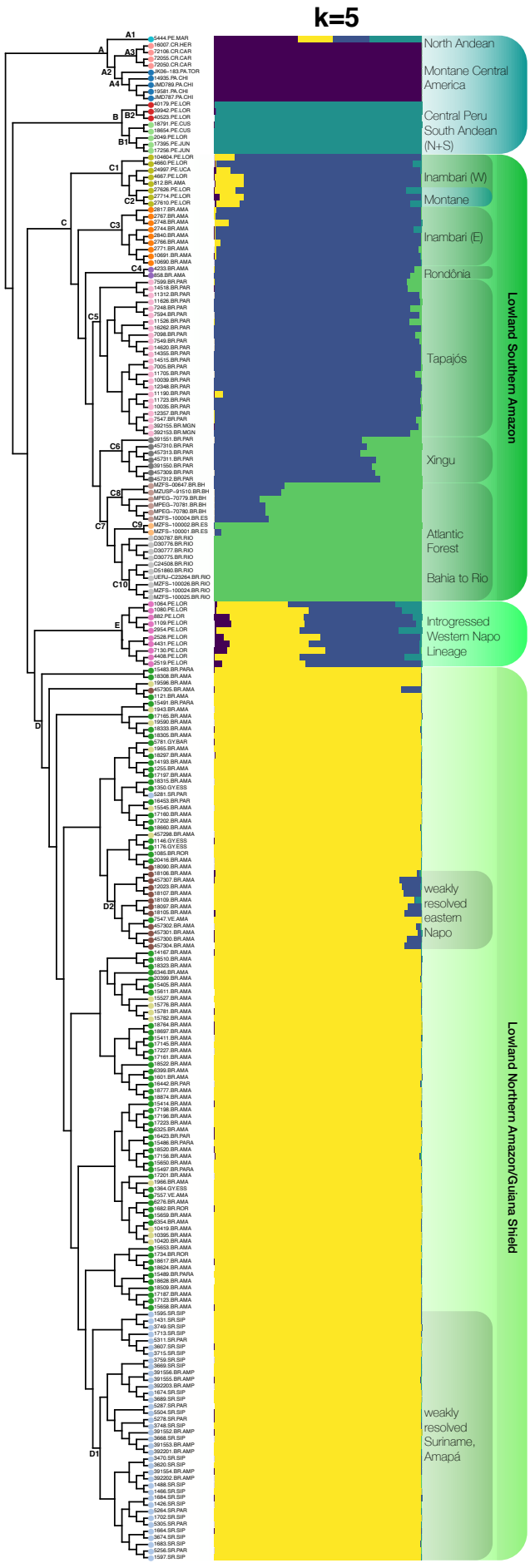
k=5
North Andean
Montane Central America
Central Peru South Andean (N+S)
Inambari (W)
Montane
Inambari (E)
Rondônia
Tapajós
Xingu
Atlantic Forest
Bahia to Rio
Lowland Southern Amazon
Introgressed Western Napo Lineage
weakly resolved eastern Napo
weakly resolved Suriname, Amapá
Lowland Northern Amazon/Guiana Shield
A
A1
A2
A3
A4
B
B1
B2
C
C1
C2
C3
C4
C5
C6
C7
C8
C9
C10
D
D1
D2
E

Figure 2.5. STRUCTURE output for K-5. STRUCTURE analysis of dataset 1, depicting population assignment and admixture estimates for K=5. The likelihood of each evaluated number of K clusters from 1:20 plateaued at K = 5, with the standard deviation across runs increasing rapidly after this point (Supplemental Figure 2). The five optimized clusters broadly correspond to wide biogeographic Neotropical regions which coincide with lowland areas of endemism, Central American, and Peruvian montane regions (Figure 4). Given these five clusters, each labeled focal region is inferred to have a unique combination of admixture proportions. The admixture cline inferred from the Xingu to the southern Atlantic Forest appears to be a product of isolation by distance (Supplementary Appendix), while the signature of introgression inferred for western Napo lineages appears to be a product of substantial historical introgression from a northern lineage (likely from the poorly resolved eastern Napo group D2), into a distinct Southern Amazonian lineage (see Figure 6 and discussion). The tree to the left corresponds to the RAxML result using the 50% haplotype dataset, with tip labels and colors indicating group membership to one of eighteen population-areas (matching those in Figures 3, 4). See Supplementary Figure 3 for K2-10 results.

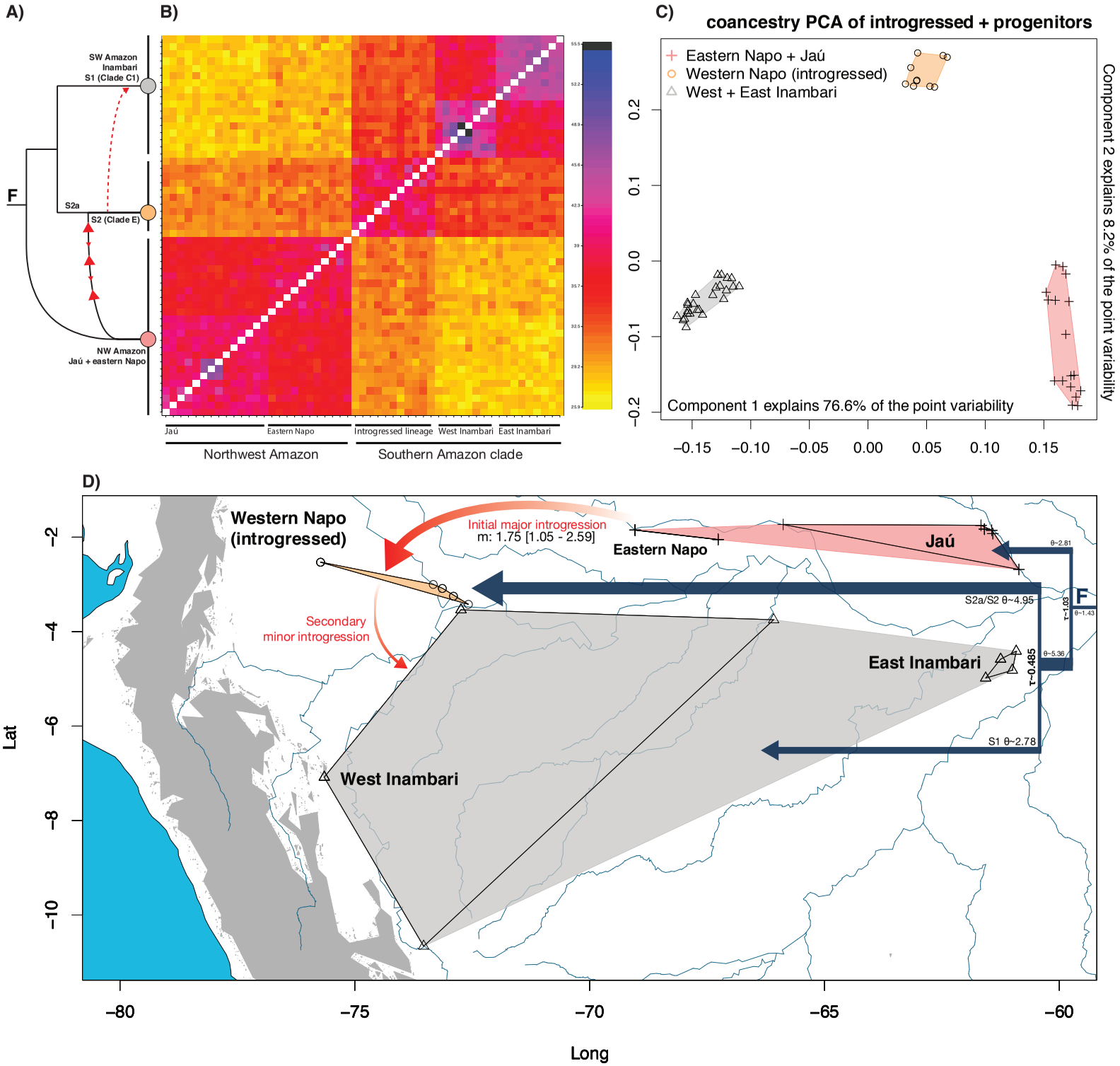
A)
B)
C)
D)
SW Amazon
Inambari
S1 (Clade C1)
F
S2a
S2 (Clade E)
NW Amazon
Jaú + eastern Napo
Jaú
Eastern Napo
Introgressed lineage
West Inambari
East Inambari
Northwest Amazon
Southern Amazon clade
coancestry PCA of introgressed + progenitors
Eastern Napo + Jaú
Western Napo (introgressed)
West + East Inambari
Component 1 explains 76.6% of the point variability
Component 2 explains 8.2% of the point variability
Western Napo
(introgressed)
Initial major introgression
m: 1.75 [1.05 - 2.59]
Eastern Napo
Jaú
Secondary
minor introgression
East Inambari
West Inambari
S2a/S2 θ~4.95
S1 θ~2.78
τ~0.485
Lat
Long

Figure 2.6. Introgressed lineage in the western Napo area of endemism. All of the available genomic evidence is consistent with the hypothesis that individuals in the western Napo area of endemism are derived from a distinct southern Amazonian lineage (S2a in Panel A) which is not represented in contemporary samples. This lineage (S2a) experienced substantial introgression from the ancestral populations of what are today eastern Napo and Jaú restricted linages. Panel A shows the phylogenetic network (in black) inferred by PhyloNet, with arrows indicating hypothetical degree and direction of historical introgression as implied by patterns of admixture. The red arrows along the PhyloNet reticulation indicate inferred introgression from the northern Amazonian lineages (clade C1 in Figure 3) into this southern Amazonian lineage (S2a). The smaller red arrows indicate potential limited backcrossing into northern lineages implied by patterns of admixture. The dashed red line connecting S2 to S1 indicates minimal implied introgression into Inambari lineages, which may have occurred after the primary introgression event, and brought northern (Clade D) alleles into SW Amazonian populations (see text and Figure 5). Panel B displays the individual level co-ancestry matrix for introgressed Napo individuals and their source/progenitor lineages; darker colors indicate greater co-ancestry. Introgressed (PH: putative hybrid) hybrids have greater co-ancestry with each of their progenitor lineages (S2a and Northern Amazon+Guiana shield (abbreviated GS)) than their progenitor lineages share with each other (PHvGS/progenitors = 1.078, PHvInambari/progenitors = 1.17, see text). In the proposed scenario, the southern progenitor lineage (S2a) is either unsampled or extinct and has not persisted sympatrically with S2. Thus, the western Inambari southern lineage (S1) comprises the closest living relatives to S2a (see discussion). Panel C summarizes co-ancestry variance as projected into component space after normalizing; the introgressed lineage is intermediate along PC1 and differentiated along PC2. The level of differentiation on PC2

corresponds to about 10% of the total variation explained by PC1 and PC2 (~85%). Panel D summarizes the minimum implied geographic extents of the groups involved (as sampled in this study). G-PhoCS demographic parameter estimates are also indicated in panel D (m: migrants per generation, when lower 95% CI > 1, τ: splitting time in generations (10^6), θ: effective population size (10^6), Supplemental Table 5). In A-D, two subpopulations are indicated for each progenitor group, as outlined with outlined minimum convex hulls in D.

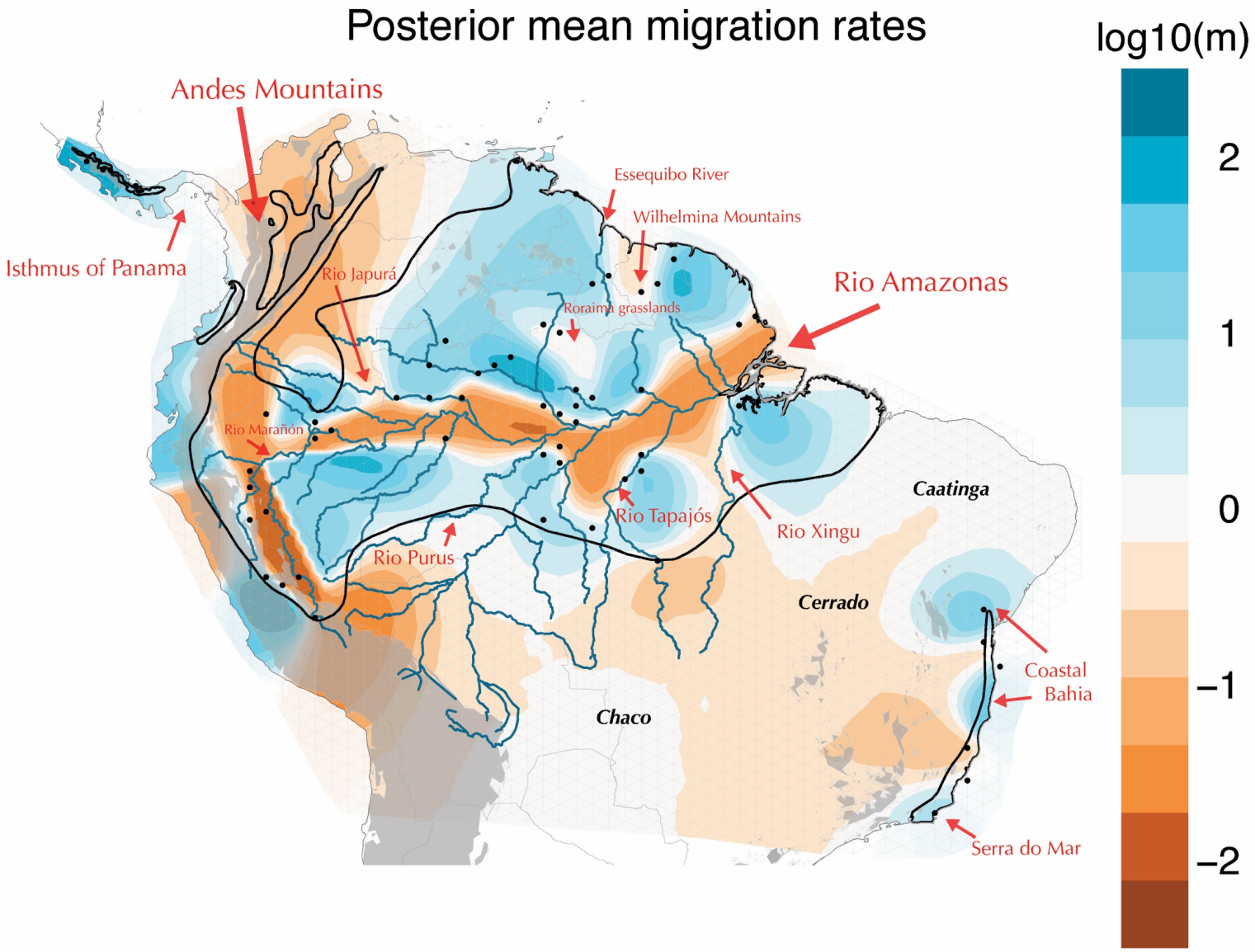
Posterior mean migration rates
log10(m)
2
1
0
−1
−2
Andes Mountains
Isthmus of Panama
Rio Japurá
Essequibo River
Wilhelmina Mountains
Roraima grasslands
Rio Amazonas
Rio Marañón
Rio Tapajós
Rio Xingu
Rio Purus
Caatinga
Cerrado
Chaco
Coastal Bahia
Serra do Mar

Figure 2.7. Estimated Effective migration surface (EEMS). The estimated migration surface links the topography and drainage system of the Neotropics to spatial patterns of genetic diversity. Shown are results estimated from a model with 2000 demes (vertices). EEMS uses an MCMC approach to estimate expected genetic dissimilarity between all pairs of individuals, integrating over all possible migration histories across the grid, and adjusting migration rates among graph edges to match the genetic differences in the data. Bluer colors indicating areas where gene flow is more likely to be able to occur (i.e., isolation by distance is predicted), and browner colors indicate areas where barriers to gene flow are highly probable. In this analysis, the Andes and the Amazon River are the most clearly inferred barriers to gene flow. Major rivers, as well as a >1000m contour (light grey) are overlaid to aid interpretation. EEMS does a very good job of explaining spatial variance in this dataset ($R^2 = 0.871$, Supplementary figure 10, 11). There are areas where it performs poorly however, particularly in the western Amazon, where the inference of a major barrier to gene flow (the Andes) is inferred a few degrees too far east, pushing other western patterns eastwards. This is likely a consequence of uneven genetic sampling in this area. Remarkably, EEMS almost perfectly infers the spatial extents of the lowland Amazonian range (range map outlined in black), despite very limited genetic sampling toward the edge of the range. EEMS also correctly detects an isolated region of corresponding to the introgressed western Napo hybrid lineage. Also noted are likely geographic barriers that correspond to estimated barrier localities.

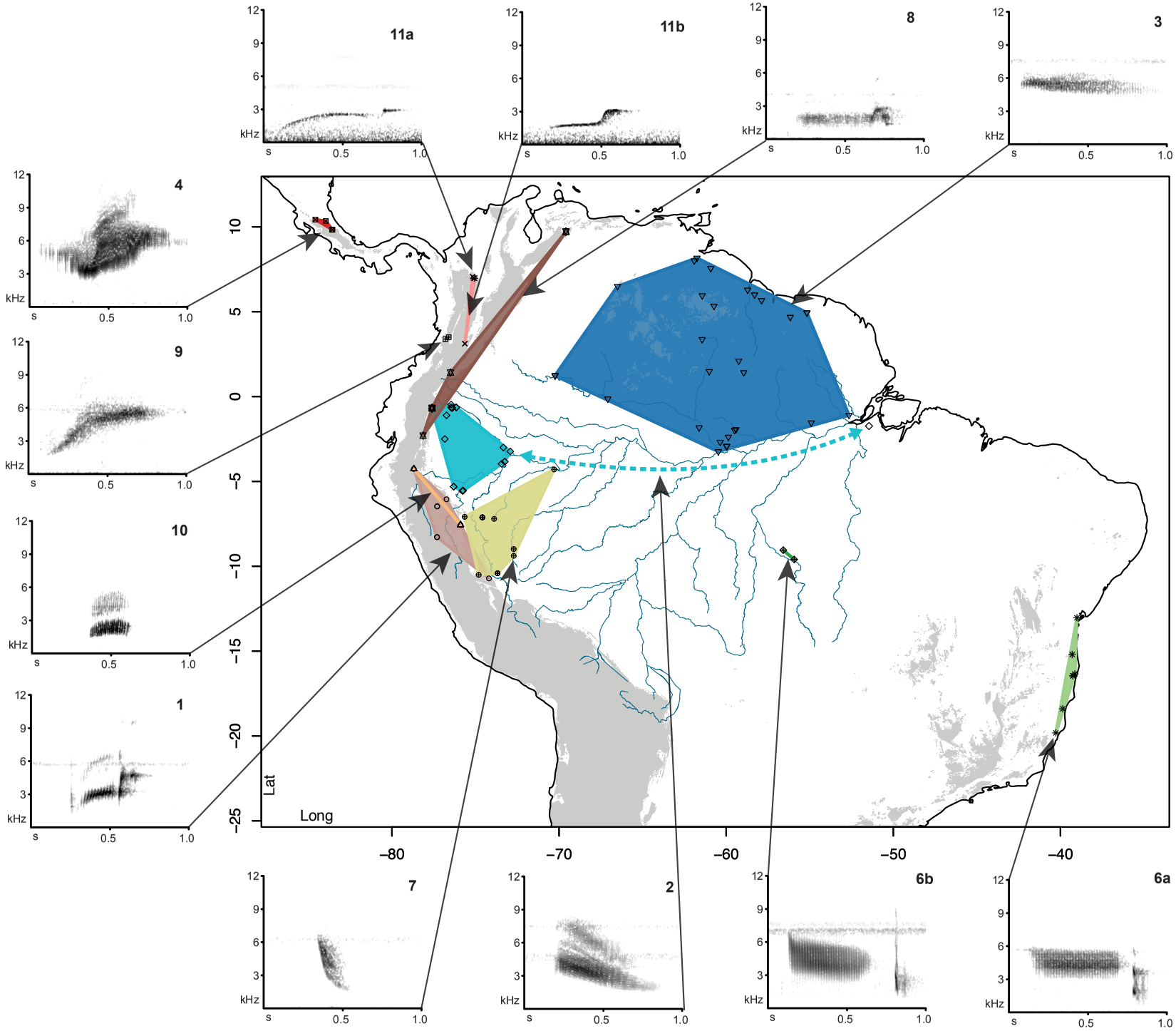
11a
11b
8
3
4
9
10
1
7
2
6b
6a
kHz
s
0.5
1.0
Lat
Long
10
5
0
−5
−10
−15
−20
−25
−80
−70
−60
−50
−40

Figure 2.8. Summary of lek vocalization phenotypes. Our analysis identified 12 qualitatively distinct lek vocalization types that can be easily diagnosed by ear, or by visual inspection of sonograms (arbitrarily labeled numerically). See Supplemental Figure 13 for vocalization measures. The inset map indicates the minimum implied ranges for each identified vocalization type, with colors and plotting symbols matching those in PCA plots (Supplemental Figures 14, 15). The thicker pale blue dashed line indicates where the 'southern Amazon' vocalization type 2 may be shared pleisiomorphically, a pattern implied by one recording from Pará, eastern Brazil, which unambiguously clusters with other recordings from the western Napo area of endemism. Vocalization type 2 may therefore occur in other unsampled areas of the southern Amazon. Several vocalization types appear to be unique to a single monophyletic lineage based on overlapping geographic ranges. Vocalization type 4 coincides with the Central American lineage (Clade A2), type 3 with the Northern Amazon + Guiana Shield clade (Clade D) excluding eastern Napo, Jaú), type 7 with the Western Inamabri lineage (Clade C1), type 1 and 10 with the South Andean Peru clades (Clade B). In our initial assessment, we identified vocalization type 6, which has a geographic range which coincides with both the southern Tapajós clade and the Atlantic Forest clade. However, upon closer consideration, we found a subtle difference between the Atlantic Forest (6a) and Tapajós (6b) regions. Type 6a recordings, which are restricted to the Atlantic Forest, have a relatively constant pitch for both the buzz and tonal notes, whereas the type 6b recordings, which are restricted to the Tapajós regions, have a descending pitch for both notes. The sharing of a similar vocal phenotype (6a and 6b) clearly links the Atlantic forest populations to the Southern Amazon, in congruence with our genetic data (Clade C7), even though these southern Tapajós individuals have a genetic affinity to other more northern Tapajós individuals. Lastly, we identified several lek vocalization types with restricted, non-overlapping

geographic ranges in regions for which we lack genetic samples. Vocal type 8 was restricted to Subtropical forests of the eastern slope of the Andes from western Venezuela to Morona-Santiago, Ecuador. Vocal type 9 was restricted to Subtropical forests of western Cauca, Colombia south to Esmeraldas, Ecuador. Lastly, vocal types 11a and 11b were restricted to Subtropical forests of Magdalena Valley, Antioquia to Huila, Colombia. It is likely they fall within the range of variation delimited by the Central America + North Andean Peru clade.

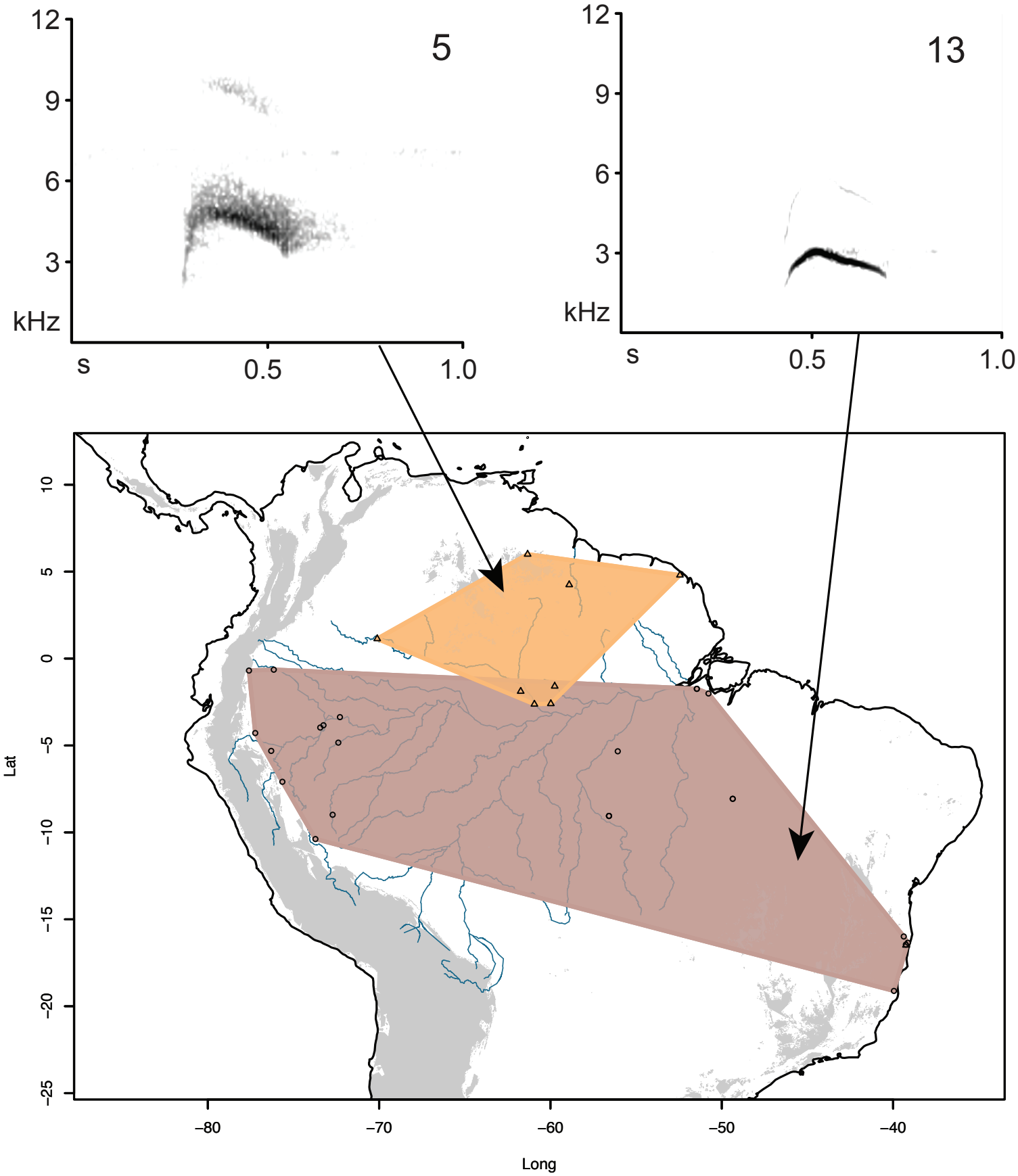
5
13
12
9
6
3
kHz
s
0.5
1.0
10
5
0
−5
−10
−15
−20
−25
Lat
−80
−70
−60
−50
−40
Long

Figure 2.9. Summary of call vocalization phenotypes. Our analysis identified 2 distinct but similar call vocalization types that can be diagnosed by ear, or by visual inspection of sonograms. See Supplemental Figure 13 for vocalization measures. The inset map indicates the minimum implied ranges for each identified call vocalization type, with colors and plotting symbols matching those in the PCA plot (Supplemental Figures 14, 15). Vocalization type 5 was primarily recorded in the northern Amazon basin, coinciding with the broad ranging Northern Amazon + Guiana Shield lineage (Clade D). From our initial unbiased classification, one recording from the Atlantic Forest (XC427315) was assigned to type 5, and is denoted here with a triangle symbol, suggesting type 5 may be shared between the Guiana Shield clade and the Atlantic Forest clade. Call vocalization type 13 was entirely restricted to but shared across diverse lowland southern Amazonian forms (Clade C).

REFERENCES

Agapow PM, Burt A. 2001. Indices of multilocus linkage disequilibrium. Molecular Ecology Notes, 1:101-102.

Andrews S. 2010. FastQC: a quality control tool for high throughput sequence data (http://www.bioinformatics.babraham.ac.uk/projects/fastqc/)

Antonelli A, Ariza M, Albert J, Andermann T, Azevedo J, Bacon C, Faurby S, Guedes T, Hoorn C, Lohmann LG, Matos-Maraví P, Ritter CD, Sanmartín I, Silvestro D, Tejedor M, ter Steege H, Tuomisto H, Werneck FP, Zizka A, Edwards SV. 2018. Conceptual and empirical advances in Neotropical biodiversity research. PeerJ, 6:e5644.

Barrera-Guzmán AO, Aleixo A, Shawkey MD, Weir JT. 2018. Hybrid speciation leads to novel male secondary sexual ornamentation of an Amazonian bird. Proceedings of the National Academy of Sciences, 115:E218-E225.

Bates JM, Zink RM. 1994. Evolution into the Andes: Molecular Evidence for Species Relationships in the Genus Leptopogon. The Auk, 111:507-515.

Berv JS, Prum RO. 2014. A comprehensive multilocus phylogeny of the Neotropical cotingas (Cotingidae, Aves) with a comparative evolutionary analysis of breeding system and plumage dimorphism and a revised phylogenetic classification. Molecular Phylogenetics and Evolution, 81:120-136.

Bioacoustics_Research_Program. 2011. Raven Pro: Interactive Sound Analysis Software (Version 1.4) [Computer software]. Ithaca, NY, The Cornell Laboratory of Ornithology. Available from http://www.birds.cornell.edu/raven.

Bollback JP. 2006. SIMMAP: Stochastic character mapping of discrete traits on phylogenies. BMC Bioinformatics, 7.

Borges SH, Da Silva JMC. 2012. A New Area of Endemism for Amazonian Birds in the Rio Negro Basin. The Wilson Journal of Ornithology, 124:15-23.

Botta F, Eriksen C, Fontaine MC, Guillot G, Yu D. 2015. Enhanced computational methods for quantifying the effect of geographic and environmental isolation on genetic differentiation. Methods in Ecology and Evolution, 6:1270-1277.

Bouckaert R, Heled J, Kühnert D, Vaughan T, Wu C-H, Xie D, Suchard MA, Rambaut A, Drummond AJ. 2014. BEAST 2: A Software Platform for Bayesian Evolutionary Analysis. PLOS Computational Biology, 10:e1003537.

Bradburd G, Coop G, Ralph P. 2017. Inferring Continuous and Discrete Population Genetic Structure Across Space. bioRxiv.

Bradburd GS, Ralph PL, Coop GM. 2013. DISENTANGLING THE EFFECTS OF GEOGRAPHIC AND ECOLOGICAL ISOLATION ON GENETIC DIFFERENTIATION. Evolution, 67:3258-3273.

Brelsford A, Milá B, Irwin DE. 2011. Hybrid origin of Audubon's warbler. Molecular Ecology, 20:2380-2389.

Brown AHD, Feldman MW, Nevo E. 1980. Multilocus Structure of Natal Populations of Hordeum Spontaneum. Genetics, 96:523-536.

Brumfield RT. 2012. Inferring the origins of lowland Neotropical birds. The Auk, 129:367-376.

Brumfield RT, Edwards SV. 2007. EVOLUTION INTO AND OUT OF THE ANDES: A BAYESIAN ANALYSIS OF HISTORICAL DIVERSIFICATION IN THAMNOPHILUS ANTSHRIKES. Evolution, 61:346-367.

Brumfield RT, Liu L, Lum DE, Edwards SV. 2008. Comparison of Species Tree Methods for Reconstructing the Phylogeny of Bearded Manakins (Aves: Pipridae, Manacus) from Multilocus Sequence Data. Systematic Biology, 57:719-731.
Burbrink FT, Gehara M. 2018. The Biogeography of Deep Time Phylogenetic Reticulation. Systematic Biology, 67:743-744.
Campagna L, Gronau I, Silveira LF, Siepel A, Lovette IJ. 2015. Distinguishing noise from signal in patterns of genomic divergence in a highly polymorphic avian radiation. Molecular Ecology, 24:4238-4251.
Campagna L, St. Clair JJH, Lougheed SC, Woods RW, Imberti S, Tubaro PL. 2012. Divergence between passerine populations from the Malvinas – Falkland Islands and their continental counterparts: a comparative phylogeographical study. Biological Journal of the Linnean Society, 106:865-879.
Capurucho JMG, Cornelius C, Borges SH, Cohn-Haft M, Aleixo A, Metzger JP, Ribas CC. 2013. Combining phylogeography and landscape genetics of Xenopipo atronitens (Aves: Pipridae), a white sand campina specialist, to understand Pleistocene landscape evolution in Amazonia. Biological Journal of the Linnean Society, 110:60-76.
Castro-Astor IN. 2014. A Phylogeographic study of two neotropical bird species, the Red-Headed Manakin (Pipna rubrocapilla) and the White-crowned Manakin (Dixiphia pipra). Biology. CUNY Academic Works, CUNY.
Castro-Astor IN, Alves MAS, Cavalcanti RB. 2007. DISPLAY BEHAVIOR AND SPATIAL DISTRIBUTION OF THE WHITE-CROWNED MANAKIN IN THE ATLANTIC FOREST OF BRAZIL. The Condor, 109:155-166.
Catchen J, Hohenlohe PA, Bassham S, Amores A, Cresko WA. 2013. Stacks: an analysis tool set for population genomics. Molecular Ecology, 22:3124-3140.
Chambers EA, Hillis DM. 2019. The Multispecies Coalescent Over-splits Species in the Case of Geographically Widespread Taxa. Systematic Biology.
Chernomor O, Minh BQ, von Haeseler A. 2016. Terrace Aware Data Structure for Phylogenomic Inference from Supermatrices. Systematic Biology, 65:997-1008.
Cheviron ZA, Hackett SJ, Brumfield RT. 2006. Sequence variation in the coding region of the melanocortin-1 receptor gene (MC1R) is not associated with plumage variation in the blue-crowned manakin (Lepidothrix coronata). Proceedings of the Royal Society B: Biological Sciences, 273:1613-1618.
Cheviron ZA, Hackett SJ, Capparella AP. 2005. Complex evolutionary history of a Neotropical lowland forest bird (Lepidothrix coronata) and its implications for historical hypotheses of the origin of Neotropical avian diversity. Molecular Phylogenetics and Evolution, 36:338-357.
Chifman J, Kubatko L. 2014. Quartet Inference from SNP Data Under the Coalescent Model. Bioinformatics, 30:3317-3324.
Chifman J, Kubatko L. 2015. Identifiability of the unrooted species tree topology under the coalescent model with time-reversible substitution processes, site-specific rate variation, and invariable sites. Journal of Theoretical Biology, 374:35-47.
Chou J, Gupta A, Yaduvanshi S, Davidson R, Nute M, Mirarab S, Warnow T. 2015. A comparative study of SVDquartets and other coalescent-based species tree estimation methods. BMC Genomics, 16:S2.
Counterman BA. 2016. Hybrid Speciation. In: Kliman RM editor. Encyclopedia of Evolutionary Biology. Oxford, Academic Press, p. 242-248.

Cracraft J. 1985. Historical Biogeography and Patterns of Differentiation within the South American Avifauna: Areas of Endemism. Ornithological Monographs:49-84.
Cracraft J, Prum RO. 1988. PATTERNS AND PROCESSES OF DIVERSIFICATION: SPECIATION AND HISTORICAL CONGRUENCE IN SOME NEOTROPICAL BIRDS. Evolution, 42:603-620.
Crother BI, Murray CM. 2011. Ontology of areas of endemism. Journal of Biogeography, 38:1009-1015.
Cunningham CW, Collins TM. 1994. Developing model systems for molecular biogeography: Vicariance and interchange in marine invertebrates. In: Schierwater B, Streit B, Wagner GP, DeSalle R editors. Molecular Ecology and Evolution: Approaches and Applications. Basel, Birkhäuser Basel, p. 405-433.
Da Silva J, Novaes F, Oren D. 2002. Differentiation of Xiphocolaptes (Dendrocolaptidae) across the river Xingu, Brazilian Amazonia: recognition of a new phylogenetic species and biogeographic implications. BULLETIN-BRITISH ORNITHOLOGISTS CLUB, 122:185-193.
da Silva JMC. 1995. Biogeographic analysis of the South American Cerrado avifauna. Steenstrupia, 21:49-67.
da Silva JMC, de Sousa MC, H. M. Castelletti C. 2004. Areas of Endemism for Passerine Birds in the Atlantic Forest, South America. Global Ecology and Biogeography, 13:85-92.
Da Silva JMC, Rylands AB, Da Fonseca GAB. 2005. The Fate of the Amazonian Areas of Endemism. Conservation Biology, 19:689-694.
de Queiroz K. 2005. Ernst Mayr and the modern concept of species. Proceedings of the National Academy of Sciences, 102:6600-6607.
Dickinson E. 2003. The Howard and Moore Complete Checklist of the Birds of the World Christopher Helm. London.
Diniz-Filho JAF, Soares TN, Lima JS, Dobrovolski R, Landeiro VL, de Campos Telles MP, Rangel TF, Bini LM. 2013. Mantel test in population genetics. Genetics and Molecular Biology, 36:475-485.
Earl DA, vonHoldt BM. 2012. STRUCTURE HARVESTER: a website and program for visualizing STRUCTURE output and implementing the Evanno method. Conservation Genet Resour, 4:359-361.
Evanno G, Regnaut S, Goudet J. 2005. Detecting the number of clusters of individuals using the software structure: a simulation study. Molecular Ecology, 14:2611-2620.
Excoffier L, Smouse PE, Quattro JM. 1992. Analysis of Molecular Variance Inferred from Metric Distances among DNA Haplotypes: Application to Human Mitochondrial DNA Restriction Data. Genetics, 131:479-491.
Fernandes A, Cohn-Haft M, Hrbek T, Farias I. 2015. Rivers acting as barriers for bird dispersal in the Amazon. Revista Brasileira de Ornitologia-Brazilian Journal of Ornithology, 22:363-373.
Fernandes AM, Gonzalez J, Wink M, Aleixo A. 2013. Multilocus phylogeography of the Wedge-billed Woodcreeper Glyphorynchus spirurus (Aves, Furnariidae) in lowland Amazonia: Widespread cryptic diversity and paraphyly reveal a complex diversification pattern. Molecular Phylogenetics and Evolution, 66:270-282.
Fjeldså J. 1992. Biogeographic patterns and evolution of the avifauna of relict high-attitude woodlands of the Andes. Steenstrupia:9-62.

Francisco MR, Gibbs HL, Galetti M, Lunardi VO, Junior PMG. 2007. Genetic structure in a tropical lek-breeding bird, the blue manakin (Chiroxiphia caudata) in the Brazilian Atlantic Forest. Molecular Ecology, 16:4908-4918.
Freile JF. 2014. First record of White-crowned Manakin Dixiphia pipra in western Ecuador. Bull. Brit. Orn. Club, 134:238-240.
Gene_Codes_Corporation. 2010. Sequencher version 5.0 sequence analysis software. Ann Arbor Michigan.
Gordon A, Hannon G. 2010. Fastx-toolkit. FASTQ/A short-reads preprocessing tools (unpublished) http://hannonlab. cshl. edu/fastx_toolkit, 5.
Goslee SC, Urban DL. 2007. The ecodist package for dissimilarity-based analysis of ecological data. Journal of Statistical Software, 22:1-19.
Gosselin T, Anderson EC, Ferchaud A-L. 2016. thierrygosselin/assigner: v.0.4.0 (Version 0.4.0). Zenodo. http://doi.org/10.5281/zenodo.197418.
Goudet J. 2005. hierfstat, a package for r to compute and test hierarchical F-statistics. Molecular Ecology Notes, 5:184-186.
Gronau I, Hubisz MJ, Gulko B, Danko CG, Siepel A. 2011. Bayesian inference of ancient human demography from individual genome sequences. Nature Genetics, 43:1031.
Gubili C, Ritter CD, Motta J, Farias IP, Bates J, Canton R, Capurucho JMG, Cornelius C, Feldheim KA, Ribas CC. 2016. Isolation and characterization of polymorphic microsatellite DNA Markers from an Amazonian white-sand vegetation specialist bird, Xenopipo atronitens (Aves: Pipridae). The Wilson Journal of Ornithology, 128:668-672.
Guillot G, Rousset F. 2013. Dismantling the Mantel tests. Methods in Ecology and Evolution, 4:336-344.
Guillot G, Schilling R, Porcu E, Bevilacqua M. 2013. Validity of covariance models for the analysis of geographical variation. arXiv:1311.4136.
Haffer J. 1969. Speciation in Amazonian Forest Birds. Science, 165:131-137.
Haffer J. 1974. Avian speciation in tropical South America, with a systematic survey of the toucans (Ramphastidae) and jacamars (Galbulidae) (Publications of the Nuttall Ornithological Club No. 14, Cambridge, MA).
Haffer J. 1978. Distribution of Amazon forest birds. Bonner Zoologische Beiträge, 29:38-78.
Haffer J. 1985. Avian zoogeography of the Neotropical lowlands. Ornithological Monographs:113-146.
Haffer J. 1992. On the river effect in some forest birds of southern Amazonia. Boletim do Museu Paraense Emílio Goeldi. Nova série. Zoologia, 8:217-245.
Haffer J. 2008. Hypotheses to explain the origin of species in Amazonia. Brazilian Journal of Biology, 68:917-947.
Hartl DL, Clark AG. 1997. Principles of population genetics. Sinauer associates Sunderland, MA.
Harvey MG, Aleixo A, Ribas CC, Brumfield RT. 2017. Habitat Association Predicts Genetic Diversity and Population Divergence in Amazonian Birds. The American Naturalist, 190:631-648.
Harvey MG, Brumfield RT. 2015. Genomic variation in a widespread Neotropical bird (Xenops minutus) reveals divergence, population expansion, and gene flow. Molecular Phylogenetics and Evolution, 83:305-316.

Hazzi NA, Moreno JS, Ortiz-Movliav C, Palacio RD. 2018. Biogeographic regions and events of isolation and diversification of the endemic biota of the tropical Andes. Proceedings of the National Academy of Sciences.
Hermansen JS, Sæther SA, Elgvin TO, Borge T, Hjelle E, Sætre G-P. 2011. Hybrid speciation in sparrows I: phenotypic intermediacy, genetic admixture and barriers to gene flow. Molecular Ecology, 20:3812-3822.
Hijmans RJ, Williams E, Vennes C. 2015. Geosphere: spherical trigonometry. R package version 1.3-11. URL: https://CRAN. R-project. org/package= geosphere.
Hoang DT, Vinh LS, Chernomor O, Minh BQ, von Haeseler A. 2017. UFBoot2: Improving the Ultrafast Bootstrap Approximation. Molecular Biology and Evolution, 35:518-522.
Hooghiemstra H, Van der Hammen T. 2004. Quaternary Ice-Age dynamics in the Colombian Andes: developing an understanding of our legacy. Philosophical Transactions of the Royal Society of London. Series B: Biological Sciences, 359:173-181.
Hothorn T, Bretz F, Westfall P, Heiberger RM, Schuetzenmeister A, Scheibe S. 2013. multcomp: simultaneous inference in general parametric models. R package version 1.2-18. Foundation for Statistical Computing, Vienna, Austria.
Huelsenbeck JP, Nielsen R, Bollback JP. 2003. Stochastic Mapping of Morphological Characters. Systematic Biology, 52:131-158.
Jakobsson M, Rosenberg NA. 2007. CLUMPP: a cluster matching and permutation program for dealing with label switching and multimodality in analysis of population structure. Bioinformatics, 23:1801-1806.
Jiggins CD, Salazar C, Linares M, Mavarez J. 2008. Hybrid trait speciation and Heliconius butterflies. Philosophical Transactions of the Royal Society B: Biological Sciences, 363:3047-3054.
Jombart T. 2008. adegenet: a R package for the multivariate analysis of genetic markers. Bioinformatics, 24:1403-1405.
Kalyaanamoorthy S, Minh BQ, Wong TKF, von Haeseler A, Jermiin LS. 2017. ModelFinder: fast model selection for accurate phylogenetic estimates. Nature Methods, 14:587.
Kamvar ZN, Tabima JF, Grünwald NJ. 2014. Poppr: an R package for genetic analysis of populations with clonal, partially clonal, and/or sexual reproduction. PeerJ, 2:e281.
Kirwan GM, David N, Gregory SM, Jobling JA, Steinheimer FD, Brito GRR. 2016. The mistaken manakin: a new genus-group name for Parus pipra Linnaeus, 1758 (Aves: Passeriformes: Pipridae). Zootaxa, 4121:89-94.
Kirwan GM, Green G. 2012. Cotingas and Manakins. Princeton, NJ, Princeton University Press.
Kuhner MK. 2006. LAMARC 2.0: maximum likelihood and Bayesian estimation of population parameters. Bioinformatics, 22:768-770.
Kumar S, Subramanian S. 2002. Mutation rates in mammalian genomes. Proceedings of the National Academy of Sciences, 99:803-808.
Lamichhaney S, Han F, Webster MT, Andersson L, Grant BR, Grant PR. 2018. Rapid hybrid speciation in Darwin's finches. Science, 359:224-228.
Lanfear R, Frandsen PB, Wright AM, Senfeld T, Calcott B. 2017. PartitionFinder 2: New Methods for Selecting Partitioned Models of Evolution for Molecular and Morphological Phylogenetic Analyses. Molecular Biology and Evolution, 34:772-773.
Langmead B, Trapnell C, Pop M, Salzberg SL. 2009. Ultrafast and memory-efficient alignment of short DNA sequences to the human genome. Genome Biology, 10:R25.

Lavretsky P, Engilis A, Eadie JM, Peters JL. 2015. Genetic admixture supports an ancient hybrid origin of the endangered Hawaiian duck. Journal of Evolutionary Biology, 28:1005-1015.
Lawson DJ, Hellenthal G, Myers S, Falush D. 2012. Inference of Population Structure using Dense Haplotype Data. PLOS Genetics, 8:e1002453.
Leaché AD, Banbury BL, Felsenstein J, de Oca An-M, Stamatakis A. 2015. Short Tree, Long Tree, Right Tree, Wrong Tree: New Acquisition Bias Corrections for Inferring SNP Phylogenies. Systematic Biology, 64:1032-1047.
Leaché AD, Zhu T, Rannala B, Yang Z. 2018. The Spectre of Too Many Species. Systematic Biology:syy051-syy051.
Legendre P, Fortin M-J. 2010. Comparison of the Mantel test and alternative approaches for detecting complex multivariate relationships in the spatial analysis of genetic data. Molecular Ecology Resources, 10:831-844.
Linck EB, Battey CJ. 2017. Minor allele frequency thresholds strongly affect population structure inference with genomic datasets. bioRxiv.
Linder HP. 2001. On Areas of Endemism, with an Example from the African Restionaceae. Systematic Biology, 50:892-912.
Long C, Kubatko L. 2017. The effect of gene flow on coalescent-based species-tree inference. arXiv:1710.03806.
Luna LW, Souza TO, e Silva WAdG, Schneider H, Sampaio I. 2017. Genetic variation of the endangered Araripe Manakin (Antilophia bokermanni) indicates a history of demographic decline. Revista Brasileira de Ornitologia, 25:60-66.
Lynch Alfaro JW, Boubli JP, Paim FP, Ribas CC, Silva MNFd, Messias MR, Röhe F, Mercês MP, Silva Júnior JS, Silva CR, Pinho GM, Koshkarian G, Nguyen MTT, Harada ML, Rabelo RM, Queiroz HL, Alfaro ME, Farias IP. 2015. Biogeography of squirrel monkeys (genus Saimiri): South-central Amazon origin and rapid pan-Amazonian diversification of a lowland primate. Molecular Phylogenetics and Evolution, 82:436-454.
MacQueen J. 1967. Some methods for classification and analysis of multivariate observations. Proceedings of the Fifth Berkeley Symposium on Mathematical Statistics and Probability, Volume 1: Statistics. Berkeley, Calif., University of California Press, p. 281-297.
Malinsky M, Trucchi E, Lawson DJ, Falush D. 2018. RADpainter and fineRADstructure: Population Inference from RADseq Data. Molecular Biology and Evolution, 35:1284-1290.
Mantel N. 1967. The detection of disease clustering and a generalized regression approach. Cancer research, 27:209-220.
Marks BD, Hackett SJ, Capparella AP. 2002. Historical relationships among Neotropical lowland forest areas of endemism as determined by mitochondrial DNA sequence variation within the Wedge-billed Woodcreeper (Aves: Dendrocolaptidae: Glyphorynchus spirurus). Molecular Phylogenetics and Evolution, 24:153-167.
Marques DA, Meier JI, Seehausen O. 2019. A Combinatorial View on Speciation and Adaptive Radiation. Trends in Ecology & Evolution.
Mayr E. 1942. Systematics and the origin of species from the viewpoint of a zoologist. Columbia University Press.
McDonald DB. 2003. MICROSATELLITE DNA EVIDENCE FOR GENE FLOW IN NEOTROPICAL LEK-MATING LONG-TAILED MANAKINS. The Condor, 105:580-586.

Milá B, Tavares ES, Muñoz Saldaña A, Karubian J, Smith TB, Baker AJ. 2012. A Trans-Amazonian Screening of mtDNA Reveals Deep Intraspecific Divergence in Forest Birds and Suggests a Vast Underestimation of Species Diversity. PLOS ONE, 7:e40541.
Moore RP, Robinson WD, Lovette IJ, Robinson TR. 2008. Experimental evidence for extreme dispersal limitation in tropical forest birds. Ecology Letters, 11:960-968.
Musher LJ, Ferreira M, Auerbach AL, McKay J, Cracraft J. 2019. Why is Amazonia a ‘source’ of biodiversity? Climate-mediated dispersal and synchronous speciation across the Andes in an avian group (Tityrinae). Proceedings of the Royal Society B: Biological Sciences, 286:20182343.
Naka LN. 2011. Avian distribution patterns in the Guiana Shield: implications for the delimitation of Amazonian areas of endemism. Journal of Biogeography, 38:681-696.
Naka LN, Brumfield RT. 2018. The dual role of Amazonian rivers in the generation and maintenance of avian diversity. Science Advances, 4.
Nieto Feliner G, Álvarez I, Fuertes-Aguilar J, Heuertz M, Marques I, Moharrek F, Piñeiro R, Riina R, Rosselló JA, Soltis PS, Villa-Machío I. 2017. Is homoploid hybrid speciation that rare? An empiricist's view. Heredity, 118:513.
Noguera-urbano EA. 2016. Areas of endemism: travelling through space and the unexplored dimension. Systematics and Biodiversity, 14:131-139.
Nyári ÁS. 2007. Phylogeographic patterns, molecular and vocal differentiation, and species limits in Schiffornis turdina (Aves). Molecular Phylogenetics and Evolution, 44:154-164.
Nylander JAA, Olsson U, Alström P, Sanmartín I. 2008. Accounting for Phylogenetic Uncertainty in Biogeography: A Bayesian Approach to Dispersal-Vicariance Analysis of the Thrushes (Aves: Turdus). Systematic Biology, 57:257-268.
Ohlson JI, Fjeldså J, Ericson PGP. 2013. Molecular phylogeny of the manakins (Aves: Passeriformes: Pipridae), with a new classification and the description of a new genus. Molecular Phylogenetics and Evolution, 69:796-804.
Oliveira U, Vasconcelos MF, Santos AJ. 2017. Biogeography of Amazon birds: rivers limit species composition, but not areas of endemism. Scientific Reports, 7:2992.
Paradis E. 2010. pegas: an R package for population genetics with an integrated–modular approach. Bioinformatics, 26:419-420.
Paris JR, Stevens JR, Catchen JM, Johnston S. 2017. Lost in parameter space: a road map for stacks. Methods in Ecology and Evolution, 8:1360-1373.
Peterson BK, Weber JN, Kay EH, Fisher HS, Hoekstra HE. 2012. Double Digest RADseq: An Inexpensive Method for De Novo SNP Discovery and Genotyping in Model and Non-Model Species. PLOS ONE, 7:e37135.
Petkova D, Novembre J, Stephens M. 2015. Visualizing spatial population structure with estimated effective migration surfaces. Nature Genetics, 48:94.
Pritchard JK, Stephens M, Donnelly P. 2000. Inference of Population Structure Using Multilocus Genotype Data. Genetics, 155:945-959.
Prum RO. 1990a. Phylogenetic Analysis of the Evolution of Display Behavior in the Neotropical Manakins (Aves: Pipridae). Ethology, 84:202-231.
Prum RO. 1990b. A test of the monophyly of the manakins (Pipridae) and of the cotingas (Cotingidae) based on morphology. Occasional Papers of the Museum of Zoology of the University of Michigan, 723:1-44.
Prum RO. 1992. Syringeal morphology, phylogeny, and evolution of the neotropical manakins (Aves, Pipridae). American Museum novitates; no. 3043.

Prum RO. 1994. PHYLOGENETIC ANALYSIS OF THE EVOLUTION OF ALTERNATIVE SOCIAL BEHAVIOR IN THE MANAKINS (AVES: PIPRIDAE). Evolution, 48:1657-1675.
Pupim FN, Sawakuchi AO, Almeida RP, Ribas CC, Kern AK, Hartmann GA, Chiessi CM, Tamura LN, Mineli TD, Savian JF, Grohmann CH, Bertassoli DJ, Stern AG, Cruz FW, Cracraft J. 2019. Chronology of Terra Firme formation in Amazonian lowlands reveals a dynamic Quaternary landscape. Quaternary Science Reviews, 210:154-163.
Quintero I, Jetz W. 2018. Global elevational diversity and diversification of birds. Nature, 555:246.
R_Core_Team. 2018. R: A language and environment for statistical computing.
Rambaut A, Drummond AJ, Xie D, Baele G, Suchard MA. 2018. Posterior Summarization in Bayesian Phylogenetics Using Tracer 1.7. Systematic Biology, 67:901-904.
Räsänen ME, Salo JS, Kalliola RJ. 1987. Fluvial perturbance in the western Amazon basin: regulation by long-term sub-Andean tectonics. Science, 238:1398-1401.
Reichenbach HG. 1850. Avium Systema Naturale: Vorläufer einer Iconographie der Arten der Vögel aller Welttheile, welche, nachdem bereits fast dreitausend Abbildungen erschienen sind, ununterbrochen fortgesetzt wird. Hofmeister.
Revell LJ. 2012. Phytools: An R package for phylogenetic comparative biology (and other things). Methods in Ecology and Evolution, 3:217-223.
Ribas CC, Aleixo A, Nogueira ACR, Miyaki CY, Cracraft J. 2012. A palaeobiogeographic model for biotic diversification within Amazonia over the past three million years. Proceedings of the Royal Society B: Biological Sciences, 279:681-689.
Ribas CC, Moyle RG, Miyaki CY, Cracraft J. 2007. The assembly of montane biotas: linking Andean tectonics and climatic oscillations to independent regimes of diversification in Pionus parrots. Proceedings of the Royal Society B: Biological Sciences, 274:2399-2408.
Ridgely RS, Greenfield PJ. 2001. The birds of Ecuador: status, distribution, and taxonomy. Cornell University Press.
Ridgely RS, Tudor G. 2009. Field guide to the songbirds of South America: the passerines. University of Texas Press.
Roure B, Baurain D, Philippe H. 2013. Impact of Missing Data on Phylogenies Inferred from Empirical Phylogenomic Data Sets. Molecular Biology and Evolution, 30:197-214.
Rousset F. 1997. Genetic Differentiation and Estimation of Gene Flow from F-Statistics Under Isolation by Distance. Genetics, 145:1219-1228.
Salazar C, Baxter SW, Pardo-Diaz C, Wu G, Surridge A, Linares M, Bermingham E, Jiggins CD. 2010. Genetic Evidence for Hybrid Trait Speciation in Heliconius Butterflies. PLOS Genetics, 6:e1000930.
Santorelli S, Magnusson WE, Deus CP. 2018. Most species are not limited by an Amazonian river postulated to be a border between endemism areas. Scientific Reports, 8:2294.
Saranathan V, Hamilton D, Powell GVN, Kroodsma DE, Prum RO. 2007. Genetic evidence supports song learning in the three-wattled bellbird Procnias tricarunculata (Cotingidae). Molecular Ecology, 16:3689-3702.
Schmidt HA, Minh BQ, von Haeseler A, Nguyen L-T. 2014. IQ-TREE: A Fast and Effective Stochastic Algorithm for Estimating Maximum-Likelihood Phylogenies. Molecular Biology and Evolution, 32:268-274.

Schmidt-Lebuhn AN, Aitken NC, Chuah A. 2017. Species trees from consensus single nucleotide polymorphism (SNP) data: Testing phylogenetic approaches with simulated and empirical data. Molecular Phylogenetics and Evolution, 116:192-201.
Schumer M, Rosenthal GG, Andolfatto P. 2014. HOW COMMON IS HOMOPLOID HYBRID SPECIATION? Evolution, 68:1553-1560.
Sedano RE, Burns KJ. 2010. Are the Northern Andes a species pump for Neotropical birds? Phylogenetics and biogeography of a clade of Neotropical tanagers (Aves: Thraupini). Journal of Biogeography, 37:325-343.
Shafer ABA, Peart CR, Tusso S, Maayan I, Brelsford A, Wheat CW, Wolf JBW. 2017. Bioinformatic processing of RAD-seq data dramatically impacts downstream population genetic inference. Methods in Ecology and Evolution, 8:907-917.
Silva SM, Peterson AT, Carneiro L, Burlamaqui TC, Ribas CC, Sousa Neves T, Miranda L, Fernandes AM, D'horta FM, Araujo-Silva LE, Batista R, Bandeira CHMM, Dantas S, Ferreira M, Martins DM, Oliveira J, Rocha TC, Sardelli CH, Thom G, Rego PS, Santos MPD, Sequeira F, Vallinoto MN, Alexio ALP. 2019. A dynamic continental moisture gradient drove Amazonian bird diversification. Science Advances, in press.
Smeds L, Qvarnström A, Ellegren H. 2016. Direct estimate of the rate of germline mutation in a bird. Genome Research, 26:1211-1218.
Smith BT, McCormack JE, Cuervo AM, Hickerson MJ, Aleixo A, Cadena CD, Perez-Eman J, Burney CW, Xie X, Harvey MG, Faircloth BC, Glenn TC, Derryberry EP, Prejean J, Fields S, Brumfield RT. 2014. The drivers of tropical speciation. Nature, 515:406-409.
Smith RH. 1979. On selection for inbreeding in polygynous animals. Heredity, 43:205.
Snow D. 1961. THE DISPLAYS OF THE MANAKINS PIPRA PIPRA AND TYRANNEUTES VIRESCENS*. Ibis, 103A:110-113.
Snow DW. 1979. Tityrinae, Pipridae, Cotingidae. In: M. A. Traylor J editor. Check-list of birds of the world. Cambridge, Massachusetts, Museum of Comparative Zoology, Harvard Univ., p. 229-308.
Snow DW. 2004. Family Pipridae (Manakins). In: del Hoyo J, Elliot A, Christie DA editors. Handbook of the Birds of the World. Barcelona, Lynx Edicions, p. 110-169.
Spencer A. 2012. White-crowned Manakin vocal variation. Xeno-Cango.org.
Stamatakis A. 2014. RAxML version 8: a tool for phylogenetic analysis and post-analysis of large phylogenies. Bioinformatics, 30:1312-1313.
Standley DM, Katoh K. 2013. MAFFT Multiple Sequence Alignment Software Version 7: Improvements in Performance and Usability. Molecular Biology and Evolution, 30:772-780.
Stopher KV, Nussey DH, Clutton-Brock TH, Guinness F, Morris A, Pemberton JM. 2012. Re-mating across years and intralineage polygyny are associated with greater than expected levels of inbreeding in wild red deer. Journal of Evolutionary Biology, 25:2457-2469.
Suh A. 2016. The phylogenomic forest of bird trees contains a hard polytomy at the root of Neoaves. Zoologica Scripta, 45:50-62.
Sukumaran J, Knowles LL. 2017. Multispecies coalescent delimits structure, not species. Proceedings of the National Academy of Sciences, 114:1607-1612.
Swofford DL. 2002. Phylogenetic analysis using parsimony (*and Other Methods). Version 4. Sinauer Associates, Sunderland, Massachusetts.

Tello JG, Moyle RG, Marchese DJ, Cracraft J. 2009. Phylogeny and phylogenetic classification of the tyrant flycatchers, cotingas, manakins, and their allies (Aves: Tyrannides). Cladistics, 25:429-467.
Teske PR, Golla TR, Sandoval-Castillo J, Emami-Khoyi A, van der Lingen CD, von der Heyden S, Chiazzari B, Jansen van Vuuren B, Beheregaray LB. 2018. Mitochondrial DNA is unsuitable to test for isolation by distance. Scientific Reports, 8:8448.
Thom G, Amaral FRD, Hickerson MJ, Aleixo A, Araujo-Silva LE, Ribas CC, Choueri E, Miyaki CY. 2018. Phenotypic and Genetic Structure Support Gene Flow Generating Gene Tree Discordances in an Amazonian Floodplain Endemic Species. Systematic Biology, 67:700-718.
Thrasher DJ, Butcher BG, Campagna L, Webster MS, Lovette IJ. 2018. Double-digest RAD sequencing outperforms microsatellite loci at assigning paternity and estimating relatedness: A proof of concept in a highly promiscuous bird. Molecular Ecology Resources, 0.
Trifinopoulos J, Nguyen L-T, Minh BQ, von Haeseler A. 2016. W-IQ-TREE: a fast online phylogenetic tool for maximum likelihood analysis. Nucleic Acids Research, 44:W232-W235.
Vaidya G, Lohman DJ, Meier R. 2011. SequenceMatrix: concatenation software for the fast assembly of multi-gene datasets with character set and codon information. Cladistics, 27:171-180.
van Els P, Norambuena HV, Etienne RS. 2019. From pampa to puna: Biogeography and diversification of a group of Neotropical obligate grassland birds (Anthus: Motacillidae). Journal of Zoological Systematics and Evolutionary Research, 00: 1– 12.
Voelker G. 1999. DISPERSAL, VICARIANCE, AND CLOCKS: HISTORICAL BIOGEOGRAPHY AND SPECIATION IN A COSMOPOLITAN PASSERINE GENUS (ANTHUS: MOTACILLIDAE). Evolution, 53:1536-1552.
Wahlund S. 1928. ZUSAMMENSETZUNG VON POPULATIONEN UND KORRELATIONSERSCHEINUNGEN VOM STANDPUNKT DER VERERBUNGSLEHRE AUS BETRACHTET. Hereditas, 11:65-106.
Wallace AR. 1854. On the monkeys of the Amazon. Annals and Magazine of Natural History, 14:451-454.
Waser PM, Austad SN, Keane B. 1986. When Should Animals Tolerate Inbreeding? The American Naturalist, 128:529-537.
Weir BS, Cockerham CC. 1984. ESTIMATING F-STATISTICS FOR THE ANALYSIS OF POPULATION STRUCTURE. Evolution, 38:1358-1370.
Weir JT. 2006. DIVERGENT TIMING AND PATTERNS OF SPECIES ACCUMULATION IN LOWLAND AND HIGHLAND NEOTROPICAL BIRDS. Evolution, 60:842-855.
Wen D, Yu Y, Zhu J, Nakhleh L. 2018. Inferring Phylogenetic Networks Using PhyloNet. Systematic Biology:syy015-syy015.
Zamudio KR, Bell RC, Mason NA. 2016. Phenotypes in phylogeography: Species' traits, environmental variation, and vertebrate diversification. Proceedings of the National Academy of Sciences of the United States of America, 113:8041-8048.
Zhu J, Wen D, Yu Y, Meudt HM, Nakhleh L. 2018. Bayesian inference of phylogenetic networks from bi-allelic genetic markers. PLOS Computational Biology, 14:e1005932.

CHAPTER 3

A comprehensive phylogeny of birds (Aves) using targeted next-generation DNA sequencing[III]

Richard O. Prum[1,2]*, Jacob S. Berv[3]*, Alex Dornburg[1,2,4], Daniel J. Field[2,5], Jeffrey P. Townsend[1,6], Emily Moriarty Lemmon[7] & Alan R. Lemmon[8]

1. Department of Ecology & Evolutionary Biology, Yale University, New Haven, Connecticut 06520, USA.
2. Peabody Museum of Natural History, Yale University, New Haven, Connecticut 06520, USA.
3. Department of Ecology and Evolutionary Biology, Fuller Evolutionary Biology Program, Cornell University, and Cornell Laboratory of Ornithology, Ithaca, New York 14853, USA.
4. North Carolina Museum of Natural Sciences, Raleigh, North Carolina 27601, USA.
5. Department of Geology & Geophysics, Yale University, New Haven, Connecticut 06520, USA.
6. Department of Biostatistics, and Program in Computational Biology and Bioinformatics, Yale University, New Haven, Connecticut 06520, USA.
7. Department of Biological Science, Florida State University, Tallahassee, Florida 32306, USA.

[III] Reviewed, formatted, and accepted for publication as Prum, R.O.*, Berv, J.S.*, Dornburg, A., Field, D. J., Townsend, J.P., Lemmon, E.M., Lemmon, A. R. A comprehensive phylogeny of birds (Aves) using targeted next-generation DNA sequencing, Nature (2015), doi:10.1038/nature15697. Reprinted here with permission.

8. Department of Scientific Computing, Florida State University, Tallahassee, Florida 32306, USA.

*These authors contributed equally to this work.

Although reconstruction of the phylogeny of living birds has progressed tremendously in the last decade, the evolutionary history of Neoaves—a clade that encompasses nearly all living bird species— remains the greatest unresolved challenge in dinosaur systematics. Here we investigate avian phylogeny with an unprecedented scale of data > 390,000 bases of genomic sequence data from each of 198 species of living birds, representing all major avian lineages, and two crocodilian outgroups. Sequence data were collected using anchored hybrid enrichment, yielding 259 nuclear loci with an average length of 1,523 bases for a total data set of over 7.8 x 10^7 bases. Bayesian and maximum likelihood analyses yielded highly supported and nearly identical phylogenetic trees for all major avian lineages. Five major clades form successive sister groups to the rest of Neoaves: (1) a clade including nightjars, other caprimulgiforms, swifts, and hummingbirds; (2) a clade uniting cuckoos, bustards, and turacos with pigeons, mesites, and sandgrouse; (3) cranes and their relatives; (4) a comprehensive waterbird clade, including all diving, wading, and shorebirds; and (5) a comprehensive landbird clade with the enigmatic hoatzin (Opisthocomus hoazin) as the sister group to the rest. Neither of the two main, recently proposed Neoavian clades—Columbea and Passerea[1]— were supported as monophyletic. The results of our divergence time analyses are congruent with the palaeontological record, supporting a major radiation of crown birds in the wake of the Cretaceous–Palaeogene (K–Pg) mass extinction.

Birds (Aves) are the most diverse lineage of extant tetrapod vertebrates. They comprise over 10,000 living species[2], and exhibit an extra- ordinary diversity in morphology, ecology, and behaviour[3]. Substantial progress has been made in resolving the phylogenetic history of birds. Phylogenetic analyses of both molecular and morphological data support the monophyletic Palaeognathae (the tinamous and flightless ratites) and Galloanserae (gamebirds and waterfowl) as successive, monophyletic sister groups to the Neoaves—a diverse clade including all other living birds[4]. Resolving neoavian phylogeny has proven to be a difficult challenge because this radiation was very rapid and deep in time, resulting in very short internodes[4].

In the last decade, phylogenetic analyses of large, multilocus data sets have resulted in the proposal of numerous, novel neoavian relationships. For example, a clade consisting of diving and wading birds has been consistently recovered, as well as a large landbird clade in which falcons and parrots are successive sister groups to the perching birds[4-8]. Recently, phylogenetic analyses of 48 whole avian genomes resulted in the proposal of a novel phylogenetic resolution of the initial branching sequence within Neoaves[1]. Although this genomic study provided much needed corroboration of many neoavian clades, the limited taxon sampling precluded further insights into the evolutionary history of birds.

It has long been recognized that phylogenetic confidence depends not only on the number of characters analysed and their rate of evolution, but also on the number and relationships of the taxa sampled relative to the nodes of interest[9-11]. Theory predicts that sampling a single taxon that diverges close to a node of interest will have a far greater effect on phylogenetic resolution than will adding more characters[11]. Despite using an alignment of >40 million base pairs, sparse sampling of 48 species in the recent avian genomic analysis may not have been sufficient to confidently resolve the deep divergences among major lineages of

Neoaves. Thus, expanded taxon sampling is required to test the monophyly of neoavian clades, and to further resolve the phylogenetic relationships within Neoaves.

Here, we present a phylogenetic analysis of 198 bird species and 2 crocodilians (Supplementary Table 1) based on loci captured using anchored enrichment[12]. Our sample includes species of 122 avian families in all 40 extant avian orders[2], with denser representation of non-oscine birds (108 families) than of oscine songbirds (14 families). Effort was made to include taxa that would break up long phylogenetic branches, and provide the highest likelihood of resolving short internodes at the base of Neoaves[11]. We also sampled multiple species within groups whose monophyly or phylogenetic interrelationships have been controversial—that is, tinamous, nightjars, hummingbirds, turacos, cuckoos, pigeons, sandgrouse, mesites, rails, storm petrels, petrels, storks, herons, hawks, hornbills, mousebirds, trogons, king- fishers, barbets, seriemas, falcons, parrots, and suboscine passerines.

We targeted 394 loci centred on conserved anchor regions of the genome that are flanked by more variable regions[12]. We performed all phylogenetic analyses on a data set of 259 genes with the highest quality assemblies. The average locus was 1,524 bases in length (361–2,316 base pairs (bp)), and the total percentage of missing data was 1.84%. The concatenated alignment contained 394,684 sites. To minimize overall model complexity while accurately accounting for substitution processes, we performed a partition model sensitivity analysis with PartitionFinder[13,14], and compared a complex partition model (one partition per locus) to a heuristically optimized (rclust) partition model. Phylogenetic informativeness (PI) approaches[15,16] provided strong evidence that the phylogenetic utility of our data set was high, with low declines in PI profiles for individual loci, data set partitions, and the concatenated matrix (Supplementary Fig. 4). We estimated concatenated trees in ExaBayes[17] and RAxML[18] using a 75 partition model. Coalescent species trees were estimated

with the gene tree summation methods in STAR[19], NJst[20], and ASTRAL[21] from gene trees estimated with RAxML (see Methods.).

Our concatenated Bayesian analyses resulted in a completely resolved, well supported phylogeny. All clades had a posterior probability (PP) of 1, except for a single clade including shoebill (*Balaeniceps*) and pelican (PP = 0.54) (Fig. 1). The concatenated maximum likelihood analysis recovered a single topology that was identical to the Bayesian tree except for three clades, all of which are far from the base of Neoaves: the relationships among pigeons; among skimmers, gulls, and terns; and among pelicans, shoebill, and waders (Supplementary Fig. 1). Almost all clades in the maximum likelihood tree were maximally supported with bootstrap scores (BS) of 1.00, but nine clades within Neoaves (including four of the most inclusive neoavian clades) received support < 0.70 (Supplementary Fig. 1). Coalescent species tree analyses produced substantially different hypotheses for neoavian relationships (Supplementary Fig. 3), but most of the discordant clades received conspicuously lower bootstrap support values (0.07 < BS < 0.30). Quantifying the phylogenetic informativeness of individual loci[15, 16] revealed that these low support values were not due to homoplasy driven by saturation of nucleotide states, but rather by the low power of individual loci to resolve the entire range of internode lengths across the depth of the tree (Supplementary Figs 4 and 5; see Methods). This result was not unexpected. The low phylogenetic information content of individual genes at deep timescales has been demonstrated to impede phylogenetic resolution in a coalescent species tree framework[22,23]. Furthermore, when clades with > 0.75 bootstrap support values in the species trees are collapsed, the resulting topology is exactly congruent with the concatenated Bayesian tree (except for the relationships of tinamous among palaeognaths; Supplementary Fig. 3). Although coalescent species trees account for incomplete lineage sorting, simulations show that

species tree methods based on gene tree summation may not provide significantly better performance over concatenation methods[22].

Our phylogeny identifies many new clades, and supports many phylogenetic relationships proposed in previous studies (see detailed phylogenetic discussion in the Supplementary Information). Congruent with all recent studies, the phylogeny places palaeognaths as the sister group to the rest of birds, and the flying tinamous (Tinamidae) within the flightless ratites. This tree, however, places tinamous as the sister group to cassowary and emu alone (Fig. 1, grey). The phylogeny of Galloanserae is exactly congruent with previous studies[4] (Fig. 1, red).
Within the monophyletic Neoaves, we recover five major clades, each of which is the successive sister group to the remaining clades in the series (Fig. 1). The Strisores includes the nightjars and their nocturnal relatives with the diurnal swifts and hummingbirds (Fig. 1, brown). Four nocturnal lineages—nightjars, a neotropical oilbird- potoo clade, frogmouths, and owlet-nightjars—form successive sister groups to the diurnal swift and hummingbird clade.

The Columbaves is a novel clade that consists of two monophyletic groups recently identified by Jarvis *et al.*[1] (Fig. 1, purple). A clade consisting of turacos, bustards, and cuckoos (Otidimorphae) is sister to a clade consisting of pigeons as the sister group to sandgrouse and mesites (Columbimorphae). The third neoavian clade consists of a well recognized monophyletic group of core gruiform birds (Gruiformes; Fig. 1, yellow), with interrelationships that are consistent with previous phylogenies[4]. The Aequorlitornithes is a novel, comprehensive clade of waterbirds, including all shorebirds, diving birds, and wading birds (Fig. 1, blue). Within this group, the flamingos and grebes[1, 4-6] are the sister group to shorebirds, and the sunbittern and tropicbirds[1,4,6] are the sister group to the wading and diving birds (Fig. 1, blue). Other interrelationships within these groups are extensively congruent with the results in ref. 4 and the work of others (see Supplementary Information).

The fifth major neoavian clade, which we name Inopinaves, is a very diverse landbird clade with the same composition as previously recognized (Telluraves) [1,4-6] but with the enigmatic, neotropical hoatzin (*Opisthocomus hoazin*) as the sister group to all other landbirds (Fig. 1, green). The phylogeny of the landbirds shares many points of congruence with earlier hypotheses, including the relationships of seriemas, falcons, parrots, and perching birds[1, 4-6] and the interrelationships among oscine songbirds[24]. However, we find that hawks (Accipitriformes) are the sister group to a new clade including the rest of the landbirds, to be called Eutelluraves (see Supplementary Information).

Our divergence time analyses employed 19 phylogenetically and geologically well-constrained fossil calibrations (following recently proposed best practices[25]), documenting many deep divergences within the avian crown group (Fig. 1, grey nodes; see Supplementary Information). Our analysis supports an extremely rapid radiation of the avian crown group in the wake of the K–Pg mass extinction event (Fig. 1, Supplementary Figs. 6 and 7). Although the post-K–Pg radiation hypothesis has long been strongly supported by the avian fossil record[26,27], it has so far received little support from molecular divergence time analyses[4,28]. The tempo and mode of the extant avian radiation remains contentious. For example, an alternative calibration analysis including the fossil *Vegavis* did not support significantly different dates of divergence outside of the Galloanserae (see Supplementary Information and Supplementary Figs 10–12). Confident determination of the age of crown Aves will have to await discoveries of Mesozoic stem neognaths and palaeognaths, and detailed assessments of the influence of soft maximum bound parameterization on the age of the deepest avian divergences.

Our results indicate that the recent genome phylogeny[1] may contain some erroneous relationships induced by long branch attraction from sparse taxon sampling. Maximum likelihood analysis of our sequence data pruned down to a phylogenetically equivalent

subsample of 48 species produces relationships along the neoavian 'backbone' (Supplementary Fig. 8) that are entirely discordant with the phylogeny based on our full data set (Fig. 1). This reduced taxon analysis recovers some of the specific features of the recent genome phylogeny by Jarvis *et al.*[1] (Supplementary Fig. 8): for example, the placement of the pigeons, mesites, and sandgrouse (a subclade of Columbea[1]) outside of the rest of the Neoaves. Differences in tree topology when taxa are excluded are to be expected if early internodes in Neoaves are very short. Adding taxa that have diverged near nodes of interest has been theoretically demonstrated to constrain the possible historical substitution patterns, and increase the accuracy of phylogenetic inference[11]. By increasing our taxon sampling to include all major avian lineages, we have minimized the possibility that additional taxon sampling alone will alter the relationships in our tree.

Jarvis *et al.*[1] also identified a well supported clade consisting of the hoatzin (*Opisthocomus*) as the sister group to a crane (*Grus*) and a plover (*Charadrius*) (total evidence nucleotide tree, BS = 0.91, 0.96, respectively). However, *Grus* and *Charadrius* were the only species sampled from two very diverse neoavian orders: Gruiformes, 185 species; and Charadriiformes, 385 species[2]. Our results indicate that *Opisthocomus* is the most ancient bird lineage (~64 million years) consisting of only a single, extant species. Thus, the three taxa placed in this assemblage by Jarvis *et al.*[1] comprise three of the most ancient, and undersampled lineages within all birds, indicating the strong possibility of long branch attraction artefacts. By contrast, these same groups are represented by 26 species in our analysis, and they do not form an exclusive clade (Fig. 1).

In addition to providing a new backbone for comprehensive avian supertrees and comparative evolutionary analyses[28], this new avian phylogeny supports many interesting hypotheses about avian evolution. This phylogeny upholds the hypothesis that the ancestor of

the diurnal swifts and hummingbirds evolved from a clade that had been predominantly nocturnal for ~10 million years. Although hummingbirds have acute near-ultraviolet vision[29], the effect of extended ancestral nocturnality on the evolution of the visual system in this group of birds is unknown. Our findings also support the emerging pattern that landbirds evolved from a raptorial grade[1]. The sister group relationships of hawks to the rest of the landbirds, of owls to the diverse coraciimorph clade, and of seriemas and falcons to the parrots and passerines indicate the persistence of a raptorial ecology among ancestral landbirds. Lastly, the identification of a new, broadly comprehensive waterbird–shorebird clade indicates a striking, and previously unappreciated, level of evolutionary constraint on the ecological diversification of birds that will be exciting to investigate in the future.

Online Content Methods, along with any additional Extended Data display items and Source Data, are available in the online version of the paper; references unique to these sections appear only in the online paper.

Received 3 May; accepted 9 September 2015.

Published online 7 October 2015.

Supplementary Information is available in the online version of the paper.

Acknowledgements The research was supported by W. R. Coe Funds from Yale University to R.O.P., and by NSF grants to A.R.L. and E.M.L. We thank the ornithology curators and staff of the following collections for granting research access to the invaluable avian tissue collections that made this work possible: American Museum of Natural History, Field Museum of Natural History, Royal Ontario Museum, University of Kansas Museum of Natural History and

Biodiversity Research Center, University of Washington Burke Museum of Natural History, and Yale Peabody Museum of Natural History. We thank M. Kortyna and H. Ralicki for contributions to laboratory work, S. Gullapalli for computational assistance, and N. J. Carriero and R. D. Bjornson at the Yale University Biomedical High Performance Computing Center, which is supported by the NIH. Bird illustrations reproduced with permission from the Handbook of the Birds of the World Alive Online, Lynx Edicions, Barcelona[30]. The research was aided by discussions with R. Bowie, S. Edwards, I. Lovette, J. Musser, T. Near, and K. Zyskowski.

Author Contributions R.O.P., J.S.B., A.R.L., and E.M.L. conceived of and designed the study. R.O.P. selected the taxa studied. A.R.L. selected the loci and designed the probes. J.S.B., A.R.L., and E.M.L. collected the data. J.S.B. and A.R.L. performed the phylogenetic analyses. A.D. and J.P.T. performed the phylogenetic informativeness, and signal and noise analyses. D.J.F. selected fossil taxa for calibration, and J.S.B., D.J.F., and A.D. designed and performed the dating analyses. R.O.P. wrote the paper with contributions from all other authors.

Author Information Electronic data files and software are permanently archived at http://dx.doi.org/10.5281/zenodo.28343. Reprints and permissions information is available at www.nature.com/reprints. The authors declare no competing financial interests. Readers are welcome to comment on the online version of the paper. Correspondence and requests for materials should be addressed to R.O.P. (richard.prum@yale.edu) or J.S.B. (jsb439@cornell.edu).

METHODS

Locus selection and probe design. Anchor loci described in ref. 12 were extended such that each contained approximately 1,350 bp. In some cases neighbouring loci were joined to form a single locus. Also, loci that performed poorly in ref. 12 were removed from the locus set. This process produced 394 loci (referred to as the version 2 vertebrate loci). Genome coordinates corresponding to these regions in the Gallus gallus genome (galGal3, UCSC genome browser) were identified and sequences corresponding to this region were extracted (coordinates are available in the Zenodo archive (http://dx.doi.org/10.5281/zenodo.28343)). In order to improve the capture efficiency for passerines, we also obtained homologous sequences for Taeniopygia guttata. After aligning the Gallus and Taeniopygia sequences using MAFFT[31], alignments were trimmed to produce the final probe region alignments (alignments available in the Zenodo archive), and probes were tiled at approximately 1.5 X tiling density (probe specification will be made avail- able upon publication).

Data collection. Data were collected following the general methods of ref. 12 through the Center for Anchored Phylogenomics at Florida State University (http://www.anchoredphylogeny.com). Briefly, each genomic DNA sample was sonicated to a fragment size of ~150–350bp using a Covaris E220 focused- ultrasonicator with Covaris microTUBES. Subsequently, library preparation and indexing were performed on a Beckman-Coulter Biomek FXp liquid-handling robot following a protocol modified from ref. 32. One important modification is a size-selection step after blunt-end repair using SPRIselect beads (Beckman- Coulter; 0.9 X ratio of bead to sample volume). Indexed samples were then pooled at equal quantities (typically 12–16 samples per pool), and enrichments were performed on each multi-sample pool using an Agilent Custom

SureSelect kit (Agilent Technologies), designed as specified above. After enrichment, the 12 enrichment pools were pooled in groups of three in equal quantities for sequencing on four PE150 Illumina HiSeq2000 lanes (three enrichment pools per lane). Sequencing was performed in the Translational Science Laboratory in the College of Medicine at Florida State University.

Data processing. Paired-read merging (Merge.java). Typically, between 50% and 75% of sequenced library fragments had an insert size between 150 bp and 300 bp. As 150 bp paired-end sequencing was performed, this means that the majority of the paired reads overlap and thus should be merged before assembly. The overlapping reads were identified and merged following the methods of ref. 33. In short, for each degree of overlap for each read we computed the probability of obtaining the observed number of matches by chance, and selected degree of overlap that produced the lowest probability, with a P value less than 10^{-10} required to merge reads. When reads are merged, mismatches are reconciled using base-specific quality scores, which were combined to form the new quality scores for the merged read (see ref. 33 for details). Reads failing to meet the probability criterion were kept separate but still used in the assembly. The merging process produces three files: one containing merged reads and two containing the unmerged reads.

Assembly (Assembler.java). The reads were assembled into contigs using an assembler that makes use of both a divergent reference assembly approach to map reads to the probe regions and a de novo assembly approach to extend the assembly into the flanks. The reference assembler uses a library of spaced 20-mers derived from the conserved sites of the alignments used during probe design. A preliminary match was called if at least 17 of 20 matches exist between a spaced kmer and the corresponding positions in a read. Reads obtaining a preliminary

match were then compared to an appropriate reference sequence used for probe design to determine the maximum number of matches out of 100 consecutive bases (all possible gap-free alignments between the read and the reference ware considered). The read was considered mapped to the given locus if at least 55 matches were found. Once a read is mapped, an approximate alignment position was estimated using the position of the spaced 20-mer, and all 60-mers existing in the read were stored in a hash table used by the de novo assembler. The de novo assembler identifies exact matches between a read and one of the 60- mers found in the hash table. Simultaneously using the two levels of assembly described above, the three read files were traversed repeatedly until an entire pass through the reads produced no additional mapped reads.

For each locus, mapped reads were then clustered into clusters using 60-mer pairs observed in the reads mapped to that locus. In short, a list of all 60-mers found in the mapped reads was compiled, and the 60-mers were clustered if found together in at least two reads. The 60-mer clusters were then used to separate the reads into clusters for contig estimation. Relative alignment positions of reads within each cluster were then refined in order to increase the agreement across the reads. Up to one gap was also inserted per read if needed to improve the alignment. Note that given sufficient coverage and an absence of contamination, each single-copy locus should produce a single assembly cluster. Low coverage (leading to a break in the assembly), contamination, and gene duplication, can all lead to an increased number of assembly clusters. A whole-genome duplication, for example, would increase the number of clusters to two per locus.

Consensus bases were called from assembly clusters as follows. For each site an unambiguous base was called if the bases present were identical or if the poly- morphism of that site could be explained as sequencing error, assuming a binomial probability model with the probability of error equal to 0.1 and alpha equal to 0.05. If the polymorphism could not be explained as sequencing error, the ambiguous base was called that corresponded to all of the observed bases at that site (for example, 'R' was used if 'A' and 'G' were observed). Called bases were soft-masked (made lowercase) for sites with coverage lower than five. A summary of the assembly results is presented in a spreadsheet in the electronic data archive (http:// dx.doi.org/10.5281/zenodo.28343; Prum_AssemblySummary_Summary.xlsx).

Contamination filtering (IdentifyGoodSeqsViaReadsMapped.r, GatherALL ConSeqsWithOKCoverage.java). In order to filter out possible low-level contami- nants, consensus sequences derived from very low coverage assembly clusters (,10reads) were removed from further analysis. After filtering, consensus sequences were grouped by locus (across individuals) in order to produce sets of homologues.

Orthology (GetPairwiseDistanceMeasures.java, plotMDS5.r). Orthology was then determined for each locus as follows. First, a pairwise distance measure was computed for pairs of homologues. To compute the pairwise distance between two sequences, we computed the percent of 20-mers observed in the two sequences that were found in both sequences. Note that the list of 20-mers was constructed from consecutive 20-mers as well as spaced 20-mers (every third base), in order to allow increased levels of sequence divergence. Using the distance matrix, we clustered the sequences using a neighbour-joining algorithm, but allowing at most one sequence

per species to be in a given cluster. Clusters containing fewer than 50% of the species were removed from downstream processing.

Alignment (MAFFT). Sequences in each orthologous set were aligned using MAFFT v7.023b[31] with "–genafpair" and "–maxiterate 1000" flags.

Alignment Trimming (TrimAndMaskRawAlignments3). The alignment for each locus was then trimmed/masked using the following procedure. First, each alignment site was identified as 'good' if the most common character observed was present in >40% of the sequences. Second, 20 bp regions of each sequence that contained <10 good sites were masked. Third, sites with fewer than 12 unmasked bases were removed from the alignment. Lastly, entire loci were removed if both outgroups or more than 40 taxa were missing. This filter yielded 259 trimmed loci containing fewer than 2.5% missing characters overall.

Model selection and phylogenetic inference. To minimize the overall model complexity while accurately accounting for substitution processes, we performed a partition-model sensitivity analysis with the development version of PartitionFinder v2.0 (ref. 13), sensu[14], and compared a complex partition-model (one partition per gene) to a heuristically optimized (relaxed clustering with the RAxML option for accelerated model selection) partition-model using BIC. Based on a candidate pool of potential partitioning strategies that spanned a single partition for the entire data set to a model allowing each locus to represent a unique partition, the latter approach suggested that 75 partitions of our data set represented the best-fitting partitioning scheme, which reduced the number of necessary model parameters by 71%, and hugely decreased computation time.

We analysed each individual locus in RAxML v8.0.20 (ref. 18), and then the concatenated alignment, using the two partitioning strategies identified above with both maximum likelihood and Bayesian based approaches in RAxML v8.0.20, and ExaBayes v1.4.2 9 (ref. 34). For each RAxML analysis, we executed 100 rapid bootstrap inferences and thereafter a thorough ML search using a GTR_{G4} model of nucleotide substitution for each data set partition. Although this may potentially over-parameterize a partition with respect to substitution model, the influence of this form of model over-parameterization has been found to be negligible in phylogenetic inference[35]. For the Bayesian analyses, we ran four Metropolis-coupled ExaBayes replicates for 10 million generations, each with three heated chains, and sampling every 1,000 generations (default tuning and branch swap parameters; branch lengths among partitions were linked). Convergence and proper sampling of the posterior distribution of parameter values were assessed by checking that the effective sample sizes of all estimated parameters and branch lengths were greater than 200 in the Tracer v1.6 software[36] (most were greater than 1,000), and by using the 'sdsf' and 'postProcParam' tools included with the ExaBayes package to ensure the average standard deviation of split frequencies and potential scale reduction factors across runs were close to zero and one, respectively. Finally, to check for convergence in topology and clade posterior probabilities, we summarized a greedily refined majority-rule consensus tree (default) from 10,000 post burn-in trees using the ExaBayes 'consense' tool for each run independently and then together. Analyses of the reduced data set referenced in the main text were conducted using the same partition-model as the full data set.

To explore variation in gene tree topology and to look for outliers that might influence combined analysis, we calculated pairwise Robinson-Foulds[37] (RF) and Matching Splits (MS) tree distances implemented in TreeCmp[38]. We then visualized histograms of tree distances and

multidimensional scaling plots in R, and estimated neighbour-joining 'trees-of-trees' in the Phangorn R package sensu lato[39,40]. Using RF and MS distances, outlier loci were identified as those that occurred in the top 10% of pairwise distances for >30 comparisons to other loci (~10%) in the data set. We also identified putative outlier loci using the kdetrees.complete function of the kdetrees R package[41]. All three methods identified 13 of the same loci as potential outliers; however removal of these loci from the analysis had no effect on estimating topology or branch lengths.

Coalescent species tree analyses. Although fully parametric estimation (for example, *BEAST, see ref. 42) of a coalescent species tree with hundreds of genes and hundreds of taxa is not currently possible, we estimated species trees using three gene-tree summation methods that have been shown to be statistically consistent under the multispecies coalescent model[43]. First, we used the STRAW web server[44] to estimate bootstrapped species trees using the STAR[19] and NJ-ST[20] algorithms (also available through STRAW). The popular MP- EST[45] method cannot currently work for more than ~50 taxa. STAR takes rooted gene trees and uses the average ranks of coalescence times[19] to build a distance matrix from which a species tree is computed with the neighbour-joining method[46]. By contrast, NJst applies the neighbour-joining method to a distance matrix computed from average gene-tree internode distances, and relaxes the requirement for input gene trees to be rooted[20].

We also summarized a species tree with the ASTRAL 4.7.6 algorithm. With simulated data, ASTRAL has been shown to outperform concatenation or other summary methods under certain amounts of incomplete lineage sorting[21]. For very large numbers of taxa and genes, ASTRAL uses a heuristic search to find the species tree that agrees with the largest number of

quartet trees induced by the set of input gene trees. For analysis with ASTRAL, we also attempted to increase the resolution of individual gene trees (Supplementary Fig. 2) by generating supergene alignments using the weighted statistical binning pipeline of refs 47, 48 with a bootstrap score of 0.75 as a bin threshold.

STAR, NJst (not shown), and the binned ASTRAL (Supplementary Fig. 3) analysis produced virtually identical inferences when low support branches (<0.75) were collapsed, and differed only with respect to the resolution of a few branches. NJst resolved the Passeroidea (Fringilla plus Spizella) as the sister group to a paraphyletic sample of Sylvioidea (Calandrella, Pycnonotus, and Sylvia), while STAR does not resolve this branch. Comparing STAR/NJst to ASTRAL, we find five additional differences: (1) within tinamous, STAR/NJst resolves Crypturellus as sister to the rest of the tinamous, whereas ASTRAL resolves Crypturellus as sister to Tinamus (similar to ExaBayes/RAxML); (2) STAR/NJst resolves pigeons as sister to a clade containing Mesitornithiformes and Pteroclidiformes, while ASTRAL does not resolve these relationships; (3), STAR/NJst fails to resolve Oxyruncus and Myiobius as sister genera, while ASTRAL does (similar to RAxML/ExaBayes); (4), in STAR/NJst, bee-eaters (Merops) are resolved as the sister group to coraciiforms (congruent with ref. 4), while ASTRAL resolves bee-eaters as sister to the rollers (Coracias) (similar to RAxML/ExaBayes); (5) lastly, in STAR/NJst, buttonquail (Turnix) is resolved as sister to the most inclusive clade of Charadriiformes not including Burhinus, Charadrius, Haematopus, and Recurvirostra, while in ASTRAL, buttonquail is resolved as sister to a clade containing Glareola, Uria, Rynchops, Sterna, and Chroicocephalus (similar to RAxML/ExaBayes).

Although lower level relationships detected with concatenation are generally recapitulated in the species trees, few of the higher level, or interordinal, relationships are resolved. This lack of resolution of the gene-tree species-tree based inferences relative to the inferences based on concatenation are not surprising, as it is increasingly recognized that the phylogenetic information content required to resolve the gene-tree histories of individual loci becomes scant at deep timescales[47]. Despite our extensive taxon sampling and the slow rate of nucleotide substitution that characterizes loci captured using anchored enrichment[12], no single locus was able to fully resolve a topology, and this lack of information will challenge the accuracy of any coalescent-based summary approach relative to concatenation[49-54]. Finally, all summation methods tested here assume a priori that the only source of discordance among gene trees is deep coalescence, and violations of this assumption may introduce systematic error in phylogeny estimation[54].

Phylogenetic informativeness. Site-specific evolutionary rates, $\lambda_{i..j}$, were calculated for each locus using the program HyPhy[55] in the PhyDesign web interface[56] in conjunction with a guide chronogram generated by a nonparametric rate smoothing algorithm[57] applied to our concatenated RAxML tree. Using these rates to predict whether an alignment will yield correct, incorrect, or no resolution of a given node, we quantified the probability of phylogenetically informative changes (ψ)[16] contributing to the resolution of the earliest divergences in Neoaves. Estimates generated under a three character state model[58] reveal that the majority of loci have a strong probability of ψ, and suggest a high potential for most loci and partitions containing multiple loci (assigned by PartitionFinder) to correctly resolve this internode. The potential for resolution as a consequence of phylogenetic signal is therefore high relative to the potential for

saturation and misleading inference induced by stochastic changes along the subtending lineages (Supplementary Fig. 4a).

To assess the information content of the loci across the entire topology, we profiled their phylogenetic informativeness (PI)[15], (Supplementary Fig. 4b). There was considerable variation in PI across loci (Supplementary Fig. 4). In all cases, the loci with the lowest values of ψ are categorized by substantially lower (60–90%) values of PI, rather than sharp declines in their PI profiles. The absence of a sharp decline in the PI profile suggests that a lack of phylogenetic information, rather than rapid increases in homoplasious sites, underlie low values of the probability of signaly[59].

Because declines in PI can be attributed to increases in homoplasious site patterns[59], we further assessed the phylogenetic utility of data set partitions by quantifying the ratio of PI at the most recent common ancestor of Neoaves to the PI at the most recent common ancestor of Aves (Supplementary Fig. 4c). Values of this ratio that are less than 1 correspond to a rise in PI towards the root. Values close to 1 correspond to fairly uniform PI. Values greater than 1 correspond to a decline in PI towards the root. Sixty-six out of 75 partitions demonstrated less than a 50% percent decline in PI, and only six partitions demonstrated a decline of PI greater than 75% (Supplementary Fig. 4c). As all but a few nodes in this study represent divergences younger than the crown of Neoaves, these ratios of PI suggest that the predicted impact of homoplasy on our topological inferences should be minimal.

As PI profiles do not directly predict the impact of homoplasious site patterns on topological resolution[16,60], we evaluated probabilities of ψ for focal nodes using both the concatenated data set as well as individual loci that span the variance in locus lengths.

Concordant with expectations from the PI profiles, all quantifications strongly support the prediction that homoplasy will have a minimal impact on topological resolution for the concatenated data set across a range of tree depths and internode distances (ψ = 1.0 for all nodes), while individual loci vary in their predicted utility (Supplementary Fig. 4d). As the guide tree does not represent a true known tree, we additionally quantified ψ across a range of tree depths and internode distances to test if our predictions of utility are in line with general trends in the data. Concordant with our results above, the concatenated data set is predicted to be of high phylogenetic utility at all timescales (ψ = 1.0 for all nodes), while the utility of individual loci begins to decline for small internodes at deep tree depths (Supplementary Fig. 5).

Estimating a time-calibrated phylogeny. We estimated a time-calibrated tree with a node dating approach in BEAST 1.8.1 (ref. 42) that used 19 well justified fossil calibrations phylogenetically placed by rigorous, apomorphy-based diagnoses (see the descriptions of avian calibration fossils in the Supplementary Information). We used a starting tree topology based on the ExaBayes inference (Fig. 1), and prior node age calibrations that followed a lognormal parametric distribution based on occurrences of fossil taxa. To prevent BEAST from exploring topology space and only allow estimation of branch lengths, we turned off the subtree-slide, Wilson–Balding, and narrow and wide exchange operators[61,62]. Finally, we applied a birth–death speciation model with default priors.

As rates of molecular evolution are significantly variable across certain bird lineages[63-65], we applied an uncorrelated relaxed clock (UCLN) to each partition of the data set where rates among branches are distributed according to a lognormal distribution[66]. All dating analyses were

performed without crocodilian outgroups to reduce the potential of extreme substitution rate heterogeneity to bias rate and consequent divergence time estimates of the UCLN model[67].

All calibrations were modelled using soft maximum age bounds to allow for the potential of our data to overwhelm our user-specified priors[68]. Soft maximum bounds are the preferred method for assigning upper limits on the age of phylogenetic divergences[69]. As effective priors necessarily reflect interactions between user specified priors, topology, and the branching-model, they may not precisely reflect the user-specified priors[70]. To correct for this potential source of error, we carefully examined the effective calibration priors by first running the prepared BEAST XML without any nucleotide data (until all ESS values were above 200). We then iteratively adjusted our user-defined priors until all of the effective priors (as examined in the Tracer software) reflected the intended calibration densities. Finally, using the compare.phylo function in the Phyloch R package, we examined how the inclusion of molecular data influenced the divergence time estimates relative to the effective prior (Supplementary Fig. 9; see below).

Defining priors. Our initial approach was to set a prior's offset to the age of its associated fossil; the mean was then manually adjusted such that 95% of the calibration density fell more recently than the K–Pg boundary at 65 Ma (million years ago) (the standard deviation was fixed at 1 Ma). In general, priors constructed this way generated calibration densities that specified their highest density peak (their mode) about 3–5 million years older than the age of the offset.

We applied a loose gamma prior to the node reflecting the most recent common ancestor of crown birds—we used an offset of 60.5 Ma (the age of the oldest known definitive, uncontroversial crown bird fossil; the stem penguin *Waimanu*), and adjusted the scale and shape of the prior such that 97.5% of the calibration density fell more recently than 86.5 Ma[71] (see

below and Supplementary Information for discussion of the .65 Ma putative crown avian Vegavis). This date (86.5 Ma) reflects the upper bound age estimate of the Niobrara Formation—one of many richly fossiliferous Mesozoic deposits exhibiting many crownward Mesozoic stem birds, without any trace of avian crown group representatives. The Niobrara, in particular, has produced hundreds of stem birds and other fragile skeletons, without yielding a single crown bird fossil, and therefore represents a robust choice for a soft upper bound for the root divergence of the avian crown[71-73]. Previous soft maxima employed for this divergence have arbitrarily selected the age of other Mesozoic stem avians (that is, *Gansus yumenensis*, 110 Ma) that are phylogenetically stemward of the Niobrara taxa[28]. Although the implementation of very ancient soft maxima such as the age of Gansus are often done in the name of conservatism, the extremely ancient divergence dates yielded by such analyses illustrate the misleading influence of assigning soft maxima that are vastly too old to be of relevance to the divergence of crown group birds[74]. However, this problem has been eliminated in some more recent analyses[75].

All of the fossil calibrations employed in our analysis represent neognaths; rootward divergences within Aves (for example the divergence between Palaeognathae and Neognathae, and Galloanserae and Neoaves) cannot be confidently calibrated due to a present lack of fossils representing the palaeognath, neognath, galloanserine, and neoavian stem groups. As such, the K–Pg soft bound was only applied to comparatively apical divergences within neognaths. Although the question of whether major neognath divergences occurred during the Mesozoic has been the source of controversy[76-78], renewed surveys of Mesozoic sediments for definitive crown avians or even possible crown neoavians have been unsuccessful (with the possible exception of Vegavis; see Supplementary Information), and together with recent divergence dating analyses have cast doubt on the presence of neoavian subclades before the K–Pg mass extinction[1,74,79].

Further, recent work has demonstrated the tendency of avian divergence estimates to greatly exceed uninformative priors, resulting in spuriously ancient divergence dating results (for example, refs 28, 75, 76, 80). These results motivated our implementation of the 65 Ma soft bound for our neoavian calibrations.

Contrary to expectation, when we compared the effective prior on the entire tree to the final summary derived from the posterior distribution of divergence times (Supplementary Fig. 9), we found no overall trend of posterior estimated ages post- dating prior calibrations. In fact, the inclusion of our molecular data decreases the inferred ages of almost all of the deepest nodes in our tree. A similar result has been obtained for mammals by using large amounts of nuclear DNA sequences[81]. Future work investigating the interplay of the density of genomic sampling and the application of various calibration age priors will be indispensible for sensitivity analyses to help us further develop a robust timescale of avian evolution. However, the pattern of posterior versus prior age estimates observed in our study raises the prospect that the new class of data used in this study (that is, semi-conserved anchor regions) may exhibit some immunity to longstanding problems associated with inferring avian divergence times, such as systematically over-estimating the antiquity of extant avian clades.

Implementing BEAST and summarizing a final calibrated tree. In addition to making predictions about the phylogenetic utility of a locus or partition towards topological resolution, PI profiles have recently also been used to mitigate the influence of substitution saturation on divergence time estimates[82]. Given the variance in PI profile shapes for captured loci and their subsequent partition assignments (Supplementary Fig. 4c), and observations that alignments and subsets of data alignments characterized by high levels of homoplasy can mislead branch length

estimation[83,84], we limited our divergence time estimates to 36 partitions that did not exhibit a decline in informativeness towards the root of the tree. We ran BEAST on each partition separately until parameter ESS values were greater than 200 (most were greater than 1,000) to ensure adequate posterior sampling of each parameter value. After concatenating 10,000 randomly sampled post burn-in trees from each of these completed analyses, we summarized a final MCC tree with median node heights in TreeAnnotator v1.8.1 (ref. 42). Supplementary Fig. 6 shows the full, calibrated Bayesian tree (Fig. 1) with 95% HPD confidence intervals on the node ages, and Supplementary Fig. 7 shows the distribution of estimated branching times, ranked by median age (using clade numbers from Fig. 1). All computations were carried out on 64-core PowerEdge M915 nodes on the Louise Linux cluster at the Yale University Biomedical High Performance Computing Center.

Data reporting. No statistical methods were used to predetermine sample size.

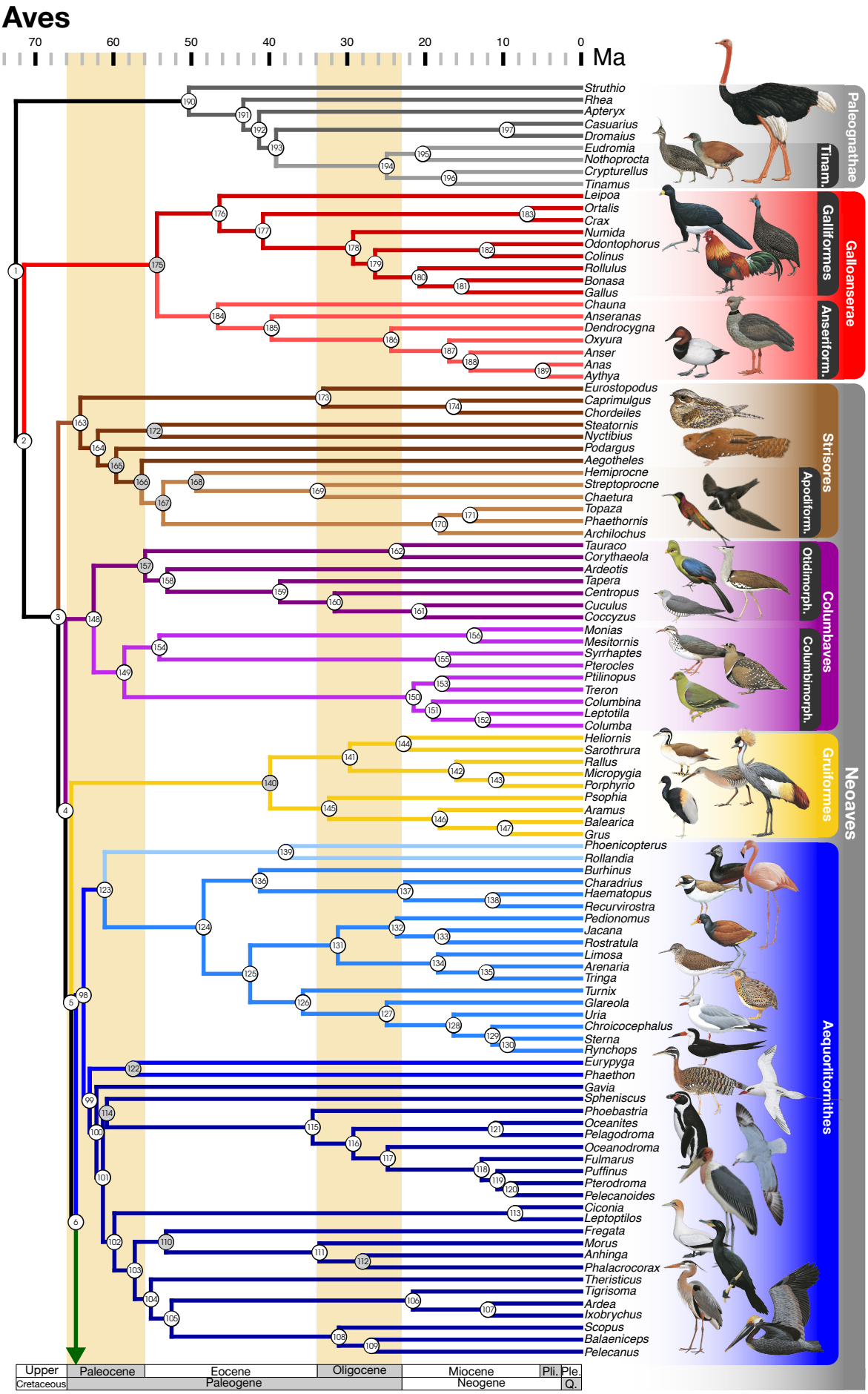
Aves
70
60
50
40
30
20
10
0
Ma
Struthio
Rhea
Apteryx
Casuarius
Dromaius
Eudromia
Nothoprocta
Crypturellus
Tinamus
Leipoa
Ortalis
Crax
Numida
Odontophorus
Colinus
Rollulus
Bonasa
Gallus
Chauna
Anseranas
Dendrocygna
Oxyura
Anser
Anas
Aythya
Eurostopodus
Caprimulgus
Chordeiles
Steatornis
Nyctibius
Podargus
Aegotheles
Hemiprocne
Streptoprocne
Chaetura
Topaza
Phaethornis
Archilochus
Tauraco
Corythaeola
Ardeotis
Tapera
Centropus
Cuculus
Coccyzus
Monias
Mesitornis
Syrrhaptes
Pterocles
Ptilinopus
Treron
Columbina
Leptotila
Columba
Heliornis
Sarothrura
Rallus
Micropygia
Porphyrio
Psophia
Aramus
Balearica
Grus
Phoenicopterus
Rollandia
Burhinus
Charadrius
Haematopus
Recurvirostra
Pedionomus
Jacana
Rostratula
Limosa
Arenaria
Tringa
Turnix
Glareola
Uria
Chroicocephalus
Sterna
Rynchops
Eurypyga
Phaethon
Gavia
Spheniscus
Phoebastria
Oceanites
Pelagodroma
Oceanodroma
Fulmarus
Puffinus
Pterodroma
Pelecanoides
Ciconia
Leptoptilos
Fregata
Morus
Anhinga
Phalacrocorax
Theristicus
Tigrisoma
Ardea
Ixobrychus
Scopus
Balaeniceps
Pelecanus
Paleognathae
Tinam.
Galloanserae
Galliformes
Anseriform.
Strisores
Apodiform.
Columbaves
Otidimorph.
Columbimorph.
Gruiformes
Neoaves
Aequorlitornithes
Upper Cretaceous
Paleocene
Eocene
Paleogene
Oligocene
Miocene
Neogene
Pli.
Ple.
Q.

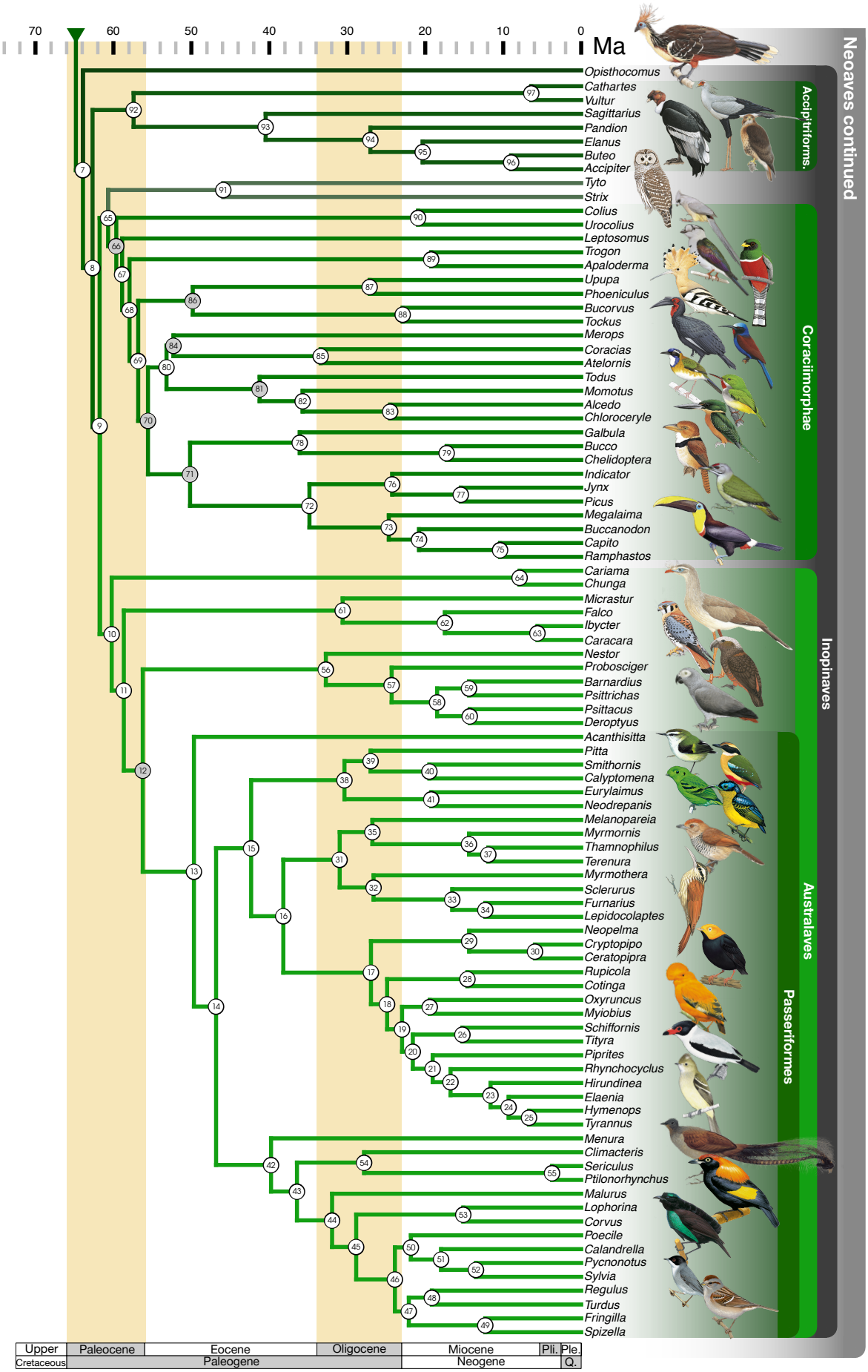
70
60
50
40
30
20
10
0
Ma
Neoaves continued
Accipitriforms.
Coraciimorphae
Inopinaves
Australaves
Passeriformes
Opisthocomus
Cathartes
Vultur
Sagittarius
Pandion
Elanus
Buteo
Accipiter
Tyto
Strix
Colius
Urocolius
Leptosomus
Trogon
Apaloderma
Upupa
Phoeniculus
Bucorvus
Tockus
Merops
Coracias
Atelornis
Todus
Momotus
Alcedo
Chloroceryle
Galbula
Bucco
Chelidoptera
Indicator
Jynx
Picus
Megalaima
Buccanodon
Capito
Ramphastos
Cariama
Chunga
Micrastur
Falco
Ibycter
Caracara
Nestor
Probosciger
Barnardius
Psittrichas
Psittacus
Deroptyus
Acanthisitta
Pitta
Smithornis
Calyptomena
Eurylaimus
Neodrepanis
Melanopareia
Myrmornis
Thamnophilus
Terenura
Myrmothera
Sclerurus
Furnarius
Lepidocolaptes
Neopelma
Cryptopipo
Ceratopipra
Rupicola
Cotinga
Oxyruncus
Myiobius
Schiffornis
Tityra
Piprites
Rhynchocyclus
Hirundinea
Elaenia
Hymenops
Tyrannus
Menura
Climacteris
Sericulus
Ptilonorhynchus
Malurus
Lophorina
Corvus
Poecile
Calandrella
Pycnonotus
Sylvia
Regulus
Turdus
Fringilla
Spizella
Upper
Cretaceous
Paleocene
Eocene
Paleogene
Oligocene
Miocene
Neogene
Pli.
Ple.
Q.

Figure 3.1. Phylogeny of birds. Time-calibrated phylogeny of 198 species of birds inferred from a concatenated, Bayesian analysis of 259 anchored phylogenomic loci using ExaBayes[17]. Figure continues on the opposite page from green arrow at the bottom of this panel. Complete taxon data in Supplementary Table 1. Higher taxon names appear at right. All clades are supported with posterior probability (PP) of 1.0, except for the Balaeniceps– Pelecanus clade (PP = 0.54; clade 109). The five major, successive, neoavian sister clades are: Strisores (brown), Columbaves (purple), Gruiformes (yellow), Aequorlitornithes (blue), and Inopinaves (green). Background colours mark geological periods. Ma, million years ago; Ple, Pleistocene; Pli, Pliocene; Q., Quaternary. Clade numbers refer to the plot of estimated divergence dates (Supplementary Fig. 7). Fossil age-calibrated nodes are shown in grey. Illustrations of representative bird species[30] are depicted by their lineages. See Supplementary Information for details and further discussion. **Please refer to the published version of this article for higher quality vector art.**

REFERENCES

1. Jarvis, E. D. et al. Whole-genome analyses resolve early branches in the tree of life of modern birds. Science 346, 1320–1331 (2014).
2. Gill, F. & Donsker, D. IOC World Bird List (v5.1) http://dx.doi.org/10.14344/ IOC.ML.5.1 (2015).
3. Gill, F. B. Ornithology 2nd edn (W. H. Freeman and Co., 1995).
4. Hackett, S. J. et al. A phylogenomic study of birds reveals their evolutionary history. Science 320, 1763–1768 (2008).
5. Ericson, P. G. P. et al. Diversification of Neoaves: integration of molecular sequence data and fossils. Biol. Lett. 2, 543–547 (2006).
6. McCormack, J. E. et al. A phylogeny of birds based on over 1,500 loci collected by target enrichment and high-throughput sequencing. PLoS ONE 8, e54848 (2013).
7. Mayr, G. Paleogene Fossil Birds (Springer, 2009).
8. Mayr, G. Metaves, Mirandornithes, Strisores and other novelties — a critical review of the higher-level phylogeny of neornithine birds. J. Zoological Syst. Evol. Res. 49, 58–76 (2011).
9. Graybeal, A. Is it better to add taxa or characters to a difficult phylogenetic problem? Syst. Biol. 47, 9–17 (1998).
10. Heath, T.A., Hedtke, S.M. & Hillis, D.M. Taxon sampling and the accuracy of phylogenetic analyses. Journal of Systematics and Evolution 46, 239–257 (2008).
11. Townsend, J. P. & Lopez-Giraldez, F. Optimal selection of gene and ingroup taxon sampling for resolving phylogenetic relationships. Syst. Biol. 59, 446–457 (2010).
12. Lemmon, A.R., Emme, S.A. & Lemmon, E.M. Anchored hybrid enrichment for massively high-throughput phylogenomics. Syst. Biol. 61, 727–744 (2012).
13. Lanfear, R., Calcott, B., Ho, S.Y. & Guindon, S. PartitionFinder: combined selection of partitioning schemes and substitution models for phylogenetic analyses. Mol. Biol. Evol. 29, 1695–1701 (2012).
14. Berv, J.S. & Prum, R.O. Acomprehensive multilocus phylogeny of the neotropical cotingas (Cotingidae, Aves) with a comparative evolutionary analysis of breeding system and plumage dimorphism and a revised phylogenetic classification. Mol. Phylogenet. Evol. 81, 120–136 (2014).
15. Townsend, J.P. Profiling phylogenetic informativeness. Syst. Biol. 56,222–231 (2007).
16. Townsend, J. P., Su, Z. & Tekle, Y. I. Phylogenetic signal and noise: predicting the power of a data set to resolve phylogeny. Syst. Biol. 61, 835–849 (2012).
17. Aberer, A.J., Kobert, K. & Stamatakis, A. ExaBayes: massively parallel Bayesian tree inference for the whole-genome era. Mol. Biol. Evol. 31, 2553–2556 (2014).
18. Stamatakis, A. RAxML version 8: a tool for phylogenetic analysis and post-analysis of large phylogenies. Bioinformatics 30, 1312–1313 (2014).
19. Liu, L., Yu, L., Pearl, D.K. & Edwards, S.V. Estimating species phylogenies using coalescence times among sequences. Syst. Biol. 58, 468–477 (2009).
20. Liu, L. & Yu, L. Estimating species trees from unrooted gene trees. Syst. Biol. 60, 661–667 (2011).
21. Mirarab, S. et al. ASTRAL: genome-scale coalescent-based species tree estimation. Bioinformatics 30, i541–i548 (2014).
22. Tonini, J., Moore, A., Stern, D., Shcheglovitova, M. & Ortí, G. Concatenation and species tree methods exhibit statistically indistinguishable accuracy under a range of simulated

conditions. PLOS Currents Tree of Life 1, http://dx.doi.org/ 10.1371/currents.tol.34260cc27551a527b124ec5f6334b6be (2015).
23. Mirarab, S., Bayzid, M. S. & Warnow, T. Evaluating summary methods for multilocus species tree estimation in the presence of incomplete lineage sorting. Syst. Biol. http://dx.doi.org/10.1093/sysbio/syu063 (2014).
24. Barker, F. K., Cibois, A., Schikler, P., Felsenstein, J. & Cracraft, J. Phylogeny and diversification of the largest avian radiation. Proc. Natl Acad. Sci. USA 101, 11040–11045 (2004).
25. Parham, J.F. et al. Best practices for justifying fossil calibrations. Syst.Biol. 61, 346–359 (2012).
26. Longrich, N.R.,Tokaryk, T. & Field, D.J. Mass extinction of birds at the Cretaceous–Paleogene (K–Pg) boundary. Proc. Natl Acad. Sci. USA 108, 15253–15257 (2011).
27. Feduccia, A.The Origin and Evolution of Birds 2nd edn (Yale Univ. Press, 1999).
28. Jetz, W., Thomas, G.H., Joy, J.B., Hartmann, K. & Mooers, A.O. The global diversity of birds in space and time. Nature 491, 444–448 (2012).
29. Goldsmith,T.H.Hummingbirdsseenearultravioletlight.Science207,786–788 (1980).
30. delHoyo, J., Elliott, A., Sargatal, J., Christie, D.A. & deJuana, E. Handbook of the Birds of the World Alive (Lynx Edicions, 2015).
31. Katoh, K. & Standley, D.M. MAFFT multiple sequence alignment software version 7: improvements in performance and usability. Mol. Biol. Evol. 30, 772–780 (2013).
32. Meyer, M. & Kircher M. Illumina sequencing library preparation for highly multiplexed target capture and sequencing. Cold Spring Harb Protoc. http:// dx.doi.org/10.1101/pdb.prot5448 (2010).
33. Rokyta, D. R., Lemmon, A. R., Margres, M. J. & Arnow, K. The venom-gland transcriptome of the eastern diamondback rattlesnake (Crotalus adamanteus). BMC Genomics 13, 312 (2012).
34. Misof, B. et al. Phylogenomics resolves the timing and pattern of insect evolution. Science 346, 763–767 (2014).
35. Dornburg, A., Santini, F. & Alfaro, M.E. The influence of model averaging on clade posteriors: an example using the triggerfishes (Family Balistidae). Syst. Biol. 57, 905–919 (2008).
36. Tracer.v1.6 http://beast.bio.ed.ac.uk/Tracer(2014).
37. Robinson, D. F. & Foulds, L. R. in Combinatorial Mathematics VI in Lecture Notes in Mathematics, Vol. 748 (eds Horadam A. F. & Wallis W. D.) Ch. 12 119–126 (Springer, 1979).
38. Bogdanowicz, D., Giaro, K. & Wróbel, B. TreeCmp: comparison of trees in polynomial time. Evol. Bioinform. 8, 475–487 (2012).
39. Nye, T. M. W. Trees of Trees: an approach to comparing multiple alternative phylogenies. Syst. Biol. 57, 785–794 (2008).
40. Schliep, K. P. phangorn: phylogenetic analysis in R. Bioinformatics 27, 592–593 (2011).
41. Weyenberg, G., Huggins, P. M., Schardl, C. L., Howe, D. K. & Yoshida, R. KDETREES: non-parametric estimation of phylogenetic tree distributions. Bioinformatics 30, 2280–2287 (2014).
42. Drummond, A. J., Suchard, M. A., Xie, D. & Rambaut, A. Bayesian phylogenetics with BEAUti and the BEAST 1.7. Mol. Biol. Evol. 29, 1969–1973 (2012).

43. Rannala, B. & Yang, Z. Bayes estimation of species divergence times and ancestral population sizes using DNA sequences from multiple loci. Genetics 164, 1645–1656 (2003).
44. Shaw, T.I., Ruan, Z., Glenn, T.C. & Liu, L. STRAW: species tree analysis webserver. Nucleic Acids Res. 41, W238–W241 (2013).
45. Liu, L., Yu, L. & Edwards, S. A maximum pseudo-likelihood approach for estimating species trees under the coalescent model. BMC Evol. Biol. 10, 302 (2010).
46. Saitou, N. & Nei, M. The neighbor-joining method: a new method for reconstructing phylogenetic trees. Mol. Biol. Evol. 4, 406–425 (1987).
47. Mirarab, S., Bayzid, M.S., Boussau, B. & Warnow, T. Statistical binning enables an accurate coalescent-based estimation of the avian tree. Science 346 (2014).
48. Mirarab, S., Bayzid, M. S. & Warnow, T. Evaluating summary methods for multilocus species tree estimation in the presence of incomplete lineage sorting. Syst. Biol., (2014).
49. Bayzid, M.S. &Warnow, T. Naïve binning improves phylogenomic analyses. Bioinformatics 29, 2277–2284 (2013).
50. DeGiorgio, M. & Degnan, J. H. Fast and consistent estimation of species trees using supermatrix rooted triples. Mol. Biol. Evol. 27, 552–569 (2010).
51. Kimball, R.T., Wang, N., Heimer-McGinn, V., Ferguson, C. & Braun, E.L. Identifying localized biases in large datasets: a case study using the avian tree of life. Mol. Phylogenet. Evol. 69, 1021–1032 (2013).
52. McCormack, J.E. et al. A phylogeny of birds based on over 1,500 loci collected by target enrichment and high-throughput sequencing. PLoS ONE 8, e54848 (2013).
53. Springer, M.S. & Gatesy, J. Land plant origins and coalescence confusion. Trends Plant Sci. 19, 267–269 (2014).
54. Tonini J., Moore A., Stearn D. ,Shcheglovitova M. & Ortí, G. Concatenation and species tree methods exhibit statistically indistinguishable accuracy under a range of simulated conditions. PLOS Currents Tree of Life 1 (2015).
55. Pond, S. L. K. & Muse, S. V. in Statistical Methods in Molecular Evolution (ed. Nielsen, R.) 125–181 (Springer, 2005).
56. López-Giráldez, F. & Townsend, J.P. PhyDesign:an online application for profiling phylogenetic informativeness. BMC Evol. Biol. 11, 152 (2011).
57. Sanderson, M. A nonparametric approach to estimating divergence times in the absence of rate constancy. Mol. Biol. Evol. 14, 1218 (1997).
58. Simmons, M. P., Carr, T. G. & O'Neill, K. Relative character-state space, amount of potential phylogenetic information, and heterogeneity of nucleotide and amino acid characters. Mol. Phylogenet. Evol. 32, 913–926 (2004).
59. Townsend, J.P. & Leuenberger, C. Taxon sampling and the optimal rates of evolution for phylogenetic inference. Syst. Biol. 60, 358–365 (2011).
60. Klopfstein, S., Kropf, C. & Quicke, D.L.J.An evaluation of phylogenetic informativeness profiles and the molecular phylogeny of Diplazontinae (Hymenoptera, Ichneumonidae). Syst. Biol. 59, 226–241 (2010).
61. Drummond, A.J. & Bouckaret, R.R. Bayesian Evolutionary Analysis With BEAST (Cambridge Univ. Press, 2015).
62. Hsiang, A.Y.et al.The origin of snakes: revealing the ecology, behavior, and evolutionary history of early snakes using genomics, phenomics, and the fossil record. BMC Evol. Biol. 15, 87 (2015).

63. Phillips, M.J., Gibb, G.C., Crimp, E.A. & Penny, D. Tinamous and moa flock together: mitochondrial genome sequence analysis reveals independent losses of flight among ratites. Syst. Biol. 59, 90–107 (2010).
64. Pereira, S.L. & Baker, A.J. A mitogenomic time scale for birds detects variable phylogenetic rates of molecular evolution and refutes the standard molecular clock. Mol. Biol. Evol. 23, 1731–1740 (2006).
65. Nam, K. et al. Molecular evolution of genes in avian genomes. Genome Biol. 11, R68 (2010).
66. Drummond, A. J., Ho, S. Y. W., Phillips, M. J. & Rambaut, A. Relaxed phylogenetics and dating with confidence. PLoS Biol. 4, e88 (2006).
67. Dornburg, A., et al. Relaxed clocks and inferences of heterogeneous patterns of nucleotide substitution and divergence time estimates across whales and dolphins (Mammalia: Cetacea). Mol. Biol. Evol. 29, 721–736 (2012).
68. Yang, Z. & Rannala, B. Bayesian estimation of species divergence times under a molecular clock using multiple fossil calibrations with soft bounds. Mol. Biol. Evol. 23, 212–226 (2006).
69. Ho, S. Y. W. Calibrating molecular estimates of substitution rates and divergence times in birds. J. Avian Biol. 38, 409–414 (2007).
70. Heled, J. & Drummond, A. J. Calibrated tree priors for relaxed phylogenetics and divergence time estimation. Syst. Biol. 61, 138–149 (2012).
71. Benton, M. J. & Donoghue, P. C. J. Paleontological evidence to date the tree of life. Mol. Biol. Evol. 24, 26 (2007).
72. Clarke, J. A. Morphology, phylogenetic taxonomy, and systematics of Ichthyornis and Apatornis (Avialae: Ornithurae). Bull. Am. Mus. Nat. Hist. 286, 1–179 (2004).
73. Field, D. J., LeBlanc, A., Gau, A. & Behlke, A. D. B. Pelagic neonatal fossils support viviparity and precocial life history of Cretaceous mosasaurs. Palaeontology 58, 401–407 (2015).
74. Mayr, G. The age of the crown group of passerine birds and its evolutionary significance — molecular calibrations versus the fossil record. Syst. Biodivers. 11, 7–13 (2013).
75. Jetz, W. et al. Global distribution and conservation of evolutionary distinctness in birds. Curr. Biol. 24, 919–930 (2014).
76. Hedges, S. B., Parker, P. H., Sibley, C. G. & Kumar, S. Continental breakup and the ordinal diversification of birds and mammals. Nature 381, 226–229 (1996).
77. Benton, M. J. Early origins of modern birds and mammals: molecules vs. morphology. Bioessays 21, 1043–1051 (1999).
78. Hope, S. in Mesozoic Birds: Above the Heads of Dinosaurs (eds Chiappe L. M. & Witmer L. M.) 339–388 (Univ. of California Press, 2002).
79. Longrich, N. R., Tokaryk, T. & Field, D. J. Mass extinction of birds at the Cretaceous–Paleogene (K–Pg) boundary. Proc. Natl Acad. Sci. USA 108, 15253–15257 (2011).
80. Baker, A. J., Pereira, S. L. & Paton, T. A. Phylogenetic relationships and divergence times of Charadriiformes genera: multigene evidence for the Cretaceous origin of at least 14 clades of shorebirds. Biol. Lett. 3, 205–209 (2007).
81. dos Reis, M. et al. Phylogenomic datasets provide both precision and accuracy in estimating the timescale of placental mammal phylogeny. Proc. R. Soc. B 279, 3491–3500 (2012).
82. Dornburg, A., Townsend, J. P., Friedman, M. & Near, T. J. Phylogenetic informativeness reconciles ray-finned fish molecular divergence times. BMC Evol. Biol. 14, 169 (2014).

83. Brandley, M. C. et al. Accommodating heterogenous rates of evolution in molecular divergence dating methods: an example using intercontinental dispersal of Plestiodon (Eumeces) lizards. Syst. Biol. 60, 3–15 (2011).
84. Phillips, M. J. Branch-length estimation bias misleads molecular dating for a vertebrate mitochondrial phylogeny. Gene 441, 132–140 (2009).

CHAPTER 4

Genomic Signature of an Avian Lilliput Effect across the K-Pg Extinction[IV]

Jacob S. Berv[1*], Daniel J. Field[2,3*]

[1]† Department of Ecology & Evolutionary Biology, Cornell University, Ithaca NY USA

[2] Department of Geology & Geophysics, Yale University, New Haven CT USA

[3]†Milner Centre for Evolution, Department of Biology and Biochemistry, University of Bath, Bath, United Kingdom

*Correspondence to: Jacob S. Berv (jsb439@cornell.edu) and Daniel J. Field (d.j.field@bath.ac.uk)

†Current address

*These authors contributed equally to this work.

[IV] Reviewed, formatted, and accepted for publication as Berv, J.S. Field, D. J., Genomic Signature of an Avian Lilliput Effect across the K-Pg Extinction, Systematic Biology (2018), doi:10.1093/sysbio/syx064. Reprinted here with permission. Note: the version of the text as it appears here may differ slightly from that of the published article because it is derived from the last revision documents. Please refer to the published article when reading.

Abstract: Survivorship following major mass extinctions may be associated with a decrease in body size—a phenomenon called the Lilliput Effect. Body size is a strong predictor of many life history traits (LHTs), and is known to influence demography and intrinsic biological processes. Pronounced changes in organismal size throughout Earth history are therefore likely to be associated with concomitant genome-wide changes in evolutionary rates. Here, we report pronounced heterogeneity in rates of molecular evolution (varying up to ~20-fold) across a large-scale avian phylogenomic dataset, and show that nucleotide substitution rates are strongly correlated with body size and metabolic rate. We also identify potential body size reductions associated with the Cretaceous-Paleogene (K-Pg) transition, consistent with a Lilliput Effect in the wake of that mass extinction event. We posit that selection for reduced body size across the K-Pg extinction horizon may have resulted in transient increases in substitution rate along the deepest branches of the extant avian tree of life. This 'hidden' rate acceleration may result in both strict and relaxed molecular clocks over-estimating the age of the avian crown group through the relationship between life history and demographic parameters that scale with molecular substitution rate. If reductions in body size (and/or selection for related demographic parameters like short generation times) are a common property of lineages surviving mass extinctions, this phenomenon may help resolve persistent divergence time debates across the tree of life. Furthermore, our results suggest that selection for certain life history traits may be associated with deterministic molecular evolutionary outcomes.

Keywords: mass extinction, life history evolution, birds, molecular clocks, divergence times, metabolic rate, body size, K-Pg

Resolving conflicts between estimates of clade ages derived from molecular divergence time analyses and the known fossil record is a persistent challenge of contemporary systematics. While discrepancies between molecular clock and fossil ages have been identified in many major clades (e.g. Metazoa: Fontanillas et al. 2007, Actinopterygii: Dornburg et al. 2014, Angiospermi: Beaulieu et al. 2015, Mammalia: Phillips 2015) a particularly controversial example involves the age of crown birds (Cracraft et al. 2015, Ksepka and Phillips 2015) – the most recent common ancestor (MRCA) of all living birds, and all of that ancestor's descendants. This debate is compounded by the absence of fossils assignable to the stem lineages of the two deepest clades within crown birds, Palaeognathae and Neognathae. As such, variable assignments of maximum age constraints have generated widely differing estimates for the age of crown birds (varying from <75 Ma (e.g. Prum et al. 2015) to >160 Ma (e.g. Cracraft et al. 2015); notably, more ancient than the ~150 Ma stemward avialan *Archaeopteryx lithographica*). These varying estimates of the avian root age often influence age estimates of more exclusive descendent clades: older root age maxima tend to draw the radiation of the major subclade Neoaves into the Cretaceous (e.g. Jetz et al. 2012), thereby generating uncertainty about the role of the K-Pg mass extinction in shaping extant avian diversity. With little paleontological evidence to support the extensive radiation of crown birds in the Mesozoic, however, these estimates remain highly contentious (Mayr 2009).

While conflicts between 'rocks and clocks' may be partially reconciled by many factors (e.g. morphological lag time, taxon sampling, data quality; see supplementary appendix for detailed discussion, doi:10.5061/dryad.nr654), a mechanistic hypothesis for pervasive discrepancies between avian molecular divergence times and the fossil record is still wanting. Although the Mesozoic avian fossil record may be undersampled with respect to crown birds,

this interpretation is unlikely to fully explain existing divergence time discrepancies. The Mesozoic fossil record of crownward stem birds argues against the up to ~100 million-year missing fossil record advocated by unconstrained divergence time analyses without a maximum age prior on the root (Benton 1999, Cracraft et al. 2015), and generally supports a much younger estimate for the avian root age. Reconciling molecular divergence time estimates with the known crown bird fossil record thus suggests a hidden acceleration of the avian molecular clock at some point in avian evolutionary history (e.g. Alroy 1999, Benton 1999, e.g. Bromham 2003). However, a plausible mechanism for such an acceleration has yet to be articulated, casting doubt on this interpretation (Easteal 1999).

Mass extinction events have been characterized by marked reductions in body size among surviving lineages relative to their pre-extinction antecedents (Twitchett 2007). This phenomenon, known as the 'Lilliput Effect' (Urbanek 1993), is difficult to observe directly in many clades (including birds) because it requires an exceptionally well-sampled fossil record immediately before and after an extinction event. The challenge is exaggerated when surviving lineages are predicted to be very small-bodied, and therefore subject to taphonomic bias against their preservation and discovery (Brown et al. 2013). Body size is correlated to constellation of traits related to life history and demography, including generation length, population size, longevity, and metabolic rate (Simpson 1944, Western and Ssemakula 1982, Brown 1995, Roff 2002). As a result, pronounced changes in body size may be correlated with changes in rates of nucleotide substitution, an expectation that stems from the nearly neutral theory of molecular evolution (Kimura 1968, Ohta 1973, Nabholz et al. 2013, Figuet et al. 2016), as well as the metabolic theory of ecology (e.g. Brown et al. 2004; see supplement for a detailed discussion). Invoking the Lilliput Effect as a hypothesis to explain a hidden period of increased substitution

rates in a clade implies two general predictions: 1) that small body sizes are associated with faster substitution rates, and 2) that survivors of a mass extinction are characterized by reduced size relative to their pre-extinction relatives.

Here, we use simulations and ancestral reconstructions to address whether a 'Lilliput Effect rate-process' among bird lineages surviving the K-Pg event could be contributing to enduring discrepancies between avian divergence time estimates derived from molecular sequence data and the crown group fossil record. First, we combine paleontological data with ancestral state reconstructions (ASR) to suggest that a pulse of body size reduction may have occurred early in the evolutionary history of the avian crown group, possibly associated with the K-Pg transition. We then re-examine the hypothesis that substitution rate variation in birds is related to LHT (life history trait) evolution (e.g. Nabholz et al. 2016). Drawing on our results, we propose that body size-related changes in LHTs associated with the K-Pg mass extinction led to substitution rate perturbations among surviving lineages. We suggest that observed increases in nucleotide substitution rates could be a result of dwarfing within surviving lineages (thereby inducing lineage-specific rate accelerations), and/or of size-biased extinction affecting the distribution of substitution rates among surviving lineages (thereby generating clade-wide effects).

To our knowledge, the present study is the first to detect significant and potentially independent effects of body size and metabolic rate on avian substitution rate while controlling for other life history variables. We illustrate the impact of our findings on divergence time estimation by demonstrating that the association between body size and LHT evolution can have a pronounced effect on estimates of the antiquity of avian clades. In addition to presenting a new biological hypothesis to reconcile the avian crown age debate, the results we report may have

macroevolutionary implications relevant to studies of divergence times and diversification in the wake of mass extinctions in other clades across the tree of life.

Materials and Methods

Life history correlations

Life history data were obtained from the AnAge senescence database Build 13 (De Magalhães and Costa 2009, Tacutu et al. 2013). We collated the following data: (1) age at sexual maturity (days), (2) incubation time (days), (3) number of eggs laid per year, (4) mass at hatching (grams), (5) growth rate (1/days), (6), maximum recorded longevity (years), and (7) total metabolic rate (watts). For genera that were present in both Prum et al. (2015) and the AnAge database, we used average values per genus; otherwise we used family-level averages. Body mass (grams, species average) data were collected from Dunning Jr (1992). This yielded a data matrix with ~49% missing data overall (with no missing data for body mass, Supplemental Table 1).

We investigated correlations among life history traits (LHTs) and overall substitution rate using Coevol 1.4b, a Bayesian MCMC tool that estimates the correlation structure among the rate of molecular evolution and a set of quantitative traits. These parameters are jointly modeled as a multivariate Brownian process that incorporates evolutionary relationships (Lartillot and Poujol 2011, Lartillot and Delsuc 2012). A number of recent studies have investigated substitution rate processes such as dn/ds (e.g. Figuet et al. 2016) and kr/kc (e. g. Weber et al. 2014b), or mitochondrial rates (e.g. Nabholz et al. 2016); our analyses focus on the overall rate of nucleotide substitution in anchored enrichment loci (Lemmon et al. 2012, Prum et al. 2015).

We estimated correlations among log-transformed data in pairwise (i.e., one-to-one or marginal), and partial (i.e., controlling for all covariates) comparisons. We used the time-calibrated tree and sequence data from Prum et al. (2015) with fixed branch lengths, and the ten data partitions exhibiting the lowest declines in phylogenetic informativeness (the 'top-ten dataset' described in Prum et al. (2015), representing a ~41kb sample of largely exonic nuclear sequence data). Using data filtered by PI ensures that results are minimally biased by saturation (Dornburg et al. 2014). The sequence data were modeled as a single concatenated data matrix, as Coevol 1.4b does not allow for the unlinking of data partitions. At least 4 independent replicates were compared for each analysis, and adequate sampling of the posterior was assessed by ensuring convergence and effective sample size (ESS) values > 200.

Body Size Evolution

To investigate body size transitions early in the evolutionary history of crown birds, we compared reconstructions of early crown bird body sizes to end-Cretaceous body sizes of the crownward-most portion of the avian stem. First, we estimated mean body sizes for an assemblage of 18 crownward Cretaceous fossils found within 300 Ka of the K-Pg boundary (latest Maastrichtian). These fossils provide a snapshot of avian (*sensu lato*) diversity immediately before the K-Pg mass extinction event, and constitute one of the most diverse Mesozoic avifaunas known (Longrich et al. 2011). We generated body mass estimates (and associated 95% prediction intervals) for the 18 ornithothoracine fossils comprising the Longrich et al. (2011) dataset using updated predictive body mass equations for fossil birds (Field et al. 2013). The most precise osteological correlates of body mass were applied to each fossil, depending on which skeletal elements were preserved (see supplement).

Measures of a clade's central tendency can sometimes be misleading when used in phylogenetic comparisons (e.g. Felsenstein 1985). However, the relationships among the fragmentary Maastrichtian fossil taxa are largely unresolved (Longrich et al. 2011), which precludes directly incorporating information about their phylogeny into the present analysis. Instead, we used a model comparison approach (see *Trait Evolution* below). Ancestral body sizes within crown birds were estimated under a Brownian motion model in fitContinuousMCMC (Harmon et al. 2008) using the time-calibrated avian phylogeny from Prum et al. (2015) and data from sources described in the next section. We also compared these estimates to reconstructions conditioned on inferred rates of molecular evolution using Coevol 1.4b (see *Trait Evolution* and Figure 1) that were generated as part of the analyses described in the previous section (e.g. Lartillot and Poujol 2011, Lartillot and Delsuc 2012).

Influence of body size on divergence time estimates

We used multiple approaches to study the effect of body size and life history evolution on divergence time estimates. First, to simulate how different scenarios of size-biased extinction may influence molecular clock estimates of clade age, we performed simple divergence time analyses using BEAST 1.8.3 (Drummond et al. 2012). By using a prior rate estimate, we illustrate scenarios in which both relaxed and strict clocks that are unaware of life history evolution may generate clade age estimates that are systematically over- or underestimated. For these analyses, we generated three topological constraint trees by subsampling taxa from each of the seven major clades identified by Prum et al. (2015) (Palaeognathae, Galloanserae, Strisores, Columbaves, Gruiformes, Aequorlitornithes, Inopinaves). Four taxa were selected from each of these clades in each analysis; the four smallest in the clade, the four largest, and the four closest

to median clade body size (Simulation A). We restricted our sampling to four taxa per subclade to minimize the number of overlapping taxa in the three topological constraints, and to ensure that node density artifacts would not bias our estimates of clade age (Hugall and Lee 2007).

We performed divergence time analyses on each of the size-partitioned datasets to generate three estimates of the avian root age. Using the taxon samples and topological constraints described above, we first estimated the age of the avian MRCA using a strict clock (clock.rate parameter) set to the mean rate of 0.0005 s/s/Ma inferred from the Prum et al. (2015) phylogeny, using the standard birth-death tree prior and GTR+Γ_8 substitution model. We then performed a similar analysis employing relaxed dating methods under an uncorrelated relaxed lognormal clock (Drummond et al. 2006) to allow for lineage-specific rate variation. The ucld.mean parameter was set to follow a normal distribution with mean of 0.0005 s/s/Ma and standard deviation of 0.0001.

Next, we investigated the sensitivity of molecular clock ages to life history-biased extinction for the major subclade Neoaves (for which the fossil record is consistent with a post K-Pg radiation). We repeated the above analyses for low, median, and heavy taxon partitions within major neoavian subclades. For these analyses we included all available members from the sequential outgroups to Neoaves (Paleognathae and Galloanserae; Simulation B). This approach held the size-rate relationship constant in the two sister lineages to Neoaves, allowing us to evaluate how different scenarios of life history-biased extinction along the Neoaves stem group (which likely crossed the K-Pg boundary; Jarvis et al. 2014, Claramunt and Cracraft 2015, Prum et al. 2015) may be responsible for biasing previous estimates of the root age of Neoaves. Simulation B yielded median neoavian MRCA age estimates that were virtually identical to

those of Simulation A, so they are presented as part of the supplementary discussion (see Supplementary Figure 7).

To test the hypothesis that size reduction within surviving lineages accelerated the rate of molecular evolution along the deepest internodes within the crown bird tree, we sought to estimate avian divergence times while simultaneously accounting for the portion of the molecular clock that may be explained by life history evolution. To reduce the size of branch length parameter space, we set tight uniform priors (2 Ma intervals) derived from the median posterior age estimates from Prum et al. (2015) around the 19 nodes previously used for fossil-informed age constraints by Prum et al. (2015), and performed analyses with a birth-death speciation prior and the autocorrelated relaxed clock in Coevol 1.4b (Lartillot and Poujol 2011, Lartillot and Delsuc 2012). An uninformative gamma prior was applied to the root node (mean = 1000, SD = 1000). We performed sets of three analyses: 1) with no size or LHT data, 2) including body size but no other LHT data 3) including the full body size and LHT data matrix. We ran multiple independent MCMC chains for each comparison. We then compared estimates of the mean posterior age estimates of all nodes both with and without life history data. Despite lengthy attempts to reanalyze the avian evolutionary timescale in Coevol 1.4b to directly test for lineage-specific rate accelerations, these analyses failed to converge (see supplementary discussion). Nevertheless, our correlational analyses allowed us to generate predictions of evolutionary body size changes across the K-Pg required to accommodate the molecular rate perturbations implied by the Prum et al. (2015) dataset (see *Trait Evolution*).

Trait evolution

To evaluate the choice of the Brownian motion model assumed in Coevol 1.4b (Lartillot and Poujol 2011, Lartillot and Delsuc 2012), we followed Slater et al. (2012) and compared four commonly used models of trait evolution using the 'bayesian fitContinuousMCMC' function in Geiger (Harmon et al. 2008). These models included Brownian motion (BM), a single-optimum Ornstein–Uhlenbeck model (called SSP, for single stationary peak, in Geiger), and two variants of the early burst model described in (Harmon et al. 2010). The latter two models accommodate rapid character evolution near the clade MRCA, followed by a linear or exponential decrease in the rate of evolution. To increase the efficiency of the MCMC search, model proposal widths were iteratively tweaked until MCMC acceptance rates were between 25-75%. All chains were run until ESS values were > 200. We also repeated this analysis using the maximum likelihood function 'ace' in ape (Paradis et al. 2004).

To assess support for K-Pg-related body size reduction along the backbone of the crown bird phylogeny, we used an information theoretic approach (using the 'fitContinuousMCMC' and 'aicm' functions), implemented in Geiger (Harmon et al. 2008) to rank hypotheses of trait evolution using Brownian motion. In one model, we applied body size priors (using uniform priors) to the Neornithes, Neognathae, and Neoaves MRCA nodes to match our latest Maastricthian mean body size estimate. This model represents a scenario in which body size did not evolve along the neornithine backbone relative to the latest Maastricthian assemblage (model A). In another model, we parameterized those nodes to match the median posterior estimates from an unconstrained Brownian motion model (model B, a pseudo 'null'). In a third model, we applied body size priors to the Neornithes, Neognathae, and Neoaves MRCA nodes to match the Neornithes MRCA estimate from an unconstrained Brownian motion model (model C).

Integrating information from the fossil record into ancestral state reconstructions increases reconstruction accuracy (Slater et al. 2012, Hsiang et al. 2015, Mitchell 2015). To improve our ASRs, we generated body mass priors derived from the set of 19 fossils used for time calibration points in Prum et al. (2015) and applied them to the calibrated nodes from that study. We generated priors by estimating body masses and associated 95% prediction intervals using the most precise osteological correlates of body mass given available measurements (see supplemental table 3, Figure 1; Field et al. 2013). For each fossil, we derived a mean and standard deviation to use as a normal prior in Geiger, assuming estimated upper or lower 95% prediction bounds are 1.96 standard deviations away from the mean. Because the 95% prediction intervals for these mass estimates are slightly asymmetric around the mean body size estimate (as size estimates cannot go below zero), we performed two alternative analyses using either the upper or lower bound priors, resulting in normal prior distributions (required by Geiger) that were either slightly wider (upper bound), or slightly narrower (lower bound).

Finally, while we acknowledge the well-explored difficulties of inferring accurate ancestral states for continuously varying traits (e.g. Webster and Purvis 2002), the accuracy of ASR has also been suggested to increase with increasing phylogenetic signal (see Fig. 2 in Litsios and Salamin 2012). Thus, we calculated phylogenetic signal (Pagel's λ, Pagel 1999, Blomberg's K, Blomberg et al. 2003) for body size using the 'phylosig()' function in phytools (Revell 2012) and α from an Ornstein-Uhlenbeck process (Hansen 1997) modeled using the 'fitContinuous' function in Geiger (Harmon et al. 2008).

Results

Substitution rate variation

For Bayesian uncorrelated-lognormal relaxed clock analyses (UCLD) in BEAST, a coefficient of variation (CoV) is recorded that provides information about how clock-like the underlying sequence data are. The CoV is defined as the clock's standard deviation divided by the mean clock rate, and values below 0.1 are considered to be strong evidence for a strict clock (Drummond and Bouckaret 2015). Re-examination of the output from Prum et al. (2015) indicates a strong rejection of clock-like evolution (mean: 0.93, 95% HPD: 0.41-2.16), and suggests that, on average, lineages vary by ~93% of the clock mean. Supplemental Figure 3 illustrates the median rates estimated for all branches, which vary by a factor of ~20 in the Prum et al. (2015) BEAST analysis. While the estimation of uncorrelated clock rates is inherently uncertain (Lartillot et al. 2016), with wide, overlapping HPD intervals, examining rates inferred to fall within the fastest 2.5% and slowest 2.5% (dashed lines in Supplemental Figure 3) revealed clear body size associations.

Life history correlations

When examined in pairwise comparisons, all LHTs, except for total metabolic rate (pp ~ 0.3, Supplemental Table 2), were significantly correlated with overall substitution rate at almost maximal posterior probability (pp~1.0). Bayesian analyses do not require corrections for multiple hypothesis testing (Gelman et al. 2012). All LHTs were inferred to be correlated to each other at maximal posterior probability (Supplemental Figure 6). Including phylogeny in the model slightly reduced the average effect size (average $R^2 = 0.33$) under the available Brownian motion model of evolution, compared to uncorrected linear regressions (average $R^2 = 0.40$, all significant with Bonferroni correction).

Partial correlations (controlling for all other covariates) detected that substitution rate is inversely correlated with adult body mass, and positively correlated with metabolic rate (R^2 = 0.1, pp = 0.97 and R^2 = 0.2, pp = 0.96, respectively, Supplemental Table 2). An additional analysis which allowed GC content to vary across lineages (-gc option in Coevol 1.4b; Lartillot and Delsuc 2012), while also controlling for metabolic rate, suggested that adult body mass may explain a substantial portion of the variance in overall substitution rate (partial mass R^2 = 0.45, pp = 0.99; partial metabolic rate R^2 = 0.22, pp = 0.91). We suggest this increase in R^2 may indicate that accounting for GC-biased gene conversion (e.g. Romiguier et al. 2010, Weber et al. 2014a) allows life history effects to explain more of the variance in substitution rate. Interestingly, Weber et al. (2014a) and Nabholz et al. (2013) also noted that patterns of GC content evolution in birds are consistent with body size reduction through time.

Body size evolution

We estimated mean body sizes for an assemblage of crownward bird fossils found within 300 Ka of the K-Pg boundary (latest Maastrichtian). This assemblage constitutes the only described diverse avifauna constrained to sediments closely preceding the end-Cretaceous mass extinction (Longrich et al. 2011). We estimate the median body size within this avifauna to have been ~959g (mean = 1,380g, Figure 1a). This estimate greatly exceeds the mean (~300g) and median (~37g) body masses of extant crown group birds (Dunning Jr 1992). With the caveat that this result represents a preliminary effort to address the plausibility of avian body size change across the end-Cretaceous mass extinction event, this pattern is consistent with the hypothesis that crown birds and their closest stem group relatives may have been relatively large immediately preceding the K-Pg mass extinction. The Latest Maastrichtian fossil assemblage has

intrinsic limitations, particularly regarding potential taphonomic and taxonomic biases (see our supplement for a discussion of this topic); however, the apparently strong influence of inferred body size transitions on molecular divergence time analyses (see 'Life history correlations' and 'Influence of body size on divergence time estimates' below) render these results of interest, and should stimulate continued research on this subject.

For uncalibrated body size reconstructions, Brownian motion was preferred over the next best model by ~80 AICM units (Raftery et al. 2006), and received 100% model weight (consistent with Harmon et al. 2010). Across models, absolute estimates of body size evolution between the neornithine, neognath, and neoavian MRCAs were nearly identical, suggesting that the observed pattern of size reduction leading to the neoavian MRCA is not driven solely by the assumptions of Brownian motion. Analyses that included body size priors based on Cenozoic crown bird fossils yielded very similar results (Figure 1a). All models detected a trend of substantial size reduction (by almost an order of magnitude) relative to our estimate for the latest Maastrichtian avifauna, followed by explosive body size evolution in the Paleocene (Figure 1b, c).

For calibrated analyses using the set of priors based on the 95% upper bound fossil body mass, Brownian motion was again selected as the preferred model (dAIC ~17, weight = 99.99%). The reconstructed states for the three deepest nodes within Neornithes were slightly smaller than those in ASR analyses without fossil calibrations, and became smaller still when using the tighter 95% lower bound mass priors (Figure 1). The Neornithes MRCA (median) was reconstructed as ~553g in the upper-bound fossil calibrated analysis (~617g in uncalibrated), ~50% smaller than our median body size estimate for the pre-K-Pg assemblage. The Neognathae MRCA and Neoaves MRCA exhibit additional ~10% and ~50% reductions in inferred body size from

internode to internode (upper-bound fossil calibrated results: 553g, 299g, respectively; uncalibrated: 564g, 339g, respectively).

Intriguingly, Coevol ASRs, which are in effect calibrated by the inferred correlation between rate of molecular evolution and body mass (in this case, using the examined model with highest explanatory power, included body mass, metabolic rate, and GC variation, R^2=0.45, above), generated median posterior estimates of ancestral body masses that were substantially smaller than the LM (latest Maastrichtian) estimate: Neornithes MRCA (352.75 g), Neognathae MRCA (372.45 g), Neoaves (195 g) (Figure 1, Supplemental Figure 8)**.** These estimates represent predictions of the ancestral body masses that would have been required to accommodate the high rates of molecular evolution implied by the Prum et al. (2015) phylogeny. Notably, the body mass estimate for the Neoaves MRCA is smaller than that inferred for all of the fossil taxa in the LM fossil assemblage, save one (~ 192g estimated for *Cimolopteryx minima*, a crown-grade ornithurine; Longrich et al. 2011). When Coevol detects a statistically significant correlation between a trait and substitution rate, ancestral state reconstructions that do not accommodate this correlation can be statistically rejected (*N. Lartillot*, personal communication, Supplemental Figure 8). Coevol 1.4b, however, cannot combine normally distributed node-based trait priors with rate-trait relationships, so we could not conduct analyses that combined our fossil mass priors with this additional source of information.

Statistical support for body size reduction near the K-Pg boundary is strong across multiple analyses (see Figure 1). For model A (latest Maastrichtian constraint), the AICM = 1285; for model B (null), AICM = 1249; for model C (Neornithes constraint), AICM = 1259. Because the AICM scores for model B << Model C << Model A, we find that a model which accommodates substantial size reduction relative to the latest Maastricthian body size estimate,

and size reduction along the neornithine backbone, represents a statistically significant improvement in model fit ($^{\Delta}AICM_{A\text{-}B}$ ~36, $^{\Delta}AICM_{B\text{-}C}$ ~26 AICM). Trend model support for size reduction along the neornithine backbone was similar (e.g., $^{\Delta}AICM_{B\text{-}C}$ ~20). Additionally, body size exhibits significant ($p << 0.05$) and high phylogenetic signal ($\lambda = 0.93$, $K = 1.49$, $\alpha = 0.00$) in our dataset, further implying that our data are generally consistent with a Brownian motion model of evolution, and are perhaps phylogenetically conservative ($K > 1$, Losos 2008, Revell et al. 2008).

Influence of body size on divergence time estimates

Simulations of different life history-biased extinction scenarios using sets of low, median, and high mass taxa with a strict clock set to the mean inferred rate of the Prum et al. (2015) analysis reveal that a difference of ~37.5 Ma in estimated avian root age can be explained by differences in substitution rate related to body mass (Figure 3). Our simple approach allowed us to generate three estimates of the neornithine MRCA age that represent the within-clade body size disparity of extant birds. Further, the observed discordance associated with estimates of clade age and average clade mass can be described by a simple linear function ($n=3$, $R^2=0.99$, $p=0.04$, clade age = 162.06 – 9.18(ln(average clade mass)). The 'low mass' taxon partition yielded a median posterior root age of 115.7 Ma, while 'median' and 'heavy' partitions yielded estimates of 94.8 Ma and 78.3 Ma, respectively, with narrow, non-overlapping HPD intervals of 5-10 Ma (Figure 3). Repeating these analyses with uncorrelated relaxed clocks generated the same pattern of median estimates (low = 125.3 Ma; median = 100.8 Ma; high = 81.6 Ma). As was the case for Neornithes, strict and relaxed clock estimates for the root age of Neoaves

revealed a striking association with body size, (e.g, strict clock: low = 68.9 Ma, median = 61.5, heavy = 44.8 Ma; Figure 3 & Supplemental Figure 7).

In general, we suggest that median mass taxon partitions may represent more accurate estimates of divergence times, insomuch as they may be less likely to be biased by extreme rates of molecular evolution. However, we do not intend that the results (i.e. age estimates) of these analyses be interpreted strictly; they are intended to demonstrate the largely unexplored sensitivity of molecular clock estimates of clade age to evolutionary perturbations in body size.

Discussion

Our data strongly support the hypothesis that macroevolutionary fluctuations in avian body size may induce substantial changes in nucleotide substitution rates in birds (Martin and Palumbi 1993, Smith and Donoghue 2008), and confirm the hypothesis that smaller-bodied birds exhibit higher rates of nucleotide sequence evolution (e.g. Figuet et al. 2016, Nabholz et al. 2016). Thus, a hidden period of nucleotide substitution rate acceleration may be partly explained by selection for small body size closely associated with the K-Pg extinction event. We propose a Lilliput-rate-process as a mechanistic hypothesis to explain a portion of the 'rocks and clocks' discrepancy in estimates of the avian crown age.

LHT correlates of total substitution rate in birds

The present study illustrates how an underappreciated source of molecular clock error—life history's connection to demography, and ultimately mutation rate—may have deterministic effects on substitution rates. In our analyses, body size and metabolic rate exhibited consistently significant associations with the rate of nucleotide evolution when other LHTs were controlled

for. When controlling for body size, metabolic rate (BMR) is a measure of mass-specific metabolic rate, which scales inversely with body size (Reynolds and Lee 1996, McNab 2012), and may be positively and causally associated with mutation rate (Martin and Palumbi 1993, Mindell et al. 1996, Gillooly et al. 2005, Gillooly et al. 2007). Our analyses detect such a positive association (Figure 2; see supplement). Smaller bodied birds would also be subject to additive substitution rate effects induced by demographic processes (i.e., shorter generation time, and in the context of the K-Pg, reduced population size). The negative association we observe between substitution rate and body size in partial correlations may be indicative of such a demographic signal. Thus, the present work may represent the first illustration of independent effects of body size and metabolic rate on avian substitution rate. Finally, because the anchored enrichment data used in this analysis may include some sites evolving non-neutrally (Lemmon et al. 2012), we suggest that our results may be conservative, as selection (acting in different directions) affecting the rate of molecular evolution is less clearly correlated with life history evolution (Martin and Palumbi 1993, Smith and Donoghue 2008).

Substitution rate variation

Our re-analyses of the Prum et al. (2015) dataset suggest that a model with ~20x rate heterogeneity is required to describe genomic rate variation across the avian tree of life (Supplemental Figure 1, 2; also, see supplemental discussion on the Niobrara Formation-informed crown prior). Among the branches falling within the fastest 1% are those leading to tinamous (Tinamidae), Neoaves (at least the stem of which likely crosses the K-Pg), swifts (Apodidae), and perching birds (Passeriformes), while those falling within the slowest 1% include the branches leading to Ciconiiformes (storks and kin), Cathartidae (New World

vultures), and Procellariiformes (tubenoses). This pattern is consistent with branch length estimates derived from the classic DNA-DNA hybridization studies of Sibley and Ahlquist (1990); the fastest (99th rate percentile) represents lineages that include extant taxa that are generally small and short-lived, while the opposite is true for the lineages found in the 1st percentile.

Our analysis also corroborates prior findings (e.g. Baker et al. 2007, Hackett et al. 2008) of an extremely long branch length (extremely fast substitution rate) for the lineage leading to *Turnix*, the cause of which has yet to be fully understood. The inferred pace of molecular evolution in *Turnix* is so extreme that it is unlikely to be due to life history evolution alone—this question merits further investigation.

Notably, we infer the stem lineage leading to the generally large-bodied Paleognathae (the sister group to all other birds, which likely crosses the K-Pg boundary), to exhibit a rate falling above the fastest 2.5 percentile of branch rates across the entire avian phylogeny. In the context of the present study, this result implies that the early ancestors of crown Paleognathae that survived the K-Pg extinction were small-bodied (and probably volant, Faux and Field 2017), with molecular evolutionary rates like those of ancestral tinamous or neoavians (this has recently been independently corroborated with paleogenomic approaches, see: Mitchell et al. 2014, Yonezawa et al. 2016).

Yonezawa et al. (2016) report an ancestral paleognath MRCA size of 3.8-5.5 kg; our analyses infer an ancestor that is smaller (Coevol: ~2.9 kg, Supplemental Figure 8). Notably, Yonezawa et al. (2016) suggest that the young age (~50 Ma) inferred for crown Paleognathae in Prum et al. (2015) relative to other studies may be due to incorrect rooting; instead, we suggest that it may be a result of convergent molecular rate decelerations experienced among large

flightless ratites. This result has important implications for the study of palaeognath macroevolution and biogeography that are beyond the scope of the present work. However, evidence that the paleognath stem lineage may be among the fastest evolving lineages in the avian tree (because of ancestrally small body size) supports the hypothesis that prior molecular clock age estimates for the Neornithes MRCA may be upwardly biased.

Convergent evolution of extremely large size in several paleognath lineages during the Cenozoic (Mitchell et al. 2014, Yonezawa et al. 2016) likely biases ASRs against the hypothesis of a small bodied paleognath ancestor, and will make it difficult to test such hypotheses without presently elusive fossil corroboration. If the ancestral paleognath was indeed small (perhaps even smaller than our estimates), our illustration of size reduction along deep neornithine internodes may be correspondingly inflated. However, such a scenario would still support the underlying hypothesis that lineages evolving at fast rates towards the base of the neornithine phylogeny are at least partly responsible for driving age overestimations. Clearer constraints on the antiquity of the various paleognath subclades—as well as a timeline of independent body size increases among ratites—await the discovery and accurate phylogenetic interpretation of additional paleognath fossils.

Using molecular clocks to estimate the antiquity of the avian crown

Reconciling clade ages estimated from the fossil record and molecular clocks is critical for testing hypotheses linking major events in Earth history with patterns of biological diversification (e.g. Claramunt and Cracraft 2015), as well as any model-based phylogenetic comparative analyses which use branch length information (e.g. Jetz et al. 2012). For example, rejecting an association between the explosive radiation of Neoaves and the mass extinction of

non-avian dinosaurs at the K-Pg boundary demands that methodological artifacts cannot explain the discrepancy between molecular clocks and the fossil record. The degree to which size-biased extinction and/or lineage-specific rate accelerations may contribute to clade age overestimations remains an open question. Our linear equation from Fig. 3 suggests that a decrease in 'average clade size' of ~1.3kg to ~250g along the neornithine backbone could induce a clade age increase of ~15 Ma (although we emphasize that this is a rough estimate). Therefore, pulsed selection against large body size in the context of the K-Pg event could explain rate increases among surviving lineages.

Further, the inclusion of appropriately parameterized crown group fossil time-calibrations are predicted to alleviate–but not eliminate–this source of bias, as they are generally applied with hard minimum and (critically) infinite maximum ages that allow age estimates to be pushed farther back in cases of substitution rate accelerations. Worryingly, if strongly elevated substitution rates driven by selection for reduced body size across the K-Pg boundary did indeed take place, even the most sophisticated relaxed clock methods currently available will likely fail to detect them. Further complicating the problem for birds, as previously stated, is the fact that there are presently no fossils that can be used to directly calibrate the minimum ages of the Paleognathae, Neognathae, or Neoaves stem lineages, or the age of the Neornithes MRCA. To accommodate this problem, Prum et al. (2015) employed an informative but soft-bound prior on the root of Neornithes, reflecting the conspicuous absence of avian crown group fossils in the Late Cretaceous Niobrara Formation. This deposit has produced hundreds of crownward stem bird fossils, and reflects the complete absence of any known crown birds from the entirety of the Mesozoic until ~67 Ma across all environments and continents. Applying this prior compresses

the age of the neornithine MRCA by ~30 Ma, and induces high substitution rates at the base of the tree (see supplemental discussion).

Phillips (2015) provides an argument in favor of using such 'appropriately conservative' priors in the face of pronounced age overestimates relative to the fossil record. We note here as well that such a calibration choice may be justified when three lines of evidence are satisfied: 1) an observation of extreme branch length extension incompatible with the fossil record, 2) evidence of a correlation between life history and substitution rate, and 3) evidence of consistent patterns of life history evolution occurring across relevant nodes. We suggest that all three of these points are satisfied in the case of crown group birds. Future investigation of these patterns will require the additional development and refinement of tools for the simultaneous estimation of divergence times, substitution rates, and their relationship with life history traits under different character and relaxed clock models (e.g. Lartillot et al. 2016).

The Lilliput Effect

The pervasiveness of the Lilliput Effect as a macroevolutionary phenomenon associated with mass extinction events has been questioned (Brayard et al. 2010, Huang et al. 2010). However, considering the expected difficulty of directly observing evidence of the Lilliput Effect in crown bird fossils flanking the K-Pg mass extinction boundary, the present lack of fossil evidence directly informing avian body size change cannot be used to reject the possibility of a marked filtering of body sizes among avian survivors of the extinction event. Given the apparently profound influence of the K-Pg mass extinction on crownward representatives of the avian stem group (Longrich et al. 2011), as well as the striking selection against large body size among many surviving lineages (McKinney 1990, Van Valen 1994, Archibald 2013, Wilson

2013), avian survivors may have been subject both to strong ecological selection for reduced body size and marked population size reductions in the immediate wake of the extinction event (e.g. Friedman 2009, Sallan and Galimberti 2015). Increased rates of nucleotide substitution are also predicted to be associated with reduced population size (e.g. Lanfear et al. 2013b). Indeed, the conspicuous rarity of fossil birds in the immediate aftermath of the K-Pg (Mayr 2009) may be jointly explained by reduced population sizes (Hull et al. 2015) and the diminished preservation potential of smaller survivors (Brown et al. 2013).

We suggest that spuriously ancient molecular divergence time estimates may be explained either by the selective extinction of relatively large-bodied taxa across an extinction horizon, and/or by size reduction of surviving lineages following a mass extinction event. We propose that both mechanisms can lead to accelerations in the rate of molecular evolution that manifest as branch length artifacts. The observation of pronounced molecular clock age overestimates relative to the fossil record in the context of the K-Pg mass extinction may therefore indicate a telltale genomic signature of the Lilliput Effect in birds and other extant clades that crossed the K-Pg boundary.

Macrogenetic Evolution

Considering our results, we can speculate that if the K-Pg acted as a LHT filter favoring relatively small survivors, the explosive post-K-Pg diversification of crown Neoaves into newly vacant niche space may have been promoted by high genetic diversity generated by rapid rates of molecular evolution in surviving lineages. Similarly, the net rate of diversification in birds appears to be correlated to rates of molecular evolution (Lanfear et al. 2010). As noted by Jablonski (2008): "...small body sizes might increase sensitivity to geographic barriers and thus

promote speciation even as accompanying large population sizes decrease species-extinction probability." The nature of the relationships among life history strategies, genetic diversity, and evolutionary rates implies that a lineage's adaptive potential in the face of marked environmental perturbations may be mediated by these interactions (Simpson 1944, Lee et al. 2013, Benson et al. 2014, Romiguier et al. 2014).

Our analyses also suggest that the cataclysmic K-Pg transition may have driven a rapid reduction of body size among ancestral crown bird lineages, following the protracted reduction in body size among progressively crownward dinosaurs throughout the Mesozoic (Brusatte et al. 2014, Lee et al. 2014, Puttick et al. 2014). Historical contingencies resulting in mass extinction and faunal body size change, like the Chicxulub asteroid impact (Alvarez et al. 1979), may therefore lead to deterministic macroevolutionary outcomes, such as pronounced changes in molecular substitution rates via associations with LHTs. Phenotypic convergence (or life history-biased extinction) toward reduced body size among lineages surviving a mass extinction may consequently result in convergent molecular substitution rate accelerations.

As hunting and habitat destruction have disproportionately affected large taxa in the Anthropocene (Duncan et al. 2002, Jablonski 2004), will the impact of human activity parallel the effects of the K-Pg transition on avian evolution? Larger-bodied species have a demonstrably higher risk of extinction than small species (Gaston and Blackburn 1995, Faurby and Svenning 2016), and populations of hundreds of bird species have declined precipitously despite conservation efforts (Barnosky et al. 2011, McLellan et al. 2014). Indeed, the fact that numerous large-bodied avian clades (e.g., Dromornithidae, Teratornithidae, Sylviornithidae, Aptornithidae, Aepyornithidae) have been lost throughout the Holocene implies that the diversity of birds available to sample today is biased towards smaller taxa exhibiting faster average rates of molecular evolution relative to avian diversity

merely thousands of years ago. The extent to which selection for demographic and life history traits across mass extinction boundaries influences rates of molecular evolution represents an important area of future macroevolutionary investigation in many clades. Such work may reveal fundamental insights into how, and when, Earth's modern biodiversity arose.

Supplementary Material: Supplementary material, including data files and/or online-only appendices, can be found in the Dryad data repository (doi:10.5061/dryad.nr654).

Funding: This research was supported by a National Science Foundation Graduate Research Fellowship and Doctoral Dissertation Improvement Grant to JSB (DGE-1650441, DEB-1700786), and a National Sciences and Engineering Council of Canada Graduate Scholarship to DJF. JSB was also supported by a Cornell Laboratory of Ornithology Athena Grant.

Acknowledgments: The research was aided by discussions with I. Lovette, R. O. Prum, J. R. Shipley, L. Campagna, D. Toews, E. Miller, N. Hofmeister, N. Mason, A. Lees, C. Edwards, J. Lewis, J. Gauthier, L. Arcila Hernández, E. Funk, P. Donoghue, R. Benson, A. Farris, A. McCune, A. Agrawal, N. Lartillot, and we are especially thankful to A. Dornburg for helpful comments and analytical suggestions. We are grateful to Simon Ho, Michael S.Y. Lee and an anonymous reviewer for comments that substantially improved this manuscript. Analyses were performed at the Yale University Biomedical High Performance Computing Center, supported by NIH grants RR19895 and RR029676-01. JSB and DJF designed and performed the research, and contributed equally to the manuscript.

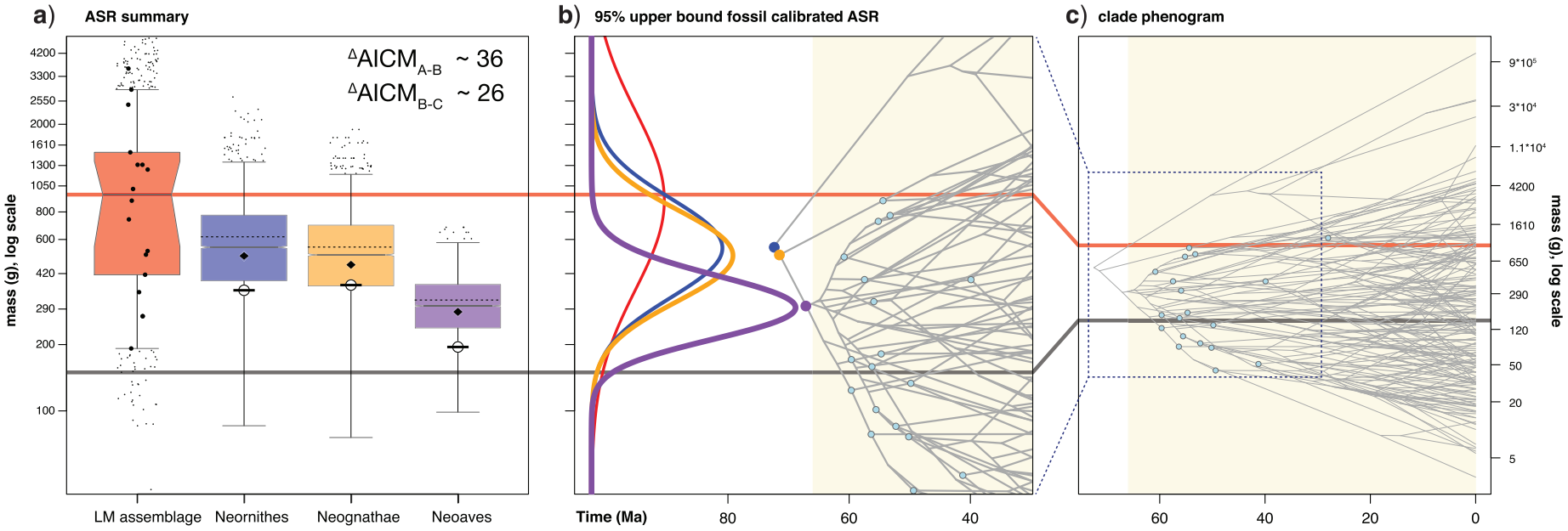
a) ASR summary
b) 95% upper bound fossil calibrated ASR
c) clade phenogram
ΔAICM A-B ~ 36
ΔAICM B-C ~ 26
mass (g), log scale
4200
3300
2550
2000
1610
1300
1050
800
600
420
290
200
100
LM assemblage
Neornithes
Neognathae
Neoaves
Time (Ma)
80
60
40
60
40
20
0
9*10⁵
3*10⁴
1.1*10⁴
4200
1610
650
290
120
50
20
5
mass (g), log scale

Figure 4.1. Avian body size evolution in association with the K-Pg boundary.

a): Ancestral state reconstructions of body size for the three most inclusive nodes within crown birds, compared to the body size distribution of a fossil avifauna from the latest Maastrichtian (LM assemblage; Longrich et al. 2011). For the LM assemblage, a sample of outliers are indicated from a simulated normal distribution, while large black dots indicate mass point estimates for fossil taxa (Supplemental figure 4). Dashed horizontal lines (black) within boxplots to the right of the LM assemblage indicate median posterior estimates from reconstructions excluding fossil body size priors; these are slightly larger than those from analyses directly incorporating fossils (using 95% upper bound priors; posterior distributions summarized by colored boxplots), suggesting that including fossil information increases the magnitude of inferred changes between the center of the LM assemblage and the reconstructions for early neornithine nodes. Median size estimates using 95% lower bound priors indicated by diamonds. Crossed circles indicate median size estimates conditioned on the correlation between rates of molecular evolution and body size, as inferred in Coevol 1.4b (Lartillot and Poujol 2011).

The red horizontal line that passes through panels a-c) indicates the median value of the LM assemblage (~1kg), and the dark grey horizontal line that passes through panel a-c) indicates the median mass of extant taxa in this dataset (~150g, somewhat larger than the median mass of extant Neornithes, ~37g). The depicted progression of body size reduction represents an improvement of up to 36 AICM units relative to a model that constrains the three deepest nodes to the mean LM estimate ($^{\Delta}AICM_{A\text{-}B} \sim 36$). $^{\Delta}AICM_{B\text{-}C} \sim 26$: an alternative model that enforces the Neornithes constraint. Boxplot colors match curves in panel b).

b): Reconstructed body size changes in close association with the K-Pg boundary (Cenozoic indicated in pale yellow). On the left, the red curve indicates a normal distribution fit

to the body size distribution of the LM assemblage. Blue, orange, and purple curves trace the posterior distributions estimated for body size of the three most inclusive nodes in the crown avian phylogeny (matched to their respective nodes with colored circles). Right side of panel b): zoomed-in 'phenogram' of body size evolution (to compare with the full range of phenotype evolution displayed in panel c)). Pale blue dots indicate Cenozoic nodes calibrated by body size priors in this study. **Please refer to the published version of this article for higher quality vector art.**

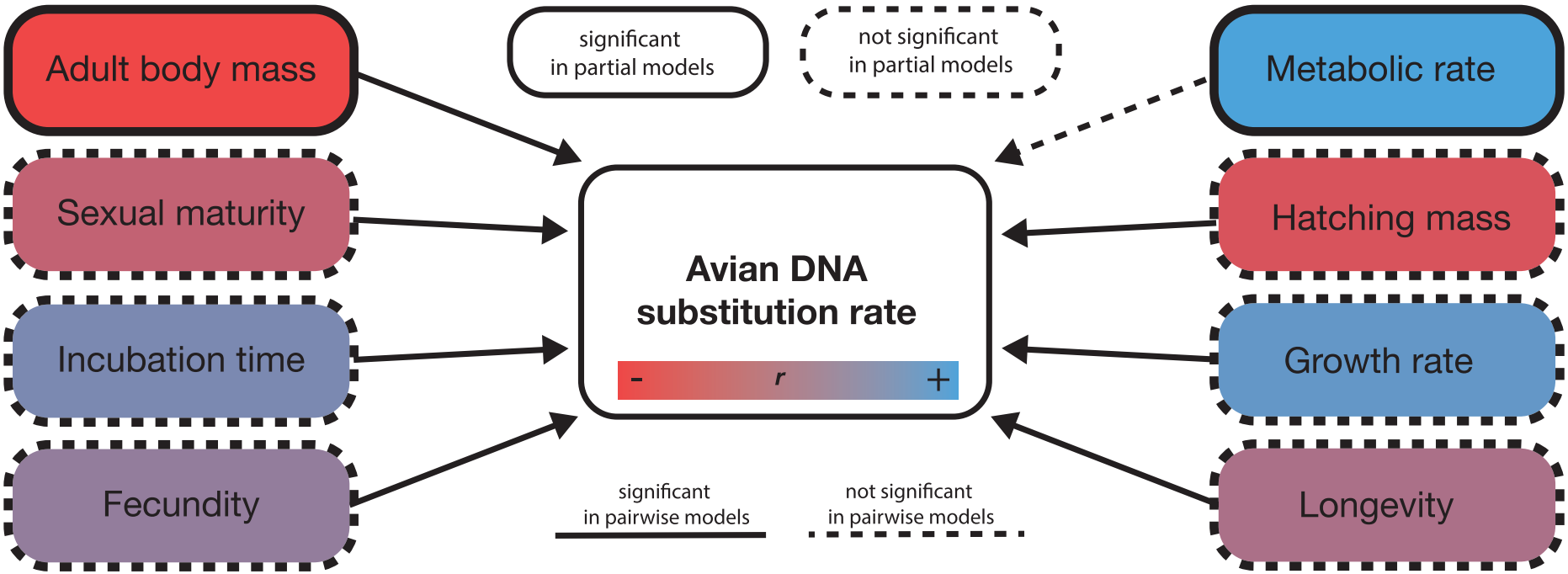
Adult body mass
Sexual maturity
Incubation time
Fecundity
significant
in partial models
not significant
in partial models
Avian DNA
substitution rate
-
r
+
significant
in pairwise models
not significant
in pairwise models
Metabolic rate
Hatching mass
Growth rate
Longevity

Figure 4.2. Model of the inferred correlation structure among life history traits and overall rate of nucleotide substitution (from Coevol 1.4b, Lartillot and Delsuc 2012). Body mass and metabolic rate remain statistically significant in partial correlations. Each link represents a test of a statistical association between a life history parameter and overall nuclear substitution rate (following Lanfear et al. 2013a). Solid arrows indicate that the relationships are statistically significant (posterior probability > 0.95 (positive relationship) or < 0.05 (negative relationship)) in pairwise comparisons, while dashed arrows indicate non-significance. Solid borders indicate a significant relationship in a partial correlation (controlling for all other covariates) while dashed borders indicate non-significance. The colors range from red to blue, and are scaled by the magnitude of the inferred partial correlation coefficient, *r* (red = negative, blue = positive). Correlation coefficients and associated posterior probability are reported in Supplemental Table 2. **Please refer to the published version of this article for higher quality vector art.**

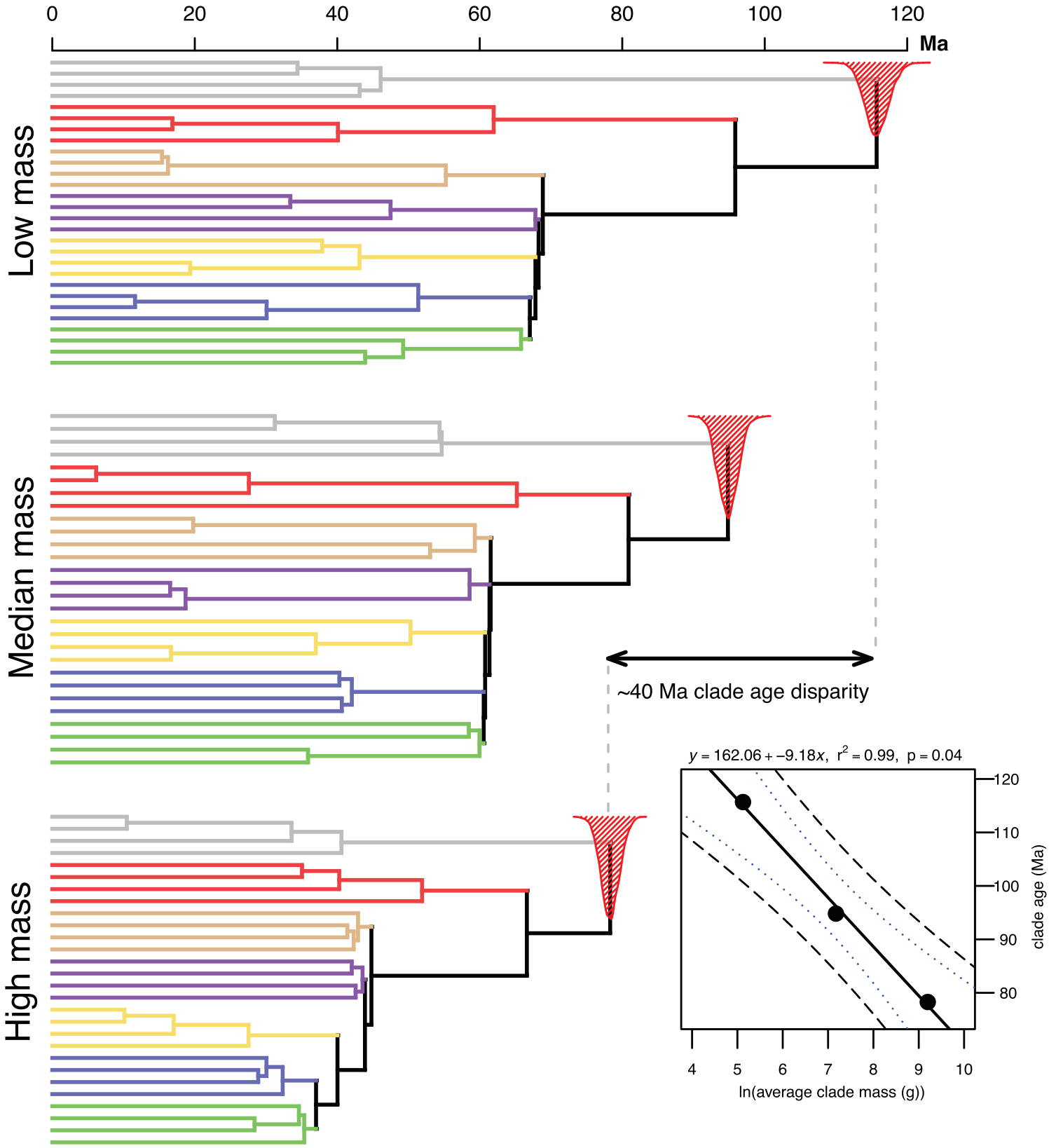
0
20
40
60
80
100
120
Ma
Low mass
Median mass
High mass
~40 Ma clade age disparity
y = 162.06 + −9.18x, r2 = 0.99, p = 0.04
120
110
100
90
80
clade age (Ma)
4
5
6
7
8
9
10
ln(average clade mass (g))

Figure 4.3. Simulations illustrating the influence of body size bias on molecular divergence time estimates. Strict molecular clock analyses of low mass, median mass, and high mass taxon samples for crown birds reveal that approximately ~40 Ma of root age disparity can be explained by differences in substitution rate related to body mass alone (relaxed clock analyses described in the text generated similar results). These analyses imply that extinction of large-bodied taxa can contribute to error in estimates of divergence times by biasing the distribution of substitution rates represented by surviving lineages. The 'low mass' taxon partition yields a median root age of 115.7 Ma, while 'median' and 'heavy' partitions yield estimates of 94.8 Ma and 78.3 Ma, respectively, with narrow, non-overlapping HPD intervals. Regression analysis (inset) reveals that the relationship may be explained by a simple linear function (R^2= 0.99, n=3, p=0.04). The fitted regression line through estimates of the clade MRCA uses the mean clade mass per simulation as a predictor. Also shown are 90% confidence and prediction (dashed lines) intervals. Shading reflects the major clades identified in Prum et al. (2015). **Please refer to the published version of this article for higher quality vector art.**

REFERENCES

Alroy J. 1999. The Fossil Record of North American Mammals: Evidence for a Paleocene Evolutionary Radiation. Systematic Biology, 48:107-118.

Alvarez L, Alvarez W, Asaro F, Michel H. 1979. Extraterrestrial cause for the Cretaceous-Tertiary extinction: Experiment and theory:1095-1108.

Archibald JD. 2013. Dinosaur extinction and the end of an era: what the fossils say. Columbia University Press.

Baker AJ, Pereira SL, Paton TA. 2007. Phylogenetic relationships and divergence times of Charadriiformes genera: multigene evidence for the Cretaceous origin of at least 14 clades of shorebirds. Biology Letters, 3:205-210.

Barnosky AD, Matzke N, Tomiya S, Wogan GOU, Swartz B, Quental TB, Marshall C, McGuire JL, Lindsey EL, Maguire KC, Mersey B, Ferrer EA. 2011. Has the Earth/'s sixth mass extinction already arrived? Nature, 471:51-57.

Beaulieu JM, O'Meara BC, Crane P, Donoghue MJ. 2015. Heterogeneous Rates of Molecular Evolution and Diversification Could Explain the Triassic Age Estimate for Angiosperms. Systematic Biology, 64:869-878.

Benson RBJ, Campione NsE, Carrano MT, Mannion PD, Sullivan C, Upchurch P, Evans DC. 2014. Rates of Dinosaur Body Mass Evolution Indicate 170 Million Years of Sustained Ecological Innovation on the Avian Stem Lineage. PLoS Biol, 12:e1001853.

Benton MJ. 1999. Early origins of modern birds and mammals: molecules vs. morphology. BioEssays, 21:1043-1051.

Blomberg SP, Garland T, Ives AR. 2003. TESTING FOR PHYLOGENETIC SIGNAL IN COMPARATIVE DATA: BEHAVIORAL TRAITS ARE MORE LABILE. Evolution, 57:717-745.

Brayard A, Nützel A, Stephen DA, Bylund KG, Jenks J, Bucher H. 2010. Gastropod evidence against the Early Triassic Lilliput effect. Geology, 38:147-150.

Bromham L. 2003. Molecular Clocks and Explosive Radiations. Journal of Molecular Evolution, 57:S13-S20.

Brown CM, Evans DC, Campione NE, O'Brien LJ, Eberth DA. 2013. Evidence for taphonomic size bias in the Dinosaur Park Formation (Campanian, Alberta), a model Mesozoic terrestrial alluvial-paralic system. Palaeogeography, Palaeoclimatology, Palaeoecology, 372:108-122.

Brown JH. 1995. Macroecology. University of Chicago Press.

Brown JH, Gillooly JF, Allen AP, Savage VM, West GB. 2004. Toward a metabolic theory of ecology. Ecology, 85:1771-1789.

Brusatte Stephen L, Lloyd Graeme T, Wang Steve C, Norell Mark A. 2014. Gradual Assembly of Avian Body Plan Culminated in Rapid Rates of Evolution across the Dinosaur-Bird Transition. Current Biology, 24:2386-2392.

Claramunt S, Cracraft J. 2015. A new time tree reveals Earth history’s imprint on the evolution of modern birds. Science Advances, 1.

Cracraft J, Houde P, Ho SYW, Mindell DP, Fjeldså J, Lindow B, Edwards SV, Rahbek C, Mirarab S, Warnow T, Gilbert MTP, Zhang G, Braun EL, Jarvis ED. 2015. Response to Comment on “Whole-genome analyses resolve early branches in the tree of life of modern birds”. Science, 349:1460-1460.

De Magalhães JP, Costa J. 2009. A database of vertebrate longevity records and their relation to other life-history traits. Journal of Evolutionary Biology, 22:1770-1774.

Dornburg A, Townsend JP, Friedman M, Near TJ. 2014. Phylogenetic informativeness reconciles ray-finned fish molecular divergence times. BMC Evolutionary Biology, 14:1-14.
Drummond AJ, Bouckaret RR. 2015. Bayesian evolutionary analysis with BEAST. Cambridge University Press.
Drummond AJ, Ho SYW, Phillips MJ, Rambaut A. 2006. Relaxed Phylogenetics and Dating with Confidence. PLoS Biol, 4:e88.
Drummond AJ, Suchard MA, Xie D, Rambaut A. 2012. Bayesian phylogenetics with BEAUti and the BEAST 1.7. Molecular biology and evolution, 29:1969-1973.
Duncan RP, Blackburn TM, Worthy TH. 2002. Prehistoric bird extinctions and human hunting. Proceedings of the Royal Society of London B: Biological Sciences, 269:517-521.
Dunning Jr JB. 1992. CRC handbook of avian body masses. CRC press.
Easteal S. 1999. Molecular evidence for the early divergence of placental mammals. BioEssays, 21:1052-1058.
Faurby S, Svenning J-C. 2016. Resurrection of the Island Rule: Human-Driven Extinctions Have Obscured a Basic Evolutionary Pattern. The American Naturalist, 0:000-000.
Faux C, Field D, J. 2017. Distinct developmental pathways underlie independent losses of flight in ratites. Biology Letters.
Felsenstein J. 1985. Phylogenies and the Comparative Method. The American Naturalist, 125:1-15.
Field DJ, Lynner C, Brown C, Darroch SAF. 2013. Skeletal Correlates for Body Mass Estimation in Modern and Fossil Flying Birds. PLoS ONE, 8:e82000.
Figuet E, Nabholz B, Bonneau M, Mas Carrio E, Nadachowska-Brzyska K, Ellegren H, Galtier N. 2016. Life History Traits, Protein Evolution, and the Nearly Neutral Theory in Amniotes. Molecular Biology and Evolution.
Fontanillas E, Welch JJ, Thomas JA, Bromham L. 2007. The influence of body size and net diversification rate on molecular evolution during the radiation of animal phyla. BMC Evolutionary Biology, 7:1-12.
Friedman M. 2009. Ecomorphological selectivity among marine teleost fishes during the end-Cretaceous extinction. Proceedings of the National Academy of Sciences, 106:5218-5223.
Gaston KJ, Blackburn TM. 1995. Birds, Body Size and the Threat of Extinction. Philosophical Transactions of the Royal Society B: Biological Sciences, 347:205-212.
Gelman A, Hill J, Yajima M. 2012. Why we (usually) don't have to worry about multiple comparisons. Journal of Research on Educational Effectiveness, 5:189-211.
Gillooly JF, Allen AP, West GB, Brown JH. 2005. The rate of DNA evolution: Effects of body size and temperature on the molecular clock. Proceedings of the National Academy of Sciences, 102:140-145.
Gillooly JF, McCoy MW, Allen AP. 2007. Effects of metabolic rate on protein evolution. Biology Letters, 3:655-660.
Hackett SJ, Kimball RT, Reddy S, Bowie RCK, Braun EL, Braun MJ, Chojnowski JL, Cox WA, Han K-L, Harshman J. 2008. A phylogenomic study of birds reveals their evolutionary history. Science, 320.
Hansen TF. 1997. Stabilizing Selection and the Comparative Analysis of Adaptation. Evolution, 51:1341-1351.
Harmon LJ, Losos JB, Jonathan Davies T, Gillespie RG, Gittleman JL, Bryan Jennings W, Kozak KH, McPeek MA, Moreno-Roark F, Near TJ, Purvis A, Ricklefs RE, Schluter D, Schulte Ii JA, Seehausen O, Sidlauskas BL, Torres-Carvajal O, Weir JT, Mooers AØ. 2010.

Early bursts of body size and shape evolution are rare in comparative data. Evolution, 64:2385-2396.
Harmon LJ, Weir JT, Brock CD, Glor RE, Challenger W. 2008. GEIGER: investigating evolutionary radiations. Bioinformatics, 24:129-131.
Hsiang AY, Field DJ, Webster TH, Behlke AD, Davis MB, Racicot RA, Gauthier JA. 2015. The origin of snakes: revealing the ecology, behavior, and evolutionary history of early snakes using genomics, phenomics, and the fossil record. BMC Evolutionary Biology, 15:87.
Huang B, Harper DA, Zhan R, Rong J. 2010. Can the Lilliput Effect be detected in the brachiopod faunas of South China following the terminal Ordovician mass extinction? Palaeogeography, Palaeoclimatology, Palaeoecology, 285:277-286.
Hugall A, F. , Lee M, S. Y. 2007. The Likelihood Node Density Effect and Consequences for Evolutionary Studies of Molecular Rates. Evolution, 61:2293-2307.
Hull PM, Darroch SAF, Erwin DH. 2015. Rarity in mass extinctions and the future of ecosystems. Nature, 528:345-351.
Jablonski D. 2004. Extinction: past and present. Nature, 427:589-589.
Jablonski D. 2008. Species Selection: Theory and Data. Annual Reviews, 39:501-524.
Jarvis ED, Mirarab S, Aberer AJ, Li B, Houde P, Li C, Ho SYW, Faircloth BC, Nabholz B, Howard JT, Suh A, Weber CC, da Fonseca RR, Li J, Zhang F, Li H, Zhou L, Narula N, Liu L, Ganapathy G, Boussau B, Bayzid MS, Zavidovych V, Subramanian S, Gabaldón T, Capella-Gutiérrez S, Huerta-Cepas J, Rekepalli B, Munch K, Schierup M, Lindow B, Warren WC, Ray D, Green RE, Bruford MW, Zhan X, Dixon A, Li S, Li N, Huang Y, Derryberry EP, Bertelsen MF, Sheldon FH, Brumfield RT, Mello CV, Lovell PV, Wirthlin M, Schneider MPC, Prosdocimi F, Samaniego JA, Velazquez AMV, Alfaro-Núñez A, Campos PF, Petersen B, Sicheritz-Ponten T, Pas A, Bailey T, Scofield P, Bunce M, Lambert DM, Zhou Q, Perelman P, Driskell AC, Shapiro B, Xiong Z, Zeng Y, Liu S, Li Z, Liu B, Wu K, Xiao J, Yinqi X, Zheng Q, Zhang Y, Yang H, Wang J, Smeds L, Rheindt FE, Braun M, Fjeldsa J, Orlando L, Barker FK, Jønsson KA, Johnson W, Koepfli K-P, O'Brien S, Haussler D, Ryder OA, Rahbek C, Willerslev E, Graves GR, Glenn TC, McCormack J, Burt D, Ellegren H, Alström P, Edwards SV, Stamatakis A, Mindell DP, Cracraft J, Braun EL, Warnow T, Jun W, Gilbert MTP, Zhang G. 2014. Whole-genome analyses resolve early branches in the tree of life of modern birds. Science, 346:1320-1331.
Jetz W, Thomas GH, Joy JB, Hartmann K, Mooers AO. 2012. The global diversity of birds in space and time. Nature, 491:444-448.
Kimura M. 1968. Evolutionary Rate at the Molecular Level. Nature, 217:624-626.
Ksepka DT, Phillips MJ. 2015. Avian Diversification Patterns across the K-Pg Boundary: Influence of Calibrations, Datasets, and Model Misspecification. Annals of the Missouri Botanical Garden, 100:300-328.
Lanfear R, Ho SYW, Jonathan Davies T, Moles AT, Aarssen L, Swenson NG, Warman L, Zanne AE, Allen AP. 2013a. Taller plants have lower rates of molecular evolution. Nature Communications, 4:1879.
Lanfear R, Ho SYW, Love D, Bromham L. 2010. Mutation rate is linked to diversification in birds. Proceedings of the National Academy of Sciences, 107:20423-20428.
Lanfear R, Kokko H, Eyre-Walker A. 2013b. Population size and the rate of evolution. Trends in Ecology & Evolution, 29:33-41.
Lartillot N, Delsuc F. 2012. Joint reconstruction of divergence times and life-history evolution in placental mammals using a phylogenetic covariance model. Evolution, 66:1773-1787.

Lartillot N, Phillips MJ, Ronquist F. 2016. A mixed relaxed clock model. Philosophical Transactions of the Royal Society of London B: Biological Sciences, 371.
Lartillot N, Poujol R. 2011. A Phylogenetic Model for Investigating Correlated Evolution of Substitution Rates and Continuous Phenotypic Characters. Molecular Biology and Evolution, 28:729-744.
Lee MSY, Cau A, Naish D, Dyke GJ. 2014. Sustained miniaturization and anatomical innovation in the dinosaurian ancestors of birds. Science, 345:562-566.
Lee MSY, Soubrier J, Edgecombe Gregory D. 2013. Rates of Phenotypic and Genomic Evolution during the Cambrian Explosion. Current Biology, 23:1889-1895.
Lemmon AR, Emme SA, Lemmon EM. 2012. Anchored Hybrid Enrichment for Massively High-Throughput Phylogenomics. Systematic Biology, 61:727-744.
Litsios G, Salamin N. 2012. Effects of Phylogenetic Signal on Ancestral State Reconstruction. Systematic Biology, 61:533-538.
Longrich NR, Tokaryk T, Field DJ. 2011. Mass extinction of birds at the Cretaceous–Paleogene (K–Pg) boundary. Proceedings of the National Academy of Sciences, 108:15253-15257.
Losos JB. 2008. Phylogenetic niche conservatism, phylogenetic signal and the relationship between phylogenetic relatedness and ecological similarity among species. Ecology Letters, 11:995-1003.
Martin AP, Palumbi SR. 1993. Body size, metabolic rate, generation time, and the molecular clock. Proceedings of the National Academy of Sciences, 90:4087-4091.
Mayr G. 2009. Paleogene Fossil Birds. Berlin, Springer.
McKinney ML. 1990. Trends in body-size evolution. Evolutionary trends:75-118.
McLellan R, Iyengar L, Jeffries B, Oerlemans N, Network GF, Network WF. 2014. Living Planet Report 2014: species and spaces, people and places. World Wide Fund for Nature.
McNab BK. 2012. Extreme measures: the ecological energetics of birds and mammals. University of Chicago Press.
Mindell DP, Knight A, Baer C, Huddleston CJ. 1996. Slow rates of molecular evolution in birds and the metabolic rate and body temperature hypotheses. Molecular Biology and Evolution, 13:422-426.
Mitchell JS. 2015. Extant-only comparative methods fail to recover the disparity preserved in the bird fossil record. Evolution, 69:2414-2424.
Mitchell KJ, Llamas B, Soubrier J, Rawlence NJ, Worthy TH, Wood J, Lee MSY, Cooper A. 2014. Ancient DNA reveals elephant birds and kiwi are sister taxa and clarifies ratite bird evolution. Science, 344:898-900.
Nabholz B, Lanfear R, Fuchs J. 2016. Body mass-corrected molecular rate for bird mitochondrial DNA. Molecular Ecology, 25:4438–4449.
Nabholz B, Uwimana N, Lartillot N. 2013. Reconstructing the Phylogenetic History of Long-Term Effective Population Size and Life-History Traits Using Patterns of Amino Acid Replacement in Mitochondrial Genomes of Mammals and Birds. Genome Biology and Evolution, 5:1273-1290.
Ohta T. 1973. Slightly Deleterious Mutant Substitutions in Evolution. Nature, 246:96-98.
Pagel M. 1999. Inferring the historical patterns of biological evolution. Nature, 401:877-884.
Paradis E, Claude J, Strimmer K. 2004. APE: Analyses of Phylogenetics and Evolution in R language. Bioinformatics, 20:289-290.
Phillips MJ. 2015. Geomolecular Dating and the Origin of Placental Mammals. Systematic Biology.

Prum RO, Berv JS, Dornburg A, Field DJ, Townsend JP, Lemmon EM, Lemmon AR. 2015. A comprehensive phylogeny of birds (Aves) using targeted next-generation DNA sequencing. Nature, 526:569-573.
Puttick MN, Thomas GH, Benton MJ. 2014. HIGH RATES OF EVOLUTION PRECEDED THE ORIGIN OF BIRDS. Evolution, 68:1497-1510.
Raftery AE, Newton MA, Satagopan JM, Krivitsky PN. 2006. Estimating the integrated likelihood via posterior simulation using the harmonic mean identity. Memorial Sloan-Kettering Cancer Center, Dept. of Epidemiology & Biostatistics Working Paper Series, Working Paper 6.
Revell LJ. 2012. phytools: an R package for phylogenetic comparative biology (and other things). Methods in Ecology and Evolution, 3:217-223.
Revell LJ, Harmon LJ, Collar DC. 2008. Phylogenetic Signal, Evolutionary Process, and Rate. Systematic Biology, 57:591-601.
Reynolds PS, Lee RM. 1996. Phylogenetic Analysis of Avian Energetics: Passerines and Nonpasserines Do Not Differ. The American Naturalist, 147:735-759.
Roff DA. 2002. Life history evolution. Sunderland, MA, Sinaur Associates.
Romiguier J, Gayral P, Ballenghien M, Bernard A, Cahais V, Chenuil A, Chiari Y, Dernat R, Duret L, Faivre N, Loire E, Lourenco JM, Nabholz B, Roux C, Tsagkogeorga G, Weber AAT, Weinert LA, Belkhir K, Bierne N, Glemin S, Galtier N. 2014. Comparative population genomics in animals uncovers the determinants of genetic diversity. Nature, 515:261-263.
Romiguier J, Ranwez V, Douzery EJP, Galtier N. 2010. Contrasting GC-content dynamics across 33 mammalian genomes: Relationship with life-history traits and chromosome sizes. Genome Research, 20:1001-1009.
Sallan L, Galimberti AK. 2015. Body-size reduction in vertebrates following the end-Devonian mass extinction. Science, 350:812-815.
Sibley CG, Ahlquist JE. 1990. Phylogeny and classification of birds: a study in molecular evolution. Yale University Press.
Simpson GG. 1944. Tempo and mode in evolution. Columbia University Press.
Slater GJ, Harmon LJ, Alfaro ME. 2012. Integrating fossils with molecular phylogenies improves inference of trait evolution. Evolution, 66:3931-3944.
Smith SA, Donoghue MJ. 2008. Rates of Molecular Evolution Are Linked to Life History in Flowering Plants. Science, 322:86-89.
Tacutu R, Craig T, Budovsky A, Wuttke D, Lehmann G, Taranukha D, Costa J, Fraifeld VE, de Magalhães JP. 2013. Human Ageing Genomic Resources: Integrated databases and tools for the biology and genetics of ageing. Nucleic Acids Research, 41:D1027-D1033.
Twitchett RJ. 2007. The Lilliput effect in the aftermath of the end-Permian extinction event. Palaeogeography, Palaeoclimatology, Palaeoecology, 252:132-144.
Urbanek A. 1993. Biotic crises in the history of Upper Silurian graptoloids: A Palaeobiological model. Historical Biology, 7:29-50.
Van Valen LM. 1994. Concepts and the nature of selection by extinction: is generalization possible. The mass extinction debates: how science works in a crisis. Stanford University Press, Stanford, Calif:200-216.
Weber CC, Boussau B, Romiguier J, Jarvis ED, Ellegren H. 2014a. Evidence for GC-biased gene conversion as a driver of between-lineage differences in avian base composition. Genome Biology, 15:549.

Weber CC, Nabholz B, Romiguier J, Ellegren H. 2014b. Kr/Kc but not dN/dS correlates positively with body mass in birds, raising implications for inferring lineage-specific selection. Genome Biology, 15:1-13.
Webster AJ, Purvis A. 2002. Testing the accuracy of methods for reconstructing ancestral states of continuous characters. Proceedings of the Royal Society of London. Series B: Biological Sciences, 269:143-149.
Western D, Ssemakula J. 1982. Life history patterns in birds and mammals and their evolutionary interpretation. Oecologia, 54:281-290.
Wilson GP. 2013. Mammals across the K/Pg boundary in northeastern Montana, USA: dental morphology and body-size patterns reveal extinction selectivity and immigrant-fueled ecospace filling. Paleobiology, 39:429-469.
Yonezawa T, Segawa T, Mori H, Campos PF, Hongoh Y, Endo H, Akiyoshi A, Kohno N, Nishida S, Wu J, Jin H, Adachi J, Kishino H, Kurokawa K, Nogi Y, Tanabe H, Mukoyama H, Yoshida K, Rasoamiaramanana A, Yamagishi S, Hayashi Y, Yoshida A, Koike H, Akishinonomiya F, Willerslev E, Hasegawa M. 2016. Phylogenomics and Morphology of Extinct Paleognaths Reveal the Origin and Evolution of the Ratites. Current Biology.

APPENDIX 1

SUPPLEMENTARY MATERIAL FOR CHAPTER 1

Additional data files can be accessed at the online version of this article

http://dx.doi.org/10.1016/j.ympev.2014.09.001

Electronic Supplement

A comprehensive multilocus phylogeny of the Neotropical cotingas (Cotingidae, Aves) with a comparative evolutionary analysis of breeding system and plumage dimorphism and a revised phylogenetic classification

Jacob S. Berv[1] and Richard O. Prum*

Department of Ecology and Evolutionary Biology, and Peabody Museum of Natural History, Yale University, P. O. Box 208105, New Haven, CT USA 06520

[1]Current Address:
Department of Ecology and Evolutionary Biology
Fuller Evolutionary Biology Program,
Cornell University, and
Cornell Laboratory of Ornithology
159 Sapsucker Woods Road,
Ithaca, NY USA 14850
jsb439@cornell.edu

*Corresponding Author: richard.prum@yale.edu

Supplementary Appendix

Design of genera-specific primers for ancient DNA amplification

Because no genetic data had previously been collected for the taxa represented by toepads and because some of these samples were many decades old, we designed genera-specific primers to amplify DNA from these degraded sources. We chose to focus our efforts on amplifying fragments of the mitochondrial ND2 gene, with the goal of obtaining at least some sequence data from as many taxa as possible. First, we chose 2-4 closely related taxa (based on putative relationship to the taxa in question) from our genetic dataset that had been collected from fresh tissue. Sequences were aligned in Sequencher 5.01 (Gene Codes Corporation, Ann Arbor, MI, USA), and alignments were visually scanned for areas of conservation. We used the Primer3Plus web application (Untergasser et al., 2007) to choose primers from the consensus sequence of a given alignment, and primers were subsequently filtered to align with areas of pre-defined conservation. For each toepad sample, ND2 was amplified in 3-8 pairs of overlapping fragments. PCR products often required secondary re-amplification to be visually quantified on an agarose gel prior to sequencing. In many cases, separation from secondary products via gel extractions was necessary to isolate the correct fragment. Like with sequences derived from fresh tissue, all ND2 consensus sequences were translated in the correct reading frame to verify no pre-mature stop codons or indels were present, and that overlapping sections of sequences were identical. Using these methods, we were able to amplify >80% of the 1041 bp of ND2 for the majority of taxa.

DNA extraction, PCR and Sequencing

Total genomic DNA was isolated from frozen tissue samples using a QIAGEN DNeasy extraction kit and standard spin-column protocols. We extracted genomic DNA from 21 museum skins using a modified QIAGEN protocol designed to maximize yield from dried collagen-rich tissue: All DNA extractions from toe pads were performed in an ancient DNA facility at Yale University with sterile technique. First, we sampled 1-3 rice-grain size slivers of avian toepads, prioritizing fleshy tissue from the hallux. After a rinse with double distilled water, these samples were digested in 360 µL of Buffer ATL, 40 µL of 20 mg/mL Proteinase K and 20-40 µL of 1M DTT (Dithiothreitol) for 24-72 hours until the tissue was completely lysed. Additional 20 µL aliquots of Proteinase K were added as necessary after each 24-hour period of digestion. Digestion was followed by the addition of 400 µL of Buffer AL, double washes with 500 µL of Buffer AW1 and AW2, and elution of the final extract with 40 µL of Buffer AE heated to 70°C. To increase the likelihood of detecting contamination, we used negative (blank) controls during extraction and subsequent PCR.

Target loci from tissue extractions were amplified using the polymerase chain reaction (PCR) with the primers listed in Supplemental Table 1 and Promega GoTaq™ Flexi DNA polymerase M3001 kits. Each 13 µl reaction contained 4.94 µl of ddH_20, 2.5 µl of 5X Green GoTaq Buffer, 0.5 µl of 10 mM Invitrogen dNTP mix, 0.5 µl of 10 mM forward primer, 0.5 µl of 10 mM reverse primer, 0.0625 µl GoTaq™ Flexi polymerase, 2.5 µl of 25 mM $MgCl_2$, and 1.5 µl of DNA template. Reactions were run on an MJ

thermal cycler with the following reaction program: initial denaturation for 2 min at 95°C, followed by 45 cycles of: 95°C for 30 seconds, annealing temperatures of 54-50°C (depending on primer T_m) with touch-down (i.e. 60°C 5x, 58°C 5x, 56°C 5x, 54°C 25x) for 30 seconds, and an extension phase at 72°C for 1 minute and 15 seconds. Cycling was followed by a final extension step of 72°C for 7 minutes and a hold at 4°C.

Many genera specific primers were designed for amplification of degraded DNA sequences from toe pads of various species (see Supplementary Electronic Appendix). For PCR amplifications from toepad extractions, we used Thermo Scientific Phusion Hot Start II High-Fidelity DNA polymerase #F-549L kits with the following reagent proportions: For a 20 μl reaction, we combined 11.2 μl ddH_20, 4 μl of 5x Phusion HF Buffer, 1 μl of 10 mM forward primer, 1 μl of 10 mM reverse primer, 0.4 μl of Invitrogen dNTP mix, 0.4 μl of Phusion Hot Start II™ DNA polymerase, and 2 μl of DNA template. Reactions were prepared in a sterile ancient DNA facility and processed on Eppendorf thermal cyclers with the following program: initial denaturation and activation of Hot Start polymerase at 98°C for 30 seconds, followed by 40 cycles of: 98°C for 10 seconds, annealing temperatures of 54-48°C (depending on primer T_m) with touch-down for 20 seconds, and extension at 72°C for 15 seconds. Cycling was followed by a final extension phase at 72°C for 10 minutes and a hold at 4°C.

All PCR products were visualized and quantified on a 1.5% agarose gel before being enzymatically processed with USB Shrimp Alkaline Phosphatase (SAP) and Exonuclease I (EXO) under the following ratios: for a 12 μl reaction, we mixed 8.5 μl of PCR product, 0.68 μl of EXO, 0.68 μl of SAP and 2.04 μl of ddH_20. This solution was cycled at 37°C for 15 minutes, followed by an enzyme inactivation step at 80°C for 15 minutes.

Forward and reverse strands were sequenced for each sample using ABI Big Dye Terminator chemistry on a 3730*xl* 96-Capillary Genetic Analyzer (Applied Biosystems) at the DNA Analysis Facility on Science Hill at Yale University. Sequences were aligned in Sequencher 5.0.1 (Gene Codes Corporation, Ann Arbor, MI, USA) and trimmed to the correct size by aligning the appropriate primer sequences. All coding sequences were checked for premature stop codons to check that nuclear pseudo-genes had not been amplified (Sorenson and Quinn, 1998). Heterozygous sites in the nuclear introns were scored using standard ambiguity codes. Sequences were aligned using a combination of Sequencher's built in alignment algorithm and the ClustalW2 (Larkin et al., 2007) plug-in, followed by correction by eye. Final consensus sequences were exported in nexus format alignments, and then were concatenated in and exported from Mesquite 2.75 (Maddison and Maddison, 2011) for subsequent analysis.

Distance matrix calculations

Because a number of our samples contained missing data, we used the pairwise-deletion function in MEGA v5.1 to calculate overall genetic distances using sites that were present in both taxa for each pairwise comparison. In some cases, such as for species with data from toepads only, distances were estimated from a single locus. Here, we report extreme "average" values calculated using pairwise-deletion, and p-distances computed from comparisons of individual loci. Within Cotingidae, intraspecific variation ranged from 0.15%: *Carpodectes antoniae — Carpodectes nitidus* (ND2); *Xipholena*

atropurpurea — Xipholena lamellipennis (ND2), to 27%: *Lipaugus uropygialis — Pipreola jucunda* (ND2-23%, G3PDH-8.2%), *Lipaugus uropygialis — Pipreola chlorolepidota* (ND2-22.8%, G3PDH-6.1%). Two additional interspecific comparisons exhibited uncorrected distances of < 1%: *Procnias averano — Procnias nudicollis,* 0.30% (ND2-0.37%, G3PDH-0.0%), *Procnias albus — Procnias tricarunculata,* 0.55% (ND2-0.82%, CYTB-0.29%, G3PDH-0.88%, MYO-0.07%). Approximately 10% of all pairwise comparisons (228/2212) were differentiated by more than 20% raw sequence divergence. Among the Cotingid genera, overall net distances ranged from 2.7% (*Cephalopterus-Pyroderus*) to 22% (*Phibalura-Porphyrolaema*). Within genera, *Xipholena* exhibits the least amount of within-group mean distance (0.83%), while *Pipreola* exhibits the most (10.1%).

Thirteen pairs of intraspecific comparisons showed differentiation of less than 1%. There were no nucleotide differences observed between replicates of *Lipaugus uropygialis* from Peru and Bolivia (266 bp ND2), or from replicates of *Phibalura flavirostris flavirostris* from Brazil and *P. f. boliviana* from Bolivia (283 bp ND2). Likewise, there were no differences among three individuals of *Procnias albus* from Venezuela, Guyana, and Brazil. *Procnias averano averano* from Brazil differed in 0.53% of 932 bp of ND2 from *Procnias averano carnobarba* specimens from Trinidad. *Porphyrolaema porphyrolaema* from Sucumbios, Ecuador, was 0.06% (ND2-0.096%, MYO-0.0%) different from a Loreto, Peru specimen. *Cotinga cayana* from Rondonia, Brazil, was 0.13% (CYTB-0.01%, ND2-0.0, MYO-0.442%) different from a Loreto, Peru specimen, and *Cotinga maynana* from Morona-Santiago, Ecuador was 0.19% (CYTB-0.19%, ND2-0.19%) different from a Loreto, Peru specimen. *Lipaugus vociferans* from Venezuela and Bolivia had 0.32% genetic differentiation (ND2-0.48%, CYTB-0.38%, G3PDH-0.0%, MYO-0.28%). *Pyroderus scutatus scutatus* from Paraguay and *Pyroderus scutatus masoni* from Peru were 0.9% different (ND2-1.5%, MYO-0.0%, G3PDH-0.9%). *Pipreola lubmoirskii* from Peru and Ecuador were 0.23% differentiated (ND2-0.1%, CYTB-0.5%, G3PDH-0.0%, MYO-0.14%). Finally, samples of *Pipreola lubomirskii* from Peru and Ecuador were weakly (0.23%) differentiated (ND2-0.1%, CYTB-0.49%, G3PDH-0.0%, MYO-0.141%)

Although these populations are not currently recognized as distinct subspecies, *Ampelioides tschudii* from San Martin, Peru and from Azuay, Ecuador exhibited 1.2% differentiation in mtDNA (CYTB-1.5%, ND2-1.1%). Lastly, *Pipreola riefferii confusa* from Cajamarca, Peru and *Pipreola riefferii melanolaema* from Venezuela showed 4.6% genetic differentiation, including substantial genetic differentiation in one nuclear intron (ND2-6.0%, CYTB-7.0%, G3PDH-5.6%, MYO-0.0%).

Assessing topological variation across loci

We explored topological discordance among gene trees using the Compare2Trees and METATREE web-applets (Nye et al., 2006; Nye, 2008). The Compare2Trees algorithm is analogous to sequence alignment, in which topologies are aligned by pairing branches in one tree with the best matching branch in a second, and similarity score out of 100% is returned (Nye et al., 2006). Prior to each topological comparison, we pruned terminals that were not present in both trees as a result of missing data. We used the METATREE software to investigate patterns of discordance across loci and their

similarity to combined analyses. In sum, the 'meta-NJ' algorithm clusters phylogenies with similar topologies to produce a 'tree of trees' network diagram that describes the pattern of discordance among input trees (Nye, 2008).

The average pairwise discordance (topological dissimilarity) among gene trees in this study was moderate (11 %), and ranged from 6.2% (mtDNA-RAG1), to 16.2% (MYO-G3PDH) (Supplemental Table 8). The meta-tree network for individual loci was somewhat star-like, with three internal nodes connecting all five loci, indicating moderate levels of gene tree discordance (Nye, 2008). Consistent with the pairwise comparisons above, MYO and G3PDH both had the longest branches (which are proportional to the number of steps needed to change one topology into another) indicating the highest relative level of discordance. When the analysis was re-run and the topologies from the Bayesian species tree and concatenated analysis were included, they clustered in different parts of the network; the species tree was placed as an internal node along the branch leading to the mtDNA tree, and the concatenated topology was placed sister to MYO (96.1% similarity) (Supplemental Figure 9).

Additional reconstruction results

When examined across the posterior distribution of 3.5 X 10^4 trees, the results from our reconstructions of breeding system and plumage dimorphism evolution were consistent with those derived from the MCC topology alone — we report the mean $-\ln l$ followed by the 2.5% and 97.5% percentiles: For breeding system evolution; one-rate, $-\ln l = 17.03$ [16.15-17.68], AIC = 36.06; two-rate, $-\ln l = 16.49$ [15.45-17.16], AIC = 36.98; ($\chi_1^2 = 1.08, p = 0.30, \Delta\text{AIC} = 0.92$). For dimorphism evolution; one-rate, $-\ln l = 27.06$ [25.62-29.98], AIC = 56.12; two-rate, $-\ln l = 25.36$ [24.16-28.04], AIC = 54.72 ($\chi_1^2 = 3.4, p = 0.07, \Delta\text{AIC} = -1.4$).

Supplemental Figure 1. Species tree chronogram. This analysis was calibrated with molecular substitution rate priors (relaxed lognormal) on CYTB, ND2, G3PDH, MYO, and RAG1. The time scale below is in millions of years, and bars at nodes represent the 95% HPD (highest posterior density) error around the age estimate.

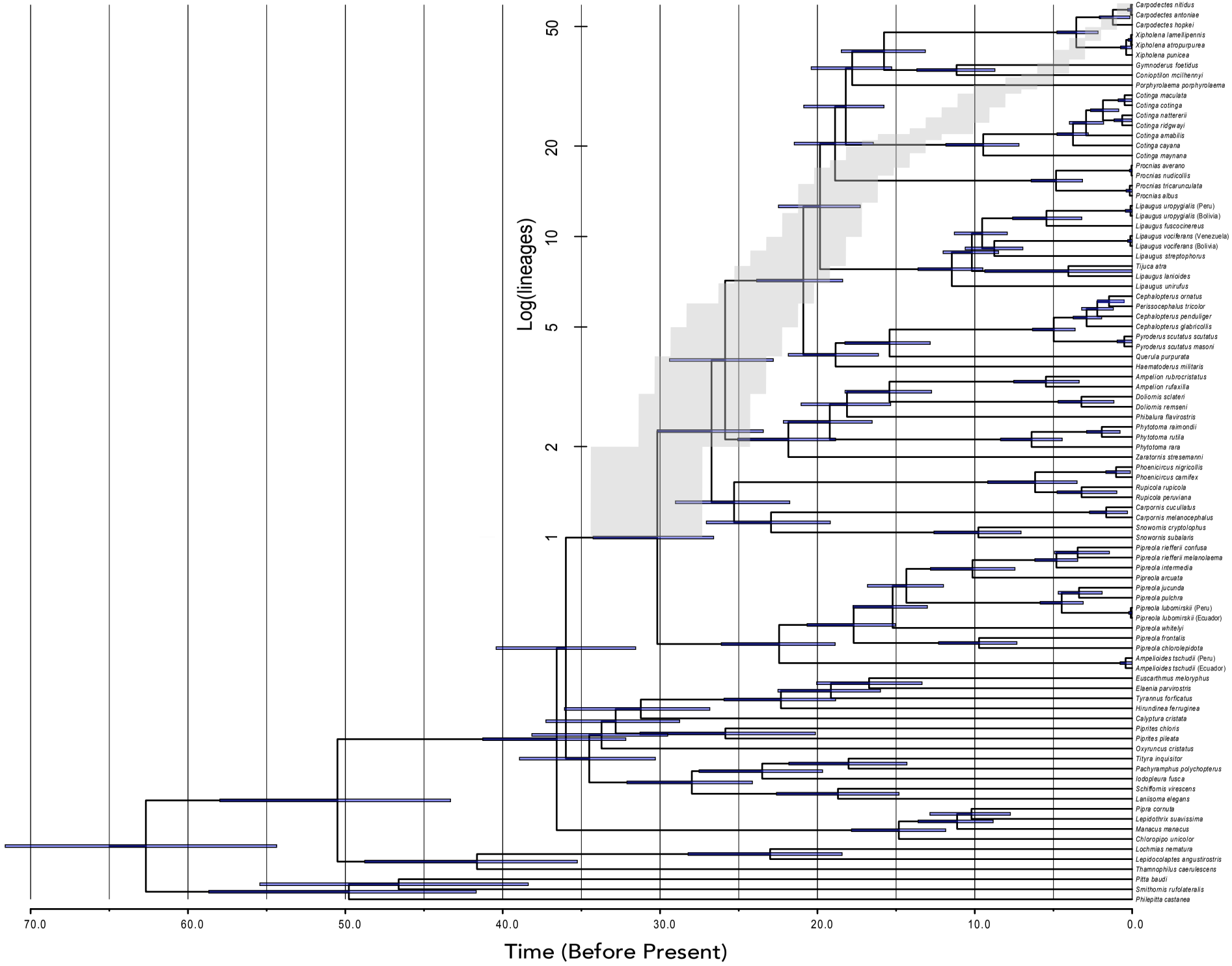

Supplemental Figure 2. Concatenated Bayesian topology. Asterisks indicate nodes that received greater than 90% posterior probability AND a bootstrap score of greater than 70. Branch lengths are proportional to genetic distance.

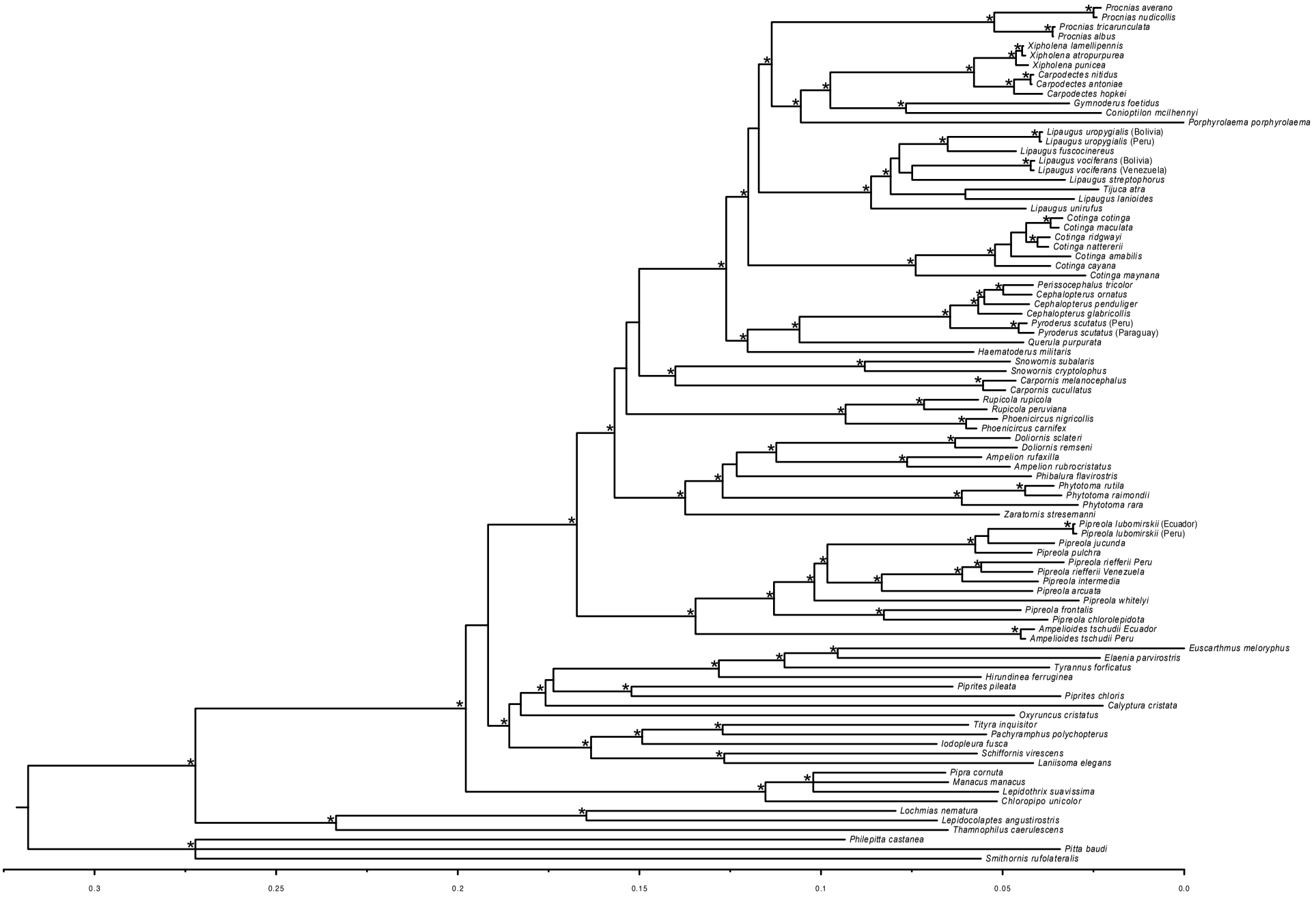

Supplemental Figures 3-8. Individual gene trees generated by MrBayes 3.2.1

RAG1

MrBayes

Scheme C3

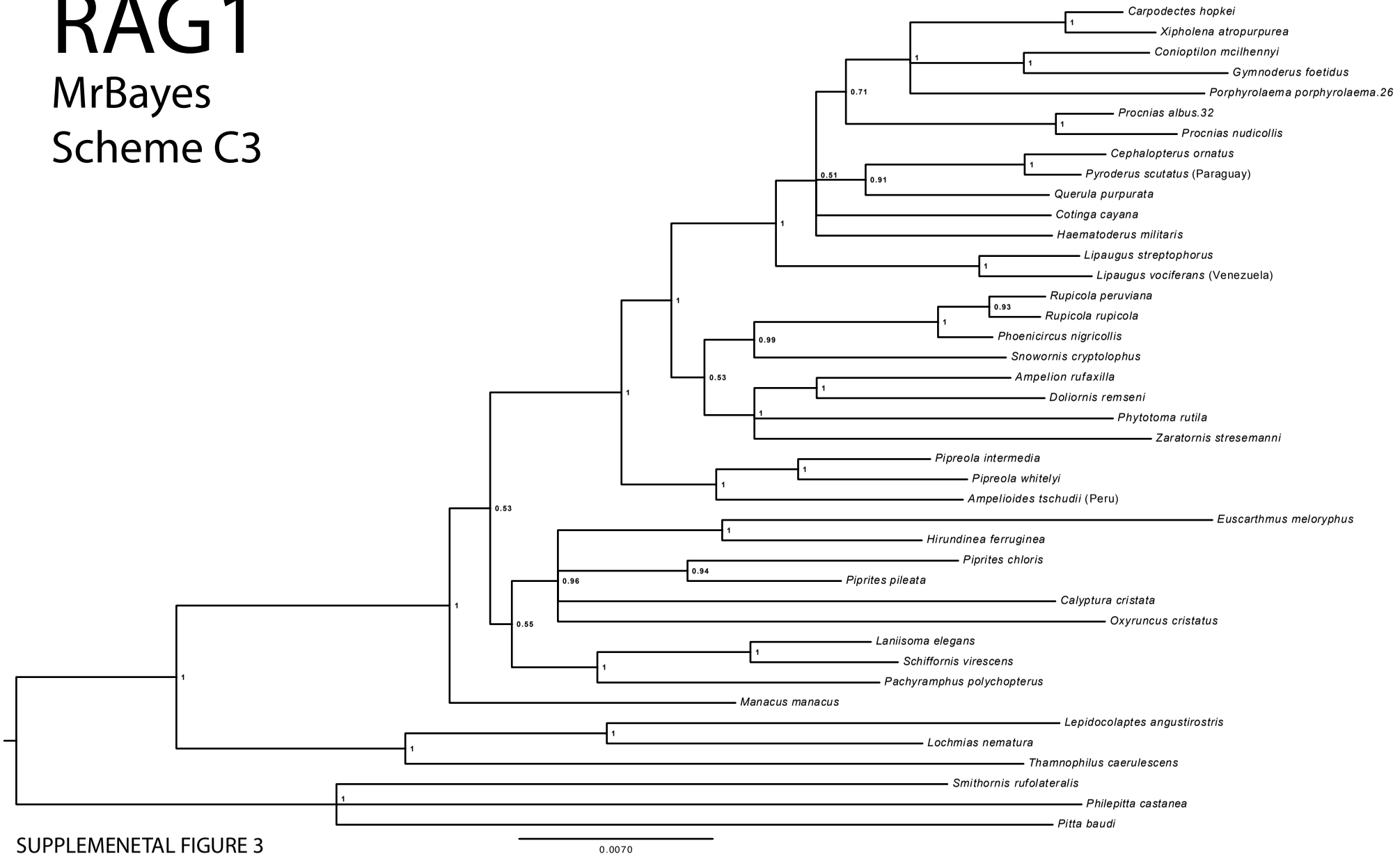

SUPPLEMENETAL FIGURE 3

Supplemental Figures 3-8. Individual gene trees generated by MrBayes 3.2.1

MYO

MrBayes

Scheme C3

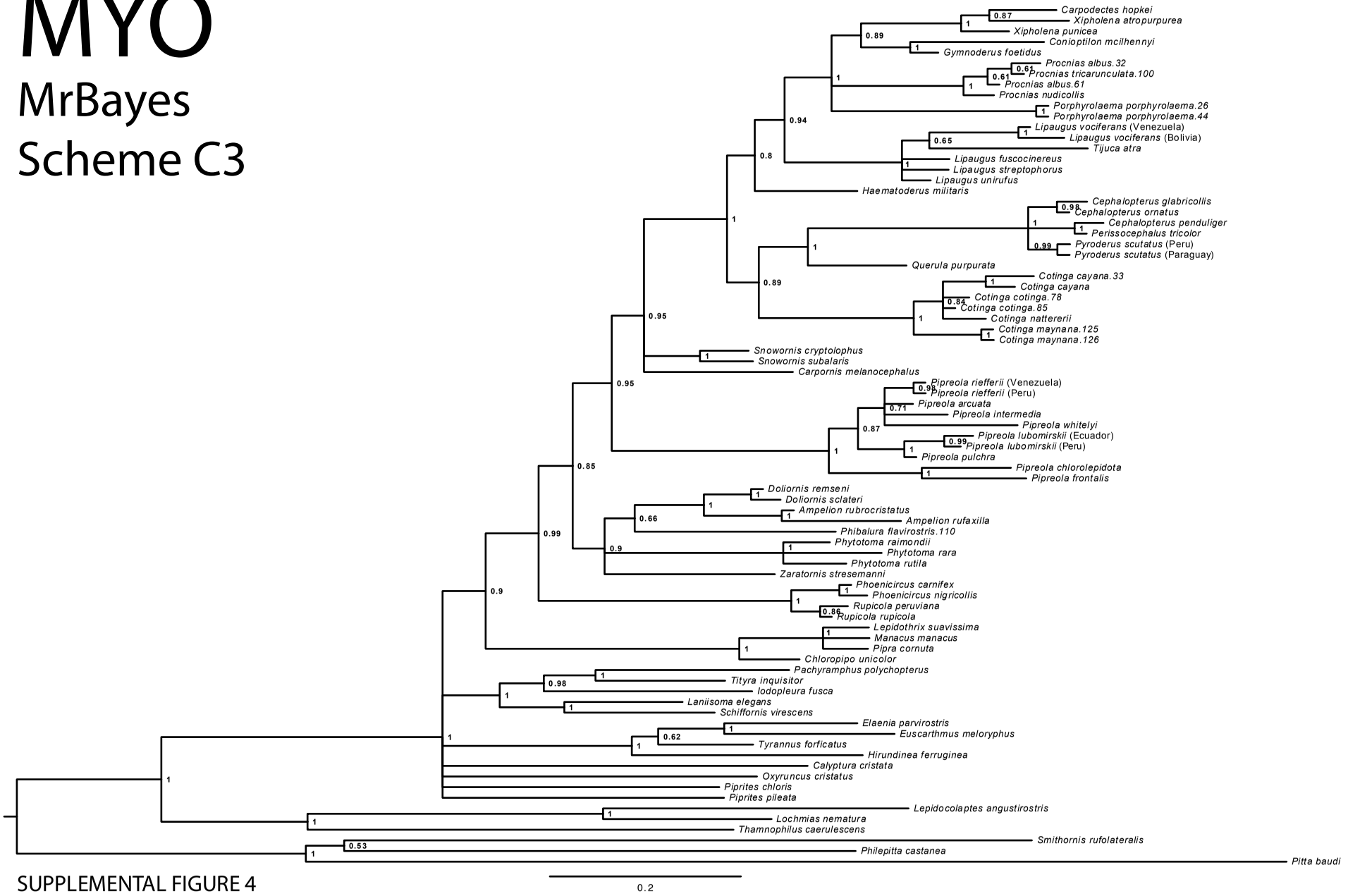

SUPPLEMENTAL FIGURE 4

Supplemental Figures 3-8. Individual gene trees generated by MrBayes 3.2.1

RAG2

MrBayes
Scheme C3

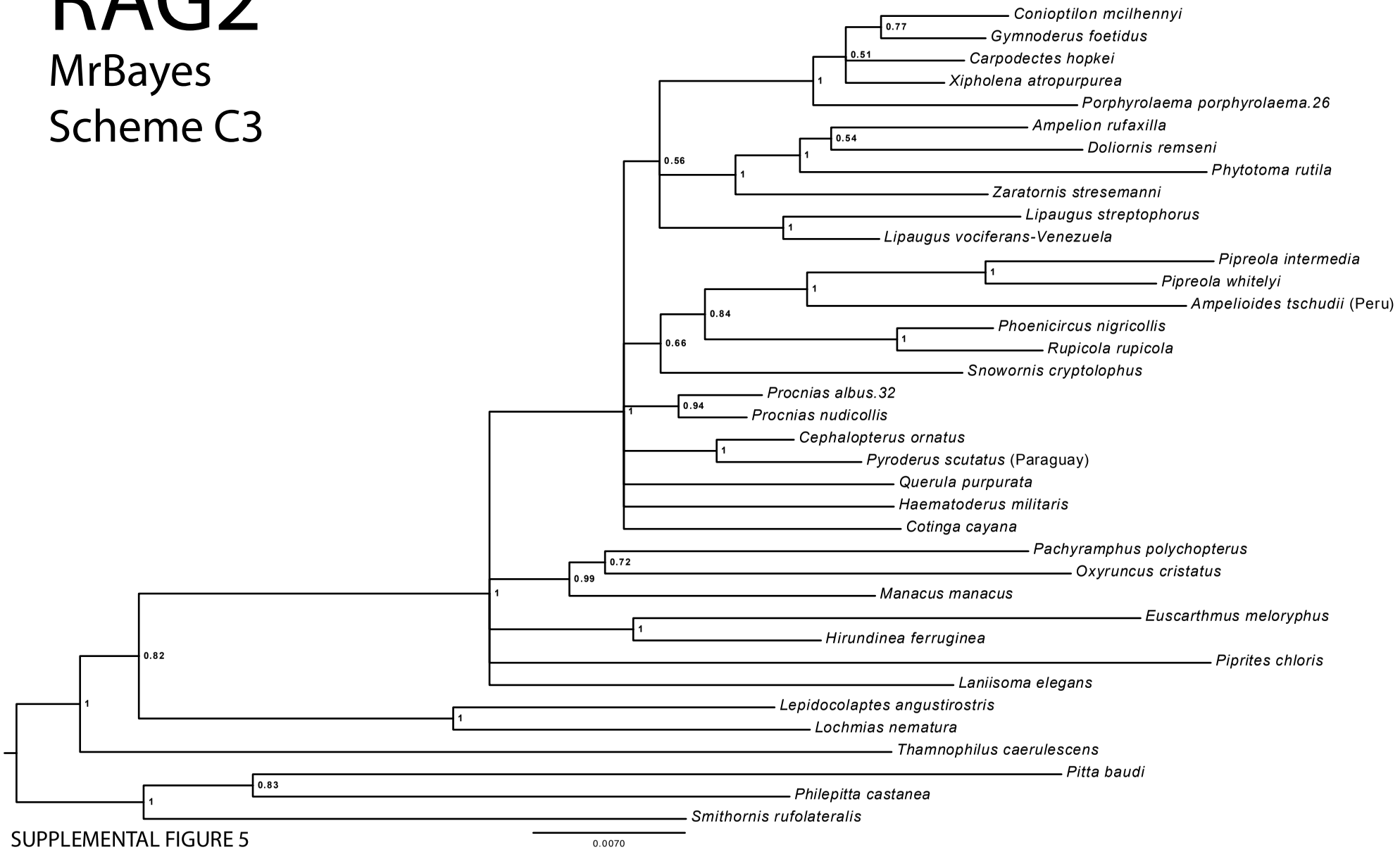

SUPPLEMENTAL FIGURE 5

Supplemental Figures 3-8. Individual gene trees generated by MrBayes 3.2.1

G3PDH

MrBayes

Scheme C3

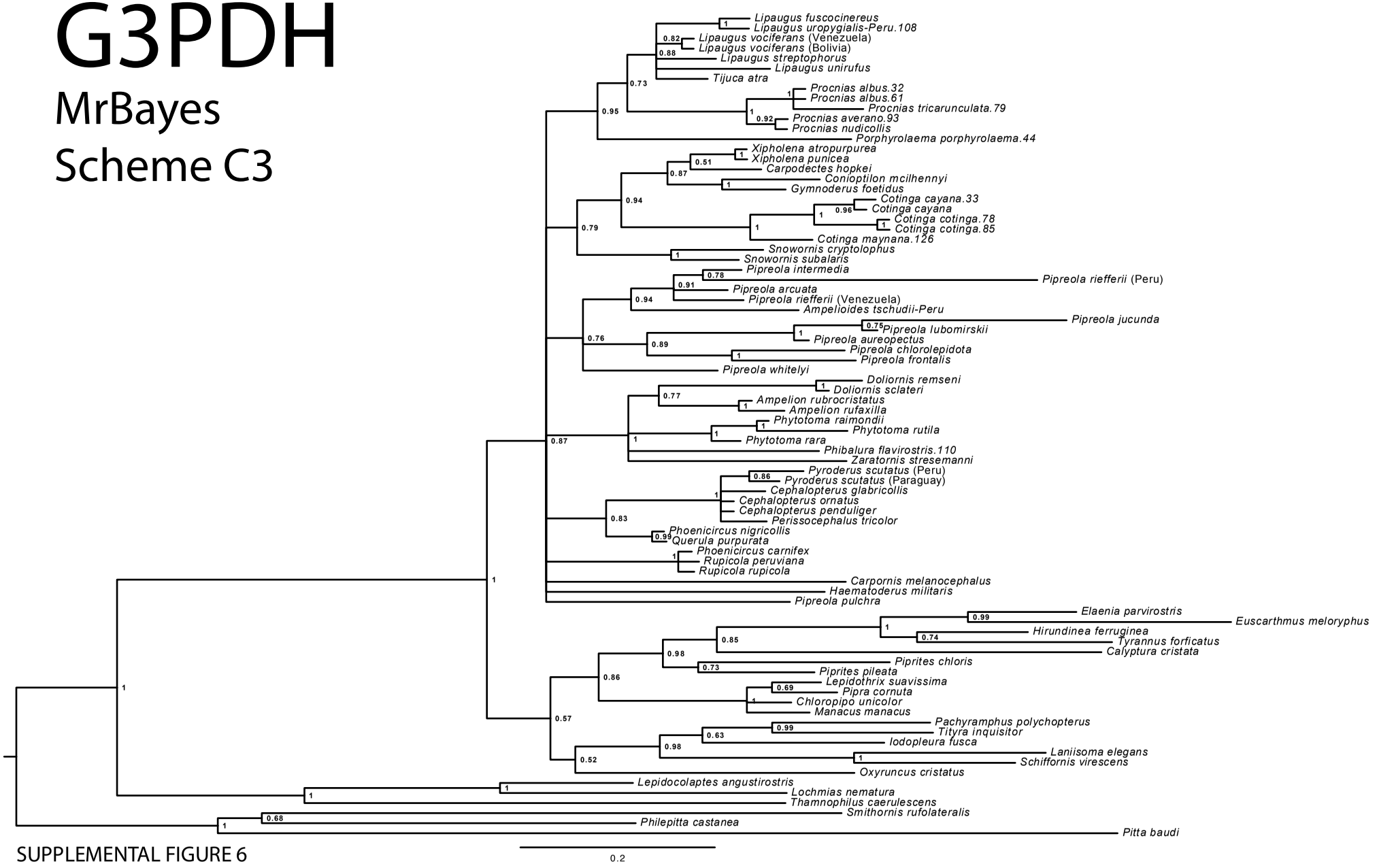

SUPPLEMENTAL FIGURE 6

Supplemental Figures 3-8. Individual gene trees generated by MrBayes 3.2.1

ND2

MrBayes

Scheme C3

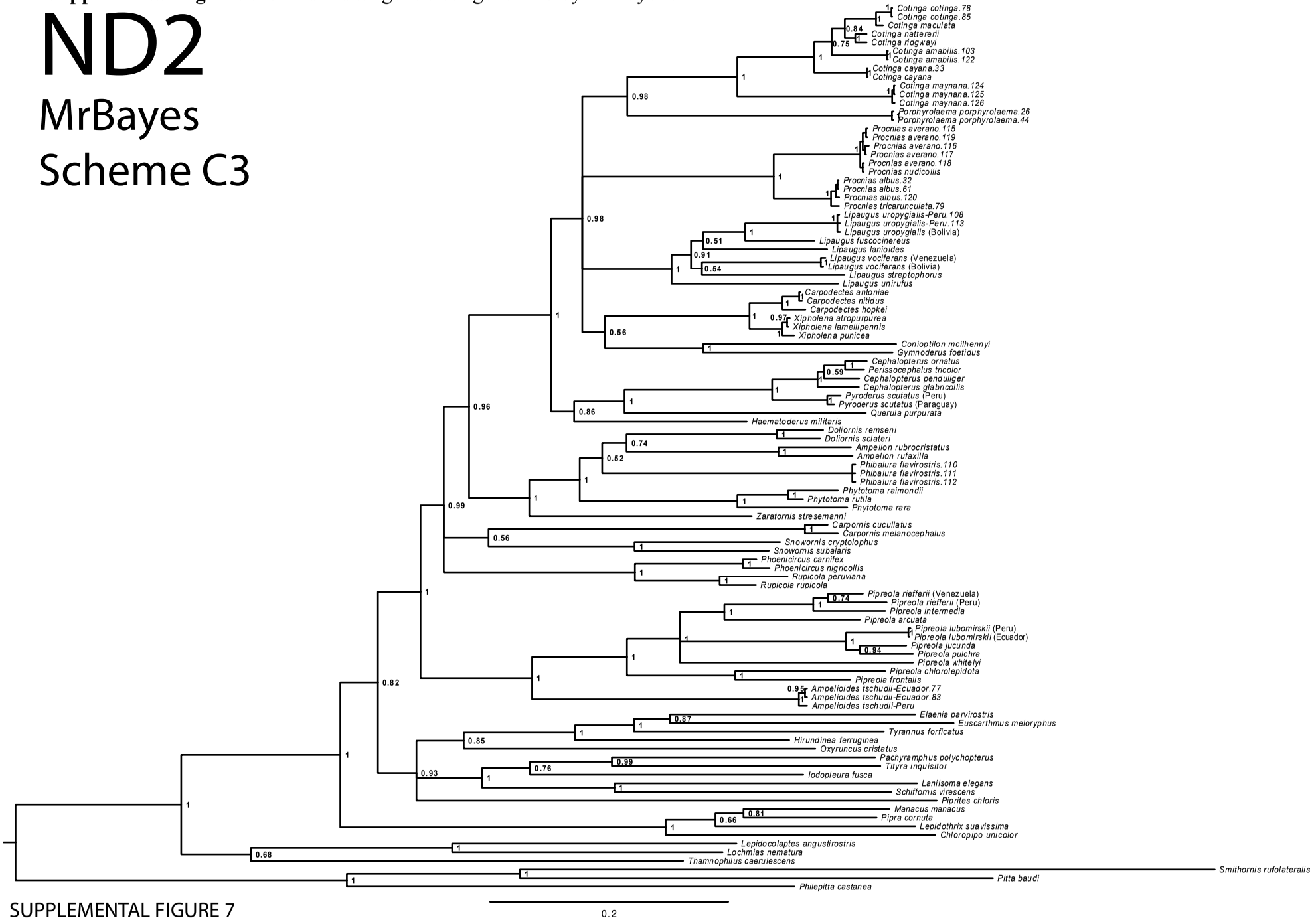

SUPPLEMENTAL FIGURE 7

Supplemental Figures 3-8. Individual gene trees generated by MrBayes 3.2.1

CYTB

MrBayes
Scheme C3

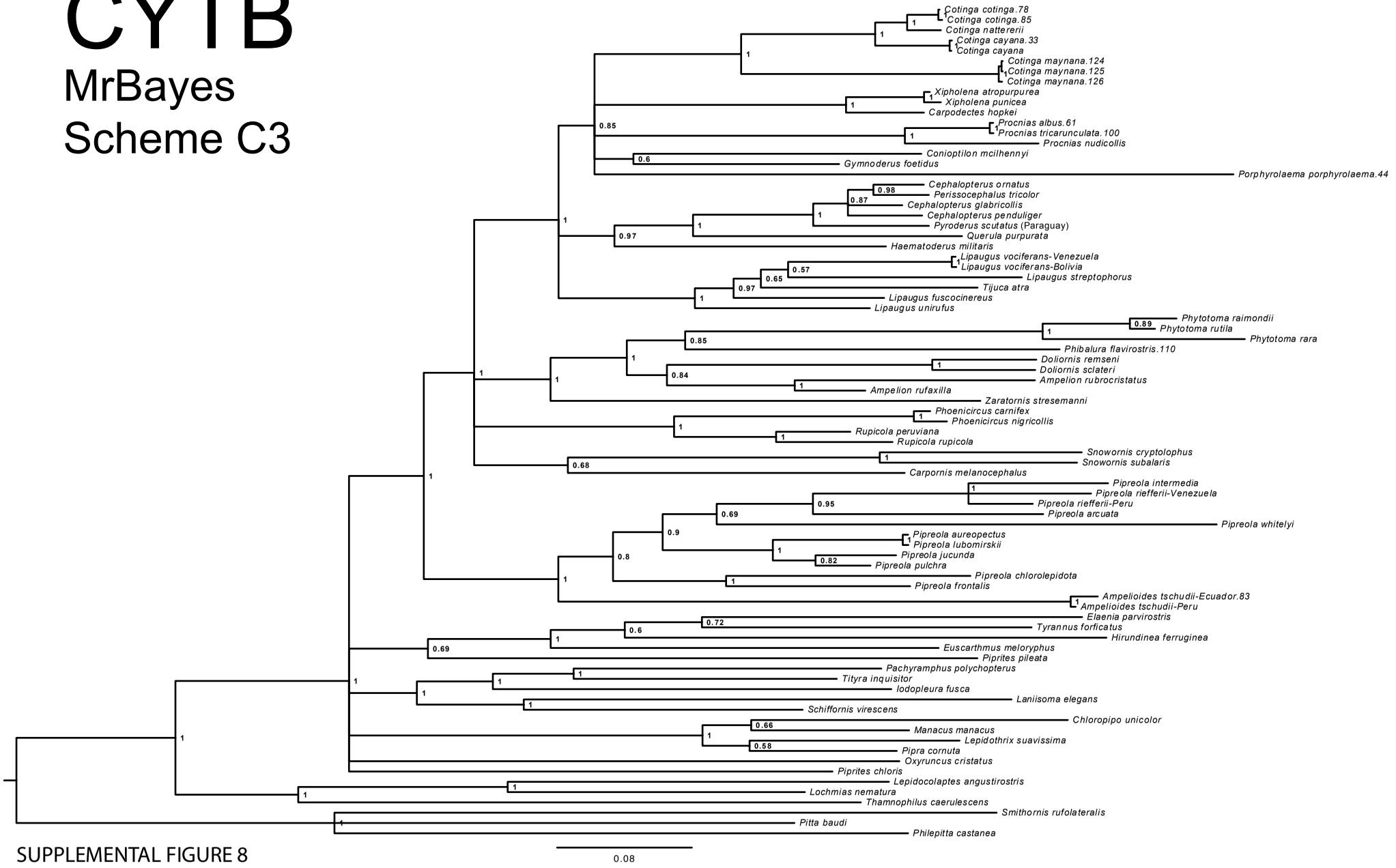

SUPPLEMENTAL FIGURE 8

Supplemental Figure 9. MetaTree 'tree of trees.'

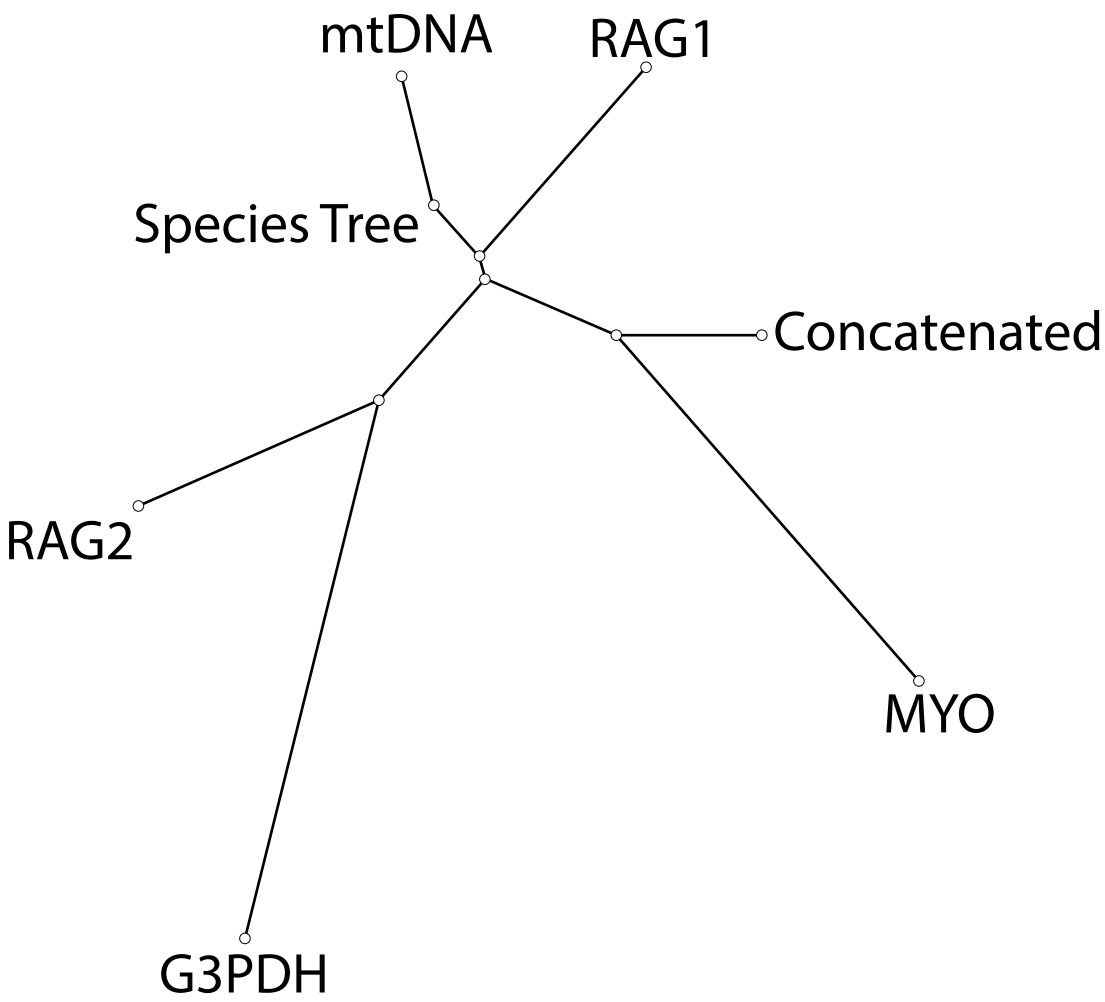

Supplemental Table 1. Table of primers used in this study to amplify and sequence ND2, CYTB, MYO, and G3PDH. * Denotes primers that were modified from their source for this study. Primers for PCR amplifications from toepad extractions are not listed.

Locus	Primer Name	Sequence (5'-3')	Source
CYTB	H15915	AACTGCAGTCATCTCCGGTTTACAAGAC	Edwards and Wilson (1990)
CYTB	H658	TCTTTGATGGAGTAGTAGGGGTGGAATGG	Johansson et al. (2002)
CYTB	L14841	AAAAAGCTTCCATCCAACATCTCAGCATGAAA	Kocher et al. (1989)
CYTB	P5L	CCTTCCTCCACGAAACAGGCTCAAACAACCC	Johansson et al. (2002)
CYTB	L14996_cot	AAYATYTCAGCMTGATGAAACTTYGG	Sorenson et al. (2003)*
G3PDH	G3p13B	TCCACCTTTGATGCGGGTGCTGGCAT	Fjeldså et al. (2003)
G3PDH	G3p14B	AAGTCCACAACACGGTTGCTGTA	Fjeldså et al. (2003)
G3PDH	G3PintL1	GAACGACCATTTTGTCAAGCTGGTT	Fjeldså et al. (2003)
MYO	Myo2	GCCACCAAGCACAAGATCCC	Irestedt et al. (2002)
MYO	Myo3	CGGAAGAGCTCCAGGGCCTT	Irestedt et al. (2002)
MYO	Myo3f	TTCAGCAAGGACCTTGATAATGACTT	Irestedt et al. (2002)
ND2	H1056	GTYTAAGGCTTTGAAGGCCTTCGG	Hernan Vasquez (personal comm.)
ND2	H1056u	RTYTAAGGCTTTGAAGGCCTTYGG	Hernan Vasquez (personal comm.)
ND2	H5766	RGAKGAGAARGCYAGGATYTTKCG	Johnson and Sorenson (1998)
ND2	H6313	ACTCTTRTTTAAGGCTTTGAAGGC	Johnson and Sorenson (1998)
ND2	H6313_cot	CTCTTRTTTAAGGCTTTGAAGGC	Johnson and Sorenson (1998)*
ND2	L5125u	TATCGGGCCCATACCCCGAAWAT	Hernan Vasquez (personal comm.)
ND2	L5216	GGCCCATACCCCGRAAATG	Sorenson and Payne (2001)
ND2	L5758	GGNGGNTGAATRGGNYTNAAYCARAC	Johnson and Sorenson (1998)

Supplemental Table 2. Table of substitution rates, base frequencies, and model parameters α and p(*I*). Reported values are those for scheme S1 for each locus as calculated in *BEAST. VS is the number of variable sites, and PS is the number of parsimony-informative sites in the alignment.

Locus	Relative substitution rates						Base Frequencies				α	p(*I*)	VS	PS
	A-C	A-G	A-T	C-G	C-T	G-T	A	C	G	T				
ND2	0.04	3.39	0.11	0.08	1.00	0.30	0.34	0.39	0.04	0.23	0.59	0.24	630	581
CYTB	0.03	1.53	0.09	0.08	1.00	0.11	0.34	0.41	0.04	0.20	0.62	0.42	567	490
RAG1	0.14	1.00	0.14	0.14	1.00	0.14	0.32	0.20	0.23	0.25	0.79	0.33	391	141
RAG2	0.15	0.76	0.07	0.30	1.00	0.15	0.31	0.20	0.23	0.26	0.66	0.22	183	55
MYO	0.17	1.00	0.17	0.17	1.00	0.17	0.31	0.20	0.22	0.27	1.11	-	199	125
G3PDH	0.23	0.14	1.30	0.45	1.00	0.26	0.32	0.28	0.17	0.23	1.77	-	190	89

Supplemental Table 3. Partition Schemes by locus for *BEAST analysis. The schemes that were chosen as 'optimal' by the BIC in PartitionFinder v1.01 are bolded. The maximally partitioned scheme S3 was chosen in all cases with the exception of RAG2 (intermediately partitioned S2).

Scheme	Partition	Model selection results			BIC
S3	**ND2-1, 2, 3**	**TVM+I+G**	**TRN+I+G**	**GTR+G**	**55902**
S2	ND2-1+2, 3	GTR+I+G	GTR+G	-	56035
S1	ND2-1+2+3	TVM+I+G	-	-	57100
S3	**CYTB-1, 2, 3**	**SYM+I+G**	**TIM+I+G**	**TIM+I+G**	**47081**
S2	CYTB-1+2, 3	TVM+I+G	TIM+I+G	-	47175
S1	CYTB-1+2+3	GTR+I+G	-	-	48667
S3	**RAG1-1, 2, 3**	**K81uf+G**	**HKY+I+G**	**HKY+G**	**23775**
S2	RAG1-1+2, 3	TVM+I+G	HKY+G	-	23797
S1	RAG1-1+2+3	K81uf+I+G	-	-	24224
S3	RAG2-1, 2, 3	HKY+G	TVMef+I+G	K80+G	10630
S2	**RAG2-1+2, 3**	**TVM+I+G**	**K80+G**	-	**10624**
S1	RAG2-1+2+3	TVM+I+G	-	-	10781
	G3PDH	GTR+G	-	-	9907
	MYO	HKY+G	-	-	11499

Supplemental Table 4. Partition schemes for concatenated analyses. The table depicts the three partition schemes that were compared with PartitionFinder v1.01. Scheme C1 (minimally partitioned), top left. Scheme C2 (maximally partitioned), bottom. Scheme C3 (optimally partitioned), top right. The optimal scheme (C3) was selected by choosing the scheme with the lowest BIC score.

Scheme C1	**Models**	**Scheme C3**	**Models**
ND2	GTR+I+G	CYTB-1+ND2-1	GTR+I+G
CYTB	GTR+I+G	CYTB-2+ND2-2	HKY+I+G
RAG1	HKY+I+G	CYTB-3+ND2-3	GTR+I+G
RAG2	K80+I+G	RAG1-1+RAG2-1	HKY+I+G
MYO	HKY+G	RAG2-2+RAG2-2	GTR+I+G
G3PDH	HKY+G	MYO+RAG1-3+RAG2-3	HKY+G
-	-	G3PDH	HKY+G
BIC	165469	**BIC**	**161920**

Scheme C2	**Models**		
ND2-1, 2, 3	GTR+I+G	HKY+I+G	GTR+G
CYTB-1, 2, 3	GTR+I+G	GTR+I+G	GTR+I+G
RAG1-1, 2, 3	HKY+I+G	HKY+I+G	HKY+G
RAG2-1, 2, 3	HKY+G	K80+I+G	K80+G
G3PDH	HKY+G	-	-
MYO	HKY+G	**BIC**	162099

Supplemental Table 5. Table of information criterion for all tested partitioning schemes output from PartitionFinder v1.01. Scheme C1-C3 represent different schemes tested for concatenated analysis in MrBayes or RAxML (descriptions in text). Schemes S1-S3 represent the different schemes tested for each locus for *BEAST species tree inference (descriptions in text). The optimal scheme was chosen in each case by selecting the scheme with the lowest BIC score.

Scheme	lnL	AIC	AICc	BIC	Params	Sites	Subsets
C1	-81589	163692	163710	165469	257	7437	6
C2	-79632	159901	159929	162099	318	7437	14
C3	-79752	160046	160067	**161920**	271	7437	7
S1-ND2	-27813	56051	56160	57100	212	1041	1
S2-ND2	-27243	54931	55053	56035	223	1041	2
S3-ND2	-27152	54763	54895	**55902**	230	1041	3
S1-CYTB	-23739	47815	47874	48667	169	1143	1
S2-CYTB	-22964	46282	46348	47175	177	1143	2
S3-CYTB	-22892	46153	46224	**47081**	184	1143	3
S1-RAG1	-11770	23711	23716	24224	86	2871	1
S2-RAG1	-11524	23237	23243	23797	94	2871	2
S3-RAG1	-11497	23190	23197	**23775**	98	2871	3
S1-RAG2	-5109	10377	10389	10781	80	1152	1
S2-RAG2	-5019	10205	10218	**10624**	83	1152	2
S3-RAG2	-5012	10196	10210	10630	86	1152	3
G3PDH	-4436	9212	9428	**9907**	170	440	1
MYO	-5203	10733	10820	**11499**	164	790	1

Supplemental Table 6. Table of rate calibrations used in this study. Mean rates and standard deviations are reported in % change per million years. All rates were converted to substitutions/site/million years for use in BEAST.

Gene	%/ MY	SD (%/MY)	Group	Source
ND2	2.3	0.37	Monarchidae	VanderWerf et al. (2010)
CYTB	2.07	0.2	Passerines	Weir and Schluter (2008)
MYO	0.15	0.0093	Furnariidae, Tyrannidae	Fjeldså et al. (2007); Ohlson et al. (2008)
G3PDH	0.24	0.054	Fringillidae	Lerner et al. (2011)
RAG1	0.07	0.0182	Fringillidae	Lerner et al. (2011)
RAG2	-	-	-	-

Supplemental Table 7. Ucld.mean is the mean of the branch rates under the uncorrelated lognormal relaxed molecular clock (in substitutions/site/million years). Ucld.stdev is the standard deviation of the relaxed clock. * Indicates that the frequency histogram did not include zero (the result is significant).

Locus	ucld.mean	ucld.stdv
ND2	0.01125	0.11
CYTB	0.01158	0.24*
RAG1	0.00043	0.16
RAG2	0.00053	0.17
MYO	0.00070	0.39*
G3PDH	0.00127	0.54*

Supplemental Table 8. Matrix of Topological similarity estimates across loci and Bayesian species tree/concatenated analyses. Similarity scores were generated using the Compare2Trees web applet. [1]Species tree topology. [2]Concatenated topology.

	mtDNA	**G3PDH**	**RAG1**	**RAG2**	**MYO**	**ST[1]**	**Concat[2]**
mtDNA	-	87.5%	93.8%	93.3%	89.0%	97.8%	95.0%
G3PDH		-	85.5%	88.7%	83.8%	88.5%	89.5%
RAG1			-	91.5%	89.2%	94.9%	92.5%
RAG2				-	87.8%	92.7%	93.0%
MYO					-	90.4%	96.1%
ST						-	91.5%
Concat							-

Supplemental Table 9. Average p-distance matrix across all cotingas
Provided as separate XLSX file

Supplemental Table 10. Coding of cotinga breeding biology characters
Provided as separate XLSX file

Supplemental References:

Edwards, S.V., Wilson, A.C., 1990. Phylogenetically informative length polymorphism and sequence variability in mitochondrial DNA of Australian songbirds (Pomatostomus). Genetics 126, 695-711.

Fjeldså, J., Irestedt, M., Jønsson, K.A., Ohlson, J.I., Ericson, P.G., 2007. Phylogeny of the ovenbird genus Upucerthia: a case of independent adaptations for terrestrial life. Zoologica Scripta 36, 133-141.

Fjeldså, J., Zuccon, D., Irestedt, M., Johansson, U.S., Ericson, P.G.P., 2003. Sapayoa aenigma: a New World representative of 'Old World suboscines'. Proceedings of the Royal Society of London. Series B: Biological Sciences 270, S238-S241.

Irestedt, M., Fjeldså, J., Johansson, U.S., Ericson, P.G.P., 2002. Systematic relationships and biogeography of the tracheophone suboscines (Aves: Passeriformes). Molecular Phylogenetics and Evolution 23, 499-512.

Johansson, U.S., Irestedt, M., Parsons, T.J., Ericson, P.G.P., 2002. Basal phylogeny of the Tyrannoidea based on comparisons of cytochrome *b* and exons of nucelar c-myc and RAG-1 genes. Auk 119, 984-995.

Johnson, K.P., Sorenson, M.D., 1998. Comparing Molecular Evolution in Two Mitochondrial Protein Coding Genes (Cytochromeband ND2) in the Dabbling Ducks (Tribe: Anatini). Molecular Phylogenetics and Evolution 10, 82-94.

Kocher, T.D., Thomas, W.K., Meyer, A., Edwards, S.V., Pääbo, S., Villablanca, F.X., Wilson, A.C., 1989. Dynamics of mitochondrial DNA evolution in animals: amplification and sequencing with conserved primers. Proceedings of the National Academy of Sciences 86, 6196-6200.

Larkin, M., Blackshields, G., Brown, N., Chenna, R., McGettigan, P., McWilliam, H., Valentin, F., Wallace, I., Wilm, A., Lopez, R., 2007. Clustal W and Clustal X version 2.0. Bioinformatics 23, 2947-2948.

Lerner, H.R., Meyer, M., James, H.F., Hofreiter, M., Fleischer, R.C., 2011. Multilocus resolution of phylogeny and timescale in the extant adaptive radiation of Hawaiian honeycreepers. Current Biology 21, 1838-1844.

Maddison, W., Maddison, D., 2011. Mesquite: a modular system for evolutionary analysis. Version 2.75. Mesquite website. Available at mesquiteproject.org.

Nye, T.M.W., 2008. Trees of Trees: An Approach to Comparing Multiple Alternative Phylogenies. Systematic Biology 57, 785-794.

Nye, T.M.W., Liò, P., Gilks, W.R., 2006. A novel algorithm and web-based tool for comparing two alternative phylogenetic trees. Bioinformatics 22, 117-119.

Ohlson, J., Fjeldså, J., Ericson, P.G., 2008. Tyrant flycatchers coming out in the open: phylogeny and ecological radiation of Tyrannidae (Aves, Passeriformes). Zoologica Scripta 37, 315-335.

Sorenson, M.D., Oneal, E., García-Moreno, J., Mindell, D.P., 2003. More taxa, more characters: the hoatzin problem is still unresolved. Molecular Biology and Evolution 20, 1484-1498.

Sorenson, M.D., Payne, R.B., 2001. A SINGLE ANCIENT ORIGIN OF BROOD PARASITISM IN AFRICAN FINCHES: IMPLICATIONS FOR HOST-PARASITE COEVOLUTION. Evolution 55, 2550-2567.

Sorenson, M.D., Quinn, T.W., 1998. Numts: A Challenge for Avian Systematics and Population Biology. The Auk 115, 214-221.

Untergasser, A., Nijveen, H., Rao, X., Bisseling, T., Geurts, R., Leunissen, J.A., 2007. Primer3Plus, an enhanced web interface to Primer3. Nucleic acids research 35, W71-W74.

VanderWerf, E.A., Young, L.C., Yeung, N.W., Carlon, D.B., 2010. Stepping stone speciation in Hawaii's flycatchers: molecular divergence supports new island endemics within the elepaio. Conservation Genetics 11, 1283-1298.

Weir, J.T., Schluter, D., 2008. Calibrating the avian molecular clock. Molecular Ecology 17, 2321-2328.

APPENDIX 2

SUPPLEMENTARY MATERIAL FOR CHAPTER 2

Additional data files will be archived online at time of publication. Until then readers are advised to contact Jacob Samuel Berv for additional materials not included herein.

Supplementary Appendices for:

Genomic phylogeography of the White Crowned Manakin *Pseudopipra pipra* (Aves: Pipridae) illuminates a continental-scale radiation out of the Andes

Author Affiliations:

Jacob S. Berv[1,5*], Leonardo Campagna[1], Teresa J. Feo[2], Ivandy Castro Astor[3], Camila Ribas[4], Richard O. Prum[5], Irby J. Lovette[1]

1. Fuller Evolutionary Biology Program, Cornell Lab of Ornithology, 159 Sapsucker Woods Road, Ithaca, NY 14850, USA. Department of Ecology and Evolutionary Biology, Cornell University, 215 Tower Road, Ithaca, NY 14853, USA.

2. Department of Vertebrate Zoology, MRC-116, National Museum of Natural History, Smithsonian Institution, Washington, DC 20013, USA.

3. Department of Biology, City College of New York and CUNY Graduate Center, City University of New York, New York, NY 10031, USA

4. Coordenacão de Biodiversidade, Instituto Nacional de Pesquisas da Amazônia, Manaus, AM, Brazil

5. Department of Ecology and Evolutionary Biology, and Peabody Museum of Natural History, Yale University, New Haven, Connecticut, 06520, USA.

*Correspondence to: Jacob S. Berv (jsb439@cornell.edu)

Supplementary Appendix

Section 1

Expanded Taxonomic Summary

Pseudopipra coracina (Sclater 1856) **Andean White-crowned Manakin**

Distribution: Subtropical Andes from Venezuela south to Esmeraldas, Ecuador and San Martín, Peru.

Phylogenetic Position: Clade A1, plus multiple unsampled subspecies from the Colombian and Ecuadorian Andes (Fig. 3).

Comments: This apparently monophyletic group of northern Andean populations includes five currently recognized subspecies, each of which may be a distinct species. Three of these subspecies–*coracina, minima,* and *occulta*– have unique, highly differentiated vocal types, and diagnosable plumage differences. The vocal type of *bolivari* is unknown.

P. c. coracina (Sclater 1856)

Distribution: Subtropical forests of the eastern slope of the Andes from western Venezuela to Morona-Santiago, Ecuador.

Phylogenetic Position: Based on mtDNA sampled, a member of Clade A1.

Plumage: Males are moderately glossy on the back. White crown feathers are long with extensive black bases. Crowns are sometimes slightly grayish. Females are olive green with lighter yellow belly, and olive gray crown with more olive cheeks.

Lek Vocal Type: 8 (*errrwer*).

Call Vocal Type: Unknown

P. c. minima (Chapman 1914)

Distribution: Subtropical forests of western Cauca, Colombia south to Esmeraldas, Ecuador

Phylogenetic Position: Not Sampled, but a likely member of Clade A1.

Plumage: Males are moderately glossy; crown feathers are entirely white to their bases. No females were observed. Chapman (1914) reported that *minima* is smaller than *anthracina*, and that males lack prominent gray tips on undertails. Freile (2014) reported one specimen of a female from San Javier, Esmeraldas, Ecuador (100 meters) and provisionally identified it as *minima.* The specimen is bright olive above and below with a slightly grayish olive grown. However, this specimen is from a substantially lower altitude than Colombian records of *minima*, so it may represent an altitudinal migrant or a distinct population.

Lek Vocal Type: 9 (*reeee*)

Call Vocal Type: Unknown

P. c. bolivari (de Schauensee 1950)

Distribution: Subtropical forests of southern Córdoba, Colombia. (Not Sampled)

Phylogenetic Position: Not Sampled, but a likely member of Clade A1.

Plumage: None observed. Apparently known only from the type specimen from Cerro Murucucú, Córdoba, Colombia. de Schauensee (1950) described this male specimen as

having entirely white feathers in the forecrown, like *minima* and *unica,* but hindcrown feathers basally black like *coracina.*
Lek Vocal Type: Unknown
Call Vocal Type: unknown

P. c. unica (de Schauensee 1945)
Distribution: Subtropical forests of Magdalena Valley, Antioquia to Huila, Colombia.
Phylogenetic Position: Not Sampled, but a likely member of Clade A1.
Plumage: Males are moderate glossy, with long crown feathers that are white to their bases. Females are olive green above, and slightly gray on the crown; underparts uniform olive. de Schauensee (1945) described *unica* as glossier than coracina, with longer tail and very long crest.
Lek Vocal Type: 11a (*weer-dink*) and 11b (*shureeep*)
Call Vocal Type: unknown

P. c. occulta (Zimmer 1936)
Distribution: Eastern slope of the Andes from Zamora-Chinchipe, Ecuador (Freile 2014) south to San Martín, and Huánuco, Peru, west of the Rio Huallaga
Phylogenetic Position: Clade A1 (Fig. 3)
Plumage: Males are glossy with dark gray bases to crown feathers. Females are dark olive with dark gray crown and gray throat. Zimmer (1936) described occulta as similar to *comata* but adult males with the occipital feathers slightly shorter and with the crown and occipital feathers sooty at the base instead of entirely white.
Lek Vocal Type: 1 (*trill-dink*) and 10 (*bree*)
Call Vocal Type: unknown

Pseudopipra anthracina (Ridgway 1906) **Western White-crowned Manakin**
Distribution: Subtropical Costa Rica to Western Panama
Phylogenetic Position: Clade A2 (Fig. 3)
Plumage: Males less lustrous on back than all other *Pseudopipra* populations, white crown feathers gray or dark gray at base. Female are olive green with slaty crown and face. Ridgway (1906) considered *anthracina* to have shorter wings, smaller beak, less lustrous plumage than *pipra* with undertails tipped with gray.
Lek Vocal Type: 4 (*jureeee*)
Call Vocal Type: unknown

Pseudopipra comata (Berlepsch and Stolzmann 1894) **Junín White-crowned Manakin**
Distribution: Subtropical Andes of Peru from Cerro Azul, Loreto (east and south of the Rio Huallaga) to southern Huánuco, Pasco, Junín, and northern Cusco.
Phylogenetic Position: Clade B (Fig. 3).
Plumage: Males are glossy black above, crown feathers longer and entirely white to their bases. Females are bright olive green above, gray on crown and face, slightly gray on throat, dark olive below, and slightly dark gray on the belly.
Lek Vocal Type: One record, statistically similar to type 1 (*trill-dink*)

Call Vocal Type: unknown
Comment: *P. comata* is also composed of two well differentiated subclades. The northern clade (B1) is known from Cerro Azul in Loreto, Peru. The southern clade (B2) is known from extreme southern Huánuco (Cerros del Sira, 9˚30'S 74˚47'W; AMNH 820866, 820952), Pasco, Junín, and Cusco. The type locality of *comata* is Vitoc, Junín within the southern clade. Further investigation plumage and behavioral is necessary to determine whether the Cerro Azul populations should be recognized as a distinct, new taxon.

Pseudopipra pygmaea *(*Zimmer 1936) **Huallaga White-crowned Manakin**
Distribution: Tropical forest of Lower Rio Huallaga Valley, Peru
Phylogeneic Position: Sister to Clade F (mtDNA)
Plumage: Males: Glossy, with black bases to crown feathers. Females are olive above and gray below with a band of olive across the chest; crown and face only slightly darker than back, not gray. Zimmer (1936) described males as having long crest with gray bases, crown sometimes slightly ashy; females are much paler than *occulta*; throat and belly decidedly more whitish, breast paler duller green; lighter even than *microlopha*.
Lek Vocal Type: 2 (*deeeer*)
Call Vocal Type: 13
Comment: Lowland populations along the Rio Huallaga have been named *pygmaea* (Zimmer 1936). Our four samples of *pygmaea* from Jeberos, Peru did not yield sufficient quality DNA for RADseq, but all four had a phylogenetically distinct mtDNA haplotype which placed this lineage as the sister group to all other lowland populations of *Pseudopipra*. These populations have song type 2, which appears to be shared plesiomorphically with *P. discolor* and *P. microlopha separabilis* from Para, Brazil.

Pseudopipra discolor (Zimmer 1936) **Napo White-crowned Manakin**
Distribution: Tropical forest in Napo, Ecuador and northern Loreto, Peru south to the Rio Marañón.
Phylogenetic Position: Clade E (Fig. 3)
Distribution: Tropical forest in Napo, Ecuador south to the Rio Marañón
Plumage: Males are glossy black above, white crown feathers with black or dark gray bases. Females are dusky olive overall, slightly grayer on crown, and grayer belly. Zimmer (1936) described male *discolor* as glossier and bluer above than *pipra.*
Lek Vocal Type: 2 (*deeeer*)
Call Vocal Type: 13
Comment: This lineage was found to have both a distinct, unique history, with subsequent introgression with adjacent populations of the northern Amazonian clade. The nature of this introgression indicates this lineage may be best recognized as a distinct hybrid species.

Pseudopipra pipra (Linneaus 1758) **Northern White-crowned Manakin**
Distribution: Tropical forest of eastern Colombia, southern Venezuela, the Guianas, and Brazil north of the Amazon. West to the right (north) bank of the Rio Putumayo, Colombia.
Phylogenetic Position: Clade D (Fig. 3).

Plumage: Males are glossy black above, crown feathers longer with extensive black bases. Females are dark olive above, olive below, grayer on belly, and occasionally only slightly darker gray on crown.
Lek Vocal Type: 3 (*buzzzz*)
Call Vocal Type: 5 (*zeee*)

Pseudopipra microlopha (Zimmer 1929) **Southern White-crowned Manakin**
Distribution: Tropical forest of eastern Peru south of the Rio Marañón, and south of the Amazon east to Pará, Brazil, and subtropical forests between the Rio Huallaga and Rio Ucayali
Phylogenetic Position: Paraphyletic, including Clade C without Clade C7 (Fig. 3).
Comments: A paraphyletic group (with respect to *P. cephaleucos* from Brazilian Atlantic forest) which includes three, currently recognized subspecies, and four additional genetically well-supported monophyletic subgroups that may be recognized as new taxa. Furthermore, we identified a genetically distinct montane clade from the highlands between Rio Huallaga and Rio Ucayali that has not been previously described, and may have distinct plumage and vocal characters.

P. m. **undescribed subspecies**
Distribution: Subtropical forest from the highlands between Rio Huallaga and Rio Ucayali All samples are from a single locatlity: 77 km WNW Contamana, Loreto, Peru; 7.08333˚ S, 75.65˚ W).
Phylogenetic Position: Clade C2 (Fig. 3)
Plumage: Not examined.
Lek Vocal Type: Unknown
Call Vocal Type: 13

P. m. microlopha (Zimmer 1929)
Distribution: Eastern Peru south of the Rio Marañón and Rio Huallaga west to Rio Juruá and Rio Purus, Brazil.
Phylogenetic Position: Apparently paraphyletic, Clade C1 excluding C2 (Fig. 3)
Plumage: Males are glossy black above, with black or dark gray bases to white crown feathers. Females are dark olive above, occasionally with slightly gray crown, olive below, and graying on the belly.
Lek Vocal Type: 7 (*jeer*)
Call Vocal Type: 13

P. m. **undescribed subspecies**
Distribution: Right (east) bank of the Rio Purus to the left (west) bank Rio Madeira
Phylogenetic Position: Clade C3 (Fig. 3)
Plumage: Not examined.
Lek Vocal Type: Unknown
Call Vocal Type: 13

P. m. **undescribed subspecies**

Distribution: Right (east) bank of the Rio Madeira to the left (west) bank the Rio Tapajos.
Phylogenetic Position: (Clade C4, Fig. 3)
Plumage: Not examined.
Lek Vocal Type: Unknown
Call Vocal Type: 13

***P. m.* undescribed subspecies**
Distribution: Right (east) bank of the Rio Tapajos to the left (west) bank of the Rio Xingu
Phylogenetic Position: Clade C5 (Fig. 3)
Plumage: Not examined.
Lek Vocal Type: 6b
Call Vocal Type: 13

P. m. separabilis (Zimmer 1936)
Distribution: Right (east) bank of the Rio Xingu east to central and southern Pará.
Phylogenetic Position: Clade C6 (Fig. 3)
Plumage: Males are moderately glossy above, crown long with large, dark gray feather bases. Predefinitive male plumage light olive above, gray below, with medium gray crown.
Females are light olive above, light grayish below with olive wash on the breast. Zimmer (1939) Zimmer (1939) commented that adult males and females not distinguishable from *separabilis,* but he identified the distinct predefinitive male plumage
Lek Vocal Type: 2
Call Vocal Type: 13

Pseudopipra cephaleucos (Thunberg 1822) **Atlantic White-crowned Manakin**
Distribution: Tropical forest from Bahia south to northern Rio de Janeiro, Brazil.
Phylogenetic Position: Clade C7 (Fig. 3)
Plumage: Males are glossy black with a long and slightly gray crown. Crown feather have extensive dark gray bases. Predefinitive males have olive backs, pure white or grayish white crowns, and slate gray on the face, throat, and belly. Females have olive back, dusky gray on head, gray below, slightly olive on breast, lighter on belly.
Lek Vocal Type: 6a (*zeeeee-tonk*)
Call Vocal Type: 13

Section 2
Additional results and discussion

Additional phylogenetic results and comments on mutational spectra

At the level the concatenated alignments, the '20% missing' dataset had a total of 2,548 132bp loci (340,956 sites), 7.92% missing sites, 8,063 parsimony informative sites, and 5,709 variable parsimony-uninformative sites. The '50% missing' dataset had a total of 4,763 132 bp loci (626,868 sites), 20.48% missing sites, 15,365 parsimony informative sites, and 11,221 variable parsimony-uninformative sites. The '80%' missing dataset had a total of 7,907 132 bp loci (1,039,632 sites), 38.89% missing sites, 24,450 parsimony informative sites, and 17,839 variable parsimony-uninformative sites. Across these datasets, alpha from the GTR+G model was << 1 (0.069, SD=6.033×10^{-4}), indicating high among site rate heterogeneity for these ddRAD loci. Chi-square tests of base compositional heterogeneity rejected the hypothesis of compositional homogeneity (Chi-sq= 7822.93, df=702, P << 0.05), with slight bias observed on the AT-GC axis of compositional variation (A: 0.24968, C: 0.25225, G: 0.24301, T: 0.24301, on the largest 80% dataset). Maximum likelihood estimates of transition rates were ~8x transversion rates (A<-->G: 7.34 x G <--> T, C <--> T: 8.13 x G <--> T), as estimated in RAxML. Estimated rates among other nucleotide classes were ~1 relative to the fixed G <--> T rate, suggesting that the available GTR model in RAxML is likely over-parameterized for ddRAD data.

Reconstruction of mitochondrial ND2 gene tree

After obtaining mitochondrial DNA sequences for 168 individuals (Supplementary Table 1), we aligned these sequences using MAAFT (Standley and Katoh 2013). The alignment was visually inspected in Sequencher (Gene_Codes_Corporation 2010), and then analyzed in IQ-TREE 1.6.10 (Schmidt et al. 2014, Chernomor et al. 2016, Trifinopoulos et al. 2016, Hoang et al. 2017, Kalyaanamoorthy et al. 2017). We partitioned by codon position and generated a maximum likelihood tree using the MFP+MERGE model search and partitioning option, with 1000 ultrafast bootstrap replicates. MFP+MERGE detected that an optimal scheme comprised of three partition-models for each of the three codon positions (CP1: TIM2+F+I; CP2: TIM2+F+G4; CP3: TIM2+F+G4). Nodes recovered with ultrafast bootstrapped < 95 were collapsed. The recovered topology was entirely congruent with the topology presented in the main text as derived from ddRAD data, with a few exceptions (Supplementary Figure 14). Our mtDNA dataset included individuals from subspecies *coracina* and *pygmaea* which were derived from low quality tissue samples (and hence were not suitable for ddRAD sequencing). This enabled us to make a preliminary assessment of their phylogenetic affinities (main text), though nuclear genomic data should be collected in future studies. Notably, the introgressed western Napo lineage has mtDNA haplotypes which are members of the southern amazon clade (BS 98), which is consistent with the scenario of hybrid origin and introgression we develop in the main text. Because mtDNA is inherited matrilineally, a potential implication of this pattern is that the introgressed Napo lineage (S2a/S2 in Figure 6) was created when southern progenitor females were introgressed with northern males.

Reconstruction of ancestral elevational habit

We performed a Bayesian stochastic character mapping analysis (Huelsenbeck et al. 2003, Bollback 2006) to estimate the ancestral habit of *Pseudopipra*. In brief, we coded lineages as montane (>1000m) or lowland (< 1000m), applied a bi-directional Mk model

('ARD') and performed 100 simulations (see supplemental R code) using the RAxML topology. We used the SIMMAP implementation in phytools (Revell 2012). These analyses unambiguously reconstructed the ancestral habit of *Pseudopipra* to be montane.

STRUCTURE - additional results

The Evanno method applied to the whole dataset detected a significant shift in the rate of change of the log probability of the data between K1 and K2, indicating a deep hierarchical split in the data. As STRUCTURE infers the degree of admixture among individuals, this assignment is not directly comparable to K-means phenetic cluster solutions, which lump individuals categorically based on overall genetic similarity. That said, there was broad overlap in cluster assignment.

Descriptive Population Genetic Statistics – methods

For population genetic statistics, we considered eighteen population-areas (Figure 3, 4). Most of these populations are delimited by clear geographic barriers (e.g., rivers in the cases of previously identified areas of endemism, the Andes, or the Cerrado belt) and have strong phylogenetic support. Two subgroups within the broad Northern Amazonian + Guiana Shield lowland clade were defined on the basis of low-support monophyly in the RAxML analysis *and* coincidence with geographic features. One of these comprised individuals unambiguously assigned to northern Amazonian clade in phylogenetic analysis, but which were also restricted to the eastern Napo area of endemism, east of the Rio Putumayo (brown dots in Figures 3, 4, 'weakly resolved eastern Napo' – abbreviated in R code and Supplementary Figures as 'GSNapo'). The second comprised individuals found near the coasts in Suriname and the Brazilian state of Amapá, east of the Essequibo river (pale blue dots in Figures 3, 4: 'Suriname + Amapá' – abbreviated in R code and Supplementary Figures as 'GSSR'). Another subgroup was defined on the basis of restriction to the Jaú area of endemism (pale yellow dots in Figures 3, 4: 'unresolved Jaú' – abbreviated in R code and Supplementary Figures as 'GSImeri'). Lastly, a fourth group of individuals included all other individuals in the lowland northern Amazon clade, restricted to the Guiana Shield (green dots in Figure 3, 4: 'weakly resolved Guiana Shield' – abbreviated in R code and Supplementary Figures as 'GS'), comprising individuals east of the Jaú group (above), and west of those in the Suriname + Amapá group. The primary geographic barriers in this region separating western and eastern Guiana Shield populations seems to be the Guiana Highlands, which is where tepuis are found, as well as the Essequibo river.

For these descriptive analyses, we focus on the aforementioned eighteen areas as units of comparison because focusing on broader populations delimited by cluster analyses would likely generate statistics biased by population sub-structure—i.e, lower than expected heterozygosities (Wahlund 1928). Further, groups delimited by broader cluster assignments may be more reflective of ancestral populations, and therefore not indicative of presently restricted groups (ie, inappropriately moving migrants back to their source populations, Kuhner 2006). Statistics were calculated using dataset 2, as this includes that largest number of putatively unlinked markers (the first SNP from each of 2,581 ddRAD loci), unless otherwise indicated.

To estimate a measure of genetic diversity across these sampling regions, we calculated the rarefied allelic richness per population (restricted to populations comprising > 5 individuals) using the allelic.richness function in the hierfstat R package (Goudet 2005), after removing all sites with missing genotypes (Supplemental R Script).

We also calculated the inbreeding coefficient F_{IS}, defined as $(H_S - H_I)/H_S$, where H_I is the mean expected heterozygosity per individual within subpopulations, and H_S is the mean expected heterozygosity within random mating populations (Goudet 2005). We generated 100,000 bootstrapped estimates of F_{IS}, sampling over loci per population, using the boot.ppfis function in hierfstat (Goudet 2005). For recently hybrid individuals, F1s should be more outbred (relative heterozygosity) than their parental genotypes. We tested the hypothesis that the introgressed western Napo population is composed of recently introgressed individuals by estimating the inbreeding coefficient for a simulated F1 population, comprised of the progenitor lineages discussed in the main text. We generated a simulated F1 population using the hybridize function in adegenet (Jombart 2008), and then estimated it's inbreeding coefficient as described above to compare to empirical estimates from source populations.

To perform a preliminary assessment of the potential for evolutionary processes deviating from the assumptions of Hardy-Weinberg equilibrium, we applied the hw.test function in the pegas R package (Paradis 2010) with 1000 Monte Carlo permutations of alleles to compute an exact p value for each locus within each population. To assess the assumption of linkage intrinsic to most model-based analyses in this study, we computed the Standardized Index of Association $\bar{r}_d$ (Brown et al. 1980, Agapow and Burt 2001) within populations using the poppr summary function in the poppr R package (Kamvar et al. 2014), and estimated p values with 1000 permutations. We estimated pairwise Weir and Cockerham's (Weir and Cockerham 1984) F_{st} among all 18 areas, and evaluated significance using 1000 bootstrapped datasets to estimate 95% confidence intervals using the 'assigner' R package (Gosselin et al. 2016).

Lastly, we quantified differentiation among two hierarchical strata recapitulating 1) deep coalescent structure (6 groups as identified by SVDquartets (~K5 from STRUCTURE + putative introgressed Napo hybrids as a separate group), and 2) populations identified in phylogenetic analyses which coincide with geographic barriers (18 groups), with analysis of molecular variance (AMOVA) (Excoffier et al. 1992). We used the poppr.amova wrapper function in the poppr R package (Kamvar et al. 2014) to perform AMOVA on adegenet genind objects, set to use the ade4 implementation of AMOVA with 1000 permutations to assess significance. For AMOVA calculations we used dataset 1, to minimize within individual variance.

Descriptive population genetic statistics – results

Missing data (dataset2) was quite low across areas (mean: ~9.5%, SD: 5.3% and ranged from ~2.4% (Jaú subgroup of the Guiana Shield clade) to a maximum of 20.5% (Costa Rica, though this was somewhat of an outlier – 75% of these areas had less than 13% missing data overall). Despite the fact that our sampling scheme among areas delimited by geographic boundaries had high variance relative to the mean (mean: 12.94 [1 - 70], SD: 16.95284, CoV: 1.31), the sum rarefied estimates of allele counts in each of 13 areas (with > 5 individuals, and after filtering out all sites with missing genotypes) were

similar. For dataset 2 (2581 SNPs): mean number of alleles: 297.76, SD: 6.44, CoV: 0.022. The greatest allelic diversity was found in the Jaú (n=14, 305.75 alleles) and introgressed western Napo population (n=10, 303.8 alleles). The lowest allelic richness was found to be in the Rio (n=10, 287.15) and Bahia (n=6, 285.48 alleles) Atlantic Forest populations, followed closely by Panamanian populations (n=5, 292 alleles). These results are generally consistent with our EEMS analysis (Supplementary Figure 12). Summary table below:

Population	**Alleles**
Atlantic Forest (Bahia)	285.4848
Atlantic Forest (Rio)	287.1516
Central America (Panama)	292.0000
South Andean Peru (South)	294.0000
Eastern Inambari endemic	297.4178
Xingu endemic	297.5155
Weakly resolved Guiana Shield (western)	299.4562
Weakly resolved Suriname + Amapá	299.5588
Inambari endemic (western)	302.4655
Weakly resolved eastern Napo	302.4864
Tapajós endemic	303.7529
Western Napo introgressed lineage	303.7964
Unresolved Jaú	305.7571

Most populations were detected to be significantly inbred ($F_{IS} > 1$**,** Supplementary Figure 9), with lower 95% confidence intervals > 0. Panamanian, Costa Rican, South Andean (North clade), Rondônia, and Espírito Santo clades had 95% confidence intervals which overlapped zero, and thus cannot be confidently inferred to have positive or negative F_{IS}. The simulated F1 population, however, did have significantly negative F_{IS}, as predicted. This pattern implies that the introgressed western Napo population, which was detected to have a significantly positive F_{IS}, is not likely to include recently introgressed individuals. Indeed, the confidence intervals for eastern Napo, Jaú, Inambari and western Napo popularions, are generally overlapping, with similar means (mean of mean estimates ~0.17, SD of mean estimates ~0.02, Supplementary Figure 9).

Pairwise population estimates of Weir and Cockerham's F_{st} ranged from essentially undifferentiated, to almost entirely distinct. At the most extreme: comparing the geographically proximate eastern Napo and Jaú populations (both weakly resolved in phylogenetic analyses, but likely sister) --F_{st}: 0.0045. By contrast, comparing an Atlantic forest Espírito Santo population to a population in Panama indicates an F_{st} of 0.81, or almost entirely differentiated. Overall, population average F_{st} was very high: 0.196 [0.188-0.204] (Supplementary Figure 10).

After correcting for multiple tests with the Benjamin & Hochberg correction, exact tests of Hardy-Weinberg equilibrium suggested most loci in most populations were in equilibrium. However, a small number of loci in the western Guiana group (123 loci), Suriname+Amapá (53 loci) and Tapajós (14 loci) areas were identified as being out of Hardy-Weinberg equilibrium. Estimates of $\bar{r}_d$ within these populations indicated that there

was no strong evidence of linkage among loci within populations, except for the Tapajós area, in which weak linage was detected ($\bar{r}_d$: 0.005956, p= 0.000999).

Lastly, an AMOVA detected significant population differentiation at all evaluated levels, including between coalescent units (well supported clades form SVDquartets) (~32%) and between samples within coalescent units (~5%) ($p < 0.001$ for all). Re-running the same AMOVA with evolutionary distances estimated with RAxML branch lengths (instead of the default allelic distance) indicated the same pattern, but with more of the variance explained by coalescent and population level strata (41.3% and 12.6% respectively). Both AMOVA analyses detected a significant proportion of the variance attributable to within sample variance (62% and 46% respectively).

Isolation by distance and the effect of geography

The evolutionary history of *Pseudopipra* within the Amazon basin appears to be deeply connected to the South American landscape, adding additional support to a rich body of literature endorsing this hypothesis (Cracraft and Prum 1988, Brumfield 2012). For virtually all evaluated cases, we find significant effects of geographic barriers on structuring genetic variation within this species complex, including the Amazon River and most associated tributaries (Supplementary Table 2b and Figure 7). Further afield, the 'dry-diagonal' Cerrado belt appears to have strongly isolated Atlantic Forest lineages from their southeastern Amazonian Xingu relatives, as do the Andes exhibit a disproportionate effect on divergence between Peruvian foothills populations and Central American lineages (with the caveat that our sampling in that area is sparse, so our power to infer spatial patterns is necessarily limited).

The establishment of the Amazonian river system has recently been questioned as a driver of species—level variation across key areas in the Neotropics (Oliveira et al. 2017, Santorelli et al. 2018). These recent studies used distributional data to infer the effects of key proposed barriers and concluded that while large rivers clearly limit some Amazonian species—the large number of exceptions to this 'rule' point towards alternative speciation mechanisms as the norm, rather than as the exception. Indeed, rivers can plausibly function as contemporary species limits without being the source of such limits (Santorelli et al. 2018). In the case of *Pseudopipra,* river barriers have clearly contributed to contemporary patterns of genetic diversity, regardless of whether or not the formation of the Amazonian drainage system was the primary driver of generating that diversity. Importantly, studies which rely on distributional data alone are limited in that their statistical power is entirely contingent on the accuracy of species and subspecies delimitation. In the biogeographic context of the Amazon, this is likely to be enormously underestimated for birds (Brumfield 2012, Smith et al. 2014). This fundamental limitation in our knowledge of cryptic avian diversity is therefore likely to bias inferences derived from distributional data, which is based on mostly untested species limits. Indeed, most studies that use genetic data to investigate the effect of river or other physical barriers in structuring Neotropical avian diversity have inferred strong, though varying effects (e.g. Moore et al. 2008, Harvey and Brumfield 2015, Naka and Brumfield 2018).

A number of authors have also noted that the practice of identifying genetic clusters with model based approaches often fail to appropriately account for the effects of isolation by distance (Guillot et al. 2013), and various methods are in development to improve our

ability to model such correlated phenomena (Bradburd et al. 2013, Botta et al. 2015, Petkova et al. 2015, Bradburd et al. 2017). STRUCTURE in particular has been highlighted as potentially suffering from over-estimating K as a consequence of spatial autocorrelation in widely distributed genetic data (Bradburd et al. 2017). Our STRUCTURE analysis appears to exhibit this behavior for the southern Amazon, with a genetic cline of admixture that falls on a longitudinal gradient across the southern Amazon and ends in the well differentiated Atlantic Forest Rio population. While it is plausible that isolation by distance, combined with physical barriers to gene flow, could generate a similar pattern (as implied by our phylogenetic analyses), it is important to keep this caveat in mind when interpreting STRUCTURE results. For example, STRUCTURE may suggest that a scenario of K2 with an admixture gradient between two populations is preferred, when K1 with an isolation by distance effect may be a better description and more biologically plausible model for the data (Bradburd et al. 2017). The degree to which this kind of spatial autocorrelation confounds STRUCTURE-like analyses at large remains an open and important area of inquiry. Our EEMS analysis attempts to circumvent this issue entirely, assuming a more biologically realistic process of continuous differentiation across a heterogeneous landscape, however it does not provide unambiguous insight into hypotheses of species delimitation.

Notes on congruent patterns with Ceratopipra

Within the manakins, a recent molecular phylogeny (Ohlson et al. 2013) placed *Pseudopipra* as sister to the genus *Ceratopipra*, which includes five well-recognized species that are extensively codistribtuted with *Pseudopipra.* The breakpoints among these *Ceratopipra* species are highly concordant with the breakpoints among the genetic clusters within the *Pseudopipra* complex that we have presented here, implying that these taxa have many components of their phylogeographic history in common. *Pesudopipra* is the Andean sister group to the lowland Ceratopipra, which has itself expanded into montane habitats twice (*corunta* and *chloromeros*). By contrast, *Pseudopipra* expanded from the Andes into the lowlands.

Ceratopipra erythrocephala is distributed in the northern Amazon, and *C. rubrocapilla* has a range encompassing the southern Amazon and the Atlantic Forest. *C. mentalis* is distributed in Central America and south-ward into the Chocó and the western edges of Columbia and Ecuador *C. chloromeros* has a narrow distribution in the lower montane forests of the southern Peruvian and northern Bolivia Andes. The distributions of *C. erythrocephala* and *rubrocapilla* are extensively with the Guianan Shield and Southern Amazonian clades of *Pseudopipra*. However, the *Pseudopipra* radiation also has some important differences from *Ceratopipra. C. cornuta* is distributed in montane forests of tepuis in Venezuela and western Guyuna, at altitudes where *Pseudopipra* does not occur. In contrast, *Pseudopipra* has extensive montane populations in the Andes from Peru to Colombia, and *C. chloromeros* is only distributed in the easterns slope of the Andes in Peru and Bolivia. *C. mentalis* is found in lowland tropical forest at lower altitudes than the lower montane populations of *Pseudopipra* in Central America. Furthermore, the Chocó population of *Pseudopipra* is also lower montane in distribution, and not continuous with Central America. Lastly, the phylogenetic relationships among the differentiated lineages of *Ceratopipra* and *Pseudopipra* are not congruent. In *Ceratopipra,* the northern and southern

Amazonian lineages are not sister taxa. Rather, the northern Amazonian *erythrocephala* is sister to the Central American and Chocó *mentalis,* and southern Amazonian *rubrocapilla* is sister to the Andean *chloromeros* (Ohlson 2013).

Vocal variation

Pseudopipra vocalizations have 1-3 buzzy or tonal notes. We measured: 1) starting frequency, 2) ending frequency, 3) minimum frequency, 4) maximum frequency, 5) number of notes, and 6) duration of the entire vocalization (see Supplementary Figure 13). To obtain a conservative estimate of the number of individuals sampled, we took measurements of one vocalization from each recording. When there were multiple recordings by the same recordist on the same day and location, only one of the recordings was measured. Some recordists raised the possibility that the tonal notes, particularly the 'tonk' in vocal type 1, may be a mechanical sound, but further research is required to determine which sounds are vocalizations and which are mechanical sonations. We performed principal components analysis (PCA) and logistic regression on the vocal measurements to test for significant differences between the vocal types and to reduce the dimensionality of the data for comparison to results from analysis of genetic data. The PCA analysis was performed using the princomp function and the logistic regression was performed using the glm function, both in the stats R package (R_Core_Team 2018). The geographic distribution of each vocal type was assessed using latitude and longitude coordinates included in the metadata of each recording. When no coordinates were available, we determined latitude and longitude based on the description of the locality. Because no sound records were directly associated with genetic samples in this study, we used geographic proximity to vocalization recordings and localization to areas of endemism or areas bounded by clear physical barriers to associate vocal types to genetic samples. This approach assumes that genetically and geographically proximate individuals are likely to share the same vocal type and enabled us to perform a preliminary assessment of how variation in vocalizations maps onto existing genetic variation. Testing the fine-scale association of genetic and vocalization boundaries will require extensive field sampling of both traits from individual manakins.

Literature Cited

Agapow PM, Burt A. 2001. Indices of multilocus linkage disequilibrium. Molecular Ecology Notes, 1:101-102.

Bollback JP. 2006. SIMMAP: Stochastic character mapping of discrete traits on phylogenies. BMC Bioinformatics, 7.

Botta F, Eriksen C, Fontaine MC, Guillot G, Yu D. 2015. Enhanced computational methods for quantifying the effect of geographic and environmental isolation on genetic differentiation. Methods in Ecology and Evolution, 6:1270-1277.

Bradburd G, Coop G, Ralph P. 2017. Inferring Continuous and Discrete Population Genetic Structure Across Space. bioRxiv.

Bradburd GS, Ralph PL, Coop GM. 2013. DISENTANGLING THE EFFECTS OF GEOGRAPHIC AND ECOLOGICAL ISOLATION ON GENETIC DIFFERENTIATION. Evolution, 67:3258-3273.

Brown AHD, Feldman MW, Nevo E. 1980. Multilocus Structure of Natal Populations of Hordeum Spontaneum. Genetics, 96:523-536.

Brumfield RT. 2012. Inferring the origins of lowland Neotropical birds. The Auk, 129:367-376.

Chernomor O, Minh BQ, von Haeseler A. 2016. Terrace Aware Data Structure for Phylogenomic Inference from Supermatrices. Systematic Biology, 65:997-1008.

Cracraft J, Prum RO. 1988. PATTERNS AND PROCESSES OF DIVERSIFICATION: SPECIATION AND HISTORICAL CONGRUENCE IN SOME NEOTROPICAL BIRDS. Evolution, 42:603-620.

Excoffier L, Smouse PE, Quattro JM. 1992. Analysis of Molecular Variance Inferred from Metric Distances among DNA Haplotypes: Application to Human Mitochondrial DNA Restriction Data. Genetics, 131:479-491.

Gene_Codes_Corporation. 2010. Sequencher version 5.0 sequence analysis software. Ann Arbor Michigan.

Gosselin T, Anderson EC, Ferchaud A-L. 2016. thierrygosselin/assigner: v.0.4.0 (Version 0.4.0). Zenodo. http://doi.org/10.5281/zenodo.197418.

Goudet J. 2005. hierfstat, a package for r to compute and test hierarchical F-statistics. Molecular Ecology Notes, 5:184-186.

Guillot G, Schilling R, Porcu E, Bevilacqua M. 2013. Validity of covariance models for the analysis of geographical variation. arXiv:1311.4136.

Harvey MG, Brumfield RT. 2015. Genomic variation in a widespread Neotropical bird (Xenops minutus) reveals divergence, population expansion, and gene flow. Molecular Phylogenetics and Evolution, 83:305-316.

Hoang DT, Vinh LS, Chernomor O, Minh BQ, von Haeseler A. 2017. UFBoot2: Improving the Ultrafast Bootstrap Approximation. Molecular Biology and Evolution, 35:518-522.

Huelsenbeck JP, Nielsen R, Bollback JP. 2003. Stochastic Mapping of Morphological Characters. Systematic Biology, 52:131-158.

Jombart T. 2008. adegenet: a R package for the multivariate analysis of genetic markers. Bioinformatics, 24:1403-1405.

Kalyaanamoorthy S, Minh BQ, Wong TKF, von Haeseler A, Jermiin LS. 2017. ModelFinder: fast model selection for accurate phylogenetic estimates. Nature Methods, 14:587.

Kamvar ZN, Tabima JF, Grünwald NJ. 2014. Poppr: an R package for genetic analysis of populations with clonal, partially clonal, and/or sexual reproduction. PeerJ, 2:e281.

627 Kuhner MK. 2006. LAMARC 2.0: maximum likelihood and Bayesian estimation of population
628 parameters. Bioinformatics, 22:768-770.
629 Moore RP, Robinson WD, Lovette IJ, Robinson TR. 2008. Experimental evidence for extreme
630 dispersal limitation in tropical forest birds. Ecology Letters, 11:960-968.
631 Naka LN, Brumfield RT. 2018. The dual role of Amazonian rivers in the generation and
632 maintenance of avian diversity. Science Advances, 4.
633 Ohlson JI, Fjeldså J, Ericson PGP. 2013. Molecular phylogeny of the manakins (Aves:
634 Passeriformes: Pipridae), with a new classification and the description of a new genus.
635 Molecular Phylogenetics and Evolution, 69:796-804.
636 Oliveira U, Vasconcelos MF, Santos AJ. 2017. Biogeography of Amazon birds: rivers limit
637 species composition, but not areas of endemism. Scientific Reports, 7:2992.
638 Paradis E. 2010. pegas: an R package for population genetics with an integrated–modular
639 approach. Bioinformatics, 26:419-420.
640 Petkova D, Novembre J, Stephens M. 2015. Visualizing spatial population structure with
641 estimated effective migration surfaces. Nature Genetics, 48:94.
642 R_Core_Team. 2018. R: A language and environment for statistical computing.
643 Revell LJ. 2012. Phytools: An R package for phylogenetic comparative biology (and other
644 things). Methods in Ecology and Evolution, 3:217-223.
645 Santorelli S, Magnusson WE, Deus CP. 2018. Most species are not limited by an Amazonian
646 river postulated to be a border between endemism areas. Scientific Reports, 8:2294.
647 Schmidt HA, Minh BQ, von Haeseler A, Nguyen L-T. 2014. IQ-TREE: A Fast and Effective
648 Stochastic Algorithm for Estimating Maximum-Likelihood Phylogenies. Molecular
649 Biology and Evolution, 32:268-274.
650 Smith BT, McCormack JE, Cuervo AM, Hickerson MJ, Aleixo A, Cadena CD, Perez-Eman J,
651 Burney CW, Xie X, Harvey MG, Faircloth BC, Glenn TC, Derryberry EP, Prejean J,
652 Fields S, Brumfield RT. 2014. The drivers of tropical speciation. Nature, 515:406-409.
653 Standley DM, Katoh K. 2013. MAFFT Multiple Sequence Alignment Software Version 7:
654 Improvements in Performance and Usability. Molecular Biology and Evolution, 30:772-
655 780.
656 Trifinopoulos J, Nguyen L-T, Minh BQ, von Haeseler A. 2016. W-IQ-TREE: a fast online
657 phylogenetic tool for maximum likelihood analysis. Nucleic Acids Research, 44:W232-
658 W235.
659 Wahlund S. 1928. ZUSAMMENSETZUNG VON POPULATIONEN UND
660 KORRELATIONSERSCHEINUNGEN VOM STANDPUNKT DER
661 VERERBUNGSLEHRE AUS BETRACHTET. Hereditas, 11:65-106.
662 Weir BS, Cockerham CC. 1984. ESTIMATING F-STATISTICS FOR THE ANALYSIS OF
663 POPULATION STRUCTURE. Evolution, 38:1358-1370.
664

Supplementary Figures and Tables

Supplementary Table 1. Specimen data table (separate file)

Supplementary Table 2a. Results from Mantel tests

Supplementary Table 2a.

Region	locality code	mantel r	two-tailed p	lower 2.5% limit	upper 97.5% limit	log.d	perm	significant (p < 0.001)
Full dataset		0.748	0.0001	0.729	0.763	F	10000	*
Central America - Costa Rica	CACR	0.459	0.2551	0.017	1.000	F	10000	-
Central America - Panama	CAPA	0.694	0.1019	0.021	0.921	F	10000	-
North Andean – Marañón	CAMA	NA	NA	NA	NA	F	10000	-
South Andean Peru (North)	CPN	-0.261	1	-0.261	-0.261	F	10000	-
South Andean Peru (South)	CPS	0.816	0.0993	0.618	0.998	F	10000	-
weakly resolved Guiana Shield	GS	0.099	0.0947	0.058	0.134	F	10000	-
unresolved Jaú	GSIMERI	0.096	0.243	0.043	0.166	F	10000	-
weakly resolved eastern Napo	GSNAPO	0.313	0.0513	0.177	0.560	F	10000	-
weakly resolved Suriname + Amapá	GSSR	0.069	0.2483	0.032	0.121	F	10000	-
Western Napo introgressed lineage	PH	0.508	0.017	0.340	0.754	F	10000	-
Western Inambari endemic	INAMBARI	0.608	0.001	0.382	0.848	F	10000	*
Eastern Inambari endemic	INAMBARIE	0.004	0.981	-0.196	0.244	F	10000	-
Rondônia endemic	RONDONIA	NA	NA	NA	NA	F	10000	-
Tapajós endemic	TAPAJOS	0.250	0.0148	0.182	0.313	F	10000	-
Xingu endemic	XINGU	0.079	0.8572	-0.170	0.275	F	10000	-
Atlantic Forest – Bahia	AFBAHIA	0.484	0.0173	0.173	0.804	F	10000	-
Atlantic Forest – Espírito Santo	AFES	NA	NA	NA	NA	F	10000	-
Atlantic Forest – Rio	AFRIO	0.701	0.0007	0.615	0.782	F	10000	*

Region	locality code	mantel r	two-tailed p	lower 2.5% limit	upper 97.5% limit	log.d	perm	significant (p < 0.001)
Full dataset		0.391	0.0001	0.379	0.401	T	10000	*
Central America - Costa Rica	CACR	0.459	0.253	0.017	1.000	T	10000	-
Central America - Panama	CAPA	0.519	0.2532	0.021	0.919	T	10000	-
North Andean – Marañón	CAMA	NA	NA	NA	NA	T	10000	-
South Andean Peru (North)	CPN	-0.261	1	-0.261	-0.261	T	10000	-
South Andean Peru (South)	CPS	0.810	0.032	0.669	0.998	T	10000	-
weakly resolved Guiana Shield	GS	0.091	0.0022	0.063	0.119	T	10000	-
unresolved Jaú	GSIMERI	0.536	0.0001	0.319	0.684	T	10000	*
weakly resolved eastern Napo	GSNAPO	0.313	0.0479	0.161	0.574	T	10000	-
weakly resolved Suriname + Amapá	GSSR	0.065	0.1054	0.026	0.117	T	10000	-
Western Napo introgressed lineage	PH	0.248	0.091	0.102	0.407	T	10000	-
Western Inambari endemic	INAMBARI	0.714	0.0008	0.499	0.952	T	10000	*
Eastern Inambari endemic	INAMBARIE	-0.004	0.9801	-0.304	0.213	T	10000	-
Rondônia endemic	RONDONIA	NA	NA	NA	NA	T	10000	-
Tapajós endemic	TAPAJOS	0.247	0.0011	0.115	0.353	T	10000	-
Xingu endemic	XINGU	0.079	0.854	-0.112	0.275	T	10000	-
Atlantic Forest – Bahia	AFBAHIA	0.481	0.0693	0.298	0.885	T	10000	-
Atlantic Forest – Espírito Santo	AFES	NA	NA	NA	NA	T	10000	-
Atlantic Forest – Rio	AFRIO	0.747	0.0012	0.676	0.912	T	10000	-

Supplementary Table 2b. Results from partial Mantel tests

Supplementary Table 2b.

Approximate Barrier	Comparison (populations)	partial mantel r	two-tailed p	lower 2.5% limit	upper 97.5% limit	log.d	perm	significant (p < 0.001)
Cordillera de Talamanca	Costa Rica vs Panama	-0.159	0.2972	-0.267	0.155	F	10000	-
Andes (1)	Central America vs Marañón	-0.591	0.0967	-0.729	-0.434	F	10000	-
Andes (2)	Central America vs (Marañón + South Andean Peru)	0.041	0.4030	-0.248	0.137	F	10000	-
Andes (3)	Central America vs (Everything else)	-0.267	0.0001	-0.295	-0.229	F	10000	*
Rio Ucayali	South Andean Peru vs Inambari	-0.906	0.0001	-0.940	-0.872	F	10000	*
Eastern Marañón + Hauallaga Rivers	Introgressed western Napo vs Inambari	-0.896	0.0001	-0.917	-0.878	F	10000	*
Rio Putumayo	Introgressed western Napo vs eastern Napo	-0.744	0.0001	-0.826	-0.702	F	10000	*
Rio Purus	Western Inambari vs eastern Inambari	-0.603	0.0001	-0.720	-0.044	F	10000	*
Rio Madeira	Eastern Inambari vs Rondônia	-0.550	0.0001	-0.697	-0.129	F	10000	*
Rio Tapajós	Rondônia vs Tapajós	-0.175	0.0441	-0.233	-0.114	F	10000	-
Rio Xingu	Tapajós vs Xingu	-0.318	0.0004	-0.383	-0.240	F	10000	*
Cerrado (1)	All pooled pops vs pooled Atlantic Forest	-0.183	0.0008	-0.229	-0.112	F	10000	*
Cerrado (2)	Xingu vs Bahia	-0.565	0.0001	-0.609	-0.434	F	10000	*
Rio Japurá	Eastern Napo vs Jaú	-0.151	0.0146	-0.297	-0.109	F	10000	-
Rio Negro	Jaú vs central Guiana Shield	-0.053	0.3107	-0.088	-0.012	F	10000	-
Rio Essequibo	central Guiana Shield vs eastern Guiana shield	-0.350	0.0001	-0.391	0.060	F	10000	*
Rio Amazonas	All pooled lowland N vs all pooled lowland S	-0.912	0.0001	-0.918	-0.907	F	10000	*

Approximate Barrier	Comparison (populations)	partial mantel r	two-tailed p	lower 2.5% limit	upper 97.5% limit	log.d	perm	significant (p < 0.001)
Cordillera de Talamanca	Costa Rica vs Panama	-0.744	0.0001	-0.802	-0.693	T	10000	*
Andes (1)	Central America vs Marañón	-0.996	0.0001	-0.997	-0.963	T	10000	*
Andes (2)	Central America vs (Marañón + South Andean Peru)	-0.829	0.0001	-0.942	-0.781	T	10000	*
Andes (3)	Central America vs (Everything else)	-0.464	0.0001	-0.495	-0.420	T	10000	*
Rio Ucayali	South Andean Peru vs Inambari	-0.910	0.0001	-0.938	-0.883	T	10000	*
Rio Marañón + Solimões	Introgressed western Napo vs Inambari	-0.880	0.0001	-0.900	-0.862	T	10000	*
Rio Putumayo	Introgressed western Napo vs eastern Napo	-0.900	0.0001	-0.941	-0.884	T	10000	*
Rio Purus	Western Inambari vs eastern Inambari	-0.833	0.0001	-0.863	-0.811	T	10000	*
Rio Madeira	Eastern Inambari vs Rondônia	-0.751	0.0001	-0.814	-0.650	T	10000	*
Rio Tapajós	Rondônia vs Tapajós	-0.316	0.0001	-0.388	-0.211	T	10000	*
Rio Xingu	Tapajós vs Xingu	-0.703	0.0001	-0.754	-0.655	T	10000	*
Cerrado (1)	All pooled pops vs pooled Atlantic Forest	-0.721	0.0001	-0.745	-0.702	T	10000	*
Cerrado (2)	Xingu vs Bahia	-0.934	0.0001	-0.952	0.070	T	10000	*
Rio Japurá	Eastern Napo vs Jaú	-0.399	0.0001	-0.490	-0.329	T	10000	*
Rio Negro	Jaú vs central Guiana Shield	-0.036	0.4825	-0.069	0.001	T	10000	-
Rio Essequibo	central Guiana Shield vs eastern Guiana shield	-0.470	0.0001	-0.503	-0.444	T	10000	*
Rio Amazonas	All pooled lowland N vs all pooled lowland S	-0.915	0.0001	-0.921	-0.911	T	10000	*

Supplementary Table 3: Song measures (separate file)

Supplementary Table 4: Song recording metadata (separate file)

Supplementary Table 5: G-PhoCS parameters

Supplementary Table 5a, θ: effective population size

	Western Napo	Eastern Napo	Inambari	MRCA Western Napo, Inambari	MRCA Inambari, Eastern Napo
median	4950840	2807467.5	2797062.5	5356300	1429540
95% HPD Interval LOW	4527457.5	2498760	2566870	4658055	1352200
95% HPD Interval HIGH	5378937.5	3132990	3044770	6047630	1512647.5

Supplementary Table 5b, τ: splitting time in generations

	MRCA Western Napo, Inambari, Eastern Napo	
median	484600	1025420
95% HPD Interval LOW	442610	954030
95% HPD Interval HIGH	532120	1099450

Supplementary Table 5c, m : migration rate (migrants per generation)

	Eastern Napo to	Inapari to Eastern	apo to West	Western Napo to Eastern Napo	Inambari to Western Napo	Western Napo to Inambari
median	0.0663	0.4196	1.7508	0.3671	0.0000	0.0000
95% HPD Interval LOW	0.0000	0.2670	1.0470	0.0000	0.0000	0.0000
95% HPD Interval HIGH	0.1763	0.6109	2.5872	0.8184	0.0056	0.0028

Supplementary Figure 1. GBIF occurrence records.
Here, we plot all GBIF occurrence records at the time of writing (in black) with our sampling localities (in red). The BirdLife approximate range map is shown in light green, and our modifications to this map are shown in pink to account for major inaccuracies in the available genus range map. This figure is provided primarily to illustrate that the BirdLife range map is inaccurate in the western Amazon, in Loreto, Peru, where our analyses detect an introgressed hybrid lineage.

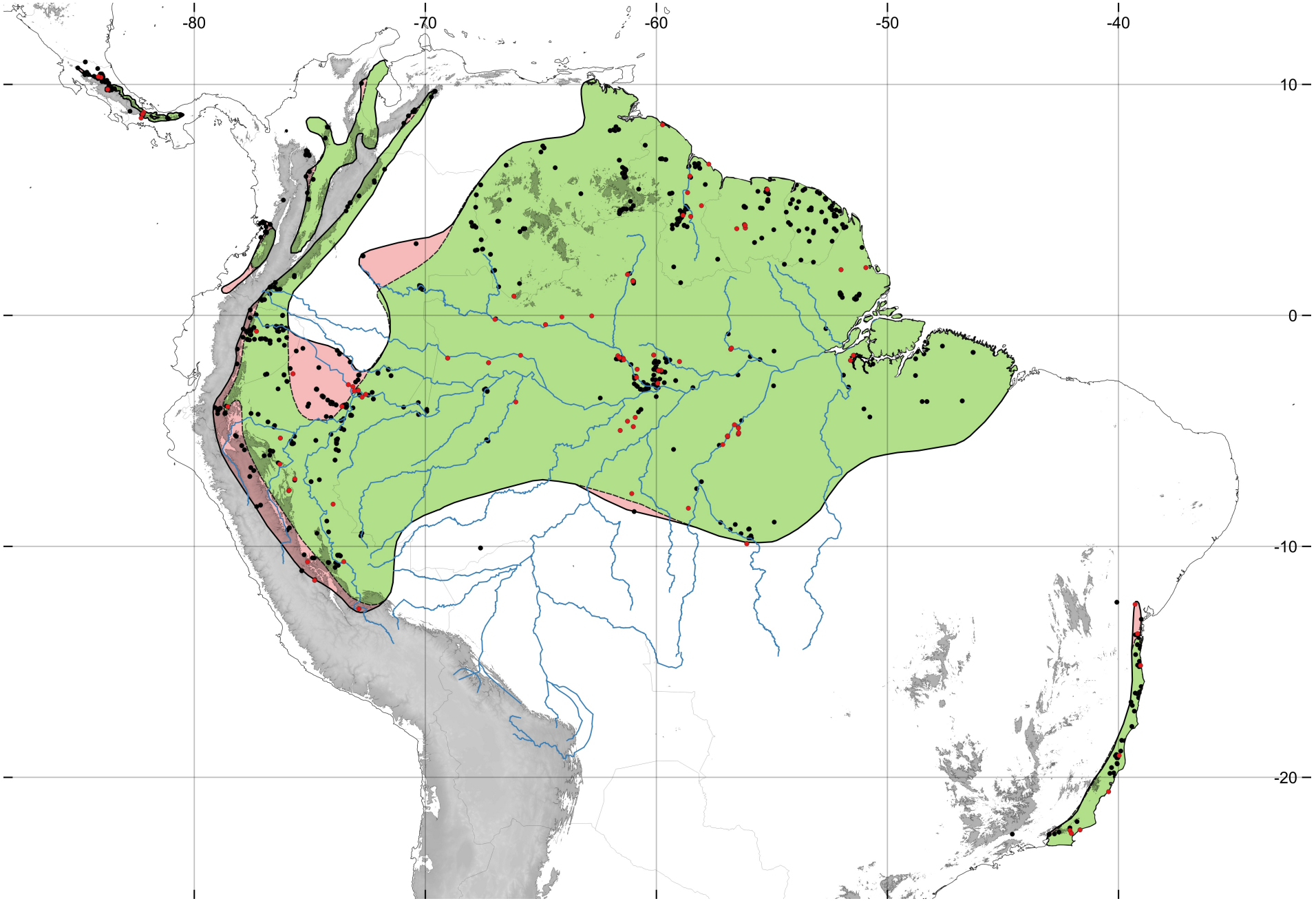
-80
-70
-60
-50
-40
10
0
-10
-20

Supplementary Figure 2. K-means clustering of SNP data
In this figure, the PCoA projections of the SNP data are indicated on the top row, with minimum convex hulls (minimum implied range) and plotting symbols indicating the optimal K-means K5 clustering solution. PCoA explained 13-17% of the variance in the SNP data on the first two axes, and K-means clustering assignments derived from each dataset recovers nearly identical population assignments. Clustering of dataset 1 (1960 SNPs, 0.05 MAF) was identical to the clustering solutions for datasets 2 and 3, except for the assignment of one important individual (5444.PE.MAR), which links Central American lineages to our San Martín specimen in North Andean, Peru. Plotting symbols and colored convex hulls reflect cluster assignment (Hull colors are synonymous only across plotted columns, see supplementary R script). For datasets 2 (2581 SNPs) and 3 (5099 SNPs), K-means clustering detected the following groups: all Guiana Shield (Clade D in Figure 3), Atlantic Forest (Clade C7), South Andean Peru (Clade B), Southern Amazon including the western Napo population (Clade C + Clade E in Figure 3), and Central America (Clade A1 in Figure 3).

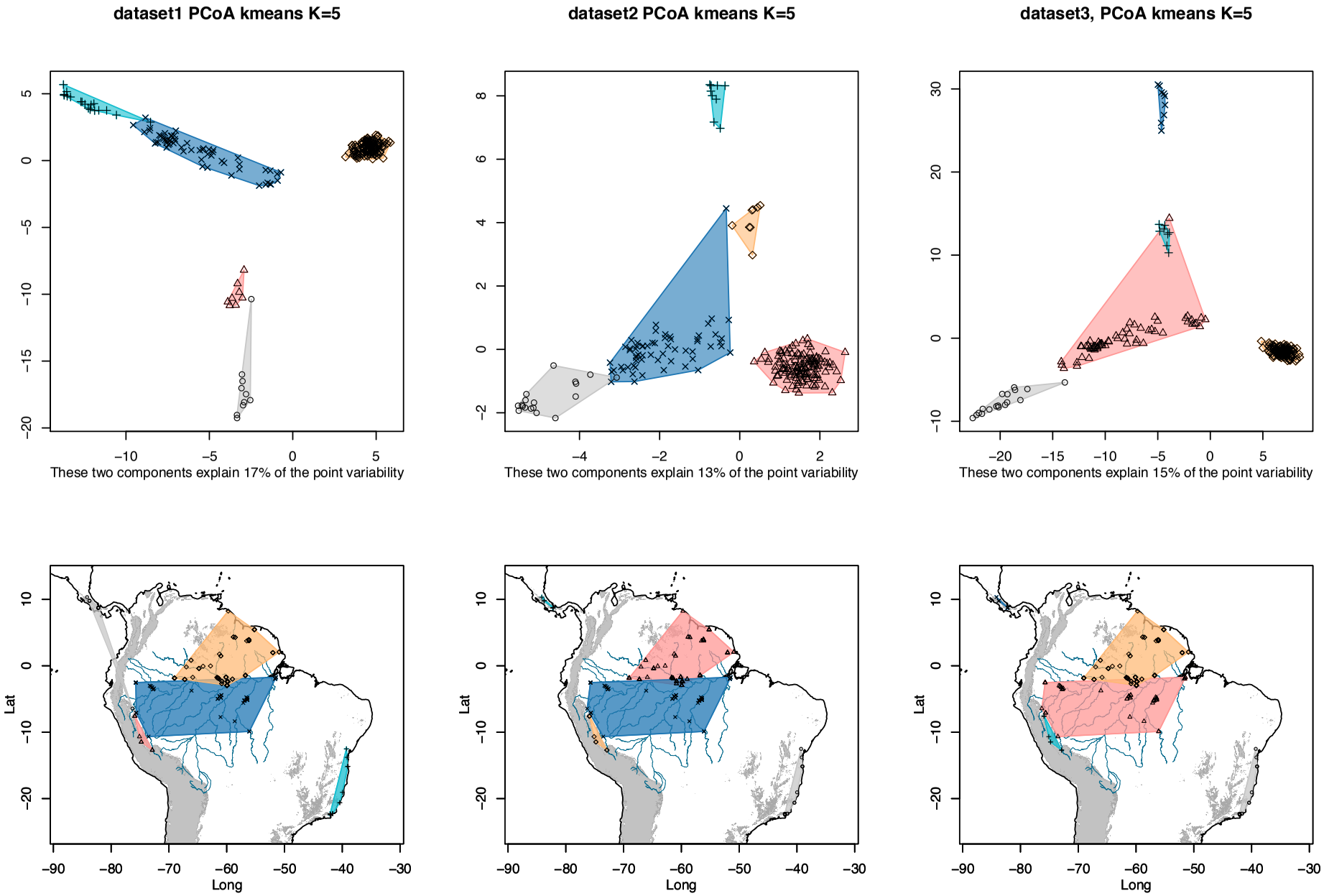
dataset1 PCoA kmeans K=5
These two components explain 17% of the point variability
dataset2 PCoA kmeans K=5
These two components explain 13% of the point variability
dataset3, PCoA kmeans K=5
These two components explain 15% of the point variability
Lat
Long

Supplementary Figure 3 – log likelihoods of STRUCTURE runs
Summarized log likelihood values across STRUCTURE runs for each value of K, with a plateau starting at K~5, and variance across runs increasing dramatically after K10.

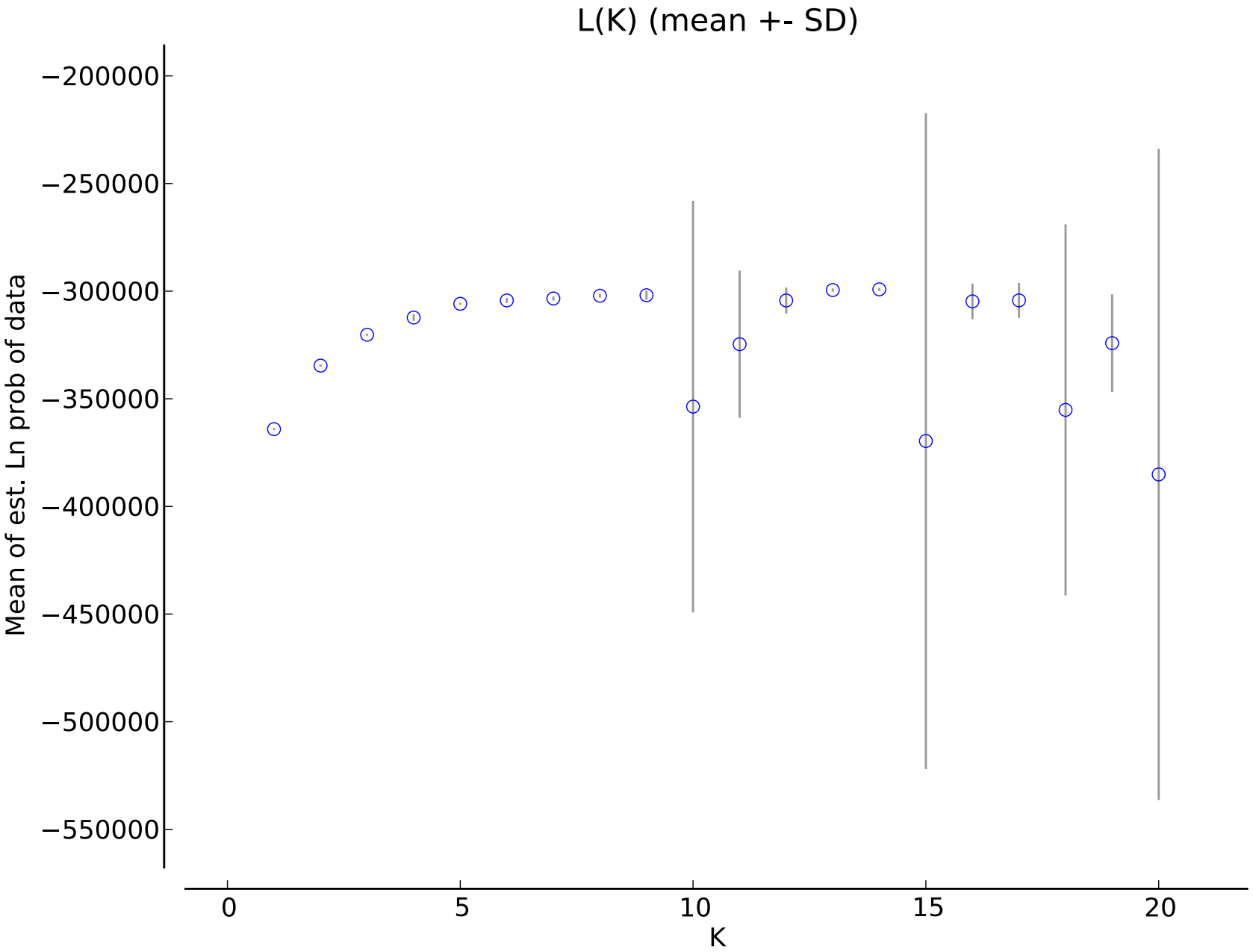
L(K) (mean +- SD)
Mean of est. Ln prob of data
−200000
−250000
−300000
−350000
−400000
−450000
−500000
−550000
0
5
10
15
20
K

Supplementary Figure 4. STRUCTURE output for k2-10

Full STRUCTURE output for dataset 1, indicating population assignments and admixture for K2-10. The likelihood of each evaluated number of K clusters from 1:20 plateaued at K = 5, with the standard deviation across runs increasing rapidly after this point (Supplementary Figure 3). See results text for descriptions of these analyses. At K2, the first partition divides the dataset into broad northern and southern Amazonian groups, with all Andean and Central American samples assigned to predominantly southern Amazonian genetic provenance, with some northern admixture. Western Napo individuals are detected as an approximately even mixture of northern and southern Amazonian genomes. At K5, the five identified clusters broadly correspond to wide biogeographic Amazonian regions which encompass multiple areas of endemism (see text). For each barplot, colors are sampled randomly from a 20 color viridis color palette for each run (i.e., they are not synonymous across values of K, see supplementary R script). The tree below corresponds to the RAxML result using the 50% haplotype dataset, with tip labels and colors indicating group membership to one of eighteen population-areas. Colored tip labels correspond to clade label colors in Figures 3 and 4. At higher K, the broad-scale population assignments inferred at K5 are similar, however additional admixture components are inferred for most groups. The introgressed western Napo clade is eventually placed into its own cluster at K9-10.

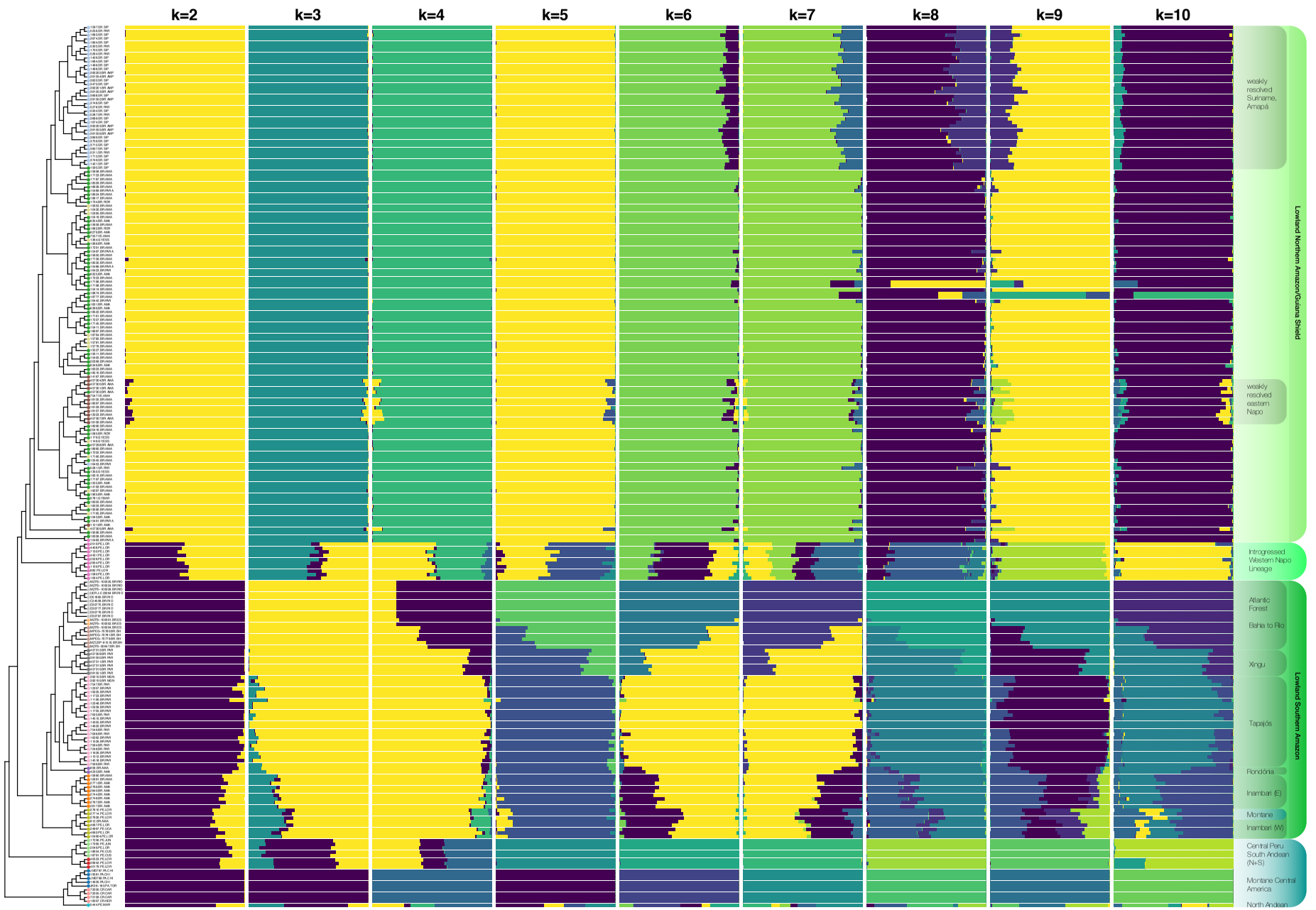
k=2
k=3
k=4
k=5
k=6
k=7
k=8
k=9
k=10
Lowland Northern Amazon/Guiana Shield
weakly resolved Suriname, Amapá
weakly resolved eastern Napo
Introgressed Western Napo Lineage
Lowland Southern Amazon
Atlantic Forest
Bahia to Rio
Xingu
Tapajós
Rondônia
Inambari (E)
Montane
Inambari (W)
Central Peru South Andean (N+S)
Montane Central America
North Andean

Supplementary Figure 5. fineRADstructure population assignment dendrogram
Clustering dendrogram generated from fineRADstructure population assignment. Note: this is not a phylogenetic hypothesis, but rather, a clustering based on genomic similarity which considers data from the full co-ancestry matrix. Tip labels correspond to population codes used internally for R scripts and other analyses. Each of these codes has a 1:1 correspondence with the labeled localities in Figures 3 and 4:

CAMA: North Andean – San Martín, Peru
CACR: Central America - Costa Rica
CAPA: Central America - Panama
CPS: South Andean Peru (South)
CPN: South Andean Peru (North)
INAMBARI: Western Inambari endemic
INAMBARIE: Eastern Inambari endemic
RONDONIA: Rondônia endemic
TAPAJOS: Tapajós endemic
XINGU: Xingu endemic
AFBAHIA: Atlantic Forest – Bahia
AFES: Atlantic Forest – Espírito Santo
AFRIO: Atlantic Forest – Rio
PH (putative hybrid): Western Napo introgressed lineage
GSIMERI: unresolved Jaú
GSNAPO: weakly resolved eastern Napo
GS: weakly resolved Guiana Shield
GSSR: weakly resolved Suriname + Amapá

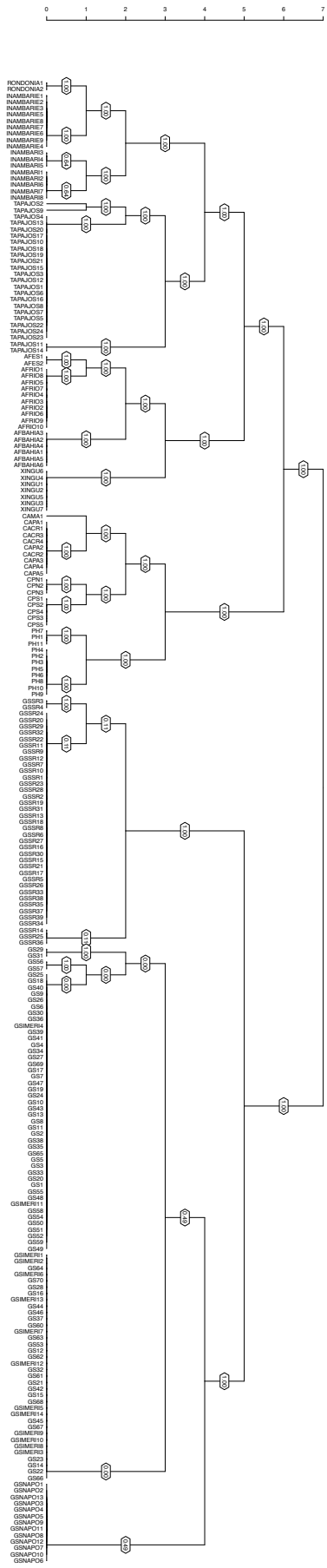
0
1
2
3
4
5
6
7
RONDONIA1
RONDONIA2
INAMBARIE1
INAMBARIE2
INAMBARIE3
INAMBARIE5
INAMBARIE8
INAMBARIE7
INAMBARIE6
INAMBARIE9
INAMBARIE4
INAMBARI3
INAMBARI4
INAMBARI5
INAMBARI1
INAMBARI2
INAMBARI8
INAMBARI7
INAMBARI6
TAPAJOS2
TAPAJOS9
TAPAJOS4
TAPAJOS13
TAPAJOS20
TAPAJOS17
TAPAJOS10
TAPAJOS18
TAPAJOS19
TAPAJOS21
TAPAJOS15
TAPAJOS3
TAPAJOS12
TAPAJOS1
TAPAJOS6
TAPAJOS16
TAPAJOS8
TAPAJOS7
TAPAJOS5
TAPAJOS22
TAPAJOS24
TAPAJOS23
TAPAJOS11
TAPAJOS14
AFES1
AFES2
AFRIC1
AFRIC8
AFRIC5
AFRIC7
AFRIC4
AFRIC3
AFRIC2
AFRIC6
AFRIC9
AFRIC10
AFBAHIA3
AFBAHIA2
AFBAHIA4
AFBAHIA1
AFBAHIA5
AFBAHIA6
XINGU6
XINGU4
XINGU1
XINGU2
XINGU5
XINGU3
XINGU7
CAMA1
CAPA1
CACR1
CACR3
CACR4
CAPA2
CACR2
CAPA3
CAPA4
CAPA5
CPN1
CPN2
CPN3
CPS1
CPS2
CPS4
CPS3
CPS5
PH7
PH1
PH11
PH4
PH2
PH3
PH5
PH6
PH8
PH10
PH9
GSSR3
GSSR4
GSSR24
GSSR20
GSSR29
GSSR32
GSSR22
GSSR11
GSSR9
GSSR12
GSSR7
GSSR10
GSSR1
GSSR23
GSSR28
GSSR2
GSSR19
GSSR31
GSSR13
GSSR18
GSSR8
GSSR6
GSSR27
GSSR16
GSSR30
GSSR15
GSSR21
GSSR17
GSSR5
GSSR26
GSSR33
GSSR38
GSSR35
GSSR37
GSSR39
GSSR34
GSSR14
GSSR25
GSSR36
GS29
GS31
GS56
GS57
GS25
GS18
GS40
GS9
GS26
GS6
GS30
GS36
GSIMER84
GS39
GS41
GS4
GS34
GS27
GS69
GS17
GS7
GS47
GS19
GS24
GS10
GS43
GS13
GS8
GS11
GS2
GS38
GS35
GS65
GS5
GS3
GS33
GS20
GS1
GS55
GS48
GSIMER11
GS58
GS54
GS50
GS51
GS52
GS59
GS49
GSIMER1
GSIMER2
GS64
GSIMER6
GS70
GS28
GS16
GSIMER13
GS44
GS46
GS37
GS60
GSIMER7
GS63
GS53
GS12
GS62
GSIMER12
GS32
GS61
GS21
GS42
GS15
GS68
GSIMER5
GSIMER14
GS45
GS67
GSIMER9
GSIMER10
GSIMER8
GSIMER3
GS23
GS14
GS22
GS66
GSNAPO1
GSNAPO2
GSNAPO13
GSNAPO3
GSNAPO4
GSNAPO5
GSNAPO9
GSNAPO11
GSNAPO8
GSNAPO12
GSNAPO7
GSNAPO10
GSNAPO6

Supplementary Figure 6. chromoPainter co-ancestry matrix
The raw co-ancestry matrix from the full haplotyle dataset, output from the fineRADstructure program. See Supplementary Figure 5 caption for descriptions of localities, matching those in Figure 3 and 4.

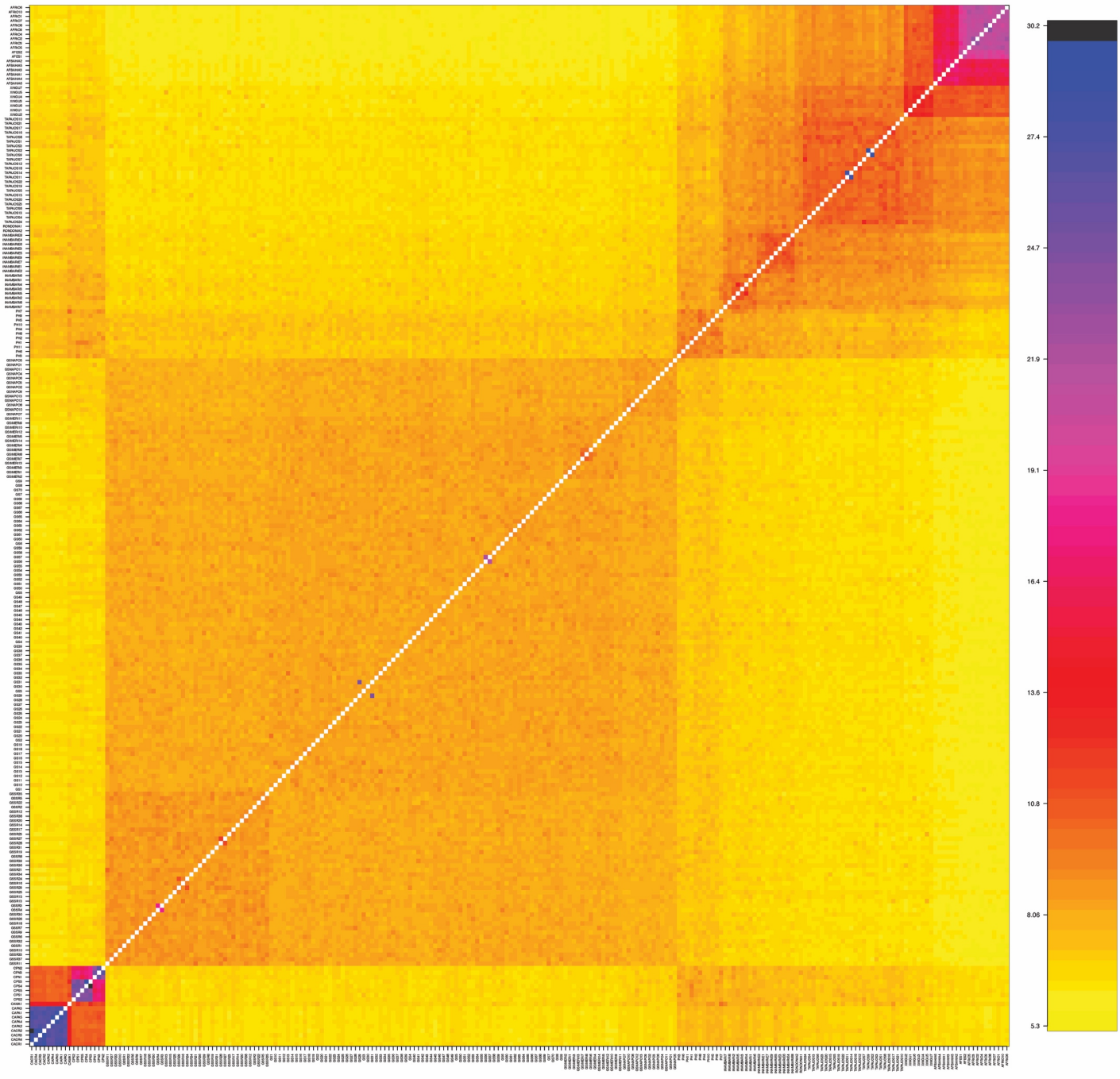
30.2
27.4
24.7
21.9
19.1
16.4
13.6
10.8
8.06
5.3

Supplementary Figure 7. chromoPainter co-ancestry matrix
The co-ancestry matrix from the full haplotyle dataset, with values averaged across 18 focal population-areas. See Supplementary Figure 5 caption for descriptions of localities, matching those in Figure 3 and 4.

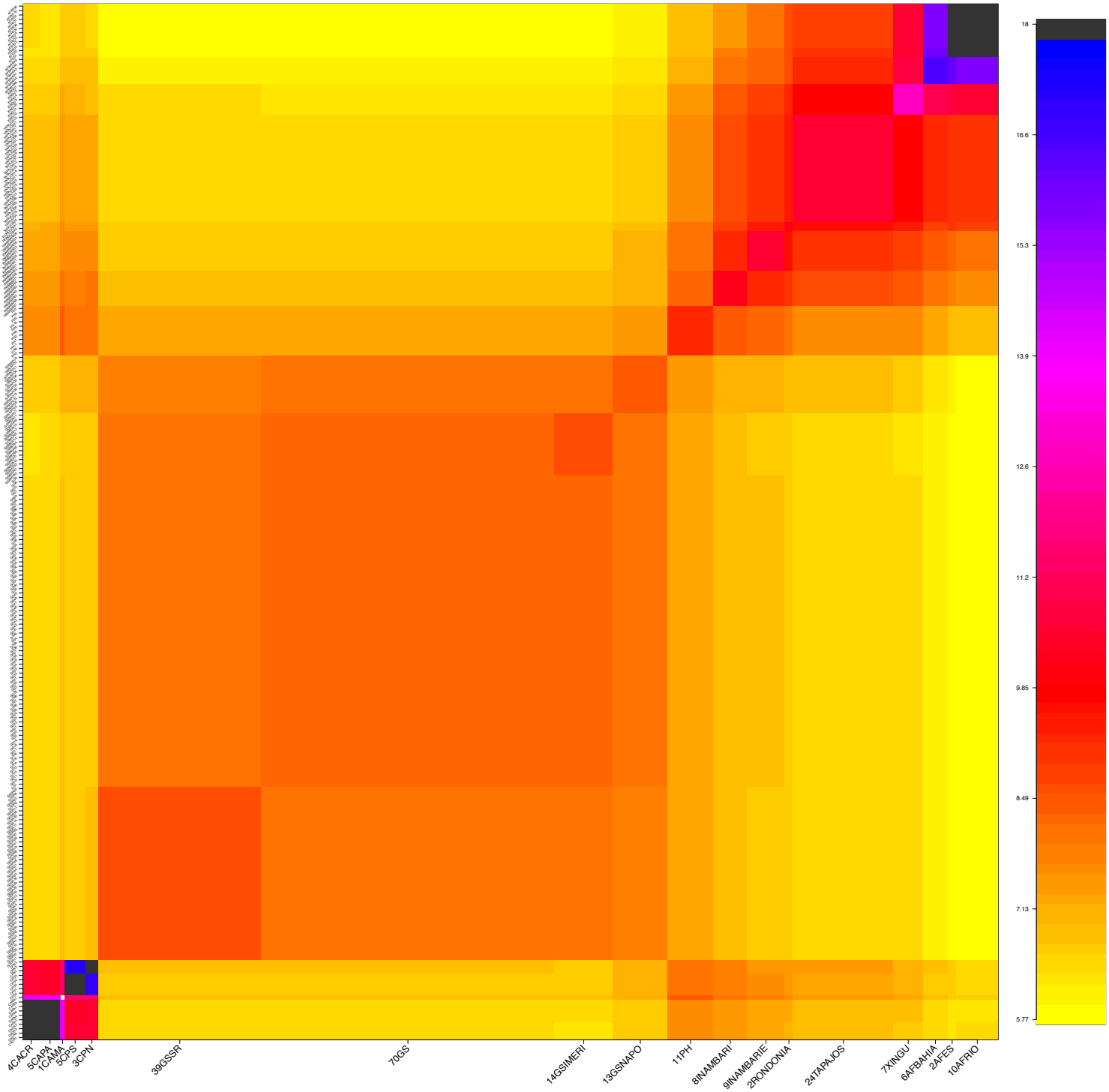
18
16.6
15.3
13.9
12.6
11.2
9.85
8.49
7.13
5.77
4CACR
5CAPA
1CAMA
5CPS
3CPN
39GSSR
70GS
14GSIMERI
13GSNAPO
11PH
8INAMBARI
9INAMBARIE
2RONDONIA
24TAPAJOS
7XINGU
6AFBAHIA
2AFES
10AFRIO

Supplementary Figure 8. K-means clustering of the full dataset co-ancestry matrix
The Lawson et al. (2012) 'normalized PCA' approach provided with the fineRADstructure software captured 89% of the variance in the genetic data on the first four component axes (axis 1: 51.4%, axis 2, 24.9%, axis 3: 7.77%, axis 4: 4.94%). Thus, the co-ancestry matrix reflects substantially more information than standard PCoA/PCA of SNP data (Supplementary Figure 2). K-means phenetic clustering of the co-ancestry matrix more finely partitions the genetic data and explains a much greater proportion of the overall genetic variance than K-means clustering of the raw SNP data. Top row: normalized PCA projection of all individuals on the first two component axes, which capture ~76% of the point variability. Plotting symbols and colored convex hulls reflect cluster assignment. Hull colors are sampled randomly from a 20-color palette for each dataset (i.e., they are synonymous only across plot columns, see supplementary R script).

The leftmost pair of plots indicate membership to one of eighteen focal population-areas (i.e., not K-means assignments, see Supplemental Appendix text for justification) and are shown as minimum convex hulls in co-ancestry PC space (top) as well as projected onto a map (bottom, also shown in Figure 4). The center pair of plots shows the K-means clustering solution of the co-ancestry matrix when K is fixed to 18 (i.e., not based on BIC scores). Intriguingly, this produces a similar set of groups as shown in the leftmost pair.

In the rightmost two plots, we show the K-means optimum clustering solution of the co-ancestry matrix, with a BIC minimum plateau of ~8. This set of groups is generally concordant with hierarchical strata determined in earlier analyses, but also further partitioned relative to standard PC analyses on our SNP data. This clustering solution identified 1) Central America (Clade A2 in Figure 3), 2) South Andean Peru + San Martín (North Andean Peru); (Clade B + Clade A1 in Figure 3), 3) western Napo (Clade E in Figure 3), 4) Inambari + Rondônia (Clades C1, C3, and C4 in Figure 3), 5) Tapajós + Xingu (Clades C5 + C6 in Figure 3), 6) eastern Napo, Jaú, western Guiana shield, 7) Suriname + Amapá (Clade D in Figure 3) and 8) the Atlantic Forest (Clade C7), as separate groups which explain a majority of the variance in the data. Notably, this solution is entirely compatible with our phylogenetic hypothesis, except for the clustering of our single San Martín sample with geographically proximate Peruvian populations, rather than Central American populations (see discussion). This solution generally recapitulates subspecies boundaries (Figure 2).

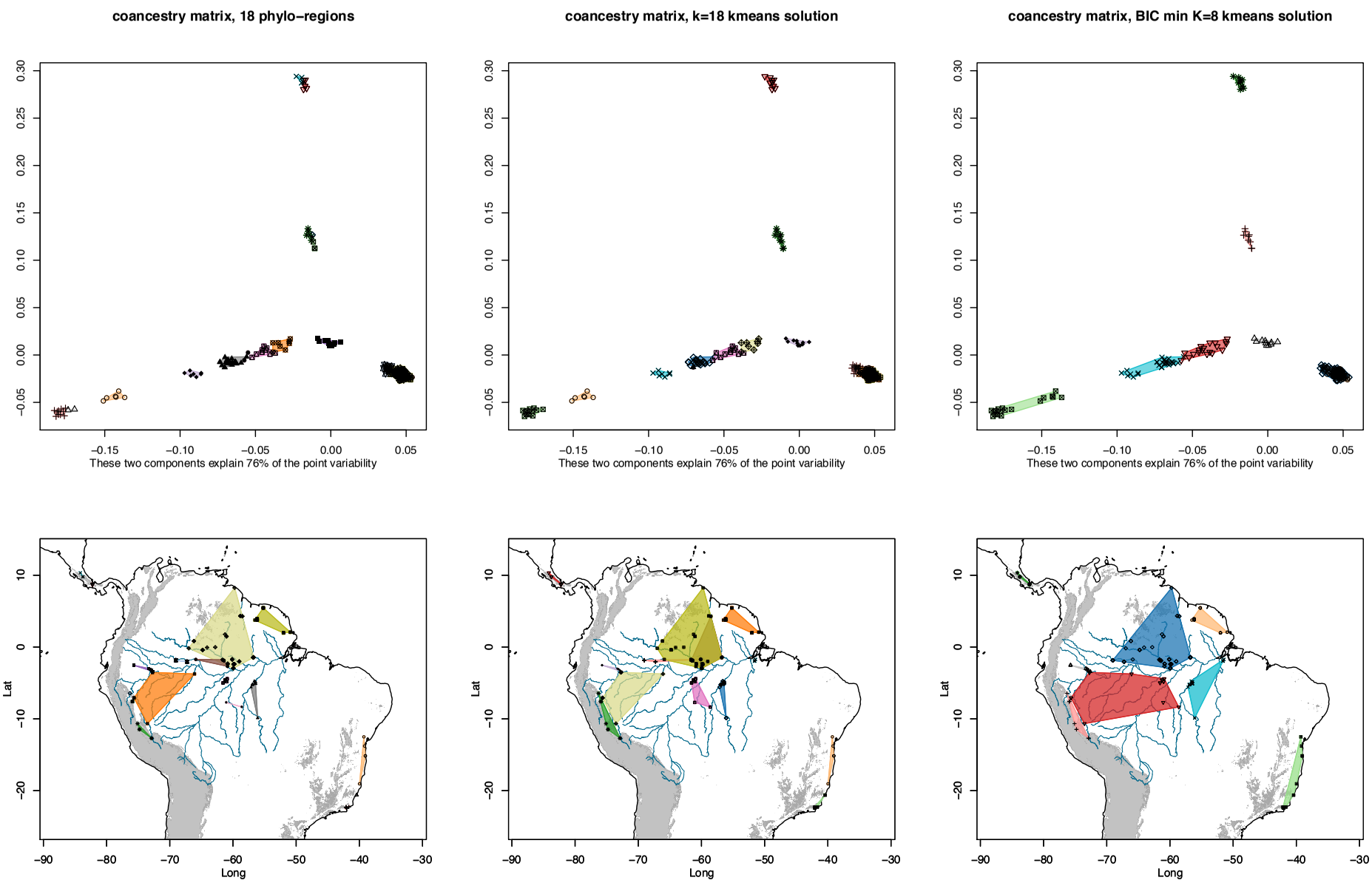
coancestry matrix, 18 phylo−regions
coancestry matrix, k=18 kmeans solution
coancestry matrix, BIC min K=8 kmeans solution
These two components explain 76% of the point variability
Lat
Long

Supplementary Figure 9. Estimates of Inbreeding coefficients F_{IS}
Most populations were detected to be significantly inbred ($F_{IS} > 1$), with lower 95% confidence intervals > 0. Panamanian, Costa Rican, South Andean (North clade), Rondônia, and Espírito Santo clades had 95% confidence intervals which overlapped zero, and thus cannot be confidently inferred to have positive or negative F_{IS}. The simulated F1 (SIMF1) population however, did have significantly negative F_{IS}, as predicted. This pattern implies that the introgressed western Napo population, which was detected to have a significantly positive F_{IS}, is not likely to include recently introgressed individuals. The confidence intervals for eastern Napo, Jaú, Inambari and western Napo popularions are generally overlapping, with similar means (mean of mean estimates ~0.17, SD of mean estimates ~0.02). Locality codes below:

CAMA: North Andean – San Martín (North Andean Peru)
CACR: Central America - Costa Rica
CAPA: Central America - Panama
CPS: South Andean Peru (South)
CPN: South Andean Peru (North)
INAMBARI: Western Inambari endemic
INAMBARIE: Eastern Inambari endemic
RONDONIA: Rondônia endemic
TAPAJOS: Tapajós endemic
XINGU: Xingu endemic
AFBAHIA: Atlantic Forest – Bahia
AFES: Atlantic Forest – Espírito Santo
AFRIO: Atlantic Forest – Rio
PH (putative hybrid): Western Napo introgressed lineage
GSIMERI: unresolved Jaú
GSNAPO: weakly resolved eastern Napo
GS: weakly resolved Guiana Shield
GSSR: weakly resolved Suriname + Amapá

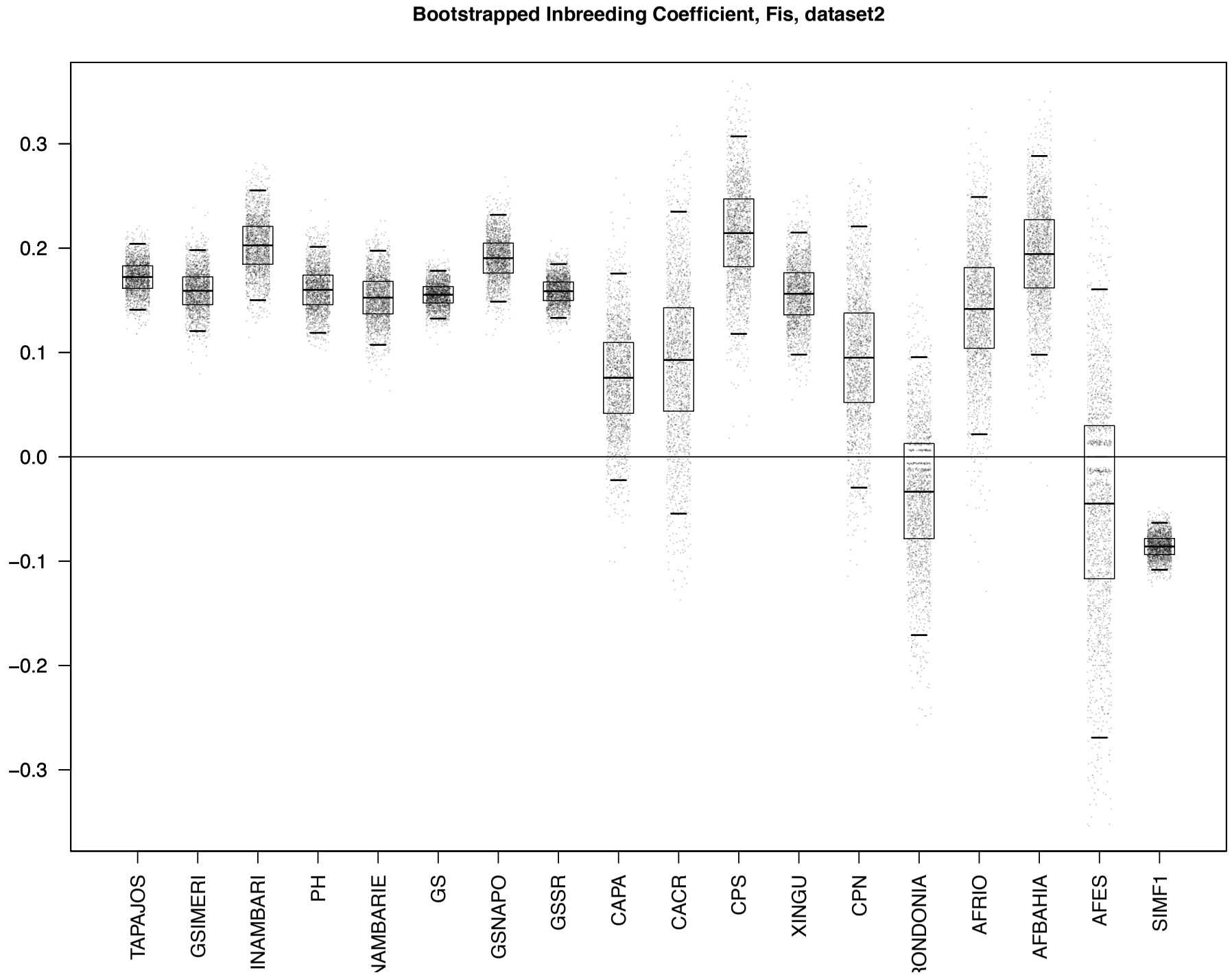
Bootstrapped Inbreeding Coefficient, Fis, dataset2
0.3
0.2
0.1
0.0
−0.1
−0.2
−0.3
TAPAJOS
GSIMERI
INAMBARI
PH
NAMBARIE
GS
GSNAPO
GSSR
CAPA
CACR
CPS
XINGU
CPN
RONDONIA
AFRIO
AFBAHIA
AFES
SIMF1

Supplementary Figure 10. Population pairwise F_{st}

We estimated pairwise Weir and Cockerham's (Weir and Cockerham 1984) F_{st} among all 18 focal areas, and evaluated significance using 1000 bootstrapped datasets to estimate 95% confidence intervals using the 'assigner' R package (Gosselin et al. 2016). Here, we show these results plotted as a pairwise distance heatmap. Average pairwise F_{st} ranged from essentially undifferentiated (F_{st}: 0.0045, comparing GSNAPO, and GSIMERI (comparing eastern Napo to Jaú)), to almost entirely differentiated (F_{st}: 0.81, comparing AFES to CAPA (comparing Espírito Santo to Panama)). Overall population F_{st} was very high ~0.196 [0.188-0.204], indicating substantial population level differentiation among focal areas for *Pseudopipra*. Locality codes are the same as those in Supplementary Figure 9.

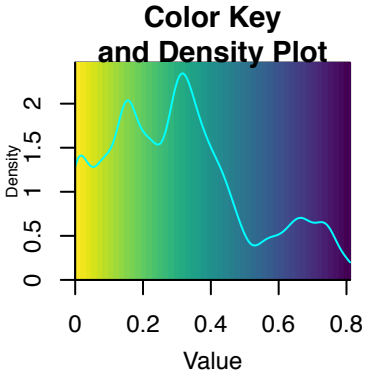
Color Key
and Density Plot
Density
0
0.5
1
1.5
2
0
0.2
0.4
0.6
0.8
Value

Fst heatmap

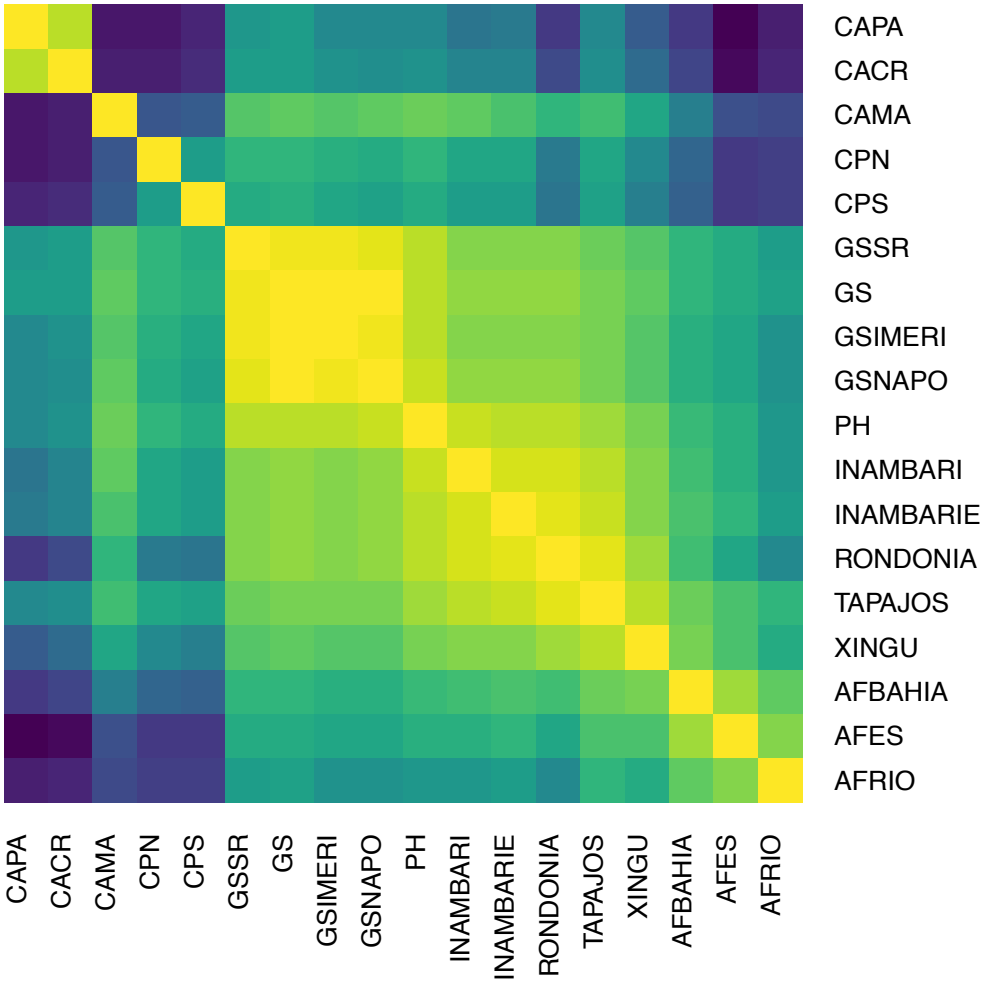
CAPA
CACR
CAMA
CPN
CPS
GSSR
GS
GSIMERI
GSNAPO
PH
INAMBARI
INAMBARIE
RONDONIA
TAPAJOS
XINGU
AFBAHIA
AFES
AFRIO

Supplementary Figure 11. EEMS model fit
Regressing the observed dissimilarity between demes against the fitted dissimilarity between demes provides an indication of model fit (Petkova et al. 2015). For the present dataset, model fit (leftmost plot) was very high ($R^2 = 0.865$). Within demes (central plot, within demes that represent more than a single individual), model fit was somewhat less, but still high ($R^2 = 0.579$). Lastly, comparing observed dissimilarity between demes against great circle distance between demes suggested a strong signal of isolation by distance operating at the scale of the entire dataset ($R^2 = 0.431$). Overall, the EEMS model does a very good job of describing spatially structured variation in this dataset.

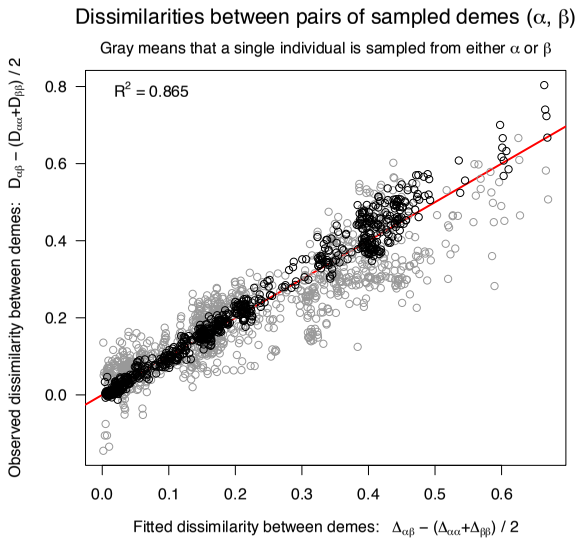
Dissimilarities between pairs of sampled demes (α, β)
Gray means that a single individual is sampled from either α or β
R² = 0.865
Observed dissimilarity between demes: Dαβ − (Dαα+Dββ) / 2
Fitted dissimilarity between demes: Δαβ − (Δαα+Δββ) / 2
0.0
0.2
0.4
0.6
0.8
0.0
0.1
0.2
0.3
0.4
0.5
0.6

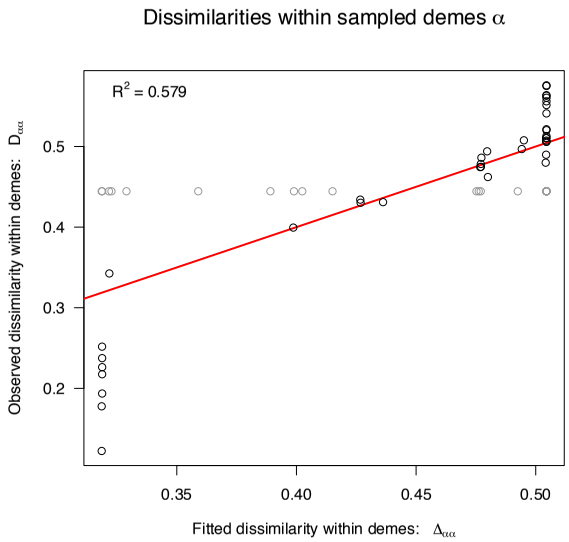
Dissimilarities within sampled demes α
R² = 0.579
Observed dissimilarity within demes: Dααα
Fitted dissimilarity within demes: Δααα
0.2
0.3
0.4
0.5
0.35
0.40
0.45
0.50

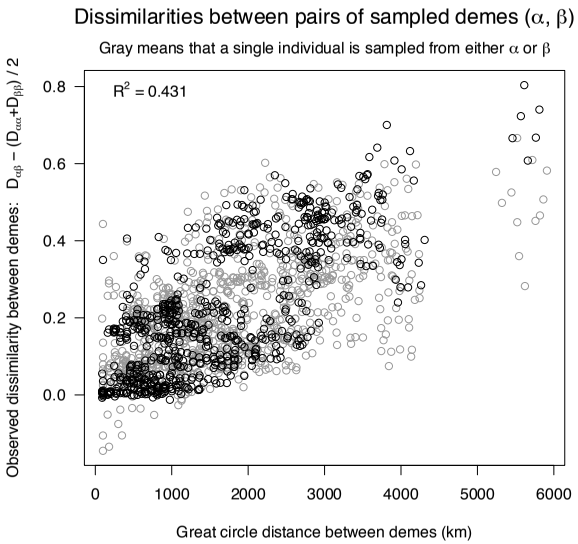
Dissimilarities between pairs of sampled demes (α, β)
Gray means that a single individual is sampled from either α or β
R² = 0.431
Observed dissimilarity between demes: Dαβ − (Dαα+Dββ) / 2
Great circle distance between demes (km)
0.0
0.2
0.4
0.6
0.8
0
1000
2000
3000
4000
5000
6000

Supplementary Figure 12. EEMS estimated genetic diversity
Two broad clusters of relatively high genetic diversity (greatest heterozygosity) were detected in EEMS. The first is centered along the Amazon river and was relatively uniform within the northern Amazonian basin, reflecting relatively high diversity in the Guiana shield. The second relatively high diversity group reflected the introgressed western Napo population. Areas of relatively low genetic diversity included the Atlantic Forest, the Peruvian Andes, and Central American lineages. These results are generally consistent with our estimates of allelic richness (Supplementary Appendix for details).

Posterior mean diversity rates q (on the log10 scale)

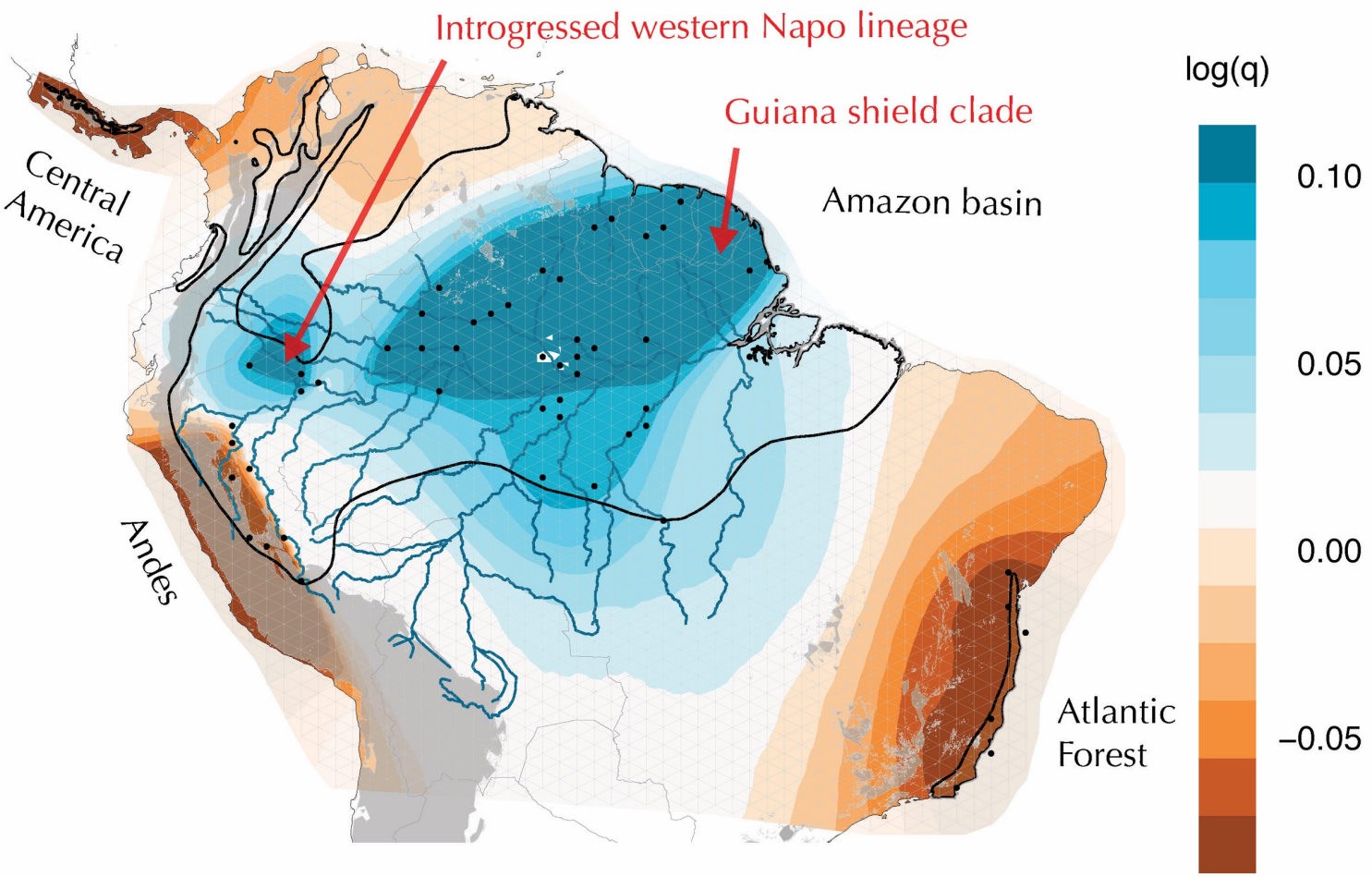

Supplementary Figure 13. Quantification of song variation
All *Pseudopipra* songs start with a single broad frequency, buzzy note. In three of the song types (Types 1, 6, and 8), the initial buzzy note is also followed by one or two shorter tonal notes. We measured: 1) starting frequency, 2) ending frequency, 3) minimum frequency, 4) maximum frequency, 5) number of notes, and 6) duration of the entire song, the buzzy note, and the tonal notes when present. To obtain a conservative estimate of the number of individuals sampled, we took measurements of one song from each recording.

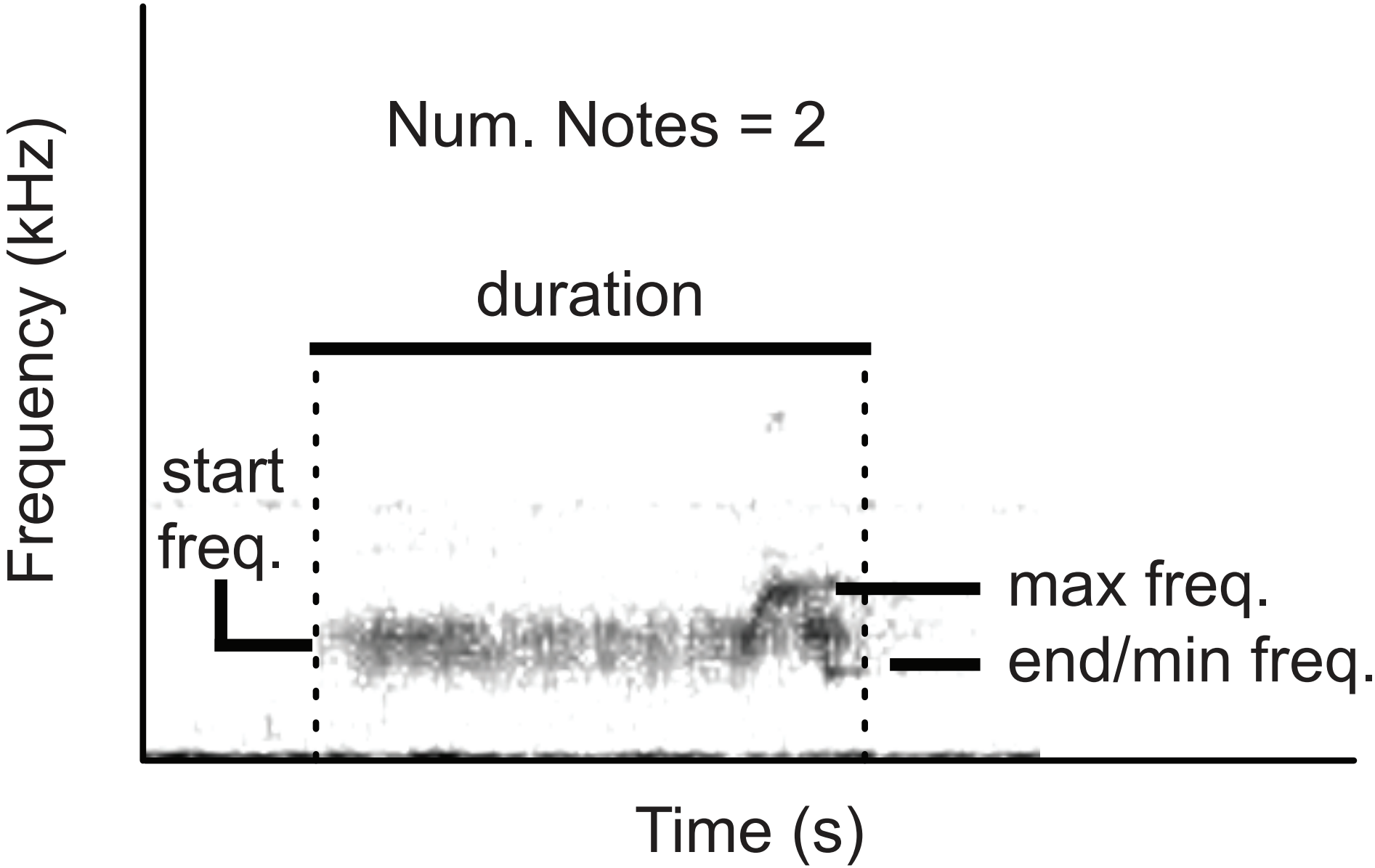
Num. Notes = 2
duration
start
freq.
max freq.
end/min freq.
Frequency (kHz)
Time (s)

Supplementary Figure 14. Expanded summary of lekking vocalization phenotypes
PCA and logistic regression on lekking vocalizations (n=114, Supplementary Table 3) found significant differences among types ($p < 0.001$). The first three axes of a PCA explained ~90% of the variation in lekking vocalization characters, with PC1 (~64%) primarily explaining variation in note number and frequency. Panels A and D show vocalization records plotted into the first and second components of a principle components analysis. Panels B and E show vocalization data points plotted into the second and third principle components. Lastly, Panels C and F are reproduced from Figure 8 and 9 in the main text. All vocal types can be quantitatively discriminated.

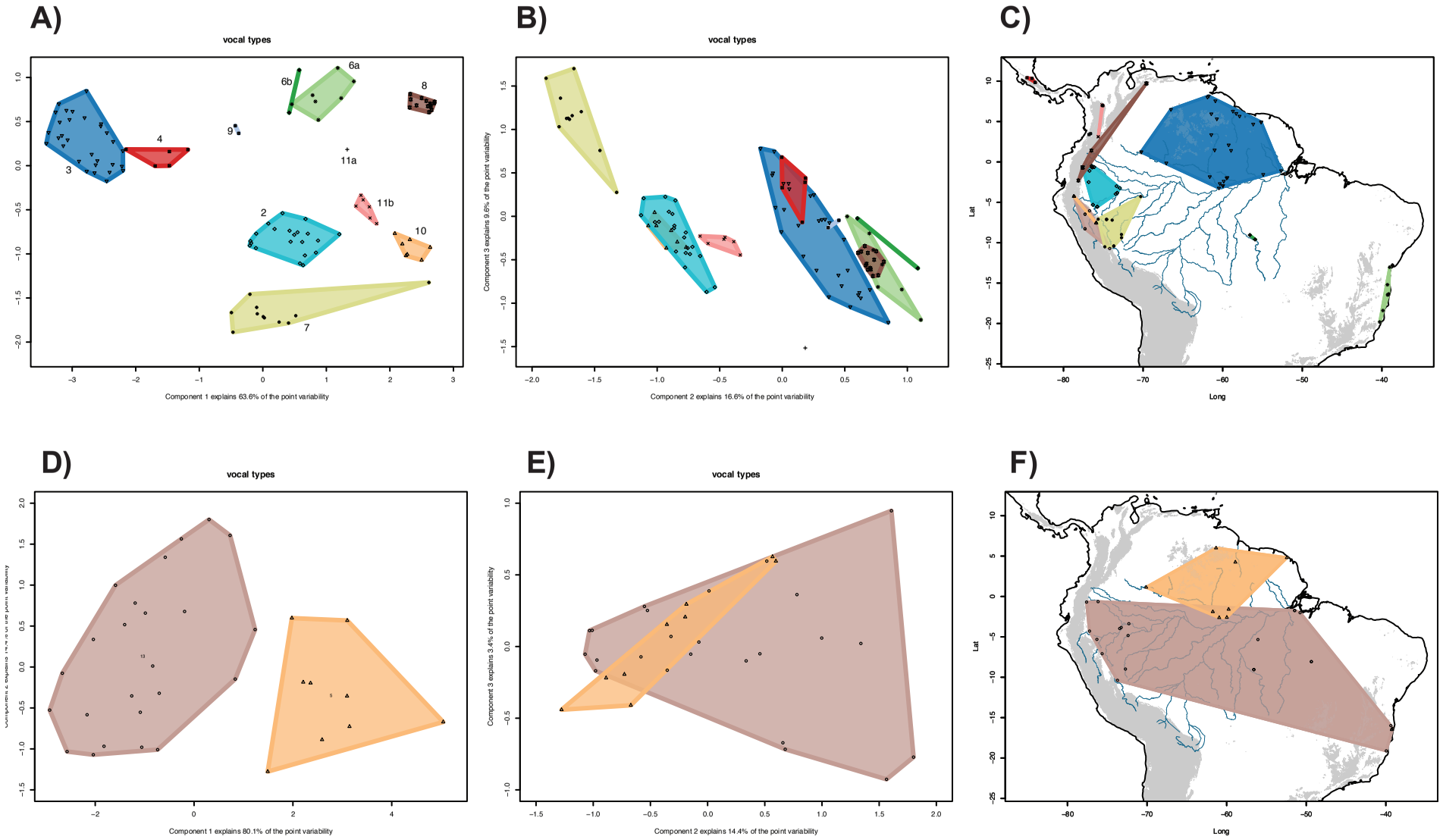
A)
vocal types
6a
6b
8
9
4
3
11a
11b
2
10
7
Component 1 explains 63.6% of the point variability
B)
vocal types
Component 3 explains 9.6% of the point variability
Component 2 explains 16.6% of the point variability
C)
Lat
Long
D)
vocal types
Component 1 explains 80.1% of the point variability
E)
vocal types
Component 3 explains 3.4% of the point variability
Component 2 explains 14.4% of the point variability
F)
Lat
Long

Supplementary Figure 15 – Vocalization Loading Plots
PCA plots from Figure 14, shown here with loading vectors projected in to principle component space. The direction and length of the vectors indicate the direction and strength of the variation in a particular direction. Panels A and B show data for lek vocalizations, while C and D show data for call vocalizations.

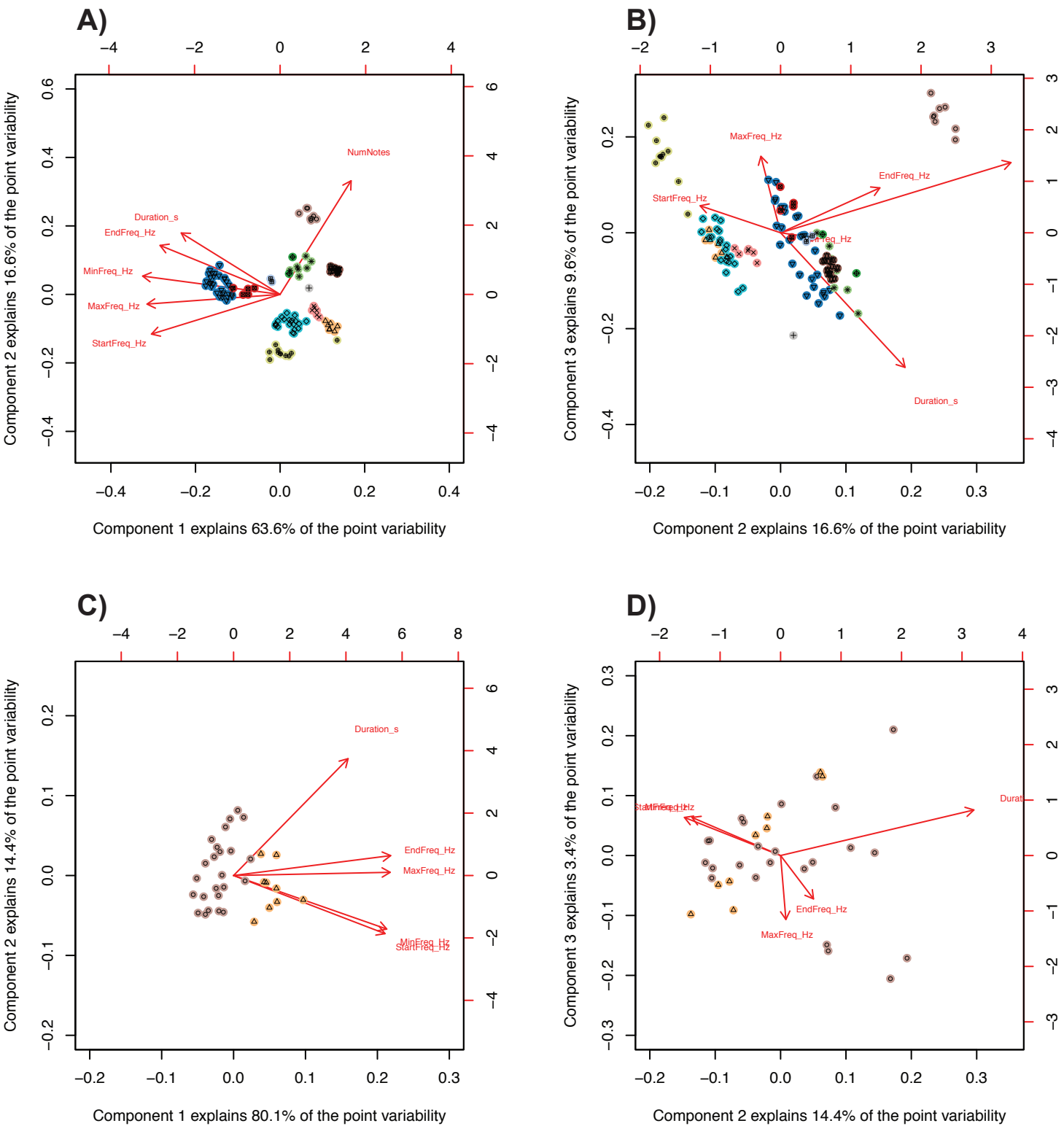
A)
NumNotes
Duration_s
EndFreq_Hz
MinFreq_Hz
MaxFreq_Hz
StartFreq_Hz
Component 2 explains 16.6% of the point variability
Component 1 explains 63.6% of the point variability
B)
MaxFreq_Hz
EndFreq_Hz
StartFreq_Hz
Duration_s
Component 3 explains 9.6% of the point variability
Component 2 explains 16.6% of the point variability
C)
Duration_s
EndFreq_Hz
MaxFreq_Hz
Component 2 explains 14.4% of the point variability
Component 1 explains 80.1% of the point variability
D)
EndFreq_Hz
MaxFreq_Hz
Component 3 explains 3.4% of the point variability
Component 2 explains 14.4% of the point variability

Supplementary Figure 16 – Mitochondrial ND2 gene tree.
Nodes with ultrafast bootstrap scores of lower than 95 are collapsed. The inferred topology is congruent with the topology presented in the main text derived from ddRAD sequencing data, with one exception: Western Napo haplotypes cluster with southern Amazonian lowland haplotypes (see results and discussion). Otherwise, there are no strongly supported conflicts (see discussion above) with our signal from nuclear genomic DNA.

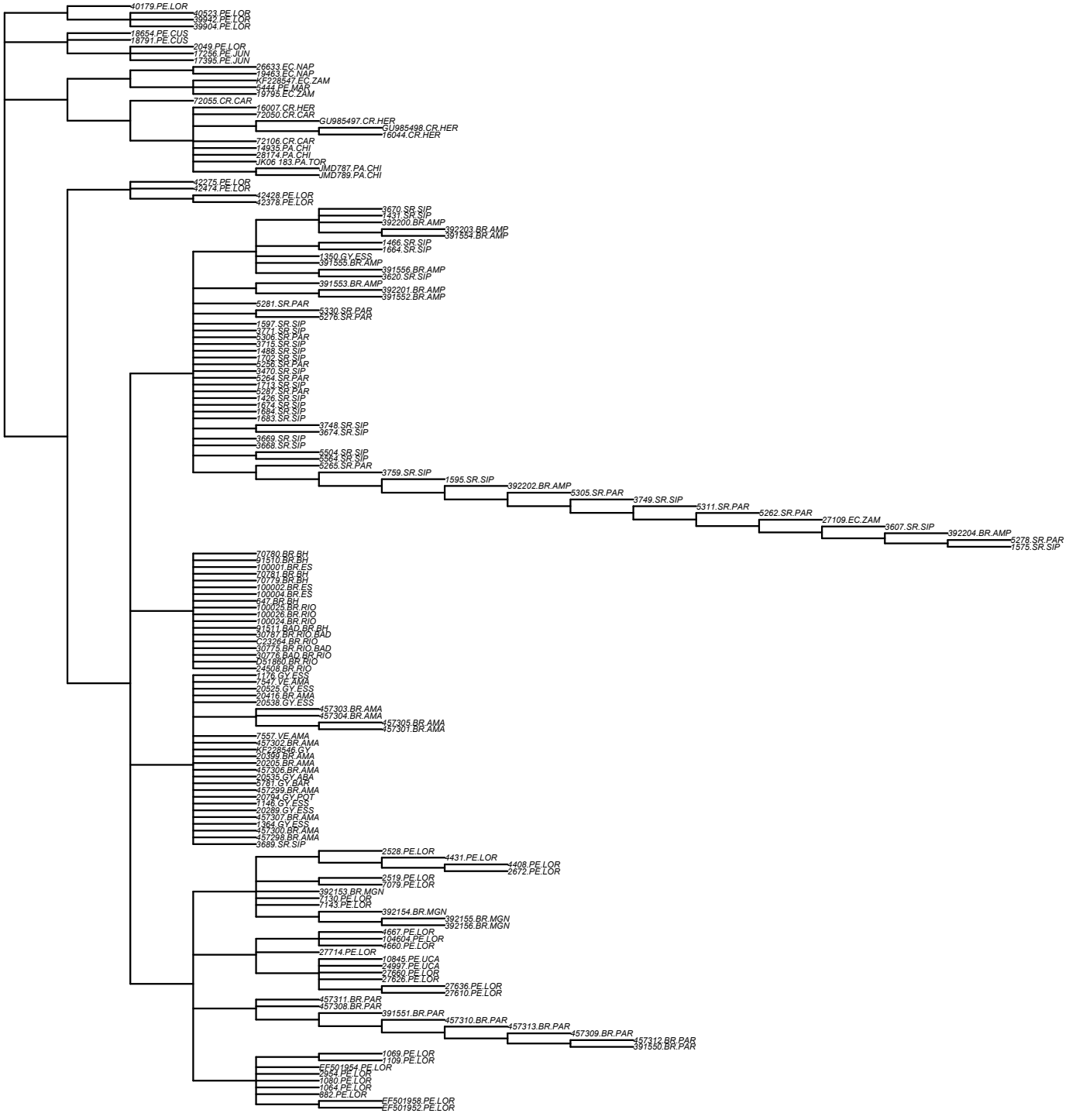
40179.PE.LOR
40523.PE.LOR
39942.PE.LOR
39904.PE.LOR
18654.PE.CUS
18791.PE.CUS
2049.PE.LOR
17256.PE.JUN
17395.PE.JUN
26633.EC.NAP
19463.EC.NAP
KF228547.EC.ZAM
4441.PE.MAD
19795.EC.ZAM
72055.CR.CAR
16007.CR.HER
72050.CR.CAR
GU985497.CR.HER
GU985498.CR.HER
16044.CR.HER
72106.CR.CAR
14935.PA.CHI
28174.PA.CHI
JK06 183.PA.TOR
JMD787.PA.CHI
JMD789.PA.CHI
42275.PE.LOR
42474.PE.LOR
42428.PE.LOR
42378.PE.LOR
3670.SR.SIP
1431.SR.SIP
392200.BR.AMP
392203.BR.AMP
391554.BR.AMP
1466.SR.SIP
1664.SR.SIP
1350.GY.ESS
391555.BR.AMP
391556.BR.AMP
3620.SR.SIP
391553.BR.AMP
392201.BR.AMP
391552.BR.AMP
5281.SR.PAR
5330.SR.PAR
5276.SR.PAR
1597.SR.SIP
1771.SR.SIP
5306.SR.PAR
3715.SR.SIP
1488.SR.SIP
1702.SR.SIP
5256.SR.PAR
3470.SR.SIP
5264.SR.PAR
1713.SR.SIP
5287.SR.PAR
1426.SR.SIP
1674.SR.SIP
1864.SR.SIP
1683.SR.SIP
3748.SR.SIP
3674.SR.SIP
3669.SR.SIP
3668.SR.SIP
5504.SR.SIP
5564.SR.SIP
5265.SR.PAR
3759.SR.SIP
1595.SR.SIP
392202.BR.AMP
5305.SR.PAR
3749.SR.SIP
5311.SR.PAR
5262.SR.PAR
27109.EC.ZAM
3607.SR.SIP
392204.BR.AMP
5278.SR.PAR
1575.SR.SIP
70780.BR.BH
91510.BR.BH
100001.BR.ES
70781.BR.BH
70179.BR.BH
100002.BR.ES
100004.BR.ES
647.BR.BH
100023.BR.RIO
100026.BR.RIO
100024.BR.RIO
91511.BAD.BR.BH
30787.BR.RIO.BAD
C23264.BR.RIO
30775.BR.RIO.BAD
30776.BAD.BR.RIO
951980.BR.RIO
24508.BR.RIO
1176.GY.ESS
7547.VE.AMA
20525.GY.ESS
20416.BR.AMA
20538.GY.ESS
457303.BR.AMA
457304.BR.AMA
457305.BR.AMA
457301.BR.AMA
7557.VE.AMA
457302.BR.AMA
KF228546.GY
20399.BR.AMA
20205.BR.AMA
457306.BR.AMA
20535.GY.ABA
5781.GY.BAR
457299.BR.AMA
20794.GY.POT
1146.GY.ESS
20289.GY.ESS
457307.BR.AMA
1364.GY.ESS
457300.BR.AMA
457298.BR.AMA
3689.SR.SIP
2528.PE.LOR
4431.PE.LOR
4408.PE.LOR
2672.PE.LOR
2519.PE.LOR
7079.PE.LOR
392153.BR.MGN
7130.PE.LOR
7143.PE.LOR
392154.BR.MGN
392155.BR.MGN
392156.BR.MGN
4667.PE.LOR
104604.PE.LOR
4660.PE.LOR
27714.PE.LOR
10845.PE.UCA
24997.PE.UCA
27660.PE.LOR
27626.PE.LOR
27636.PE.LOR
27610.PE.LOR
457311.BR.PAR
457308.BR.PAR
391551.BR.PAR
457310.BR.PAR
457313.BR.PAR
457309.BR.PAR
457312.BR.PAR
391550.BR.PAR
1069.PE.LOR
1109.PE.LOR
EF501954.PE.LOR
2554.PE.LOR
1080.PE.LOR
1064.PE.LOR
382.PE.LOR
EF501958.PE.LOR
EF501952.PE.LOR

Literature Cited

Gosselin T, Anderson EC, Ferchaud A-L. 2016. thierrygosselin/assigner: v.0.4.0 (Version 0.4.0). Zenodo. http://doi.org/10.5281/zenodo.197418.

Lawson DJ, Hellenthal G, Myers S, Falush D. 2012. Inference of Population Structure using Dense Haplotype Data. PLOS Genetics, 8:e1002453.

Petkova D, Novembre J, Stephens M. 2015. Visualizing spatial population structure with estimated effective migration surfaces. Nature Genetics, 48:94.

Weir BS, Cockerham CC. 1984. ESTIMATING F-STATISTICS FOR THE ANALYSIS OF POPULATION STRUCTURE. Evolution, 38:1358-1370.

APPENDIX 3

SUPPLEMENTARY MATERIAL FOR CHAPTER 3

Additional data files can be accessed at the online version of this article

www.nature.com/doifinder/10.1038/nature15697

and

http://dx.doi.org/10.5281/zenodo.28343

doi:10.1038/nature15697

A Comprehensive Phylogeny of Birds (Aves) using Targeted Next Generation DNA Sequencing

Richard O. Prum[1,2,*], Jacob S. Berv[3,*], Alex Dornburg[1,2,4], Daniel J. Field[2,5], Jeffrey P. Townsend[6], Emily Moriarty Lemmon[7], and Alan R. Lemmon[8]

[1] Department of Ecology & Evolutionary Biology, Yale University, New Haven CT USA
[2] Peabody Museum of Natural History, Yale University, New Haven CT USA
[3] Department of Ecology & Evolutionary Biology, Cornell University, Ithaca NY USA
[4] North Carolina Museum of Natural Sciences, Raleigh NC USA
[5] Department of Geology & Geophysics, Yale University, New Haven CT USA
[6] Department of Biostatistics, and Program in Computational Biology and Bioinformatics, Yale University, New Haven, CT USA
[7] Department of Biological Science, Florida State University, Tallahassee, FL USA
[8] Department of Scientific Computing, Florida State University, Tallahassee, FL USA

* These authors contributed equally to this work.

Online Data and Software Archive

A zip archive containing assembled sequence data, newick formatted tree files, code and scripts for generating and analyzing phylogenetic informativeness, and information on probe design and data assembly is available at Zenodo.org: http://dx.doi.org/10.5281/zenodo.28343. R code used for generating tree and supplemental figures is available on request.

Choosing Fossil Calibrations

We elected to employ traditional node-based divergence dating instead of a fossil tip-dating approach[1,2] due to the lack of a sufficiently extensive and reliable morphological data matrix for extant and fossil crown birds. Our node-dating approach followed the commonly employed method of specifying hard minimum bounds on the age of a divergence using fossils, while applying a 'soft' upper bound for date estimates[3,4]. This approach is based on the premise that the common ancestor of a clade (a node on the phylogeny) cannot be younger than its oldest fossil descendant (a child cannot be older than its parent). As a result, for a given node on the phylogeny (representing a theoretical ancestor α with two descendent lineages), only the oldest known fossil representing one of the descendant lineages of α is used for setting a hard minimum age for that divergence. More recent fossils that represent descendants of α are uninformative, since they are younger than α's youngest possible age.

In contrast to recently published divergence time analyses for crown birds[5], we sought to employ Parham *et al.*'s[6] criteria for best practices for justifying fossil calibrations in the selection of our calibration points. These criteria outline stringent phylogenetic and geochronological criteria that must be met in order for a potential

calibrating fossil to be considered strongly supported. Only fossils that have been phylogenetically placed by apomorphy-based diagnoses or comprehensive phylogenetic analyses have been included here. We provide references to up-to-date apomorphy-based diagnoses or phylogenetic analyses for each taxon listed (all of which are associated with museum specimen numbers), the most exclusive clade to which they can be referred, names of each fossil locality, and minimum-possible geochronologial ages for each fossil, inclusive of error[6]. In instances where radioisotopic dates were unavailable and fossils could only be biostratigraphically assigned to geochronological stages, the most conservative approach of selecting the minimum-possible age of the stage, inclusive of error, was implemented[6].

Our complete list of fossil calibrations comprises 19 fossil taxa, which together document many deep phylogenetic divergences within Neognathae. Although palaeognaths are well represented in Palaeogene fossil deposits in the form of members of the clade Lithornithidae[7], ambiguity regarding their monophyly and phylogenetic relationships with respect to extant palaeognaths informed our decision to exclude them from this analysis. The restriction of calibration points to Neognathae, and the lack of definitive stem neognaths or stem palaeognaths, rendered it impossible to directly calibrate the root divergence within crown Aves.

The Mesozoic fossil record of crown birds is at best extremely sparse[8,9], or possibly completely absent. Although the putative crown anseriform *Vegavis iaai* has often been used as a Late Cretaceous (66.5 Ma[10]) calibration point for Anseriformes, Neognathae, or crown Aves, recent phylogenetic analyses have cast doubt on the relationships of this taxon, and its placement within the avian crown group[11]. As a result, we decided not to include this fossil in our full analysis; however, we have conducted an additional sensitivity analysis to asses the robustness of our results to the exclusion/inclusion of the *Vegavis* calibration (see below).

In certain instances, multiple closely related extant clades exhibited Palaeogene stem group representatives deriving from similarly aged sediments. For example, the stem potoo (Pan-Nyctibiidae), *Paraprefica kelleri*, is dated at 47.5Ma, whereas the stem oilbird (Pan-Steatornithidae), *Prefica nivea*, is dated at 51.66Ma[12-14]. In this instance, the phylogenetic divergence between Nyctibiidae and Steatornithidae was calibrated using the older fossil (*Prefica nivea*), and the stem nyctibiid was not used. Similar logic resulted in, for example, the exclusion of the stem leptosomid *Plesiocathartes kelleri* in favor of the older stem representative of the Coraciidae + Brachypteraciidae clade *Primobucco mcgrewi*[15,16].

Additional Dating Analysis using *Vegavis* Calibration

Since *Vegavis* may represent a *bona fide* crown anseriform, we performed a sensitivity analysis of our dating estimate with ten data partitions that exhibited the lowest declines in phylogenetic informativeness across the tree; otherwise we used the same diagnostic criteria employed in our initial analyses. In order to include *Vegavis,* we substituted our stem galliform calibration (*Gallinuloides,* ~51.66 Ma) for a stem anatid calibration (~66.5 Ma). As in previous fossil calibrations, we used a lognormal

distribution, setting the offset to 66.5 Ma and defined 97.5% of the calibration density to fall more recently than 86 Ma (see comments on defining the soft crown prior for justification of the soft maximum we employ here).

Figure S10 shows the alternative time calibration (including *Vegavis*) for the Bayesian tree with error bars for each node age. Figure S11 compares the posterior distributions of the estimated ages of the avian crown clade with and without the *Vegavis* calibration, and Figure S12 compares the ages of all nodes in the phylogeny with and without *Vegavis*. When *Vegavis* is included, we find that the median posterior estimate of the root age is increased, but only by ~6 million years, pushing the estimate of the age of the avian crown to ~78 Ma (mean: 78.26; median: 78.00; 95% HPD interval: 71.98-84.93)(Fig. S11). However, this is not a significant change; the median estimate of the divergence time falls within the HPD confidence intervals of our initial estimate of the root age without *Vegavis* (mean: 72.72; median: 72.33; 95% HPD interval: 66.96-79.45)(Fig. S11). Examining the differences over the entire tree, we see that the only significant changes to node age estimates are restricted to those within the Galloanserae (Fig. S12); several divergences were pulled significantly closer to the end of the Cretaceous. For example, when *Vegavis* is included, the median age of the oldest split in Galloanserae is necessarily increased to ~72.5 Ma. The median posterior age estimates for most other neoavian nodes were also pushed further back in time by ~2-4 million years as a consequence of including *Vegavis*, but they also fell within the HPD confidence intervals of our analysis excluding *Vegavis* (Fig. S12).

In summary, based on an analysis of the most phylogenetically informative subset of our data using a calibration with *Vegavis*, we are confident that our age estimates are robust to the inclusion or exclusion of this particular calibration. Although crown group ages within Anseriformes are pulled further back in time, the inclusion of *Vegavis* has no significant influence on the HPD confidence for various neoavian subclades. Until more fossils become available, the age estimates of early avian diversification events will remain inherently uncertain.

Detailed Justification of Fossil Calibrations

For every specimen presented below, the clade calibrated represents the most recent common ancestor of the total group noted, and its extant sister taxon. For example, *Pulchrapollia gracilis* (stem Psittaciformes) calibrates the divergence between total group Psittaciformes and total group Passeriformes. For taxa whose phylogenetic and stratigraphic placement have already been discussed in light of best practices for fossil calibrations[17], (e.g. *Limnofregata azygosternon*[18]), only brief summaries are presented here.

Clade: Stem Pici (all Piciformes except Bucconidae and Galbulidae)
Taxon: *Rupelramphastoides knopfi*[19,20]
Cladistic justification: Analyses of discrete morphological characters diagnose *Rupelramphastoides* as a stem group representative of Pici, including the presence of a very large and narrow accessory trochlea for the retroverted fourth toe, a very narrow tarsometatarsal trochlea for the second toe, and marked ulnar papillae for the attachment of the secondary flight feathers[7]. The plesiomorphic absence of an ossified extensor

bridge on the proximal tarsometatarsus, and a mosaic of other features supports a phylogenetic position for *Rupelramphastoides* on the stem of the clade bracketed by Indicatoridae and Picidae, while the presumably plesiomorphic similarity of the tarsometatarsus of *Rupelramphastoides* and crown Ramphastidae support *Rupelramphastoides*' status as a stem group representative of Pici[7].
Stratigraphy: Frauenweiler south of Wiesloch, Germany[19]. Provenance identifiable only to geologic stage (Rupelian); thus youngest possible age of Rupelian inclusive of error is applied (following [17]).
Calibration: Minimum age of 28.3 Ma[21,22].

Clade: Stem Upupidae + Phoeniculidae
Taxon: *Messelirrisor grandis*[23,24]
Cladistic justification: Phylogenetic analyses of morphology[24].
Stratigraphy: Messel, Germany. A detailed description of the age of the Messel Pit, and the minimum age of the fossils contained within it is presented by [10].
Calibration: Minimum age of 46.6 Ma[25].

Clade: Stem Coraciidae + Brachypteraciidae
Taxon: *Primobucco mcgrewi*[16,26,27]
Cladistic justification: Morphological phylogenetic analysis[28], and phylogenetic analyses of combined morphological and molecular data[27].
Stratigraphy: Fossil Butte Member of the Green River Formation. The most complete specimen of this taxon[10] derives from the middle unit of the Fossil Butte Member; detailed age justification presented in [10].
Calibration: Minimum age of 51.57 Ma[29].

Clade: Stem Psittaciformes
Taxon: *Pulchrapollia gracilis*[30]
Cladistic justification: Based on phylogenetic analyses of morphological data [30-32], and combined analyses of morphological and molecular data[33,34].
Stratigraphy: Collected from the Walton Member of the London Clay Formation at Walton-on-the-Naze, England. Details regarding the age of the specimen ([35-37]) are summarized by [10].
Calibration: Minimum age of 53.5 Ma[10].

Clade: Stem Fregatidae
Taxon: *Limnofregata azygosternon*[38,39]
Cladistic justification: Based on analyses of osteological data, [39] identified 18 unambiguous synapomorphies of a *Limnofregata* + *Fregata* clade. These are discussed in detail in [18].
Stratigraphy: Fossil Butte Member of the Green River Formation. Several referred specimens have been recovered from the F-2 Facies, in the middle unit of the Fossil Butte Member of the Green River Formation[18,40,41]. Precise details regarding the dating of these deposits are discussed by [18].
Calibration: Minimum age of 51.58 Ma[18].

Clade: Stem Sphenisciformes
Taxon: *Waimanu manneringi*[42]
Cladistic justification: Following [10], *Waimanu* was recovered as a total group sphenisciform by multiple analyses using morphology[42] and combined data [43,44].
Stratigraphy: Basal Waipara Greensand, Waipara River, New Zealand. The top of the Waipara Greensand marks the Paleocene-Eocene boundary, and calcareous nannofossils further constrain this locality's age. Detailed age justification presented in [10].
Calibration: Minimum age of 60.5 Ma[45].

Clade: Stem Gruoidea (Aramidae + Psophiidae + Gruidae)
Taxon: *Parvigrus pohli*[7,46]
Cladistic justification: Analyses of discrete character data support the position of *Parvigrus pohli* as a stem group representative of the Gruoidea[46]. Morphological support for the gruoid affinities of *P. pohli* include an elongated and narrow sternum lacking deep incisions on its caudal margin, and a medially protruding projection on the proximal end of the first phalanx of the fourth toe[7,46]. A combination of features observable in *P. pohli* and its extinct relative *Rupelrallus saxoniensis* diagnose *P. pohli* as a stem group gruoid, including the sternal extremity of the coracoid bearing a marked depression, and a lack of coracoid pneumatic foramina. Additionally, the caudal margin of the sternum of *P. pohli* exhibits a pair of shallow incisions, in contrast to the condition observed in crown Gruoidea[7,46].
Stratigraphy: Pichovet, Vachères, France. Provenance identifiable only to geologic stage (Rupelian); thus youngest possible age of Rupelian inclusive of error is applied (following [17]).
Calibration: Minimum age of 28.3 Ma[47].

Clade: Stem Phaethontidae
Taxon: *Lithoptila abdouensis*[48]
Cladistic justification: Based on cladistic analyses of morphological data[39,48]. [93] found 10 unambiguous cranial synapomorphies for Phaethontes + *L. abdouensis*[18].
Stratigraphy: Bed IIa, Ouled Abdoun Basin, near Grand Daoui, Morocco. Provenance identifiable only to geologic stage (Thanetian), thus youngest possible age of Thanetian inclusive of error is applied (following [17]).
Calibration: Minimum age of 55.6 Ma[49].

Clade: Stem Apodidae
Taxon: *Scaniacypselus wardi*[50,51]
Cladistic justification: Phylogenetic analysis of morphology[52], and combined phylogenetic analyses of morphological and molecular data[103].
Stratigraphy: Bed R6 of the Røsnæs Clay Formation, Denmark[53]. Provenance identifiable only to geologic stage (Ypresian); thus youngest possible age of Ypresian inclusive of error is applied (following [17]). Additional details of the stratigraphic provenance presented in [10].
Calibration: Minimum age of 48.4 Ma[54-56].

Clade: Stem Podargidae

Taxon: *Fluvioviridavus platyrhamphus*[14]
Cladistic justification: Parsimony analysis of morphology, and combined morphological and molecular data, by [14]. A *F. platyrhamphus* + Podargidae clade was supported by numerous cranial synapomorphies including i) a rim surrounding the external naris that extends anterolaterally onto the dorsal surface of the beak, the absence of pterygoid-basipterygoid contact, and a well rounded posterior portion of the articular portion of the mandible[14]. Monophyly of crown group Podargidae to the exclusion of *F. platyrhamphus* was supported by several characters, including posteriorly-projecting lacrimal 'horns' at the anterior portion of the orbit, and very long lateral trabeculae and short intermediate trabeculae of the sternum[14].
Stratigraphy: Fossil Butte Member of the Green River Formation; precise details regarding the dating of these deposits are discussed by [10].
Calibration: Minimum age of 51.58 Ma[29].

Clade: Stem Steatornithidae
Taxon: *Prefica nivea*[12,13,14,53]
Cladistic justification: Discrete analyses of morphological data by [71], and morphological and combined morphological and molecular phylogenetic analyses by [14]. *P. nivea* shares a distinct mandibular morphology with *S. caripensis*, as well as an extremely short tarsometatarsus and a well-developed temporal fossae with the extant Oilbird, *Steatornis caripensis*. Additionally, these taxa share a distinctly shortened tibiotarsus, approaching the length of the carpometacarpus[14]; characters differentiating *P. nivea* and *S. caripensis* include overall body size, and an unfused ilium-synsacrum contact in *P. nivea*[12,13,57].
Stratigraphy: Fossil Butte Member of the Green River Formation; precise details regarding the dating of these deposits are discussed by [18].
Calibration: Minimum age of 51.58 Ma [29].

Clade: Stem Threskiornithidae
First: *Rhynchaeites sp.*[58]
Cladistic justification: Following [18], which lists the full suite of threskiornithid apomorphies exhibited by *Rhynchaeites*, three unambiguous synapomorphies place *Rhynchaeites* with total group Threskiornithidae (an elongate recurved bill; a schizorhinal bill with a dorsoventrally broad basal segment of the ventral bar, and a notarium consisting of at least three fused thoracic vertebrae[59,60]).
Stratigraphy: Fur Formation. Precise horizon within Fur Formation from which fossil was recovered is unknown, thus the youngest possible radiometric age for these deposits, inclusive of error, is applied. A comprehensive discussion of the age justification for the oldest known specimen of *Rhynchaeites* sp. is presented in [18].
Calibration: Minimum age of 53.9 Ma[61].

Clade: Stem Coliiformes
First: *Sandcoleus copiosus*[62,63]
Cladistic justification: Morphological phylogenetic analyses[63-66].
Stratigraphy: Sand Coulee Beds, Willwood Formation. Fossil derives from *Plesiadapis cookei* zone in [67], thus youngest possible age of this zone is applied (following [17]). Details of stratigraphic provenance and aging presented in [10].

Calibration: Minimum age of 56.22 Ma[67].

Clade: Stem Alcediniformes (Momotidae + Meropidae + Alcedinidae + Todidae)
First: *Quasisyndactylus longibrachis* [57,68,69]
Cladistic justification: Placement of *Q. longibrachis* as the extinct sister taxon to crown group Alcediniformes enjoys support from analyses of discrete anatomical characters [57,68,69]. Although a suite of anatomical features align *Q. longibrachis* with crown group Alcediniformes (the proximal end of the first phalanx of the hindtoe bears a lateral projection like all crown alcediniforms), and the cranial anatomy compares favorably with that of crown Todidae[119], the plesiomorphic morphology of the furcula supports the assignment of *Q. longibrachis* to the alcediniform stem group[109,118].
Stratigraphy: Messel, Germany. A detailed description of the age of the Messel Pit, and the minimum age of the fossils contained with in it is presented by [10].
Calibration: Minimum age of 47.5 Ma[25].

Clade: Stem Todidae
First: *Palaeotodus cf. itardiensis* [70]
Cladistic justification: The taxon *Palaeotodus* was initially erected to describe material from the early Oligocene Brule Formation of Wyoming (*P. emryi*[71]). Additional material belonging to *Palaeotodus* (*P. escampsiensis* and *P. itardiensis*) was described by [72]. A postcranial skeleton identified as *Palaeotodus* cf. *itardiensis* was described by [70], and exhibits a substantially elongate and narrow tarsometarsus approaching the length of the humerus[119], and the complete absence of a procoraoid process (the former a Todidae + Momotidae synapomorphy, the latter one shared with Todidae)[7]. [120] describes the distal tarsometatarsus as exhibiting a plesiomorphic morphology with respect to crown Todidae, suggesting that *P.* cf. *itardiensis* represents the extinct sister taxon to the todid crown group.
Stratigraphy: Frauenweiler south of Wiesloch, Germany. Provenance identifiable only to geologic stage (Rupelian); thus youngest possible age of Rupelian inclusive of error is applied (following [17]).
Calibration: Minimum age of 28.3 Ma[21,22].

Clade: Stem Phalacrocoracidae
First: *Oligocrax stoeffelensis* [39,73,74]
Cladistic justification: Based on morphological analyses by [123]. That analysis identified three unambiguous *?Borvocarbo stoeffelensis* + Phalacrocoracidae synapomorphies, discussed by [18]. Taxonomy of *?Borvocarbo stoeffelensis* has been changed to *Oligocrax stoeffelensis* following [124].
Stratigraphy: Enspel Formation. Following [18], The Enspel deposits correspond the Upper Oligocene Mammal Paleogene reference level 28 [75]. $^{40}Ar/^{39}Ar$ radiometric dating from basaltic flows bounding the Enspel deposits exhibit ages of 24.56 ± 0.04 to 24.79 ± 0.05 Ma[75].
Calibration: Minimum age of 24.52 Ma [75].

Clade: Stem Musophagidae
First: *Foro panarium*[76,77]

Cladistic justification: Based on Bayesian and parsimony phylogenetic analyses of morphological characters, both unconstrained and constrained to molecular backbone trees by [127]. That analysis identified *Foro* as sister to Musophagidae with strong statistical support from bootstrap percentages and Bayesian posterior probabilities under all unconstrained and constrained topologies. Although the extant sister taxon to Musophagidae has historically been a topic of controversy, the morphological analysis of [127] supports a close relationship between Musophagidae and Cuculidae, a hypothesis strongly supported by the independent phylogenomic dataset presented in the present study (as part of a clade that also includes the Otididae).
Stratigraphy: Fossil Butte Member of the Green River Formation. Following [126], the only known specimen derives from the "Thompson Quarry," northwest of Kemmerer, Lincoln County, Wyoming: NW1/4, SW1/4, sec.22, T22N, R117W (Kemmerer 15-minute quadrangle); 41°44'N, 110°31'W. This site is among the F-2 localities of [78]. Precise details regarding the dating of these deposits are discussed by [18].
Calibration: Minimum age of 51.58 Ma[29].

Clade: Stem Galliformes
First: *Gallinuloides wyomingensis*[79]
Cladistic justification: Phylogenetic analyses of morphological data[129,80], and combined morphological and molecular data[129]. [129] performed a series of phylogenetic analyses incorporating variants of a morphological cladistic dataset, and inclusion and exclusion of gene sequence data. In all analyses *Gallinuloides* resolved as a stem galliform, with varying degrees of statistical support. In those analyses six unambiguous synapomorphies were found to support a monophyletic Galliformes to the exclusion of *Gallinuloides*; these synapomorphies are similar to those proposed by [80] in support of the same phylogenetic position[79]. These include i) scapus claviculae of furcula narrow, ii) spina interna of sternum present, iii) apex carinae of sternum shifted caudally, iv) cotyla scapularis of coracoid shallowly excavated, v) incisura capitis of humerus enclosed distally by a ridge, vi) spatium intermetacarpale of carpometacarpus wide[79].
Stratigraphy: Fossil Butte Member of the Green River Formation; precise details regarding the dating of these deposits are discussed by [18].
Calibration: Minimum age of 51.58 Ma[29].

Clade: Stem Apodiformes
First: *Eocypselus rowei*[51,81]
Cladistic justification: [51,81] conducts two analyses under parsimony, one of a comparative morphological dataset, and one combining these morphological data with genetic data from 4 loci. The position of *Eocypselus* as a total group apodiform was supported by two unambiguous synapomorphies (a short humerus, and an ossified arcus extensorius of the tarsometatarsus), while crown apodiform monophyly was upheld to the exclusion of *Eocypselus* by eight crown group synapomorphies[131].
Stratigraphy: Smith Hollow Quarry, Fossil Butte Member, Green River Formation; precise details regarding the dating of these deposits are discussed by [18].
Calibration: Minimum age of 51.58 Ma[29].

Detailed Phylogenetic Discussion

Particular effort was made to include taxa that would break up long phylogenetic branches and provide the highest likelihood of resolving short internodes at the base of Neoaves. We also sampled multiple species within groups whose monophyly or phylogenetic relationships to other birds have been controversial– i.e. multiple species of tinamous (4 sp.), nightjars (3 sp.), hummingbirds (3 sp.), turacos (2 sp.), cuckoos (4 sp.), pigeons (5 sp.), sandgrouse (2 sp.), mesites (2 sp.), rails (3 sp.), storm petrels (3 sp.), petrels (3 sp.), storks (2 sp.), herons (3 sp.), hawks (3 sp.), hornbills (2 sp.), mousebirds (2 sp.), trogons (2 sp.), kingfishers (2 sp.), barbets (2 sp.), seriemas (2 sp.), falcons (4 sp.), parrots (5 sp.), and suboscine passerines (28 sp.).

Here, we discuss our phylogenetic results (Figs. 1, S1) in detail, and we describe points of congruence and discordance with previous hypotheses of avian phylogeny from the published literature.

Congruent with all recent studies, the concatenated phylogeny places the palaeognaths as the sister group to the rest of living birds, and the flying tinamous (Tinamidae) within the flightless ratites[82-86]. However, these studies have placed tinamous in various positions: as sister group to a cassowary (*Casuarius*), emu (*Dromaius*), and kiwi (*Apteryx*) clade[82,83], as sister to all extant palaeognaths except ostrich (*Struthio*)[85], or in the same position but as the sister group to the extinct moas[84]. Our tree places tinamous as the sister group to a cassowary-emu clade (Casuariiformes) (Fig. 1). The phylogenetic relationships among the Galloanserae (Fig. 1) are exactly congruent with Hackett *et al.*[82].

Within the monophyletic Neoaves, we identify five main clades which are each the successive sister groups to the rest of Neoaves (Fig. 1). A clade including Caprimulgiformes and Apodiformes, called Strisores (or Caprimulgimorphae[5]), is resolved as the sister to the rest of Neoaves (Fig. 1, brown). The interrelationships we recover within this clade are novel: the nightjars (Caprimulgidae), a Neotropical oilbird-potoo clade, the frogmouths (Podargidae), and the owlet-nightjars (Aegothelidae) form four successive sister groups to the monophyletic swifts (Hemiprocnidae + Apodidae) and hummingbird (Trochilidae) clades. Within nightjars, our placement of *Eurostopodus* as sister group to *Caprimulgus* and *Chordeiles* is congruent with Barrowclough *et al*.[87]. We also confirm the monophyly of swifts (*Chaetura* and *Streptoprocne*, Apodidae) with respect to the crested swifts (Hemiprocnidae). Congruent with a recent comprehensive, multilocus phylogeny of the hummingbirds[88], *Topaza* and *Phaethornis* form a clade that is sister to *Archilochus* (Fig 1).

The next neoavian clade is a novel clade that consists of two recently identified monophyletic groups, which we call Columbaves (Fig. 1, purple). The first subclade includes the turacos (*Tauraco* and *Corythaeola,* Musophagidae), the bustards (*Ardeotis,* Otididae), and the cuckoos (*Tapera, Centropus, Cuculus,* and *Coccyzus,* Cuculidae). A turaco-bustard-cuckoo clade was previously identified by Jarvis *et al.*[5] and called the Otidimorphae. Jarvis *et al*.[5] found weak support for a turaco and bustard clade (BS= 0.55) with cuckoos as their sister group. However, we find strong support for the placement of

turacos as the sister group to a clade of bustards and cuckoos. Within the cuckoos, our phylogeny is exactly congruent with Sorenson and Payne[89].

Within the Columbaves, the sister group to the Otidimorphae consists of pigeons (Columbidae) as the sister group to an Old World clade consisting of monophyletic radiations of sandgrouse (Pteroclididae) and the Malagasy mesites (Mesitornithidae). This clade was identified by Hackett *et al*.[82], and confirmed by Jarvis *et al.*[5] and called the Columbimorphae. Within the Columbimorphae, Hackett *et al*.[82] placed mesites and pigeons as sister groups, but our phylogeny agrees with Jarvis *et al*.[5] in placing mesites and sandgrouse in a clade with pigeons as their sister group. Jarvis *et al.*[5] proposed that the Otidimorphae was the sister group to the caprimulgiform+apodiform clade (Caprimulgimorphae), and that the Columbimorphae was related to flamingos and grebes. Our results do not support these proposed phylogenetic relationships.

Within pigeons, our phylogeny is congruent with the result of Johnson and Clayton[90] and Pereira *et al*.[91], except for our placement of *Columbina* as the sister group to the *Columba-Leptotila* clade instead of as the sister to all other columbids. This is one of the few areas of discordance between our Bayesian and our ML phylogenies; our ML topology is congruent with the placement of *Columbina* in Johnson and Clayton[90] and Pereira *et al*.[91] (Fig. S1).

The next neoavian clade consists of the core Gruiformes (Fig. 1, yellow) *sensu stricto* as previously proposed by Hackett *et al*[82] and others. Among the gruiforms, we find phylogenetic interrelationships that are entirely consistent with Hackett *et al*.[82]. There are two monophyletic superfamilies. The Gruoidea consists of the trumpeters (Psophiidae) as the sister group to the limpkin (Aramidae) and the cranes (*Grus* and *Balearica,* Gruidae). Within the Ralloidea, we confirm that the flufftails (*Sarothrura,* Sarothruridae) are more closely related to the sungrebes (Heliornithidae) than they are to other rails (*Rallus, Porphyrio,* and *Micropygia,* Rallidae).

Our results confirm the existence of a diverse, waterbird clade (Fig. 1, blue), similar to, but more expansive in composition than, that previously proposed[5,82,92]. This clade, which we call Aequorlitornithes, includes all diving birds, wading birds, shorebirds, and two small, eclectic, aquatic bird clades. Briefly stated, we find that The clade of (Shorebirds+(Flamingos+Grebes)) is the sister group of the clade of (all diving and wading birds +(Sunbittern+Tropicbirds))(Fig. 1). Within the charadriiform clade, the interrelationships in our Bayesian tree are exactly congruent with those found by Hackett *et al*.[82]. Our Bayesian results are completely congruent with the charadriiform phylogeny of Baker *et al*.[93], except for the relationships among terns (*Sterna*), gulls (*Chroicocephalus*), and skimmers (*Rynchops*). Our Bayesian tree has (gulls +(terns +skimmers), whereas Baker *et al*.[93] found (terns+(gulls+skimmers). Interestingly, this is one of three areas of discordance between our Bayesian and ML results, and our ML tree agrees with the Baker *et al*.[93] topology.

We confirm the monophyly of the clade including diving and wading birds[5,82,92] (called Aequornithia[94]), and we confirm the placement of the sunbittern-tropicbirds clade

(Phaethontimorphae) as the sister group to Aequornithia. Hackett *et al*.[82] placed the Kagu (*Rhynochetos*), as sister to the sunbittern (*Eurypyga*). Unfortunately, we were not able to obtain tissue of *Rhynochetos* to test this hypothesis.

Within Aequornithia, our phylogeny is exactly congruent with Jarvis *et al.*[5], and closely follows Hackett *et al*.[82]. Loons (*Gavia*) are the sister group to the rest of Aequornithia, which is composed of two main clades. Within the Procellariimorphae[5], the penguins (*Spheniscus*) are the sister group to the monophyletic tubenoses (Procellariiformes). Our extensive sampling establishes new relationships within tubenoses beyond Hackett *et al*.[82]. *Contra* Hackett *et al*., we place albatross (Diomedeidae) as the sister group to all other tubenoses. We confirm that the storm petrels are paraphyletic with respect to other petrels. *Oceanites* and *Pelagodroma* (Oceanitidae) and *Oceanodroma* (Hydrobatidae) are successive sister groups to the rest of the petrels. Lastly, the traditional petrels are paraphyletic with respect to the diving petrels (*Pelecanoides*); *Pelecanoides* is more closely related to *Pterodroma* than are *Puffinus* or *Fulmarus* (respectively). These novel relationships are not congruent with previous studies[95,96]. However, the alternative resolutions have not been highly supported in these previous studies[95,96].

The sister group to Procellariimorphae has been called the Pelecanimorphae[5]. Within this clade, our results are very similar to Hackett *et al*.[82] but with some differences between our Bayesian and ML topologies. Both trees agree with Hackett *et al*.[82] in the relationships of (frigatebirds+(boobies+(anhingas+cormorants))). The sister group to this clade has the same composition in our Bayesian and ML trees and Hackett *et al*.[82], but with some variation in topology among them. Our Bayesian tree places ibis as sister group to the rest. Our ML tree and Hackett *et al*.[82] place ibis as the sister group to herons. Our Bayesian tree, our ML tree, and Hackett *et al*.[82] find three different resolutions of the relationships among the Shoebill (*Balaeniceps*), pelicans (*Pelecanus*), and Hamerkop (*Scopus*). Our Bayesian tree finds (*Scopus*+(pelicans+*Balaeniceps*). The ML tree places (*Balaeniceps*+(pelicans+*Scopus*). Hackett *et al*.[82] found (pelicans+(*Balaeniceps*+*Scopus*).

Our results confirm the monophyly of a comprehensive clade of landbirds (Fig. 1, green), Telluraves[83], which has been supported by many recent studies[82,83,85,92,97]. However, we find that the sister group to this land bird clade is the enigmatic Hoatzin (*Opisthocomus hoazin*), and we call this new, more comprehensive clade Inopinaves (*inopina*= unexpected). Based on this phylogenetic position and our fossil calibration, *Opisthocomus* is the most ancient (~64 myo), living bird lineage that is represented today by only a single extant species. Thus, *Opisthocomus* is the longest 'long branch' in the avian tree, which has obviously contributed to the great challenges of placing it confidently within avian phylogeny.

Within Telluraves, we find that hawks and relatives (Accipitriformes *sensu stricto*[82]) is the sister group to the remaining members of the landbird clade (congruent with Kimball *et al*.'s[85] 49-locus species-tree; Fig. 5B), and not the sister group to the clade of owls, mousebirds, cuckoo-roller, trogons, bucerotiforms, coraciiforms, and piciforms[5,82,83,85,97]. Consequently, 'Afroaves'[5] is not monophyletic in our analysis. We

call this new clade of landbirds, excluding Accipitriformes, Eutelluraves. Within the accipitriforms, we uncover the same relationship as many previous studies: (New World vultures+(secretarybird+(Osprey+hawks)[5,82,83,85,97,98]. Within the hawks (Accipitridae), our topology is congruent with Griffiths *et al*.[98]. We also confirm the monophyly of the New World vultures (Cathartidae).

Eutelluraves consists of two well supported clades with increasingly well established interrelationships. Congruent with recent studies, we find that owls are the sister group to the diverse clade Coraciimorphae, comprised of (mousebirds+(cuckoo roller+(trogons+(bucerotiforms+(coraciiforms+ piciforms) [5,82,83,85,97]. Within each of these groups, our phylogeny is closely congruent with Hackett *et al*.[82], except that we find bee-eaters (*Merops*) to be the sister group to the rollers (*Coracias*) and ground-rollers (*Atelornis*), instead of the sister group to all other coraciiforms. The hornbills are the sister group to hoopoes and wood hoopoes. The coraciiforms (*sensu stricto*) form a clade that is the sister group to the monophyletic piciforms. Within the piciforms, honeyguides (Indicatoridae) are sister to woodpeckers (Picidae)[82,99], the wrynecks (*Jynx)* are the sister group to all other woodpeckers[99], and the Asian, African, and Neotropical barbets share successively closer relationships to the Neotropical toucans[100].

The last major clade of the land bird assemblage, called Australavis[101] or Australaves[5], is comprised of seriemas (Cariamidae), falcons (Falconidae) and parrots (Psittaciformes) as the successive sister groups to the monophyletic perching birds (Passeriformes). This topology has been identified consistently in several recent studies[5,82,83]. We confirm the monophyly of the extant seriemas (*Chunga*+*Cariama*). Within the falcons, our tree is exactly congruent with Griffiths *et al*.[102] Within the parrots (Psittaciformes), our topology– (*Nestor*+(*Probosciger*+((*Barnardius*+*Psittrichas*)+(*Psittacus*+*Deroptyus*))))– is largely congruent with Wright *et al*.[103], except for the placement of *Psittrichas fulgidus.* Wright *et al*.[103] found (*Barnardius*+(*Psittrichas*+(*Psittacus*+*Deroptyus*))), but their placement of *Psittrichas* was among the most poorly supported relationships in their analysis.

Congruent with previous morphological[104] and molecular[5,82,83,85] phylogenetic analyses of the passerines, the New Zealand wrens (*Acanthisitta*) are the sister group to the suboscine and oscine clades (Fig. 1). Within the Old World suboscines, our placement of the Malagasy asities (*Neodrepanis*) as sister to Asian *Eurylaimus* is congruent with previous morphological[105] and molecular[106] phylogenies. Congruent with Moyle *et al*.[106], we identify an exclusive clade including *Smithornis* and *Calyptomena* broadbills. However, pittas (*Pitta*) are placed within the broadbills as the sister group to the *Smithornis* and *Calyptomena* clade. The monophyly of all broadbills and asities, excluding the pittas, was the lowest supported node in the Moyle *et al*. phylogeny[106] (BS=0.85). This novel placement of *Pitta* should be tested further with greater taxon sampling.

Within the New World suboscines, we identified the two main tracheophone and tyrannoid clades (Fig. 1). The phylogenetic relations among the tracheophones in our tree are largely congruent with Moyle *et al*.[107] and Ohlson *et al*.[108]. Congruent with Ohlson *et al*.[108], we find *Melanopareia* to be the sister group to the thamnophilid antbirds. In

contrast, *Moyle et al*.[107] placed *Melanopareia* as sister to all other tracheophones except thamnophilids, but this relationship was poorly supported[107]. Furthermore, within antbirds, we find *Myrmornis* to be the sister group to *Terenura callinota* and *Thamnophilus ruficapillus,* whereas Moyle *et al*.[107] placed *Terenura sharpei* as the sister group to all other thamnophilids. Bravo *et al*.[109] place both *T. callinota* and *T. sharpei* in a clade as sister to all other antbirds, putting them in the new genus *Euchrepomis*. Further taxon sampling will be needed to resolve the conflict between our phylogeny and these previous analyses[107,109].

Within the tyrannoid suboscines, the relationships are quite similar to recent phylogenies by Tello *et al*.[110] and Ohlson *et al*.[108], with a few notable differences. Congruent with several recent studies[108,111], the manakins (Pipridae) and cotingas (Cotingidae) are monophyletic, successive sister groups to the rest of the tyrannoids. Within manakins, *Neopelma* is sister to *Cryptopipo* and *Ceratopipra,* which is congruent with all recent phylogenies[112-114]. The next tyrannoid lineage is a clade including the Sharpbill (*Oxyruncus*) and *Myiobius*– the Onychorhynchini of Tello *et al*.[110], or the Onychorhynchidae-Oxyruncidae clade of Ohlson *et al*.[108]. The tityrid clade (Tityridae) and *Piprites* are the next successive sister groups to the tyrant flycatcher radiation (Tyrannidae). Within tyrannids, *Rhynchocyclus* (Rhynchocyclinae) and *Hirundinea* (Hirundineinae) are successive sister groups to rest, within which *Elaenia* (Elaeniinae) is the sister group to *Hymenops* (Fluvicolinae) and *Tyrannus* (Tyranninae).

Within the oscine clade, the interrelationships among the 15 oscine passerines sampled are exactly congruent with the phylogeny of Barker *et al*.[115]. Three Australopapuan lineages comprise the first three successive sister groups to the rest of the oscines. The lyrebirds (*Menura*) are sister group to the rest. A clade including the Australian treecreepers (*Climacteris*) and the bowerbirds (*Sericulus* and *Ptilonorhynchus*) is the next, and the fairy wrens (*Malurus*) are the third. The corvoid clade (*Corvus* and *Lophorhina*) is the sister group to the Passerida clade. Within Passerida, the Sylvioidea (*Poecile, Calandrella, Pycnonotus,* and *Sylvia*) are sister groups to the Muscicapoidea (*Turdus* and *Regulus*) and the Passeroidea (*Fringilla* and *Spizella*). Within the sylvioids, our topology– (*Poecile*+(*Calandrella*+(*Pycnonotus*+*Sylvia*)))– is exactly congruent with Barker *et al*.[115].

References

1 Ronquist, F. *et al.* A Total-Evidence Approach to Dating with Fossils, Applied to the Early Radiation of the Hymenoptera. *Systematic Biology*, doi:10.1093/sysbio/sys058 (2012).

2 Hsiang, A. Y. *et al.* The origin of snakes: revealing the ecology, behavior, and evolutionary history of early snakes using genomics, phenomics, and the fossil record. *BMC Evolutionary Biology* **15**, 1-22, doi:10.1186/s12862-015-0358-5 (2015).

3 Ho, S. Y. W. & Phillips, M. J. Accounting for Calibration Uncertainty in Phylogenetic Estimation of Evolutionary Divergence Times. *Systematic Biology* **58**, 367-380, doi:10.1093/sysbio/syp035 (2009).

4 Yang, Z. & Rannala, B. Bayesian Estimation of Species Divergence Times Under a Molecular Clock Using Multiple Fossil Calibrations with Soft Bounds. *Molecular Biology and Evolution* **23**, 212-226, doi:10.1093/molbev/msj024 (2006).

5 Jarvis, E. D. *et al.* Whole-genome analyses resolve early branches in the tree of life of modern birds. *Science* **346**, 1320-1331, doi:10.1126/science.1253451 (2014).

6 Parham, J. F. *et al.* Best Practices for Justifying Fossil Calibrations. *Systematic Biology*, doi:10.1093/sysbio/syr107 (2011).

7 Mayr, G. *Paleogene Fossil Birds*. (Springer, 2009).

8 Clarke, J. A., Tambussi, C. P., Noriega, J. I., Erickson, G. M. & Ketcham, R. A. Definitive fossil evidence for the extant avian radiation in the Cretaceous. *Nature* **433**, 305-308 (2005).

9 Longrich, N. R., Tokaryk, T. & Field, D. J. Mass extinction of birds at the Cretaceous-Paleogene (K-Pg) boundary. *Proceedings of the National Academy of Sciences* **108**, 15253-15257 (2011).

10 Ksepka, D. T. & Clarke, J. Phylogenetically vetted and stratigraphically constrained fossil calibrations within Aves. *Palaeontologia Electronica* **18.1.3FC**, 1-25, doi:palaeo-electronica.org/content/fc-3 (2015).

11 O'Connor, J. K., Chiappe, L. M. & Bell, A. in *Living Dinosaurs: The evolution of modern birds* (eds G. Dyke & G. Kaiser) 39-114 (Wiley-Blackwell, 2011).

12 Olson, S. L. An early Eocene oilbird from the Green River Formation of Wyoming (Caprimulgiformes: Steatornithidae). *Doc Lab Geol Lyon* **99**, 57-69 (1987).

13 Mayr, G. The Palaeogene Old World potoo Paraprefica Mayr, 1999 (Aves, Nyctibiidae): its osteology and affinities to the New World Preficinae Olson, 1987. *Journal of Systematic Palaeontology* **3**, 359-370 (2005).

14 Nesbitt, S. J., Ksepka, D. T. & Clarke, J. A. Podargiform Affinities of the Enigmatic *Fluvioviridavis platyrhamphus* and the Early Diversification of Strisores ("Caprimulgiformes" + Apodiformes). *PLoS ONE* **6**, e26350, doi:10.1371/journal.pone.0026350.g008 (2011).

15 Mayr, G. The Madagascan "Cuckoo-Roller"(Aves: Leptosomidae) is Not a Roller-Notes on the Phylogenetic Affinities and Evolutionary History of a "Living Fossil". *Acta Ornithologica* **43**, 226-230 (2008).

16 Ksepka, D. T. & Clarke, J. A. Primobucco mcgrewi (Aves: Coracii) from the Eocene Green River Formation: New Anatomical Data from the Earliest Constrained Record of Stem Rollers. *Journal of Vertebrate Paleontology* **30**, 215-225, doi:10.1080/02724630903412414 (2010).

17 Parham, J. F. *et al.* Best practices for justifying fossil calibrations. *Syst Biol* **61**, 346 - 359 (2012).

18 Smith, N. D. & Ksepka, D. T. Five well-supported fossil calibrations within the "Waterbird" assemblage (Tetrapoda, Aves). *Palaeontologia Electronica* **18.1.7FC**, 1-21, doi:palaeo-electronica.org/content/fc-7 (2015).

19 Mayr, G. A tiny barbet-like bird from the Lower Oligocene of Germany: the smallest species and earliest substantial fossil record of the Pici (woodpeckers and allies). *Auk* **122**, 1055-1063 (2005).

20 Mayr, G. First fossil skull of a Paleogene representative of the Pici (woodpeckers and allies) and its evolutionary implications. *Ibis* **148**, 824-827 (2006).

21 Micklich, N. & Parin, N. The fish fauna of Frauenweiler (Middle Oligocene, Rupelian; Germany): First results of a review. *Instituto Español de Oceanografía, Publicaciones Especiales* **21**, 129-148 (1996).

22 Trunkó, L. & Munk, W. Geologische Beobachtungen in drei tertiären Aufschlußkomplexen im Randbereich des Mittleren Rheingrabens. *Carolinea* **56**, 9-28 (1998).

23 Mayr, G. Tiny hoopoe-like birds from the Middle Eocene of Messel (Germany). *Auk* **117**, 968-974 (2000).

24 Mayr, G. New specimens of the Eocene Messelirrisoridae (Aves: Bucerotes), with comments on the preservation of uropygial gland waxes in fossil birds from Messel and the phylogenetic affinities of Bucerotes. *Paleontol Z* **80**, 405-420 (2006).

25 Legendre, S. & Lévêque, F. in *Actes du congrès BiochroM'97.* Vol. 21 (eds Aguilar J. P., S. Legendre, & J. Michaux) 461-473 (Mem Trav Ec Prat Hautes Etudes Inst 1997).

26 Brodkorb, P. An Eocene puffbird from Wyoming. *Rocky Mountain Geology* **9**, 13-15 (1970).

27 Clarke, J. A., Ksepka, D. T., Smith, N. A. & Norell, M. A. Combined phylogenetic analysis of a new North American fossil species confirms widespread Eocene distribution for stem rollers (Aves, Coracii). *Zoological Journal of the Linnean Society* **157**, 586-611, doi:10.1111/j.1096-3642.2009.00550.x (2009).

28 Mayr, G., Mourer-Chauviré, C. & Weidig, I. Osteology and systematic position of the Eocene Primobucconidae (Aves, Coraciiformes *sensu stricto*), with first records from Europe. *J Syst Palaeontol* **2**, 1-12 (2004).

29 Smith, M. E., Caroll, A. R. & Singer, B. S. Synoptic reconstruction of a major ancient lake system: Eocene Green River Formation, western United States. *GSA Bulletin* **120**, 54-85 (2008).

30 Dyke, G. & Cooper, J. H. A new psittaciform bird from the London Clay (Lower Eocene) of England. *Palaeontology* **43**, 271-285 (2000).

31 Mayr, G. On the osteology and phylogenetic affinities of the Pseudasturidae–Lower Eocene stem-group representatives of parrots (Aves, Psittaciformes). *Zoological Journal of the Linnean Society* **136**, 715-729 (2002).

32 Barker, F. K., Dyke, G. & Kaiser, G. *Living Dinosaurs: The Evolutionary History of Modern Birds*. Vol. null (2011).

33 Ksepka, D. T. & Clarke, J. A. A new stem parrot from the Green River Formation and the complex evolution of the grasping foot in Pan-Psittaciformes. *Journal of Vertebrate Paleontology* **32**, 396-406 (2012).

34 Ksepka, D. T., Clarke, J. & Grande, L. Stem parrots (Aves, Halcyornithidae) from teh Green River Formation and a combined phylogeny of Pan-Psittaciformes. *Journal of Paleontology* **85**, 835-854 (2011).

35 King, C. The stratigraphy of the London Clay and associated deposits. *Tertiary Research, Special Paper* **6**, 1-158 (1981).

36 Rhodes, G. M., Ali, J. R., Hailwood, E. A., King, C. & Gibson, T. G. Magnetostratigraphic correlation of Paleogene sequences from northwest Europe and North America. *Geology* **27**, 451-454 (1999).

37 Westerhold, T. *et al.* On the duration of magnetochrons C24r and C25n and the timing of early Eocene global warming events: implications from the Ocean Drilling Program Leg 208 Walvis Ridge depth transect. *Paleoceanography* **22**, PA2201 (2007).

38 Olson, S. L. A lower Eocene frigatebird from the Green River Formation of Wyoming (Pelecaniformes, Fregatidae). *Smithsonian Institution Press* **No. 35** (1977).

39 Smith, N. D. Phylogenetic analysis of Pelecaniformes (Aves) based on osteological data: implications for waterbird phylogeny and fossil calibration studies. *PLoS ONE* **5**, e13354 (2010).

40 Grande, L. & Buchheim, H. P. Paleontological and sedimentological variation in early Eocene Fossil Lake. *Contributions to Geology* **30**, 33-56 (1994).

41 Grande, L. *The Lost World of Fossil Lake: Snapshots from Deep Time*. (University of Chicago Press, 2013).

42 Slack, K. E. *et al.* Early penguin fossils, plus mitochondrial genomes, calibrate avian evolution. *Molecular Biolology and Evolution* **23**, 1144-1155 (2006).

43 Ksepka, D. T., Bertelli, S. & Giannini, N. P. The phylogeny of the living and fossil Sphenisciformes (penguins). *Cladistics* **22**, 412-441 (2006).

44 Clarke, J. A. *et al.* Paleogene equatorial penguins challenge the proposed relationship between biogeography, diversity, and Cenozoic climate change. *Proceedings of the National Academy of Sciences* **104**, 11545 (2007).

45 Cooper, R. A. *The New Zealand Geological Timescale*. (2004).

46 Mayr, G. A chicken-sized crane precursor from the early Oligocene of France. *Naturwissenschaften* **92**, 389-393 (2005).

47 Cavelier, C. in *Synthèse Géologique du Sud-Est de la France* Vol. 125 (ed Debrant-Passard S.) 389-468 (Mémoires BRGM France, 1986).

48 Bourdon, E., Bouya, B. & Iarochene, M. Earliest African neornithine bird: a new species of Prophaethontidae (Aves) from the Paleocene of Morocco. *Journal of Vertebrate Paleontology* **25**, 157-170 (2005).

49 Gheerbrant, E. *et al.* The mammal localities of Grand Daoui Quarries, Ouled Abdoun Basin, Morocco, Ypresian: A first survey. *Bulletin de la Societe Geologique de France* **174**, 279-293 (2003).

50 J., M. *Cenozoic birds of the World. Part 1: Europe*. (Ninox, 2002).

51 Ksepka, D. T., Clarke, J. A., Nesbitt, S. J., Kulp, F. B. & Grande, L. *Fossil evidence of wing shape in a stem relative of swifts and hummingbirds (Aves, Pan-Apodiformes)*. Vol. 280 (2013).

52 Mayr, G. PHYLOGENY OF EARLY TERTIARY SWIFTS AND HUMMINGBIRDS (AVES: APODIFORMES). *The Auk* **120**, 145, doi:10.1642/0004-8038(2003)120[0145:POETSA]2.0.CO;2 (2003).

53 Harrison, C. J. O. A revision of the fossil swifts (Vertebrata, Aves, suborder Apodi), with descriptions of three new genera and two new species. *Mededelingen van de Werkgroep voor Tertiaire en Kwartaire Geologie* **21**, 157-177 (1984).

54 Heilmann-Clausen, C., B., N. O. & Gersner, F. Lithostratigraphy and depositional environments in the Upper Paleocene and Eocene of Denmark. *Bulletin of the Geological Society of Denmark* **33**, 287-323 (1984).

55 Schnetler, K. I. & Heilmann-Clausen, C. The molluscan fauna of the Eocene Lillebælt Clay, Denmark. *Cainozoic Research* **8**, 41-99 (2011).

56 Sheldon, E., Gravesen, P. & Nøhr-Hansen, H. Geology of the Femern Bælt area between Denmark and Germany. *Geological Survey of Denmark and Greenland Bulletin* **26**, 13-16 (2012).

57 Mayr, G. *Paleogene Fossil Birds*. Vol. null (2009).

58 Mayr, G. & Bertelli, S. A record of Rhynchaeites (Aves, Threskiornithidae) from the early Eocene Fur Formation of Denmark, and the affinities of the alleged parrot Mopsitta. *Palaeobiodiversity and Palaeoenvironments* **91**, 229-236 (2011).

59 Peters, D. S. Die "Schnepfenralle" *Rhynchaeites messelensis* Wittich 1898 ist ein Ibis. *Journal für Ornithologie* **124**, 1-27 (1983).

60 Mayr, G. A contribution to the osteology of the middle Eocene ibis *Rhynchaeites messelensis* (Aves: Threskiornithidae: Rehynchaeitinae nov. sub-fam.). *Neues Jahrbuch für Geologie und Paläontologie, Monatshefte* **2002**, 501-512 (2002).

61 Chambers, L. M. *et al.* in *Abstracts of the EGS-AGU-EUG Joint Assembly.* (2003).

62 Houde, P. & Olson, S. L. in *Papers in avian paleontology honoring Pierce Brodkorb* Vol. 36 (ed K. E. Campbell) 137-160 (Nat Hist Mus Los Angeles Cty Sci Ser, 1992).

63 Ksepka, D. T. & Clarke, J. A. Affinities of *Palaeospiza bella* and the Phylogeny and Biogeography of Mousebirds (Coliiformes). *The Auk* **126**, 245-259 (2009).

64 Mayr, G. & Mourer-Chauviré, C. Unusual tarsometatarsus of a mousebird from the Paleogene of France and the relationships of *Selmes* Peters, 1999. *Journal of Vertebrate Paleontology* **24**, 366-372 (2004).

65 Zelenkov, N. V. & Dyke, G. The fossil record and evolution of mousebirds (Aves: Coliiformes). *Palaeontology* **51**, 1403-1418 (2008).

66 Ksepka, D. T. & Clarke, J. A. New fossil mousebird (Aves: Coliiformes) with feather preservation provides insight into the ecological diversity of an Eocene North American avifauna. *Zoological Journal of the Linnean Society* **160**, 684-706 (2010).

67 Secord, R. *et al.* Geochronology and mammalian biostratigraphy of middle and upper Paleocene continental strata, Bighorn Basin, Wyoming. *American Journal of Science* **306**, 211-245 (2006).

68 Mayr, G. Coraciiforme" und "piciforme" Kleinvögel aus dem Mittel-Eozän der Grube Messel (Hessen, Deutschland). *Cour Forsch Inst Senckenberg* **205**, 1-101 (1998).

69 Mayr, G. New specimens of *Hassiavis laticauda* (Aves: Cypselomorphae) and *Quasisyndactylus longibrachis* (Aves: Alcediniformes) from the Middle Eocene of Messel, Germany. *Cour Forsch Inst Senckenberg* **252**, 23-28 (2004).

70 Mayr, G. & Knopf, C. A tody (Alcediniformes, Todidae) from the early Oligocene of Germany. *The Auk* **124**, 1294-1304 (2007).

71 Olson, S. L. Oligocene fossils bearing on the origins of the Todidae and the Momotidae (Aves: Coraciiformes). *Smithsonian Contributions to Paleobiology* **27**, 111-119 (1976).

72 C., M.-C. Les Todidae (Aves, Coraciiformes) des Phosphorites du Quercy (France). *Proc K Ned Akad Wet B* **88**, 407-414 (1985).

73 Mayr, G. A small representative of the Phalacrocoracoidea (cormorants and anhingas) from the late Oligocene of Germany. *Condor* **109**, 929-942 (2007).

74 Mayr, G. A new skeleton of the late Oligocene "Enspel cormorant"—from Oligocorax to Borvocarbo, and back again. *Palaeobiodiversity and Palaeoenvironments* **95**, 87-101, doi:10.1007/s12549-014-0167-7 (2015).

75 Mertz, D. F., Renne, P. R., Wuttke, M. & Mödden, C. A numerically calibrated reference level (MP28) for the terrestrial mammal-based biozonation of the European Upper Oligocene. *International Journal of Earth Sciences* **96**, 353-361 (2007).

76 Olson, S. L. in *Papers in avian paleontology honoring Pierce Brodkorb* Vol. 36 (ed Kenneth E. Campbell) 137-160 (Natural History Museum of Los Angeles County Science Series, 1992).

77 Field, D. J. & Hsiang, A. Y. Nearctic origins of the 'endemic' African avifauna? The necessity of fossils for avian historical biogeography. *Journal of Vertebrate Paleontology, Program and Abstracts*, 129 (2014).

78 Grande, L. Paleontology of the Green River Formation, with a review of the fish fauna. *BUlletin of the Geological Survey of Wyoming* **63**, 1-333 (1984).

79 Ksepka, D. T. Broken gears in the avian molecular clock: new phylogenetic analyses support stem galliform status for *Gallinuloides wyomingensis* and rallid affinities for *Amitabha urbsinterdictensis*. *Cladistics* **25**, 173-197 (2009).

80 Mayr, G. & Weidig, I. The early Eocene bird Gallinuloides wyomingensis – a stem group representative of Galliformes. *Acta Palaeontologica Polonica* **49**, 211-217 (2004).

81 Mayr, G. Reappraisal of *Eocypselus* - a stem group apodiform from the Early Eocene of northern Europe. *Palaeobiodiversity and Palaeoenvironments* **9**, 395-403 (2010).

82 Hackett, S. J. *et al.* A phylogenomic study of birds reveals their evolutionary history. *Science* **320**, 1763-1768 (2008).

83 Yuri, T. *et al.* Parsimony and model-based analyses of indels in avian nuclear genes reveal congruent and incongruent phylogenetic signals. *Biology* **2**, 419-444., doi:doi:10.3390/biology2010419 (2013).

84 Baker, A. J., Haddrath, O., McPherson, J. D. & Cloutier, A. Genomic support for a moa-tinamous clade and adpative morphological convergence in flightless ratites. *Molecular Biology and Evolution* **31**, 1686-1696 (2014).

85 Kimball, R. T., Wang, N., Heimer-McGinn, V., Ferguson, C. & Braun, E. L. Identifying localized biases in large datasets: A case study using the avian tree of life. *Molecular Phylogenetics and Evolution* **69**, 1021-1032, doi:doi.org/10.1016/j.ympev.2013.05.029 (2013).

86 Harshman, J. *et al.* Phylogenomic evidence for multiple losses of flight in ratite birds. *Proceedings of the National Academy of Science* **105**, 13462-13467, doi:doi:10.1073/pnas.0803242105 (2008).

87 Barrowclough, G. F., Groth, J. G. & Mertz, L. A. The RAG-1 exon in the avian order Caprimulgiformes: Phylogeny, heterozygosity, and base composition. *Molecular Phylogenetics and Evolution* **41**, 238-248 (2006).

88 McGuire, J. A. *et al.* Molecular phylogenetic and diversification of hummingbirds. *Current Biology* **24**, 1-7 (2014).

89 Sorenson, M. D. & Payne, R. B. in *The Cuckoos* (ed R. B. Payne) 68-94 (Oxford University Press, 2005).

90 Johnson, K. P. & Clayton, D. H. Nuclear and mitochondrial genes contain similar phylogenetic signal for pigeons and doves (Aves: Columbiformes). *Molecular Phylogenetics and Evolution* **14**, 141-151 (2000).

91 Pereira, S. L., Johnson, K. P., Clayton, D. H. & Baker, A. J. Mitochondrial and nuclear DNS sequences support a Cretaceous origin of Columbiformes anda dispersal-driven radiation in the Paleogne. *Syst. Biol.* **56**, 656-672, doi:DOI: 10.1080/10635150701549672 (2007).

92 Ericson, P. G. P. *et al.* Diversification of Neoaves: integration of molecular sequence data and fossils. *Biology Letters* **2**, 543-547, doi:doi: 10.1098/rsbl.2006.0523 (2006).

93 Baker, A. J., Pereira, S. L. & Paton, T. A. Phylogenetic relationships and divergence times of Charadriiformes genera: multigene evidence for the Cretaceous origin of at least 14 clades of shorebirds. *Biology Letters* **3**, 205-209, doi:doi:10.1098/rsbl.2006.0606 (2007).

94 Mayr, G. Metaves, Mirandornithes, Strisores and other novelties – a critical review of the higher-level phylogeny of neornithine birds. *Journal of Zoological Systematics and Evolutionary Research* **49**, 58-76, doi:DOI: 10.1111/j.1439-0469.2010.00586.x (2011).

95 Welch, A. J., Olson, S. L. & Fleischer, R. C. Phylogenetic relationships of the extinct St. Helena petrel, *Pterodroma rupinarum* Olson, 1975 (Procellariiformes: Procelariidae), based on ancient DNA. *Zoological Journal of the Linnean Society* **170**, 494-505 (2014).

96 Penhallurick, J. & Wink, M. Analysis of the taxonomy and nomenclature of the Procellariiformes based on complete nucleotide squences of the mitochondrial cytochrome *b* gene. *Emu* **104**, 125-147 (2004).

97 McCormack, J. E. *et al.* A phylogeny of birds based on over 1,500 loci collected by target enrichment and high-throughput sequencing. *PLoS One* **ci**, doi:10.1371/journal.pone.0054848 (2013).

98 Griffths, C. S., Barrowclough, G. F., Groth, J. G. & Mertz, L. A. Phylogeny, diversity, and classification of the Accipitridae based on DNA sequences of the RAG-1 exon. *Journal of Avian Biology* **38**, 587-602 (2007).

99 Swierczewski, E. V. & Raikow, R. J. Hind limb mophology, phylogeny, and classification of the Piciformes. *Auk* **98**, 466-480 (1981).

100 Moyle, R. G. Phylogenetics of barbets (Aves: Piciformes) based on nuclear and mitochondrial DNA sequence data. *Molecular Phylogenetics and Evolution* **30**, 187-200, doi:doi:10.1016/S1055-7903(03)00179-9 (2004).

101 Ericson, P. G. P. Evolution of terrestrial birds in three continents: biogeography and parallel radiations. *Journal of Biogeography* **39**, 813-824, doi:doi:10.1111/j.1365-2699.2011.02650.x (2012).

102 Griffiths, C. S., Barrowclough, G. F., Groth, J. G. & Mertz, L. A. Phylogeny of the Falconidae (Aves): a comparison of the efficacy of morphological, mitochondrial, and nuclear data. *Molecular Phylogenetics and Evolution* **32**, 101-109, doi:doi:10.1016/j.ympev.2003.11.019 (2004).

103 Wright, T. F. *et al.* A multilocus molecular phylogeny of the parrots (Psittaciformes): support for a gondwanan origin during the Cretaceous. *Molecular Biology and Evolution* **25**, 2141–2156, doi:doi:10.1093/molbev/msn160 (2008).

104 Raikow, R. J. Hindlimb myology and evolution of the Old World suboscine passerine birds. *Ornithological Monographs* **41**, 1-81 (1987).

105 Prum, R. O. Phylogeny, biogeography, and evolution of the broadbills (Eurylaimidae) and asities (Philepittidae) based on morphology. *Auk* **110**, 304-324 (1993).

106 Moyle, R. G., Chesser, R. T., Prum, R. O., Schikler, P. & Cracraft, J. Phylogeny and evolutionary history of the Old World suboscine birds (Aves: Eurylaimides). *American Museum Novitates* **3544**, 1-22 (2006).

107 Moyle, R. G. *et al.* Phylogeny and phylogenetic classification of the antbirds, ovenbirds, woodcreepers, and allies (Aves: Passeriformes: infraorder Furnariides). *Cladistics* **25**, 386-405 (2009).

108 Ohlson, J. I., Irestedt, M., Ericson, P. G. P. & Fjeldså, J. Phylogeny and classification of the New World suboscines (Aves, Passeriformes). *Zootaxa* **3613**, 1-35 (2013).

109 Bravo, G. A., Remsen Jr., J. V., Whitney, B. M. & Brumfield, R. T. DNA sequence data reveal a subfamily-level divergence within the Thamnophilidae (Aves: Passeriformes). *Molecular Phylogenetics and Evolution* **65**, 287-293, doi:doi.org/10.1016/j.ympev.2012.06.016 (2012).

110 Tello, J. G., Moyle, R. G., Marchese, D. J. & Cracraft, J. Phylogeny and phylogenetic classification of the tyrant flycatchers, cotingas, manakins, and their allies (Aves: Tyrannides). *Cladistics* **25**, 429-467 (2009).

111 Berv, J. S. & Prum, R. O. A comprehensive multilocus phylogeny of the Neotropical cotingas (Cotingidae, Aves) with a comparative evolutionary analysis of breeding system and plumage dimorphism and a revised phylogenetic classification. *Molecular Phylogenetics and Evolution* **81**, 120-136, doi:doi.org/10.1016/j.ympev.2014.09.001 (2014).

112 Prum, R. O., Rice, N. H., Mobley, J. A. & Dimmick, W. W. A preliminary phylogenetic hypothesis for the cotingas (Cotingidae) based on mitochondrial DNA. *Auk* **117**, 236-241 (2000).

113 McKay, B. D., Barker, F. K., Mays, H. L., Jr., Doucet, S. M. & Hill, G. E. A molecular phylogenetic hypothesis for the manakins (Aves: Pipridae). *Molecular Phylogenetics and Evolution* **55**, 733-737, doi:doi:10.1016/j.ympev.2010.02.024 (2010).

114 Ohlson, J. I., Fjeldså, J. & Ericson, P. G. P. Molecular phylogeny of the manakins (Aves: Passeriformes: Pipridae), with a new classifcation and description of a new genus. *Molecular Phylogenetics and Evolution* **69**, 796-804, doi:doi.org/10.1016/j.ympev.2013.06.024 (2013).

115 Barker, F. K., Cibois, A., Schikler, P., Felsenstein, J. & Cracraft, J. Phylogeny and diversification of the largest avian radiation. *Proceedings of the National Academy of Sciences of the United States of America* **101**, 11040-11045 (2004).

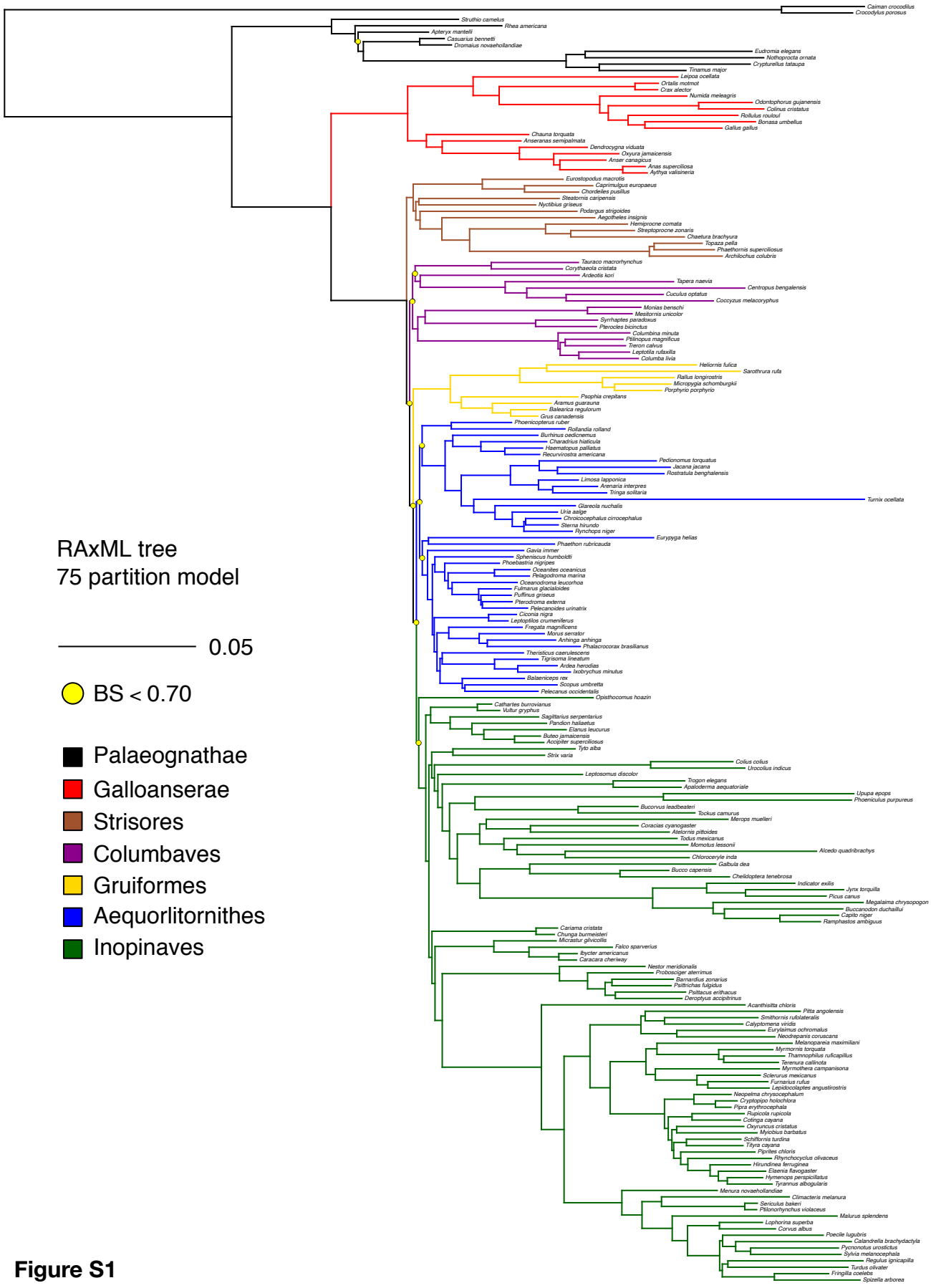
RAxML tree
75 partition model
0.05
BS < 0.70
Palaeognathae
Galloanserae
Strisores
Columbaves
Gruiformes
Aequorlitornithes
Inopinaves

Figure S1

Figure S1. Concatenated RAxML Tree. The RAxML phylogeny estimated using the 75 partition model and 100 bootstrap replicates. Branch lengths are proportional to substitutions/site, and low support nodes are highlighted in yellow. Various clades are colored according to our classification scheme: Palaeognathae (**black/gray**), Galloanserae (**red**) Strisores (**brown**), Columbaves (**purple**), Gruiformes (**yellow**), Aequorlitornithes (**blue**), and Inopinaves (**green**).

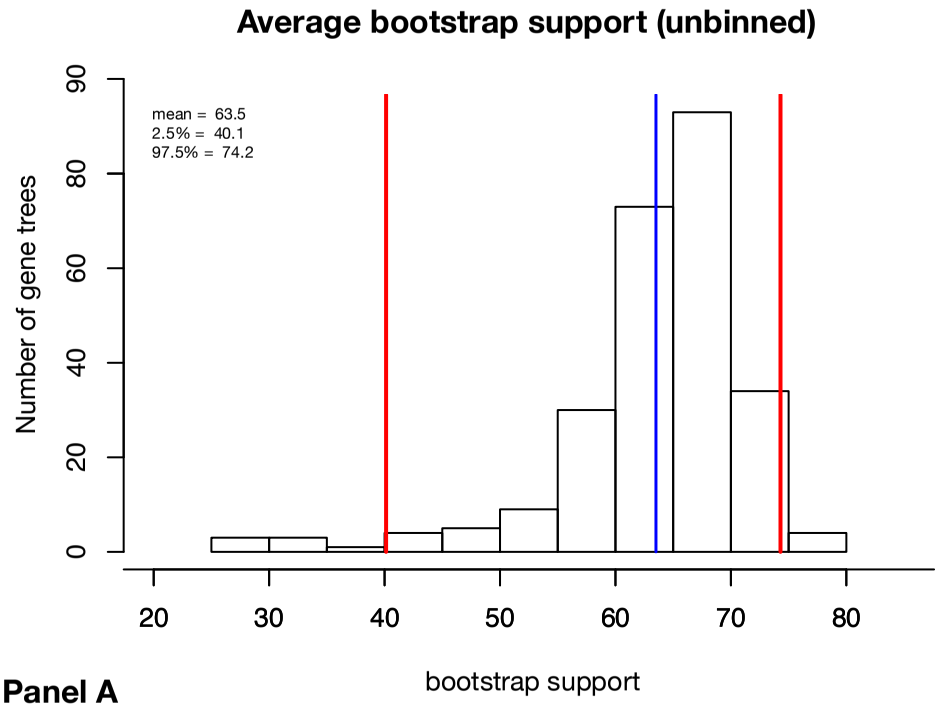

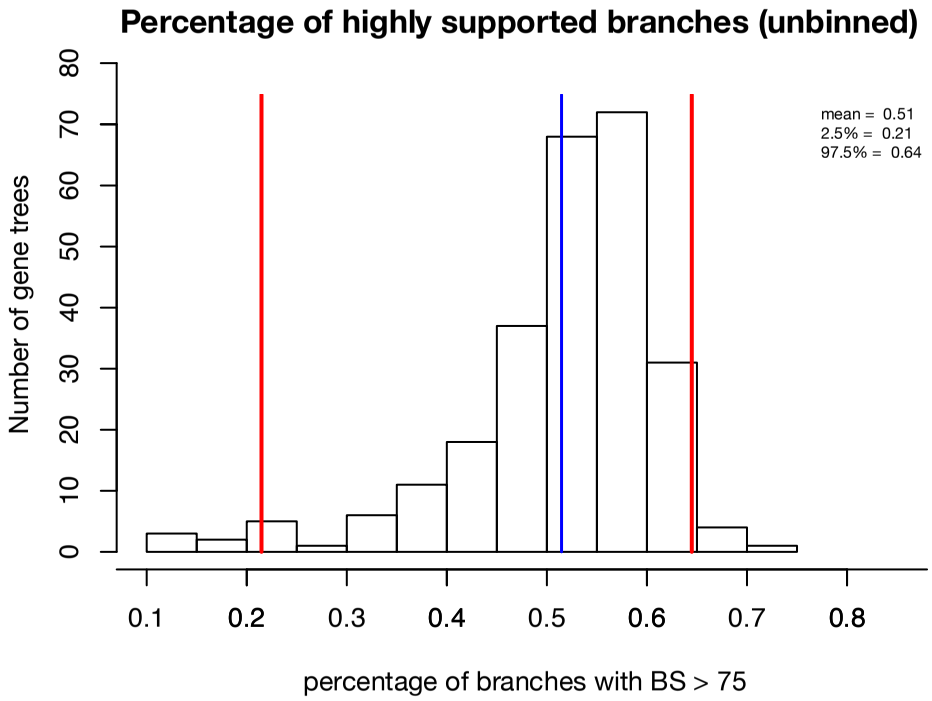

Panel A

Panel B

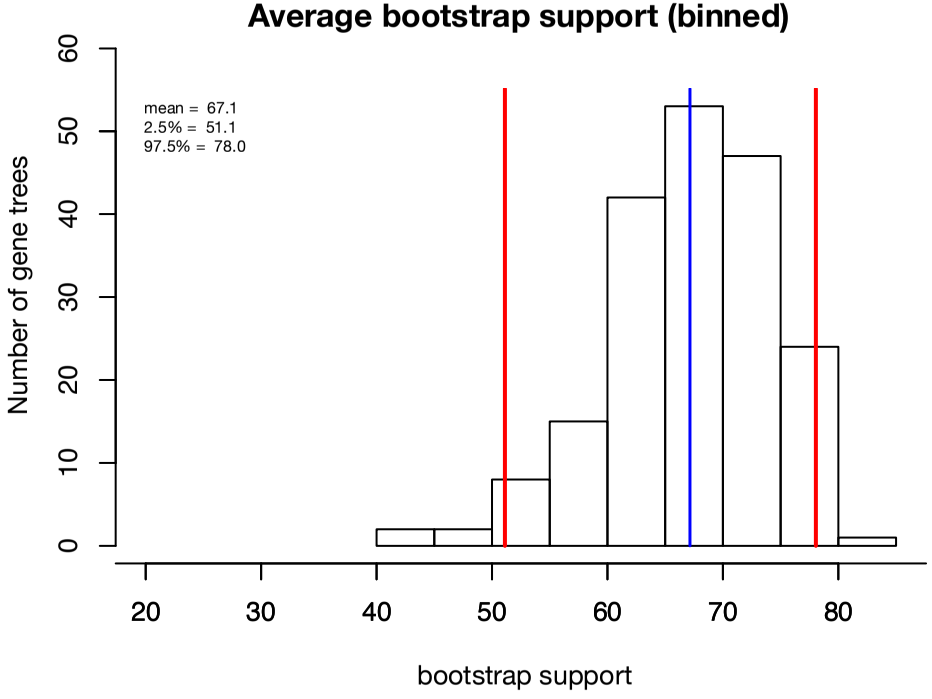

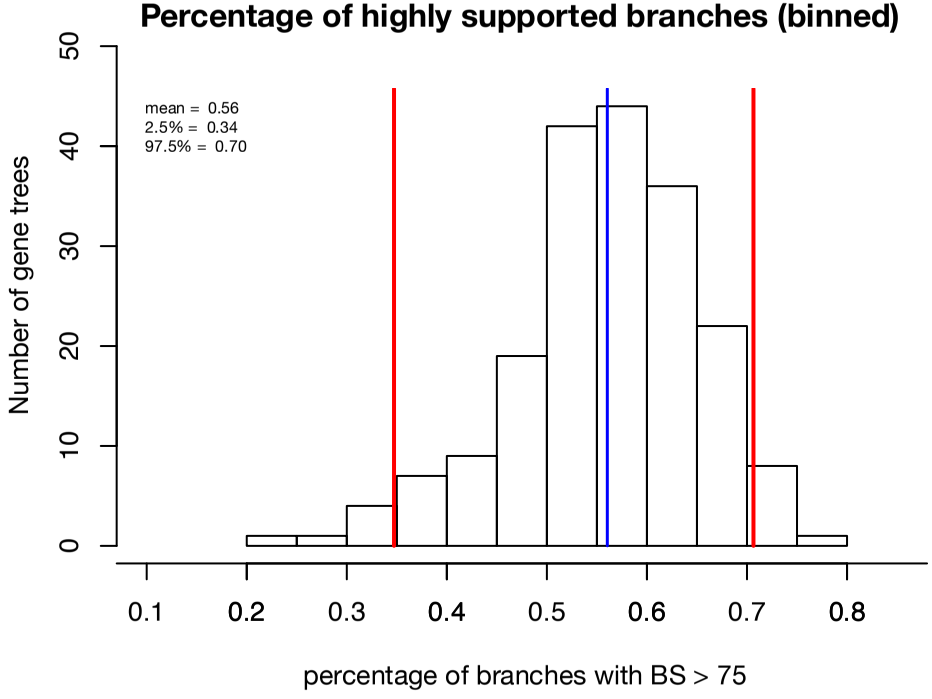

Figure S2

Figure S2. Statistical binning and bootstrap support. Histograms of average bootstrap support and the percentage of highly supported nodes across individual loci. (**A**) distributions for unbinned loci. Most loci have high average bootstrap support (~70), and most loci have a high percentage (~55%) of branches with bootstrap support > 75. (**B**) loci after binning with a bootstrap threshold of 75. Most supergenes have high average bootstrap support (~70), but the low-support tail of the distribution (**A**) has been eliminated. Most supergenes have a high percentage (~60%) of branches with bootstrap support >75.

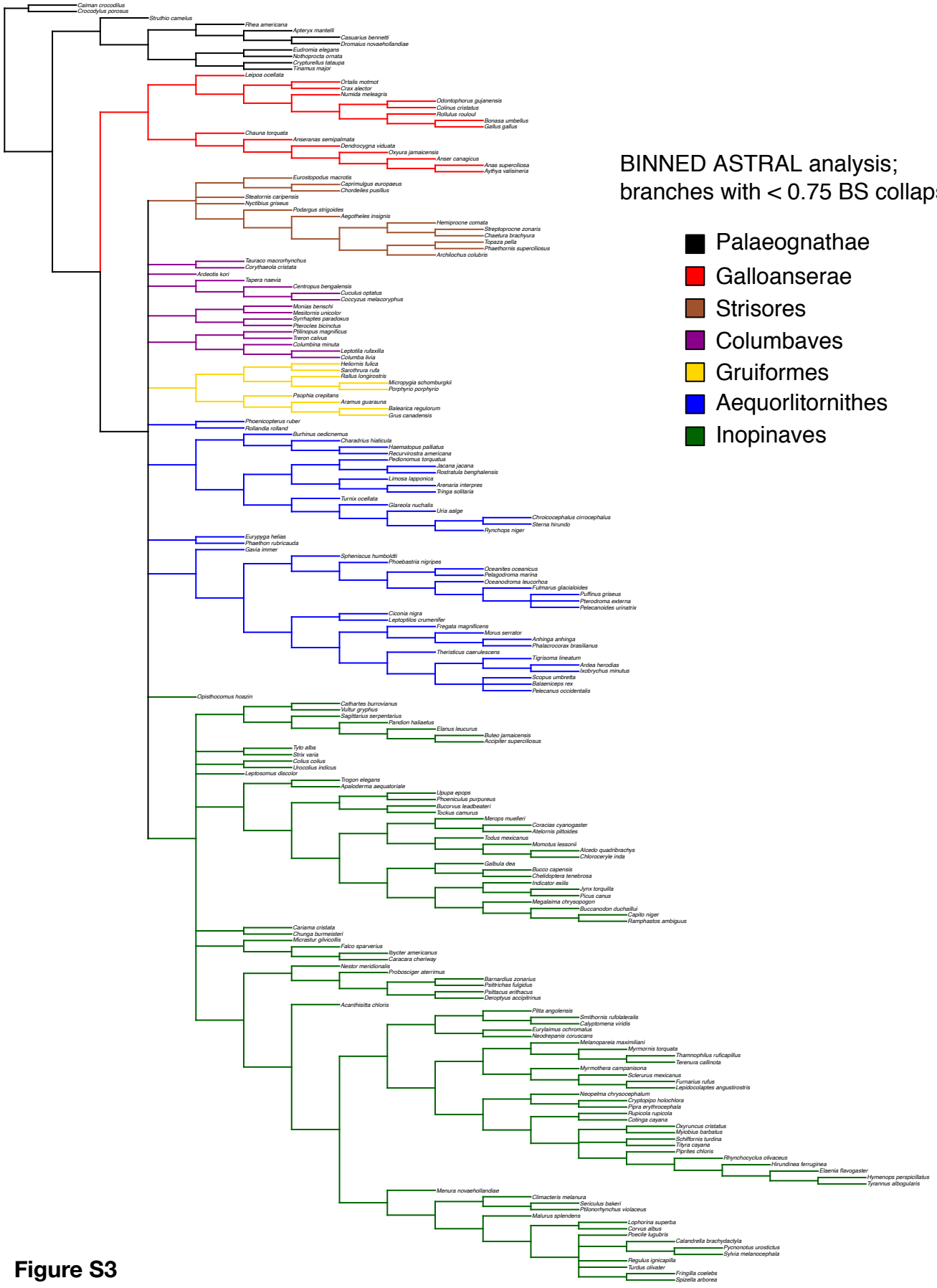

BINNED ASTRAL analysis;
branches with < 0.75 BS collapsed

- Palaeognathae
- Galloanserae
- Strisores
- Columbaves
- Gruiformes
- Aequorlitornithes
- Inopinaves

Figure S3

Figure S3. Binned ASTRAL Tree. Coalescent species tree generated with the (weighted) binned ASTRAL algorithm, with low support branches collapsed (< 75 bootstrap support). Various clades are colored according to our classification scheme: Palaeognathae (**black/gray**), Galloanserae (**red**) Strisores (**brown**), Columbaves (**purple**), Gruiformes (**yellow**), Aequorlitornithes (**blue**), and Inopinaves (**green**).

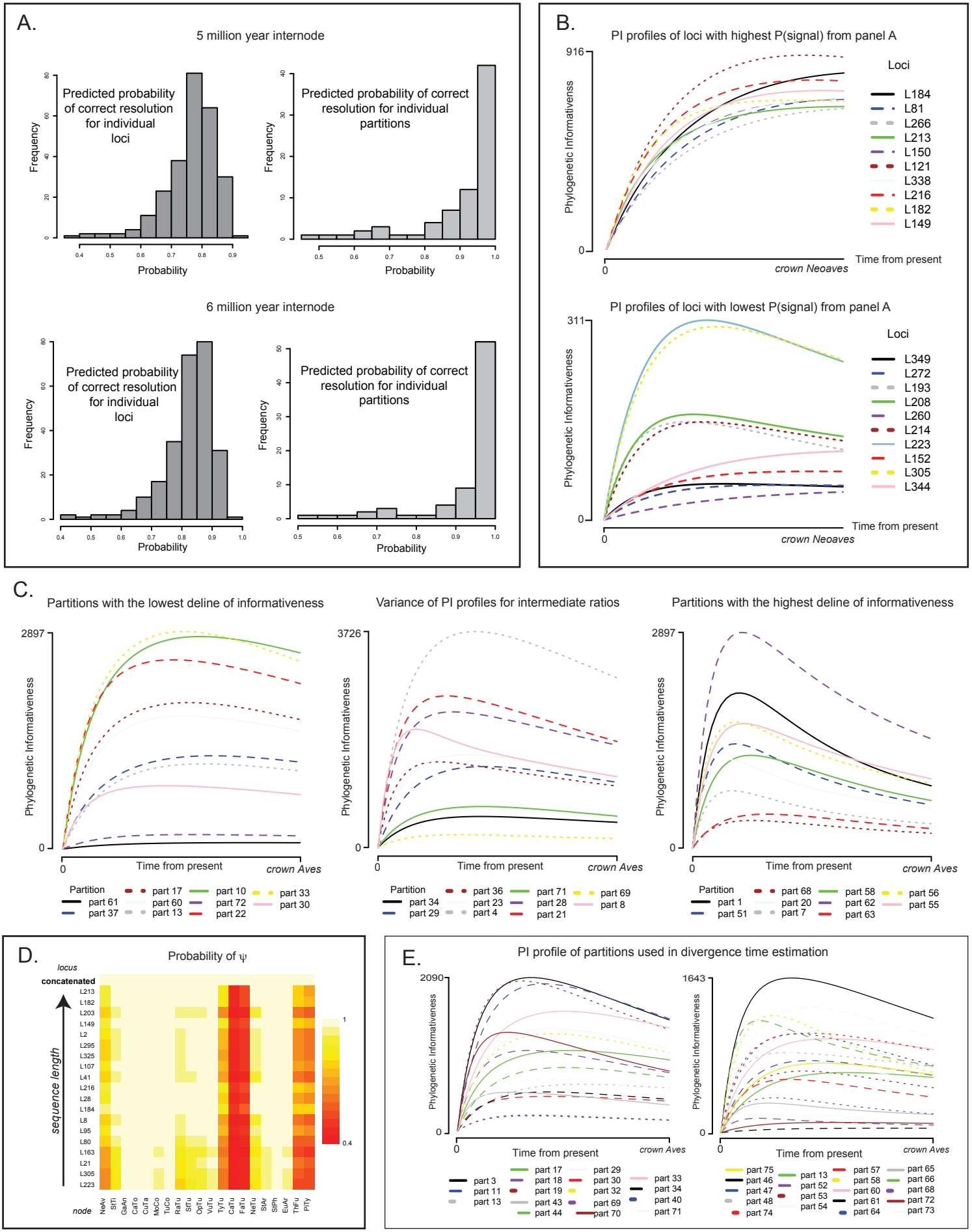
A.
5 million year internode
Predicted probability of correct resolution for individual loci
Predicted probability of correct resolution for individual partitions
Frequency
Probability
6 million year internode
B.
PI profiles of loci with highest P(signal) from panel A
Phylogenetic Informativenss
Loci
L184
L81
L266
L213
L150
L121
L338
L216
L182
L149
Time from present
crown Neoaves
PI profiles of loci with lowest P(signal) from panel A
L349
L272
L193
L208
L260
L214
L223
L152
L305
L344
C.
Partitions with the lowest deline of informativeness
Variance of PI profiles for intermediate ratios
Partitions with the highest deline of informativeness
Phylogenetic Informativeness
Time from present
crown Aves
Partition
part 61
part 37
part 17
part 60
part 13
part 10
part 72
part 22
part 33
part 30
part 36
part 34
part 29
part 23
part 4
part 71
part 28
part 21
part 69
part 8
part 1
part 51
part 68
part 20
part 7
part 58
part 62
part 63
part 56
part 55
D.
Probability of ψ
locus
concatenated
sequence length
node
E.
PI profile of partitions used in divergence time estimation
part 3
part 11
part 13
part 17
part 18
part 19
part 43
part 44
part 29
part 30
part 32
part 69
part 70
part 33
part 34
part 40
part 71
part 75
part 46
part 47
part 48
part 74
part 13
part 52
part 53
part 54
part 57
part 58
part 60
part 61
part 64
part 65
part 66
part 68
part 72
part 73

Figure S4

Figure S4. Analyses of phylogenetic informativeness of the loci captured by anchored hybrid enrichment of 198 bird species. **A**) Values of ψ of all individual loci and combinations of loci assigned to partitions by PartitionFinder for the crown of Neoaves given relative divergences corresponding to approximate internode lengths between 5 and 6 million years. **B**) Visualizations of PI profiles for the loci with the highest and lowest values of ψ. **C**) PI profiles for loci that span the variance of ratios in the PI of crown of Neoaves to Crown Aves, with low ratios corresponding to the highest decline in informativeness. **D**) Probability of ψ of individual loci that span the range of locus lengths and the concatenated dataset for focal nodes: NeAv= most recent common ancestor (MRCA) Neoaves; StTi= MRCA of *Struthio* and *Tinamus*; GaAn = MRCA of *Gallus* and *Anas*; CaTo = MRCA of *Caprimulgus* and *Topaza*; CuTa = MRCA of *Cuculus* and *Tauraco*; MoCo = MRCA of *Monias* and *Columba*; TuCo = MRCA of *Tauraco* and *Columba*; RaTu = MRCA of *Rallus* and *Turdus*; StTu = MRCA of *Sterna* and *Turdus*; OpTu = MRCA of *Opisthocomus* and *Turdus*; VuTu = MRCA of *Vultur* and *Turdus*; TyTu = MRCA of *Tyto* and *Turdus*; CaTu = MRCA of *Cariama* and *Turdus*; FaTu = MRCA of *Falco* and *Turdus*; NeTu = MRCA of *Nestor* and *Turdus*; StAr = MRCA of *Sterna* and *Ardea*; StPh = MRCA of *Sterna* and *Phoenicopterus*; EuAr = MRCA of *Eurypyga* and *Ardea*; ThFu = MRCA of *Thamnophilus* and *Furnarius*; and PiTy = MRCA of *Pitta* and *Tyrannus*. **E**) PI profiles of dataset partitions used in divergence time estimation.

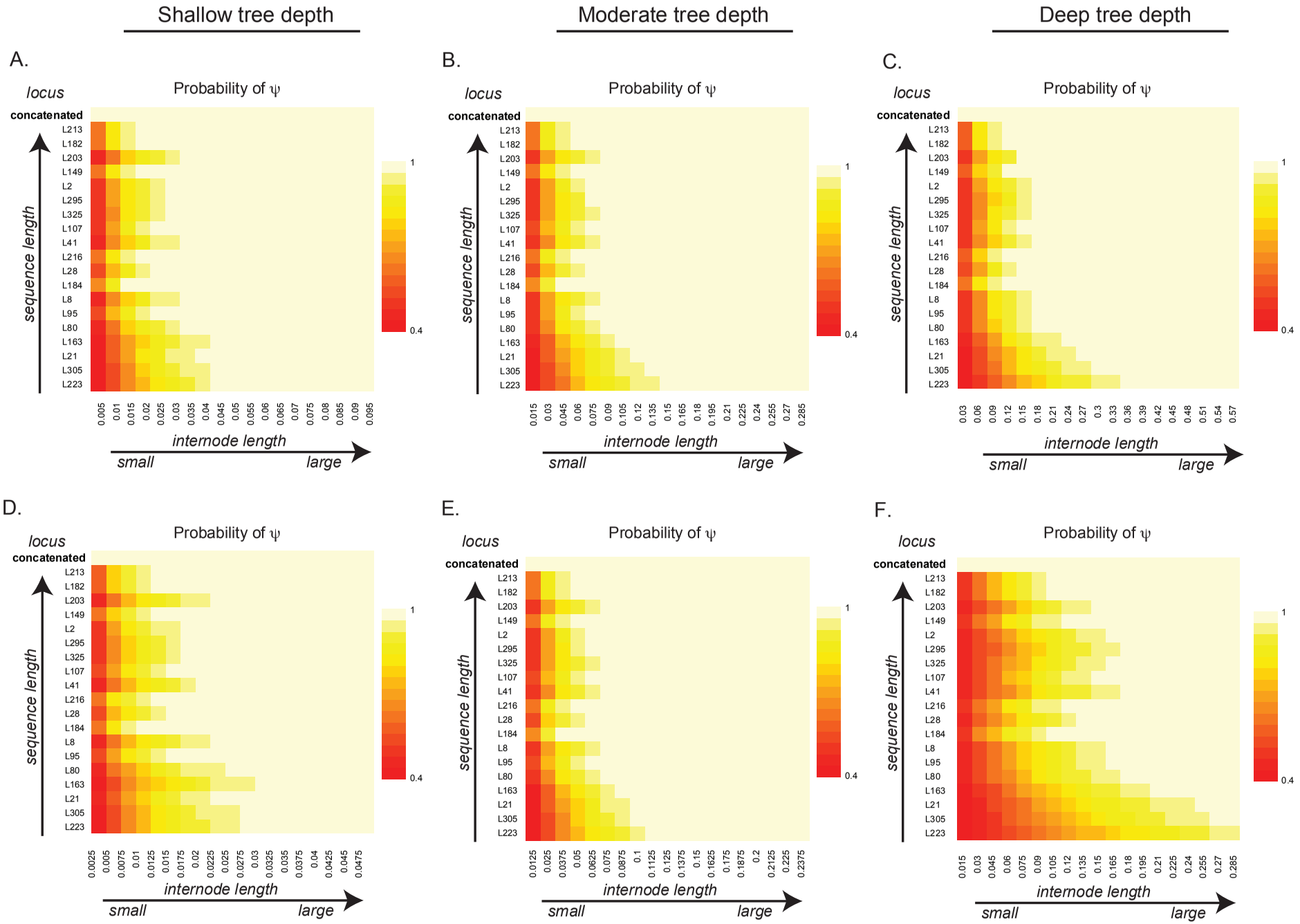
Shallow tree depth
Moderate tree depth
Deep tree depth
A.
B.
C.
D.
E.
F.
locus
concatenated
sequence length
Probability of ψ
internode length
small
large
1
0.4

Figure S5

Figure S5. Calculations of ψ values for individual loci sorted by the number of nucleotides that span the range of locus lengths and the concatenated dataset for hypothetical nodes. ψ values were quantified for a range of internode distances across a set range of tree depths: **A**) a shallow divergence occurring at 10% of the total depth, **B**) a divergence occurring at 30% of the total tree depth, **C**) a divergence occurring at 60% of the total tree depth, **D**) a divergence occurring at 5% of the total tree depth, **E**) a divergence occurring at 25% of the total tree depth, and **F**) a divergence occurring at 60% of the total tree depth with a fifty percent reduction in the range of internode distances relative to those in A.

Avian Time Tree

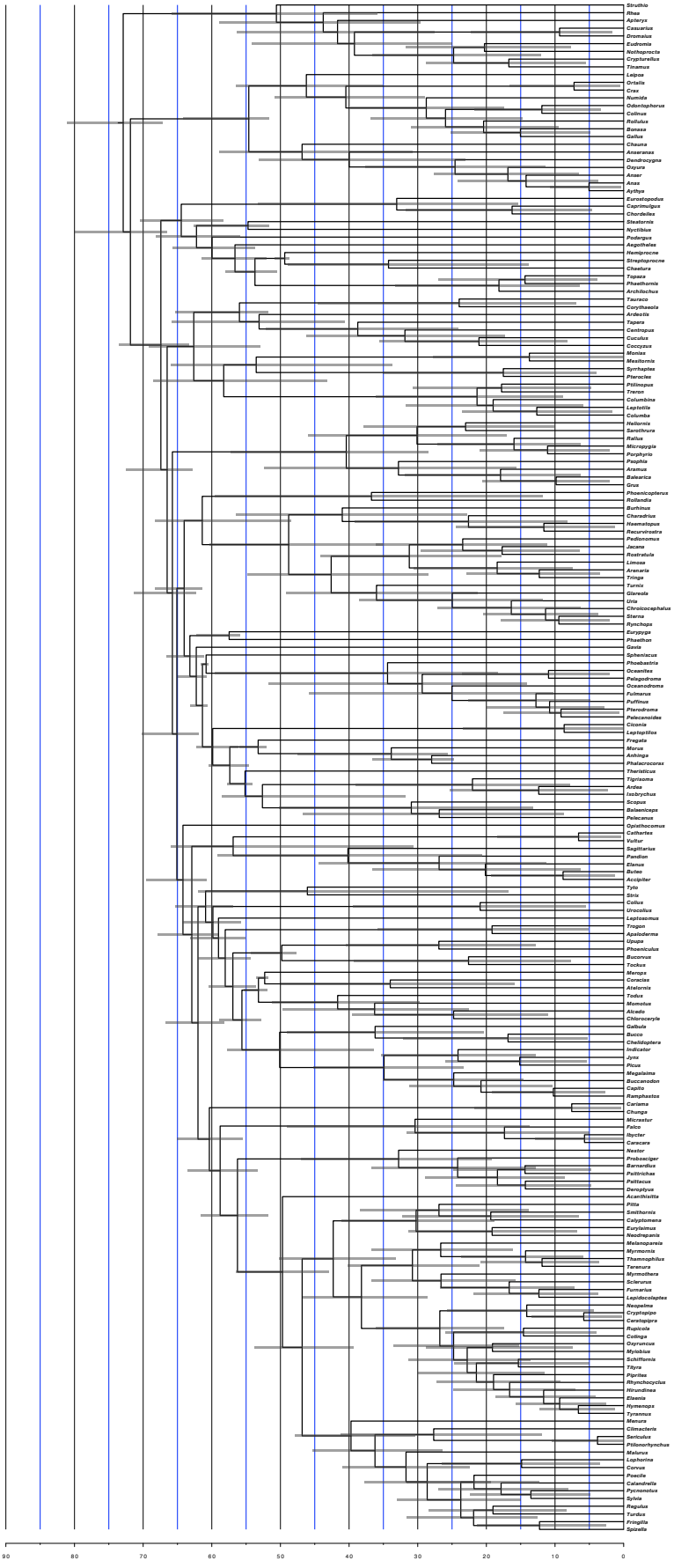

Figure S6

WWW.NATURE.COM/NATURE/S2

Figure S6. Time calibrated Bayesian Tree. The final calibrated analysis (median ages) of the ExaBayes topology and 36 data partitions (see supplemental text), shown here with error bars at each node indicating the 95% HPD confidence intervals. For an alternative calibration analysis that includes the fossil *Vegavis,* see Fig. S12.

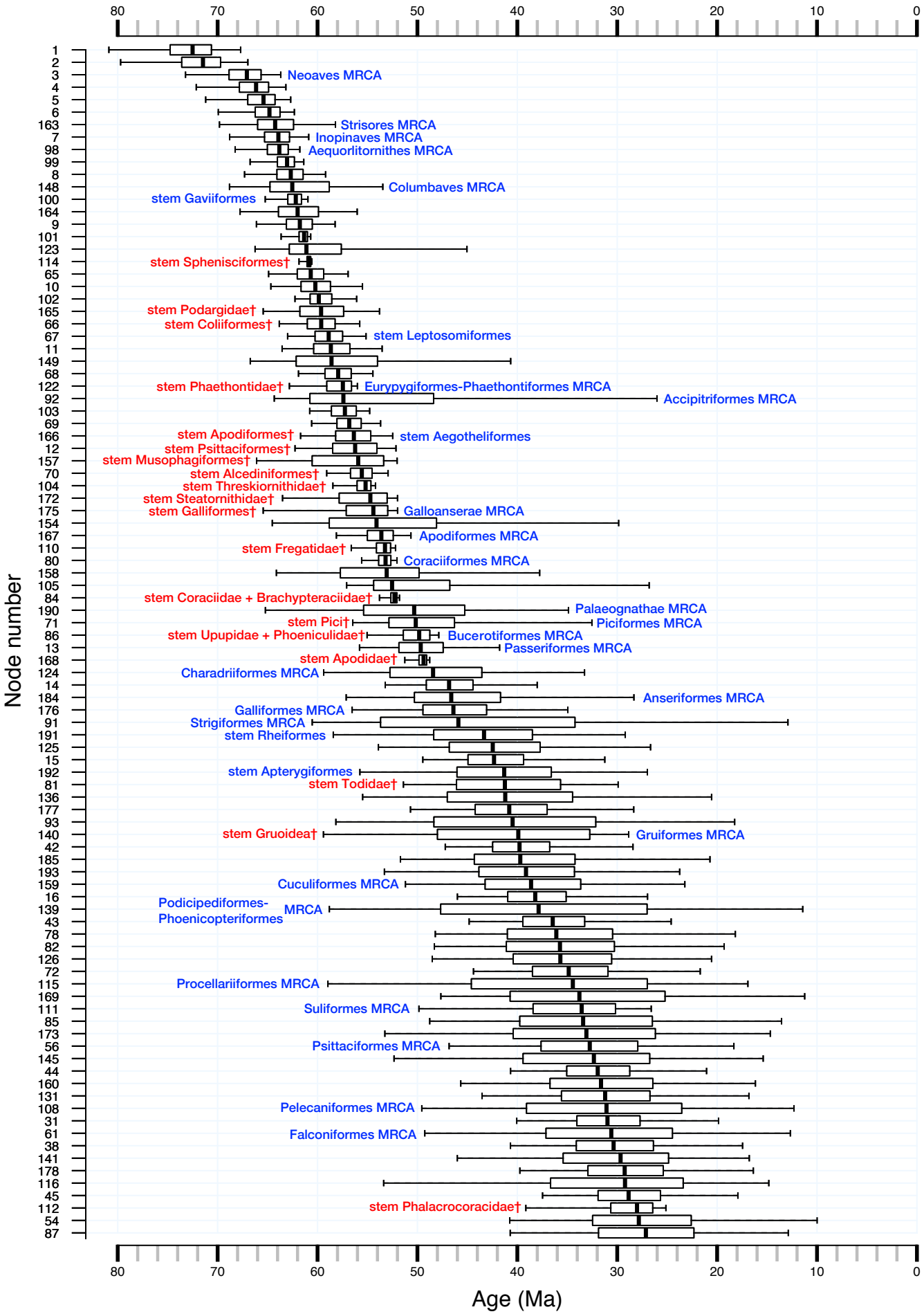

Figure S7 - Page 1

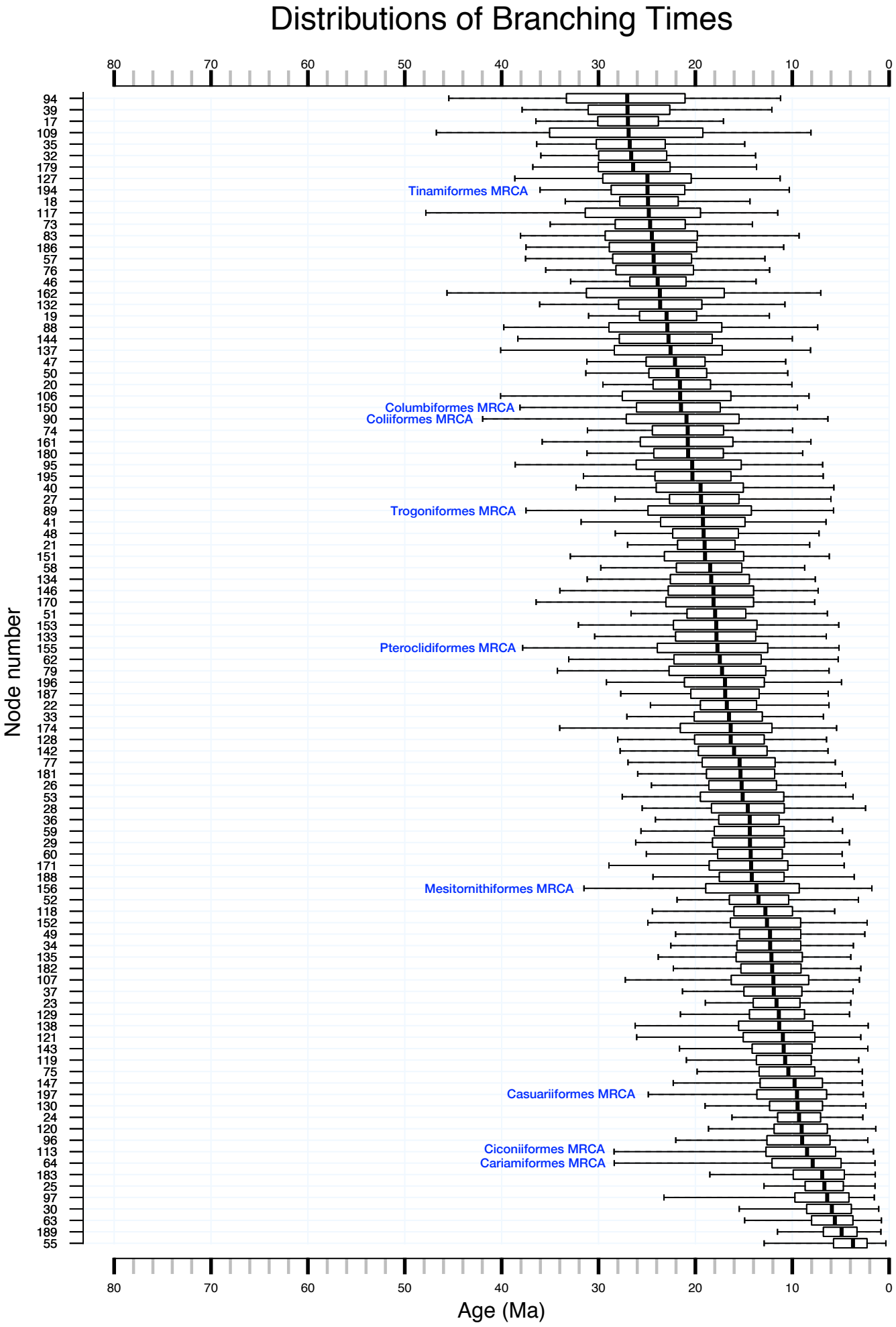

Figure S7 - Page 2

Figure S7. Posterior distributions of estimated node ages. Node numbers on the left margin refer to nodes in the Bayesian tree (Fig. 1). Boxplots represent the posterior distribution of node ages across the summarized distribution of trees from the dating analysis. Whisker lines represent 2.5 and 97.5 percentiles, while the inner box represents the interquartile range and median. Fossil calibrated nodes are labeled in red, and other key nodes at the interordinal level are labeled in blue.

RaxML re-analysis
Lineages sampled to match Jarvis et. al. 2014

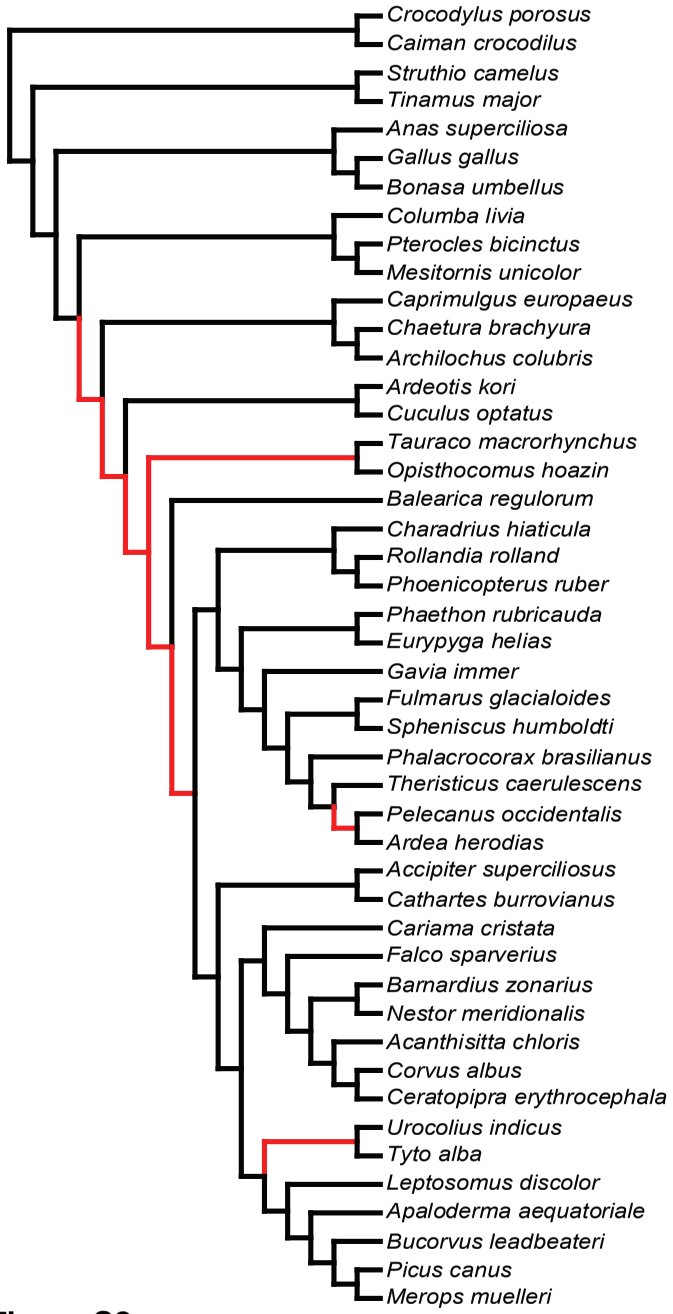

Low support branches collapsed (<75)

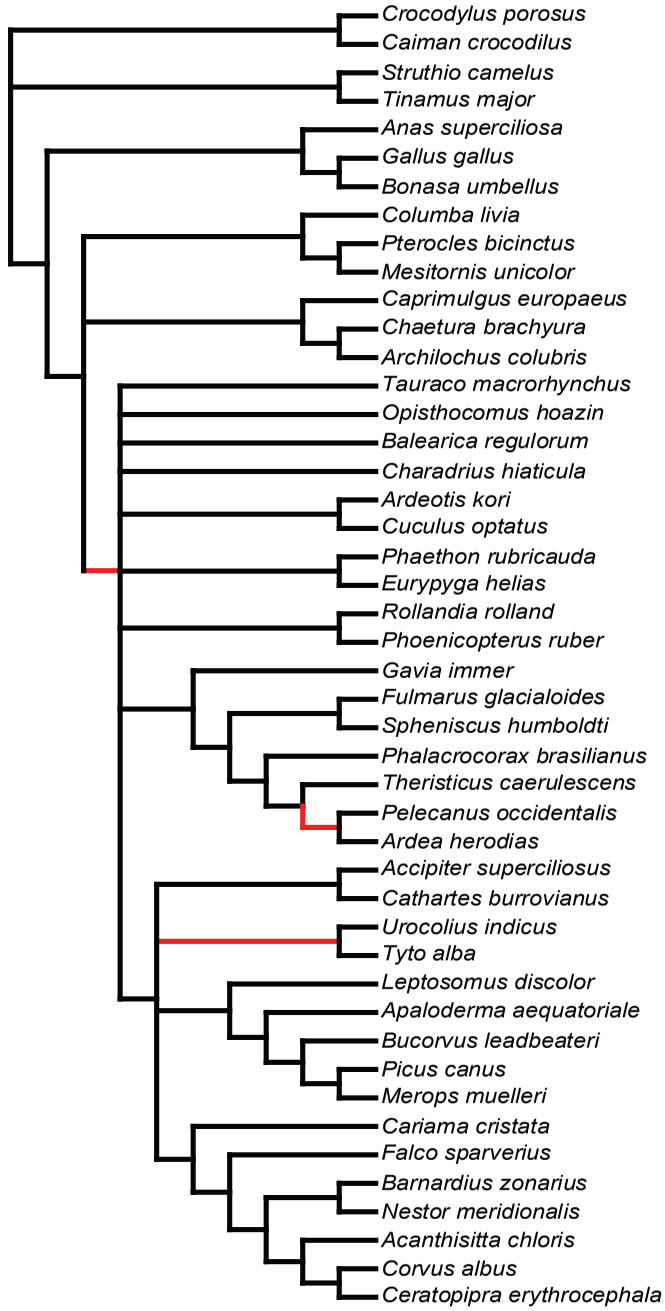

Figure S8

Figure S8. Maximum Likelihood Analysis of the Anchored Enrichment data set pruned to 48 taxa. Phylogenetic hypothesis produced with RaxML from the anchored enrichment data for a reduced sample of 48 species representing the same clades examined in a recent phylogenetic analysis of 48 whole avian genomes[5]. Red lineages mark clades that are incongruent with the Bayesian and ML trees of the full anchored enrichment data set (Fig. 1).

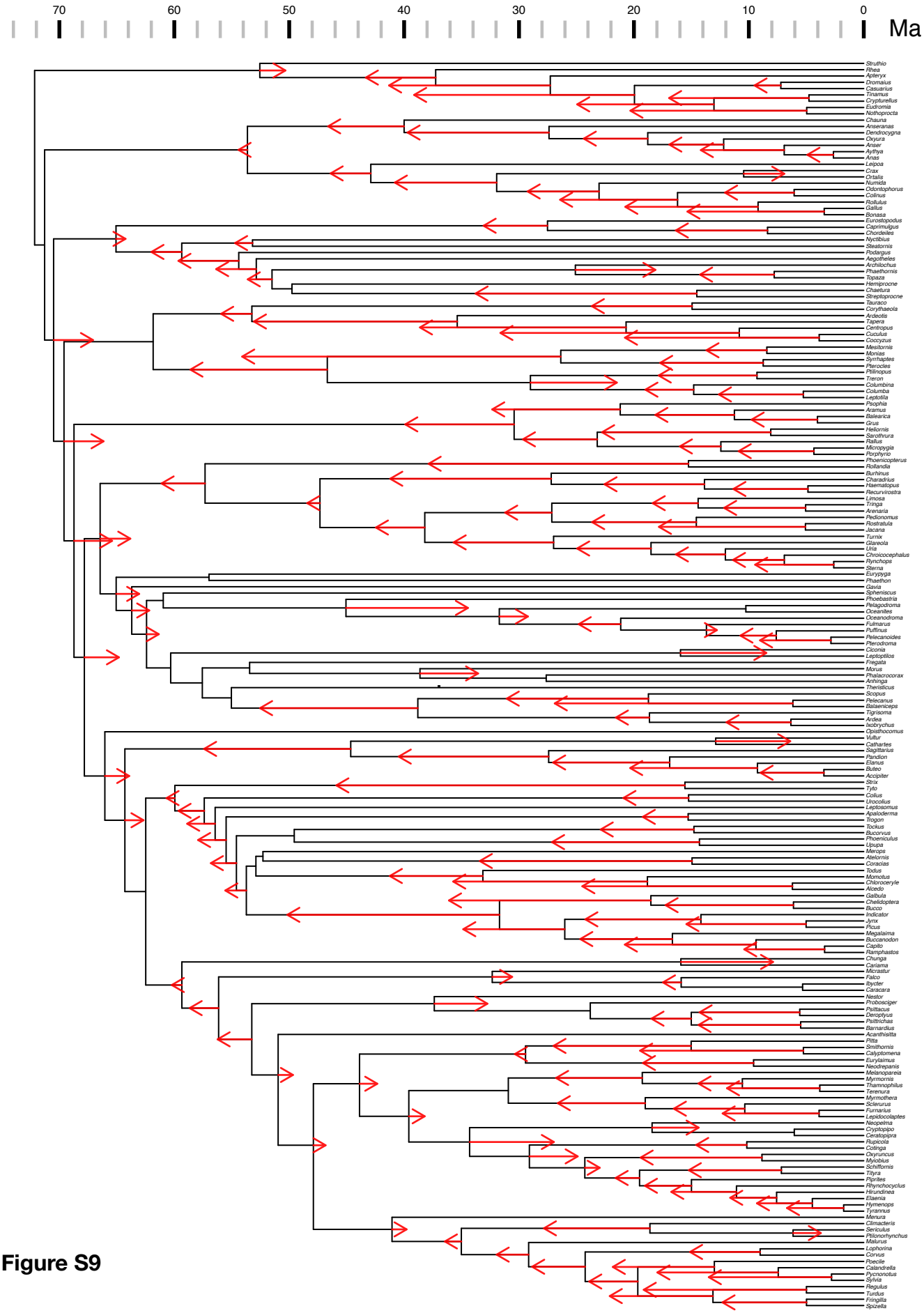
70
60
50
40
30
20
10
0
Ma
Struthio
Rhea
Apteryx
Dromaius
Casuarius
Tinamus
Crypturellus
Eudromia
Nothoprocta
Chauna
Anseranas
Dendrocygna
Oxyura
Anser
Aythya
Anas
Leipoa
Crax
Ortalis
Numida
Odontophorus
Colinus
Rollulus
Gallus
Bonasa
Eurostopodus
Caprimulgus
Chordeiles
Nyctibius
Steatornis
Podargus
Aegotheles
Archilochus
Phaethornis
Topaza
Hemiprocne
Chaetura
Streptoprocne
Tauraco
Corythaeola
Ardeotis
Tapera
Centropus
Cuculus
Coccyzus
Mesitornis
Monias
Syrrhaptes
Pterocles
Ptilinopus
Treron
Columbina
Columba
Leptotila
Psophia
Aramus
Balearica
Grus
Heliornis
Sarothrura
Rallus
Micropygia
Porphyrio
Phoenicopterus
Rollandia
Burhinus
Charadrius
Haematopus
Recurvirostra
Limosa
Tringa
Arenaria
Pedionomus
Rostratula
Jacana
Turnix
Glareola
Uria
Chroicocephalus
Rynchops
Sterna
Eurypyga
Phaethon
Gavia
Spheniscus
Phoebastria
Pelagodroma
Oceanites
Oceanodroma
Fulmarus
Puffinus
Pelecanoides
Pterodroma
Ciconia
Leptoptilos
Fregata
Morus
Phalacrocorax
Anhinga
Threskiornis
Scopus
Pelecanus
Balaeniceps
Tigrisoma
Ardea
Ixobrychus
Opisthocomus
Vultur
Cathartes
Sagittarius
Pandion
Elanus
Buteo
Accipiter
Strix
Tyto
Colius
Urocolius
Leptosomus
Apaloderma
Trogon
Tockus
Bucorvus
Phoeniculus
Upupa
Merops
Alcedo
Galbula
Chelidoptera
Bucco
Indicator
Jynx
Picus
Megalaima
Buccanodon
Capito
Ramphastos
Chunga
Cariama
Micrastur
Falco
Ibycter
Caracara
Nestor
Probosciger
Psittacus
Deroptyus
Psittrichas
Barnardius
Acanthisitta
Pitta
Smithornis
Calyptomena
Eurylaimus
Neodrepanis
Melanopareia
Myrmornis
Thamnophilus
Terenura
Myrmotherula
Sclerurus
Furnarius
Lepidocolaptes
Neopelma
Cryptopipo
Ceratopipra
Rupicola
Cotinga
Oxyruncus
Myiobius
Schiffornis
Tityra
Piprites
Rhynchocyclus
Hirundinea
Elaenia
Hymenops
Tyrannus
Menura
Climacteris
Sericulus
Ptilonorhynchus
Maluris
Lophorina
Corvus
Poecile
Calandrella
Pycnonotus
Sylvia
Regulus
Turdus
Fringilla
Spizella

Figure S9

Figure S9. Comparison of Prior and Posterior age estimates. The black base tree is derived from summarizing an MCC tree with median node heights from the distribution of trees generated when only prior calibrations are included in the BEAST analysis (i.e., it is a representation of the effective prior on the entire topology). The red arrows at each node indicate how the estimated divergence times change when our new molecular data is included in the analysis (ie, a representation of the posterior). Arrows pointing to the left indicate posterior ages that are older than their effective prior, and arrows pointing to the right indicate posterior ages that are younger. The posterior divergence time estimates of nodes with no arrows were within 1% of their effective prior.

Avian Time Tree - Testing *Vegavis*

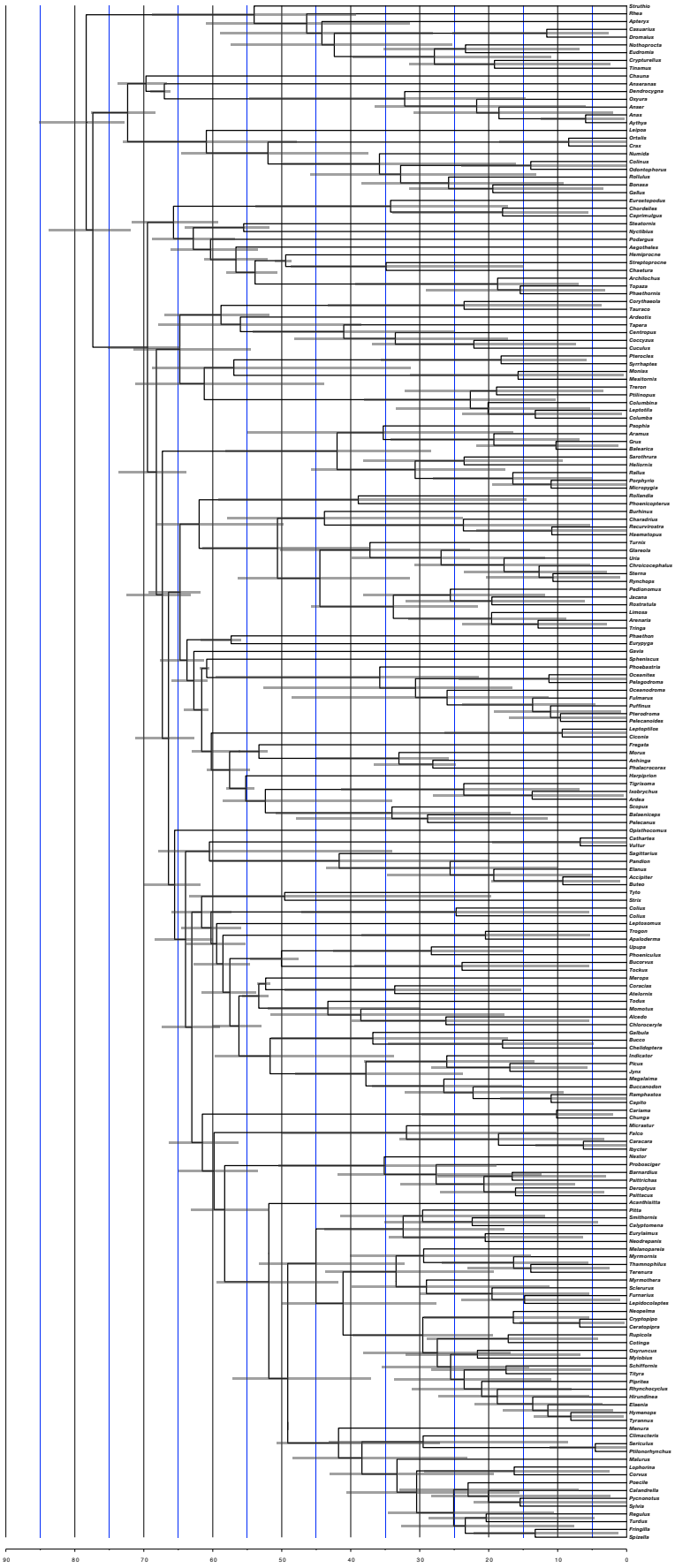

Figure S10

Figure S10. Alternative Time calibrated Bayesian Tree including *Vegavis* calibration point. A time calibrated sensitivity analysis of the ExaBayes topology and the top ten data partitions (those ten partitions which exhibited the lowest declines in phylogenetic informativeness), shown here with error bars at each node indicating the 95% HPD confidence intervals. This analysis includes the putative stem anseriform *Vegavis* (see supplemental text). For comparison to the primary analysis that excludes *Vegavis*, see Fig S12.

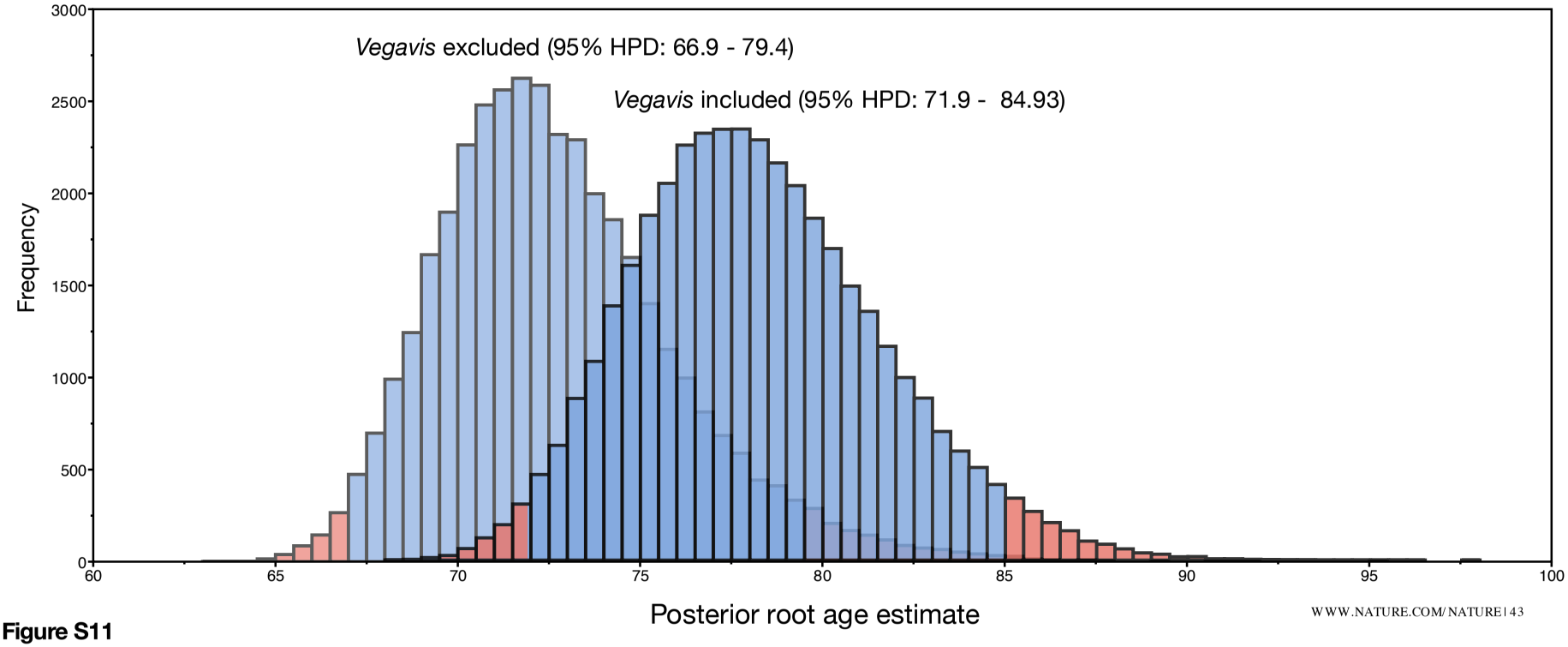
Vegavis excluded (95% HPD: 66.9 - 79.4)
Vegavis included (95% HPD: 71.9 - 84.93)
Frequency
3000
2500
2000
1500
1000
500
0
60
65
70
75
80
85
90
95
100
Posterior root age estimate
WWW.NATURE.COM/NATURE143

Figure S11

Figure S11. Comparison of Posterior age estimates of the avian crown clade with and without *Vegavis* calibration (see Supplement text). The inclusion of *Vegavis* increased the median estimated age of the avian crown clade by 6.36 MY to 78.26 MY. This revised estimate is not significantly different from our previous analysis (Fig. S6-S7), because it falls within the HPD confidence intervals of our initial estimate of the root age without the *Vegavis* calibration.

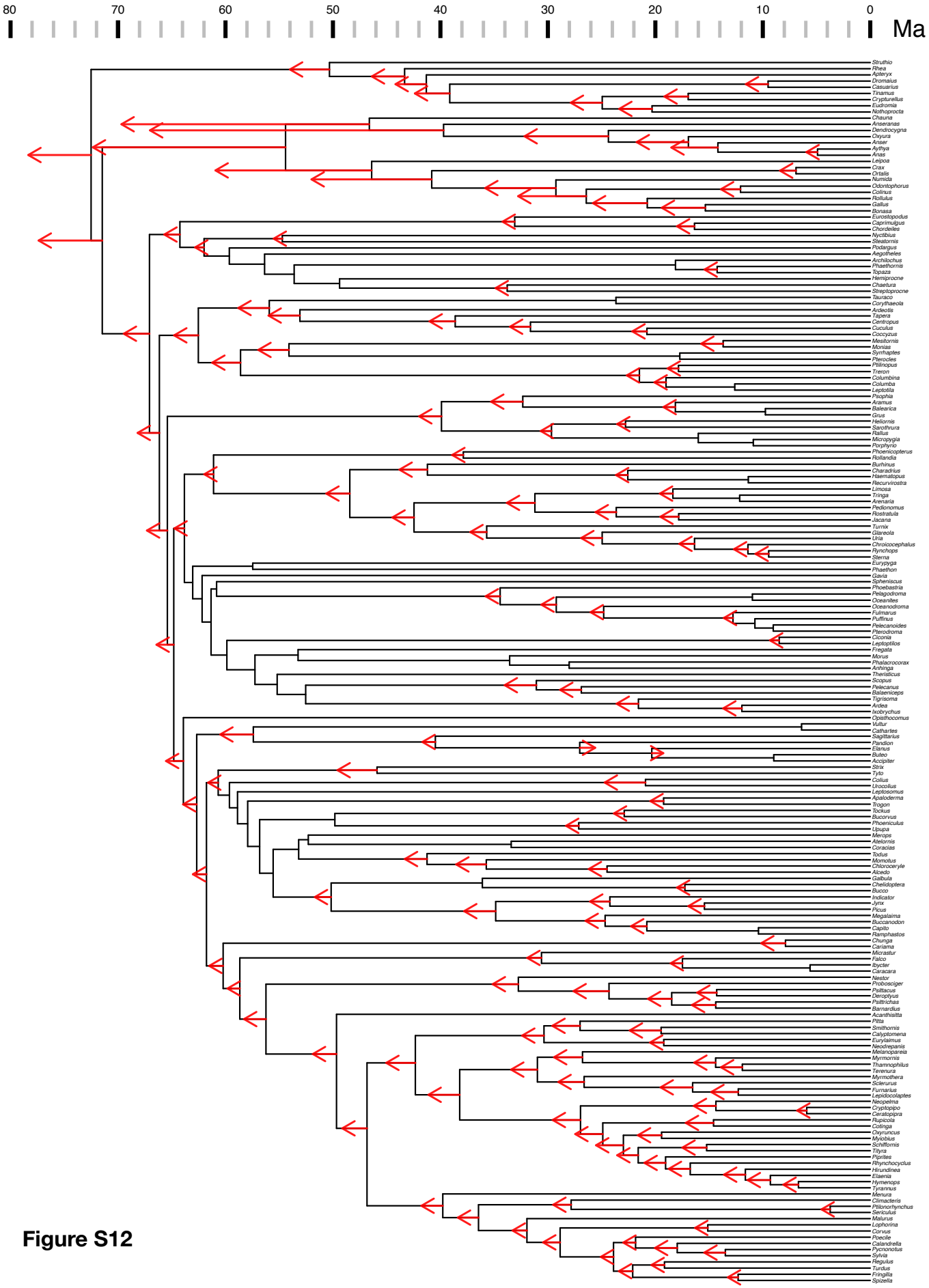
80
70
60
50
40
30
20
10
0
Ma
Struthio
Rhea
Apteryx
Dromaius
Casuarius
Tinamus
Crypturellus
Eudromia
Nothoprocta
Chauna
Anseranas
Dendrocygna
Oxyura
Anser
Aythya
Anas
Leipoa
Crax
Ortalis
Numida
Odontophorus
Colinus
Rollulus
Gallus
Bonasa
Eurostopodus
Caprimulgus
Chordeiles
Nyctibius
Steatornis
Podargus
Aegotheles
Archilochus
Phaethornis
Topaza
Hemiprocne
Chaetura
Streptoprocne
Tauraco
Corythaeola
Ardeotis
Tapera
Centropus
Cuculus
Coccyzus
Mesitornis
Monias
Synthaptes
Pterocles
Ptilinopus
Treron
Columbina
Columba
Leptotila
Psophia
Aramus
Balearica
Grus
Heliornis
Sarothrura
Rallus
Micropygia
Porphyrio
Phoenicopterus
Rollandia
Burhinus
Charadrius
Haematopus
Recurvirostra
Limosa
Tringa
Arenaria
Pedionomus
Rostratula
Jacana
Turnix
Glareola
Uria
Chroicocephalus
Rynchops
Sterna
Eurypyga
Phaethon
Gavia
Spheniscus
Phoebastria
Pelagodroma
Oceanites
Oceanodroma
Fulmarus
Puffinus
Pelecanoides
Pterodroma
Ciconia
Leptoptilos
Fregata
Morus
Phalacrocorax
Anhinga
Theristicus
Scopus
Pelecanus
Balaeniceps
Tigrisoma
Ardea
Ixobrychus
Opisthocomus
Vultur
Cathartes
Sagittarius
Pandion
Elanus
Buteo
Accipiter
Strix
Tyto
Colius
Urocolius
Leptosomus
Apaloderma
Trogon
Tockus
Bucorvus
Phoeniculus
Upupa
Merops
Atelornis
Coracias
Todus
Momotus
Chloroceryle
Alcedo
Galbula
Cheloptera
Bucco
Indicator
Jynx
Picus
Megalaima
Buccanodon
Capito
Ramphastos
Chunga
Cariama
Micrastur
Falco
Ibycter
Caracara
Nestor
Probosciger
Psittacus
Deroptyus
Psittrichas
Barnardius
Acanthisitta
Pitta
Smithornis
Calyptomena
Eurylaimus
Neodrepanis
Melanopareia
Myrmoria
Thamnophilus
Tereiura
Myrmothera
Sclerurus
Furnarius
Lepidocolaptes
Neopelma
Cryptopipo
Ceratopipra
Rupicola
Cotinga
Oxyruncus
Myiobius
Schiffornis
Tityra
Pipriles
Rhynchocyclus
Hirundinea
Elaenia
Hymenops
Tyrannus
Menura
Climacteris
Ptilonorhynchus
Sericulus
Malurus
Lophorina
Corvus
Poecile
Calandrella
Pycnonotus
Sylvia
Regulus
Turdus
Fringilla
Spizella

Figure S12

Figure S12. Comparison of divergence time estimates without (black) and with (red arrows) *Vegavis* calibration. The black base tree is the time calibrated Bayesian analysis (Fig. S6) which excludes the putative stem Anseriform *Vegavis*. The red arrows at each node indicate how the estimated divergence times change when *Vegavis* is included in the analysis as a calibration point (Fig. S10). For most nodes, ages are increased slightly by the inclusion of *Vegavis*, but significant changes are restricted to the Galloanseres (Fig. S9). The posterior divergence time estimates of nodes with no arrows were within 1% of the analysis excluding *Vegavis.*

doi:10.1038/nature15697

Supplementary Table 1 The avian taxa and outgroups analyzed in this study. Alphabetical by genus. Table provides the taxonomic family, the source institution, catalog/tissue number, and locality for each specimen. Taxonomy follows Gill and Donsker (2015; fifth ed). Crocodilian outgroup genera– *Caiman* and *Crocodylus*– are marked with an *. Institution codes (with the total number of specimens contributed to the study): **AMNH**- American Museum of Natural History (1); **ANSP**- Academy of Natural Sciences of Philadelphia (1); **FMNH**- Field Museum of Natural History (6); **KU**- University of Kansas Natural History Museum and Biodiversity Research Center (46); **ROM**- Royal Ontario Museum (3); **UWBM**- University of Washington Burke Museum of Natural History (17); **YPM**- Yale Peabody Museum of Natural History (125).

Genus	Species	Family	Inst.	Number	Locality
Acanthisitta	*chloris*	Acanthisittidae	ROM	RIFL	New Zealand: South Island
Accipiter	*superciliosus*	Accipitridae	YPM	3790	Suriname: Tafelberg
Aegotheles	*insignis*	Aegothelidae	KU	16098	Papua New Guinea: Madang
Alcedo	*quadribrachys*	Alcedinidae	YPM	495	Equatorial Guinea: Monte Alen Nat. Park
Anas	*superciliosa*	Anatidae	YPM	3154	Australia: Victoria, Melbourne
Anhinga	*anhinga*	Anhingidae	KU	3106	No Data
Anser	*canagicus*	Anatidae	YPM	6059	Captivity
Anseranas	*semipalmata*	Anseranatidae	YPM	3158	Australia: Victoria, Lara
Apaloderma	*aequatoriale*	Trogonidae	YPM	295	Equatorial Guinea: Monte Alen Nat. Park
Apteryx	*matelli*	Apterygidae	KU	14905	New Zealand: North Island
Aramus	*guarauna*	Aramidae	UWBM	90368	USA: Florida, Pinellas
Archilochus	*colubris*	Trochilidae	YPM	5465	USA: Connecticut, Shelton
Ardea	*herodias*	Ardeidae	YPM	2800	USA: Connecticut, Madison
Ardeotis	*kori*	Otididae	YPM	5967	Captivity
Arenaria	*interpres*	Scolopacidae	YPM	3383	USA: Connecticut, New Haven
Atelornis	*pittoides*	Brachypteraciidae	FMNH	384759	Madagascar: RNI d'Andohahela
Aythya	*valisineria*	Anatidae	YPM	6097	Captivity
Balaeniceps	*rex*	Balaenicipitidae	YPM	5404	Captivity

Balearica	*regulorum*	Gruidae	YPM	6296	Captivity
Barnardius	*zonarius*	Psittacidae	KU	8723	Australia
Bonasa	*umbellus*	Phasianidae	YPM	5642	USA: Alaska, Anchorage
Buccanodon	*duchaillui*	Lybiidae	YPM	522	Equatorial Guinea: Monte Alen Nat. Park
Bucco	*capensis*	Bucconidae	YPM	3690	Suriname: Tafelberg
Bucorvus	*leadbeateri*	Bucerotidae	ROM	3250	Captivity
Burhinus	*oedicnemus*	Burhinidae	YPM	1223	Greece: Crete, Chania
Buteo	*jamaicensis*	Accipitridae	YPM	86	El Salvador: San Miguel Volcano
*Caiman**	*crocodilus*	Alligatoridae	YPM	15451	Brazil: Rio Tapajós, Teles Pires
Calandrella	*brachydactyla*	Alaudidae	YPM	1245	Greece: Crete, Heraklion
Calyptomena	*viridis*	Eurylaimidae	YPM	6323	Brunei: Bukit Pagon
Capito	*niger*	Capitonidae	YPM	3617	Suriname: Tafelberg
Caprimulgus	*europaeus*	Caprimulgidae	YPM	3336	Serbia: Bujanovac, Prohor Pcinjsk
Caracara	*cheriway*	Falconidae	YPM	2938	Suriname: Sipaliwini
Cariama	*cristata*	Cariamidae	YPM	1173	Uruguay: Cerro Largo, Canada Canas
Casuarius	*bennetti*	Casuariidae	KU	6875	Papua New Guinea: base Mt. Suckling
Cathartes	*burrovianus*	Cathartidae	YPM	1066	Uruguay: Artigas, Estancia Mandiyu
Centropus	*bengalensis*	Cuculidae	KU	17932	Philipines: Batanes, Sabtang Island
Ceratopipra	*erythrocephala*	Pipridae	YPM	2249	Suriname: Sipaliwini
Chaetura	*brachyura*	Apodidae	YPM	2886	Suriname: Sipaliwini
Charadrius	*hiaticula*	Charadriidae	YPM	1289	Greece: Crete, Heraklion
Chauna	*torquata*	Anhimidae	KU	1829	Captivity
Chelidoptera	*tenebrosa*	Bucconidae	YPM	5339	Suriname: Boven Coesewijne Nature Reserve
Chloroceryle	*inda*	Alcedinidae	YPM	5303	Suriname: Boven Coesewijne Nature Reserve
Chordeiles	*pusillus*	Caprimulgidae	YPM	2276	Suriname: Sipaliwini
Chroicocephalus	*cirrocephalus*	Laridae	YPM	1192	Uruguay: Tacuarembo, Lago Rincon del Bonete
Chunga	*burmeisteri*	Cariamidae	UWBM	77230	Bolivia: Santa Cruz, Laguna Caucaya
Ciconia	*nigra*	Ciconiidae	YPM	1226	Greece: Evros, Dadia Forest Reserve

Climacterus	*melanura*	Climacteridae	KU	6178	Australia: West Australia, 20 km W of Gascoyne Jct
Coccyzus	*melacoryphus*	Cuculidae	YPM	2065	Suriname: Sipaliwini
Colinus	*cristatus*	Odontophoridae	YPM	2944	Suriname: Sipaliwini
Colius	*colius*	Coliidae	UWBM	52764	South Africa: Free State, Springfontein
Colius	*indicus*	Coliidae	UWBM	67124	South Africa: KwaZulu/Natal, Melmoth
Columba	*livia*	Columbidae	YPM	1232	Greece: Crete, Rethimno, Arkalu
Columbina	*minuta*	Columbidae	YPM	2275	Suriname: Sipaliwini
Coracias	*cyanogaster*	Coraciidae	YPM	6031	Captivity
Corvus	*albus*	Corvidae	YPM	832	Equatorial Guinea: Rio Campo
Corythaeola	*cristata*	Musophagidae	YPM	523	Equatorial Guinea: Monte Alen Nat. Park
Cotinga	*cayana*	Cotingidae	YPM	2211	Suriname: Sipaliwini
Coturnix	*coturnix*	Phasianidae	YPM	4090	Russia: Krasnodar Krai, Blagoveschenskaya
Crax	*alector*	Cracidae	YPM	1607	Suriname: Tafelberg
*Crocodylus**	*porosus*	Crocodylidae	YPM	14722	Palau: Ngerikiil
Crypturellus	*tataupa*	Tinamidae	YPM	1770	Bolivia: Santa Cruz, Warnes
Cryptopipo	*holochlora litae*	Pipridae	UWBM	76941	Panama: 51 km NNE Panama City, Rio Esperanza
Cuculus	*optatus*	Cuculidae	YPM	2497	Russia: Zabaykasky Krai, Krasny Chikoy
Dendrocygna	*viduata*	Anatidae	YPM	6026	Captivity
Deroptyus	*accipitrinus*	Psittacidae	YPM	2217	Suriname: Sipaliwini
Dromaius	*novaehollandiae*	Dromaiidae	YPM	3380	Captivity
Elaenia	*flavogaster*	Tyrannidae	YPM	5336	Suriname: Boven Coesewijne Nature Reserve
Elanus	*leucurus*	Accipitridae	KU	9309	El Salvador: Zaxatecoluca, Animas Abajo
Eudromia	*elegans*	Tinamidae	YPM	5886	Captivity
Eurostopodus	*macrotis*	Caprimulgidae	KU	18174	Philippines: Midanao, Zamboanga
Eurylaimus	*ochromalus*	Eurylaimidae	KU	12368	Malaysia: Sarawak, 25 km S Bintulu
Eurypyga	*helias*	Eurypygidae	KU	16818	No Data
Falco	*sparverius*	Falconidae	YPM	2079	Suriname: Sipaliwini

Fregata	*magnificens*	Fregatidae	KU	9129	El Salvador: Pacific Ocean, ~35 mi S Puerto Triumfo
Fringilla	*coelebs*	Fringillidae	YPM	1837	Russia: Krasnodar Krai, Solenoye
Fulmarus	*glacialoides*	Procellariidae	KU	21828	New Zealand: North Island, Aukland, Muriwai Beach
Furnarius	*rufus*	Furnariidae	YPM	988	Uruguay: Artigas, Arroyo Mandiyu
Galbula	*dea*	Galbulidae	YPM	5315	Suriname: Boven Coesewijne Nature Reserve
Gallus	*gallus*	Phasianidae	KU	2419	Captivity; from wild stock from India: Dehra Dun
Gavia	*immer*	Gaviidae	UWBM	66928	USA: Washington, Indianola
Glareola	*nuchalis*	Glareolidae	KU	19903	Sierra Leone: Outamba-Kilimi Nat. Park
Grus	*canadensis*	Gruidae	KU	21897	USA: Kansas, Stafford
Haematopus	*palliatus*	Haematopodidae	YPM	6295	USA: Connecticut, Cockenoe Island
Heliornis	*fulica*	Heliornithidae	KU	3087	No Data
Hemiprocne	*comata*	Hemiprocnidae	KU	12571	Philippines: Mindonoro, Barangay Harrison
Hirundinea	*ferruginea*	Tyrannidae	YPM	1183	Uruguay: Cerro Largo, Rio Yaguaron
Hymenops	*perspicillatus*	Tyrannidae	YPM	1087	Uruguay: Rivera, Cuchilla de Caraguata
Ibycter	*americanus*	Falconidae	YPM	3574	Suriname: Tafelberg
Indicator	*exilis*	Indicatoridae	YPM	344	Equatorial Guinea: Monte Alen Nat. Park
Ixobrychus	*minutus*	Ardeidae	YPM	730	Greece: Crete, Bramiana Lake
Jacana	*jacana*	Jacanidae	YPM	5911	Captivity
Jynx	*torquilla*	Picidae	YPM	1334	Greece: Crete, Selakano
Leipoa	*ocellata*	Megapodiidae	YPM	3178	Australia: Western Australia Jerramungup
Lepidocolaptes	*angustirostris*	Furnariidae	YPM	2273	Suriname: Sipaliwini
Leptoptilos	*crumeniferus*	Ciconiidae	KU	2661	Tanzania
Leptosomus	*discolor*	Leptosomatidae	FMNH	449184	Captivity
Leptotila	*rufaxilla*	Columbidae	YPM	1526	Suriname: Tafelberg
Limosa	*lapponica*	Scolopacidae	YPM	5370	Alaska: North Slope, Sagavanirktok River
Lophorina	*superba*	Paradisaeidae	YPM	6345	Captivity
Malurus	*splendens*	Maluridae	KU	6209	Australia: West Australia, Kabarri

Megalaima	*chrysopogon*	Megalaimidae	KU	17790	Malaysia: Sabah, Crocker Range Park
Melanopareia	*maximiliani*	Melanopareiidae	KU	2841	Paraguay: Presidente Hayes, Campo Largo
Menura	*novaehollandiae*	Menuridae	UWBM	76638	Australia: Victoria
Merops	*muelleri*	Meropidae	YPM	955	Equatorial Guinea: Wele-Nzas, Altos de Nsork NP
Mesitornis	*unicolor*	Mesitornithidae	FMNH	345610	Madagascar: Foret d'Analalava, 7 km N Manantenina
Micrastur	*gilvicollis*	Falconidae	YPM	1413	Suriname: Tafelberg
Micropygia	*schomburgkii*	Rallidae	YPM	2961	Suriname: Sipaliwini
Momotus	*lessonii*	Momotidae	YPM	111	El Salvador: Joya del Matazano, Cerro Cacahuatique
Monias	*benschi*	Mesitornithidae	FMNH	438526	Madagascar: Foret des Mikeas
Morus	*serrator*	Sulidae	YPM	3160	Australia: Victoria, Melbourne, Frankston Beach
Myiobius	*barbatus*	Tityridae	YPM	1474	Suriname: Tafelberg
Myrmornis	*torquata*	Thamnophilidae	YPM	2182	Suriname: Sipaliwini
Myrmothera	*campanisona*	Grallariidae	YPM	3677	Suriname: Tafelberg
Neodrepanis	*coruscans*	Eurylaimidae	FMNH	345711	Madagascar: Marosohy Forest,
Neopelma	*chrysocephalum*	Pipridae	YPM	1712	Suriname: Kappel Airstrip
Nestor	*meridionalis*	Psittacidae	KU	14873	New Zeland: North Island, Titirangi
Nothoprocta	*ornata*	Tinamidae	YPM	1748	Bolivia: José Manuel Pando, Berenguela
Numida	*meleagris*	Numididae	UWBM	52755	South Africa: Free State, Springfontein
Nyctibius	*griseus*	Nyctibiidae	YPM	2220	Suriname: Sipaliwini
Oceanites	*oceanicus*	Hydrobatidae	AMNH	3175	Chile: Valaparíso
Oceanodroma	*leucorhoa*	Hydrobatidae	YPM	6008	USA: Connecticut, Prospect
Odontophorus	*gujanensis*	Odontophoridae	YPM	1619	Suriname: Tafelberg
Opisthocomus	*hoazin*	Opisthocomus	KU	848	Peru: Loreto
Ortalis	*motmot*	Cracidae	YPM	2963	Suriname: Sipaliwini
Oxyruncus	*cristatus*	Oxyruncidae	YPM	3562	Suriname: Tafelberg
Oxyura	*jamaicensis*	Anatidae	YPM	3236	Captivity
Pandion	*haliaetus*	Pandionidae	UWBM	81668	USA: Washington, Everett

Pedionomus	*torquatus*	Pedionomidae	ROM	2685	Australia: Victoria
Pelagodroma	*marina*	Hydrobatidae	UWBM	62853	Australia: New South Wales, Sydney
Pelecanoides	*urinatrix*	Pelecanoididae	KU	10701	Australia
Pelecanus	*occidentalis*	Pelecanidae	KU	15014	El Salvador: Usulután, Jucuarán
Phaethon	*rubricauda*	Phaethontidae	KU	2613	Pacific Ocean: Johnston Atoll
Phaethornis	*superciliosus*	Trochilidae	YPM	1514	Suriname: Tafelberg
Phalacrocorax	*brasilianus*	Phalacrocoracidae	KU	1658	No data
Phoebastria	*nigripes*	Diomedeidae	UWBM	82096	North Pacific Ocean: 31°N 159°W
Phoenicopterus	*ruber*	Phoenicopteridae	YPM	6069	Captivity
Phoeniculus	*purpureus*	Phoeniculidae	KU	15430	Ghana: Upper West Region, Gbele Resource Reserve
Picus	*canus*	Picidae	YPM	3344	Serbia: Knjazevac, Babin Zub
Piprites	*chloris*	Incertae sedis	YPM	1616	Suriname: Tafelberg
Pitta	*angolensis*	Pittidae	KU	19788	Sierra Leone: Kambui Hills Forest Reserve
Podargus	*strigoides*	Podargidae	YPM	3161	Australia: Victoria, Melbourne
Poecile	*lugubris*	Paridae	YPM	3321	Serbia: Bujanovac, Prohor Pcinjsk
Porphyrio	*porphyrio*	Rallidae	KU	22888	Australia: Northern Territory, Roper River
Probosciger	*aterrimus*	Psittacidae	YPM	5927	Captivity
Psittacus	*erithacus*	Psittacidae	KU	1566	Cameroon
Psittrichas	*fulgidus*	Psittacidae	YPM	5253	Captivity
Psophia	*crepitans*	Psophiidae	YPM	3569	Suriname: Tafelberg
Pterocles	*bicinctus*	Pteroclididae	UWBM	53231	South Africa: Gauteng, Rustenburg
Pterodroma	*externa*	Procellariidae	KU	16363	Pacific Ocean
Ptilinopus	*magnificus*	Columbidae	YPM	6298	Captivity
Ptilonorhynchus	*violaceus*	Ptilonorhynchidae	KU	10756	Australia
Puffinus	*griseus*	Procellariidae	KU	22550	Fiji
Pycnonotus	*urostictus*	Pycnonotidae	KU	18173	Philippines: Mindanao, Zamboanga, Pasanoca NP
Rallus	*longirostris*	Rallidae	YPM	3386	USA: Connecticut, Milford
Ramphastos	*ambiguus*	Ramphastidae	YPM	6061	Captivity
Recurvirostra	*americana*	Recurvirostridae	KU	21	USA: Kansas, Rooks

Regulus	*ignicapilla*	Regulidae	YPM	1370	Greece: Crete, Chania, Omalos
Rhea	*americana*	Rheidae	UWBM	72512	Captivity
Rhynchocyclus	*olivaceus*	Tyrannidae	YPM	1698	Suriname: Kappel Airstrip
Rhynchops	*niger*	Rynchopidae	KU	15950	USA: Florida, Lee
Rollandia	*rolland*	Podicipedidae	YPM	1201	Uruguay: Colonia, Puerto de Conchillas
Rollulus	*rouloul*	Phasianidae	KU	1587	Captivity
Rostratula	*benghalensis*	Rostratulidae	KU	20061	Sierra Leone: Outamba-Kilimi Nat. Park
Rupicola	*rupicola*	Cotingidae	YPM	1452	Suriname: Tafelberg
Sagittarius	*serpentarius*	Sagittariidae	AMNH	9545	Captivity
Sarothrura	*rufa elizabethae*	Sarothruridae	FMNH	384805	Uganda: Echuya Forest Reserve
Schiffornis	*turdina*	Tityridae	YPM	3576	Suriname: Tafelberg
Sclerurus	*mexicanus*	Furnariidae	YPM	1586	Suriname: Tafelberg
Scopus	*umbretta*	Scopidae	UWBM	89784	Captivity
Sericulus	*bakeri*	Ptilonorhynchidae	KU	12230	Papua New Guinea: Madang
Smithornis	*rufolateralis*	Eurylaimidae	YPM	225	Equatorial Guinea: Monte Alen Nat. Park
Spheniscus	*humboldti*	Spheniscidae	UWBM	85124	Captivity
Spizella	*arborea*	Emberizidae	KU	21896	USA: Kansas, Lawrence
Steatornis	*caripensis*	Steatornithidae	ANSP	20224	Ecuador: Napo, Las Palmas
Sterna	*hirundo*	Sternidae	YPM	4099	Russia: Krasnodar Krai, Blagoveschenskaya
Streptoprocne	*zonaris*	Apodidae	YPM	135	El Salvador: Joya del Matazano, Cerro Cacahuatique
Strix	*varia*	Strigidae	YPM	1208	USA: Connecticut, New Haven
Struthio	*camelus*	Struthionidae	UWBM	90121	Captivity
Sylvia	*melanocephala*	Sylviidae	YPM	1354	Greece: Crete, Heraklion
Syrrhaptes	*paradoxus*	Pteroclididae	KU	20547	Mongolia: Dornu Gobi, Ulaan Badrakh Soum
Tapera	*naevia*	Cuculidae	YPM	2923	Suriname: Sipaliwini
Tauraco	*macrorhynchus*	Musophagidae	YPM	375	Equatorial Guinea: Monte Alen Nat. Park
Terenura	*callinota*	Thamnophilidae	YPM	3515	Suriname: Tafelberg

Thamnophilus	*ruficapillus*	Thamnophilidae	YPM	1193	Uruguay: Colonia, Puerto de Conchillas
Theristicus	*caerulescens*	Threskiornithidae	YPM	1174	Uruguay: Cerro Largo, Rio Yaguaron
Tigrisoma	*lineatum*	Ardeidae	YPM	2212	Suriname: Sipaliwini, Werehpai
Tinamus	*major*	Tinamidae	YPM	1774	Bolivia: Santa Cruz, Ichilo, Puerto Grether
Tityra	*cayana*	Tityridae	YPM	3044	Suriname: Sipaliwini
Tockus	*camurus*	Bucerotidae	YPM	937	Equatorial Guinea: Wele-Nzas, Altos de Nsork NP
Todus	*mexicanus*	Todidae	YPM	1994	Captivity
Topaza	*pella*	Trochilidae	YPM	1489	Suriname: Tafelberg
Treron	*calvus*	Columbidae	YPM	447	Equatorial Guinea: Monte Alen Nat. Park
Tringa	*solitaria*	Scolopacidae	YPM	999	Uruguay: Artigas, Estancia Mandiyu
Trogon	*elegans*	Trogonidae	YPM	115	El Salvador: Joya del Matazano, Cerro Cacahuatique
Turdus	*olivater*	Turdidae	YPM	1568	Suriname: Tafelberg
Turnix	*ocellatus*	Turnicidae	KU	25985	Philippines: Luzon, Gonzaga, Mt. Cagua
Tyrannus	*albogularis*	Tyrannidae	YPM	2823	Suriname: Sipaliwini
Tyto	*alba*	Tytonidae	UWBM	88784	USA: Washington, Whidbey Island
Upupa	*epops*	Upupidae	YPM	1920	Russia: Kasnodar Krai, Bugazkaya Kosa
Uria	*aalge*	Alcidae	KU	25293	USA: Oregon, Clatsop
Vultur	*gryphus*	Cathartidae	YPM	5411	Captivity

APPENDIX 4

SUPPLEMENTARY MATERIAL FOR CHAPTER 4

Additional data files can be accessed at the online version of this article

http://dx.doi.org/10.1093/sysbio/syx064

and

http://dx.doi.org/10.5061/dryad.nr654

Supplementary Appendix for

Genomic Signature of an Avian Lilliput Effect across the K-Pg Extinction

Author Affiliations:

Jacob S. Berv[1*], Daniel J. Field[2,3*]

[1]† Department of Ecology & Evolutionary Biology, Cornell University, Ithaca NY USA

[2] Department of Geology & Geophysics, Yale University, New Haven CT USA

[3]†Milner Centre for Evolution, Department of Biology and Biochemistry, University of Bath, Bath, United Kingdom

*Correspondence to: Jacob S. Berv (jsb439@cornell.edu) and Daniel J. Field (d.j.field@bath.ac.uk)

†Current address

*These authors contributed equally to this work.

Additional Background and Discussion

Context

Molecular age estimates of the deepest divergences within crown birds range from the mid (Barker et al. 2002, Jetz et al. 2012, Jarvis et al. 2014) to the Late Cretaceous (Claramunt et al. 2015, Cracraft et al. 2015, Prum et al. 2015), while the oldest definitive crown fossils are either known from the early Paleogene (Slack et al. 2006), or the latest Cretaceous (Clarke et al. 2005, Clarke et al. 2016). A similar pattern of absolute discordance in divergence time estimates has been observed for crown eutherian mammals; molecular clocks tend to favor a radiation in the Late Cretaceous (Tavare et al. 2002, Bininda-Emonds et al. 2007, Wilkinson et al. 2011), while the fossil record is consistent with a Paleogene radiation (Smith et al. 2006, O'Leary et al. 2013). This 'rocks/clocks' discrepancy is not restricted to vertebrates. The oldest fossil angiosperms date to around 140 Ma (Brenner 1996, Friis et al. 2011), while molecular clock estimates generally support a much older Triassic origin of ~200 Ma (e.g. Smith et al. 2010, Zeng et al. 2014). Indeed, discordance between the fossil record and molecular divergence time estimates may be a general property of eukaryotic life (Peterson et al. 2004, Fontanillas et al. 2007, Erwin et al. 2011, Parfrey et al. 2011); in general, deep clade ages estimated with molecular clocks frequently overshoot those suggested by the fossil record by substantial margins.

As summarized in the main text, several methodological and biological forces may be partly responsible for this phenomenon. A study's density of taxon sampling (Prum et al. 2015), the choice and placement of fossil calibrations (Parham et al. 2011), genetic data quality (Dornburg et al. 2014), and the choice of clock model (Drummond et al. 2006), have

all been implicated as potential factors contributing to discordance in divergence time estimates, and their additive contributions may help explain this pattern. However, both strict and relaxed molecular clock approaches fail to provide age estimates consistent with the fossil record in the absence of highly informative (and arguably circular) priors for many clades, including crown birds (Phillips 2015, Prum et al. 2015). Claramunt et al. (2015) illustrated that employing a tree prior that takes incomplete taxon sampling into account also has an additive effect on over-estimates of avian crown age. Additionally, the inference of pronounced incomplete lineage sorting among avian lineages in the wake of the K-Pg (Jarvis et al. 2014, Suh et al. 2015), may be partly responsible for inferred rate increases due to incorrectly mapped substitutions in analyses of concatenated gene sequences (Mendes et al. 2016).

Numerous biological forces may be responsible for driving the over-estimation of divergence time estimates from molecular sequence data. First, genetic coalescence time (the age of genetic divergence), is expected to be older than the age of morphological divergence (given that the accrual of phenotypic apomorphies takes time). Under an allopatric model of speciation, genetic differences are predicted to accumulate in daughter lineages by drift even in the absence of morphological evolution that can be detected in the fossil record (Brown et al. 2008). While the effect of this 'morphological lag time' is potentially important and should be investigated further, its effects are difficult to quantify and are likely to be clade- and context-specific.

Substitution rates

66 Others have also proposed that discrepancies between molecular clock-based ages
67 and the fossil record may be partially explained by extreme molecular rate heterogeneity
68 driven by the evolution of life history traits (e.g. Lartillot et al. 2011, Dornburg et al. 2012,
69 Steiper et al. 2012, Beaulieu et al. 2015, Phillips 2015). The association between LHTs and
70 substitution rates has been studied in many clades, and while strong correlations have
71 emerged in some cases, others remain more equivocal. As a few examples: in mammals,
72 strong associations have been detected between mtDNA and body size (Steiper et al. 2012),
73 in birds: nuDNA—no association with body size, sexual maturity or sexual maturity
74 (Lanfear et al. 2010), nuDNA- strong association with body size (Jarvis et al. 2014, Weber et
75 al. 2014), mtDNA—strong associations with longevity and body size (Nabholz et al. 2013),
76 in reptiles: mtDNA and nuDNA—strong association with body size (Bromham 2002), in
77 fishes: mtDNA—strong association with longevity (Hua et al. 2015), in flowering plants:
78 mtDNA and nuDNA—strong associations with generation time (Smith et al. 2008), in
79 invertebrates: no association with body size (Thomas et al. 2006), strong association with
80 generation time (Thomas et al. 2010).
81 Many LHTs are correlated with nucleotide substitution rates through their often-
82 strong association with demography and population genetics. For example, body size,
83 longevity, and fecundity are related to population size (e.g. Hutchinson 1959). As generally
84 derived from predictions of the nearly neutral theory of molecular evolution (Kimura
85 1968), the strength of drift scales negatively with effective population size for slightly
86 deleterious mutations, thereby increasing substitution rates as population size declines
87 (Ohta 1973, Woolfit et al. 2003, Lanfear et al. 2013)—if, as is generally accepted, most
88 mutations are deleterious and adaptive substitutions are rare, while holding other

parameters constant, e.g. Woolfit (2009). Thus, one plausible explanation for an acceleration of substitution rate in the history of bird evolution might be a pronounced reduction in the effective population sizes of lineages surviving the K-Pg. Future simulations may help shed light on the extent to which post-K-Pg population reduction may have influenced substitution rates; however, given the difficulty of inferring ancestral population sizes in the distant past, this question may never be directly testable.

Substitution rates may also be inversely related to generation time because of the 'copy error effect,' whereby genomes that are copied more often accumulate more DNA replication errors—this association has been largely established in mammals, though the relationship may not be linear (e.g. Bromham 2011). In most other sexual organisms where detailed life history data are not available, the age of sexual maturity has often been used as a proxy for generation time (Sibley et al. 1990, Bromham 2011). However, age of sexual maturity may be a poor indicator of genetic generation time and demography for iteroparus species like birds (it should only be taken as the lower bound for genetic generation time, as age to maturation does not typically scale at the same rate as longevity, e.g. Lehtonen et al. 2014). Indeed, the age of sexual maturity was not significantly correlated with substitution rate when controlling for other LHTs in our analysis (Figure 2). Our detection of significant associations between other parameters and substitution rate in pairwise comparisons may thus be interpreted as the result of their co-variation with adult body size (e.g. Martin et al. 1993, Lehtonen et al. 2014). The significant negative association we detect between body size and substitution rate while controlling for other LHTs suggests that adult body size may be a better proxy for genetic generation time or population size than other LHTs are in birds. Until more detailed life history data become

112 available for a wider diversity of extant bird species, we must rely on correlates to study
113 the relationship between LHT-driven changes in population genetics and substitution rates.
114
115 *Mutation rate, metabolic rate, and body size*
116 We avoid using the terms 'substitution rate' and 'mutation rate' interchangeably, as
117 many authors do (Barrick et al. 2013). These terms have different connotations; we use the
118 term 'mutation rate' strictly to refer to the rate at which mutations are generated, and
119 'substitution rate' to refer to the fixation rate (which can be inferred from phylogenies and
120 molecular sequence data). An increase in the mutation rate may be expected to lead to an
121 increase in the substitution rate, all else being equal (since the mutation rate represents the
122 ultimate source of genetic diversity).
123 When controlling for body size (as we do in our study), the total metabolic rate is a
124 measure of mass-specific metabolic rate, which has been proposed to scale inversely with
125 body size and positively with mutation rate, perhaps due to an increase in mutagenic
126 oxygen radicals in smaller taxa with higher mass-specific metabolic rates (Gillooly et al.
127 2005, Gillooly et al. 2007, Bromham 2011). Thus, smaller-bodied taxa (Reynolds et al. 1996,
128 McNab 2012) may be predicted to have higher intrinsic mutation rates (Gillooly et al. 2005,
129 Gillooly et al. 2007).
130 Fundamentally, this is a prediction derived from neutral theory's result that the
131 substitution rate collapses to the mutation rate for neutral mutations, independent of
132 population size (Kimura 1968). If the underlying avian mutation rate scales positively with
133 mass-specific metabolic rates, the substitution rate for neutral mutations may be expected
134 to increase with decreasing body size. Our analyses show that substitution rates in birds do

scale positively with mass-specific metabolic rates. While these results do not constitute a direct test of this mechanism (in lieu of an estimator of the true mutation rate in this study), they are consistent with the hypothesis that higher mass-specific metabolic rates in small taxa may drive a higher mutation rate (and thus an elevated substitution rate as well).

In sum, the effects of the relationship between body size and population dynamics, as well as intrinsic biological processes such as metabolic rates, may be predicted to *additively* contribute to increases in overall substitution rate under selection for small body and/or population size. Notably, in extant communities, body size is often inversely correlated with population size or abundance (e.g. White et al. 2007). Therefore, a macroevolutionary decrease in body size may be expected to be correlated with an increase in population size and decrease in generation time, thus acting to neutralize effects on substitution rate. We consider this scenario unlikely, given that the K-Pg likely decimated population sizes among surviving lineages. However, even if population sizes among survivers were high, increases in mass-specific metabolic rate due to selection for smaller body size in the extinction's aftermath may still have acted to increase overall substitution rate. Our analyses support the hypothesis that the mutation rate, and not only the substitution rate, may be higher in smaller-bodied birds.

Despite the difficulty of completely disentangling the effects of these correlated phenomena (Jablonski 2008), changes leading to reductions in body size (or complete filtering of large taxa) may be expected to produce the same net effect (Romiguier et al. 2014); i.e., a transient increase in the rate of nucleotide substitution (consistent with a Lilliput-rate-process in the wake of the K-Pg mass extinction). Our results predict that

158 branch length errors induced by life history evolution should be reduced in clades that
159 have experienced relatively little life history evolution (e.g. Nabholz et al. 2016).
160
161 ***Effect of the root prior on divergence time estimation***
162 Prum et al. (2015) employed a soft gamma-distributed prior on the avian root age
163 derived from the absence of crown fossils in the Niobrara formation (sediments rich in
164 crownward stem birds and other small vertebrates (Benton et al. 2007, Field et al. 2015);
165 this, in combination with 19 fossil calibrations vetted according to recently-published best
166 practices (Parham et al. 2012), resulted in the inference of a TMRCA of ~72 Ma (95% HPD:
167 66.9-79.4 Ma) for crown birds, and HPD intervals straddling the K-Pg boundary (~66 Ma)
168 for the radiation of Neoaves.
169 To investigate the effect of this soft prior parameterization on estimates of
170 substitution rate and divergence times across the avian crown, and to investigate the
171 ability of relaxed clocks to detect extreme substitution rate shifts in the absence of
172 informative priors, we re-analyzed the Prum et al. (2015) timescale without this prior (all
173 other parameters were unchanged from the original analysis). We used sequence data from
174 the ten data partitions described in Prum et al. (2015), filtered to exhibit the lowest-
175 possible declines in phylogenetic informativeness (Townsend 2007). This dataset
176 comprises ~40kb (or ~10% of the full Prum et al. (2015) dataset) of genomic sequence
177 data, and was selected to minimize the possibility that rate inferences would be biased by
178 the effects of saturation (Nabholz et al. 2013, Dornburg et al. 2014, Prum et al. 2015). Our
179 sensitivity analysis was performed in BEAST 1.8.3 (Drummond et al. 2012) with a fixed
180 topology (following the Bayesian result from Prum et al. 2015) and a Bayesian relaxed

clock model of uncorrelated molecular rates which allows for sister or descendant lineages to sample disparate rates from a continuous lognormal distribution (Drummond et al. 2006).

Our reanalysis generated a root age estimate younger than many prior studies of avian divergence dates, yet considerably older (by about 40 million years) than the earliest-known fossil evidence of the avian crown group: median age 106.84 Ma (95% HPD 79.46-143.442)—indicating the Niobrara prior contributes ~30 Ma of branch length compression to the deepest branches in the avian phylogeny relative to an unconstrained analysis (Supplemental Figure 1). The application of the prior on the root also substantially influences the inference of extreme rates at the base of the tree in the context of the well-sampled Cenozoic calibration set used in this analysis (Prum et al. 2015).

This sensitivity analysis yielded estimates for early divergences within the major avian subclade Neoaves close to the K-Pg boundary (considering 95% HPD intervals)—with the caveat that the employed Cenozoic fossil crown group priors have soft maxima defined by the K-Pg—Supplemental Figure 1 (e.g. Prum et al. 2015). In the absence of the Niobrara prior however, median posterior ages for many of these nodes predate the K-Pg, illustrating a source of uncertainty about the role the K-Pg may have played in subsequent diversification (e.g. Jetz et al. 2012). In general however, this result is consistent with Prum et al. (2015), and is similar to the timescale inferred in a more recent study of a large nucleotide dataset with comparable taxon sampling (median root age of 96.6 Ma; 95% HPD 84.2-114.3; Claramunt et al. 2015). Claramunt et al. (2015) used over 1000 clock-like exons, 24 priors generated from 130 fossils using a novel methodology, and a birth-death

tree prior that accounted for incomplete taxon sampling, also without an explicit prior on the root age.

To test the sensitivity of our Coevol correlational analyses to the application of the Niobrara-informed soft calibration maximum, we repeated our initial correlational analyses (Figure 2 of the main text, and Supplementary Figure 6) using a time-scaled phylogeny generated without the Niobrara prior (Supplementary Figure 1B). The correlational patterns were nearly identical to the correlational analyses and results we report in the main text based on the Prum et al. (2015) time tree. In partial correlations, body size and metabolic rate remain statistically significant while other LHTs do not, and thus, overall correlational patterns do not appear to be strongly affected by application of the Niobrara prior.

Coevol estimates of the antiquity of the avian crown

In general, we used the approach outlined here and in the main text to test the hypothesis that the inclusion of body size as a covariate of substitution rate should reduce the relative ages of lineages we reconstruct as having experienced pronounced size reduction in association with the K-Pg mass extinction. While a direct test of a Lilliput-rate-process along specific avian lineages generated equivocal results due to current methodological limitations (see below), all available indirect evidence is consistent with this hypothesis. In combination, our results supporting substantial size decreases associated with the K-Pg, and multifaceted evidence supporting the hypothesis that size decreases (or the filtering out of large sizes) lead to macroevolutionary increases in substitution rates (relative to pre-extinction conditions), make a compelling case for

226 invoking the Lilliput Effect as a potential hypothesis to reconcile the rocks/clocks debate
227 across the neornithine crown.
228 In Coevol, the root age is an inherently difficult parameter to estimate (Nicolas
229 Lartillot, personal communication, Lartillot et al. 2011, Lartillot et al. 2012). Thus, we
230 attempted to validate our results by examining convergence across repeated Bayesian
231 analyses starting from different random values. Each repeated analysis ran as described in
232 the main text for >two months (>10,000 samples from the posterior) on a high-
233 performance computing cluster. Across these independent analyses with and without body
234 mass, mean MRCA age estimates for Neornithes failed to converge, and therefore could not
235 be used to identify a Lilliput-rate-process acting on the avian root node. While the results
236 from several independent chains fit our prediction (a substantial reduction in the ages of
237 the deepest nodes when including body size evolution in the model), we suggest that
238 technical limitations preventing unequivocal testing of this prediction of a Lilliput-rate-
239 process present a clear direction for future methodological refinement and analytical tool
240 development.
241 Many additional tests were performed on individual data partitions, and with
242 different combinations of fossil calibrations; none yielded reliable estimates of early avian
243 divergence times in Coevol 1.4b. A test which constrained all node ages (except for the
244 three deepest nodes in Neornithes) to match those estimated in Prum et al. (2015) revealed
245 that Coevol 1.4b explores the root age parameter space extremely slowly (and currently
246 has no option to enable user-specified tuning of this parameter). Thus, it is unable to
247 estimate this parameter with consistency within a reasonable computational timeframe for
248 this dataset (MCMC convergence diagnostics indicated low (<20) ESS values for the root

age (all other parameters > 200)). Discussions with the software developer confirmed this current technical limitation for large-scale data.

Intriguingly, across all repeated Coevol analyses, divergence times apical to the calibration points were virtually identical. The inferred lengths of apical branches experiencing life history-induced rate accelerations are therefore perhaps constrained in dating analyses by sister lineages evolving at less extreme rates and by fossil calibrations. Thus, rate increases driven by life history evolution along apical branches may not manifest as extremely long branches in the context of these constraints, whereas the deepest nodes in the avian tree, which lack such indirect or direct rate priors, can extend to implausibly ancient divergence times. This hypothesis is corroborated by our divergence time simulations that compared low, median, and heavy taxon partitions from within neoavian subclades (Simulation B, Supplemental Figure 7); while the age of Neoaves is extremely sensitive (~30 Ma), the age of Neornithes remains relatively constant (~ 95 Ma), even without fossil calibrations. As a result, age estimates for Neoaves may effectively be maximally constrained by age estimates for Neornithes (since the former is a subclade of the latter).

While Coevol is currently the most sophisticated tool for investigating the kinds of correlation structures treated in the present work, absolute ages estimated in this way are not easily comparable to those from similar analyses using other software (e.g. BEAST, see below) because they are generated with fundamentally different clock models. Age estimates derived from autocorrelated clocks that follow a Brownian rate evolution assumption (like Coevol) allow for limited variance in substitution rates across close branches, and therefore may induce older ages in the presence of rapid life history

evolution that drives extreme and uncalibrated substitution rate variation (Lartillot et al. 2016). However, in the presence of appropriately conservative calibrations (sensu Phillips 2015), relaxed clock analyses should be able to accommodate life history-induced substitution rate changes, but only for nodes apical to the calibration points (above). We illustrate this by visualizing the BEAST output from the Prum et al. (2015) divergence time estimation as a 'phenogram,' (Revell 2012), with estimated branch rates plotted at each node (Supplemental Figure 2). Supplemental Figure 3 illustrates the same distribution of rates plotted as a histogram (in gray) and a ranked list (red line with associated quartiles), and also plots inferred branch rates directly onto the Prum et al. (2015) phylogeny.

Late Cretaceous body size estimates

Body mass estimates were generated for the late Maastrichtian avifauna described by Longrich et al. (2011). This avifauna comprises 17 taxa (18 specimens, Supplemental Figure 4) from within 300,000 years of the K-Pg boundary, and represents numerous crownward stem avian lineages (including Enantiornithes, 'Palintropiformes', Hesperornithes, Ichthyornithes), and at least ten taxa phylogenetically indistinguishable from crown birds. As is unfortunately the case with the early fossil record of crown-grade birds, our study is necessarily limited with respect to the sample size of this assemblage, which represents most of the well-studied avian fossil material definitively dated to the latest Cretaceous.

Although all of these remains are comprised of fragmentary, isolated elements (and therefore are mostly phylogenetically unresolved relative to each other), the series of equations for avian body mass estimation derived by Field et al. (2013) allowed mean body

295 mass estimates, and associated 95% prediction intervals, to be derived for the coracoids
296 and tarsometatarsi represented in this dataset. Although the relatively large size of some
297 fossil taxa from this assemblage (mean = 1380.2g; median = 958.5g) could be explained by
298 bias against the preservation and discovery of small Maastrichtian bird fossils, the shape of
299 the transformed sample distribution (illustrated by the red curve in Figure 1) does not
300 suggest a skew towards larger body sizes.

301 We examined the shape of this full distribution to test for skew using a variety of
302 approaches. Using the fitdistrplus R package (Delignette-Muller et al. 2015), we fit normal,
303 lognormal, gamma, weibull, and exponential distributions to log-transformed body size
304 estimates using maximum likelihood, and found that the first three were statistically
305 preferred from the remaining two but indistinguishable from each other using AIC scores.
306 We also tested whether the kurtosis and skewness are significantly different from zero, and
307 found that they were not (one-tailed, p=0.16, and p=0.59, respectively). The Shapiro-Wilk
308 (p=0.84), Anderson-Darling (p=0.89), Cramér-von Mises (p=0.87), Pearson chi-square
309 (p=0.69), Shapiro-Francia (p=0.93), and Kolomogorv-Smirnov (p=0.91) normality tests
310 (implemented in the 'nortest' R package, Thode 2002, Gross et al. 2012) all failed to reject
311 the null hypotheses of normality, and a visualization of a normal Q-Q plot showed no
312 obvious deviations from linearity (not shown). Therefore, we suggest that, while
313 taphonomic size bias represents a legitimate challenge in paleontology, the size
314 distribution of the late Maastrichtian fossil sample investigated here does not show clear
315 evidence of being strongly skewed towards larger sizes.

316 As a final note, our sample includes two representatives of the Enantiornithes–a
317 group more distantly related to crown birds than are the other taxa in the analysis. Also

318 included are two tarsometatarsi from hesperornithines, which may have been flightless
319 and therefore possibly not reasonable analogues for early crown birds. Given that these
320 taxa are relatively large with respect to most other taxa in the sample, an additional
321 potential caveat to our fossil body size analyses is that their inclusion increases our
322 estimates of central tendency. While this is true, the effect is not large enough to change
323 our conclusions (as log transforming the data reduces the effects of extreme observations);
324 removing the two Enantiornithes from our dataset reduces that dataset mean and median
325 to 1122.75g and 820g, respectively—still substantially larger than our ASR estimates for
326 the neornithine MRCA. Further removal of the hesperornithines reduces the mean (to
327 938.4g) and median (to 636g); however, we note that these values are also still larger than
328 our ASR estimates, and still at least twice as large as our estimates for the Neoaves MRCA.
329 Moreover, we feel that removing the hesperornithines from this sample is unjustified, as
330 these are among the closest-known stem group relatives of crown birds, and including
331 them helps constrain the ancestral body size of crown birds. Although all well-represented
332 hesperornithine remains are flightless, the group was ancestrally flighted, and the pedal
333 remains in our sample preclude assessment of the flying ability of the particular
334 hesperornithine taxa in our analysis. Although the caveats noted here about potential body
335 size bias in this sample are important, we suggest the fact that some crownward stem taxa
336 are comparatively large (though still comfortably falling within the range of body size
337 variation exhibited by living flying birds) may simply reflect the fact that larger body sizes
338 were selectively filtered across the K-Pg extinction event, consistent with the hypothesis of
339 an avian Lilliput Effect.
340

Principle component analyses of life history parameters

In order to evaluate how life-history parameter co-linearity might influence estimates of the correlation structure among the eight life history parameters in this study and DNA substitution rate, we performed an additional analysis in Coevol 1.4b using the first principle component derived from a phylogenetic PCA (Revell 2010) of all eight life history axes treated here. Missing data were imputed using the Rphylopars (Bruggeman et al. 2009) R package with default settings, and the completed data matrix was subsequently analyzed using a phylogenetic PCA (using the correlation matrix) (Revell 2012). We found that PC1 explained ~70% of the variance in the dataset. Body mass and metabolic rate loaded heavily on this axis (-0.87 and -0.92, respectively). Using PC1 as a covariate of substitution rate in Coevol 1.4b (Lartillot et al. 2011, Lartillot et al. 2012) indicated that this statistically independent life history axis explained only slightly more of the variance in substitution rate (R^2=0.33, with or without GC variation considered) than did adult body mass alone (R^2=0.26) (both with pp=1.0). Thus, adult body mass is a good proxy for life history variation (Supplemental Figure 5).

Figure S1. Illustration of the effect of removing the Niobrara crown prior on the estimation of avian divergence dates under the Prum et al. (2015) node dating framework (A). Branch colors and widths are plotted as proportional to inferred rate of molecular evolution. The black base tree (in C) is the Prum et al. (2015) time tree (A), and the red arrows indicate where median posterior divergence dates are shifted when the top-10 dataset from that study is reanalyzed without the crown prior (B), while keeping all other priors consistent with those of Prum et al. (2015). While the dates of all nodes are shifted further back in time, the bulk of the change is restricted to nodes that occur close to the K-Pg boundary. Notably, the 95% HPD confidence intervals of the 7 most inclusive nodes within Neoaves (not shown) straddle the K-Pg boundary, even in the absence of an informative prior on the root, providing support for a major radiation of Neoaves related to the K-Pg mass extinction.

Supplementary Figure 1

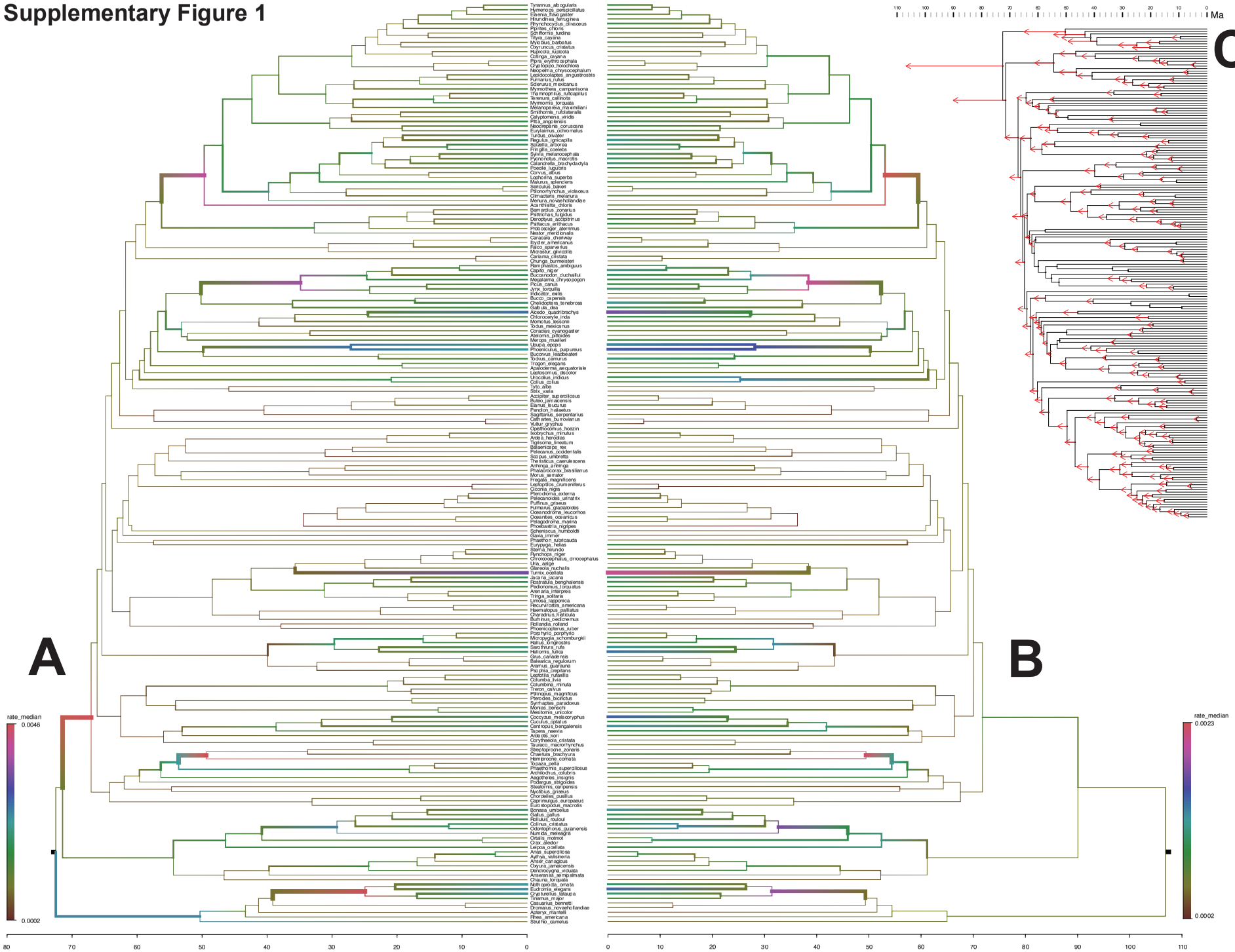

Figure S2. Visualization of the inferred branch rates from Prum et al. (2015) as a 'rateogram' (Revell 2012). Median branch rates are plotted along the vertical axis coordinates (shown here as relative rates), across time. Branch colors recapitulate those of the seven major clades depicted in Prum et al. (2015) and those in the main text Figure 3 of the present study. The dashed red line indicates the Cretaceous/Paleogene boundary, and the dotted black line indicates the oldest unambiguous crown bird fossil serving as a node calibration in Prum et al. (2015), the stem sphenisciform *Waimanu manneringi*. An additional 18 fossils were used to calibrate clade ages in Prum et al. (2015), but they are all younger than *W. manneringi*. Thus, the use of a Niobrara-informed prior to constrain the age of the root induces deep branch rates that are ~5-20x faster than the slowest-evolving lineages in these analyses.

Supplementary Figure 2

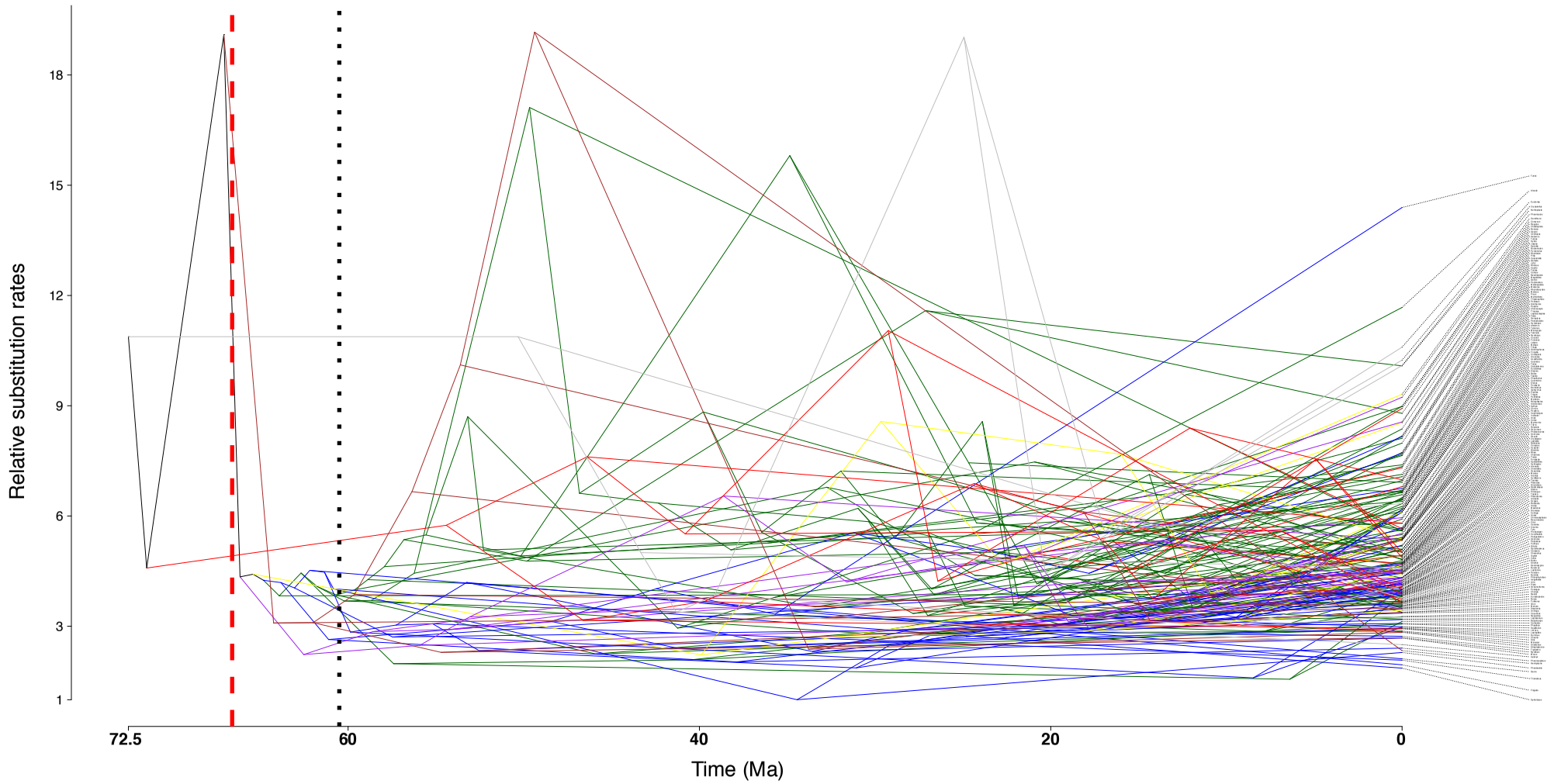

Figure S3. Visualization of the inferred substitution rates from the primary Prum et al. (2015) BEAST analysis. These rates were inferred under an uncorrelated relaxed lognormal clock model, with 19 well-justified fossil-informed prior calibrations and a Niobrara-informed calibration on the root (following the original analysis in Prum et al. 2015). On the left, rates are plotted along branches and colored and scaled in proportion to rate (also shown in Supplemental Figure 1A). The histogram, shown in grey, generally follows the shape of a lognormal distribution, indicating that the posterior distribution of rates is informed by the lognormal prior. Overlaid on the histogram are the same rate data, sorted from slowest to fastest, and then normalized by the slowest rate; rates are inferred to vary by ~20x. The black confidence intervals around this line indicate the upper and lower quartiles of the rate posterior distributions (not the 95% HPD).

Supplementary Figure 3

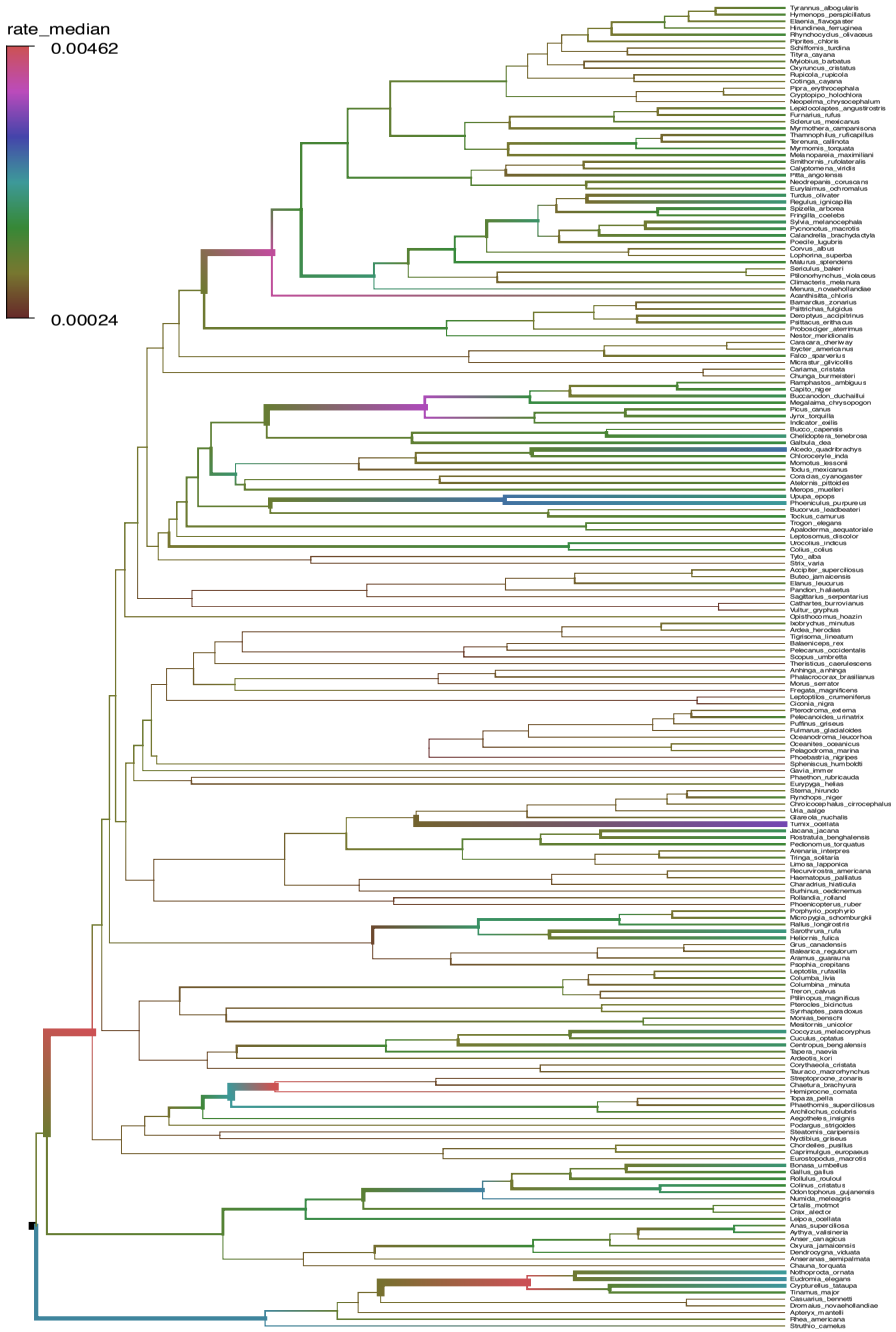

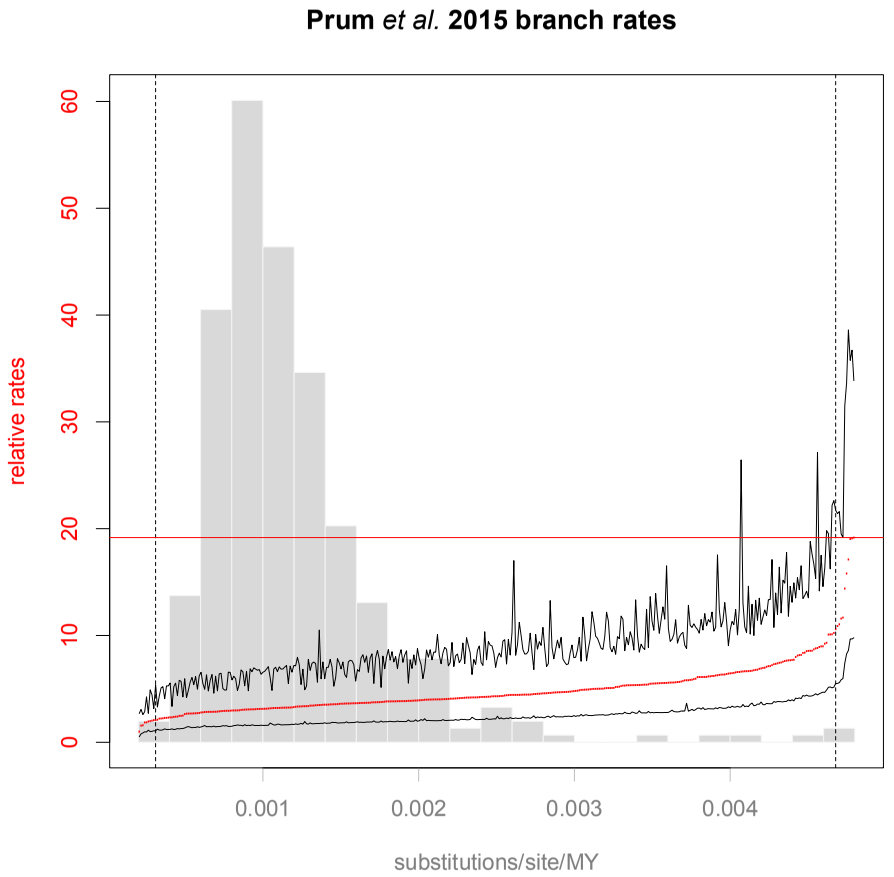

Figure S4. Mean mass estimates and associated 95% prediction intervals for the latest-Maastrichian avifauna described by Longrich et al. (2011). For isolated coracoids within this assemblage the predictive mass equation for humeral articulation facet measurements [ln(BM) = 2.44(ln HAF) + 2.00] from Field et al. (2013) was applied. For isolated tarsometatarsi, the predictive mass equation for tarsus midshaft diameter [ln(BM) = 2.38(ln TaD) + 3.12] from Field et al. (2013) was applied. The dashed line indicates the mean mass estimate for this fossil assemblage.

Supplementary Figure 4

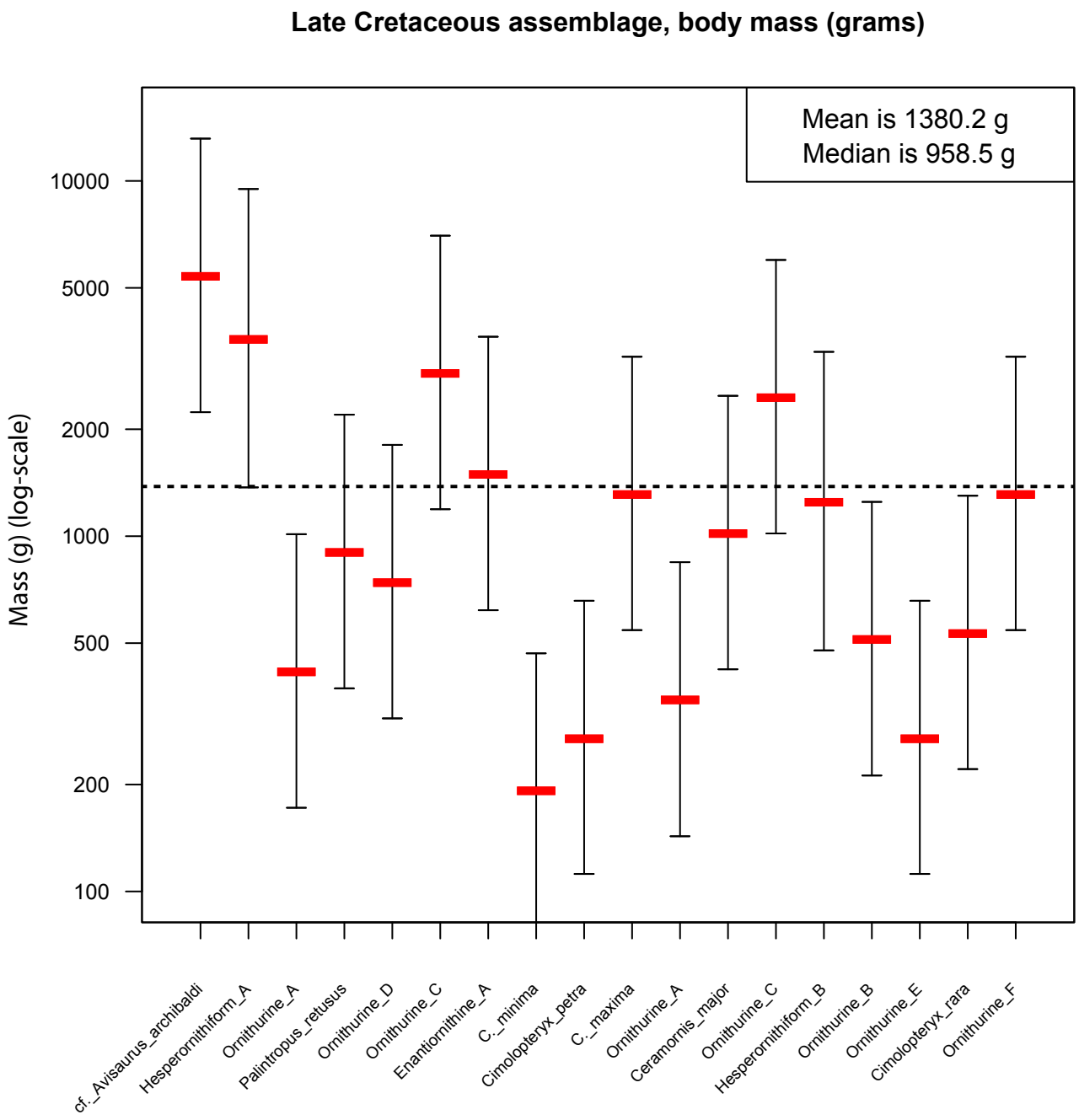

Figure S5. Left: Phylogenetic PCA (Revell 2010) of the life history data treated in the present study, with PC1 regressed against PC2 to illustrate statistical independence ($R^2 \sim 0.01$), with loadings (red arrows) of different parameters projected into component space. Middle: the proportion of variance in the dataset explained by different statistically independent components. Right: PC1 (which explains >70% of the total variance) regressed against ln(adult mass), to illustrate that body mass is a good proxy for life history variation ($R^2 \sim 0.83$).

Supplementary Figure 5

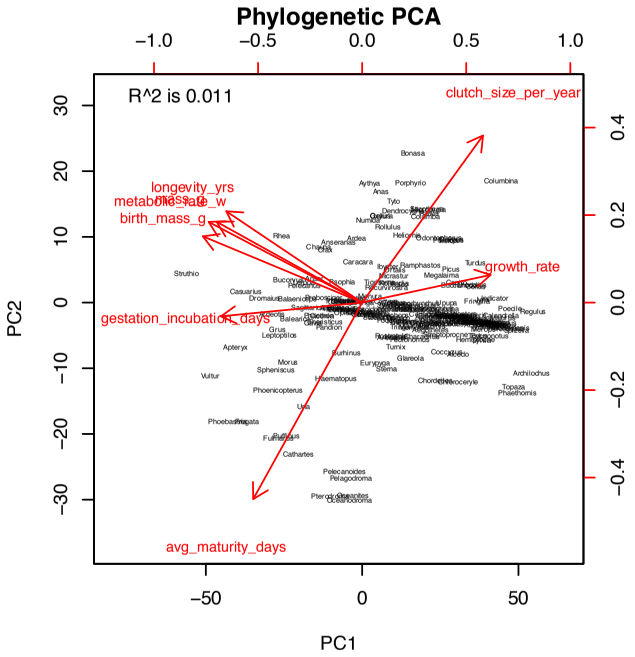

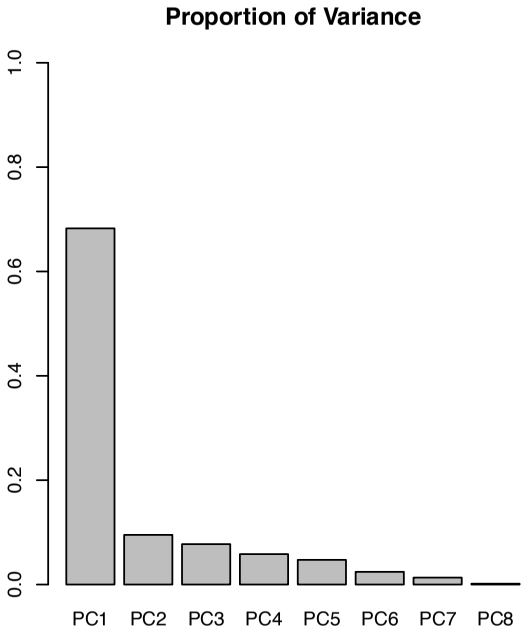

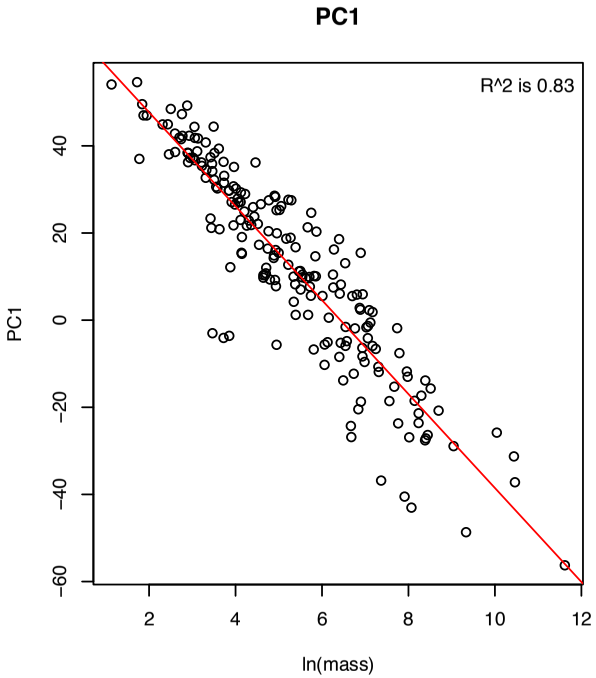

Figure S6. Pairwise scatterplot matrix of life history traits (LHTs) downloaded from the AnAge database for a sample of 198 bird species. Scatterplots of the raw, natural log-transformed data with accompanying simple linear regression (to illustrate general trends) are shown in the lower left triangle. The upper right triangle summarizes the R^2 values for simple linear regression (top), phylogenetically informed regression (middle value – pairwise regression coefficient from Coevol), and the number of missing data points in each comparison (bottom). These data are also reported in /SuppData4/coevol-data-files/all-data/mega-data-clutch-size-per-year-chain1.cov. Asterisks indicate Bonferroni-corrected significance at the 0.05 level (for the top number), and maximal posterior probabilities (pp=1.0) (middle number). The colors of the boxes in the top right triangle are scaled per the direction and strength of the correlation in the uncorrected linear regression (red, negative; blue, positive).

Supplementary Figure 6

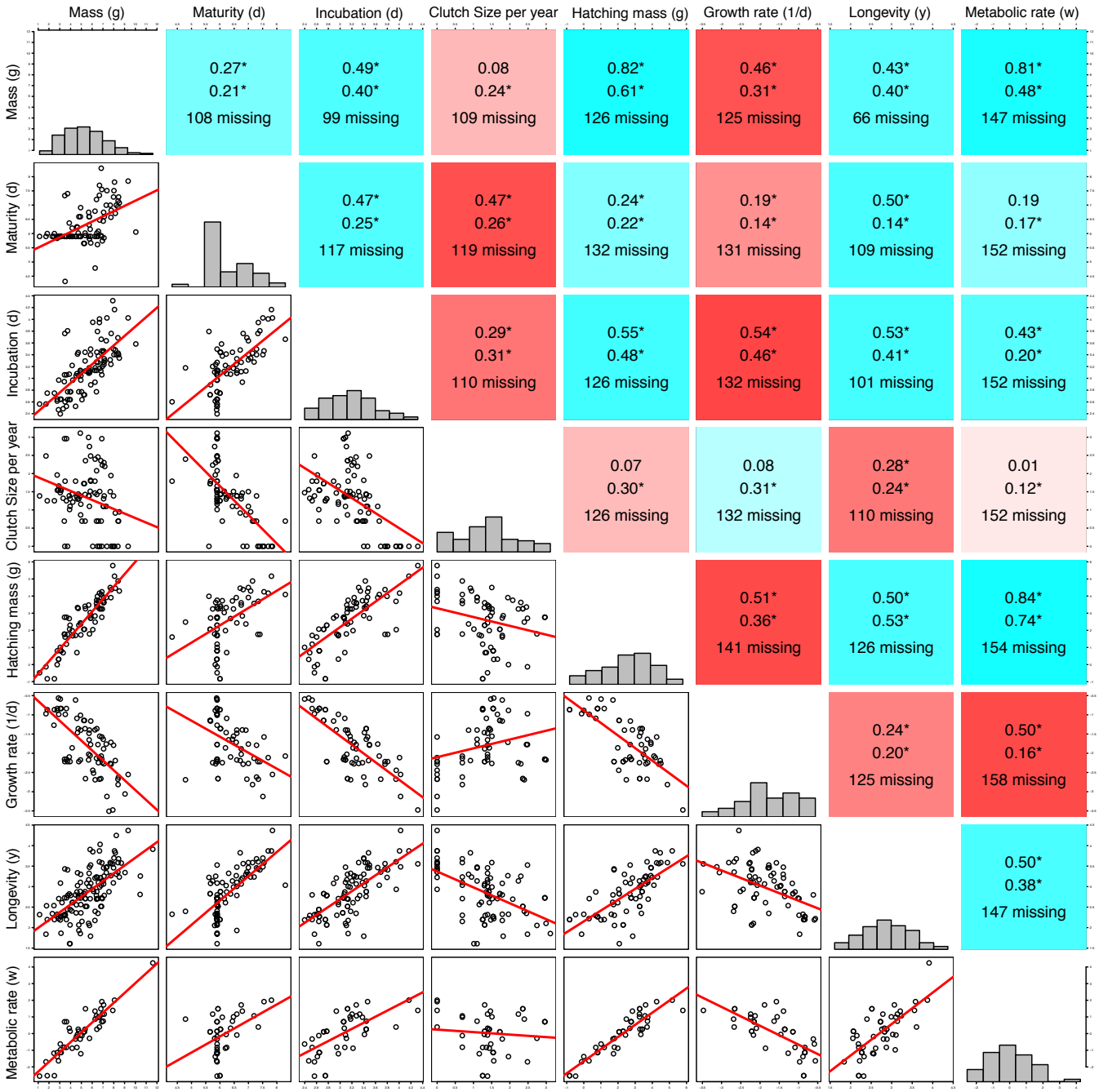

Figure S7. Simulations of the effect of size-biased extinction on the inferred age of Neoaves (Simulation B). The composition of Palaeognathae and Galloanserae (the successive sister groups to Neoaves) are held constant, and partitions of heavy (green), median (red), and low (blue) mass representatives of the major neoavian subclades were analyzed using both strict and relaxed molecular clocks. This analysis illustrates that inferred clade ages within Neoaves are strongly influenced by body size. For relaxed clock analyses, up to ~35 Ma of divergence time disparity in the age of Neoaves can be explained by substitution rate variation related to body size alone. The different median posterior estimates generated from both strict and relaxed clock simulations span a range of hypotheses invoking different effects of the K-Pg mass extinction on neoavian diversification. All simulations of this type using the median mass taxon partition are consistent with a post-K-Pg radiation of Neoaves, and are entirely congruent with the known avian crown group fossil record. While the median mass taxon partition may not represent the 'true' age of Neoaves, we suggest this estimate should be less biased by lineages evolving at either extremely high or extremely low rates of molecular evolution.

Supplementary Figure 7

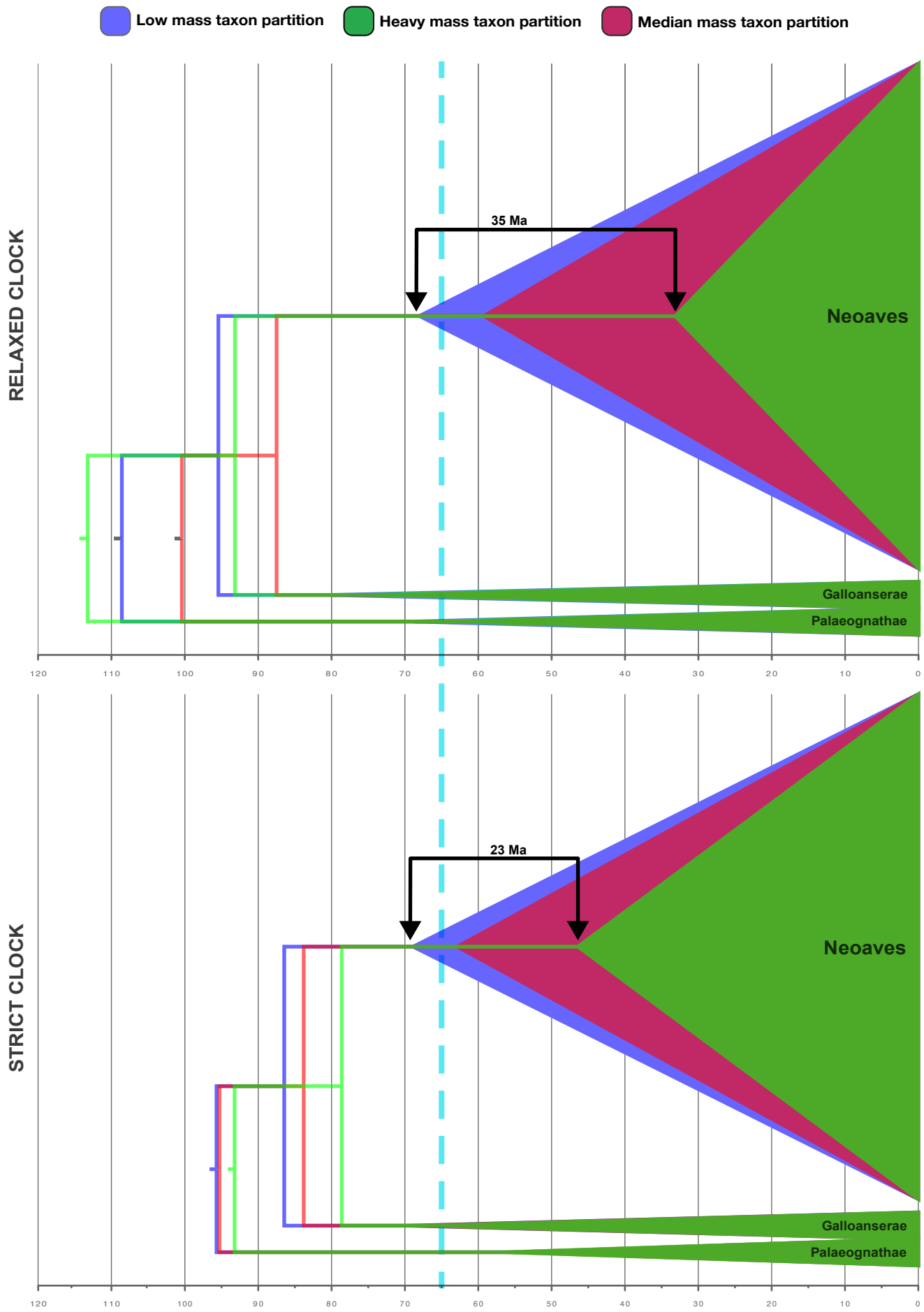

Figure S8. Ancestral body size estimates from Coevol correlational analysis. Following (Lartillot et al. 2012), we compared posterior distributions of ancestral state reconstructions generated in Coevol 1.4b (Lartillot et al. 2011). Using the model referred to in the main text which included body mass, metabolic rate, and GC content variation, we generated estimates of ancestral body size conditioned on rates of molecular evolution implied by the Prum et al. (2015) time-scaled phylogeny (histograms shown in red, with dashed line indicating the median). Histograms shown in white (with solid line indicating the median) were generated in Coevol with the '–diag' flag, which forces the covariance matrix to be diagonal (rates and traits evolve independently). As discussed in the main text, these simulations suggest that the fast rates implied by the Prum et al. (2015) phylogeny are enough to considerably reduce the estimated size reconstructions for several key nodes (e.g., Neornithes, Neognathae, and Neoaves), even beyond what is implied by independent, fossil-calibrated reconstructions (Figure 1). Because Coevol detects a statistically significant correlation between body size and substitution rate, ancestral state reconstructions that do not accommodate this correlation can be statistically rejected in this context (*N. Lartillot*, personal communication).

Supplementary Figure 8

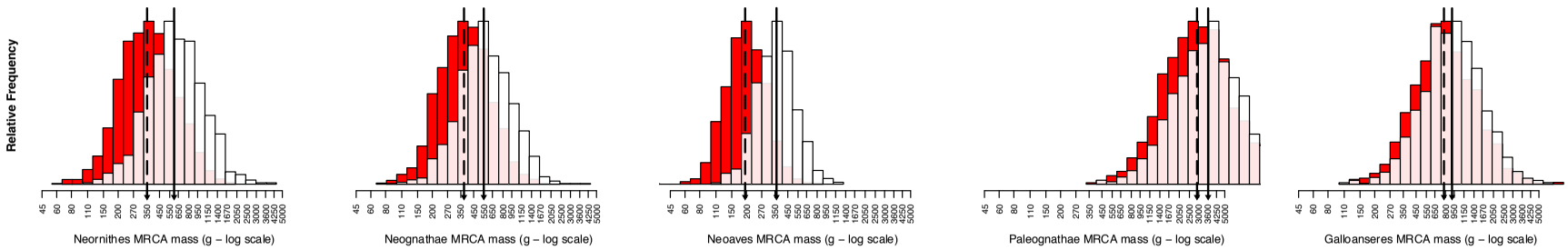

Additional Data Table S1 (separate file)

Life history data table formatted for input into the Coevol analytical software. Life history data were obtained from the AnAge senescence database Build 13 (De Magalhães et al. 2009, Tacutu et al. 2013). We collated the following data: (1) age at sexual maturity (days), (2) incubation time (days), (3) number of eggs laid per year, (4) mass at hatching (grams), (5) growth rate (1/days), (6), maximum recorded longevity (years), and (7) total metabolic rate (watts). Relative to the set of 198 avian taxa in Prum et al. (2015), when matching genera occurred in the AnAge database, we used averages at the genus level; otherwise, we used family-level averages. Body mass (grams, species average) data were collected from Dunning Jr (1992). This yielded a data matrix with ~49% missing data overall (with no missing data for body mass).

Additional Data Table S2 (separate file)

Correlation coefficients and posterior probabilities from substitution rate analysis with Coevol 1.4b (summarized in Figure 2). Raw posterior probabilities are reported as ranging from from 0.0 (100% support for a negative correlation) to 1.0 (100% support for a positive correlation). Negative correlations are reported as 1-raw in the main text.

Additional Data Table S3 (separate file)

Data table of estimated crown fossil masses used as body size priors to calibrate ASRs. Mean body mass estimates and associated 95% prediction intervals are derived from published predictive equations (Field et al. 2013). Unless otherwise noted, measurements for these taxa are taken from holotype specimens, and unless otherwise noted, published measurements were used from references noted in the table.

Additional Data File S4 (SuppData4.zip, separate file)

We provide as a zip archive the data and script files necessary to reproduce the analyses in the present work. A detailed readme txt file is included in this zip archive that outlines the analytical procedures needed to replicate the major analyses in the present work.

638 **Supplementary References**

639

640 Barker FK, Barrowclough GF, Groth JG. 2002. A phylogenetic hypothesis for passerine
641 birds: taxonomic and biogeographic implications of an analysis of nuclear DNA sequence
642 data., 269:295-308.

643 Barrick JE, Lenski RE. 2013. Genome dynamics during experimental evolution. Nat Rev
644 Genet, 14:827-839.

645 Beaulieu JM, O'Meara BC, Crane P, Donoghue MJ. 2015. Heterogeneous Rates of Molecular
646 Evolution and Diversification Could Explain the Triassic Age Estimate for Angiosperms.
647 Systematic Biology, 64:869-878.

648 Benton MJ, Donoghue PCJ. 2007. Paleontological evidence to date the tree of life. Molecular
649 Biology and Evolution, 24:26.

650 Bininda-Emonds ORP, Cardillo M, Jones KE, MacPhee RDE, Beck RMD, Grenyer R, Price SA,
651 Vos RA, Gittleman JL, Purvis A. 2007. The delayed rise of present-day mammals. Nature,
652 446:507-512.

653 Brenner GJ. 1996. Evidence for the Earliest Stage of Angiosperm Pollen Evolution: A
654 Paleoequatorial Section from Israel. In: Taylor DW, Hickey LJ editors. Flowering Plant
655 Origin, Evolution & Phylogeny. Boston, MA, Springer US, p. 91-115.

656 Bromham L. 2002. Molecular Clocks in Reptiles: Life History Influences Rate of Molecular
657 Evolution. Molecular Biology and Evolution, 19:302-309.

Bromham L. 2011. The genome as a life-history character: why rate of molecular evolution varies between mammal species. Philosophical Transactions of the Royal Society of London B: Biological Sciences, 366:2503-2513.

Brown JW, Rest JS, García-Moreno J, Sorenson MD, Mindell DP. 2008. Strong mitochondrial DNA support for a Cretaceous origin of modern avian lineages. BMC Biology, 6:1-18.

Bruggeman J, Heringa J, Brandt BW. 2009. PhyloPars: estimation of missing parameter values using phylogeny. Nucleic Acids Research, 37:W179-W184.

Claramunt S, Cracraft J. 2015. A new time tree reveals Earth history's imprint on the evolution of modern birds. Science Advances, 1.

Clarke JA, Chatterjee S, Li Z, Riede T, Agnolin F, Goller F, Isasi MP, Martinioni DR, Mussel FJ, Novas FE. 2016. Fossil evidence of the avian vocal organ from the Mesozoic. Nature, 538:502-505.

Clarke JA, Tambussi CP, Noriega JI, Erickson GM, Ketcham RA. 2005. Definitive fossil evidence for the extant avian radiation in the Cretaceous. Nature, 433:305-308.

Cracraft J, Houde P, Ho SYW, Mindell DP, Fjeldså J, Lindow B, Edwards SV, Rahbek C, Mirarab S, Warnow T, Gilbert MTP, Zhang G, Braun EL, Jarvis ED. 2015. Response to Comment on "Whole-genome analyses resolve early branches in the tree of life of modern birds". Science, 349:1460-1460.

De Magalhães JP, Costa J. 2009. A database of vertebrate longevity records and their relation to other life-history traits. Journal of Evolutionary Biology, 22:1770-1774.

678 Delignette-Muller ML, Dutang C. 2015. fitdistrplus: An R Package for Fitting Distributions.
679 2015, 64:34.

680 Dornburg A, Brandley MC, McGowen MR, Near TJ. 2012. Relaxed Clocks and Inferences of
681 Heterogeneous Patterns of Nucleotide Substitution and Divergence Time Estimates across
682 Whales and Dolphins (Mammalia: Cetacea). Molecular Biology and Evolution, 29:721-736.

683 Dornburg A, Townsend JP, Friedman M, Near TJ. 2014. Phylogenetic informativeness
684 reconciles ray-finned fish molecular divergence times. BMC Evolutionary Biology, 14:1-14.

685 Drummond AJ, Ho SYW, Phillips MJ, Rambaut A. 2006. Relaxed Phylogenetics and Dating
686 with Confidence. PLoS Biol, 4:e88.

687 Drummond AJ, Suchard MA, Xie D, Rambaut A. 2012. Bayesian phylogenetics with BEAUti
688 and the BEAST 1.7. Molecular biology and evolution, 29:1969-1973.

689 Dunning Jr JB. 1992. CRC handbook of avian body masses. CRC press.

690 Erwin DH, Laflamme M, Tweedt SM, Sperling EA, Pisani D, Peterson KJ. 2011. The Cambrian
691 Conundrum: Early Divergence and Later Ecological Success in the Early History of Animals.
692 Science, 334:1091-1097.

693 Field DJ, LeBlanc A, Gau A, Behlke ADB. 2015. Pelagic neonatal fossils support viviparity
694 and precocial life history of Cretaceous mosasaurs. Palaeontology:401-407.

695 Field DJ, Lynner C, Brown C, Darroch SAF. 2013. Skeletal Correlates for Body Mass
696 Estimation in Modern and Fossil Flying Birds. PLoS ONE, 8:e82000.

697 Fontanillas E, Welch JJ, Thomas JA, Bromham L. 2007. The influence of body size and net
698 diversification rate on molecular evolution during the radiation of animal phyla. BMC
699 Evolutionary Biology, 7:1-12.

700 Friis EM, Crane PR, Pedersen KR. 2011. Early flowers and angiosperm evolution. Cambridge
701 University Press.

702 Gillooly JF, Allen AP, West GB, Brown JH. 2005. The rate of DNA evolution: Effects of body
703 size and temperature on the molecular clock. Proceedings of the National Academy of
704 Sciences, 102:140-145.

705 Gillooly JF, McCoy MW, Allen AP. 2007. Effects of metabolic rate on protein evolution.
706 Biology Letters, 3:655-660.

707 Gross J, Ligges U. 2012. Nortest: Tests for normality. R package version 1.0–2. URL:
708 http://cran.r-project.org/package=nortest.

709 Hua X, Cowman P, Warren D, Bromham L. 2015. Longevity Is Linked to Mitochondrial
710 Mutation Rates in Rockfish: A Test Using Poisson Regression. Molecular Biology and
711 Evolution, 32:2633-2645.

712 Hutchinson GE. 1959. Homage to Santa Rosalia or Why Are There So Many Kinds of
713 Animals? The American Naturalist, 93:145-159.

714 Jablonski D. 2008. Species Selection: Theory and Data. Annual Reviews, 39:501-524.

715 Jarvis ED, Mirarab S, Aberer AJ, Li B, Houde P, Li C, Ho SYW, Faircloth BC, Nabholz B,
716 Howard JT, Suh A, Weber CC, da Fonseca RR, Li J, Zhang F, Li H, Zhou L, Narula N, Liu L,

717 Ganapathy G, Boussau B, Bayzid MS, Zavidovych V, Subramanian S, Gabaldón T, Capella-
718 Gutiérrez S, Huerta-Cepas J, Rekepalli B, Munch K, Schierup M, Lindow B, Warren WC, Ray
719 D, Green RE, Bruford MW, Zhan X, Dixon A, Li S, Li N, Huang Y, Derryberry EP, Bertelsen MF,
720 Sheldon FH, Brumfield RT, Mello CV, Lovell PV, Wirthlin M, Schneider MPC, Prosdocimi F,
721 Samaniego JA, Velazquez AMV, Alfaro-Núñez A, Campos PF, Petersen B, Sicheritz-Ponten T,
722 Pas A, Bailey T, Scofield P, Bunce M, Lambert DM, Zhou Q, Perelman P, Driskell AC, Shapiro
723 B, Xiong Z, Zeng Y, Liu S, Li Z, Liu B, Wu K, Xiao J, Yinqi X, Zheng Q, Zhang Y, Yang H, Wang J,
724 Smeds L, Rheindt FE, Braun M, Fjeldsa J, Orlando L, Barker FK, Jønsson KA, Johnson W,
725 Koepfli K-P, O'Brien S, Haussler D, Ryder OA, Rahbek C, Willerslev E, Graves GR, Glenn TC,
726 McCormack J, Burt D, Ellegren H, Alström P, Edwards SV, Stamatakis A, Mindell DP, Cracraft
727 J, Braun EL, Warnow T, Jun W, Gilbert MTP, Zhang G. 2014. Whole-genome analyses resolve
728 early branches in the tree of life of modern birds. Science, 346:1320-1331.

729 Jetz W, Thomas GH, Joy JB, Hartmann K, Mooers AO. 2012. The global diversity of birds in
730 space and time. Nature, 491:444-448.

731 Kimura M. 1968. Evolutionary Rate at the Molecular Level. Nature, 217:624-626.

732 Lanfear R, Ho SYW, Love D, Bromham L. 2010. Mutation rate is linked to diversification in
733 birds. Proceedings of the National Academy of Sciences, 107:20423-20428.

734 Lanfear R, Kokko H, Eyre-Walker A. 2013. Population size and the rate of evolution. Trends
735 in Ecology & Evolution, 29:33-41.

736 Lartillot N, Delsuc F. 2012. Joint reconstruction of divergence times and life-history
737 evolution in placental mammals using a phylogenetic covariance model. Evolution,
738 66:1773-1787.

739 Lartillot N, Phillips MJ, Ronquist F. 2016. A mixed relaxed clock model. Philosophical
740 Transactions of the Royal Society of London B: Biological Sciences, 371.

741 Lartillot N, Poujol R. 2011. A Phylogenetic Model for Investigating Correlated Evolution of
742 Substitution Rates and Continuous Phenotypic Characters. Molecular Biology and
743 Evolution, 28:729-744.

744 Lehtonen J, Lanfear R. 2014. Generation time, life history and the substitution rate of
745 neutral mutations. Biology Letters, 10.

746 Longrich NR, Tokaryk T, Field DJ. 2011. Mass extinction of birds at the Cretaceous–
747 Paleogene (K–Pg) boundary. Proceedings of the National Academy of Sciences, 108:15253-
748 15257.

749 Martin AP, Palumbi SR. 1993. Body size, metabolic rate, generation time, and the molecular
750 clock. Proceedings of the National Academy of Sciences, 90:4087-4091.

751 McNab BK. 2012. Extreme measures: the ecological energetics of birds and mammals.
752 University of Chicago Press.

753 Mendes FK, Hahn MW. 2016. Gene Tree Discordance Causes Apparent Substitution Rate
754 Variation. Systematic Biology.

755 Nabholz B, Lanfear R, Fuchs J. 2016. Body mass-corrected molecular rate for bird
756 mitochondrial DNA. Molecular Ecology, 25:4438–4449.

757 Nabholz B, Uwimana N, Lartillot N. 2013. Reconstructing the Phylogenetic History of Long-
758 Term Effective Population Size and Life-History Traits Using Patterns of Amino Acid
759 Replacement in Mitochondrial Genomes of Mammals and Birds. Genome Biology and
760 Evolution, 5:1273-1290.

761 O'Leary MA, Bloch JI, Flynn JJ, Gaudin TJ, Giallombardo A, Giannini NP, Goldberg SL, Kraatz
762 BP, Luo Z-X, Meng J, Ni X, Novacek MJ, Perini FA, Randall ZS, Rougier GW, Sargis EJ, Silcox
763 MT, Simmons NB, Spaulding M, Velazco PM, Weksler M, Wible JR, Cirranello AL. 2013. The
764 Placental Mammal Ancestor and the Post–K-Pg Radiation of Placentals. Science, 339:662-
765 667.

766 Ohta T. 1973. Slightly Deleterious Mutant Substitutions in Evolution. Nature, 246:96-98.

767 Parfrey LW, Lahr DJG, Knoll AH, Katz LA. 2011. Estimating the timing of early eukaryotic
768 diversification with multigene molecular clocks. Proceedings of the National Academy of
769 Sciences, 108:13624-13629.

770 Parham JF, Donoghue PCJ, Bell CJ, Calway TD, Head JJ, Holroyd PA, Inoue J, Irmis RB, Joyce
771 WG, Ksepka DT, Patane JSL, Smith ND, Tarver JE, van Tuinen M, Yang Z, Angielczyk KD,
772 Greenwood JM, Hipsley CA, Jacobs L, Makovicky PJ, Muller J, Smith KT, Theodor JM,
773 Warnock RCM, Benton MJ. 2012. Best practices for justifying fossil calibrations. Syst Biol,
774 61:346 - 359.

775 Parham JF, Donoghue PCJ, Bell CJ, Calway TD, Head JJ, Holroyd PA, Inoue JG, Irmis RB, Joyce
776 WG, Ksepka DT, Patané JSL, Smith ND, Tarver JE, van Tuinen M, Yang Z, Angielczyk KD,
777 Greenwood JM, Hipsley CA, Jacobs L, Makovicky PJ, Müller J, Smith KT, Theodor JM,
778 Warnock RCM. 2011. Best Practices for Justifying Fossil Calibrations. Systematic Biology.

779 Peterson KJ, Lyons JB, Nowak KS, Takacs CM, Wargo MJ, McPeek MA. 2004. Estimating
780 metazoan divergence times with a molecular clock. Proceedings of the National Academy of
781 Sciences of the United States of America, 101:6536-6541.

782 Phillips MJ. 2015. Geomolecular Dating and the Origin of Placental Mammals. Systematic
783 Biology.

784 Prum RO, Berv JS, Dornburg A, Field DJ, Townsend JP, Lemmon EM, Lemmon AR. 2015. A
785 comprehensive phylogeny of birds (Aves) using targeted next-generation DNA sequencing.
786 Nature, 526:569-573.

787 Revell LJ. 2010. Phylogenetic signal and linear regression on species data. Methods in
788 Ecology and Evolution, 1:319-329.

789 Revell LJ. 2012. phytools: an R package for phylogenetic comparative biology (and other
790 things). Methods in Ecology and Evolution, 3:217-223.

791 Reynolds PS, Lee RM. 1996. Phylogenetic Analysis of Avian Energetics: Passerines and
792 Nonpasserines Do Not Differ. The American Naturalist, 147:735-759.

793 Romiguier J, Gayral P, Ballenghien M, Bernard A, Cahais V, Chenuil A, Chiari Y, Dernat R,
794 Duret L, Faivre N, Loire E, Lourenco JM, Nabholz B, Roux C, Tsagkogeorga G, Weber AAT,

795 Weinert LA, Belkhir K, Bierne N, Glemin S, Galtier N. 2014. Comparative population
796 genomics in animals uncovers the determinants of genetic diversity. Nature, 515:261-263.

797 Sibley CG, Ahlquist JE. 1990. Phylogeny and classification of birds: a study in molecular
798 evolution. Yale University Press.

799 Slack KE, Jones CM, Ando T, Harrison GL, Fordyce RE, Arnason U, Penny D. 2006. Early
800 Penguin Fossils, Plus Mitochondrial Genomes, Calibrate Avian Evolution. Molecular Biology
801 and Evolution, 23:1144-1155.

802 Smith SA, Beaulieu JM, Donoghue MJ. 2010. An uncorrelated relaxed-clock analysis suggests
803 an earlier origin for flowering plants. Proceedings of the National Academy of Sciences,
804 107:5897-5902.

805 Smith SA, Donoghue MJ. 2008. Rates of Molecular Evolution Are Linked to Life History in
806 Flowering Plants. Science, 322:86-89.

807 Smith T, Rose KD, Gingerich PD. 2006. Rapid Asia–Europe–North America geographic
808 dispersal of earliest Eocene primate Teilhardina during the Paleocene–Eocene Thermal
809 Maximum. Proceedings of the National Academy of Sciences, 103:11223-11227.

810 Steiper ME, Seiffert ER. 2012. Evidence for a convergent slowdown in primate molecular
811 rates and its implications for the timing of early primate evolution. Proceedings of the
812 National Academy of Sciences, 109:6006-6011.

813 Suh A, Smeds L, Ellegren H. 2015. The Dynamics of Incomplete Lineage Sorting across the
814 Ancient Adaptive Radiation of Neoavian Birds. PLoS Biol, 13:e1002224.

815 Tacutu R, Craig T, Budovsky A, Wuttke D, Lehmann G, Taranukha D, Costa J, Fraifeld VE, de
816 Magalhães JP. 2013. Human Ageing Genomic Resources: Integrated databases and tools for
817 the biology and genetics of ageing. Nucleic Acids Research, 41:D1027-D1033.

818 Tavare S, Marshall CR, Will O, Soligo C, Martin RD. 2002. Using the fossil record to estimate
819 the age of the last common ancestor of extant primates. Nature, 416:726-729.

820 Thode HC. 2002. Testing for normality. CRC press.

821 Thomas JA, Welch JJ, Lanfear R, Bromham L. 2010. A Generation Time Effect on the Rate of
822 Molecular Evolution in Invertebrates. Molecular Biology and Evolution, 27:1173-1180.

823 Thomas JA, Welch JJ, Woolfit M, Bromham L. 2006. There is no universal molecular clock
824 for invertebrates, but rate variation does not scale with body size. Proceedings of the
825 National Academy of Sciences, 103:7366-7371.

826 Townsend JP. 2007. Profiling phylogenetic informativeness. Systematic Biology, 56:222-
827 231.

828 Weber CC, Nabholz B, Romiguier J, Ellegren H. 2014. Kr/Kc but not dN/dS correlates
829 positively with body mass in birds, raising implications for inferring lineage-specific
830 selection. Genome Biology, 15:1-13.

831 White EP, Ernest SKM, Kerkhoff AJ, Enquist BJ. 2007. Relationships between body size and
832 abundance in ecology. Trends in Ecology & Evolution, 22:323-330.

833 Wilkinson RD, Steiper ME, Soligo C, Martin RD, Yang Z, Tavaré S. 2011. Dating Primate
834 Divergences through an Integrated Analysis of Palaeontological and Molecular Data.
835 Systematic Biology, 60:16-31.

836 Woolfit M. 2009. Effective population size and the rate and pattern of nucleotide
837 substitutions. Biology Letters.

838 Woolfit M, Bromham L. 2003. Increased Rates of Sequence Evolution in Endosymbiotic
839 Bacteria and Fungi with Small Effective Population Sizes. Molecular Biology and Evolution,
840 20:1545-1555.

841 Zeng L, Zhang Q, Sun R, Kong H, Zhang N, Ma H. 2014. Resolution of deep angiosperm
842 phylogeny using conserved nuclear genes and estimates of early divergence times. Nat
843 Commun, 5.
844